May 2014

The Effect of localized low concrete strength on flexural strength of RC beams

Feng Xie
Syracuse University

ABSTRACT

In reinforced concrete (RC) beams, localized low concrete strength may occur under certain conditions, e.g., poor construction practice that results in concrete honeycombing. The performance of beams with localized poor zones has received considerable attention in civil engineering research. This report presents the response of beams with various localized poor zones along the length of simply supported flexural members. A finite element model approach is developed and calibrated against two experimental beam test data, conducted by others. Solid 65 elements for modeling the concrete and Link180 elements for modeling the steel reinforcing bars are combined together with spring elements between reinforcing steel and concrete. The modified Hognestad Model is adopted for describing the concrete properties, and the properties of steel followed a perfect elasto-plastic model. To model the bond between concrete and reinforcing steel bars, nonlinear spring element Combin39 is used to connect the concrete nodes and steel nodes. For the bond spring elements, the bond stress and slip curves are in accordance with the recent researches by CEB-FIP.

To simulate concrete degradation effect, the concrete strength at different locations is reduced. In this paper, the beam is divided into three major regions, one is sensitive to bending moment, one is sensitive to shear, and the third region is sensitive to bond slip. The variables investigated under this study also included four types of concrete strength and three different rebar sizes. A total of 30 FEM beams are investigated. The results of this research suggest that the most critical region to have

low concrete strength, along the beam length, is the bond slip zone near the supports, as reflected on the ductility of the load-deflection curves. A new generalized empirical model is developed with the objective to predict the load reduction effect of the localized concrete problem.

Keywords: Construction defects; Bond slip; Low strength concrete; reinforced concrete; Finite element modeling; localized damaged concrete; Nonlinear analysis

The Effect of localized low concrete strength on flexural strength of RC beams

by

Feng Xie

B.S., China University of Geosciences, 2012

Thesis

Submitted in partial fulfillment of the requirements for the degree of
Master of Science in Civil Engineering.

Syracuse University
May 2014

ACKNOWLEDGMENT

The author would like to gratefully and sincerely thank his supervisor, Dr. Riyad Aboutaha, Professor of Department of Civil Engineering at the Syracuse University. He helped the author a lot throughout the entire research period with his knowledge, guidance and support. The author would also like to thank Professor Lui, Professor Salem and Professor Murthy for teaching him advanced knowledge in civil engineering and being his committee member. In addition, the help from author's friend, Lu Wang, Fares Jnaid, Sara, Sara Sotoud, Sudipta Ghorai are also acknowledged.

TABLE OF CONTENTS

LIST OF FIGURES

LIST OF TABLES

LIST OF CONVERSION FACTORS

U.S Customary Units to S.I Metric Units

Overall Geometry	
Spans	1 ft = 0.3048 m
Displacements	1 in. = 25.4 mm
Surface Area	1 ft^2 = 0.0929 m^2
Volume	1 ft^3 = 0.0283 m^3
	1 yd^3 = 0.765 m^3
Structural Properties	
Cross-sectional dimensions	1 in. = 25.4 mm
Area	1 $in.^2$ = 645.2 mm^2
Section modulus	1 $in.^3$ = 16.39 x 10^3 mm^3
Moment of inertia	1 $in.^4$ = 0.4162 x 10^6 mm^4
Material Properties	
Density	1 lb/ft^3 = 16.03 kg/m^3
Modulus and stress	1 $lb/in.^2$ =0.006895 N/mm^2
	1 $kip/in.^2$ =6.895 N/mm^2
Loadings	
Concentrated loads	1 lb = 4.448 N
	1 kip = 4.448 kN
Density	1 lb/ft^3 = 0.1571 kN/m^3
Linear loads	1 kip/ft = 14.59 kN/m
Surface loads	1 lb/ft^2 = 0.0479 kN/m^2
	1 kip/ft^2 = 47.9 kN/m^2
Stresses and Moments	
Stress	1 $lb/in.^2$ = 0.006895 N/mm^2
	1 $kip/in.^2$ = 6.895 N/mm^2
Moment or torque	1 ft-lb = 1.356 N-m
	1 ft-kip = 1.356 kN-m

Note: 1 N/mm^2 = 1 MPa

Chapter 1 INTRODUCTION

1.1 Background

Reinforced concrete structures are widely used over the world due to its cost-effective benefit. They can work well as designed because the behavior of reinforced concrete structures could be easily predicated if constructed as designed and well maintenance. However, poor construction practice could cause problems, such as honeycombing in concrete, and create zones of low concrete strength. Many of the bridges built in United States are reinforced concrete bridges. But one in nine of the nation's bridges are rated as structurally deficient. In the nation's 102 largest metropolitan regions, over two hundred million trips are taken daily across these deficient bridges. (ASCE | 2013 Report Card for America's Infrastructure). To avoid unexpected failure of these concrete structures, we need to investigate the effect of localized low concrete strength on flexural strength of RC beams and the safety performance of those deteriorated RC beams.

Experimental investigation is a fundamental research approach because it gives firm evidences supporting proposed formula, which is invaluable in the preliminary design stages. But they are time-consuming and costly. With the advent of digital technics and FEM method, researchers can now simulate the RC beams through finite element modeling and obviate the need for large scale of experiments.

1.2 Objective and Scope

The objective of this paper is to investigate the effects of localized poor concrete zones on the strength of reinforced concrete beams. It covers the methodology about

modeling reinforced concrete finite element in ANSYS. Different kinds of concrete and steel models will be discussed. To save analysis time and maintain the solution accuracy, half of the simply supported beam is modeled. The impacts of following parameters on the flexural strength of RC beams were studied.

1) Inferior concrete zone location. In a reinforced concrete beam, different locations are sensitive to different failure modes. The analytical beam was divided into three different regions. First one at the middle of the beam, whose length is 500mm, is sensitive to bending moment. The second region 500mm long is sensitive to shear. And the remaining 550mm long part makes up the third region, which is sensitive to bond failure.
2) Rebar size. The interaction between reinforcement and concrete for large rebar and small rebar are different. Therefore, 16mm, 25mm and 32mm rebar sizes are used for the bottom reinforcement. The response of under-reinforced, moderately-reinforced and over-reinforced concrete beam were investigated.
3) Concrete strength. The concrete strength has effect on the bond strength and the ultimate flexural capacity of the beam. Weak concrete has poor aggregate interlock and poor crushing ability. Four types of concrete strengths were investigated in the paper, 10MPa, 20MPa, 30MPa and 42.7 MPa.

The influence of localized low concrete strength on flexural strength of RC beams will be presented based on the integrated experimental and finite element investigations.

Chapter 2 LITERATURE REVIEW

2.1 Localized Concrete Degradation

Concrete is a manufactured material that has two types of construction methods, cast-in-place and precast concrete. Precast concrete is built in the factory and transferred to the construction site for erection in final position. As it is built in factory, it has stable physical characteristics and few defects. On the other hand, the quality of cast-in-place concrete can be affected by the various factors related to site condition that affect the quality of the concrete. Some construction errors are trivial and can be ignored or easily fixed. But the others which affect the strength of concrete should be investigated and fixed. The typical defects that lower the strength of the concrete are listed below.

2.1.1 Excess Concrete Mix Water

Concrete is a composite material consist of cement, aggregate and water. The cement water ratio could significantly affect the strength of the concrete. Excessive water content is one the most common construction defect. Although excessive water will increase the flowability of concrete, it will also reduce the concrete strength, increase the porosity and creep of concrete, and reduce the abrasion resistance of concrete (Guide to Concrete Repair, 1996).

2.1.2 Construction Defects

Honeycomb and rocket pocket, are concrete whose mortar failed to bond the aggregates and leave voids inside the concrete due to lack of vibration or poor construction practice, which results in localized low strength concrete zones.

Form failure – When constructing cast in place concrete, forms have to be set up before pouring concrete. If the forms are not properly set up and sealed, then the mortar would leak through formwork joints, which creates inferior concrete zones.

Finishing defects - after the concrete has been poured, construction work has to flatten the finish of concrete. During the finishing procedure, they will add some water to the surface of the concrete. This will generate a porous permeable and low durability concrete. On the other hand, a poorly finished concrete surface is susceptible to premature spalling.

2.1.3 Cavitation Damage

Cavitation damage occurs when high velocity water flows encounter discontinuities on the flow surface .When water flow into a discontinued path, it will lift off the flow surface and create negative pressure zones and results in bubbles of water vapor. These bubbles will go on traveling and collapse against a concrete surface, a zone of very high pressure impact occurs over an infinitely small area of the surface .In that case, particles of concrete will be removed by such high impacts and form another discontinuity which then can create more extensive cavitation damage.

2.2 Concrete

2.2.1 Behavior of Concrete

Concrete is a heterogeneous composite material made up of cement, mortar and aggregates. The thermo-chemical reaction between these components results in a unique building material. It has high compressive strength but low in tensile strength.

For the purpose of analysis and design, however, concrete is often considered a homogeneous material at the macroscopic scale.

The nonlinear behavior of concrete under uniaxial monotonic loading can be explained by the creation and propagation of micro-cracks (Kotsovos and Newman, 1977). Concrete exhibits a large amount of micro-cracks even before application of any external loading. The response of concrete while loading in microscopic scale is illustrated in Figure 2-1. At first stage when the concrete is constructed or cured, a large amount of micro-cracks are formed between coarse aggregates and mortar before the application of any external loading. The segregation, shrinkage or thermal expansion of the mortar induce stress and strain concentration and initial many of these cracks. Since those aggregate and cement paste components have different elastic moduli and thermal coefficient (Figure 2-1a). When the external load beyond micro-cracks initiation threshold is applied, additional micro-cracks are formed (Figure 2-1b). As the external load continues to grow, the micro-cracks grow and spread until they merge into the matrix after a certain threshold is reached (Figure 2-1c). With the cracks' size grow, they will coalesce with each other and form major cracks which eventually lead to concrete failure (Figure 2-1d).

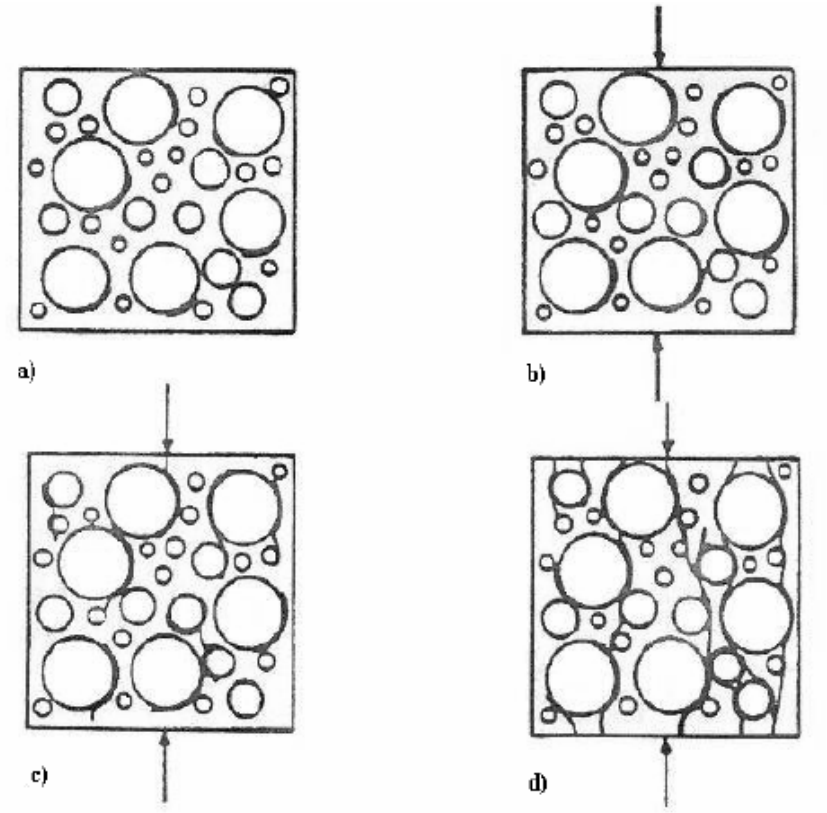

Figure 2-1 Aggregate-matrix interface: a) prior to loading, b) 65% of ultimate load, c) 85% of ultimate load, d) failure load, (Kotsovos and Newman, 1977)

2.2.2 Modulus of Elasticity for Concrete

The elastic modulus for concrete is a deformation capability of concrete. The modulus of elasticity for concrete is sensitive to the modulus of elasticity of the aggregate. It could be changed due to the different aggregates, cement matrix, and density.

According to ACI code 318-11 and 318M-11, the recommended modulus of elasticity for normal weight concrete is:

$$E_c = 57,000\sqrt{f'_c} \text{ (in psi)} \quad (2.1)$$

$$E_c = 4700\sqrt{f'_c} \text{ (in MPa)} \quad (2.2)$$

For a more accurate estimation, the modulus of elasticity for different types of concrete could be achieved base on the work done by Adrian Pauw (1960):

$$E_c = w_c^{1.5} 33 \sqrt{f'_c} \text{ (in psi)} \quad (2.3)$$

$$E_c = w_c^{1.5} 0.043 \sqrt{f'_c} \text{ (in MPa)} \quad (2.4)$$

2.2.3 Stress Strain Relationship for Concrete

There are many mathematical constitutive models for concrete in use in finite element analysis today. They are classified as four different types: orthotropic models, nonlinear elasticity models, plastic models and endochronic models. (Desayi, 1964, POPOVICS 1970, Bažant and Arthur 1982, Kwak, 1990, Reddiar, 2000, and Chen, 2007)

A typical uniaxial tension stress-strain curve is shown in Figure 2-2 (Peterson, 1981). It can be clearly seen that the tensile stress strain relationship for concrete behave in brittle manner. In general, elasticity portion of the tensile part is 60-80% of the ultimate tensile strength and the tensile strength is significantly lower than the compressive strength.

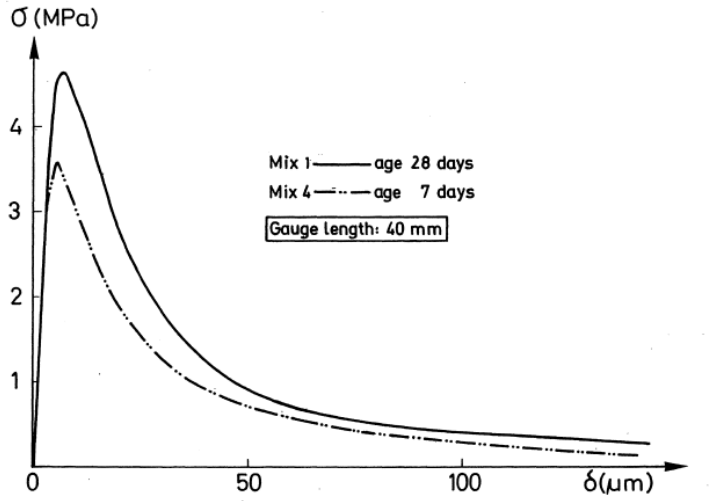

Figure 2-2 Mean stress-deformation curves representing different ages of the (Peterson, 1981)

Many empirical formulas have been proposed to describe the uniaxial compression stress-strain relationship for concrete. Different concrete constitutive formulas are reviewed and summarized by other researchers.

Figure 2-3 shows the modified hognestad model that used by Kwak (1990) in his proposed finite element modeling method. This model consists of three branches. It starts with linear segment until reaches $0.6\sigma_{ip}$, when the cracks at nearby aggregate surface start to connect to each other in the form of mortar cracks and other bond cracks continue to grow slowly. A linear portion follows previous till the stress gets to peak stress σ_{ip}. Beyond the peak is a linear descending branch represents the strain softening.

where

σ_{ip} = from the biaxial failure surface of concrete, where I is equal to 1 or 2.

ε_{ip} is the strain at the compressive strength

ε_{iu} = strain at ultimate stage

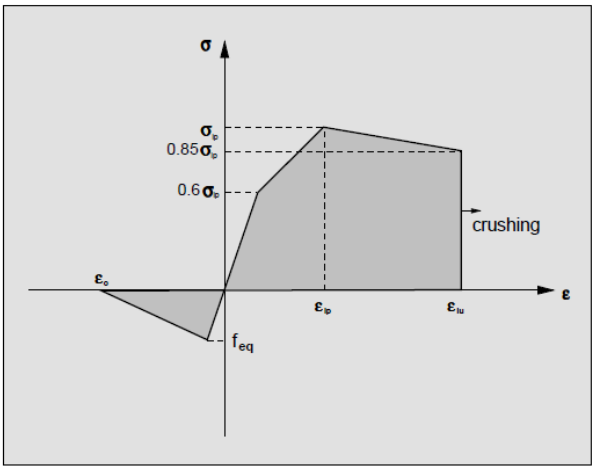

Figure 2-3 STRESS-STRAIN RELATION OF CONCRETE (Kwak, 1990)

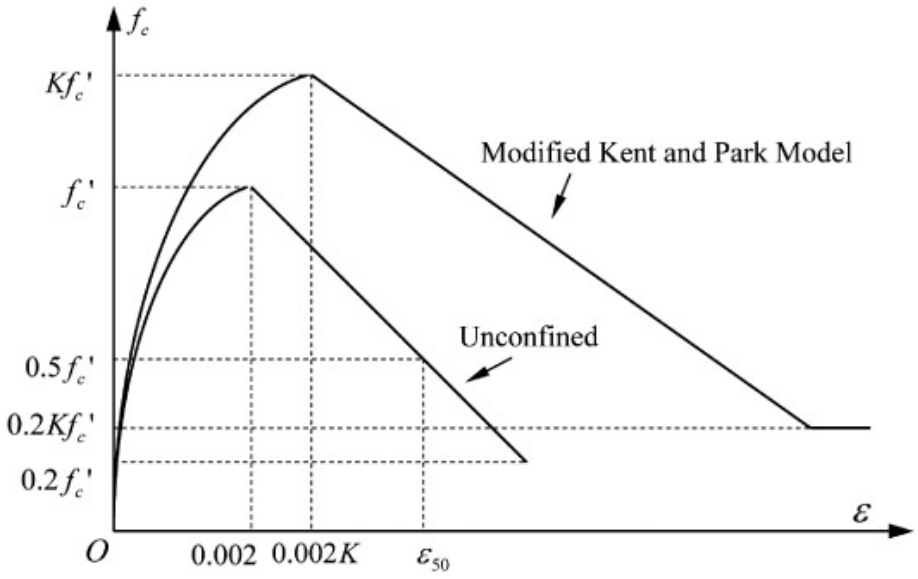

Figure 2-4 Modified Kent and Park model for monotonic stress—strain relationship of confined concrete (C. Hsu, 2010)

The concrete model in Figure 2-4 is the modified Kent and Park material model proposed by Scott and Park (1982) for confined concrete to incorporated with degraded linear unloading and reloading paths according to the work of Karsan and Jirsa (1969)

$$\text{For} \quad \varepsilon \le 0.002K, \quad f_c = Kf'_c\left[\frac{2\varepsilon}{0.002K} - \left(\frac{\varepsilon}{0.002K}\right)^2\right] \tag{2.5}$$

$$\text{For} \quad \varepsilon \ge 0.002K, f_c = Kf'_c\left[1 - Z\left(\varepsilon - 0.002K\right)\right] \ge 0.2Kf_c \tag{2.6}$$

where

$$K = 1 + \frac{\rho_s f_{yh}}{f'_c} \tag{2.7}$$

$$Z = \frac{0.5}{\frac{3 + 0.29f'_c}{145f'_c - 1000} + \frac{3}{4}\rho_s\sqrt{\frac{b''}{S} - 0.002K}} \tag{2.8}$$

f_c = longitudinal compressive stress in concrete (MPa)

f'_c = concrete compressive cylinder strength (MPa)

ε = longitudinal compressive strain in concrete

ρ_s = ratio of volume of hoop reinforcement to volume of concrete core

b'' = width of concrete core measured to outside of peripheral hoop (mm)

f_{yh} = yield stress of the confining stirrups (MPa)

S = spacing of the confining stirrups (mm)

2.3 Reinforcing Steel

2.3.1 Behavior of Reinforcing Steel

In reinforced concrete structures, steel is mainly used for providing tension force compensating the concrete weakness. The behavior of reinforcing steel is

comparatively simple and can be considered as a homogeneous material with generally well defined material properties. Thus it can be described sufficiently by models with simple stress-strain relations.

2.3.2 Steel Stress Strain Relationship

Elasto-plastic model is the basic model for steel (as shown in Figure 2-5). The steel has an initial linear elastic portion in the first stage, whose stress in proportion to the strain times the steel elasticity. It neglects the strength increase due to strain hardening effect, and models the later deformation of stress as a horizontal segment. Two parameters, from either σ_y , ε_y , or E_{steel} , are sufficient to describe the model. This model can well match the behavior of low-carbon steels with low yield strength.

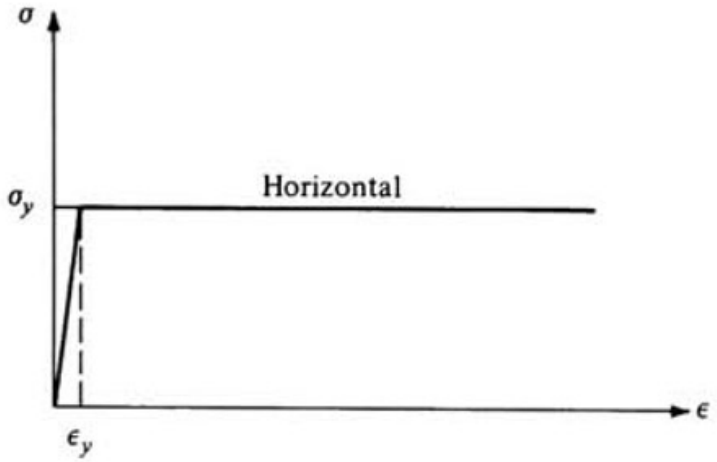

Figure 2-5 Elastic perfectly plastic model (Chen, 2007)

Figure 2-6 presents the linear elastic, linear strain hardening model for reinforcing bars. This mode exhibits two portions. The initial elastic portion has stiffness equal to the elastic modulus of reinforcement E_{s1}. And the linear strain hardening part has stiffness equal to the strain-hardening modulus of reinforcement E_{s2}. This model

has been incoporated in Kawk(1990) and Taqieddin (2008) proposed finite element models.

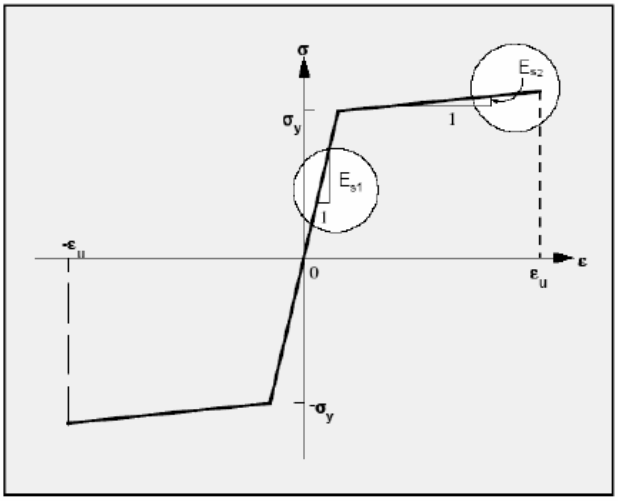

Figure 2-6 Linear elastic, linear strain hardening steel stress-strain relation (Taqieddin, 2008)

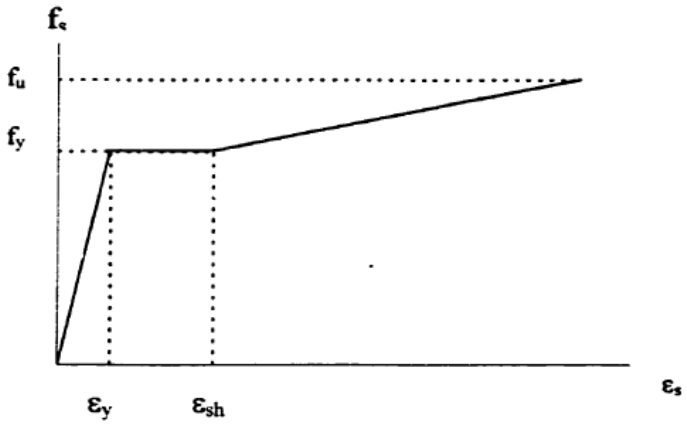

Figure 2-7 Trilinear approximation model (Chen, 2007)

Figure 2-7 displays the trilinear approximation model. This model has three segments, initial elastic part, the yield plateau part, and strain-hardening part. The stiffness of the first part follows the elastic modulus of steel E_{s1}. The second level branch ends at the commencement of strain hardening. And the linear strain-hardening

part follows a stiffness of the strain-hardening modulus of steel E_{s2}. This model was used in Gan's finite element analysis (2000).

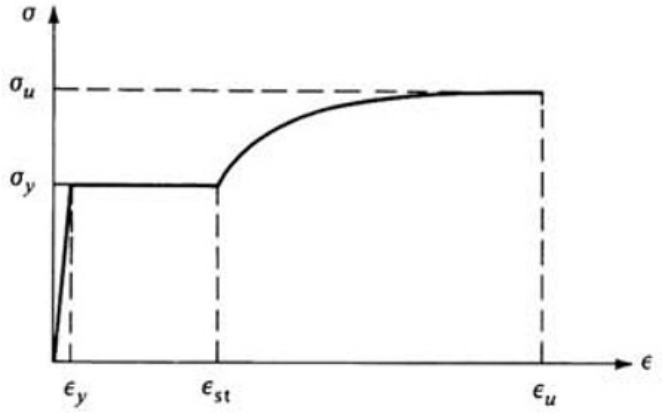

Figure 2-8 Compressive model (Chen, 2007)

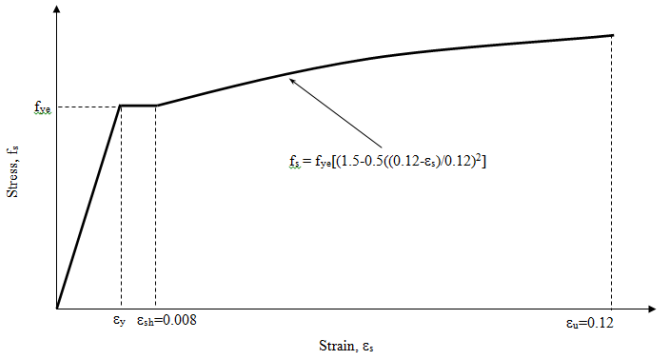

Figure 2-9 Example of compressive model (Kim, 2004)

Complete model is extracted from the trend of actual experiment data (Figure 2-8). Therefore, it fits well with the experimental results. However, the parameters for the strain-hardening part to determine the complete model have to be gained in experiment, which make it difficult to use in some cases. Figure 2-9 presents the model used by Kim (2004). The formula for his reinforcement stress-strain during strain hardening is

$$f_s = f_{ye}\left(1.5 - 0.5\left(\frac{\left(0.12 - \varepsilon_s\right)}{0.12}\right)^2\right) \tag{2.9}$$

where f_s = nominal stress of reinforcement

f_{ye} = yielding stress (psi) of reinforcement

ε_y = strain when steel yields

ε_{sh} = strain when the strain-hardening starts

ε_u = assumed ultimate reinforcement strain

2.4 Bond

2.4.1 General

Reinforced concrete is a composite material. In order to behave as one material system, reinforcement and concrete must be well bonded together. Basically, the bond force is generated through three major ways, the mechanical interaction between lugs and concrete, the chemical adhesion from concrete paste and friction between rough surfaces of reinforcing bars and concrete. Concrete is the one which exert the bond force onto the reinforcement. And reinforcement carries the transferred tension force. In most cases today, the reinforcements are deformed bars because they provide better mechanical bond strength.

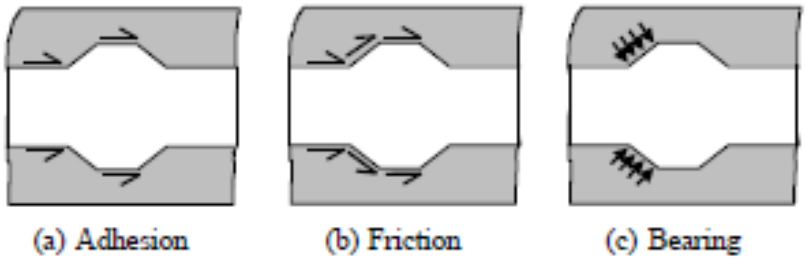

Figure 2-10 Bond force (LUNDGREN, 1999)

2.4.2 Mechanics of Bond

Lutz and Gergely (1967) researched the fundamentals of bond and slip. In general, the bond force was initially generated from the combined mechanical interaction and chemical adhesion. This adhesion acts until slip or movement of the steel relative to the adjacent concrete occurs. After the chemical adhesion is destroyed, the rib of rebar bearing against the concrete will prevent the rebar from slipping. For

deformed bar, the interlock between bar ribs and concrete contribute to the major portion of bond force. They also concluded that there are two kinds of slip in deformed bars: (1) the concrete in front of ribs are pushed away along the surface of the rebar (wedging action); (2) the concrete crushed by the moving ribs. However, experiments indicates that when the rib face angle is larger than 40 degrees, there is no wedging action take place and all concrete crushed by the moving ribs, the slip takes place through the crushing of the crushing the porous concrete face. When the ribs have a face angle less than 30 degrees, the friction between deformed bars is insufficient to prevent the concrete from lateral movement. In this case, the slip is due mainly to the relative movement along the surface of the ribs.

Usually, deformed bars have face angle larger than 40 degrees. And the slip mechanism is mostly due to the crushing of the adjacent concrete.

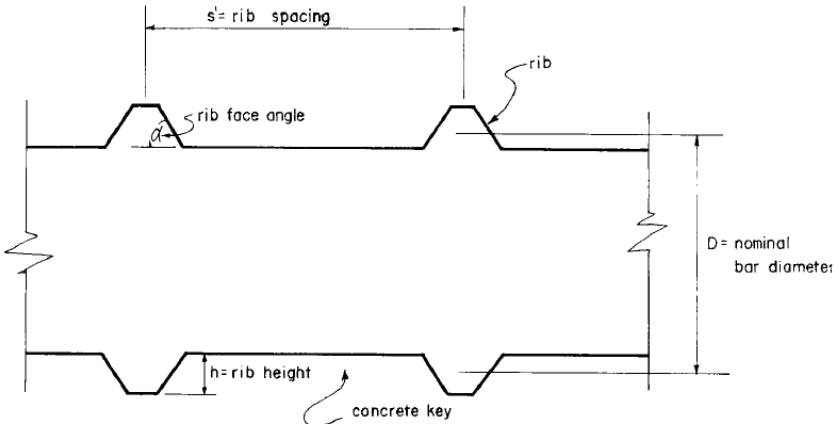

Figure 2-11 Geometry of bar deformations (Lutz and Gergely, 1967)

GOTO (1971) investigated the crack stress around deformed tension bars and showed the stress distribution for tensile members as illustrated in Figure 2-12.

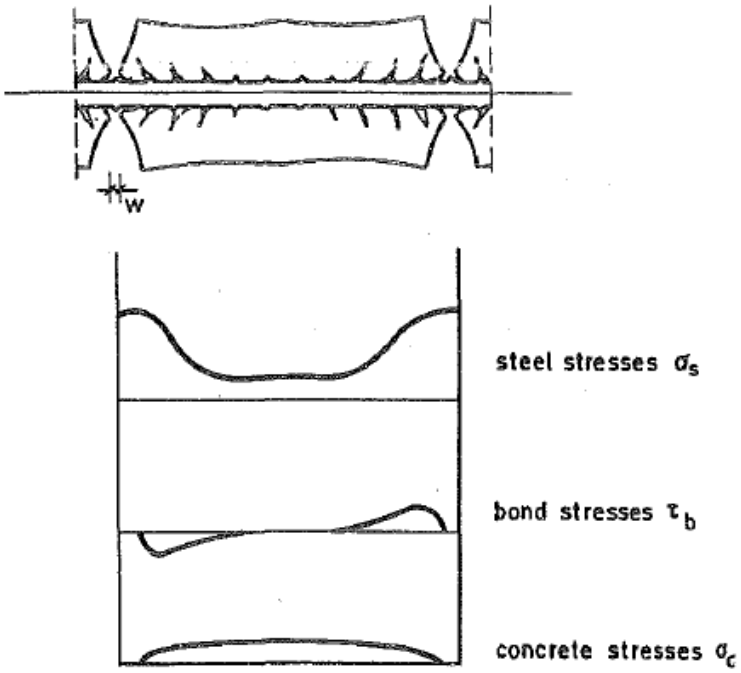

Figure 2-12 Reinforced Concrete Tensile Member with Crack Formation from Goto (1971) and Corresponding Stress Distribution

Nilson (1968) reported a bond stress slip trend obtained from considerable scatter of experimental data, and abstracted the following equation from trend.

$$\tau = 3.606*10^6\Delta - 5.356*10^9\Delta^2 + 1.986*10^{12}\Delta^3 \quad (2.10)$$

Where

τ is the nominal bond stress in psi

Δ is the local bond slip in inches

Differential the equation (2.10) with respect to Δ, yields

$$\frac{d\tau}{d\Delta} = 3.606*10^6 - 10.712*10^9\Delta + 5.985*10^{12}\Delta^2 \quad (2.11)$$

Equation (2.11) shows the stiffness of the bond force between reinforcing bars and concrete.

Later Nilson (1972) summarized the work he done earlier and proposed another model for the bond. The model was described:

$$\tau = 3100\left(1.43x + 1.50\right)\Delta f'_c \qquad (2.12)$$

Where

τ is the nominal bond stress, and satisfy $\tau < \left(1.43x + 1.50\right) f'_c$

x is the distance from the loaded end in inches

f'_c is the concrete strength in psi

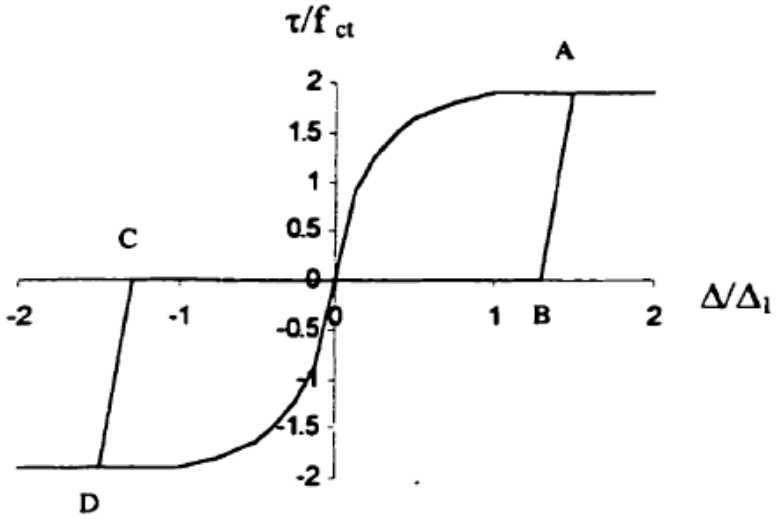

Figure 2-13 Relationship of local bond stress and slip

Mirza and Houde (1979) investigated the influence of bar size, concrete strength and the thickness of the concrete cover. They found that the slip linearly increases as the stress in steel increases. Then the stress experiences a horizontal segment.

Before the peak value

$$\tau = 1.95\times10^{6}\Delta - 2.35\times10^{9}\Delta^{2} + 1.39\times10^{12}\Delta^{3} - 0.33\times10^{15}\Delta^{4} \quad (2.13)$$

Differentiating equation (2.13) with respect to the slip d, one obtains

$$\frac{d\tau}{d\Delta} = 1.95\times10^{6} - 4.70\times10^{9}d + 4.17\times10^{12}d^{2} - 1.32\times10^{15}d^{3} \quad (2.14)$$

Where:

τ =nominal bond stress (psi)

Δ=local slip (inch)

2.4.3 Eligehausen, Popov, and Bertero (1983)

In 1983, Eligehausen and his team investigated a series of reinforced beam with 25mm rebar size and extracted a practical model based on their experiment data. The details of the bond stress slip model under monotonic loading for confined concrete are illustrated in Figure 2-14. The mode can be described as following relationships:

$$\tau = \tau_1\left(\frac{s}{s_1}\right)^{\alpha} \quad \text{for } s \le s_1 \quad (2.15)$$

$$\tau = \tau_1 \quad \text{for } s_1 \le s \le s_2 \quad (2.16)$$

$$\tau = \tau_2 - \frac{(\Delta - \Delta_2)}{(\Delta_3 - \Delta_2)} * (\tau_2 - \tau_f) \quad \text{for } \Delta_2 \le \Delta \le \Delta_3 \quad (2.17)$$

$$\tau = \tau_f \quad \text{for } \Delta \geq \Delta_3 \tag{2.18}$$

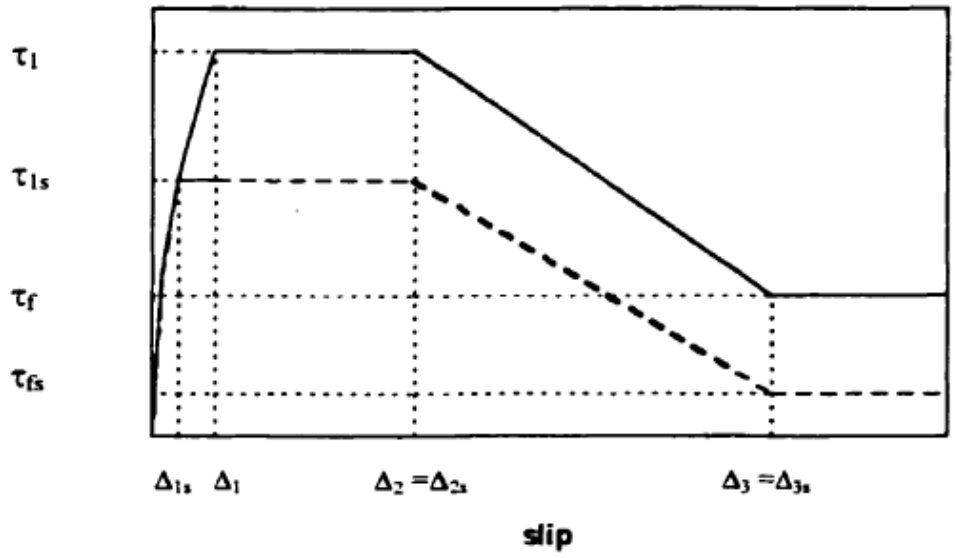

Figure 2-14 Bond strees-slip relationship (Eligehausen, 1983)

Figure 2-15 shows the actual average data Eligehausen (1983) achieved for the average bond stress slip relationship of the 25mm reinforced beam.

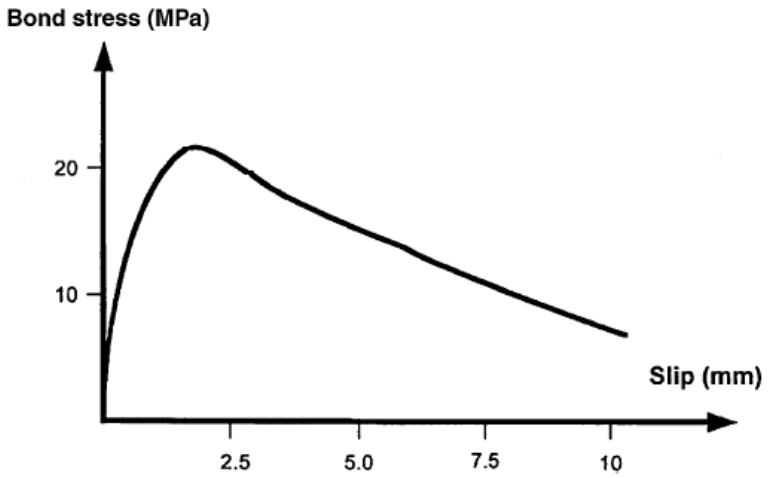

Figure 2-15 Bond stress-slip curve for bar loaded monotonically and failing by pullout (ACI 408R-03, 2003) (Note: 1 MPa = 145 psi; 1 mm = 0.0394 in.)

2.4.4 CEB FIP Model (reproved 2010)

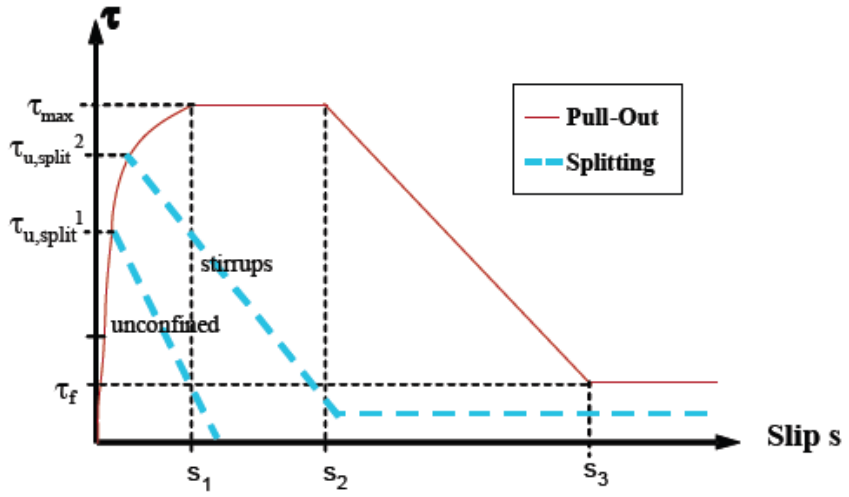

Figure 2-16 Analytical bond stress-slip relationship, monotonic loading (CEB-FIP, 2010)

The CEB committee proposed a bond stress-slip model in 1990. Later in 2010, Rolf Eligehausen and John Cairns proposed a modified bond model, as shown in Figure 2-16 (CEB-FIP, 2010).

The model is a piecewise function in terms of relative displacement s, which can describe the bond stresses between concrete and reinforcing bars for pull-out and splitting failure. The relative displacements are obtained from (2.19) to (2.22)

$$\tau_0 = \tau_{\max}\left(\frac{s}{s_1}\right)^{\alpha} \qquad \text{for } 0 \le s \le s_1 \qquad (2.19)$$

$$\tau_0 = \tau_{\max} \qquad \text{for } s_1 \le s \le s_2 \qquad (2.20)$$

$$\tau_0 = \tau_{\max}\left(\tau_{\max} - \tau_f\right)\frac{\left(s - s_2\right)}{\left(s_3 - s_2\right)} \qquad \text{for } s_2 \le s \le s_3 \qquad (2.21)$$

$$\tau_f \qquad \text{for } s_3 < s \qquad (2.22)$$

The parameters for the CEB-FIP model can be obtained in the Table 2-1, which are valid for ribbed reinforcing steel with a related rib area $A_{sr} \approx A_{sr,\min}$ according to relevant international standards. Depending on the failure mode, pull-out or splitting, different parameters are applied.

Table 2-1 Parameters for defining the mean bond stress-slip

	1	2	3	4	5	6
	Pull-Out (PO)		**Splitting (SP)**			
	$\varepsilon_s < \varepsilon_{s,y}$		$\varepsilon_s < \varepsilon_{s,y}$			
	Good bond cond.	**All other bond cond.**	**Good bond cond.**		**All other bond cond.**	
			unconfined	**stirrups**	**unconfined**	**stirrups**
τ_{max}	$2.5\sqrt{f_{ck}}$	$1.25\sqrt{f_{ck}}$	$7.0\cdot\left(\frac{f_{ck}}{20}\right)^{0.25}$	$8.0\cdot\left(\frac{f_{ck}}{20}\right)^{0.25}$	$5.0\cdot\left(\frac{f_{ck}}{20}\right)^{0.25}$	$5.5\cdot\left(\frac{f_{ck}}{20}\right)^{0.25}$
s_1	1.0mm	1.8mm	$s(\tau_{max})$	$s(\tau_{max})$	$s(\tau_{max})$	$s(\tau_{max})$
s_2	2.0mm	3.6mm	s_1	s_1	s_1	s_1
s_3	c_{clear} [1)]	c_{clear} [1)]	$1.2s_1$	$0.5c_{clear}$ [1)]	$1.2s_1$	$0.5c_{clear}$ [1)]
α	0.4	0.4	0.4	0.4	0.4	0.4
τ_f	$0.40\tau_{max}$	$0.40\tau_{max}$	0	$0.4\tau_{max}$	0	$0.4\tau_{max}$

[1)] c_{clear} is the clear distance between ribs

The values in Table 2-1, columns 1 and 2 (pull-out failure) are valid for well confined concrete (concrete cover $\geqslant$ 5 Ø, clear spacing between bars $\geqslant$ 10Ø).

The values in Table 2-1, columns 3 to 6 (splitting failure) are valid for Ø $\leqslant$ 20mm, $\frac{c_{\max}}{c_{\min}}$ = 2.0, c_{min} = Ø and K_{tr} = 2% in case of stirrups. For definition of K_{tr} see(2.23)

$$\tau_{u,split} = \eta_2 \cdot 6.54 \cdot \left(\frac{f_{ck}}{20}\right)^{0.25} \cdot \left(\frac{20}{\varnothing}\right)^{0.2} \cdot \left(\left(\frac{c_{\min}}{\varnothing}\right)^{0.33} \cdot \left(\frac{c_{\max}}{c_{\min}}\right)^{0.1} + 8K_{tr}\right) \qquad (2.23)$$

where:

η_2 =1.0 for good bond conditions,

=0.7 for all other bond conditions

f_{ck} is characteristic cylinder concrete compressive strength (N/mm^2)

$\varnothing$ is diameter of the bar (mm)

$c_{min} = \min\{c_x, c_y, c_{si}\}$

$c_{max} = \max\{c_x, c_{si}\}$

and

$$K_{tr} = \frac{n_1 A_{sv}}{(n_b \varnothing s_v)}$$

where:

n_1 is number of legs of confining reinforcement at a section

A_{sv} is cross sectional area of one leg of a confining bar [mm^2]

S_v = longitudinal spacing of confining reinforcement [mm^2]

n_b = number of anchored bars or pairs of lapped bars

$\varnothing$ is diameter of the anchored bar or of the smaller of a pair of lapped bars [mm^2]

2.5 Reinforced Concrete Structure

Reinforced concrete structure consists of two different materials, namely, concrete and steel. Concrete is strong in compression and inexpensive, but weak in tension. On the other side, reinforcement is strong in both tension and compression, and can be incorporated inside concrete to work as tension component though it's expensive. Combing these two materials can create economic and robust composite material.

The response of a typical reinforced concrete simply supported beam is a nonlinear curve as shown in Figure 2-17. The response of the load-deflection curve can be roughly divided into three stages, the uncracked elastic stage, the crack propagation stage and plastic (yielding or crushing) stage (Chen, 2007).

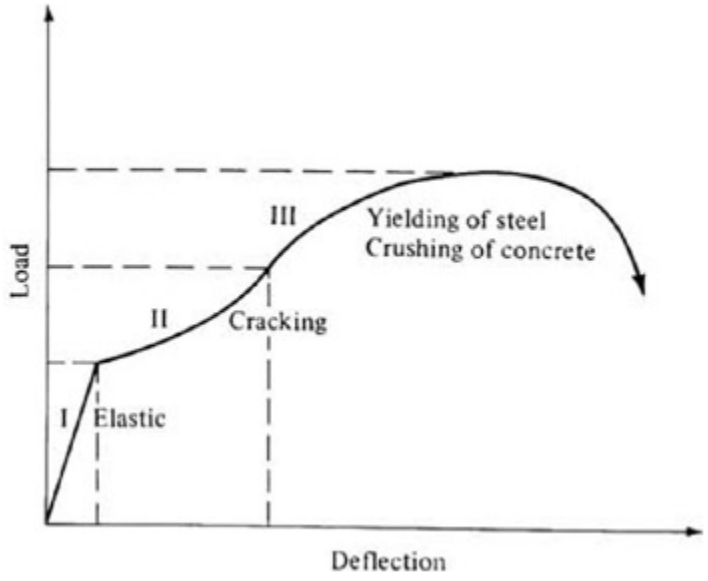

Figure 2-17 Typical load-deflection relationship of a reinforced concrete beam (Chen, 2007)

The nonlinear response of RC structures can be described as follows:

- Cracking of concrete in tension
- Yielding of the reinforcement or concrete crushing in compression

However, there are still some other factors which will contribute to the nonlinear response of the reinforced concrete structure:

- Interaction of the components of reinforced concrete, such as bond-slip between reinforcing bars and surrounding concrete
- The time-dependent effects of creep, shrinkage and temperature variation

- The actual tension stress-strain relationship of concrete is different from that in compression
- The mechanical properties vary with different concrete age at loading and on environmental conditions
- The material properties of concrete and steel are strain-rate dependent to some extent

2.6 Finite Element Modeling for RC Beams

Ngo and Scordelis (1967) have done the earliest landmark publication on the application of the finite element method to the analysis of RC structures. A simply supported beam was analyzed, in their study. Concrete and reinforcement are modeled separately by constant strain triangle elements, and a special link element was used to bond the concrete and reinforcement nodes at the same coordinate to describe the bond-slip effect. The principal stresses in concrete, in reinforcement and bond stresses in interface were determined through linear analysis with beams have predefined crack patterns.

There are basically two approaches to model the interface mechanism in RC structure (KWAK, 1990). First is bond link element. The bond can be modeled as 1-D, 2-D or 3-D dimensionless spring elements linking a reinforcing steel node with the concrete node at the same location. The multiple springs at the same location must be orthogonal to each other.

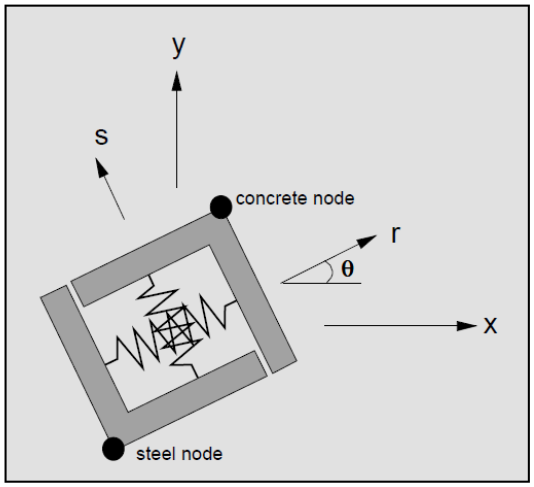

Figure 2-18 2-D BOND LINK ELEMENT (KWAK, 1990)

The second method is bond zone element. The bond contact element is modeled through the contact surface between reinforcing nodes and immediate vicinity of concrete nodes by special constitutive equations, which represents the interlocking properties of the bond zone, the friction effect of different steel bars shape (deformed or not). The bond contact element constructed by the material law must describes the behavior of the interface between reinforcing steel and concrete and provides a continuous connection for them.

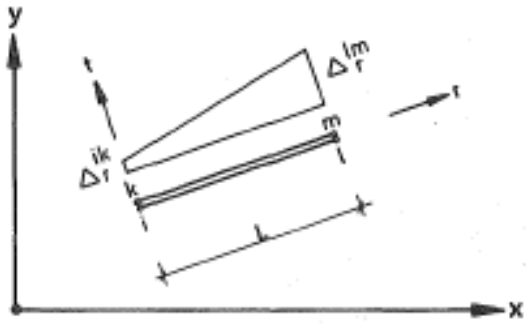

Figure 2-19 Contact Element

The development of analytical model for the response of RC structures is sophisticated because (Kwak and Filippou, 1997):

- The different constituent materials, concrete and reinforcing steel have different have differences in short and long term behavior.
- Reinforcing steel and concrete interact in a complex way through bond-slip and aggregate interlock.

Smeared crack

Cracking is one of the most difficult parts in modeling reinforced concrete using finite element method. Rashid (1968) proposed the concept of “smeared” crack in the study of Ultimate strength of prestressed concrete pressure vessels.

There are two different types of smeared crack: fixed crack and rotating crack. Fixed crack method assumed the crack forms perpendicular to the principal tensile stress direction of concrete when the tension stress exceeds concrete tensile strength and the crack orientation stay the same during subsequent loading. This model has numerical problem caused by the singularity of the material stiffness matrix and the results cannot match experimental data very well (Jain and Kennedy, 1974). Introducing a cracked shear modulus can overcome this problem, eliminating the singularity of the material stiffness matrix.

Discrete crack

Discrete crack model builds the crack element separately from the concrete model. When the iteration goes on in analysis, the crack elements are required to recalculate and develop new crack elements. Although this method can simulate the

real behavior of concrete better than the smeared crack model, it requires intensive computational work.

Gilbert and Warner (1978) used the smeared cracked crack model in their analysis for the tension softening effect of reinforced concrete slabs. They firstly found that the analytical solution is greatly affected by the size of finite element mesh and the by the amount of tension stiffening of concrete.

Many other finite element analysis methods have been proposed in recent years. (Kwak, 1990; Gregoria, 2007; Taqieddin, 2008). Since those methods require to define custom element base on their algorithm, their proposed models will not be included in this paper.

There are many software packages that can execute finite element modeling and analysis in the applications of reinforced concrete structures such as ANSYS, ABAQUS, DIANA, ATENA, and MIDAS FEA.

In general, there are two methods to model the reinforcement, smeared reinforcement model and discrete reinforcement model.

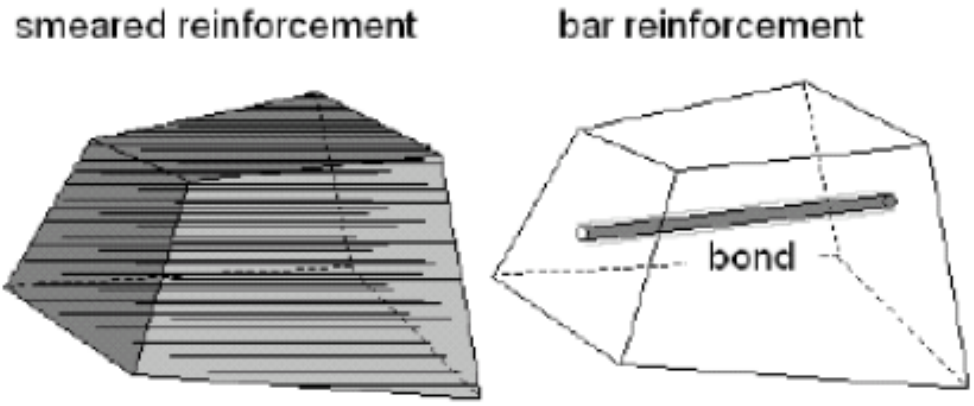

Figure 2-20 Different Reinforcement Models (Mordini, 2006)

Many research attempted to apply finite element modeling to analyze reinforced concrete structures such as beams and slabs using different packages. Montoya (2000) have compared different methods to model finite element confined concrete using SPARCS. Jendele (2006) presented an approach to model the reinforcement bar with bond using ATENA. Mordini (2006) incorporated his proposed model 3D-PARC with ABAQUS and achieved good solution. Kim (2004) modeled analytical beams using ANSYS to investigated the ductility of carbon fiber reinforced polymer (CFRP) strengthened reinforced concrete beams and achieved a solution well matched the experiment results. With the help of DIANA, Hasegawa (2004) modeled the beams subjected to diagonal tension failure and achieved good results matching experiments data in 2004. Later in 2010 Hasegawa (2010) proposed a bond stress-slip model and testified the finite element data obtained from DIANA with the experiment data done by Podgorniak-Stanik (1998).

The solutions of the perfect bond model, Eligehausen model, and bi-linear model using ANSYS have been investigated by KHALFALLAH (2008).

2.7 Development Length

Reinforcing bars require certain amount of length to fully develop its tensile characteristic in reinforced concrete structure. To better understand the high relative rib area bars in normal and high-strength concrete, Zuo and Darwin (2000) proposed a new development model based on the experiment data.

In addition, ACI 318-11 Building Code Requirements for Structural Concrete also provide a development length formulas for deformed bars and deformed wire in tension, l_d, shall be determined from:

Table 2-2 Development length in customs units

Spacing and cover	No. 6 and smaller bars and deformed wires	No. 7 and larger bars
Clear spacing of bars or wires being developed or spliced not less than d_b, clear cover not less than d_b, and stirrups or ties throughout ℓ_d not less than the Code minimum or Clear spacing of bars or wires being developed or spliced not less than $2d_b$ and clear cover not less than d_b	$\left(\frac{f_y \psi_t \psi_e}{25\lambda\sqrt{f'_c}}\right) d_b$	$\left(\frac{f_y \psi_t \psi_e}{20\lambda\sqrt{f'_c}}\right) d_b$
Other cases	$\left(\frac{3 f_y \psi_t \psi_e}{50\lambda\sqrt{f'_c}}\right) d_b$	$\left(\frac{3 f_y \psi_t \psi_e}{40\lambda\sqrt{f'_c}}\right) d_b$

According to the ACI 318M-11, the development length for deformed bars and deformed wire in tension, shall be determined from:

Table 2-3 Development length in metric unit

Spacing and cover	No. 19 and smaller bars and deformed wires	No. 22 and larger bars
Clear spacing of bars or wires being developed or spliced not less than d_b, clear cover not less than d_b, and stirrups or ties throughout ℓ_d not less than the Code minimum or Clear spacing of bars or wires being developed or spliced not less than $2d_b$ and clear cover not less than d_b	$\left(\frac{f_y \psi_t \psi_e}{2.1\lambda\sqrt{f'_c}}\right) d_b$	$\left(\frac{f_y \psi_t \psi_e}{1.7\lambda\sqrt{f'_c}}\right) d_b$
Other cases	$\left(\frac{f_y \psi_t \psi_e}{1.4\lambda\sqrt{f'_c}}\right) d_b$	$\left(\frac{f_y \psi_t \psi_e}{1.1\lambda\sqrt{f'_c}}\right) d_b$

A general detail provision is also provided in ACI 318M-11 code,

$$l_d = \left(\frac{f_y}{1.1\lambda\sqrt{f'_c}} \times \frac{\psi_t \psi_e \psi_s}{\left(\frac{c_b + K_{tr}}{d_b} \right)} \right) \times d_b \qquad (2.24)$$

in which the confinement term $\left(\frac{c_b + K_{tr}}{d_b} \right)$ shall not be taken greater than 2.5, and

$$K_{tr} = \frac{40 A_{tr}}{sn} \qquad (2.25)$$

where

A_{tr} = total cross sectional area of all transverse reinforcement (mm^2)

s = maximum C-C spacing of transverse reinforcement within the development length

n = number of longitudinal bars being developed along the plane of splitting

ψ_t = modifier for reinforcement location

ψ_e = modifier for epoxy coated reinforcing

The product, $\psi_t \psi_e$ should ne exceed 1.7

ψ_s = modifier for bar size

λ = modifier for light weight concrete

Chapter 3 EXPERIMENT DETAILS

3.1 Dimensions and Reinforcement Arrangement of the Specimens

Before investigate the localized concrete damaged deterioration, we have to verify the veracity of the finite element model. A recent experiment done by Lim Hwee Sin (2011) was chosen as reference experiment. In his research, the performance of lightweight concrete was carefully investigated. The reference group with normal concrete beam was chosen as reference beam in this research as well.

Although several simply supported beam were investigated experimentally, in the reference paper, beam No.1,the most simple and symmetric case, was chosen as the reference specimen to compare with the result of finite element model. The dimensions of the reference beam are illustrated in Figure 3-1 and Figure 3-2. The section of the beam is 300mm high and 150mm wide. The span length of the beam is 2800mm from support to support.

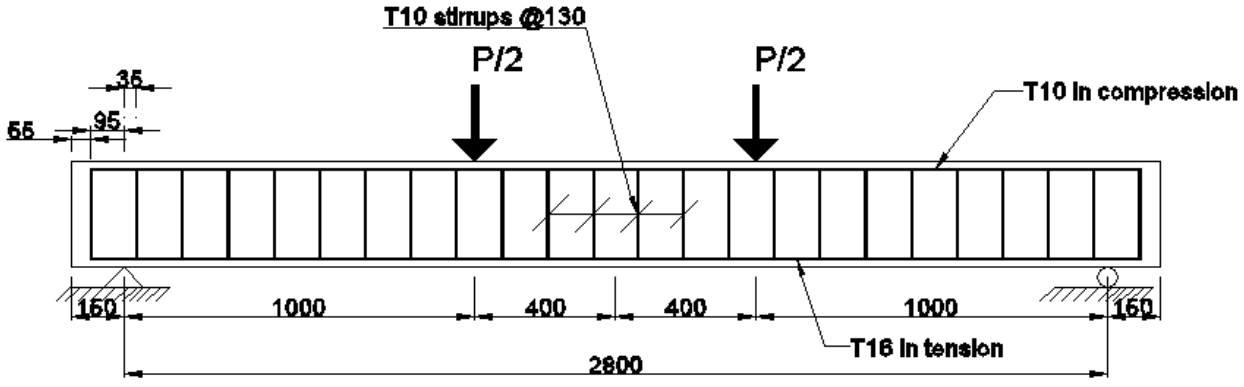

Figure 3-1 Detailing of the reference beam (modified Sin, 2011)

Figure 3-2 Cross section of the reference beam (modified Sin, 2011)

3.2 Material Properties of the Specimens

3.2.1 Concrete

For the reference normal concrete (fresh concrete density around 2400 kg/m^3) the concrete strength is given as 42.7 MPa, based on 100mm (4 in) cube laboratory result in the reference paper. The elastic modulus of the concrete is roughly determined as 30.927 GPa according to the ACI 318-11M.

3.2.2 Reinforcing Steel

Top reinforcement and stirrups are both 10mm rebars, whose yielding strength is 550MPa and elastic modulus is 185GPa. The bottom reinforcement are 16mm rebars, whose yielding strength is 512MPa and elastic modulus is 183GPa.

3.3 Loading History of the Specimens

The load deflection curve for the case no.1 is presented as Figure 3-3. In the first stage, the first crack occurs when applied load reaches 15.1kN and deflection is 9.4mm. After cracking, the RC beam experiences stiffness softening and the stiffness of RC beam decreases because the cracking concrete release the tension stress they carry

and leaves the reinforcement carry tension alone. At service stage, the load deflection curve increases linearly. Basically, the bottom reinforcement carries the incremental tension force and concrete in top carry the incremental compression force. At the third stage, when the steel reaches its yielding point 512MPa, at an applied load of 100.3kN and deflection of15.4mm, steel experiences plastification and elongation and thus the load deflection curve display a comparatively horizontal segment. After the deformation of concrete exceeds a certain amount, the RC beam experiences a load capacity drop and continues deformation until its total collapse when the applied load ends at 107.2kN and deflection is 39.5mm.

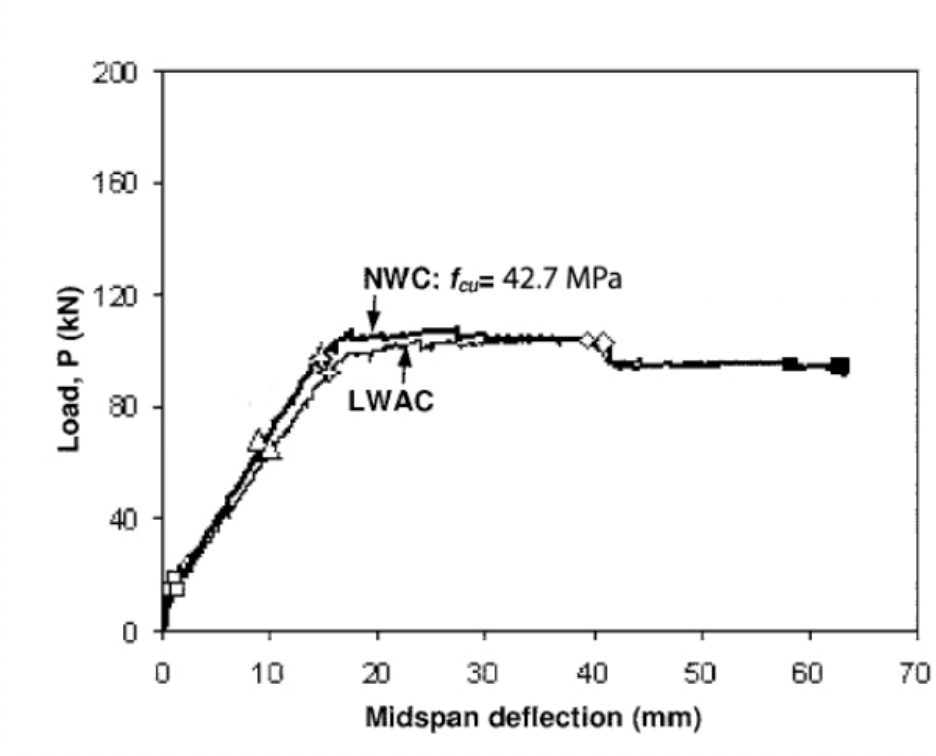

Figure 3-3 Load Deflection curve for the case 16-0 (Lim Hwee Sin, 2011)

3.4 ACI Code Model

In addition to the experiment result, the recommend values based on ACI code should also be evaluated so as to have a brief concept about the parameter that will be

used in later finite element analysis. Table 3-1 is pulled from the reference paper and lists all the result for the normal concrete beam.

Table 3-1 Test results at different stages of loading (Lim Hwee Sin, 2011)

Beam no.	Concrete strength f_{cu},* MPa	Elastic modulus E_c, MPa	Cracking load P_{cr}, kN	At assumed service			At yielding		At ultimate		At failure		Concrete strain capacity ε_{cu}
				Load P_s,† kN	Deflection δ_s, mm	Maximum crack width w_{max}, mm	Load P_y, kN	Deflection δ_y, mm	Load P_u, kN	Deflection δ_u, mm	Load P_f, kN	Deflection δ_f, mm	
1	42.7	25.1	15.1	66.7	9.4	0.20	100.3	15.4	107.2	39.5	92.7‡	63.3	0.0038
2	67.6	33.1	15.3	118.0	11.5	0.20	170.3	17.6	189.3	25.7	160.9	43.9	0.0023
3	77.5	34.8	20.2	117.8	11.6	0.25	180.7	20.0	189.3	38.1	160.2	39.5	0.0028
4	28.3	16.1	10.1	47.1	9.3	0.30	72.3	15.7	75.3	36.1	67.6‡	72.7	0.0028

3.4.1 Minimum Reinforcement

According to the ACI 318M-11, the provided reinforcement should satisfy minimum reinforcement requirement at every section of a flexural member.

$$A_{s,\min} = \frac{0.25\sqrt{f'_c}}{f_y} b_w d \tag{3.1}$$

And not less than $1.4 b_w d / f_y$, using above equations the minimum reinforcement can be achieved in Table 3-2.

Table 3-2 Minimum Reinforcement

Case No	f'c (MPa)	fy (MPa)	bw (mm)	d (mm)	As(min)
1	42.7	512	150	275	131.6158

3.4.2 Ultimate Load Capacity

In the ACI Code, at ultimate state, an equivalent concrete stress block is recommended for stress distribution of concrete in the compression zone,

$$a = \frac{A_s f_y}{0.85 f'_c b} \tag{3.2}$$

$$M_n = A_s f_y \left(d - \frac{a}{2} \right) \tag{3.3}$$

Where $A_s = 2 \times 200.96 =$ 401.92mm^2 f_y =512MPa, f'_c =42.7MPa, b=150mm

Substitute the parameters above into the equations, get

a = 37.798mm^2

M_n =52.701kN*m

$$M_n = \frac{P_{ACI}}{2} \times 1.4 - \frac{P_{ACI}}{2} \times 0.4 \tag{3.4}$$

$$P_{ACI} = \frac{2 \times M_n}{1m} = 105.402\text{kN} \tag{3.5}$$

3.5 Supplemental shear bond failure experiment

3.5.1 Dimension

Bogdan A. Podgorniak-Stanik (1998) has done an extensive experiment program to investigate the shear behavior of reinforced and prestressed concrete members. Case BN50of his is used in this paper to testify the veracity of the finite element method when it comes to shear bond failure. The dimension of the beam is illustrated in Figure 3-4 and Figure 3-5. The beam has no stirrups due to the purpose of investigating the shear bond failure in the experiment. Only tension reinforcement are provided here,

they are two 20M rebar at the bottom corner and one 25M at the bottom middle. The depth of the beam is 500m, including 50mm concrete cover in vertical and horizontal direction. The width of the beam is 300mm and the span of the beam is 2700mm. Support are placed 150mm away from the end of the beam at each side. The concentrated load is applied in the top middle of the beam. The concrete strength of this beam is 37MPa.

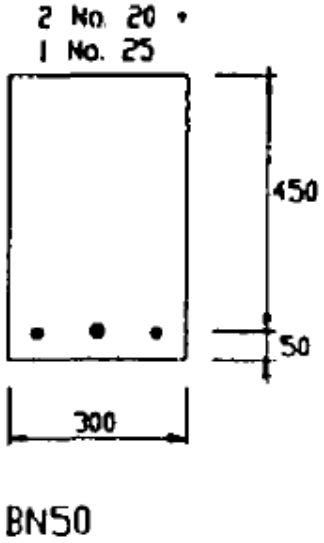

Figure 3-4 Cross sectional detailing of bond experiment (Stanik, 1998)

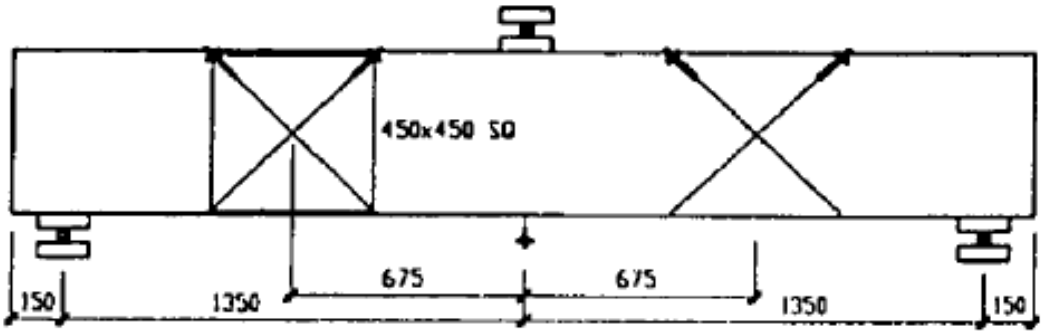

Figure 3-5 Elevation detailing of bond experiment (Stanik, 1998)

3.5.2 Response and failure mode

The load is applied incrementally and the deflection of the beam is recorded at each stage. In the BN50 test, there are 6 load stages in total. And the load deflection response of the BN50 case is shown in Figure 3-6. The ultimate load at the final stage is 266kN.

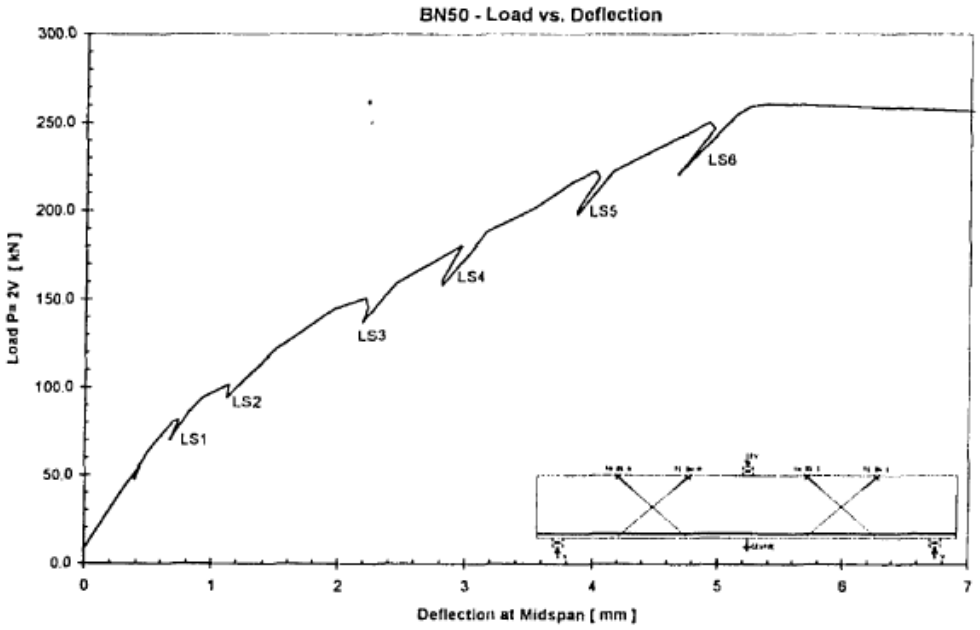

Figure 3-6 Load deflection response (Stanik, 1998)

The details of the beam at final stage are presented in Figure 3-7. There are many diagonal cracks caused by shear on the beam. And a longitudinal splitting crack is observed at the right end of the beam at the final stage, which indicates that the beam is subjected to a shear bond failure.

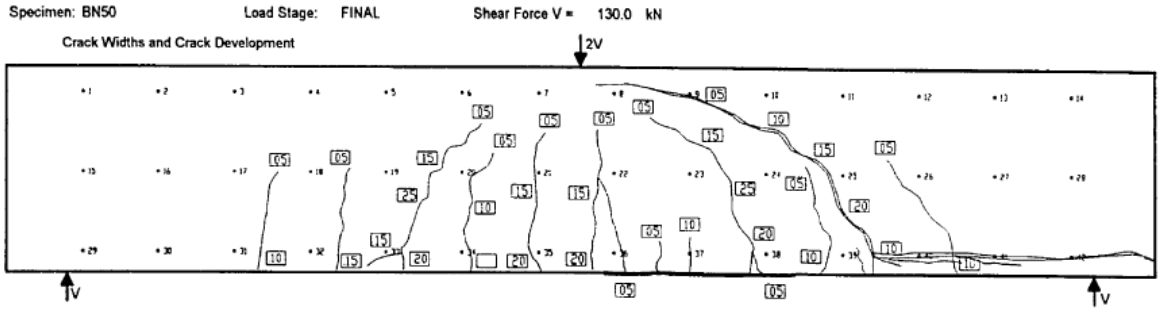

Figure 3-7 failure mode of BN50 at final stage (Stanik, 1998)

Chapter 4 FINITE ELEMENT MODELING

4.1 General

Finite element is a powerful tool in scientific research. Different types of model can be modeled to simulate the different behavior of real materials. Some simplified models are adopted in this paper in order to increase the computational efficiency of the model.

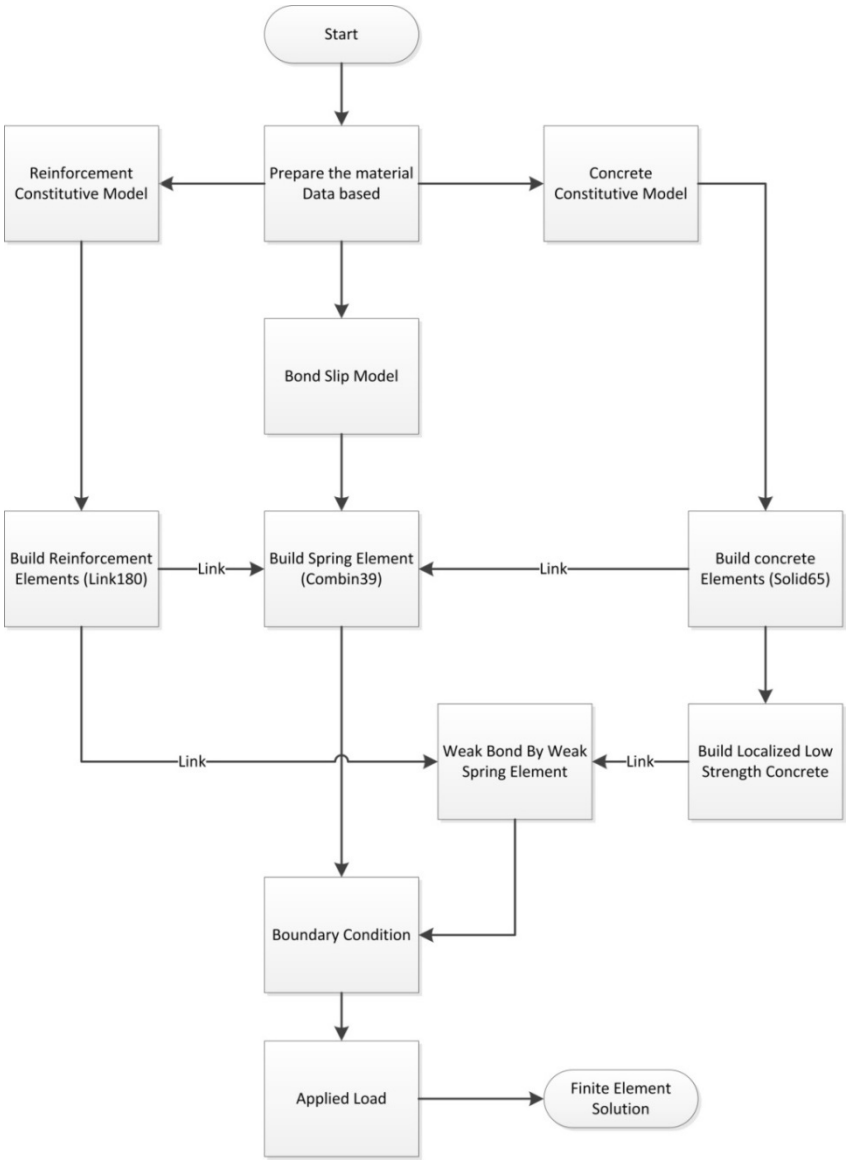

Figure 4-1 Finite Element Modeling flowchart

4.2 Concrete Elements

SOLID65 is an 8 node element, as shown in Figure 4-2, whose each node has three degrees of freedom: translations in the nodal x, y, and z directions. It is capable of cracking in tension and crushing in compression. It works well with reinforcing steel elements. The reinforcement element must be 1-D element capable of tension and compression and up to 3 reinforcement elements can be defined at each solid65 node. The nonlinear material properties are the most important feature of this element. The concrete is capable of cracking (in three orthogonal directions), crushing, plastic deformation, and creep.

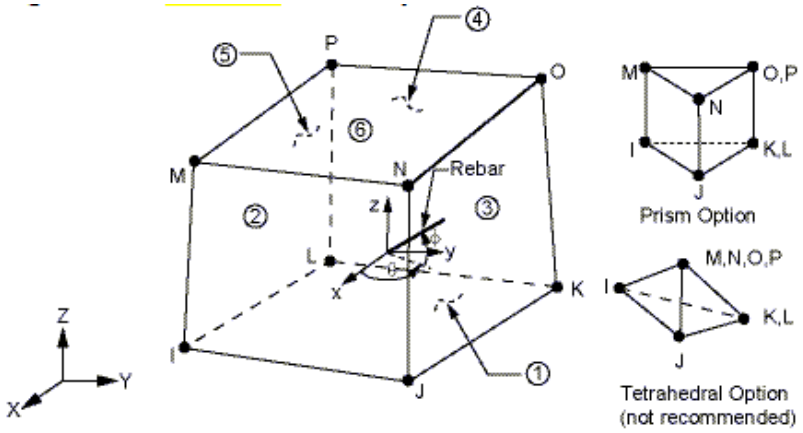

Figure 4-2 SOLID65 Geometry

Since most of the concrete defects are difficult to quantitatively described, and some of them are minor and can be easily fixed or ignored, until now, there is still few research investigate the relationship between the construction defects of concrete and material properties, for instance, the honeycombing effects on concrete strength. Therefore, in this paper, the concrete strength of concrete f'_c is assumed to be 20MPa, 30MPa, 42.7MPa.

Restricted to the software package, and considering the computational efficiency. Smeared crack model is applied throughout all the concrete elements.

The shear modulus of concrete is determined by 0.2 according to some researchers. Barzegar and Schnobrich, (1986) showed that the variable shear modulus would not affect the results, but it could improve the accuracy of the crack pattern.

For the computational efficiency of the model, a modified hognestad concrete model was used. The model is illustrated in Figure 4-3

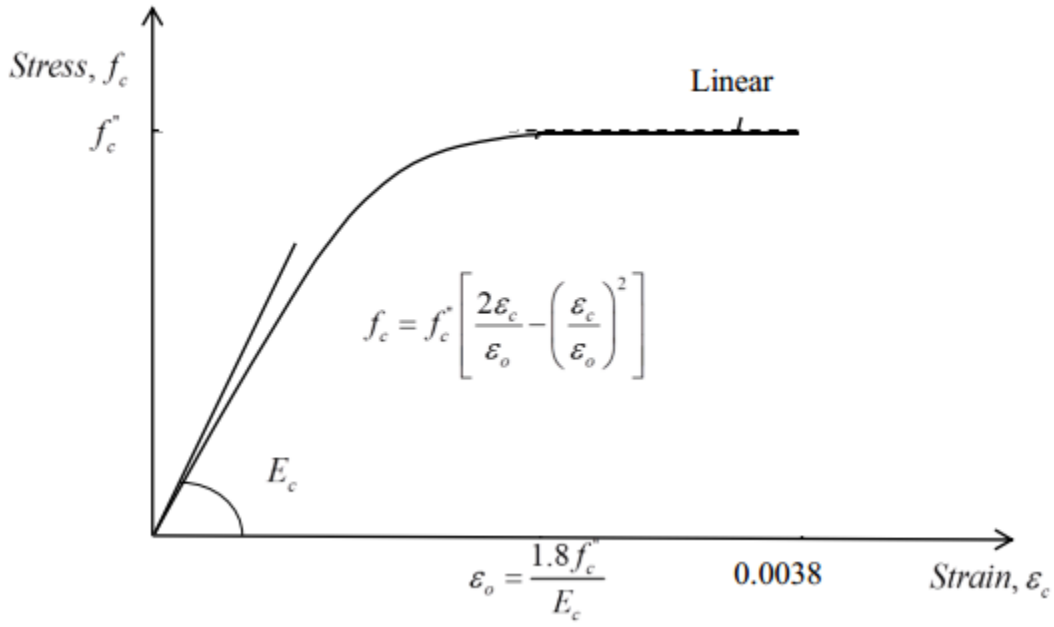

Figure 4-3 Modified hognestad

The parabola part follows equation (Macgregor, 2006),

$$f_c = f'_c\left[\frac{2\varepsilon_c}{\varepsilon_0} - \left(\frac{\varepsilon_c}{\varepsilon_0}\right)^2\right] \quad (4.1)$$

Linear part is assumed to be linear plastic because technically ANSYS does not accept negative stiffness for the constitutive model of concrete.

In addition, there are some assumptions and restrictions for the solid65 element.

(1) Cracking is permitted in three orthogonal directions at each integration point.

(2) The cracking is treated as a “smeared band” of cracks, rather than discrete cracks. In addition, the cracking is modeled through an adjustment of material properties after cracking occurs at an integration point.

(3) The concrete material is assumed to be initially isotropic.

(4) The reinforcement is assumed to be “smeared” throughout the element.

A modified Willam and Warnke (1975) failure criterion is adopted for this concrete element. The criterion for failure of concrete due to a multiaxial stress state can be expressed in the form

$$\frac{F}{f_c} - S \geq 0 \qquad (4.2)$$

Where:

F = a function of the principal stress state (σ_{xp}, σ_{yp}, σ_{zp})

S = failure surface expressed in terms of principal stress and five input parameters f_t, f_c, f_{cb}, f_1 and f_2 defined in

f_c =uniaxial crushing strength

σ_{xp}, σ_{yp}, σ_{zp} = principal stresses

f_t = Ultimate uniaxial tensile strength

f_c =Ultimate uniaxial compressive strength

f_{cb} =Ultimate biaxial compressive strength

f_1 = Ultimate compressive strength for a state of biaxial

f_2 = Ultimate compressive strength for a state of uniaxial

The failure of concrete is categorized into four domains:

- The Domain (Compression - Compression - Compression)

  When any node in concrete is subjected to triple compression, $0 \geq \sigma_1 \geq \sigma_2 \geq \sigma_3$, the F can be taken as

$$F = F_1 = \frac{1}{\sqrt{15}}\left[(\sigma_1 - \sigma_2)^2 + (\sigma_2 - \sigma_3)^2 + (\sigma_3 - \sigma_1)^2\right]^{\frac{1}{2}} \tag{4.3}$$

  And S is described as,

$$S = S_1 = \frac{2r_2(r_2^2 - r_1^2)\cos\eta + r_2(2r_1 - r_2)\left[4(r_2^2 - r_1^2)\cos^2\eta + 5r_1^2 - 4r_1r_2\right]^{\frac{1}{2}}}{4(r_2^2 - r_1^2)\cos^2\eta + (r_2 - 2r_1)^2} \tag{4.4}$$

- The Domain (Tension - Compression - Compression)

  When any node in concrete is subjected to tension, compression and compression, $\sigma_1 \geq 0 \geq \sigma_2 \geq \sigma_3$ the F can be taken as

$$F = F_2 = \frac{1}{\sqrt{15}}\left[(\sigma_2 - \sigma_3)^2 + \sigma_2^2 + \sigma_3^2\right]^{\frac{1}{2}} \tag{4.5}$$

  And S is described as,

$$S = S_2 = \left(1 - \frac{\sigma_1}{f_t}\right)\frac{2p_2(p_2^2 - p_1^2)\cos\eta + p_2(2p_1 - p_2)\left[4(p_2^2 - p_1^2)\cos^2\eta + 5p_1^2 - 4p_1p_2\right]^{\frac{1}{2}}}{4(p_2^2 - p_1^2)\cos^2\eta + (p_2 - 2p_1)^2} \tag{4.6}$$

- The Domain (Tension - Tension - Compression)

When any node in concrete is subjected to tension, tension and compression, $\sigma_1 \geq \sigma_2 \geq 0 \geq \sigma_3$ the F can be taken as

$$F = F_3 = \sigma_i;\ i = 1,2 \tag{4.7}$$

And S is described as,

$$S = S_3 = \frac{f_t}{f_c}\left(1 + \frac{\sigma_3}{f_c}\right);\ i = 1,2 \tag{4.8}$$

Cracking occurs in the plane perpendicular to principal stress σ1, If the failure criterion is satisfied for i = 1. The Cracking will occurs in the planes perpendicular to principal stresses σ1 and σ2, If the failure criterion for both i = 1, 2 is satisfied.

- The Domain (Tension - Tension - Tension)

  When any node in concrete is subjected to tension, tension and tension, $\sigma_1 \geq \sigma_2 \geq \sigma_3 \geq 0$ the F can be taken as

$$F = F_4 = \sigma_i;\ i = 1,2,3 \tag{4.9}$$

  and S is described as

$$S = S_4 = \frac{f_t}{f_c} \tag{4.10}$$

  The cracking will occurs up to three planes perpendicular to principal stresses σ1, σ2, and σ3, when failure criterion is satisfied in directions i.(i= 1,2,3)

4.3 Steel Elements

Although discrete reinforcement model allows for the investigation of bond-slip behavior of reinforcement with respect to the adjacent concrete in a higher accuracy when compared to the smeared steel model, it is more computationally expensive. In this paper, smeared steel modeling method is adopted and can generate good result with less computational work.

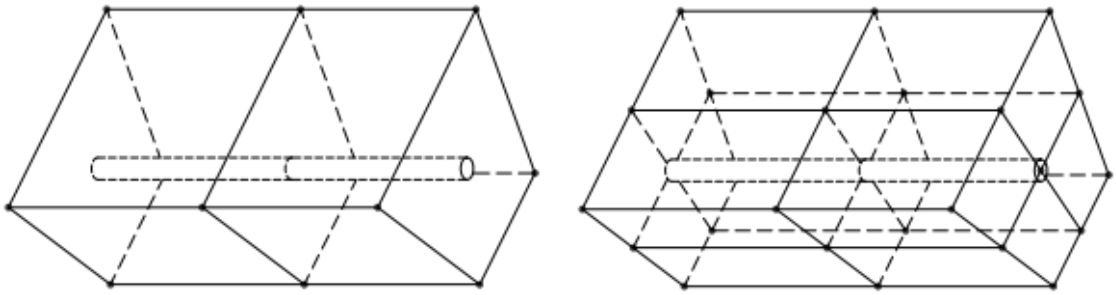

Figure 4-4 Left: embedded reinforcement model (smeared model), Right: discrete reinforcement model (Naito, 2001)

. Link180 is the element type that can be used in ANSYS to modeling the discrete steel. LINK180 is a 3-D spar element that can be used in various engineering applications. The application ranges from trusses, sagging cables, links, springs etc. This element is capable of carrying uniaxial tension-compression. It has two nodes as shown in Figure 4-5, and each node has three degrees of freedom: translations in the nodal x, y, and z directions.

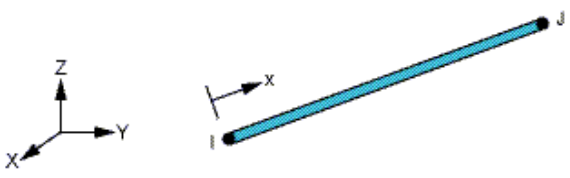

Figure 4-5 LINK180 Geometry

4.4 Bond between Concrete and Steel

COMBIN39 element is used in this paper to model the bond behavior between reinforcement and concrete. Combin39 is a unidirectional element with 2 nodes. It is capable of being dimensionless and incorporating nonlinear generalized force-deflection. The element has longitudinal or torsional capability in 1-D, 2-D, or 3-D applications. The longitudinal option is a uniaxial tension-compression element with up to three degrees of freedom at each node: translations in the nodal x, y, and z directions.

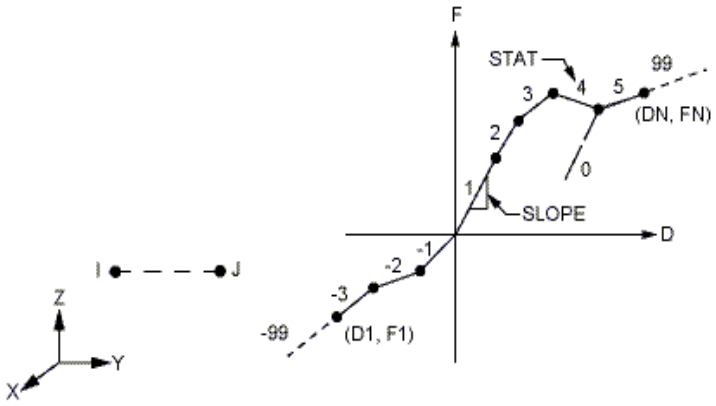

Figure 4-6 COMBIN39 Geometry

CEB-FIP (2010) model is the most acceptable bond model presents the interface characteristic between reinforcement and concrete at present with simple form. Therefore, the bond model for the bond behavior of average reinforcement is constructed based on CEB-FIP (2010) proposed model.

4.5 Boundary Condition

In the reference beam, the left support is set to model the boundary condition of the finite element beam same as the reference beam, all the nodes at middle bottom are set to be symmetry. They could move downward but restricted to the symmetry axis.

By setting the symmetry axis, all the nodes and element in the other half of the beam can be saved without accuracy decrease.

4.6 Failure

4.6.1 Failure Mode

Debonding failure: a sudden loss of bond between reinforcing bars and concrete in anchorage zones. Generally, in a well-developed bond condition, the shape of bond stress is approximate to parabolic and the bond stress and support end is zero. But in a lack-developed bond condition, bond stress near the support is not zero, which is a sign that indicates the shortage of development length. And the shape of bond stress is approximate horizontal near support and descends when it comes close to the middle of the beam.

Flexural failure: for a ductile flexural failure that the reinforcement yields firstly before the concrete crush, the load deflection will present an obvious horizontal segment during the reinforcement plastification. For a brittle flexural failure, whose load deflection curve will terminate in a sudden, the stress and strain in the critical section should be investigated to make sure it’s a flexural failure.

4.6.2 Failure Criteria

Flexural failure: flexural failure is an expected failure mode for reinforced beam. When the load increases, the beam reinforcement reaches its yielding stress and starts to deform. Yielding of reinforcement exhibits a leveling branch in the load deflection curve of structure.

Shear bond failure: In a flexural failure or a pure shear failure, before the reinforcement yield and concrete crush, the reinforcement nodes right above the support should only experience a small amount of movement during the loading. After the reinforcement yield or concrete crush, the reinforcements resist the deformation and the nodes above the support may start to move dramatically. However, in a shear bond failure, when the load increases, the concrete provide bond resistance and prevent the reinforcement from movement. When the load increase to a certain amount, before the reinforcement yield and less than the concrete shear resistance, the bond force in reinforcement are not enough to hold the reinforcement in its position, then the nodes right above the support will start to move dramatically. Soon the beam fails due to the relative movement between reinforcement and concrete. This situation is considered a bond failure.

The distinctive characteristic of a bond failure is the bond stress shape along the reinforcement.

A normal flexural failure whose reinforcement could develop its stress sufficiently would look like a wave, which has several peaks and troughs. The relative movement between concrete and reinforcement at the end is extremely small. Because in the real world, the high ribs of deformed bars are designed to create high mechanical bond stress through interlock mechanism between concrete and reinforcement.

However, for a beam which does not provide enough development length. The bond stress along the reinforcement of the beam will a triangle or trapezoid shape, whose relative movement between reinforcement and concrete at the end are relatively high than other place.

4.7 Case Summary

To understand effect of localized low concrete strength on flexural strength of RC beams, 30 beams with different parameters have been set up as listed in Table 4-1.

Table 4-1 Cases summary

Case Summary			
Case Name	Bottom Reinforcement	Honeycombing Location	Strength of Concrete(MPa)
16-0	2x16mm	None	42.7
16-1-10	2x16mm	1	10
16-1-20	2x16mm	1	20
16-1-30	2x16mm	1	30
16-2-10	2x16mm	2	10
16-2-20	2x16mm	2	20
16-2-30	2x16mm	2	30
16-3-10	2x16mm	3	10
16-3-20	2x16mm	3	20
16-3-30	2x16mm	3	30
25-0	2x25mm	None	42.7
25-1-10	2x25mm	1	10
25-1-20	2x25mm	1	20
25-1-30	2x25mm	1	30
25-2-10	2x25mm	2	10
25-2-20	2x25mm	2	20
25-2-30	2x25mm	2	30
25-3-10	2x25mm	3	10
25-3-20	2x25mm	3	20
25-3-30	2x25mm	3	30
32-0	2x32mm	None	42.7
32-1-10	2x32mm	1	10
32-1-20	2x32mm	1	20
32-1-30	2x32mm	1	30
32-2-10	2x32mm	2	10
32-2-20	2x32mm	2	20
32-2-30	2x32mm	2	30
32-3-10	2x32mm	3	10
32-3-20	2x32mm	3	20
32-3-30	2x32mm	3	30

4.8 Finite Element Mesh

Due to the computer hardware performance and analysis time limit, only half of the reference simply supported beam was modeled in ANSYS, as shown in Figure 4-7 and Figure 4-8. For the reinforced concrete element solid65, the recommended minimum element size for the core part is larger than 50mm (2in) to avoid load concentration. Therefore, within the core concrete, the division of the longitudinal direction is set to be 65mm to fit for the placement of the stirrups. The longitudinal division for the extended concrete end at left was divided into two parts. In the X-Y plane, the element size of the core concrete is set to be 50mm along the X axis and Y axis. The element size for outer concrete cover is set to be 25mm to meet the reference beam. Moreover, to reduce the load concentration at point where the loads are applied, a high stiffness steel cushion is added to distribute the load evenly. At the left end near the support, an additional high stiffness steel cushion is also added to avoid concentration here.

Figure 4-7 Finite Element Meshing

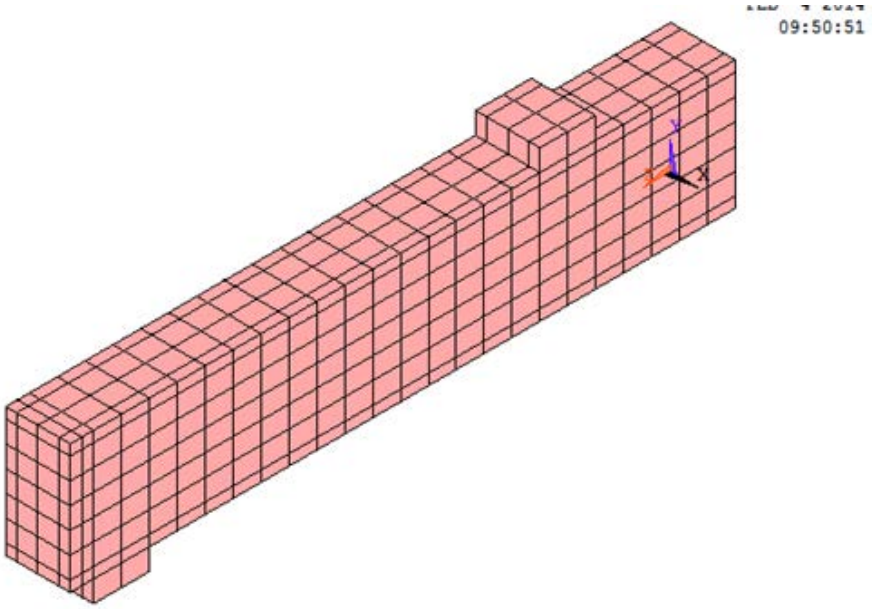

Figure 4-8 Isotropic view of finite element meshing

4.9 Division of the beam

The beam is divided into three regions. Middle bending region, shear sensitive region, bond sensitive region.

4.10 Validation of FEM

The meshing finite element model could affect the numerical analysis result. Before the analytical model were tested and investigated, the effect of element meshes have to be studied firstly to guarantee the accuracy of the finite element model. Three types of smeared element meshes (details listed in Table 4-2) were used in meshes study here, half beam coarse mesh, half beam fine mesh, full beam fine mesh.

Table 4-2 details of different mesh

	Node number	Element number	bond condition between concrete and reinforcement
half beam coarse model	754	605	Fully Bonded
half beam fine model	2115	1024	Via spring elements
Full beam fine model	21385	18440	Fully bonded

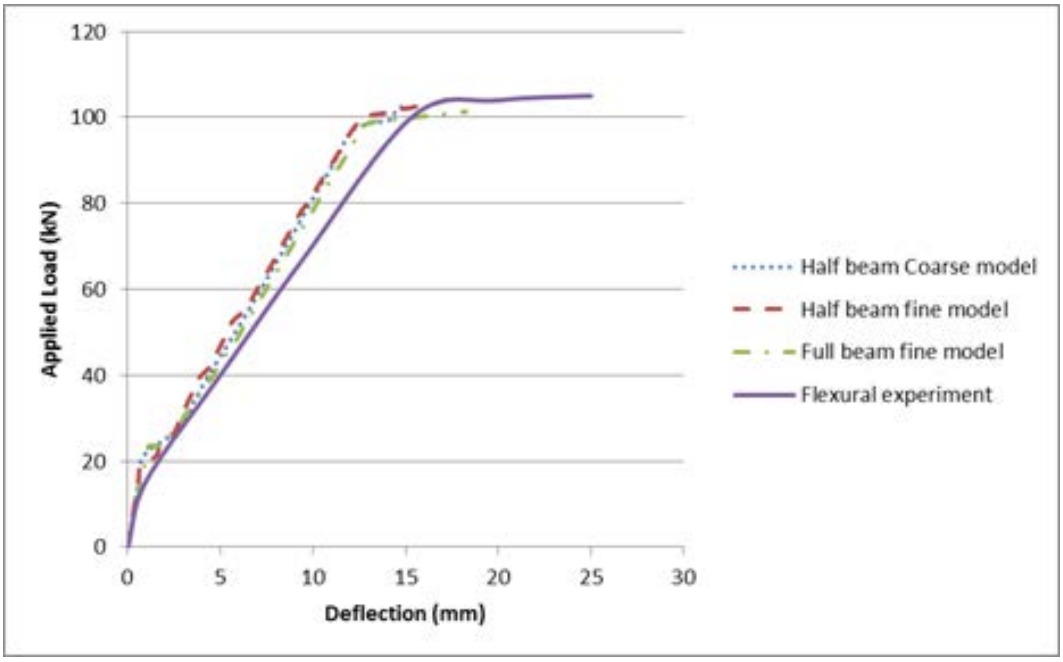

Figure 4-9 Element Mesh Study and flexural strength verification

The load-deflection curve results of these beams are listed in Figure 4-9. Although the full beam fine model consists of tremendous nodes and elements, the response of the beams are almost the same. And they are all close to the experiment results. Hence, it is unnecessary to use the full beam model with fine mesh to achieve little improvement in accuracy at the expense of computing time three to four times greater.

The element mesh of half beam fine model, shown in Figure 4-7 and Figure 4-8 was chose to study the flexural strength of RC beams, in later analysis.

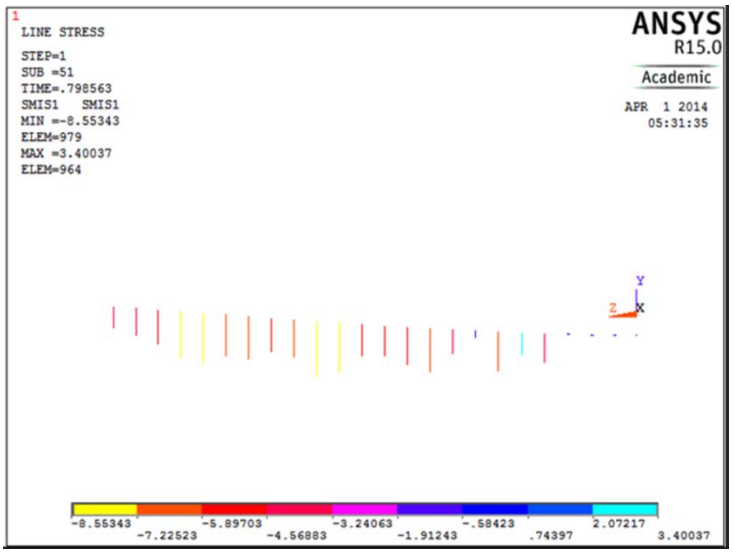

Figure 4-10 Bond stress in the half beam fine model

The bond force in the half beam fine model is illustrated in Figure 4-9. Figure 4-10 shows the actual bond stress in the real world from the experiment done by Mainst, 1951. Considering that the experiment result represents only half bond stress of the beam, the parabolic shape of spring force with several peaks and troughs match the experiment one well, and the spring force terminate where the load applied is the same as the experiment one.

Figure 4-11 Bond stress in a deformed bar when loading (MAINST, 1951)

Another finite element model has been set up to simulate the BN50 beam fail in shear with splitting cracks. The solution of the finite element mode is presented in Figure 4-11. As can be seen, the solution also matches the shear failure beam very well.

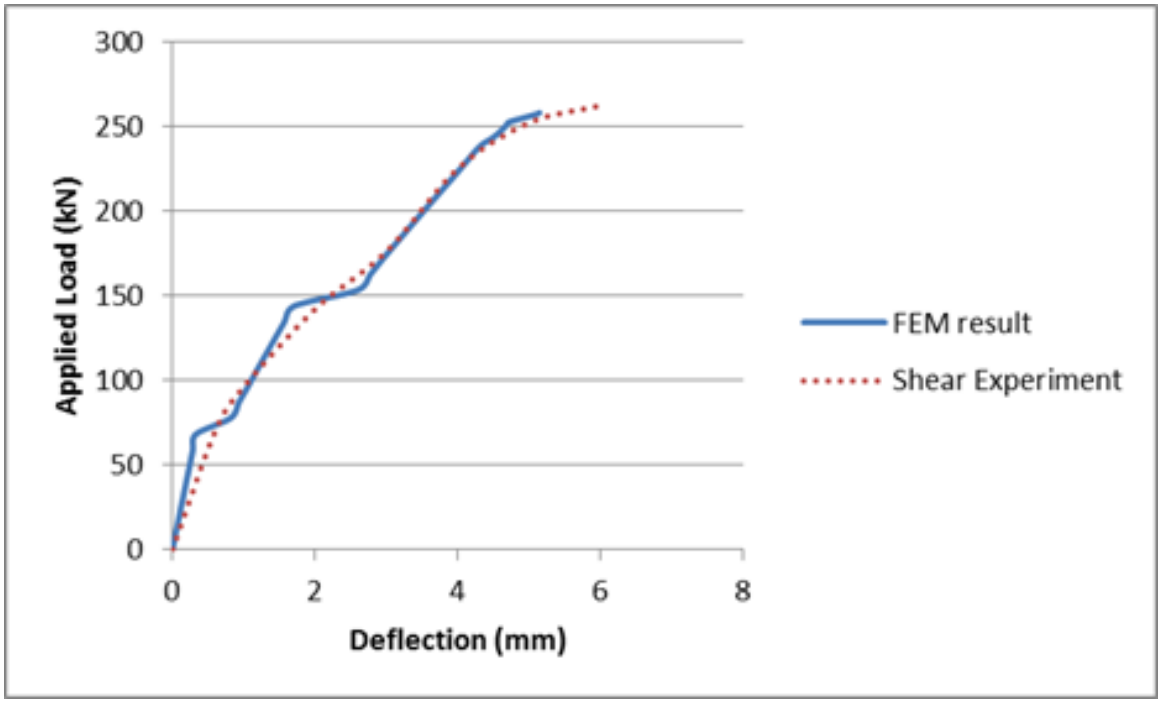

Figure 4-12 finite element model against shear failure with splitting cracks

In summary, the scheme of how to verify the finite element model is illustrated in Figure 4-12.

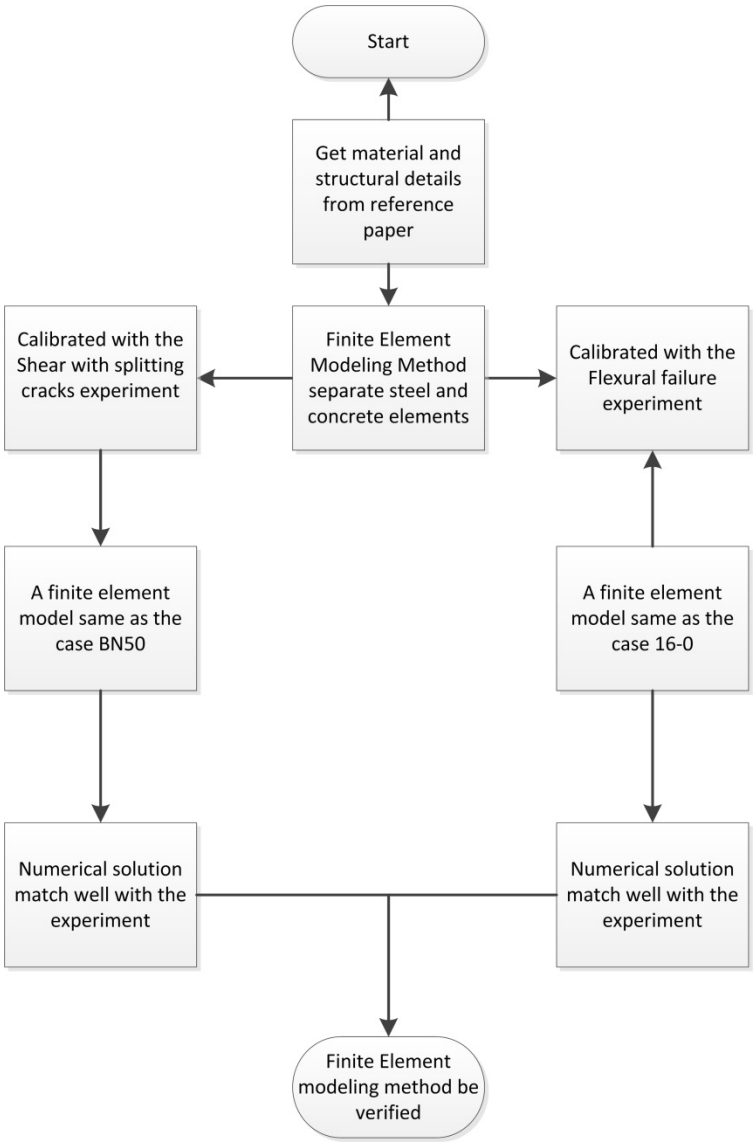

Figure 4-13 Verification flowchart

Chapter 5 RESULT ANALYSIS

5.1 General

This chapter presents the failure mechanism for each beam case, in detail. In order to investigate the details of failure, up to eight aspects of the RC beams at the ultimate state were revealed. The load deflection curve shows the response history of the RC beam to the applied load. The ultimate load, ultimate deflection and the variation of stiffness can be seen in the load deflection curve. The reinforcement stress diagram exhibits the stress in steel in GPa. Normally, when the stress of steel reached 0.512GPa, the steel is considered to have yielded and the RC structure supposed to have a horizontal segment in its load deflection response curve. The Von Mises stress diagram displays the equivalent Von Mises stress in concrete. It is related to the principal stress by equation:

$$\sigma_e = \sqrt{[\frac{(\sigma_1-\sigma_2)^2+(\sigma_2-\sigma_3)^2+(\sigma_3-\sigma_1)^2}{2}]} \quad (5.1)$$

where σ_1, σ_2, σ_3 = First, second, third principal stress

The equivalent Von Mises stress presents the highest compression position in concrete. But the concrete crushing failure criteria is defined by William and Warnke (1975) failure criterion described in last chapter.

The 3rd principal strain chart presents the total mechanical strain of 3rd principal strain. The XZ shear strain chart shows the total mechanical strain in the longitudinal direction along the reinforcement. They could tell which part of the concrete are subjected to larger strain. And the Crack Ⅰ, Ⅱ, Ⅲ shows the details of crack pattern.

The failure of the concrete is determined by modified Willam and Warnke theory, which will be described in concrete element modeling section. The scheme of how to investigate the failure mode for the RC beams is shown below in Figure 5-1.

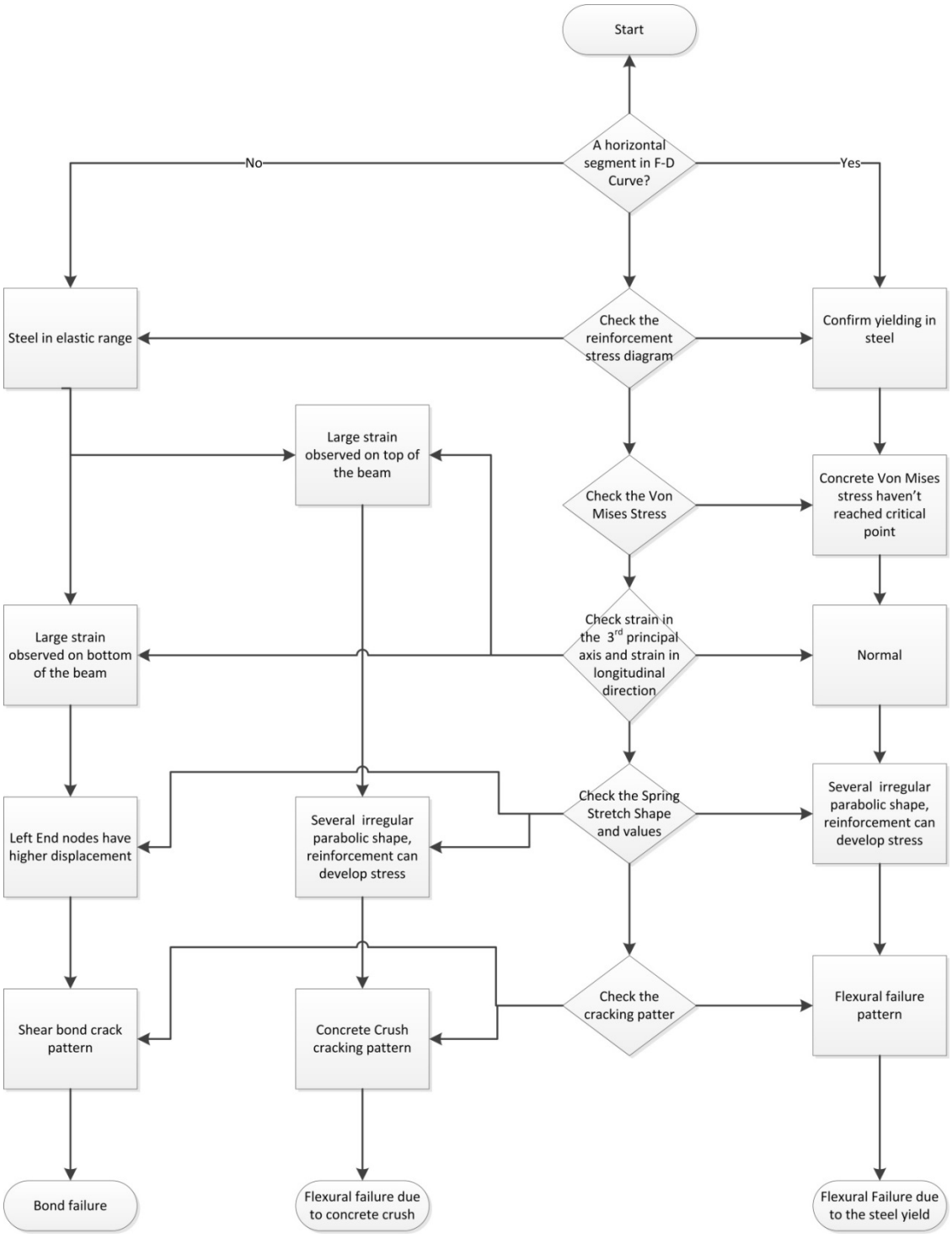

Figure 5-1 Failure Mode Investigation Flowchart

5.2 Results Analyses

5.2.1 Case 16-0

Case 16-0 was the reference beam for all the FEM cases with 16mm rebar. Table D-1exhibits the detailed dimensions and honeycombing location for this case. The concrete of this case is assumed to be in good condition, 42.7MPa strength throughout the entire beam. Loading were applied near the middle of the beam. The ultimate load and corresponding deflection at mid-span were 104.21kN and 17.33mm. And a horizontal segment could be observed in the load deflection curve, which indicated the yielding of steel. The details of the beam at ultimate stage were illustrated from Figure D-1 to Figure D-8. The steel stress diagram indicated the stress in reinforcement had reached 512MPa, which was the yielding point, also verified the horizontal response in the load deflection diagram. The Von Mises stress diagram indicated that the concrete hadn't reached its critical stress yet. The spring stretch graph displayed a parabolic shape with several peak and trough, which indicated steel could develop its strength well. Cracking figures showed the typical flexural failure cracking along the bottom of the entire beam. From all the facts above, it could be concluded that case 16-0 experienced a flexural failure that the reinforcement yield firstly and then the concrete crush later.

5.2.2 Case 16-1-10

Case 16-1-10 was assumed to have low strength concrete at the middle portion of the beam. Table D-2 shows the detailed dimensions and honeycombing location for this case. The strength of concrete at the middle was assumed to be 10MPa, and the rest concrete were still in good condition, 42.7MPa. Loading were applied near the

middle of the beam. The ultimate load and corresponding deflection at mid-span were 53.62kN and 8.36mm. The load deflection curve stopped in a sudden when the applied load reached 53.62kN. The details of the beam at ultimate stage were showed from Figure D-9 to Figure D-16. The steel stress diagram indicated the stress in reinforcement hadn't reached its yielding position yet. The 3rd principal total mechanical strain diagram and XZ shear total mechanical strain indicated that the top concrete near the middle of the beam experienced concentrated compression. The Von Mises stress diagram also indicated that the top concrete near middle of the beam experienced a critical situation. The spring stretch graph displayed a parabolic shape, which indicated steel could develop its strength well. Cracking figures showed that most of the cracks occurred at the middle portion of this beam, where the low strength concrete located. From all the facts above, it could be concluded that case 16-1-10 experienced a flexural failure, the top-right corner of the concrete in Region (1) crushed before the reinforcement yield at the final stage.

5.2.3 Case 16-1-20

Case 16-1-20 was assumed to have low strength concrete at the middle portion of the beam. Table D-3 shows detailed dimensions and honeycombing location for this case. The strength of concrete at the middle was assumed to be 20MPa, and the rest concrete were in good condition, 42.7MPa. Loading were applied near the middle of the beam. The ultimate load and corresponding deflection at mid-span were 94.14kN and 13.68mm. When the stiffness tends to drop dramatically, the load deflection curve stopped, which indicated crush of concrete. The details of the beam at ultimate stage were displayed from Figure D-17 to Figure D-24. The steel stress diagram indicated the

stress in reinforcement had reached 512MPa, which is the yielding stress. However, the Von Mises stress diagram also indicated that the concrete reached its critical stress. The spring stretch graph displayed a parabolic shape, which indicated that steel could develop its strength well. Cracking figures showed the typical flexural failure cracking along the bottom of the entire beam. From all the facts above, it could be concluded that case 16-1-20 experienced a flexural failure. Both concrete and reinforcement govern the failure status.

5.2.4 Case 16-1-30

Case 16-1-30 was assumed to have low strength concrete at the middle portion of the beam. It is assumed that all reinforcements are smeared through the concrete elements. Table D-4 shows detailed dimensions and honeycombing location for this case. The strength of concrete at the middle was assumed to be 30MPa, and the rest concrete were in good condition, 42.7MPa. Loading were applied near the middle of the beam. The ultimate load and corresponding deflection at mid-span were 101.23kN and 20.28mm. And a horizontal segment could be observed in the load deflection curve, which indicated the yielding of steel. The details of the beam at ultimate stage were displayed from Figure D-25 to Figure D-32. The steel stress diagram indicated the stress in reinforcement had reached 512MPa, which is the yielding stress, this also verified the horizontal response in the load deflection diagram. The Von Mises stress diagram indicated that the concrete hadn’t reached its critical stress yet. The spring stretch graph displayed a parabolic shape, which indicated that steel could develop its strength well. Cracking figures showed the typical flexural failure cracking along the bottom of the entire beam. From all the facts above, it could be concluded that case 16-

1-30 experienced a flexural failure, the reinforcement yield firstly and then the concrete crush later.

5.2.5 Case 16-2-10

Case 16-2-10 was assumed to have low strength concrete at the shear sensitive portion, region (2), of the beam. Table D-5 shows detailed dimensions and honeycombing location for this case. The concrete at the portion (2) was assumed to be 10MPa, and the rest concrete were in good condition, 42.7MPa. Loading were applied near the middle of the beam. The ultimate load and corresponding deflection at mid-span were 60.26kN and 8.42mm. The load deflection curve stopped in a sudden when the applied load reached 60.26kN. The details of the beam at ultimate stage were showed from Figure D-33 to Figure D-40. The steel stress diagram indicated the stress in reinforcement hadn't reached its yielding position, 512MPa. The 3rd principal total mechanical strain diagram and XZ shear total mechanical strain indicated that the top-right corner of the concrete in portion (2) experienced critical compression. The Von Mises stress diagram also indicated that the top-right corner of the concrete in portion (2) was in a critical situation. The spring stretch graph displayed a parabolic shape, which indicated that steel could develop its strength well. Cracking figures showed that most of the cracks occurred at the portion (2) of this beam, where the low strength concrete located. From all the facts above, it could be concluded that case 16-2-10 experienced a flexural compression failure, the top-right corner of the concrete in Region (2) crushed at ultimate stage before the reinforcement yield.

5.2.6 Case 16-2-20

Case 16-2-20 was assumed to have low strength concrete at the shear sensitive portion, region (2), of the beam. Table D-6 shows detailed dimensions and honeycombing location for this case. The concrete at the portion (2) was assumed to be 20MPa, and the rest concrete were in good condition, 42.7MPa. Loading were applied near the middle of the beam. The ultimate load and corresponding deflection at mid-span were 95.97kN and 12.60mm. The load deflection curve stopped in a sudden when the applied load reached 95.97kN. The details of the beam at ultimate stage were showed from Figure D-41 to Figure D-48. The steel stress diagram indicated the stress in reinforcement hadn't reached its yielding position, 512MPa. The 3rd principal total mechanical strain diagram indicated that the top-right corner of the concrete in portion (2) experienced a critical compression. The Von Mises stress diagram also indicated that the top-right corner of the concrete in portion (2) was in a critical situation. The spring stretch graph displayed a parabolic shape, which indicated that steel could develop its strength sufficiently. Cracking figures showed that some flexural cracks occurred at the bottom of the beam, and many cracks occurred within the portion (2) of this beam, where the low strength concrete located. From all the facts above, it could be concluded that case 16-2-20 experienced a flexural failure, the top-right corner of the concrete in Region (2) crushed at ultimate stage before the reinforcement yield.

5.2.7 Case 16-2-30

Case 16-2-30 was assumed to have low strength concrete at the shear sensitive portion of the beam, region (2). Table D-7 shows detailed dimensions and honeycombing location for this case. The concrete at the portion (2) was assumed to be

30MPa, and the rest concrete were in good condition, 42.7MPa. Loading were applied near the middle of the beam. The ultimate load and corresponding deflection n at mid-span were 102.17kN and 24.8mm. And a horizontal segment could be observed in the load deflection curve, which indicated the yielding of steel. The details of the beam at ultimate stage were illustrated from Figure D-49 to Figure D-56. The steel stress diagram indicated the stress in reinforcement reached 512MPa, which was the yielding position, this also verified then horizontal response in the load deflection diagram. The Von Mises stress diagram indicated that the concrete didn't reach its critical stress. The spring stretch graph displayed a parabolic shape whose steel could develop its strength sufficiently. Cracking figures showed the typical flexural failure cracking along the bottom of the entire beam. From all the facts above, it could be concluded that case 16-2-30 experienced a flexural failure that the reinforcement yield firstly and then the concrete crush later.

5.2.8 Case 16-3-10

Case 16-3-10 was assumed to have low strength concrete at the bond sensitive portion of the beam, region (3). Table D-8 shows detailed dimensions and honeycombing location for this case. The concrete at the portion (3) was assumed to be 10MPa, and the rest concrete were in good condition, 42.7MPa. Loading were applied near the middle of the beam. The ultimate load and corresponding deflection at mid-span were 72.27kN and 8.98mm. The load deflection curve stopped in a sudden when the applied load reached 72.27kN. The details of the beam at ultimate stage were illustrated from Figure D-57 to Figure D-64. The steel stress diagram indicated the

stress in reinforcement didn't reach 512MPa, which was the yielding position. The Von Mises stress diagram indicated that the weak concrete at the interface next to normal concrete experienced a critical stress. The spring stretch graph displayed a parabolic shape with peak at the middle of the beam, which indicated steel is still capable of developing its strength. Cracking figures showed the many flexural failure cracks occurred firstly. And lots of cracks took place near the support end, where the localized low strength concrete located. From all the facts above, it could be concluded that case 16-3-10 experienced a flexural failure, the top-right corner of the concrete in Region (1) crushed at ultimate stage before the reinforcement yield.

5.2.9 Case 16-3-20

Case 16-3-20 was assumed to have low strength concrete at the bond sensitive portion of the beam. Table D-9 shows detailed dimensions and honeycombing location for this case. The concrete at the portion (3) was assumed to be 20MPa, and the rest concrete were in good condition, 42.7MPa. Loading were applied near the middle of the beam. The ultimate load and corresponding deflection at mid-span were 103.81kN and 18.97mm. And a horizontal segment could be observed in the load deflection curve, which indicated the yielding of steel. The details of the beam at ultimate stage were displayed from Figure D-65 to Figure D-72. The steel stress diagram indicated the stress in reinforcement reached 512MPa, which was the yielding position; this also verified the horizontal response in the load deflection diagram. The Von Mises stress diagram indicated that the concrete didn't reach its critical stress. The yielding of reinforcement caused a comparatively large displacement in spring stretch diagram. But the reinforcement should be able to develop its strength sufficiently. Cracking figures

showed the typical flexural failure cracking along the bottom of the entire beam. From all the facts above, it could be concluded that case 16-3-20 experienced a flexural failure that the reinforcement yield firstly and then the concrete crush later.

5.2.10 Case 16-3-30

Case 16-3-30 was assumed to have low strength concrete at the bond sensitive portion of the beam. Table D-10 shows detailed dimensions and honeycombing location for this case. The concrete at the portion (3) was assumed to be 30MPa, and the rest concrete were in good condition, 42.7MPa. Loading were applied near the middle of the beam. The ultimate load and corresponding deflection at mid-span were 103.82kN and 18.02mm. And a horizontal segment could be observed in the load deflection curve, which indicated the yielding of steel. The details of the beam at ultimate stage were presented from Figure D-73 to Figure D-80. The steel stress diagram indicated the stress in reinforcement reached 512MPa, which was the yielding position. This also verified response in the load deflection diagram. The Von Mises stress diagram indicated that the concrete didn't reach its critical stress. The spring stretch graph displayed a parabolic shape, which indicated that steel could develop its strength sufficiently. Cracking figures showed the typical flexural failure cracking along the bottom of the entire beam. From all the facts above, it could be concluded that case 16-3-20 experienced a flexural tension failure that the reinforcement yield firstly and then the concrete crush later.

5.2.11 Case 25-0

Case 25-0 was the reference beam for the FEM cases with 25mm rebar. Table D-11 shows detailed dimensions and honeycombing location for this case. The concrete

of this case is assumed to be in good condition, 42.7MPa throughout the entire beam. Loading were applied near the middle of the beam. The ultimate load and corresponding deflection at mid-span were 178.92kN and 12.92mm. The load deflection curve terminated abruptly when the applied load reached 178.92kN. The details of the beam at ultimate stage were showed from Figure D-81 to Figure D-88. The steel stress diagram indicated the stress in reinforcement didn't reach the yielding position, 512MPa. And the Von Mises stress diagram indicated that the concrete didn't reach its critical point. But the XZ shear total mechanical strain displayed a strain concentration along the longitudinal reinforcement. And the spring stretch graph displayed a bond failure trapezoid shape which indicated that the development length was insufficient for the steel to develop its stress. The Cracking figures showed some flexural cracking developed along the bottom of the entire beam. From all the facts above, it could be concluded that case 25-0 experienced a bond failure, the bond slip initialed before the reinforcement developed its strength.

5.2.12 Case 25-1-10

Case 25-1-10 was assumed to have low strength concrete at the bending sensitive portion of the beam, region (1). Table D-12 shows detailed dimensions and honeycombing location for this case. The strength of concrete at the middle was assumed to be 10MPa, and the rest concrete were in good condition, 42.7MPa. Loading were applied near the middle of the beam. The ultimate load and corresponding deflection at mid-span were 60.94kN and 4.97mm. The load deflection curve stopped in a sudden when the applied load reached 60.94kN. The details of the beam at ultimate stage were presented from Figure D-89 to Figure D-96. The steel stress diagram

indicated the stress in reinforcement didn't reach its yielding position, which was 512MPa. The 3rd principal total mechanical strain diagram indicated that the top middle concrete next to the normal concrete experienced critical compression. The Von Mises stress diagram also indicated the top middle concrete next to the normal concrete experienced a critical situation. The spring stretch graph displayed a parabolic flexural failure shape with some peaks and troughs, which indicated that steel was capable of developing its strength. Cracking figures showed that most of the cracks occurred at the middle portion of this beam, where the low strength concrete located. From all the facts above, it could be concluded that case 25-1-10 experienced a flexural failure, the top-left corner of the concrete in Region (1) crushed at ultimate stage before reinforcement yield.

5.2.13 Case 25-1-20

Case 25-1-20 was assumed to have low strength concrete at the middle portion of the beam. Table D-13 shows detailed dimensions and honeycombing location for this case. The strength of concrete at the middle was assumed to be 20MPa, and the rest concrete were in good condition, 42.7MPa. Loading were applied near the middle of the beam. The ultimate load and corresponding deflection at mid-span were 95.18N and 7.07mm. The load deflection curve stopped in a sudden when the applied load reached 95.18kN. The details of the beam at ultimate stage were displayed from Figure D-97 to Figure D-104. The steel stress diagram indicated the stress in reinforcement didn't reach its yielding position, which was 512MPa. The 3rd principal total mechanical strain diagram and XZ shear total mechanical strain indicated that the top concrete experienced critical compression. The Von Mises stress diagram also indicated that the

top concrete at middle of the beam experienced critical situation. The spring stretch graph displayed a parabolic flexural failure shape, which indicated that steel could well develop its strength. Cracking figures showed that normal flexural cracks occurred along the bottom of this beam. From all the facts above, it could be concluded that case 25-1-20 experienced a flexural failure, the top of the concrete in region (1) crushed at ultimate stage before reinforcement yield.

5.2.14 Case 25-1-30

Case 25-1-30 was assumed to have low strength concrete at the middle portion of the beam. Table D-14 shows detailed dimensions and honeycombing location for this case. The strength of concrete at the middle was assumed to be 30MPa, and the rest concrete were in good condition, 42.7MPa. Loading were applied near the middle of the beam. The ultimate load and corresponding deflection at mid-span were 161.03kN and 12.39mm. The load deflection curve stopped in a sudden when the applied load reached 161.03kN. The details of the beam at ultimate stage were displayed from Figure D-106 to Figure D-112. The steel stress diagram indicated the stress in reinforcement didn't reach its yielding position, which was 512MPa. The 3rd principal total mechanical strain diagram indicated that the top concrete at the middle part experienced high compression. The Von Mises stress diagram also indicated that the top concrete at middle experienced high stress. The XZ shear strain graph shows a concentrated high strain along the reinforcement. In addition, the spring stretch graph still expressed a trapezoid shape, which indicated that steel was not able to develop its strength at this point. Cracking figures showed that many flexural cracks occurred along

the bottom of this beam. From all the facts above, it could be concluded that case 25-1-30 experienced a bond failure.

5.2.15 Case 25-2-10

Case 25-2-10 was assumed to have low strength concrete at the shear sensitive portion of the beam. Table D-15 shows detailed dimensions and honeycombing location for this case. The concrete at the portion (2) was assumed to be 10MPa, and the rest concrete were in good condition, 42.7MPa. Loading were applied near the middle of the beam. The ultimate load and corresponding deflection at mid-span were 67.93kN and 5.30mm. The load deflection curve stopped in a sudden when the applied load reached 67.93kN. The details of the beam at ultimate stage were demonstrated from Figure D-113 to Figure D-120. The steel stress diagram indicated the stress in reinforcement didn't reach its yielding position, which was 512MPa. The 3rd principal total mechanical strain diagram and XZ shear total mechanical strain indicated that the top-right corner of the concrete in portion (2) experienced critical compression. The Von Mises stress diagram also indicated that the top-right corner of the concrete in portion (2) was in a critical situation. The spring stretch graph showed a parabolic shape with one peak, this indicated that steel could develop its strength sufficiently. Cracking figures showed that most of the cracks occurred at the portion (2) of this beam, where the low strength concrete located. From all the facts above, it could be concluded that case 25-2-10 experienced a flexural compression failure, the top-right corner of the concrete in Region (2) crushed at ultimate stage before the reinforcement yield.

5.2.16 Case 25-2-20

Case 25-2-20 was assumed to have low strength concrete at the shear sensitive portion of the beam, region (2). Table D-16 shows detailed dimensions and honeycombing location for this case. The concrete at the portion (2) was assumed to be 20MPa, and the rest concrete were in good condition, 42.7MPa. Loading were applied near the middle of the beam. The ultimate load and corresponding deflection at mid-span were 115.15kN and 8.22mm. The load deflection curve stopped in a sudden when the applied load reached 115.15kN. The details of the beam at ultimate stage were demonstrated from Figure D-121 to Figure D-128. The steel stress diagram indicated the stress in reinforcement didn't reach its yielding position. The 3rd principal total mechanical strain diagram that the top of the concrete in portion (2) experienced critical compression. The Von Mises stress diagram also indicated that the top of the concrete in portion (2) was in a critical situation. The spring stretch graph presented a parabolic shape whose steel could sufficiently develop its strength. Cracking figures showed that most of the cracks occurred at the portion (2) of this beam, where the low strength concrete located. From all the facts above, it could be concluded that case 25-2-20 experienced a flexural compression failure, the top of the concrete in middle region crushed at ultimate stage before reinforcement yield.

5.2.17 Case 25-2-30

Case 25-2-30 was assumed to have low strength concrete at the shear sensitive portion of the beam, portion (2). Table D-17 shows detailed dimensions and honeycombing location for this case. The concrete at the portion (2) was assumed to be 30MPa, and the rest concrete were in good condition, 42.7MPa. Loading were applied

near the middle of the beam. The ultimate load and corresponding deflection at mid-span were 167.37kN and 12.21mm. The load deflection curve stopped in a sudden when the applied load reached 167.37kN. The details of the beam at ultimate stage were illustrated from Figure D-129 to Figure D-136. The steel stress diagram indicated the stress in reinforcement didn't reach its yielding position. The 3rd principal total mechanical strain diagram indicated that top of the concrete in portion (2) experienced high compression. The Von Mises stress diagram indicated that the top of the concrete in portion (2) was in a high compression. The spring stretch graph displayed a trapezoid shape whose steel could not develop its strength. Cracking figures showed that many flexural cracks occurred along the bottom of entire beam. From all the facts above, it could be concluded that case 25-2-30 experienced a bond failure.

5.2.18 Case 25-3-10

Case 25-3-20 was assumed to have low strength concrete at the bond sensitive part of the beam, volume (3). Table D-18 shows detailed dimensions and honeycombing location for this case. The concrete at the portion (3) was assumed to be 10MPa, and the rest concrete were in good condition, 42.7MPa. Loading were applied near the middle of the beam. The ultimate load and corresponding deflection at mid-span were 101.57kN and 7.26mm. Once the applied load got to 101.57kN, the load deflection curve stopped. The details of the beam at ultimate stage were showed from Figure D-137 to Figure D-144. The steel stress diagram indicated the stress in reinforcement didn't reach 512MPa, which was the yielding position. The Von Mises stress diagram indicated that the concrete didn't reach its critical stress. The spring stretch graph displayed a deboning failure shape; the spring stretch at the left end is

extreme high, especially the nodes at left end. This indicated that the steel can't develop its strength within this development length and the relative movement between reinforcement and concrete had already initialed. Cracking figures showed the most of the cracks occurred at the left portion of the beam, where the localized low strength concrete located. From all the facts above, it could be concluded that case 25-3-10 experienced a bond failure.

5.2.19 Case 25-3-20

Case 25-3-20 was assumed to have low strength concrete at the bond sensitive portion of the beam. Table D-19 shows detailed dimensions and honeycombing location for this case. The concrete at the portion (3) was assumed to be 20MPa, and the rest concrete were in good condition, 42.7MPa. Loading were applied near the middle of the beam. The ultimate load and corresponding deflection at mid-span were 128.90kN and 9.06mm. When the applied load increased to 128.90kN, the load deflection curve stopped. The details of the beam at ultimate stage were displayed from Figure D-145 to Figure D-152. The steel stress diagram indicated the stress in reinforcement didn't reach 512MPa, which was the yielding position. The Von Mises stress diagram indicated that the concrete didn't reach its critical stress. The spring stretch graph displayed a deboning failure shape; the spring stretch at the left end is extreme high, especially the nods at left end. This indicated that the steel can't develop its strength within this development length and the relative movement between reinforcement and concrete had already initialed. Cracking figures showed the most of the cracks occurred at the left portion of the beam, where the localized low strength concrete located. From all the facts above, it could be concluded that case 25-3-20 experienced a bond failure.

5.2.20 Case 25-3-30

Case 32-3-10 was assumed to have low strength concrete at the bond sensitive portion of the beam. Table D-20 shows detailed dimensions and honeycombing location for this case. The concrete at the portion (3) was assumed to be 10MPa, and the rest concrete were in good condition, 42.7MPa. Loading were applied near the middle of the beam. The ultimate load and corresponding deflection at mid-span were 173.98kN and 12.80mm. And the load deflection curve stopped when the applied load reached 173.98kN. The details of the beam at ultimate stage were showed from Figure D-153 to Figure D-160. The steel stress diagram indicated the stress in reinforcement didn't reach 512MPa, which was the yielding position. The Von Mises stress diagram indicated that the concrete didn't reach its critical stress. But the total mechanical shear strain in XZ plane presented a large load concentration along the tensile reinforcement. The spring stretch graph displayed a bond failure shape; the spring stretch at the left end is extreme high, especially the nods at left end. Cracking figures showed most of the shear cracking occurred in the left portion of the concrete. From all the facts above, it could be concluded that case 32-3-10 experienced a bond failure.

5.2.21 Case 32-0

Case 32-0 was the reference beam for the FEM cases with 32mm rebar. Table D-21 shows detailed dimensions and honeycombing location for this case. The concrete of this case is assumed to be in good condition, 42.7MPa throughout the entire beam. Loading were applied near the middle of the beam. The ultimate load and corresponding deflection at mid-span were 195.42kN and 10.46mm. The load deflection curve terminated abruptly when the applied load reached 195.42kN. The details of the

beam at ultimate stage were illustrated from Figure D-161 to Figure D-168. The steel stress diagram indicated the stress in reinforcement didn't reach the yielding position. And the Von Mises stress diagram indicated that the concrete didn't reach its critical point. But the XZ shear total mechanical strain displayed a strain concentration along the longitudinal reinforcement. And the spring stretch graph displayed a bond failure shape the spring stretch at the left end is extreme high, especially the nods at left end. This indicated that the development length was insufficient for the steel to develop its stress. The Cracking figures showed some flexural cracking developed along the bottom of the entire beam. From all the facts above, it could be concluded that case 32-0 experienced a bond failure.

5.2.22 Case 32-1-10

Case 32-1-10 was assumed to have low strength concrete at the middle portion of the beam. Table D-22 shows detailed dimensions and honeycombing location for this case. The strength of concrete at the middle was assumed to be 10MPa, and the rest concrete were in good condition, 42.7MPa. Loading were applied near the middle of the beam. The ultimate load and corresponding deflection at mid-span were 66.05kN and 4.19mm. The load deflection curve stopped in a sudden when the applied load reached 66.05kN. The details of the beam at ultimate stage were demonstrated from Figure D-169 to Figure D-176. The steel stress diagram indicated the stress in reinforcement didn't reach its yielding position yet. The 3rd principal total mechanical strain diagram indicated that the top concrete at middle of the beam experienced critical compression. The Von Mises stress diagram also indicated that the top concrete at middle of the beam experienced a critical situation. The spring stretch at left end was still small and

shows a parabolic shape, which indicated that the concrete failed before the beam has bond problem. Cracking figures showed that most of the cracks occurred at the middle of the beam, where the localized concrete occurred. From all the facts above, it could be concluded that case 32-1-10 experienced a flexural failure, the top concrete at middle of the beam crushed at ultimate stage before reinforcement yield.

5.2.23 Case 32-1-20

Case 32-1-20 was assumed to have low strength concrete at the middle portion of the beam. Table D-23 shows detailed dimensions and honeycombing location for this case. The strength of concrete at the middle was assumed to be 20MPa, and the rest concrete were in good condition, 42.7MPa. Loading were applied near the middle of the beam. The ultimate load and corresponding deflection at mid-span were 95.63kN and 5.32mm. The load deflection curve stopped in a sudden when the applied load reached 95.6kN. The details of the beam at ultimate stage were illustrated from Figure D-177 to Figure D-184. The steel stress diagram indicated the stress in reinforcement didn't reach its yielding position. The 3rd principal total mechanical strain diagram and XZ shear total mechanical strain indicated that the top concrete at the middle of the beam experienced critical compression. The Von Mises stress diagram also indicated that the top concrete in volume (1) experienced a critical situation. The spring stretch at left end was still small and displayed a parabolic shape, which indicated that the concrete failed before the beam has bond problem. Cracking figures showed that normal flexural cracks occurred along the bottom of this beam. From all the facts above, it could be concluded that case 32-1-20 experienced a flexural failure, the top concrete in Region (1) crushed at ultimate stage before reinforcement can yield.

5.2.24 Case 32-1-30

Case 32-1-30 was assumed to have low strength concrete at the middle portion of the beam, region (1). Table D-24 shows detailed dimensions and honeycombing location for this case. The strength of concrete at the middle was assumed to be 30MPa, and the rest concrete were in good condition, 42.7MPa. Loading were applied near the middle of the beam. The ultimate load and corresponding deflection at mid-span were 161.32kN and 9.03mm. The load deflection curve stopped in a sudden when the applied load reached 161.32kN. The details of the beam at ultimate stage were listed from Figure D-185 to Figure D-192. The steel stress diagram indicated the stress in reinforcement hadn't reached its yielding position. The 3rd principal total mechanical strain diagram and XZ shear total mechanical strain indicated that the top concrete at middle of the beam experienced high compression. The Von Mises stress diagram also indicated that the top concrete at middle of the beam experienced a high stress. The spring stretch presented a trapezoid shape, which indicated the bond problem initial before the concrete problem. Cracking figures showed that normal flexural cracks occurred along the bottom of entire beam. From all the facts above, it could be concluded that case 32-1-30 experienced a bond failure.

5.2.25 Case 32-2-10

Case 32-2-10 was assumed to have low strength concrete at the shear sensitive portion of the beam. Table D-25 shows detailed dimensions and honeycombing location for this case. The strength of concrete at the region (2) was assumed to be 10MPa, and the rest concrete were in good condition, 42.7MPa. Loading were applied near the middle of the beam. The ultimate load and corresponding deflection at mid-span were

79.69kN and 4.85mm. The load deflection curve stopped in a sudden when the applied load reached 79.69kN. The details of the beam at ultimate stage were illustrated from Figure D-193 to Figure D-200. The steel stress diagram indicated the stress in reinforcement didn't reach its yielding position. The 3rd principal total mechanical strain diagram and XZ shear total mechanical strain indicated that the top concrete in portion (2) experienced critical compression. The Von Mises stress diagram also showed that the top concrete in portion (2) was in a critical situation. The spring stretch graph displayed a parabolic shape whose steel was still capable of developing its strength. The cracking figures showed that most of the cracks occurred at the portion (2) of this beam, where the low strength concrete located. From all the facts above, it could be concluded that case 32-2-10 experienced a flexural failure, the top concrete in Region (2) crushed at ultimate stage before the reinforcement yield

5.2.26 Case 32-2-20

Case 32-2-20 was assumed to have low strength concrete at the shear sensitive portion of the beam. Table D-26 shows detailed dimensions and honeycombing location for this case. The concrete at the portion (2) was assumed to be 20MPa, and the rest concrete were in good condition, 42.7MPa. Loading were applied near the middle of the beam. The ultimate load and corresponding deflection at mid-span were 152.48kN and 8.48mm. The load deflection curve stopped in a sudden when the applied load reached 152.48kN. The details of the beam at ultimate stage were given from Figure D-201 to Figure D-208. The steel stress diagram indicated the stress in reinforcement didn't reach its yielding position. The 3rd principal total mechanical strain diagram indicated that the top-right corner of the concrete in portion (2) experienced high compression.

The Von Mises stress diagram also demonstrated that the top-right corner of the concrete in portion (2) was in high stress. The spring stretch graph showed a trapezoid shape, which indicated bond problem. Cracking figures showed that most of the cracks occurred at the portion (2) of this beam, where the low strength concrete located. From all the facts above, it could be concluded that case 32-2-20 experienced a bond failure.

5.2.27 Case 32-2-30

Case 32-2-30 was assumed to have localized low strength concrete at the shear sensitive portion of the beam. Table D-27 shows detailed dimensions and honeycombing location for this case. The concrete at the portion (2) was assumed to be 30MPa, and the rest concrete were in good condition, 42.7MPa. Loading were applied near the middle of the beam. The ultimate load and corresponding deflection at mid-span were 173.45kN and 9.4mm. And the load deflection curve stopped when the applied load reached 173.45kN. The details of the beam at ultimate stage were showed from Figure D-209 to Figure D-216. The steel stress diagram indicated the stress in reinforcement didn't reach 512MPa, which was the yielding position. The Von Mises stress diagram indicated that the concrete didn't reach its critical stress. The total mechanical strain in 3rd principal axis presented a concentration at top volume (2). The spring stretch graph displayed a trapezoid shape, which is a sign of bond problem. The cracking figures showed most of the shear cracking occurred at the left of the beam. From all the facts above, it could be concluded that case 32-2-30 experienced bond failure.

5.2.28 Case 32-3-10

Case 32-3-10 was assumed to have low strength concrete at the bond sensitive portion of the beam. Table D-28 shows detailed dimensions and honeycombing location for this case. The concrete at the portion (3) was assumed to be 10MPa, and the rest concrete were in good condition, 42.7MPa. Loading were applied near the middle of the beam. The ultimate load and corresponding deflection at mid-span were 101.98kN and 5.18mm. And the load deflection curve stopped when the applied load reached 101.98kN. The details of the beam at ultimate stage were demonstrated from Figure D-217 to Figure D-224. The steel stress diagram indicated the stress in reinforcement didn't reach 512MPa, which was the yielding position. The Von Mises stress diagram indicated that the concrete didn't reach its critical stress. The total mechanical shear strain in XZ plane presented a big strain along the tensile reinforcement, especially at left end. The spring stretch graph displayed a bond failure shape whose steel would not be able to develop its stress. Cracking figures showed most of the shear cracks occurred in the left portion of the concrete. From all the facts above, it could be concluded that case 32-3-10 experienced a bond failure.

5.2.29 Case 32-3-20

Case 32-3-20 was assumed to have low strength concrete at the bond sensitive portion of the beam. Table D-29 shows detailed dimensions and honeycombing location for this case. The concrete at the portion (3) was assumed to be 20MPa, and the rest concrete were in good condition, 42.7MPa. Loading were applied near the middle of the beam. The ultimate load and corresponding deflection at mid-span were 175.68kN and 9.57mm. And the load deflection curve stopped when the applied load reached

175.68kN. The details of the beam at ultimate stage were showed from Figure D-225 to Figure D-232. The steel stress diagram indicated the stress in reinforcement didn't reach yielding position. The Von Mises stress diagram indicated that the concrete didn't reach its critical stress. But the total mechanical shear strain in XZ plane presented a big strain concentration along the tensile reinforcement, especially at left end. The spring stretch graph displayed a bond failure shape whose steel would not be able to develop its stress. Cracking figures showed most of the shear cracking occurred in the left portion of the concrete. From all the facts above, it could be concluded that case 32-3-20 experienced a bond failure.

5.2.30 Case 32-3-30

Case 32-3-30 was assumed to have low strength concrete at the bond sensitive portion of the beam. Table D-30 shows detailed dimensions and honeycombing location for this case. The concrete at the portion (3) was assumed to be 30MPa, and the rest concrete were in good condition, 42.7MPa. Loading were applied near the middle of the beam. The ultimate load and corresponding deflection at mid-span were 183.56kN and 9.94mm. And the load deflection curve stopped when the applied load reached 183.56kN. The details of the beam at ultimate stage were displayed from Figure D-233 to Figure D-240. The steel stress diagram indicated the stress in reinforcement didn't reach yielding position. The Von Mises stress diagram indicated that the concrete didn't reach its critical stress. But the total mechanical shear strain in XZ plane presented a large strain concentration along the tensile reinforcement, especially at the left support. The spring stretch graph displayed a bond failure shape whose steel would not be able to develop its stress. Cracking figures showed many shear cracks occurred in the left

portion of the concrete. From all the facts above, it could be concluded that case 32-3-20 experienced a bond failure. Table 5-1 summaries all the details failure for these 30 cases.

Table 5-1 Cases Failure Summary

Case Failure Summary						
Case Name	Honeycombing Location	Strength of Concrete(MPa)	Ultimate Load (kN)	Ultimate Deflection (mm)	Failure Mode	P_{FEA}/P_{FEA0}
16-0	None	42.7	104.21	17.33	F-T	1.000
16-1-30	1	30	101.23	20.28	F-T	0.971
16-1-20	1	20	87.76	12.39	F-C	0.842
16-1-10	1	10	53.62	8.36	F-C	0.515
16-2-30	2	30	102.17	24.80	F-T	0.980
16-2-20	2	20	95.97	12.60	F-C	0.921
16-2-10	2	10	60.26	8.42	F-C	0.578
16-3-30	3	30	103.82	18.02	F-T	0.996
16-3-20	3	20	103.81	18.97	F-T	0.996
16-3-10	3	10	72.27	8.98	F-C	0.693
25-0	None	42.7	178.92	12.92	B	1.000
25-1-30	1	30	161.03	12.39	B	0.900
25-1-20	1	20	95.18	7.07	F-C	0.532
25-1-10	1	10	60.94	4.97	F-C	0.341
25-2-30	2	30	167.37	12.21	B	0.935
25-2-20	2	20	115.15	8.22	F-C	0.644
25-2-10	2	10	67.93	5.30	F-C	0.380
25-3-30	3	30	173.98	12.80	B	0.972
25-3-20	3	20	128.90	9.06	B	0.720
25-3-10	3	10	101.57	7.26	F-C	0.568
32-0	None	42.7	195.42	10.46	B	1.000
32-1-30	1	30	161.32	9.03	B	0.825
32-1-20	1	20	95.63	5.32	F-C	0.489
32-1-10	1	10	66.05	4.19	F-C	0.338
32-2-30	2	30	173.45	9.44	B	0.888
32-2-20	2	20	152.48	8.48	B	0.780
32-2-10	2	10	79.69	4.85	F-C	0.408
32-3-30	3	30	183.56	9.94	B	0.939
32-3-20	3	20	175.68	9.57	B	0.899
32-3-10	3	10	101.98	5.18	B	0.522

5.3 FEA Solution Comparison

5.3.1 Effects of Concrete Strength

Table 5-2 Comparison of 16mm rebar with 30MPa concrete

Case Name	Bottom Reinforcement	Deteriorated location	Strength of Concrete(MPa)	Ultimate Load (kN)	Ultimate Deflection(mm)	Failure Mode
16-0	16mm	None	42.7	104.21	17.33	F-T
16-1-30	16mm	1	30	101.23	20.28	F-T
16-2-30	16mm	2	30	102.17	24.80	F-T
16-3-30	16mm	1	30	103.82	18.02	F-T

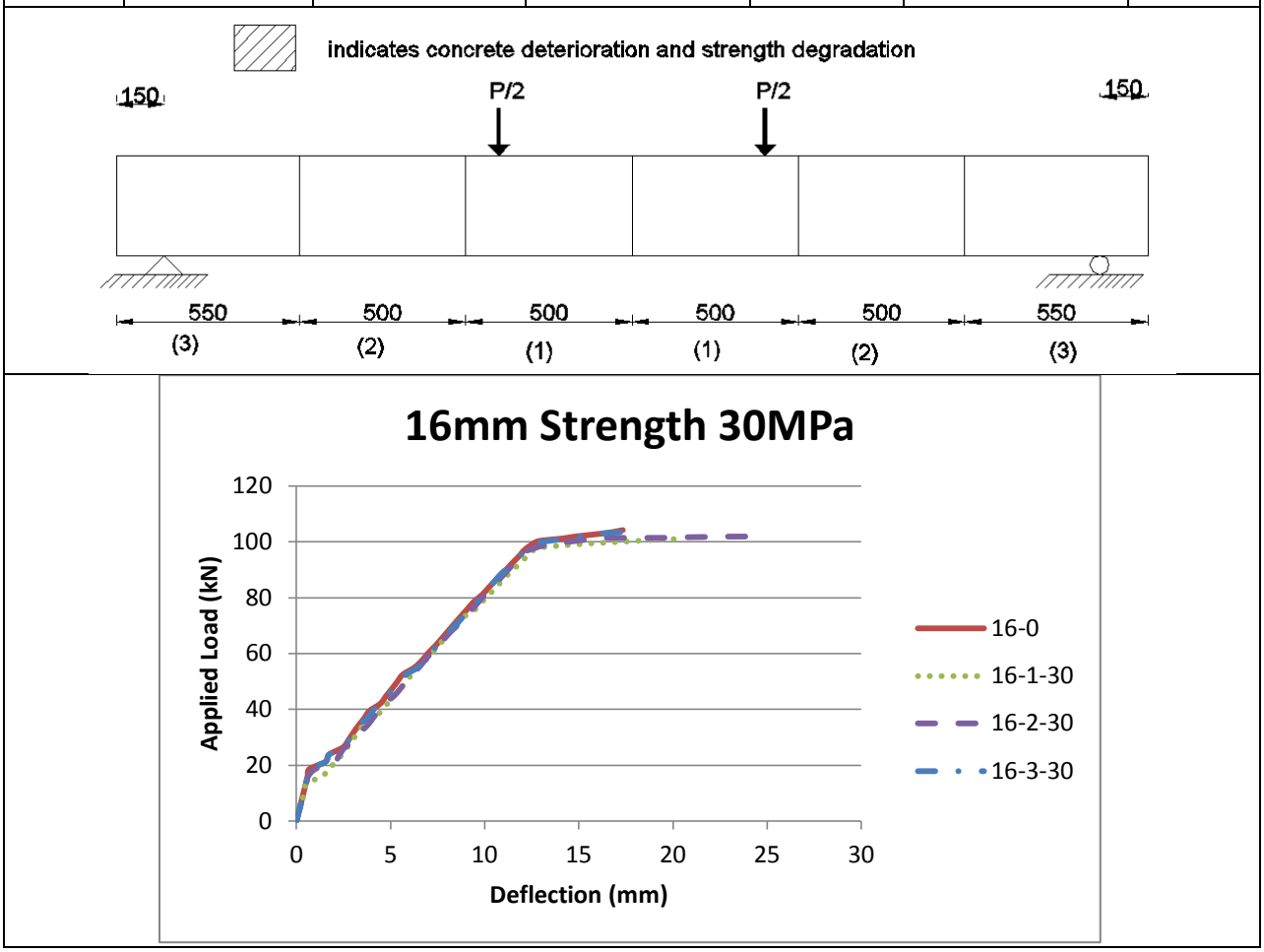

The details of localized concrete with strength 30MPa on bending sensitive, shear sensitive and bond sensitive locations are illustrated in Table 5-2. All these beams are reinforced with two 16 mm tensile rebar with localized 30Mpa concrete in the

middle. The failure modes for all these cases are reinforcement yield before the concrete crush. So wherever the localized low strength concrete occurs, reinforcement could always develop their stress until yielding occurs before the concrete crush. When the localized concrete strength is as low as 30MPa, it has little effect on the flexural strength of RC beams, and the reinforcement governs the failure of the beams.

Table 5-3 Comparison of 16mm rebar with 20MPa concrete

Case Name	Bottom Reinforcement	Deteriorated location	Strength of Concrete(MPa)	Ultimate Load (kN)	Ultimate Deflection(mm)	Failure Mode
16-0	16mm	None	42.7	104.21	17.33	F-T
16-1-20	16mm	1	20	87.76	12.39	F-C
16-2-20	16mm	2	20	95.97	12.60	F-C
16-3-20	16mm	1	20	103.81	18.97	F-T

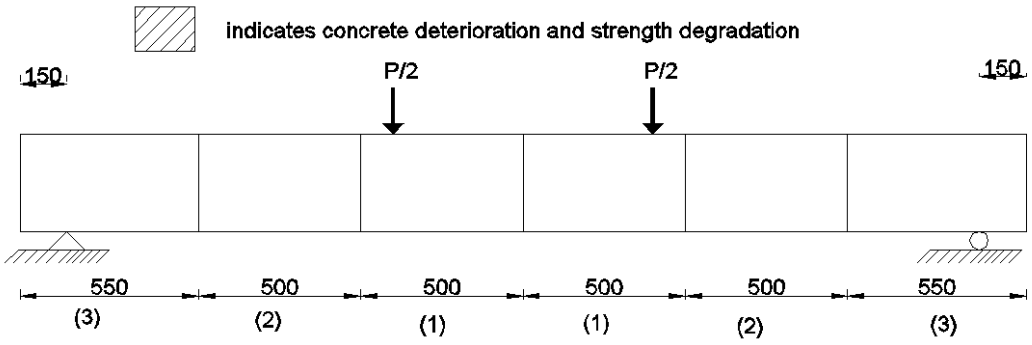

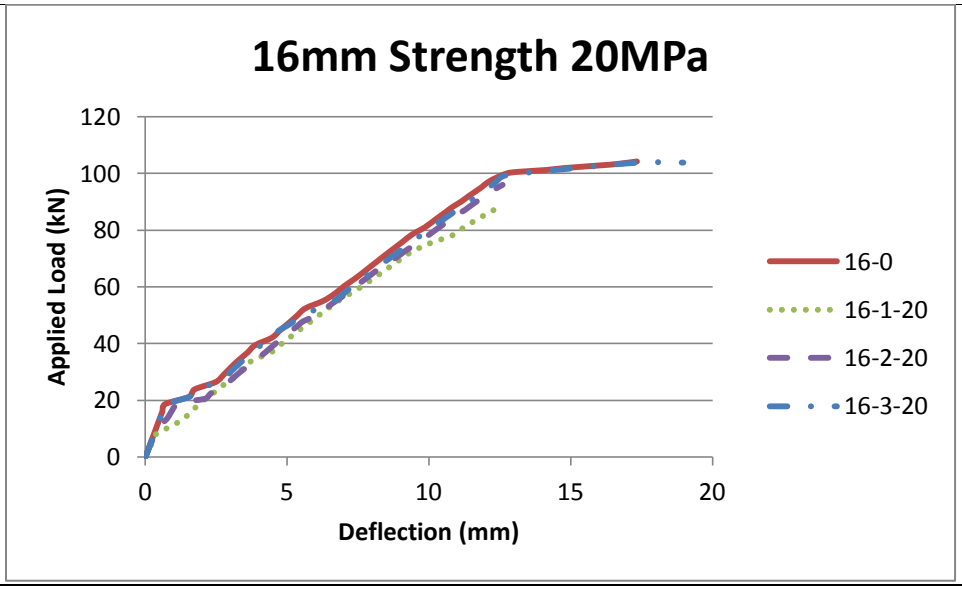

The details of localized concrete with strength 20MPa on bending sensitive, shear sensitive and bond sensitive locations are illustrated in Table 5-3. All these beams are reinforced with two 16 mm tensile rebar with localized 20Mpa concrete occurs in location (1), location (2) and location (3) separately. The failure mode of for reference beam 16-0 and 16-3-20 are that the reinforcement yield firstly and the concrete crush later. As they both used same material for their steel, which governs the failure, they share almost the same ultimate load. For the cases 16-1-20 and 16-2-20, the failure modes are that the concrete crush before the reinforcement could yield. Therefore, their ultimate loads were governed by the low strength of the localized concrete. Comparing 16-1-20 and 16-2-20, the localized low strength concrete at location (1) was more critical than location (2). In addition, these two cases share similar ultimate load because 16mm rebar are small amount of reinforcement for these beams.

Table 5-4 Comparison of 16mm rebar with 10MPa concrete

Case Name	Bottom Reinforcement	Deteriorated location	Strength of Concrete(MPa)	Ultimate Load (kN)	Ultimate Deflection(mm)	Failure Mode
16-0	16mm	None	42.7	104.21	17.33	F-T
16-1-10	16mm	1	10	53.62	8.36	F-C
16-2-10	16mm	2	10	60.26	8.42	F-C
16-3-10	16mm	1	10	72.27	8.98	F-C

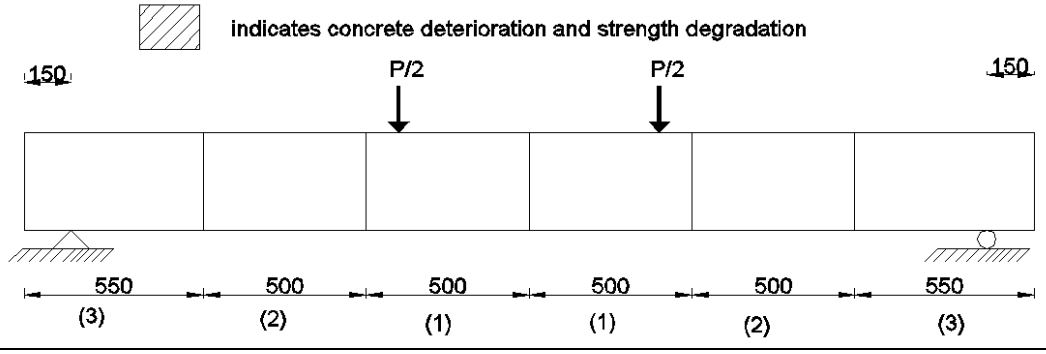

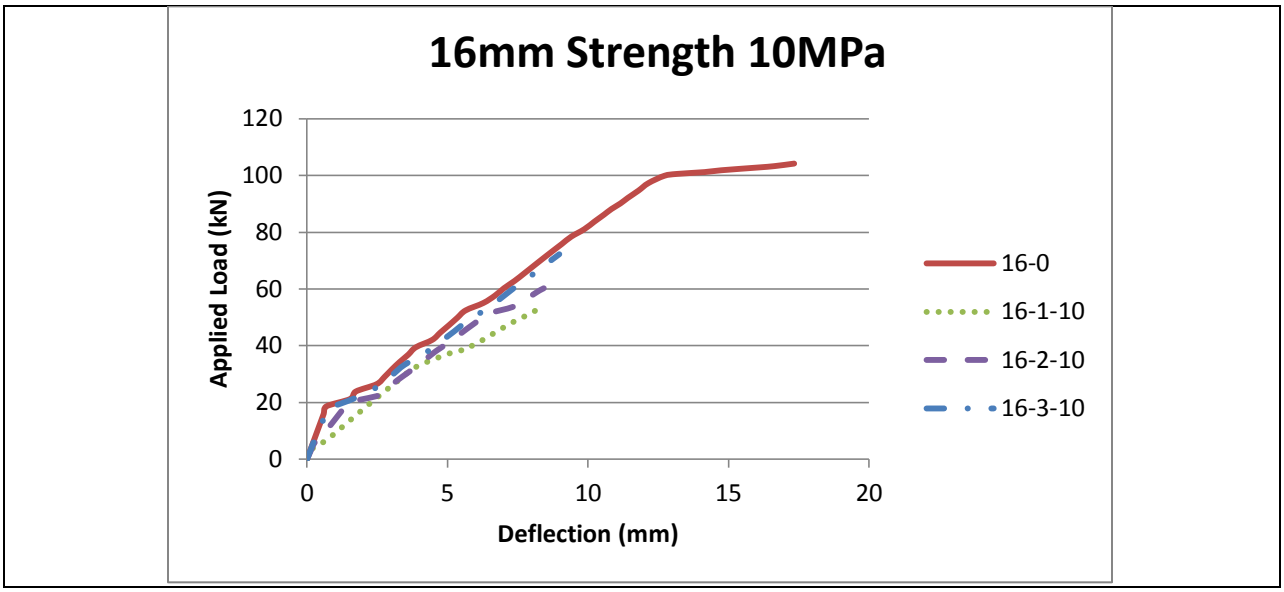

The details of localized concrete with strength 10MPa on bending sensitive, shear sensitive and bond sensitive locations are illustrated in Table 5-4. All these beams are reinforced with two 16 mm tensile rebar with localized 10Mpa concrete in the bending zone, shear zone and bond zone separately. Except the reference case 16-0, the failure mode of beam 16-1-10, 16-2-10 and 16-3-10 are that the concrete crush before the reinforcement yield. So the localized strength of concrete controls the failure of the beams. For the beams reinforced with two 16 mm rebar in tension zone, when the concrete strength get as low as 10 MPa, the impact of localized concrete at the middle is the most critical and the impact at support end is the least critical.

Table 5-5 Comparison of 25mm rebar with 30MPa concrete

Case Name	Bottom Reinforcement	Deteriorated location	Strength of Concrete(MPa)	Ultimate Load (kN)	Ultimate Deflection(mm)	Failure Mode
25-0	25mm	None	42.7	178.92	12.92	B
25-1-30	25mm	1	30	161.03	12.39	B
25-2-30	25mm	2	30	167.37	12.21	B
25-3-30	25mm	1	30	173.98	12.80	B

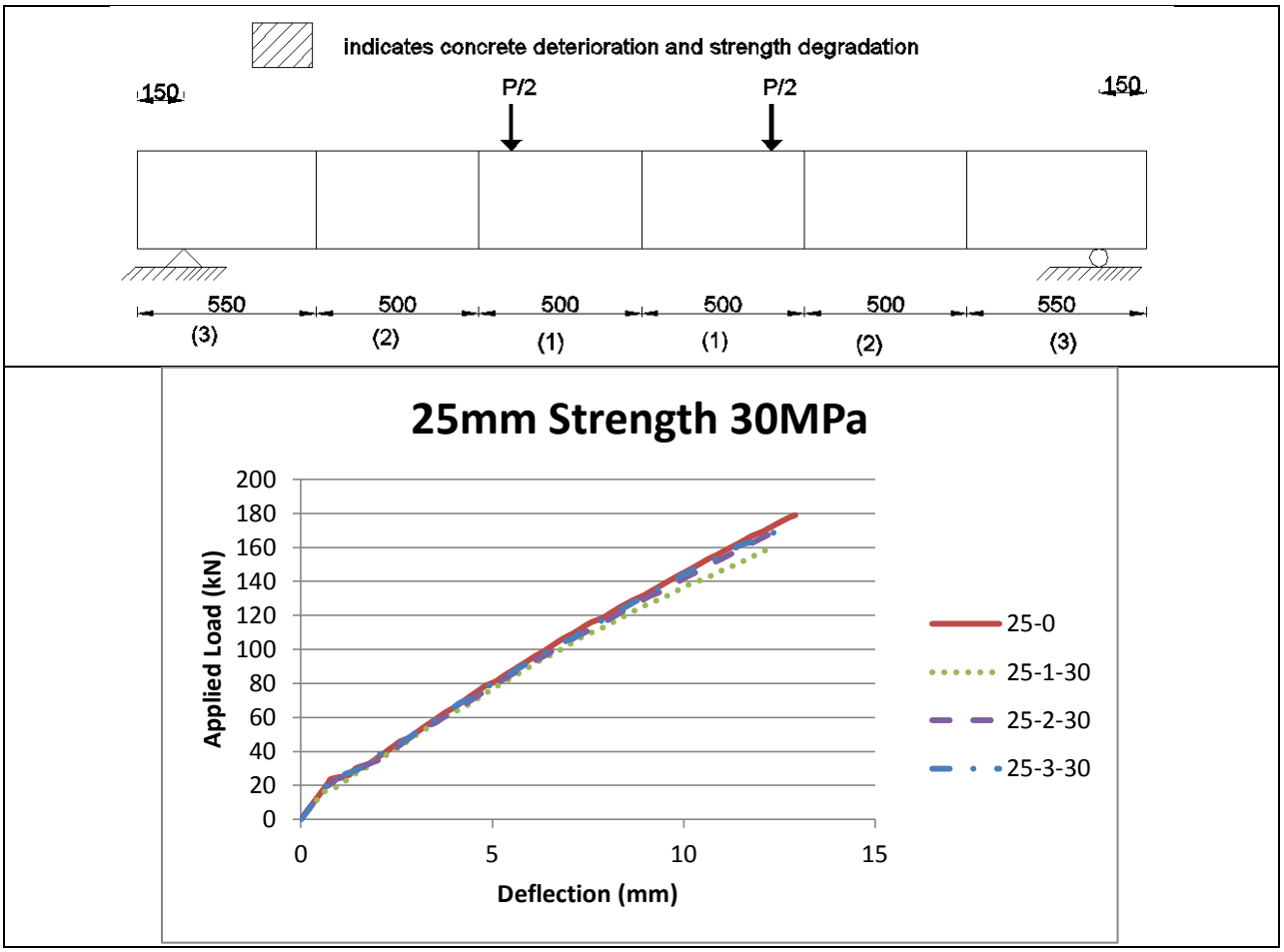

The details of localized concrete with strength 30MPa on bending sensitive, shear sensitive and bond sensitive locations are illustrated in Table 5-5. All these beams are reinforced with two 25 mm tensile rebar with localized 30Mpa concrete in the bending zone, shear zone and bond zone separately. Including the reference case 25-0, the failure modes of all beams are bond failure. For the beams reinforced with two 25 mm rebar in tension zone, when the concrete strength get as low as 30 MPa, no matter where the localized low strength concrete is, the beam will fail in bond. And the impact of localized concrete at the middle is the most critical and the impact at support end is the least critical.

Table 5-6 Comparison of 25mm rebar with 20MPa concrete

Case Name	Bottom Reinforcement	Deteriorated location	Strength of Concrete(MPa)	Ultimate Load (kN)	Ultimate Deflection(mm)	Failure Mode
25-0	25mm	None	42.7	178.92	12.92	B
25-1-20	25mm	1	20	95.18	7.07	F-C
25-2-20	25mm	2	20	115.15	8.22	F-C
25-3-20	25mm	1	20	128.90	9.06	B

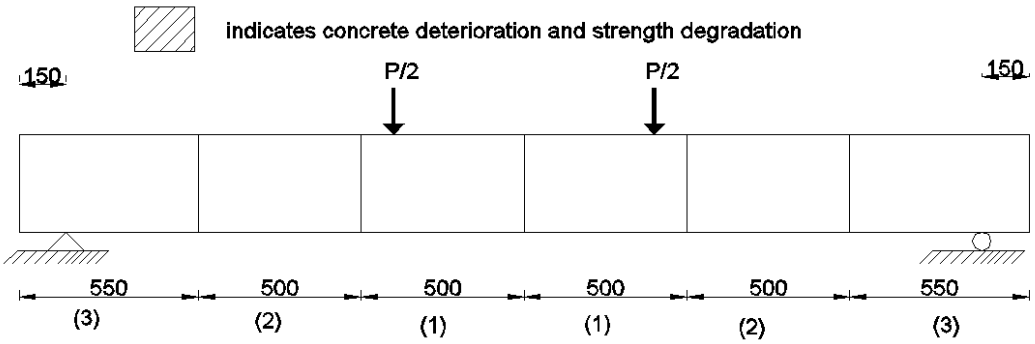

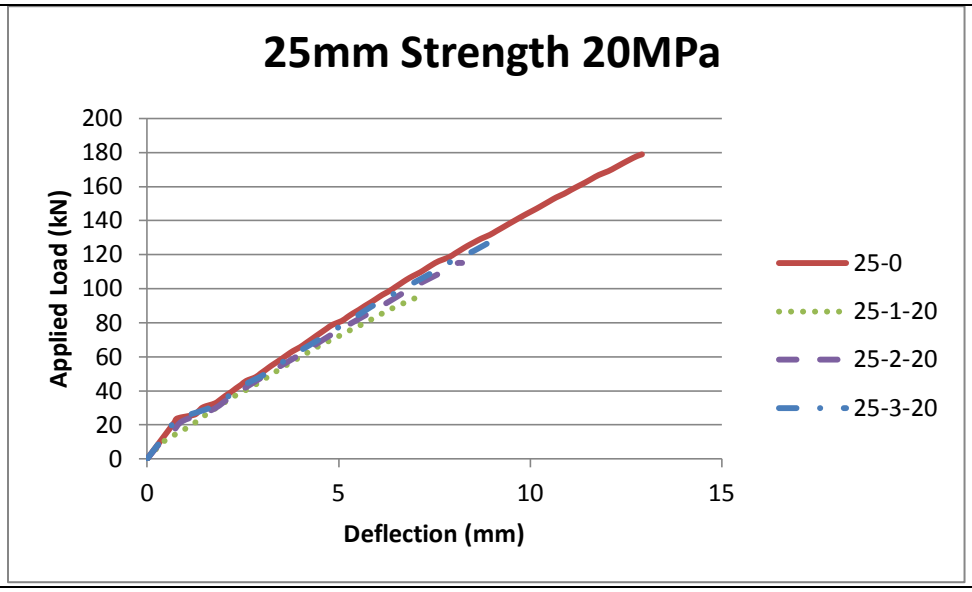

The details of localized concrete with strength 20MPa on bending sensitive, shear sensitive and bond sensitive locations are illustrated in Table 5-6. All these beams are reinforced with two 25 mm tensile rebar with localized 20Mpa concrete in the bending zone, shear zone and bond zone separately. The failure modes of beams 25-0 and 25-3-20 are bond failure. And the failure modes of 25-1-20 and 25-2-20 are flexural

failure. For the beams reinforced with two 25 mm rebar in tension zone, when the concrete strength get as low as 20 MPa, the impact of localized concrete at the middle is the most critical and the impact at support end is the least critical.

Table 5-7 Comparison of 25mm rebar with 10MPa concrete

Case Name	Bottom Reinforcement	Deteriorated location	Strength of Concrete(MPa)	Ultimate Load (kN)	Ultimate Deflection(mm)	Failure Mode
25-0	25mm	None	42.7	178.92	12.92	B
25-1-10	25mm	1	10	60.94	4.97	F-C
25-2-10	25mm	2	10	67.93	5.30	F-C
25-3-10	25mm	1	10	101.57	7.26	B

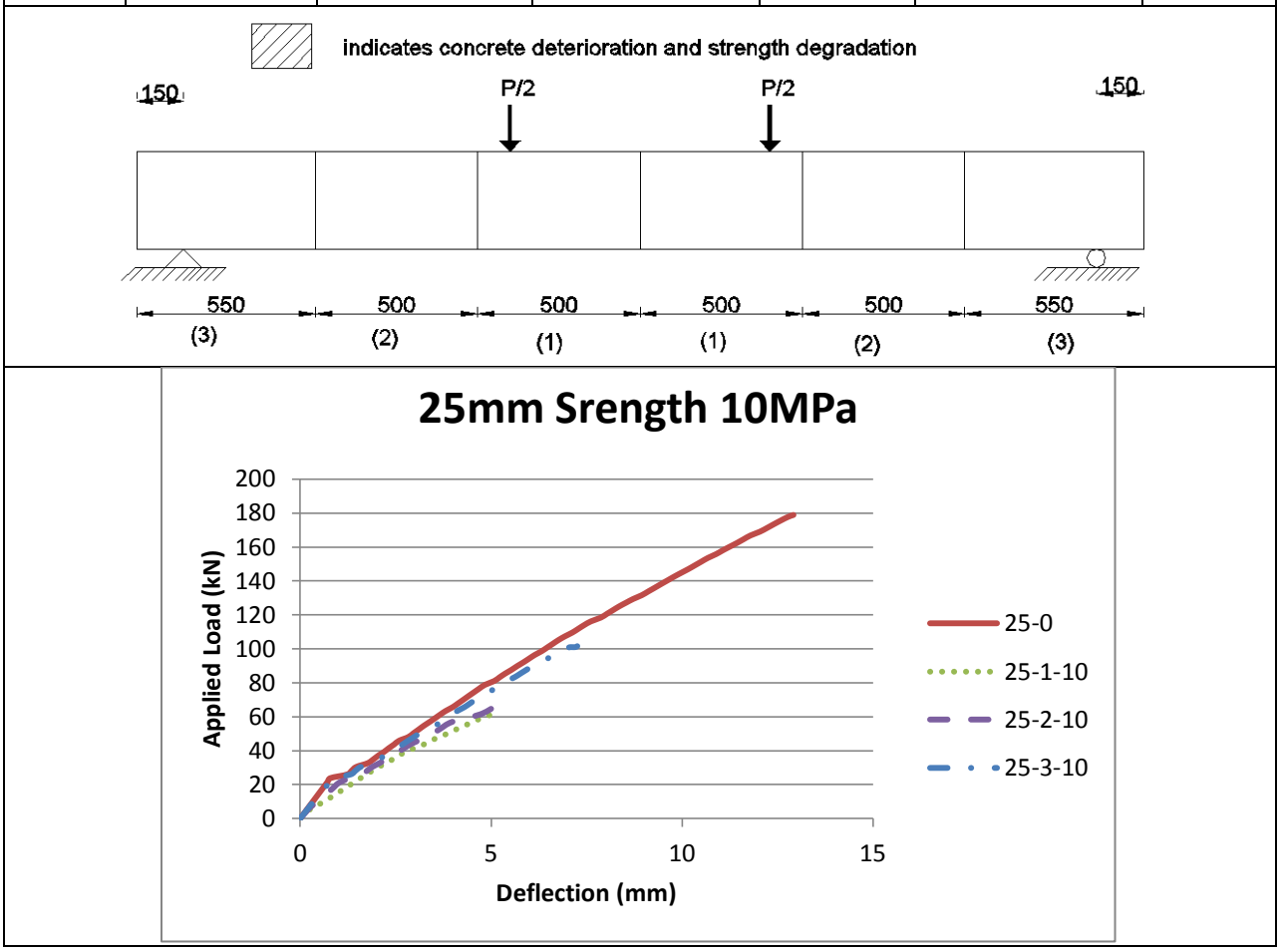

The details of localized concrete with strength 10MPa on bending sensitive, shear sensitive and bond sensitive locations are illustrated in Table 5-7. All these beams are reinforced with two 25 mm tensile rebar with localized 10Mpa concrete in the bending zone, shear zone and bond zone separately. The failure modes of beams 25-0 and 25-3-10 are bond failure. And the failure modes of 25-1-10 and 25-2-10 are flexural failure, because when the applied load increase, the middle part with low strength concrete always fails firstly. So the ultimate loads of these two cases are similar. For the beams reinforced with two 25 mm rebar in tension zone, when the concrete strength get as low as 10 MPa, the impact of localized concrete at the middle is the most critical and the impact at support end is the least critical.

Table 5-8 Comparison of 32mm rebar with 30MPa concrete

Case Name	Bottom Reinforcement	Deteriorated location	Strength of Concrete(MPa)	Ultimate Load (kN)	Ultimate Deflection(mm)	Failure Mode
32-0	32mm	None	42.7	195.42	10.46	B
32-1-30	32mm	1	30	161.32	9.03	B
32-2-30	32mm	2	30	173.45	9.44	B
32-3-30	32mm	1	30	183.56	9.94	B

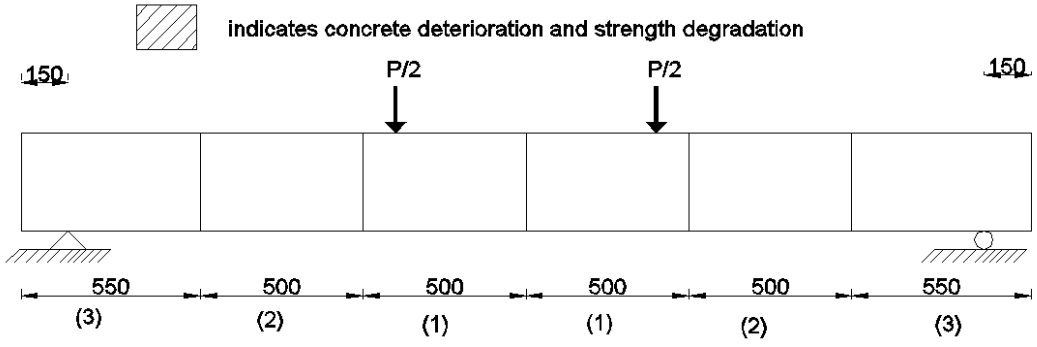

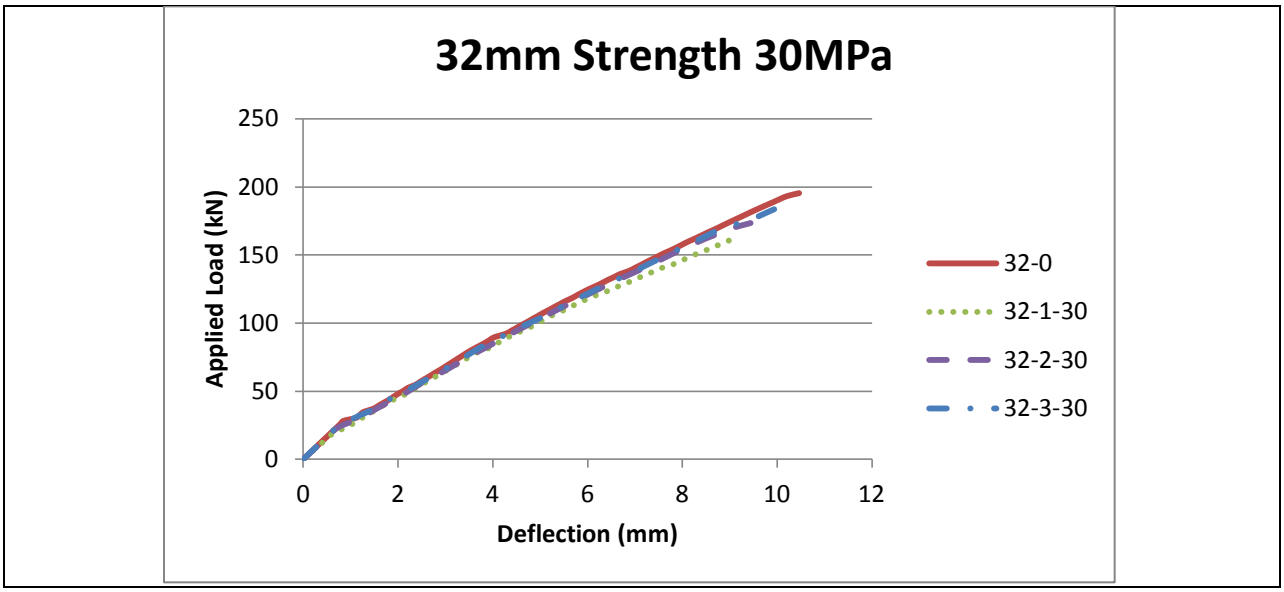

The details of localized concrete with strength 30MPa on bending sensitive, shear sensitive and bond sensitive locations are illustrated in Table 5-8. All these beams are reinforced with two 32 mm tensile rebar with localized 30Mpa concrete in the bending zone, shear zone and bond zone separately. The failure modes of all four beams are bond failure. For the beams reinforced with two 32 mm rebar in tension zone, when the concrete strength get as low as 30 MPa, there is little impact on the flexural strength of RC beams, and the impact of localized concrete at the middle is the most critical and the impact at support end is the least critical.

Table 5-9 Comparison of 32mm rebar with 20MPa concrete

Case Name	Bottom Reinforcement	Deteriorated location	Strength of Concrete(MPa)	Ultimate Load (kN)	Ultimate Deflection(mm)	Failure Mode
32-0	32mm	None	42.7	195.42	10.46	B
32-1-20	32mm	1	20	95.63	5.32	F-C
32-2-20	32mm	2	20	152.48	8.48	B
32-3-20	32mm	1	20	175.68	9.57	B

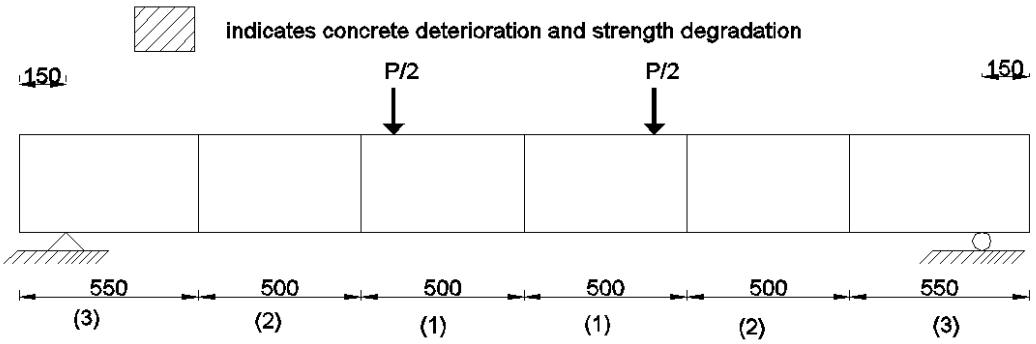

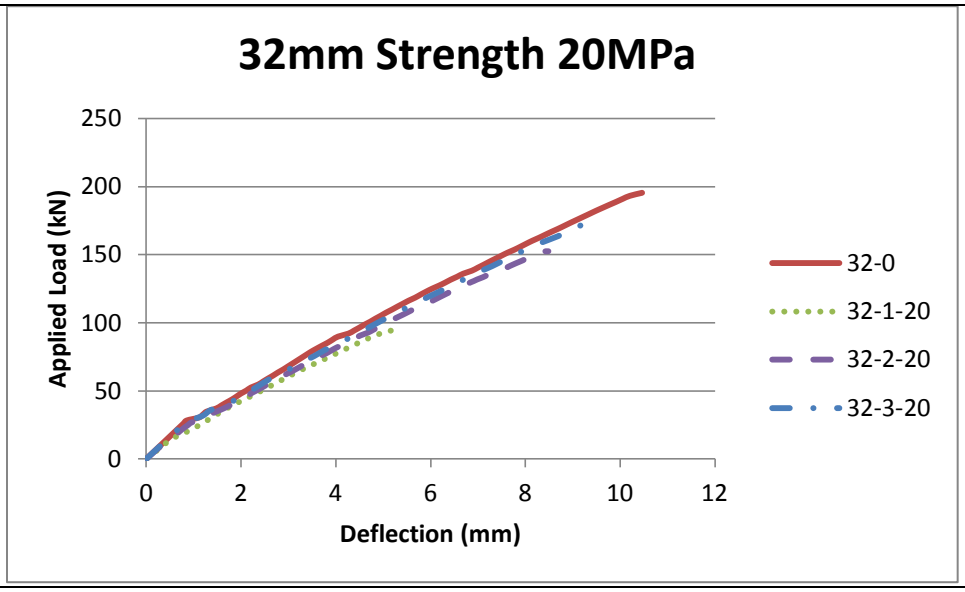

The details of localized concrete with strength 20MPa on bending sensitive, shear sensitive and bond sensitive locations are illustrated in Table 5-9. All these beams are reinforced with two 32 mm tensile rebar with localized 20Mpa concrete in the bending zone, shear zone and bond zone separately. For case 32-1-20, the concrete crush firstly because the largest compressive stress located at middle and it increases

dramatically. The failure modes of other three beams are bond failure. For the beams reinforced with two 32 mm rebar in tension zone, when the concrete strength get as low as 20 MPa, the impact of localized concrete at the middle is the most critical and the impact at support end is the least critical.

Table 5-10 Comparison of 32mm rebar with 10MPa concrete

Case Name	Bottom Reinforcement	Deteriorated location	Strength of Concrete(MPa)	Ultimate Load (kN)	Ultimate Deflection(mm)	Failure Mode
32-0	32mm	None	42.7	195.42	10.46	B
32-1-10	32mm	1	10	66.05	4.19	F-C
32-2-10	32mm	2	10	79.69	4.85	F-C
32-3-10	32mm	1	10	101.98	5.18	B

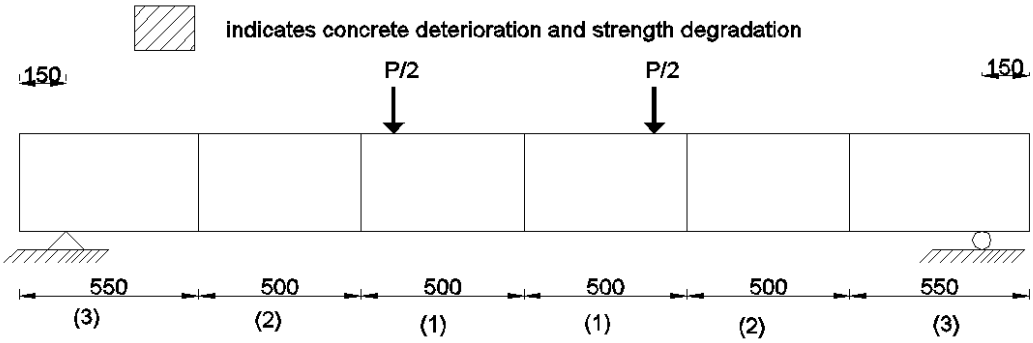

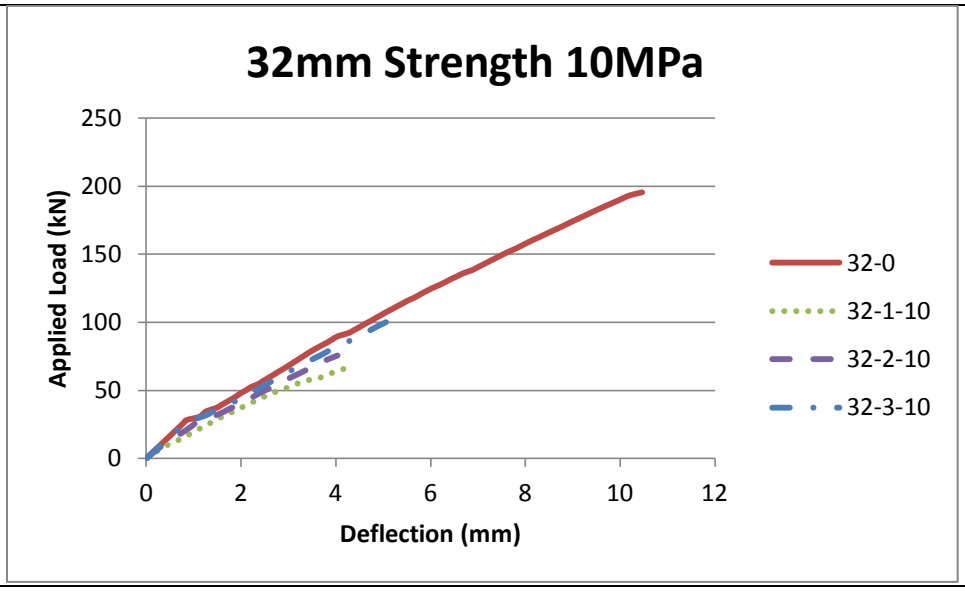

The details of localized concrete with strength 10MPa on bending sensitive, shear sensitive and bond sensitive locations are illustrated in Table 5-10. All these beams are reinforced with two 32 mm tensile rebar with localized 10Mpa concrete in the bending zone, shear zone and bond zone separately. For case 32-1-10 and 32-2-10, the concrete crush firstly because the largest compressive stress within the span and they increase dramatically. The failure modes of other two beams are bond failure. For the beams reinforced with two 32 mm rebar in tension zone, when the concrete strength get as low as 10 MPa, the impact of localized concrete within the span are the most critical and the impact at support end is the least critical.

5.3.2 Effects of Different Location

Table 5-11 Comparison of 16mm rebar with different f'_c at location (1)

Case Name	Bottom Reinforcement	Deteriorated location	Strength of Concrete(MPa)	Ultimate Load (kN)	Ultimate Deflection(mm)	Failure Mode
16-0	16mm	None	42.7	104.21	17.33	F-T
16-1-30	16mm	1	30	101.23	20.28	F-T
16-1-20	16mm	1	20	87.76	12.39	F-C
16-1-10	16mm	1	10	53.62	8.36	F-C

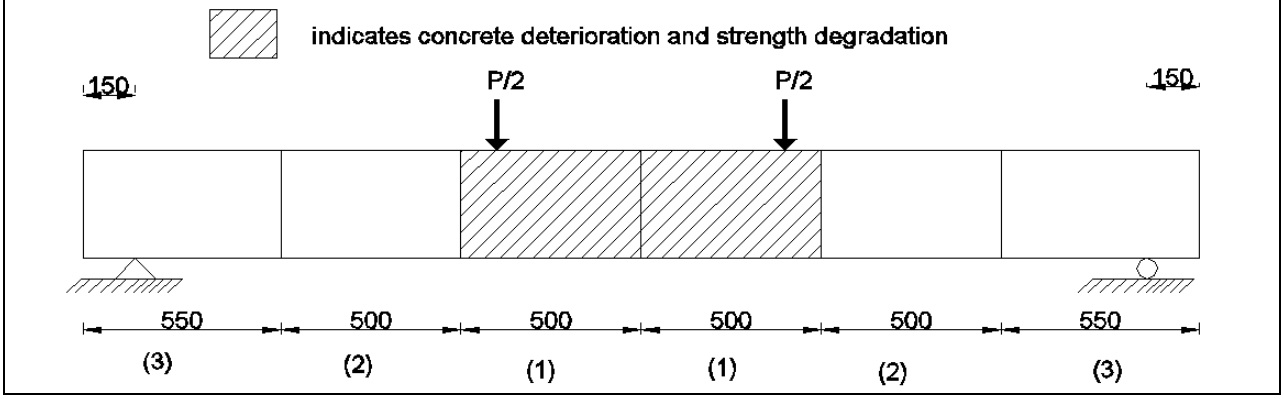

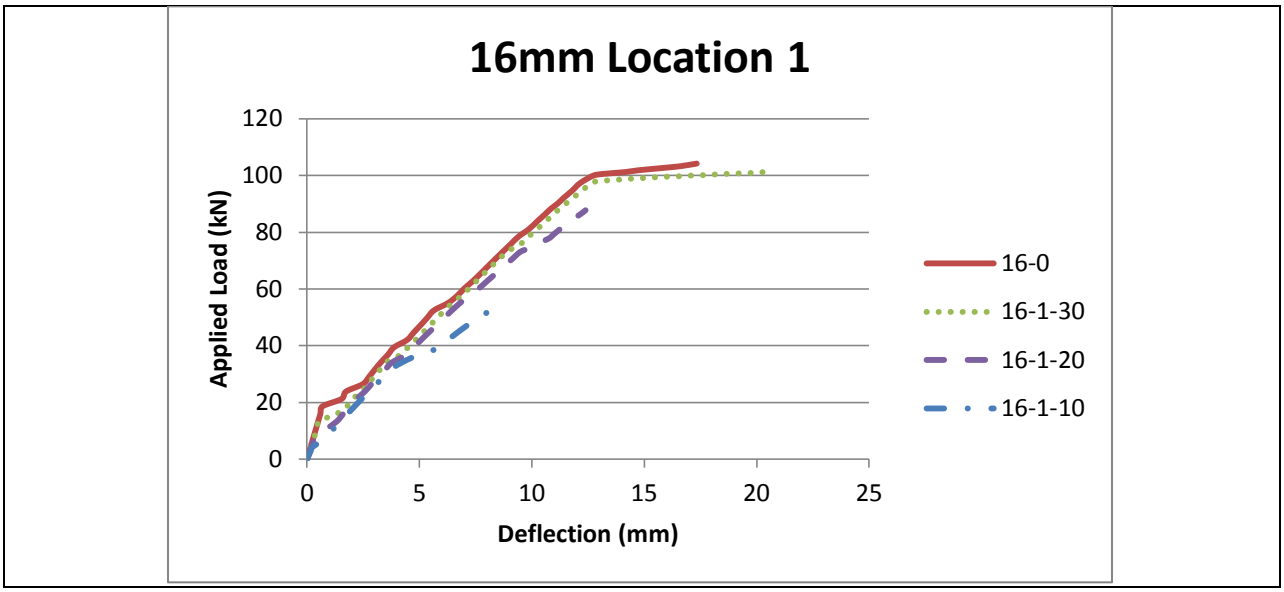

The details of different strength localized concrete on bending sensitive location (named location 1) are illustrated in Table 5-11. All these beams are reinforced with two 16 mm tensile rebar with localized low strength concrete occur in the middle of the beam. The failure modes of case 16-0 and 16-1-30 are that reinforcement yield firstly and then concrete crush. And the failure modes of case 16-1-20 and 16-1-10 are that concrete crush firstly before reinforcement yield. When the localized concrete strength is above 30MPa, it has little effect on the flexural strength of RC beams. But when the localized concrete strength is below 20MPa, the load capacity of the beam reduces based on the strength of concrete.

Table 5-12 Comparison of 16mm rebar with different f'_c at location (2)

Case Name	Bottom Reinforcement	Deteriorated location	Strength of Concrete(MPa)	Ultimate Load (kN)	Ultimate Deflection(mm)	Failure Mode
16-0	16mm	None	42.7	104.21	17.33	F-T
16-2-30	16mm	2	30	102.17	24.80	F-T
16-2-20	16mm	2	20	95.97	12.60	F-C
16-2-10	16mm	2	10	60.26	8.42	F-C

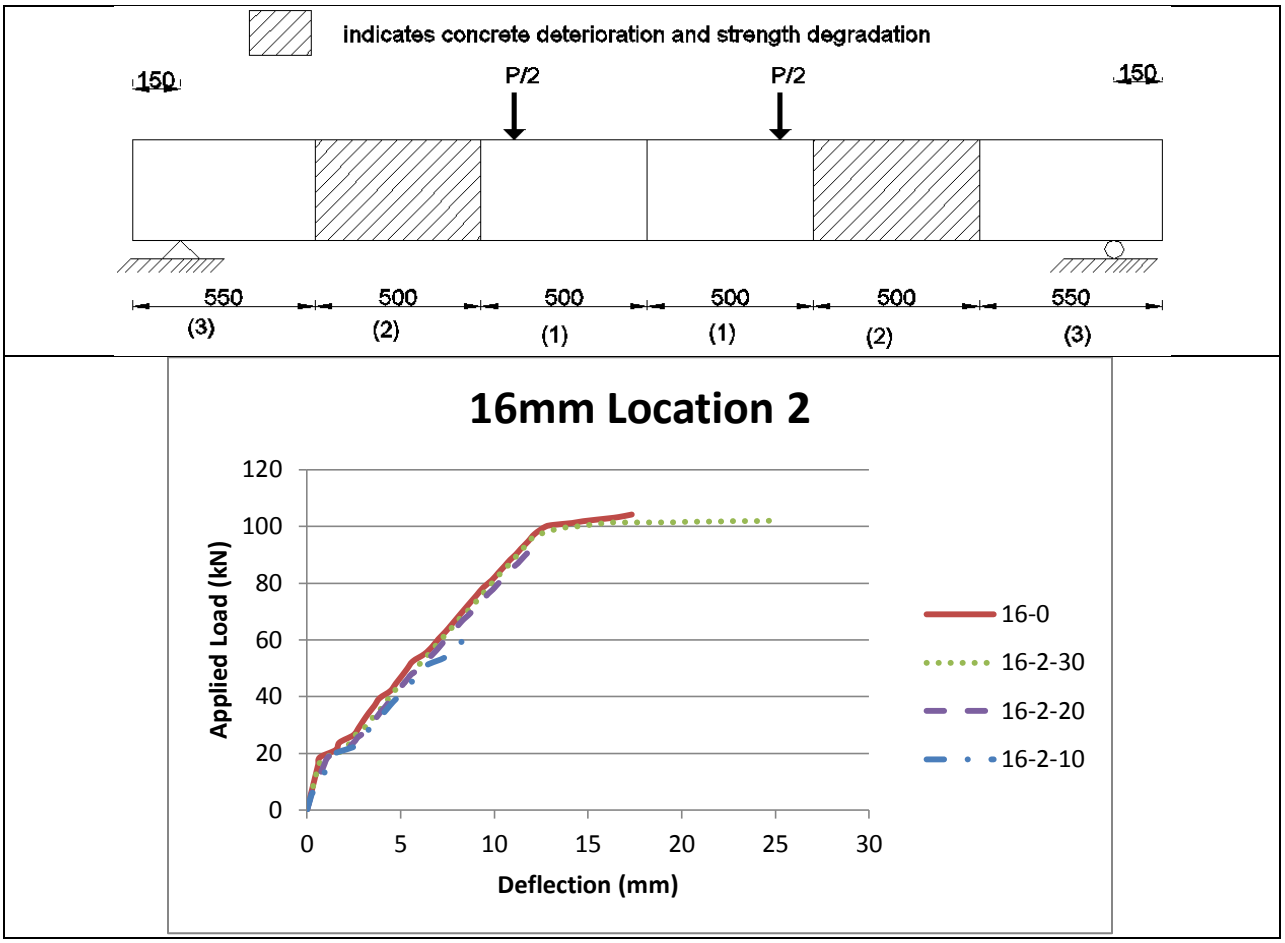

The details of different strength localized concrete on bending shear location (named location 2) are illustrated in Table 5-12. All these beams are reinforced with two 16 mm tensile rebar with localized low strength concrete occur at region (2). The failure modes of case 16-0 and 16-2-30 are that reinforcement yield firstly and then concrete crush. And the failure modes of case 16-2-20 and 16-2-10 are that concrete crush firstly before reinforcement yield. When the localized concrete strength is above 30MPa, it has little effect on the flexural strength of RC beams. But when the localized concrete strength is below 20MPa, the load capacity of the beam reduces based on the strength of concrete.

Table 5-13 Comparison of 16mm rebar with different f'_c at location (3)

Case Name	Bottom Reinforcement	Deteriorated location	Strength of Concrete(MPa)	Ultimate Load (kN)	Ultimate Deflection(mm)	Failure Mode
16-0	16mm	None	42.7	104.21	17.33	F-T
16-3-30	16mm	1	30	103.82	18.02	F-T
16-3-20	16mm	1	20	103.81	18.97	F-T
16-3-10	16mm	1	10	72.27	8.98	F-C

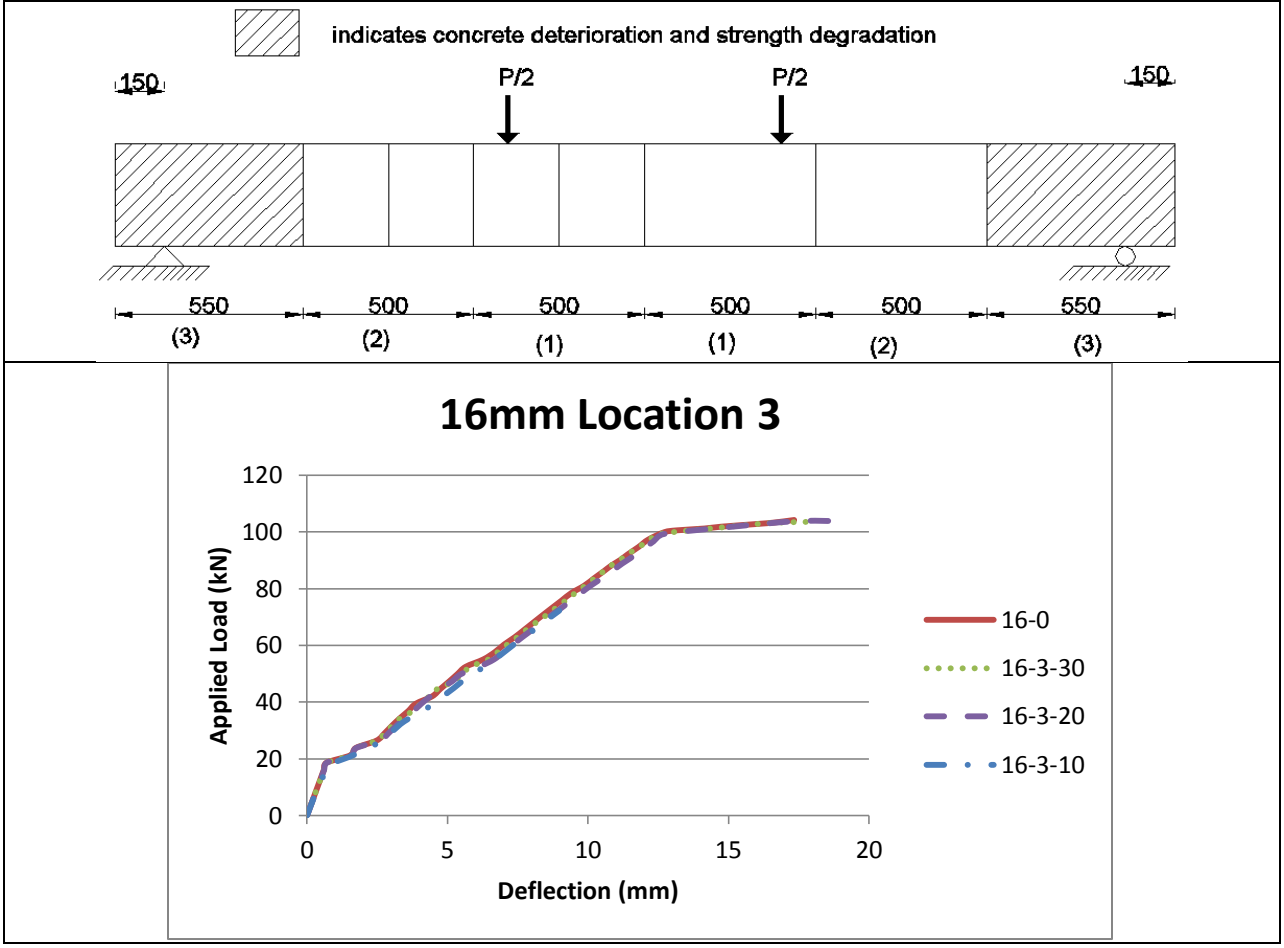

The details of different strength localized concrete on bond sensitive location (named location 3) are illustrated in Table 5-13. All these beams are reinforced with two 16 mm tensile rebar with localized low strength concrete occur at both ends. The failure modes of case 16-0, 16-3-30 and 16-3-20 are that reinforcement yield firstly and then concrete crush. And the failure modes of case 16-2-20 and 16-2-10 are that concrete

crush firstly before reinforcement yield. When the localized concrete strength is above 30MPa, it has little effect on the flexural strength of RC beams. But when the localized concrete strength is below 20MPa, the load capacity of the beam reduces based on the strength of concrete.

Table 5-14 Comparison of 25mm rebar with different f'_c at location (1)

Case Name	Bottom Reinforcement	Deteriorated location	Strength of Concrete(MPa)	Ultimate Load (kN)	Ultimate Deflection(mm)	Failure Mode
25-0	25mm	None	42.7	178.92	12.92	B
25-1-30	25mm	1	30	161.03	12.39	B
25-1-20	25mm	1	20	95.18	7.07	F-C
25-1-10	25mm	1	10	60.94	4.97	F-C

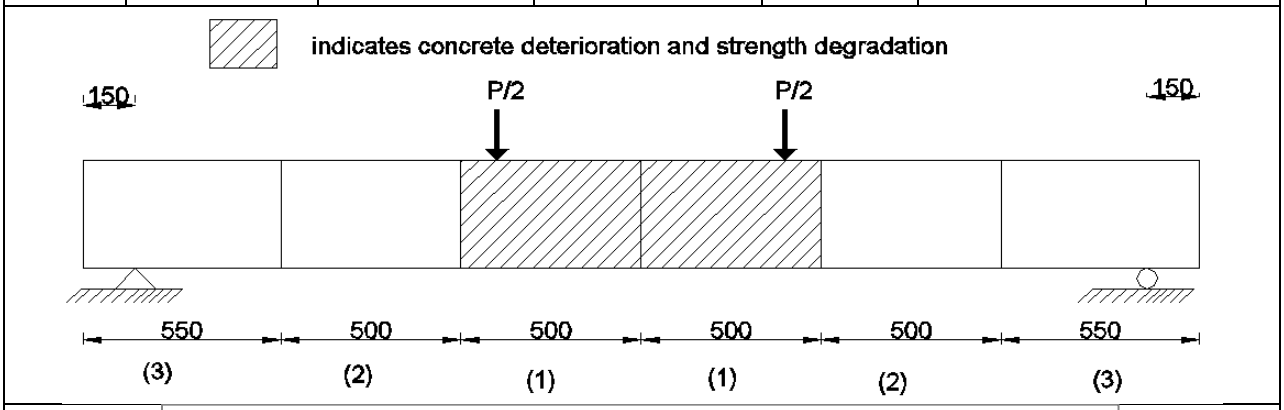

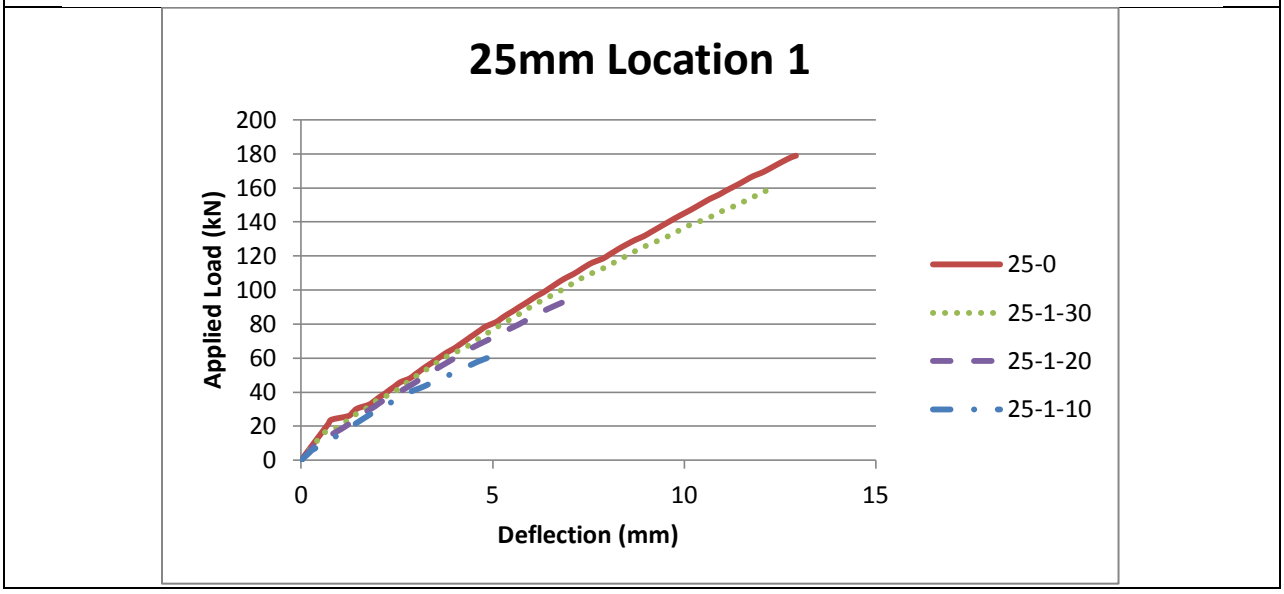

The details of different strength localized concrete on bending sensitive location (named location 1) are illustrated in Table 5-14. All these beams are reinforced with two 25 mm tensile rebar with localized low strength concrete occur in the middle of the beam. The failure modes of case 25-0 and 25-1-30 are bond failure. And the failure modes of case 25-1-20 and 25-1-10 are that concrete crush firstly before reinforcement yield. When the localized concrete strength is above 30MPa, it will fail in bond and the ultimate load decrease a little. When the localized concrete strength is below 20MPa, the beams fail in flexural and the load capacity of the beam reduces a lot.

Table 5-15 Comparison of 25mm rebar with different f'_c at location (2)

Case Name	Bottom Reinforcement	Deteriorated location	Strength of Concrete(MPa)	Ultimate Load (kN)	Ultimate Deflection(mm)	Failure Mode
25-0	25mm	None	42.7	178.92	12.92	B
25-2-30	25mm	2	30	167.37	12.21	B
25-2-20	25mm	2	20	115.15	8.22	F-C
25-2-10	25mm	2	10	67.93	5.30	F-C

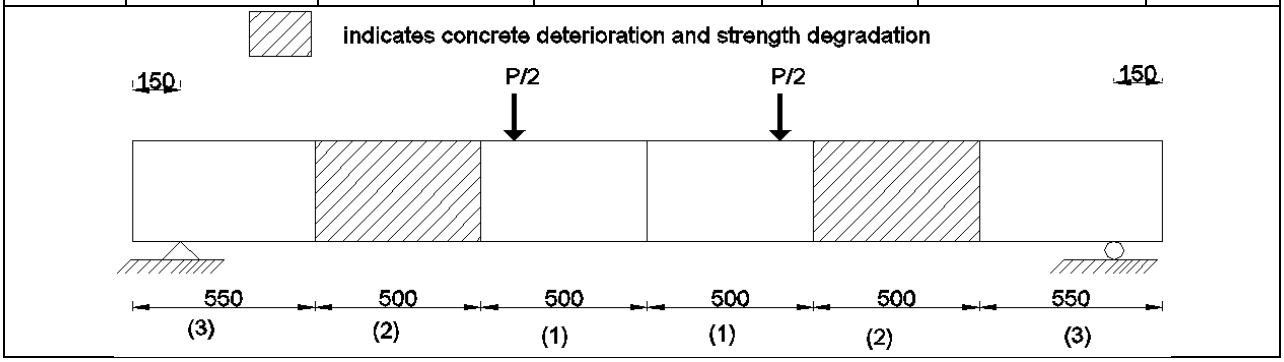

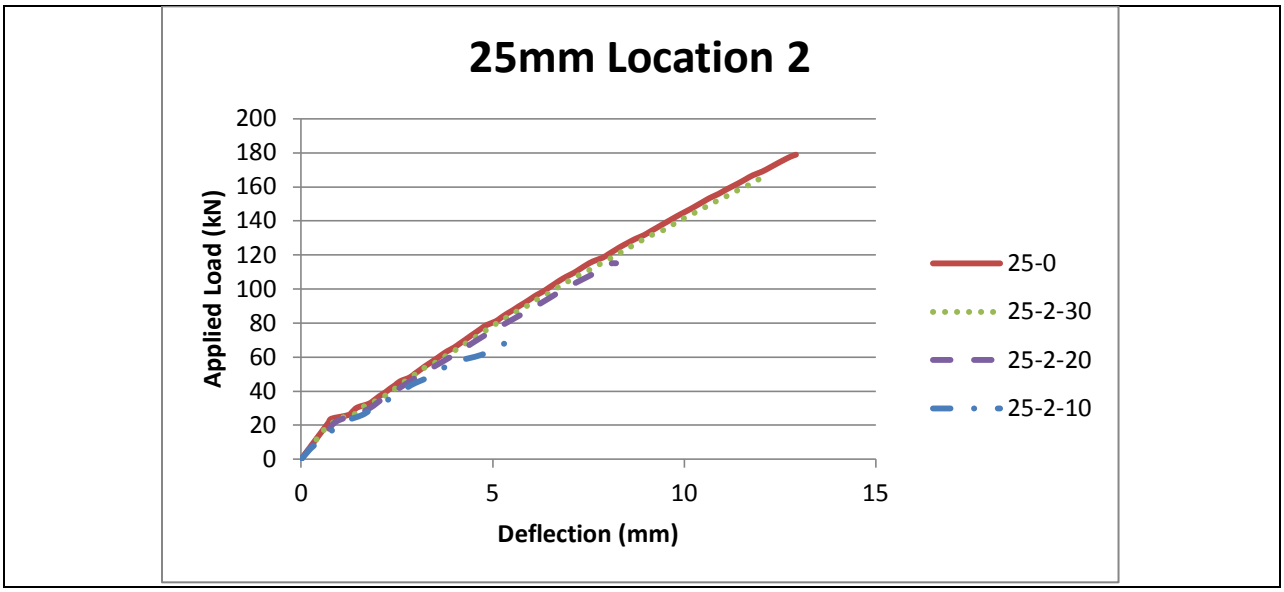

The details of different strength localized concrete on bending shear location (named location 2) are illustrated in Table 5-15. All these beams are reinforced with two 25 mm tensile rebar with localized low strength concrete occur at region (2). The failure modes of case 25-0 and 25-2-30 are bond failure. And the failure modes of case 25-2-20 and 25-2-10 are that concrete crush firstly before reinforcement yield. When the localized concrete strength is above 30MPa, beams will fail in bond and the ultimate load decrease a little. When the localized concrete strength is below 20MPa, the beams fail in flexural and the load capacity of the beam reduces a lot.

Table 5-16 Comparison of 25mm rebar with different f'_c at location (3)

Case Name	Bottom Reinforcement	Deteriorated location	Strength of Concrete(MPa)	Ultimate Load (kN)	Ultimate Deflection(mm)	Failure Mode
25-0	25mm	None	42.7	178.92	12.92	B
25-3-30	25mm	1	30	173.98	12.80	B
25-3-20	25mm	1	20	128.90	9.06	B
25-3-10	25mm	1	10	101.57	7.26	B

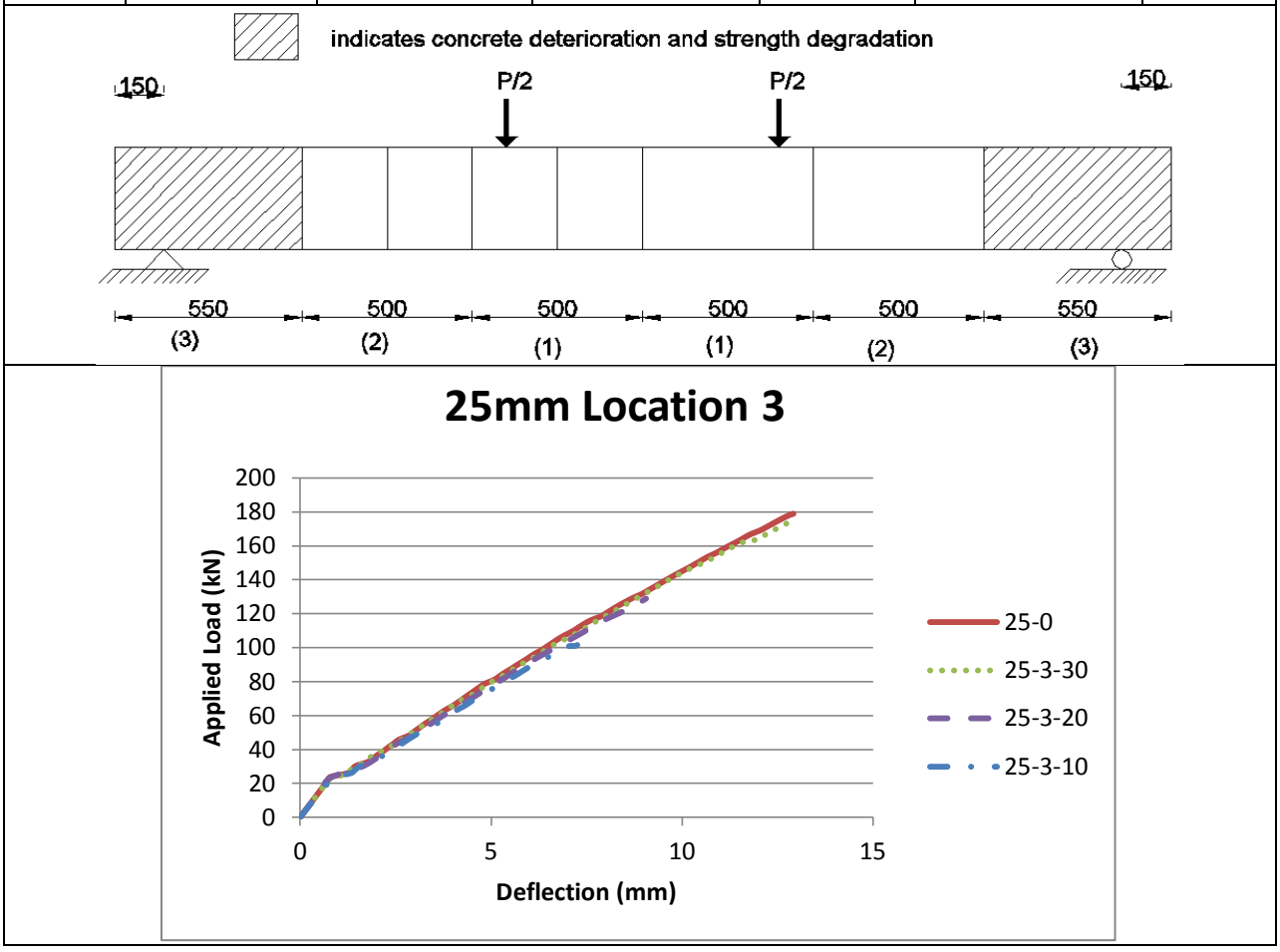

The details of different strength localized concrete on bond sensitive location (named location 3) are illustrated in Table 5-16. All these beams are reinforced with two 25 mm tensile rebar with localized low strength concrete occur at both ends. The failure modes of four beams are bond failure. As long as the localized low strength concrete

occurs at support, beams will fail in bond. And the load capacity of the beam reduces a lot based on the localized low strength of concrete.

Table 5-17 Comparison of 32mm rebar with different f'_c at location (1)

Case Name	Bottom Reinforcement	Deteriorated location	Strength of Concrete(MPa)	Ultimate Load (kN)	Ultimate Deflection(mm)	Failure Mode
32-0	32mm	None	42.7	195.42	10.46	B
32-1-30	32mm	1	30	161.32	9.03	B
32-1-20	32mm	1	20	95.63	5.32	F-C
32-1-10	32mm	1	10	66.05	4.19	F-C

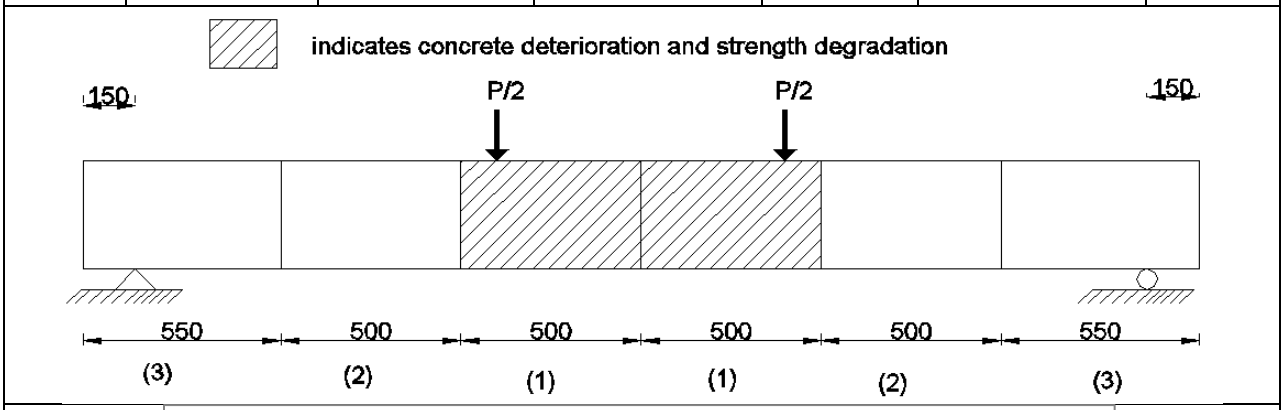

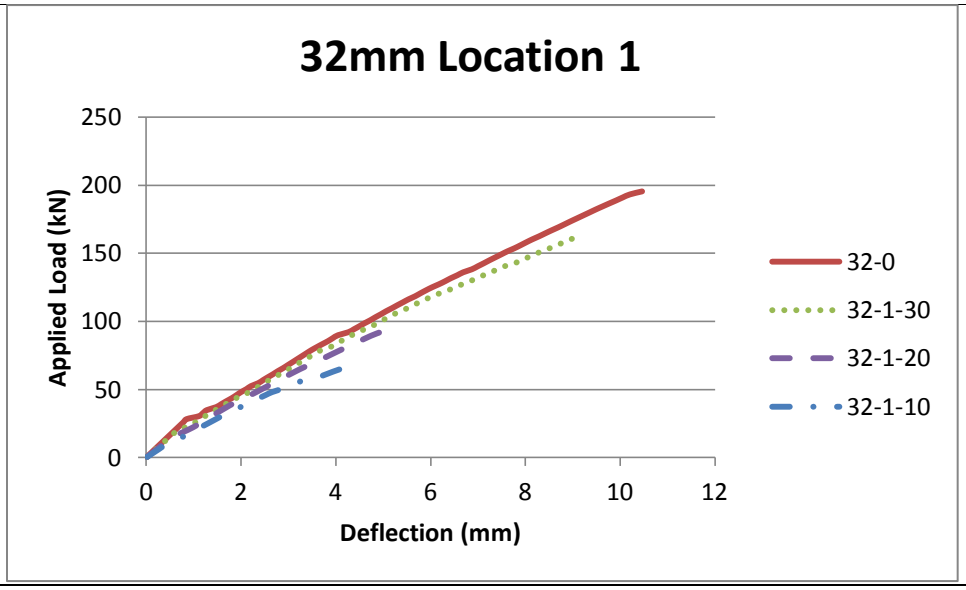

The details of different strength localized concrete on bending moment sensitive location (named location 1) are illustrated in Table 5-17. All these beams are reinforced

with two 32 mm tensile rebar with localized low strength concrete occur in the middle of the beam. The failure modes of case 32-0 and 32-1-30 are bond failure. And the failure modes of case 32-1-20 and 32-1-10 are that concrete crush firstly before reinforcement yield. When the localized concrete strength is above 30MPa, beams will fail in bond and the ultimate load decease a little. When the localized concrete strength is below 20MPa, the load capacity of the beam reduces a lot based on the strength of concrete.

Table 5-18 Comparison of 32mm rebar with different f'_c at location (2)

Case Name	Bottom Reinforcement	Deteriorated location	Strength of Concrete(MPa)	Ultimate Load (kN)	Ultimate Deflection(mm)	Failure Mode
32-0	32mm	None	42.7	195.42	10.46	B
32-2-30	32mm	2	30	173.45	9.44	B
32-2-20	32mm	2	20	152.48	8.48	B
32-2-10	32mm	2	10	79.69	4.85	F-C

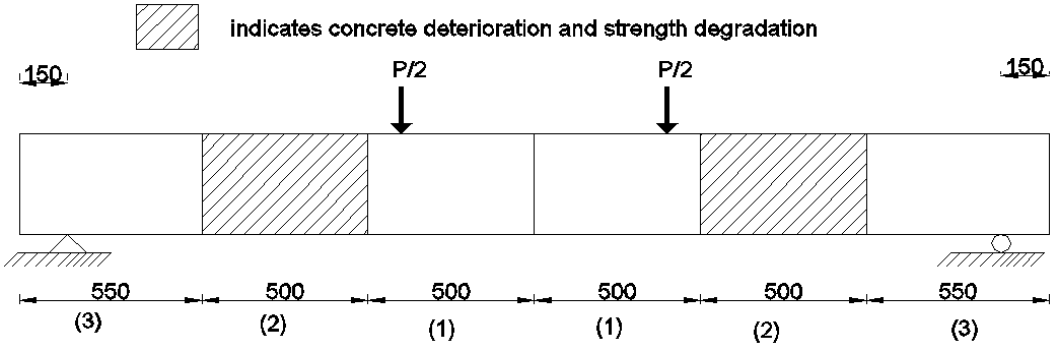

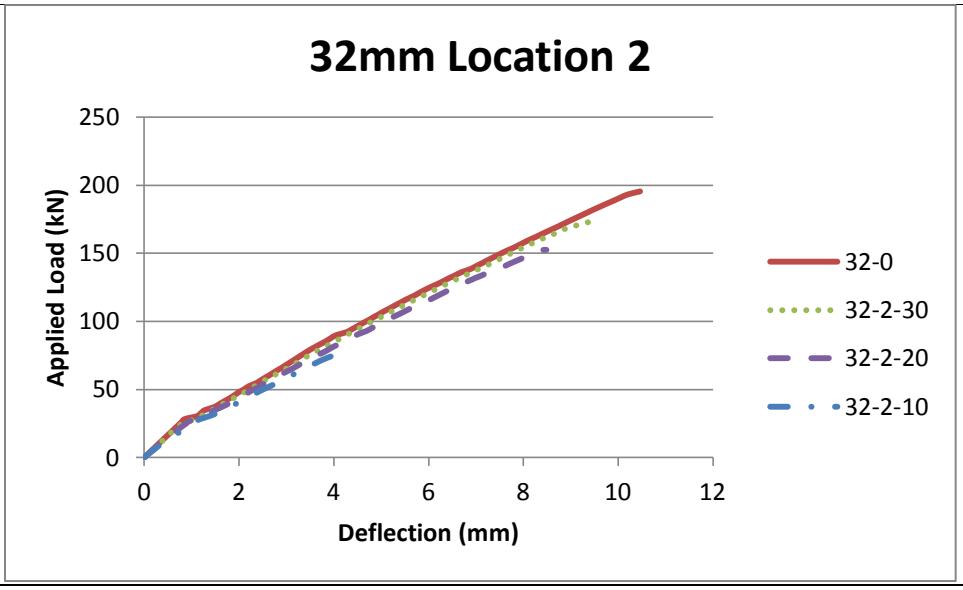

The details of different strength localized concrete on bending shear location (named location 2) are illustrated in Table 5-18. All these beams are reinforced with two 32 mm tensile rebar with localized low strength concrete occur at region (2). The failure modes of case 32-0, 32-2-30 and 32-2-20 are bond failure. And the failure mode of case 32-2-10 that concrete crushes firstly before reinforcement yield. When the localized concrete strength is above 20MPa beams will fail in bond and the ultimate load decease little by little. When the localized concrete strength is below 10MPa, the load capacity of the beam drop dramatically based on the strength of concrete.

Table 5-19 Comparison of 32mm rebar with different f'_c at location (3)

Case Name	Bottom Reinforcement	Deteriorated location	Strength of Concrete(MPa)	Ultimate Load (kN)	Ultimate Deflection(mm)	Failure Mode
32-0	32mm	None	42.7	195.42	10.46	B
32-3-30	32mm	1	30	183.56	9.94	B
32-3-20	32mm	1	20	175.68	9.57	B
32-3-10	32mm	1	10	101.98	5.18	B

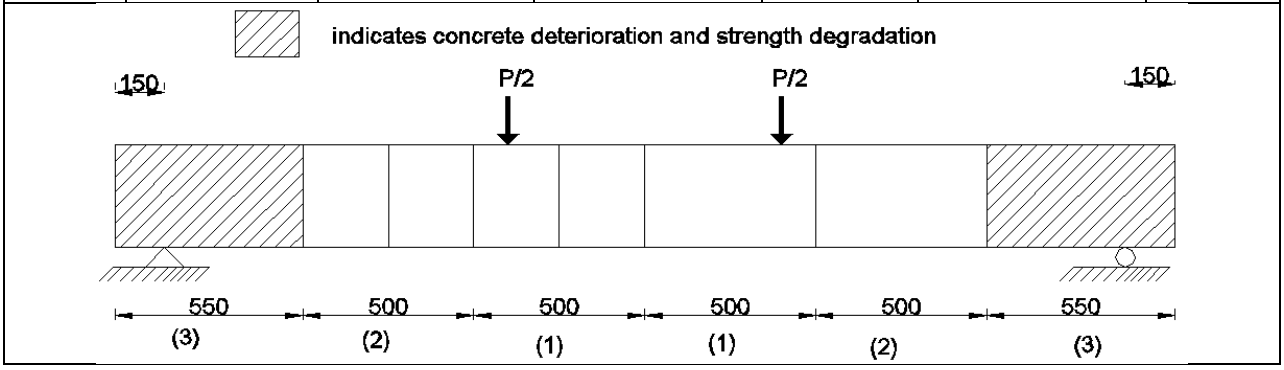

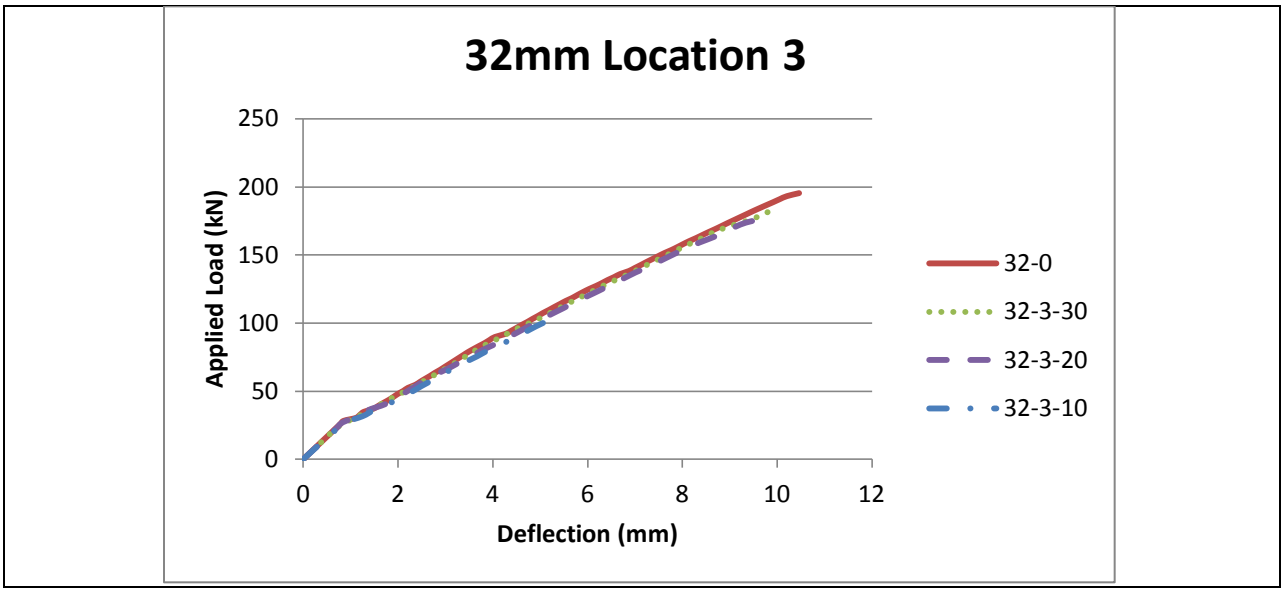

The details of different strength localized concrete on bond sensitive location (named location 3) are illustrated in Table 5-19. All these beams are reinforced with two 32 mm tensile rebar with localized low strength concrete occur at both ends. The failure modes of all four beams are bond failure. When the localized low strength concrete occur at the support end for a beam without sufficient development length, beams will still fail in bond. And the load capacity of the RC beam reduces a lot based on the localized strength of concrete.

5.3.3 Effects of Different Rebar Size

Table 5-20 Comparison of beams with 42.7MPa concrete

Case Name	Bottom Reinforcement	Deteriorated location	Strength of Concrete(MPa)	Ultimate Load (kN)	Ultimate Deflection(mm)	Failure Mode
16-0	16mm	None	42.7	104.21	17.33	F-T
25-0	25mm	None	42.7	178.92	12.92	B
32-0	32mm	None	42.7	195.42	10.46	B

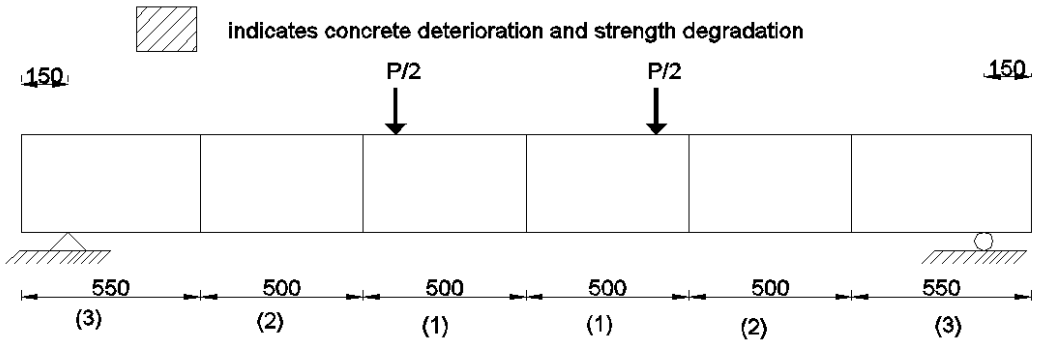

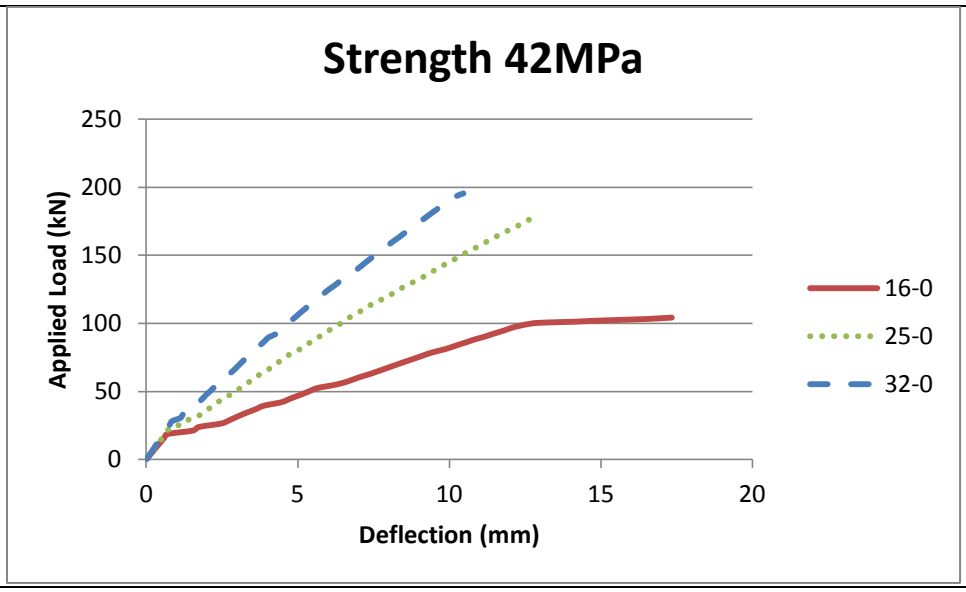

The details of localized all reference beams with different rebar size and without localized low strength concrete are illustrated in Table 5-20. The failure mode of case 16-0 is that the reinforcement yields then the concrete crush. And the failure mode of case 25-0 and 32-0 are bond failure. So their results are relatively similar.

Table 5-21 Comparison of beams with 30MPa concrete at Location (1)

Case Name	Bottom Reinforcement	Deteriorated location	Strength of Concrete(MPa)	Ultimate Load (kN)	Ultimate Deflection(mm)	Failure Mode
16-1-30	16mm	1	30	101.23	20.28	F-T
25-1-30	25mm	1	30	161.03	12.39	B
32-1-30	32mm	1	30	161.32	9.03	B

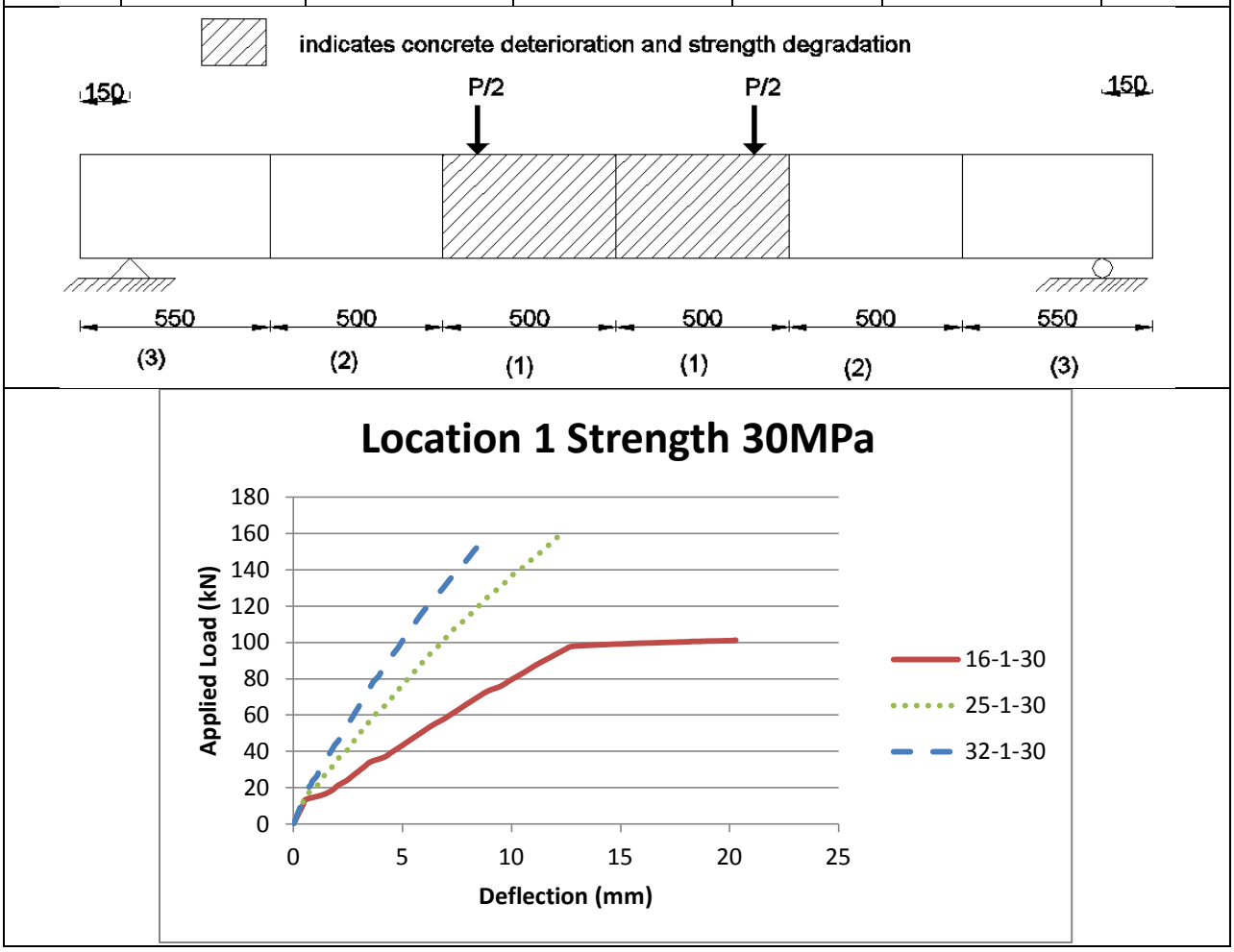

The details of beams with different rebar size when localized 30MPa concrete occurs at the bending moment sensitive zone (location 1) are illustrated in Table 5-21. The failure mode of case 16-1-30 is that the reinforcement yields then the concrete crush. And the failure mode of case 25-0 and 32-0 are bond failure. So their results are relatively similar.

Table 5-22 Comparison of beams with 20MPa concrete at Location (1)

Case Name	Bottom Reinforcement	Deteriorated location	Strength of Concrete(MPa)	Ultimate Load (kN)	Ultimate Deflection(mm)	Failure Mode
16-1-20	16mm	1	20	87.76	12.39	F-C
25-1-20	25mm	1	20	95.18	7.07	F-C
32-1-20	32mm	1	20	95.63	5.32	F-C

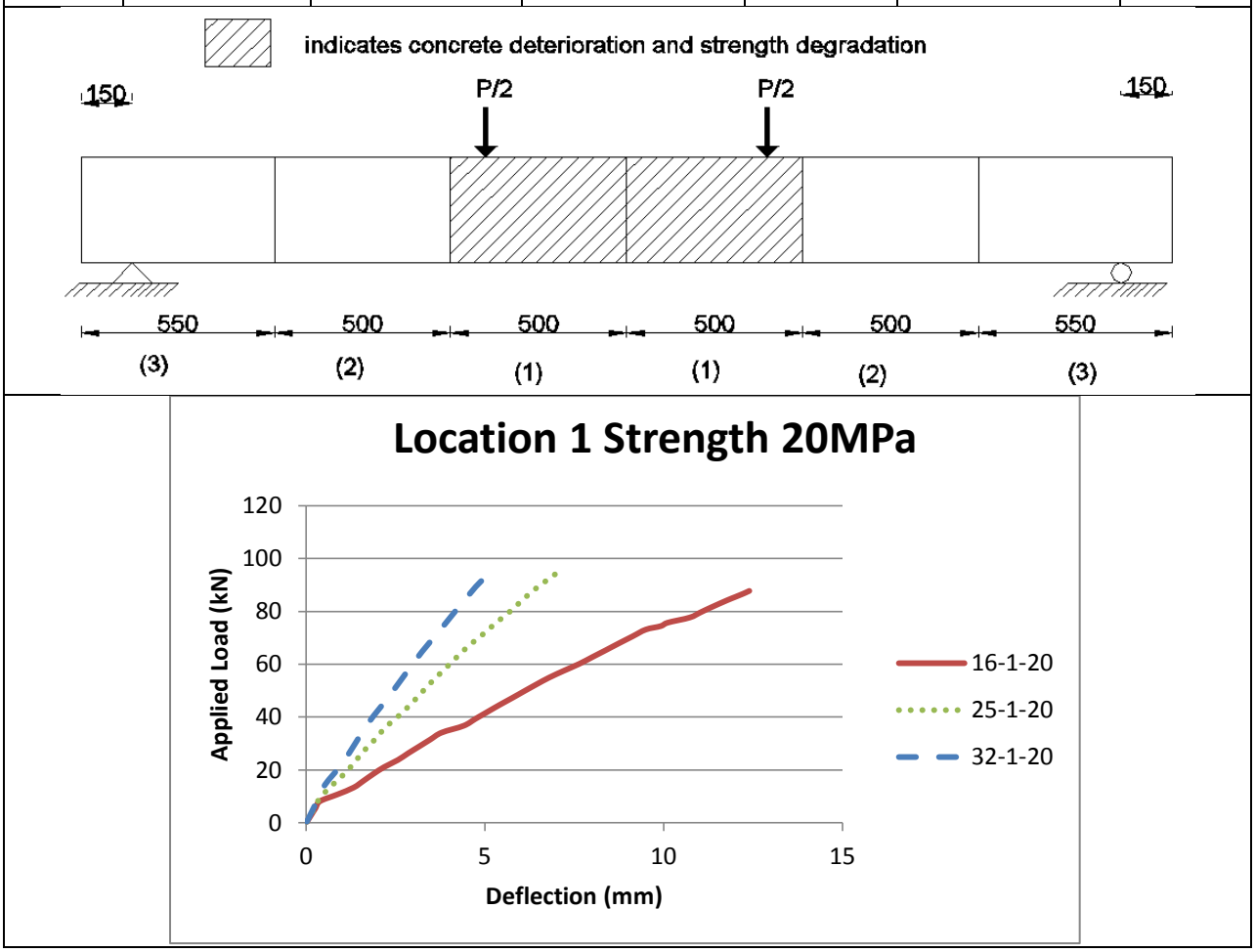

The details of beams with different rebar size when localized 20MPa concrete occurs at the bending moment sensitive zone (location 1) are illustrated in Table 5-22. The failure modes of all three cases are that the concrete crush before the reinforcement yield. For large rebar size beams, the ultimate loads govern by concrete strength as low as 20 are similar.

Table 5-23 Comparison of beams with 10MPa concrete at Location (1)

Case Name	Bottom Reinforcement	Deteriorated location	Strength of Concrete(MPa)	Ultimate Load (kN)	Ultimate Deflection(mm)	Failure Mode
16-1-10	16mm	1	10	53.62	8.36	F-C
25-1-10	25mm	1	10	60.94	4.97	F-C
32-1-10	32mm	1	10	66.05	4.19	F-C

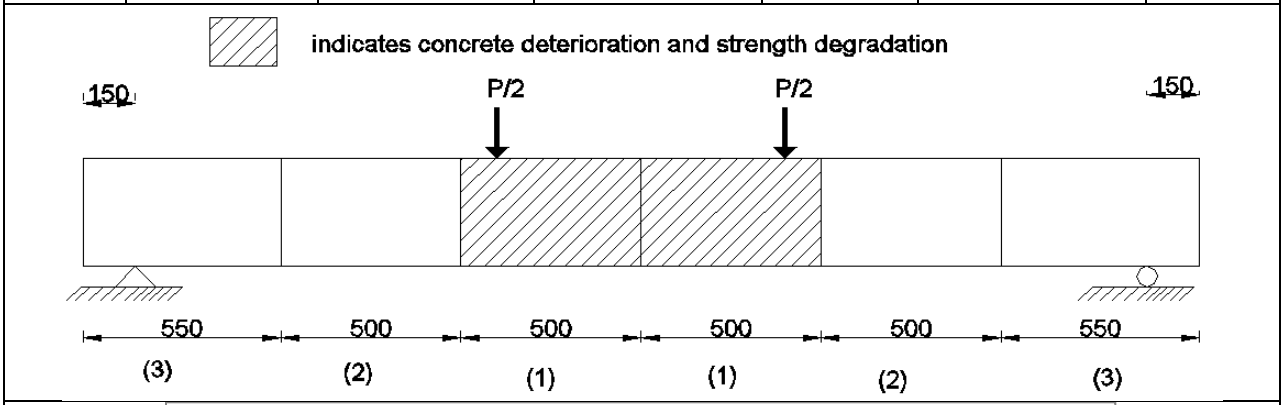

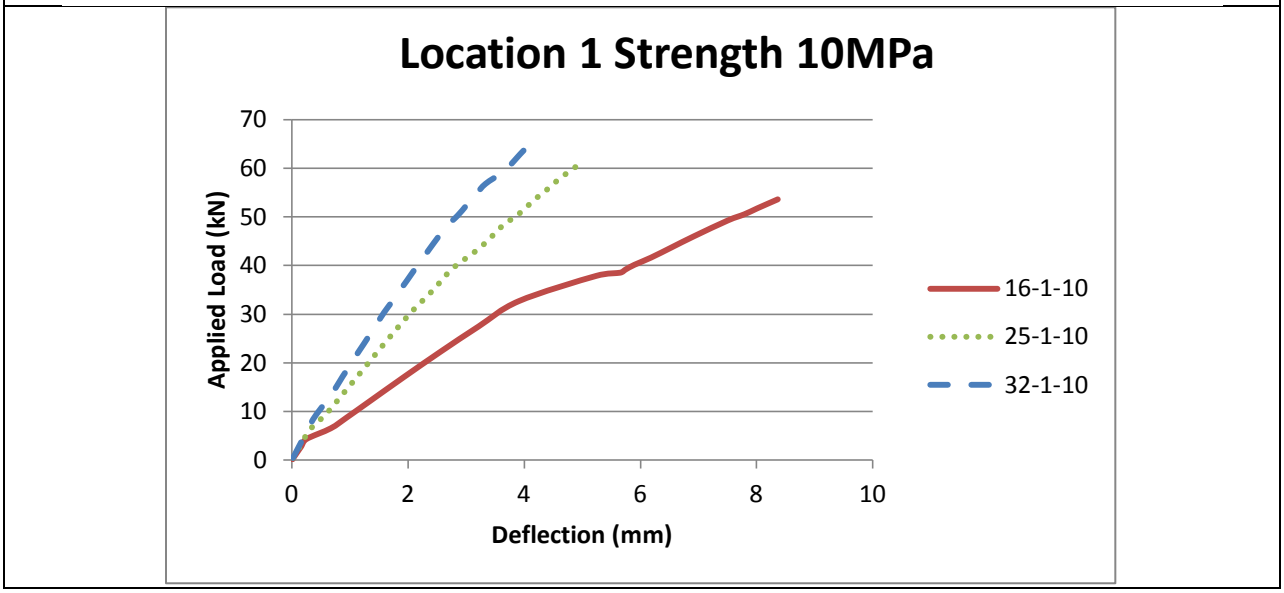

The details of beams with different rebar size when localized 10MPa concrete occurs at the bending moment sensitive zone (location 1) are illustrated in Table 5-23. The failure modes of all three cases are that the concrete crush before the reinforcement yield. When the localized strength of concrete gets as low as 10 MPa, the ultimate load capacity of RC beams decrease based on rebar size.

Table 5-24 Comparison of beams with 30MPa concrete at Location (2)

Case Name	Bottom Reinforcement	Deteriorated location	Strength of Concrete(MPa)	Ultimate Load (kN)	Ultimate Deflection(mm)	Failure Mode
16-2-30	16mm	2	30	102.17	24.80	F-T
25-2-30	25mm	2	30	167.37	12.21	F-C
32-2-30	32mm	2	30	173.45	9.44	B

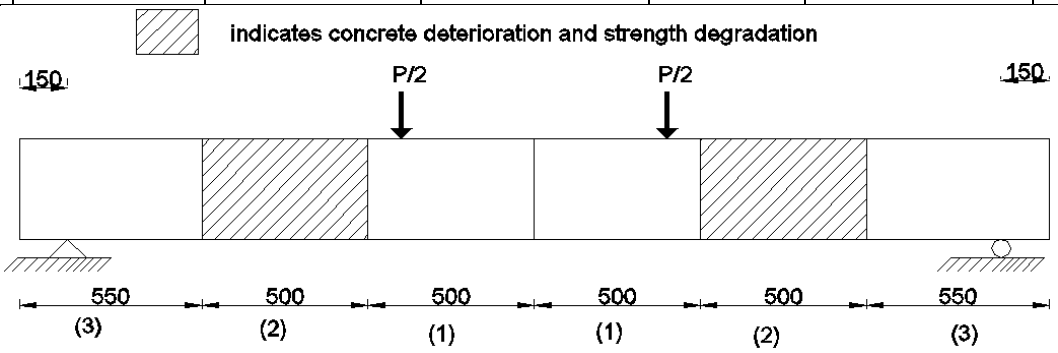

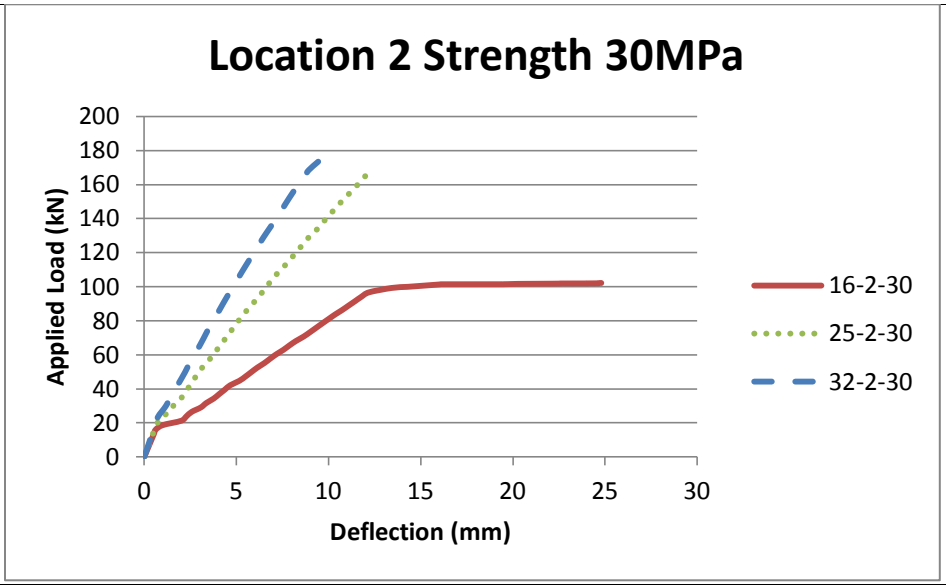

The details of beams with different rebar size when localized 30MPa concrete occurs at the shear force sensitive zone (location 2) are illustrated in Table 5-24. The failure mode of case 16-2-30 is that the reinforcement yields then the concrete crush. The failure mode for case 25-2-30 is that the concrete crush before the reinforcement yield. And the failure mode of case 32-0 is bond failure. The ultimate load capacity decreases when they are small size rebar.

Table 5-25 Comparison of beams with 20MPa concrete at Location (2)

Case Name	Bottom Reinforcement	Deteriorated location	Strength of Concrete(MPa)	Ultimate Load (kN)	Ultimate Deflection(mm)	Failure Mode
16-2-20	16mm	2	20	95.97	12.60	F-C
25-2-20	25mm	2	20	115.15	8.22	F-C
32-2-20	32mm	2	20	152.48	8.48	B

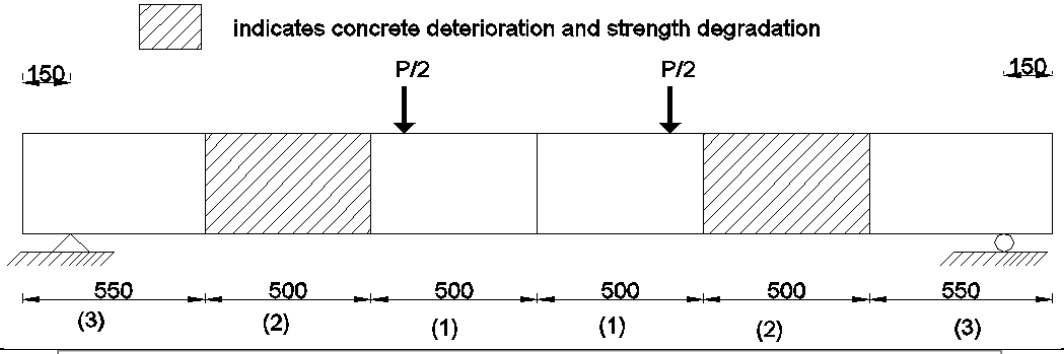

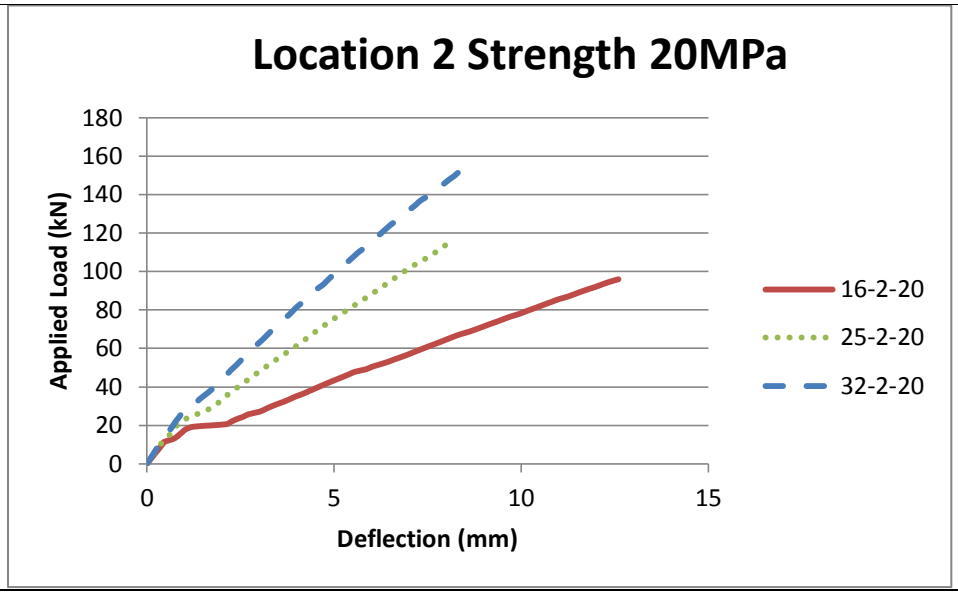

The details of beams with different rebar size when localized 20MPa concrete occurs at the shear force sensitive zone (location 2) are illustrated in Table 5-25. The failure mode of case 16-2-20 and case 25-2-20 are that the concrete crush before the reinforcement yield. And the failure mode of case 32-2-20 is bond failure. Small size rebar has less load capacity than large sizes rebar, but it has a better ductile.

Table 5-26 Comparison of beams with 10MPa concrete at Location (2)

Case Name	Bottom Reinforcement	Deteriorated location	Strength of Concrete(MPa)	Ultimate Load (kN)	Ultimate Deflection(mm)	Failure Mode
16-2-10	16mm	2	10	60.26	8.42	F-C
25-2-10	25mm	2	10	67.93	5.30	F-C
32-2-10	32mm	2	10	79.69	4.85	F-C

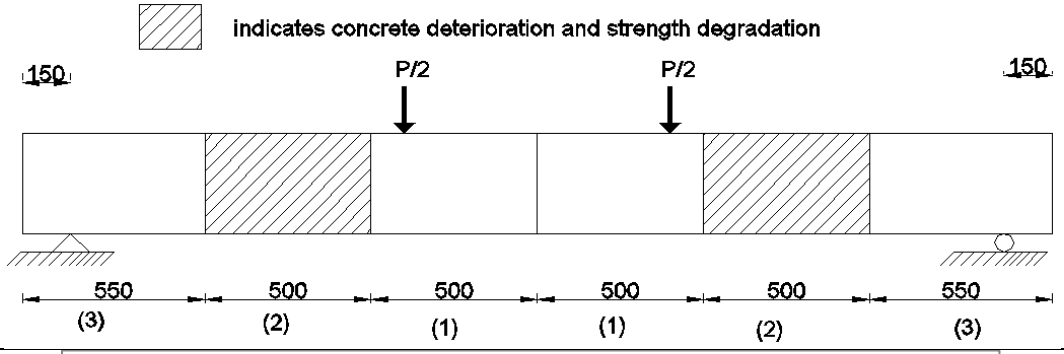

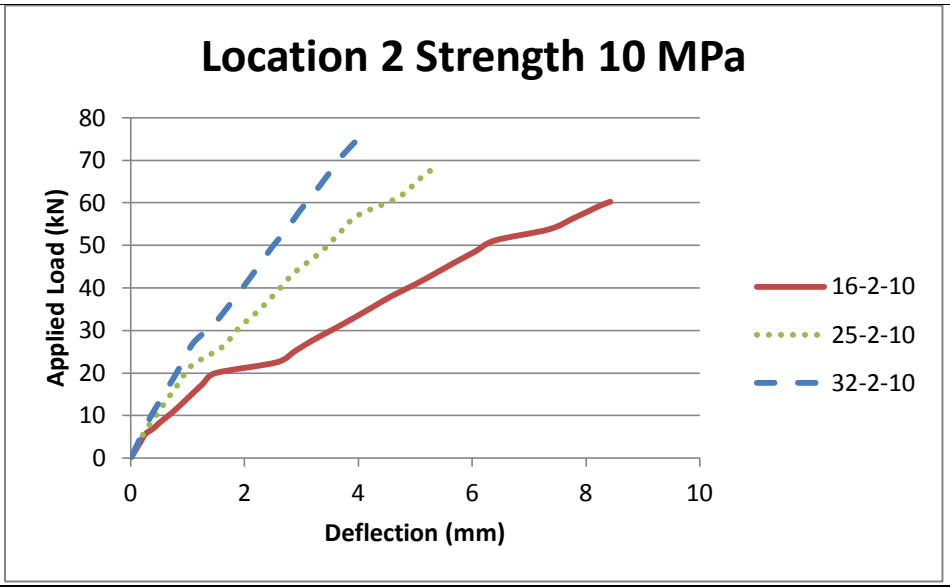

The details of beams with different rebar size when localized 10MPa concrete occurs at the shear force sensitive zone (location 2) are illustrated in Table 5-26. The failure modes of all three beams are concrete crush before the reinforcement yield. When the localized low strength concrete occurred at location 2 gets as low as 10 MP, beams will fail in flexural and the load capacity decease little by little.

Table 5-27 Comparison of beams with 30MPa concrete at Location (3)

Case Name	Bottom Reinforcement	Deteriorated location	Strength of Concrete(MPa)	Ultimate Load (kN)	Ultimate Deflection(mm)	Failure Mode
16-3-30	16mm	3	30	103.82	18.02	F-T
25-3-30	25mm	3	30	173.98	12.80	B
32-3-30	32mm	3	30	183.56	9.94	B

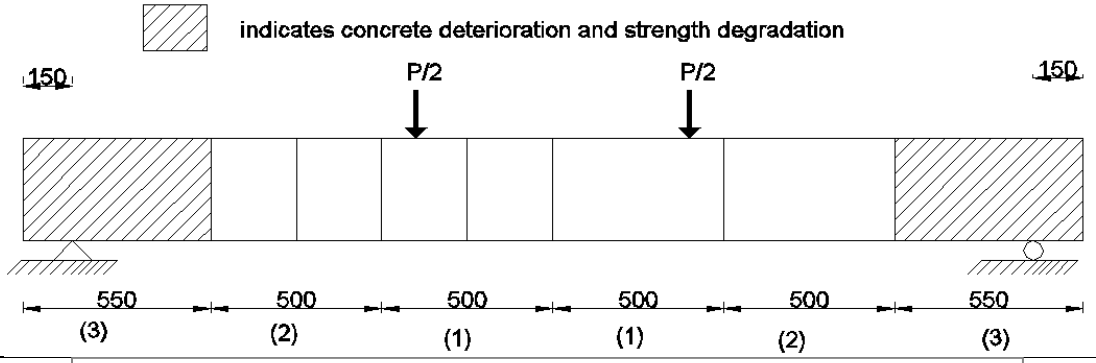

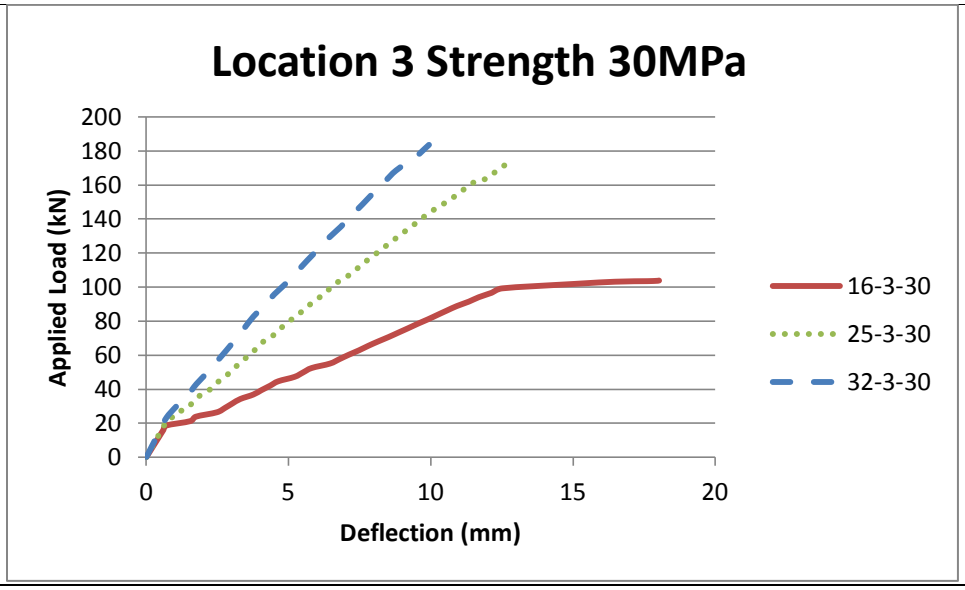

The details of beams with different rebar size when localized 30MPa concrete occurs at bond sensitive zone (location 3) are illustrated in Table 5-27. The failure mode of case 16-3-30 is that the reinforcement yields then the concrete crush. And the failure modes of other two beams are bond failure. There is a little load capacity decrease between large size rebar 25mm and 32m.

Table 5-28 Comparison of beams with 20MPa concrete at Location (3)

Case Name	Bottom Reinforcement	Deteriorated location	Strength of Concrete(MPa)	Ultimate Load (kN)	Ultimate Deflection(mm)	Failure Mode
16-3-20	16mm	3	20	103.81	18.97	F-T
25-3-20	25mm	3	20	128.90	9.06	B
32-3-20	32mm	3	20	175.68	9.57	B

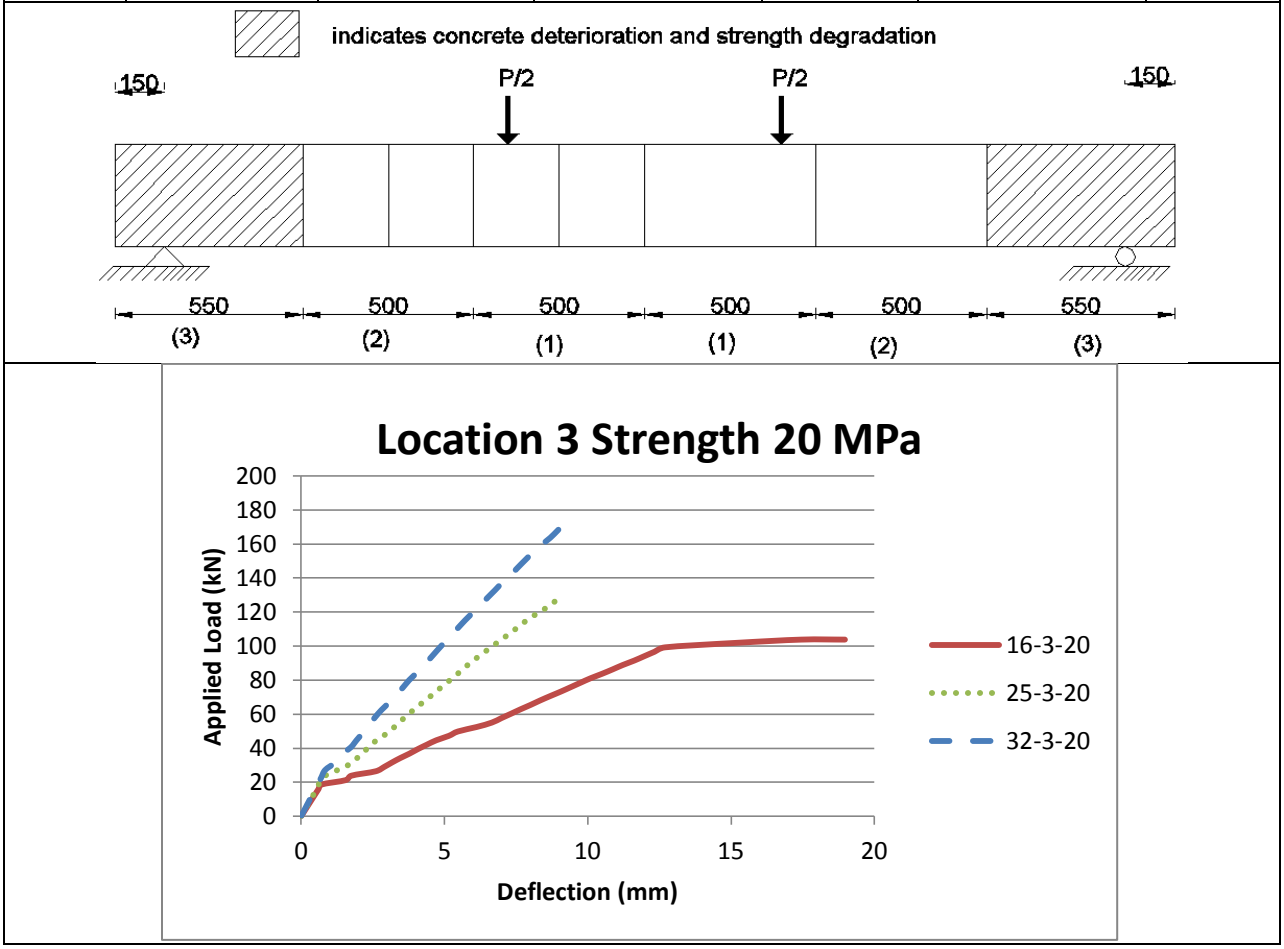

The details of beams with different rebar size when localized 20MPa concrete occurs at bond sensitive zone (location 3) are illustrated in Table 5-28. The failure mode of case 16-3-20 is that the reinforcement yields then the concrete crush. And the failure modes of other two beams are bond failure. There is a little load capacity decrease between large size rebar 25mm and 32m.

Table 5-29 Comparison of beams with 10MPa concrete at Location (3)

Case Name	Bottom Reinforcement	Deteriorated location	Strength of Concrete(MPa)	Ultimate Load (kN)	Ultimate Deflection(mm)	Failure Mode
16-3-10	16mm	3	10	72.27	8.98	F-C
25-3-10	25mm	3	10	101.57	7.26	B
32-3-10	32mm	3	10	101.98	5.18	B

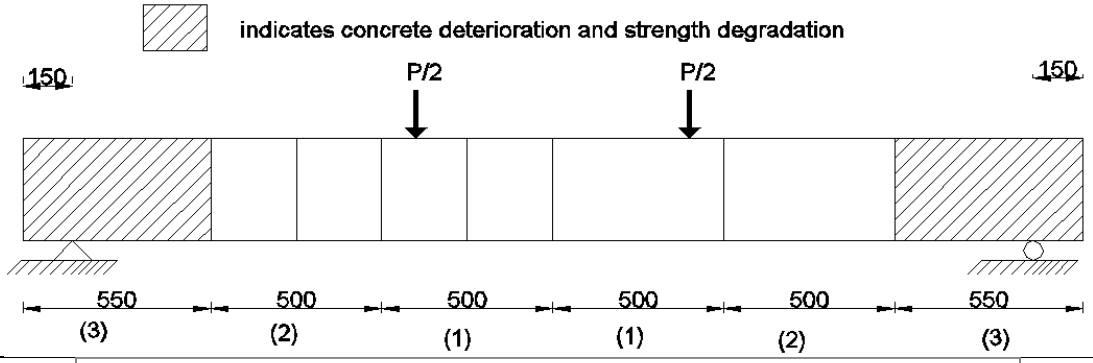

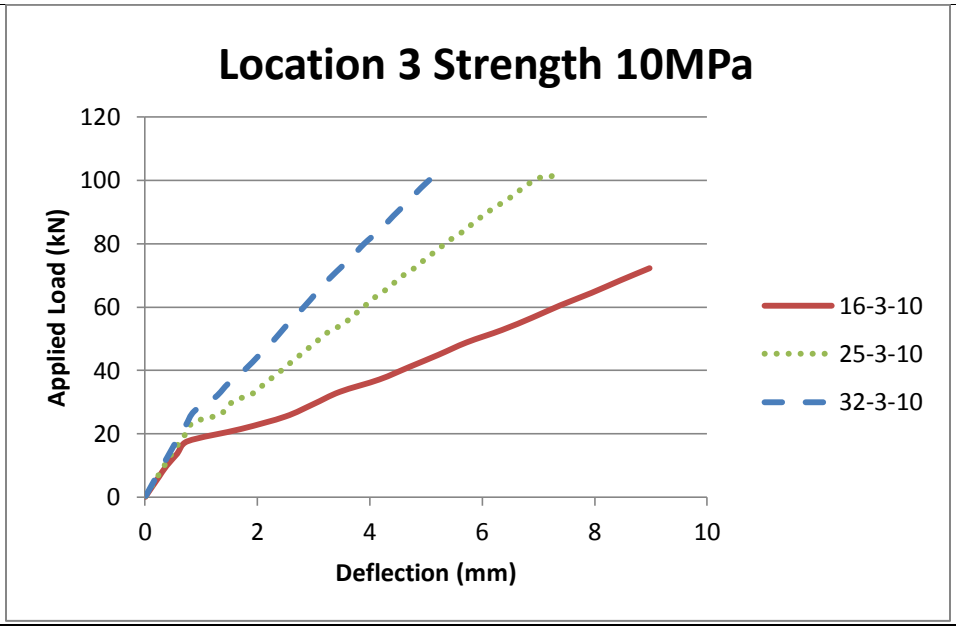

The details of beams with different rebar size when localized 10MPa concrete occurs at bond sensitive zone (location 3) are illustrated in Table 5-29. The failure mode of case 16-3-10 is that the concrete crush before the reinforcement yield. And the failure modes of other two beams are bond failure. The load capacity of 25 and 32 rebar sizes are similar.

5.4 Comparison Summary and discussion

5.4.1 Summary of flexural strength under different category

Table 5-30 Summary of flexural strength under different f'_c

Case Name	Ultimate Load(kN)	Ultimate Deflection(mm)	Failure Mode	Ratio of Residual Load
16-0	104.21	17.33	F-T	1.000
16-1-30	101.23	20.28	F-T	0.975
16-1-20	87.76	12.39	F-C	0.842
16-1-10	53.62	8.36	F-C	0.516
16-2-30	102.17	24.80	F-T	0.984
16-2-20	95.97	12.60	F-C	0.924
16-2-10	60.26	8.42	F-C	0.580
16-3-30	103.82	18.02	F-T	1.000
16-3-20	103.81	18.97	F-T	1.000
16-3-10	72.27	8.98	F-C	0.696
25-0	178.92	12.92	B	1.000
25-1-30	161.03	12.39	B	0.900
25-1-20	95.18	7.07	F-C	0.521
25-1-10	60.94	4.97	F-C	0.341
25-2-30	167.37	12.21	B	0.935
25-2-20	115.15	8.22	F-C	0.644
25-2-10	67.93	5.30	F-C	0.380
25-3-30	173.98	12.80	B	0.972
25-3-20	128.90	9.06	B	0.720
25-3-10	101.57	7.26	B	0.579
32-0	195.42	10.46	B	1.000
32-1-30	161.32	9.03	B	0.825
32-1-20	95.63	5.32	F-C	0.489
32-1-10	66.05	4.19	F-C	0.338
32-2-30	173.45	9.44	B	0.888
32-2-20	152.48	8.48	B	0.780
32-2-10	79.69	4.85	F-C	0.408
32-3-30	183.56	9.94	B	0.939
32-3-20	175.68	9.57	B	0.899
32-3-10	101.98	5.18	B	0.522

Table 5-31 Summary of flexural strength at different location

Case Name	Ultimate Load(kN)	Ultimate Deflection(mm)	Failure Mode	Ratio of Residual Load
16-0	104.21	17.33	F-T	1.000
16-1-30	101.23	20.28	F-T	0.975
16-2-30	102.17	24.80	F-T	0.984
16-3-30	103.82	18.02	F-T	1.000
16-1-20	87.76	12.39	F-C	0.842
16-2-20	95.97	12.60	F-C	0.924
16-3-20	103.81	18.97	F-T	1.002
16-1-10	53.62	8.36	F-C	0.516
16-2-10	60.26	8.42	F-C	0.580
16-3-10	72.27	8.98	F-C	0.696
25-0	178.92	12.92	B	1.000
25-1-30	161.03	12.39	B	0.900
25-2-30	167.37	12.21	B	0.935
25-3-30	173.98	12.80	B	0.972
25-1-20	95.18	7.07	F-C	0.521
25-2-20	115.15	8.22	F-C	0.644
25-3-20	128.90	9.06	B	0.720
25-1-10	60.94	4.97	F-C	0.341
25-2-10	67.93	5.30	F-C	0.380
25-3-10	101.57	7.26	B	0.579
32-0	195.42	10.46	B	1.000
32-1-30	161.32	9.03	B	0.825
32-2-30	173.45	9.44	B	0.888
32-3-30	183.56	9.94	B	0.939
32-1-20	95.63	5.32	F-C	0.489
32-2-20	152.48	8.48	B	0.780
32-3-20	175.68	9.57	B	0.899
32-1-10	66.05	4.19	F-C	0.338
32-2-10	79.69	4.85	F-C	0.408
32-3-10	101.98	5.18	B	0.522

Table 5-32 Summary of flexural strength at different rebar size

Case Name	Ultimate Load(kN)	Ultimate Deflection(mm)	Failure Mode	Ratio of Residual Load
16-0	104.21	17.33	F-T	1.000
25-0	178.92	12.92	B	1.000
32-0	195.42	10.46	B	1.000
16-1-30	101.23	20.28	F-T	0.975
25-1-30	161.03	12.39	B	0.900
32-1-30	161.32	9.03	B	0.825
16-2-30	102.17	24.80	F-T	0.984
25-2-30	167.37	12.21	B	0.935
32-2-30	173.45	9.44	B	0.888
16-3-30	103.82	18.02	F-T	1.000
25-3-30	173.98	12.80	B	0.972
32-3-30	183.56	9.94	B	0.939
16-1-20	87.76	12.39	F-C	0.842
25-1-20	95.18	7.07	F-C	0.521
32-1-20	95.63	5.32	F-C	0.489
16-2-20	95.97	12.60	F-C	0.924
25-2-20	115.15	8.22	F-C	0.644
32-2-20	152.48	8.48	B	0.780
16-3-20	103.81	18.97	F-T	1.002
25-3-20	128.90	9.06	B	0.720
32-3-20	175.68	9.57	B	0.899
16-1-10	53.62	8.36	F-C	0.516
25-1-10	60.94	4.97	F-C	0.341
32-1-10	66.05	4.19	F-C	0.338
16-2-10	60.26	8.42	F-C	0.580
25-2-10	67.93	5.30	F-C	0.380
32-2-10	79.69	4.85	F-C	0.408
16-3-10	72.27	8.98	F-C	0.696
25-3-10	101.57	7.26	B	0.579
32-3-10	101.98	5.18	B	0.522

5.4.2 Discussion

Table 5-30 summaries the flexural strength of RC beam under category of different localized strength of concrete. Table 5-31 summaries the flexural strength of RC beams under category of location where the localized low strength concrete occurs. Table 5-32 summaries the flexural strength of RC beams under category of different rebar size when localized low strength concrete occur at the same place. As can be seen from these tables, the numbers vary irregularly because the mechanism of flexural strength affected by the localized low strength concrete is complex.

Strength

When the strength of localized concrete is high enough for the reinforcement to develop its stress, there is little influence of the flexural capacity of RC beams even when the localized low strength concrete decrease.

When the strength of localized concrete is in effective range, the flexural strength of RC beams will decrease based on the reduction of localized low strength concrete.

Location

The bending zone is most critical, the shear zone is second critical zone and the bond zone is the least critical zone when the reinforcement of beams are capable of developing its strength.

If the strength of concrete is high, no matter where the localized concrete defects occur, it has little impact on the flexural strength of the RC structure because the reinforcement are still capable of development its stress to yielding point before the concrete crush.

When the concrete strength is in appropriate range, the effects of localized low strength concrete in middle of the beam, where the highest compressive stress occur, is the most critical. And the impact of localized low strength concrete at the support end is the least critical under this circumstance.

When the localized strength concrete is very low, the location of the concrete defects takes place has little impact on the flexural strength of concrete.

If the beam does not provide sufficient development length originally and the concrete defect occurs at the support end of the beam, the beam must be fail in bond as same as the original one.

Rebar Size

For small size reinforcement, no matter where the localized strength concrete occurs, there is little effect on the flexural strength of the RC members.

When the size of reinforcement is big, beams need long development length. Generally, the impacts of localized low strength concrete of larger size rebar are less than that of the small size rebar. When the rebar sizes are small, the flexural strength of RC beams will decrease a lot.

When the beam has big reinforcement, the localized low strength could be more affected by the bond problem. When the beams are reinforced with small size rebar. Bond problem will not affect the flexural strength of the RC members.

For 16mm, the bending volume is more critical than the shear sensitive region. And sometimes bond sensitive region have little effect on the flexural strength of the RC structures because the compressive stress of concrete near the support are smaller

than the middle one. Once the stirrups provide enough confinement, there will be little effect on the load capacity of the beam when concrete defects occur at the bond sensitive region.

Chapter 6 PRACTICAL MODEL

6.1 General

The practical model should be able to predict the performance of beams subjected to these failures:

Flexural Tension Control Failure – A reinforced concrete beam with localized low strength concrete problem is supposed to fail in flexural tension mode, the reinforcement yield first, then followed by concrete crush.

Flexural Compression Control Failure - If a beam is over reinforced, concrete crushes before the reinforcement yield. Then the critical failure surface of concrete is probably at the interface between localized low strength concrete and good concrete.

Bonding failure – A beam that fails in bond is a complex mechanism.

Two approaches, a specific approach which can work for particular beams and a generalized approach which can work for any beams that meets the assumptions are proposed in this report. Both of them are constructed based on results of 30 cases discussed before plus some results under boundary condition (e.g., when f'c=0 MPa, load capacity is 0).

To find out the fundamental rules of the effect of localized low strength on the flexural strength of RC beams, a new parameter, relative defect concrete position, which is the ratio of distance from center of localized poor concrete to the support end, is introduced here to describe the behavior of the RC beams (as shown in Figure 6-1).

For all the cases discussed above, when the localized low strength concrete occurred at the bond sensitive zone (support end), the center of the poor concrete to the support end was considered to be ,

$$\frac{x}{L} = \frac{200}{1400} \times \frac{1}{2} = 0.071$$

For all the cases discussed above, when the localized low strength concrete occurred at shear sensitive zone (location 2), the center of the poor concrete to the support end was considered to be ,

$$\frac{x}{L} = \frac{400 + 250}{1400} \times \frac{1}{2} = 0.232$$

For all the cases discussed above, when the localized low strength concrete occurred at bending sensitive region (location 3), the center of the poor concrete to the support end was considered to be ,

$$\frac{x}{L} = \frac{400 + 500 + 250}{1400} \times \frac{1}{2} = 0.41$$

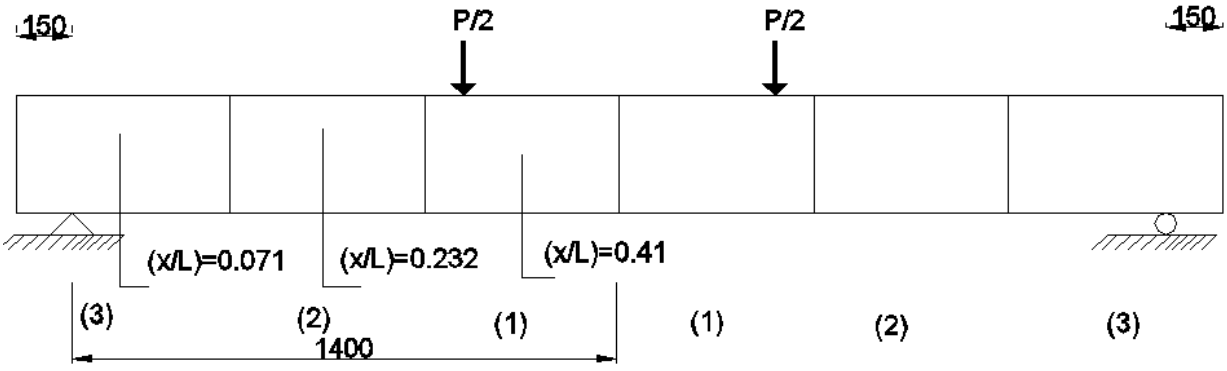

Figure 6-1 Ratio of distance from center of honeycombing to support

6.2 Specific model for existing cases

6.2.1 16mm rebar size

For all the cases 16mm, a parameter, named structural performance index, is defined by ($P_{localized}/P_{original}$). For all the cases related to 16mm rebar, the $P_{original}$ is referred to be the applied force P=104.21kN. $P_{localized}$ is referred to be the critical force for all the other cases subjected to localized low strength concrete.

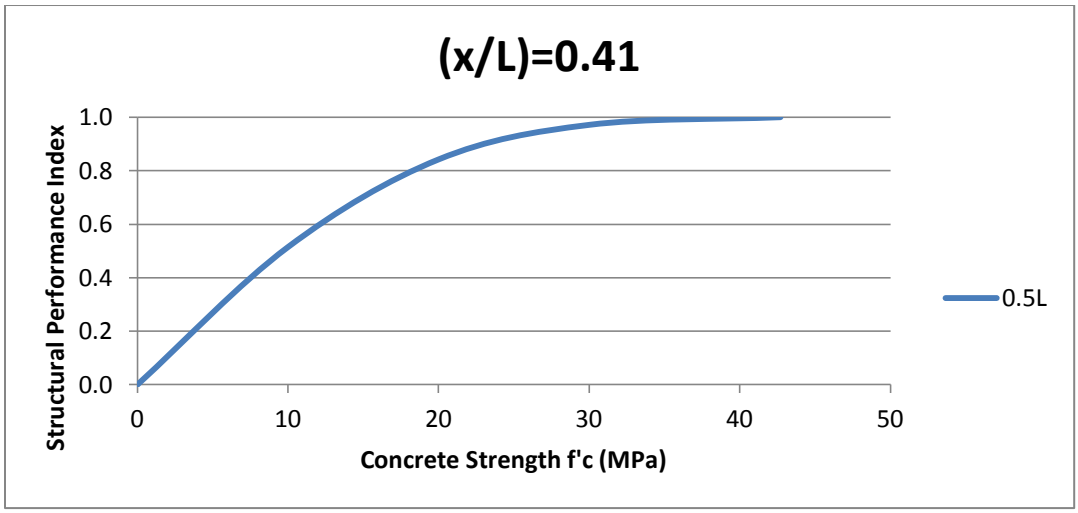

Figure 6-2 localized concrete degradation on bending region (16mm rebar)

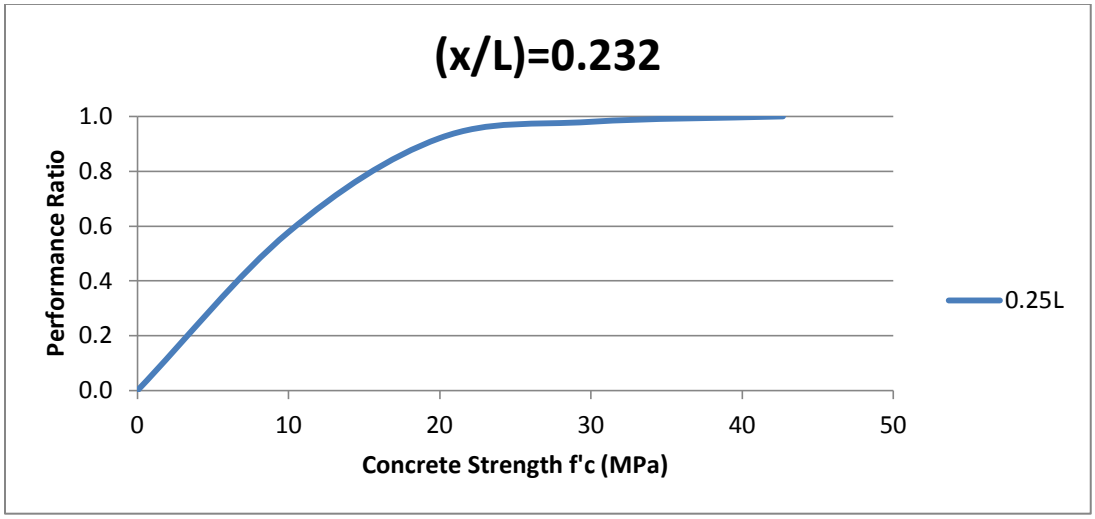

Figure 6-3 localized concrete degradation on shear region (16mm rebar)

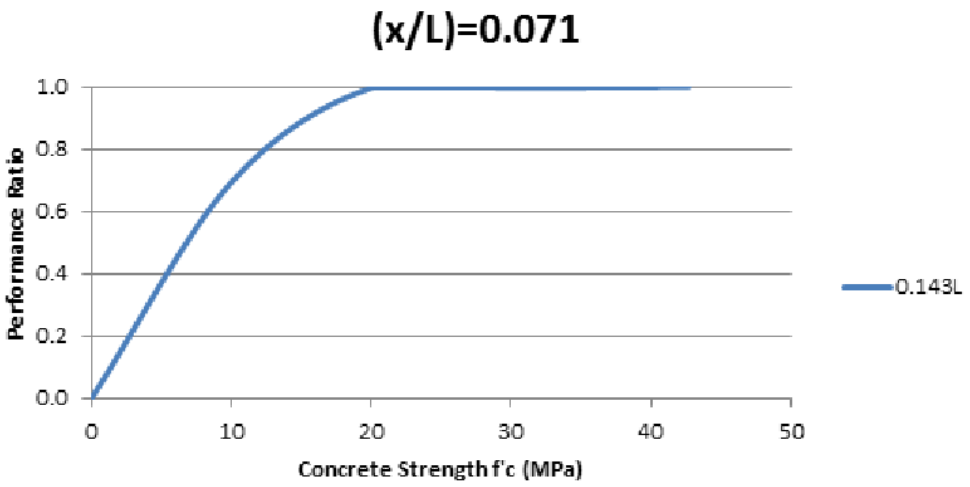

Figure 6-4 localized concrete degradation on bond region (16mm rebar)

Table 6-1 Summary of structural performance index (16mm rebar)

Structural Performance Index (16mm)		Relative defective concrete position (x/L)		
		0.41	0.232	0.071
Localized strength concrete (MPa)	42.7	1	1	1
	30	0.971	0.980	0.996
	20	0.842	0.921	0.996
	10	0.515	0.578	0.693
	0	0	0	0

Figure 6-2, Figure 6-3 and Figure 6-4 show the processed data after replacing all the original ultimate force with structural performance index, ratio of poor concrete to support end. Table 6-1 supplement the information in details. This information will be plotted in 3-D space. Then the data will then be expanded by linear interpretation to show the underlying behavior of localized degradation of beams reinforced with 16mm rebar.

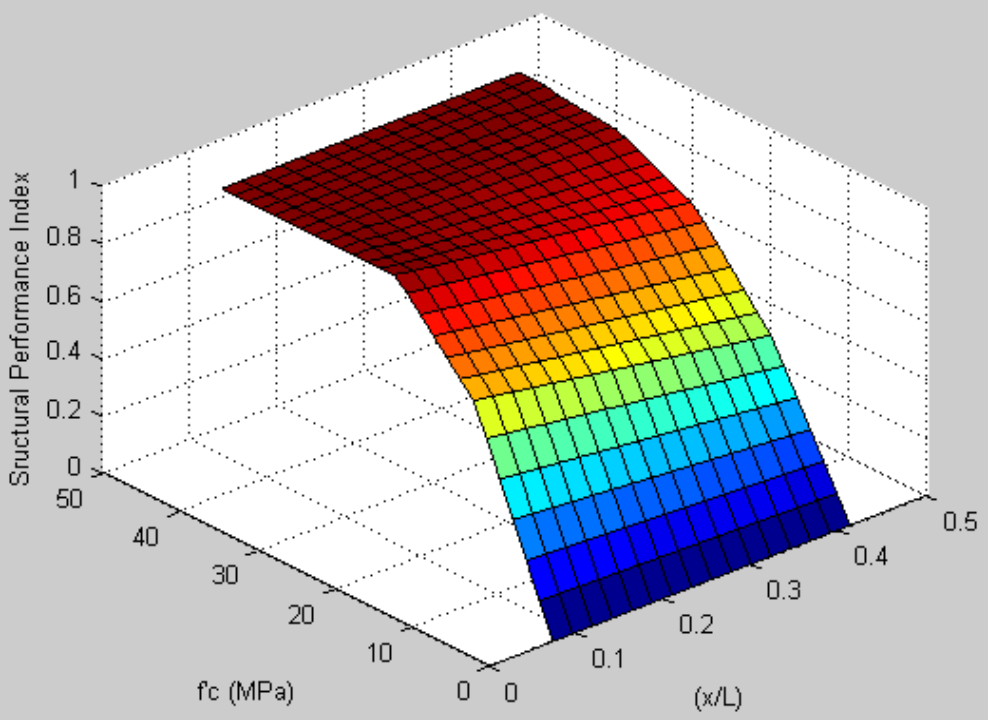

Figure 6-5 behavior of 16mm rebar under localized low f'c in 3D

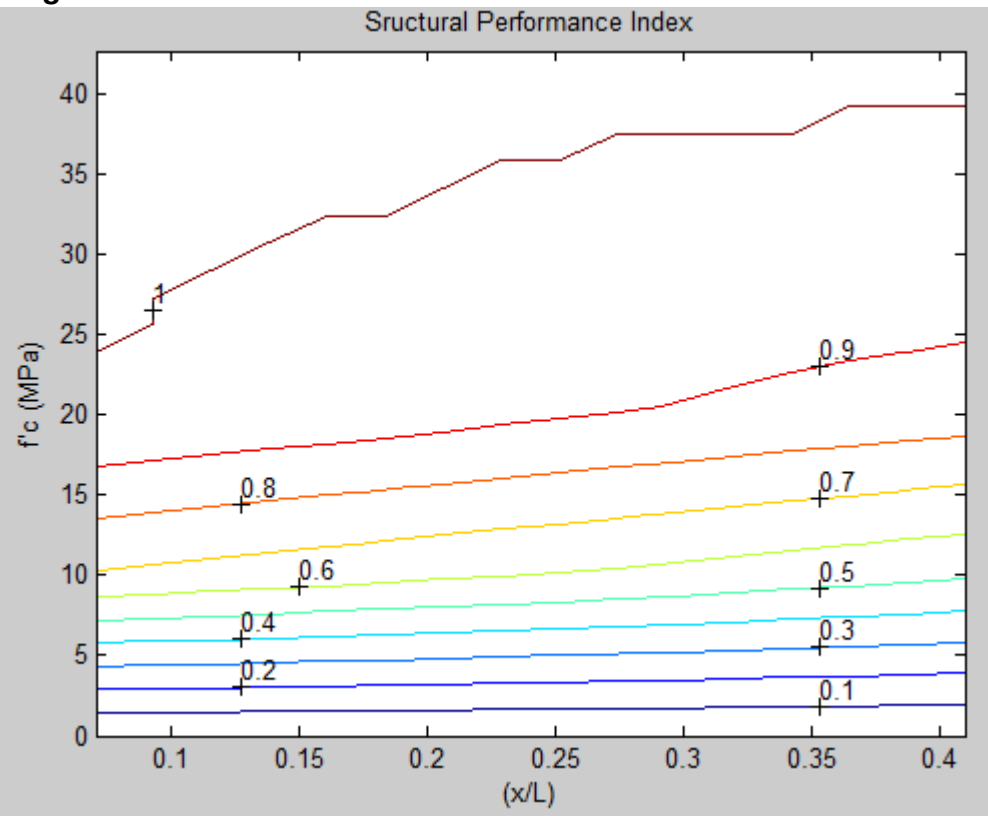

Figure 6-6 behavior of 16mm rebar under localized low f'c in 2D

After linear interpolation, particular empirical model can be achieved from the expanded data. They are presented in Figure 6-5 and Figure 6-6. This structural performance index chart can be used to primarily estimate the reduction of flexural strength for specific beams reinforced with 16mm rebar.

6.2.2 25mm rebar size

For all the cases 25mm, a parameter, named structural performance index, is defined by ($P_{localized}/P_{original}$). For all the case related to 25mm rebar, the $P_{original}$ is referred to be the applied force P=178.92kN. $P_{localized}$ is referred to be the critical force for all the other case subjected to localized low strength concrete.

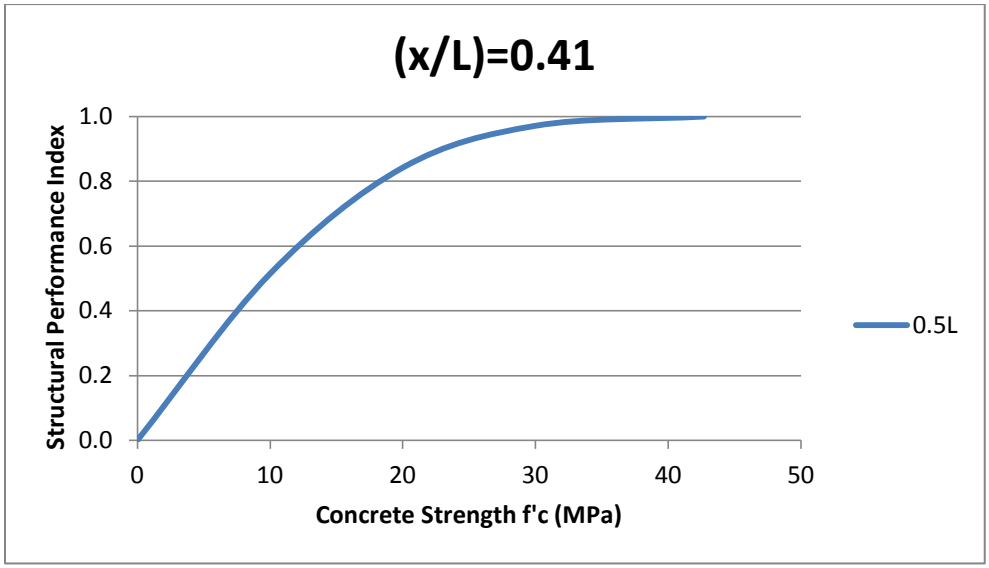

Figure 6-7 localized concrete degradation on bending region (25 mm rebar)

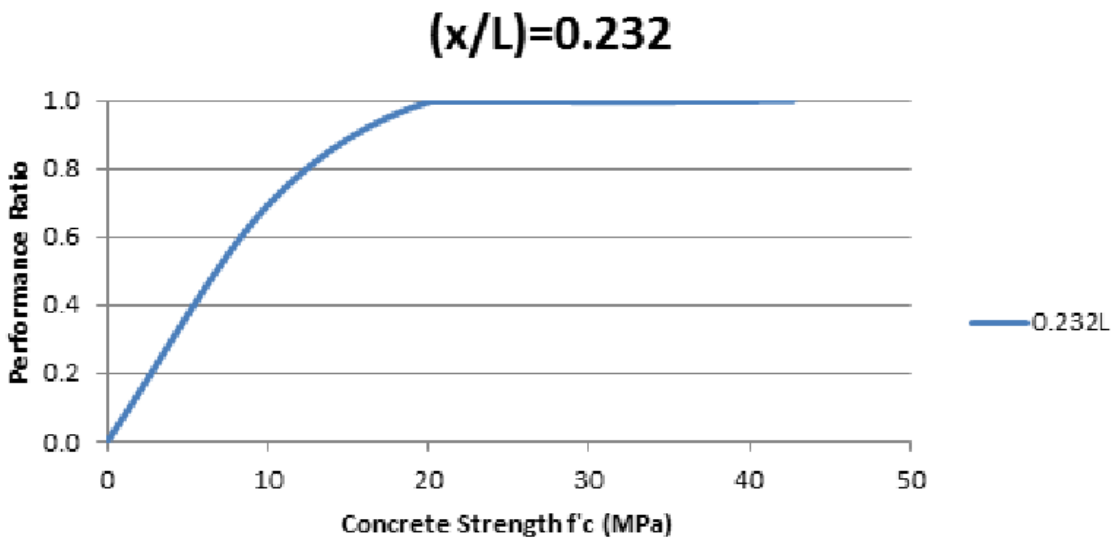

Figure 6-8 localized concrete degradation on shear region (25mm rebar)

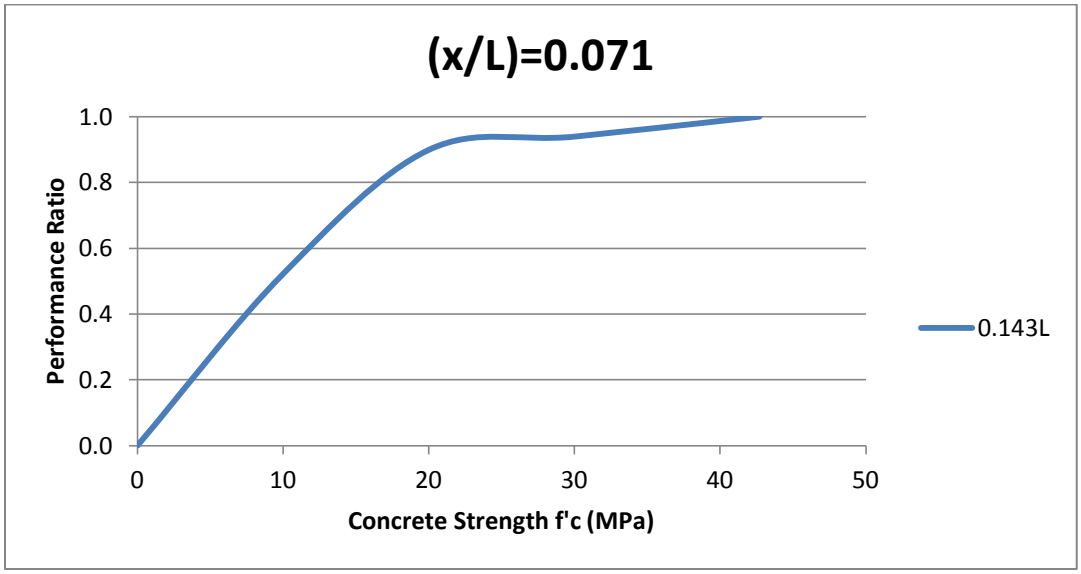

Figure 6-9 localized concrete degradation on bond region (25mm rebar)

Table 6-2 Summary of structural performance index (25mm rebar)

Structural Performance Index (25mm)		Relative defective concrete position (x/L)		
		0.41	0.232	0.071
Localized strength concrete (MPa)	42.7	1	1	1
	30	0.900	0.935	0.972
	20	0.532	0.644	0.720
	10	0.341	0.380	0.568
	0	0	0	0

Figure 6-7, Figure 6-8 and Figure 6-9 show the processed data after replacing all the original ultimate force with structural performance index, ratio of poor concrete to support end. Table 6-2 shows the information in details. This information will be plot in 3-D space. The data will be then expanded by linear interpretation to show the underlying behavior of localized degradation of beams reinforced with 25mm rebar

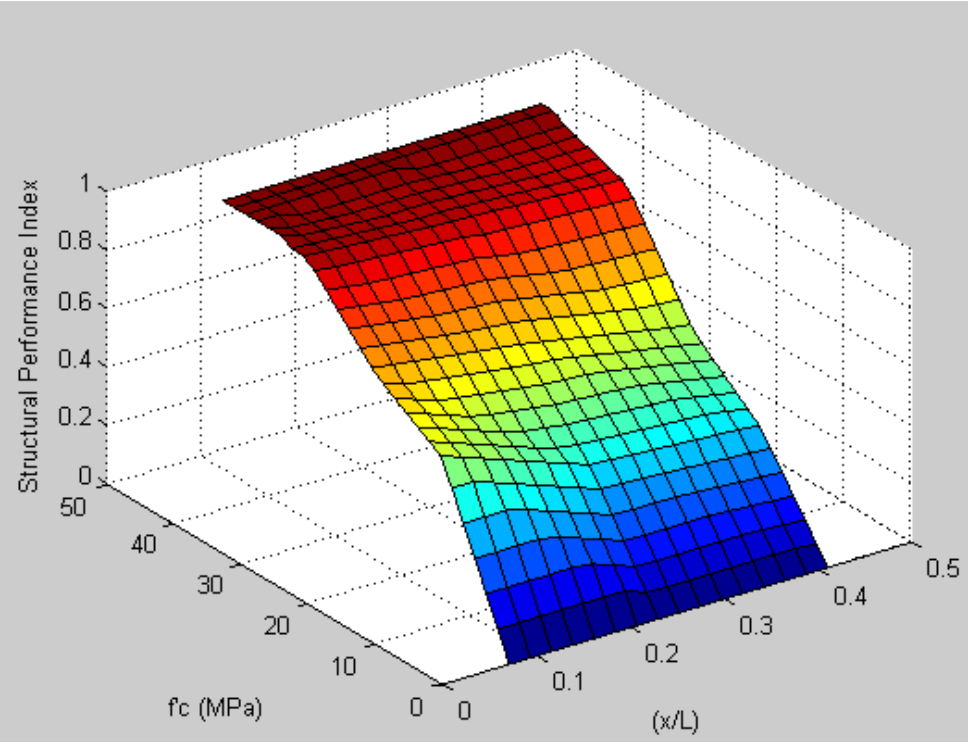

Figure 6-10 behavior of 25mm rebar under localized low f'c in 3D

After linear interpolation, empirical model can be achieved from the expanded data of 25mm. They are presented in Figure 6-10 and Figure 6-11. This structural performance index chart can be used to primarily estimate the reduction of flexural strength for specific beams reinforced with 25mm rebar.

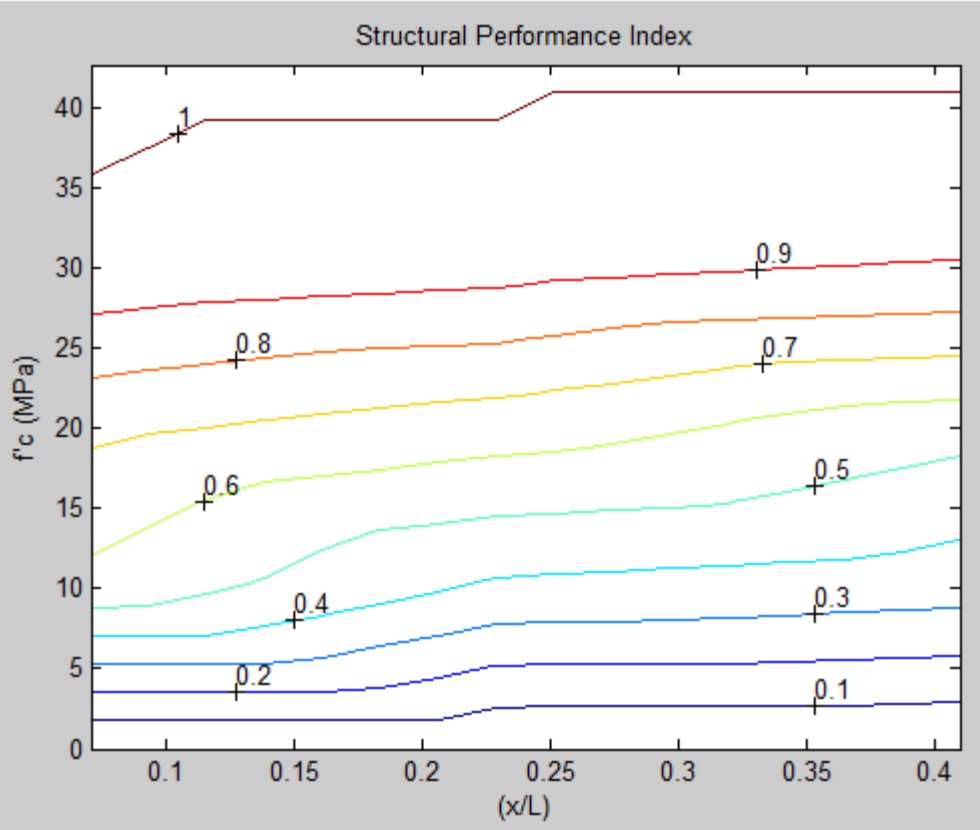

Figure 6-11 behavior of 25mm rebar under localized low f'c in 2D

6.2.3 32mm rebar size

For all the cases 32mm, a parameter, named structural performance index, is defined by (Plocalized/Poriginal). For all the cases related to 32mm rebar, the $P_{original}$ is referred to be the applied force P=195.42kN. $P_{localized}$ is referred to be the critical force for all the other case subjected to localized low strength concrete.

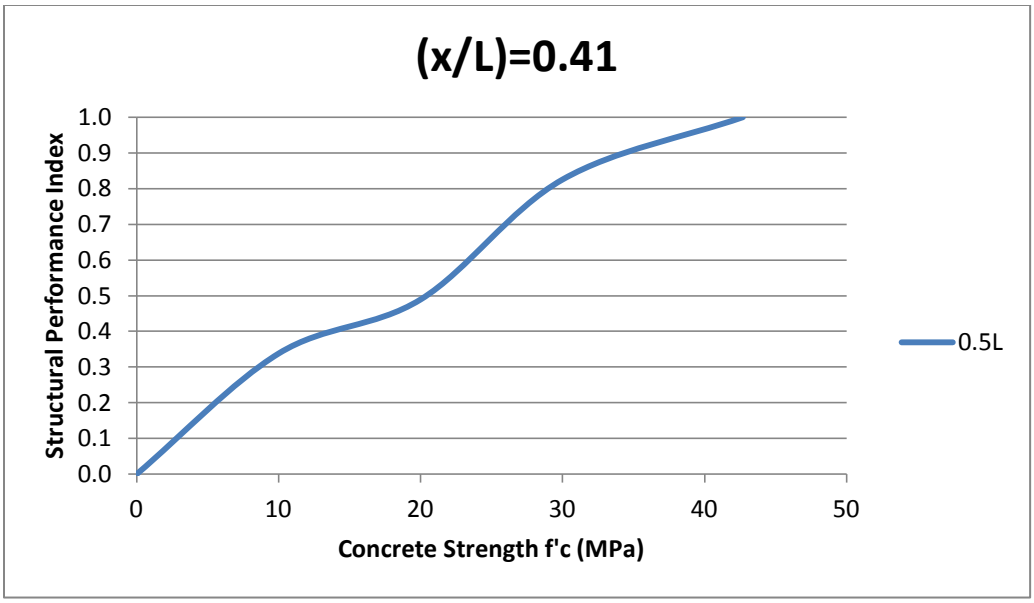

Figure 6-12 localized concrete degradation on shear region (32mm rebar)

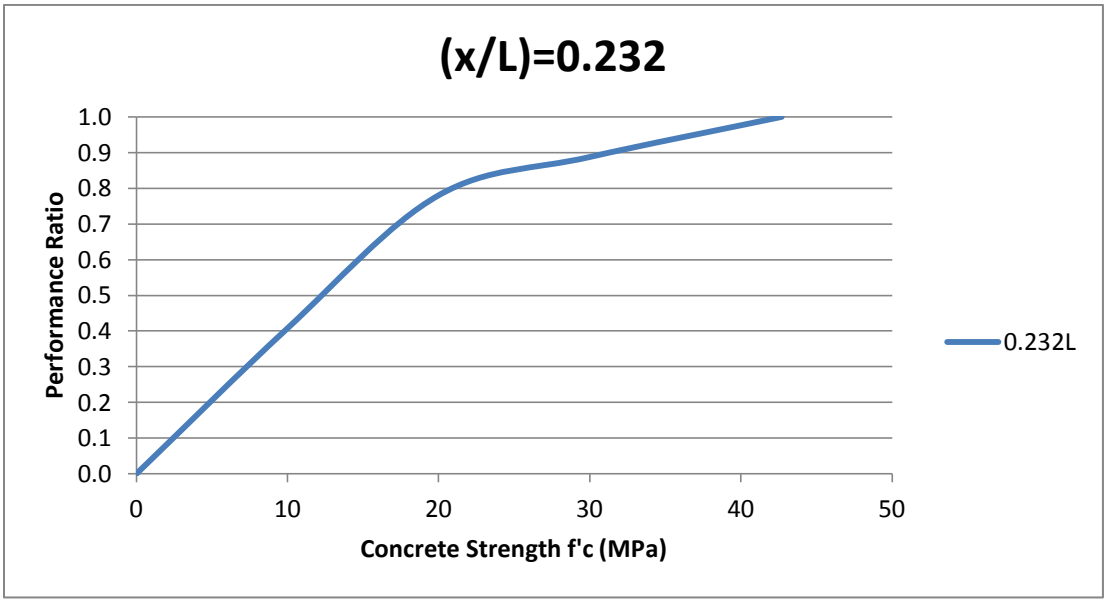

Figure 6-13 localized concrete degradation on shear region (32mm rebar)

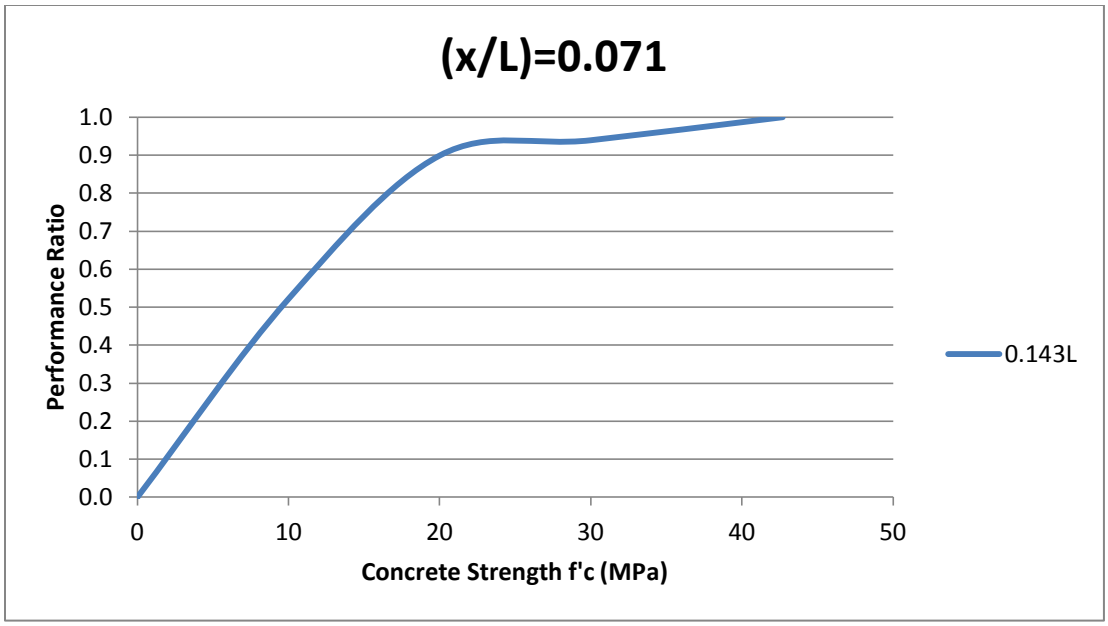

Figure 6-14 localized concrete degradation on shear region (32mm rebar)

Table 6-3 Summary of structural performance index (32mm rebar)

Structural Performance Index (32mm)		Relative defective concrete position (x/L)		
		0.41	0.232	0.071
Localized strength concrete (MPa)	42.7	1	1	1
	30	0.825	0.888	0.939
	20	0.489	0.780	0.899
	10	0.338	0.408	0.522
	0	0	0	0

Figure 6-12, Figure 6-13, and Figure 6-14 show the processed data after replacing original ultimate force with structural performance index, ratio of poor concrete to support end. And Table 6-3 shows the information in details. This information will be plotted in 3-D space. The values between lines are the structural performance indexed numbers. They indicate the percentage of remaining flexural strength compared to the original performance. The data will be then expanded by linear interpretation to show the underlying behavior of localized degradation of beams reinforced with 32mm rebar

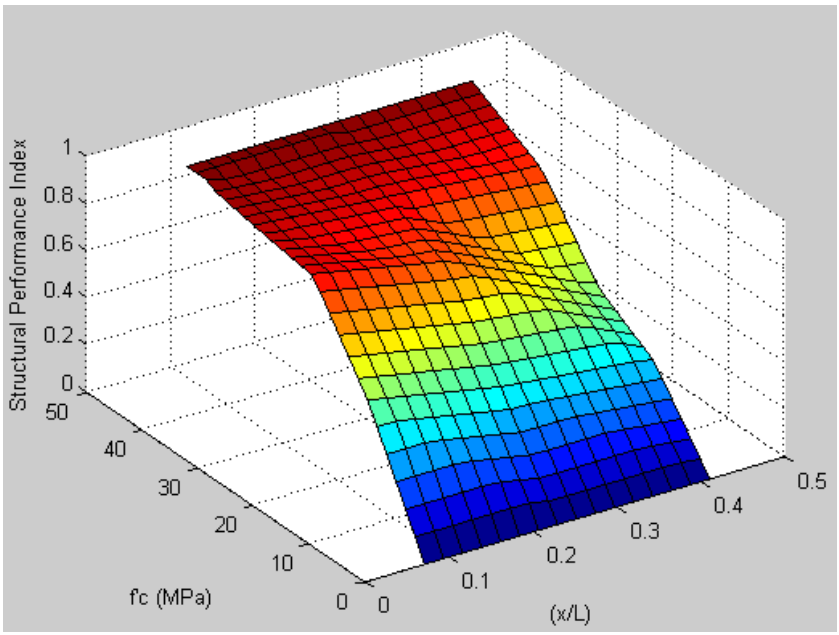

Figure 6-15 behavior of 32mm rebar under localized low f'c in 3D

After linear interpolation, empirical model can be achieved from the expanded data of 32mm. They are presented in Figure 6-15 and Figure 6-16. This structural performance index chart can be used to primarily estimate the reduction of flexural strength for specific beams reinforced with 32mm rebar.

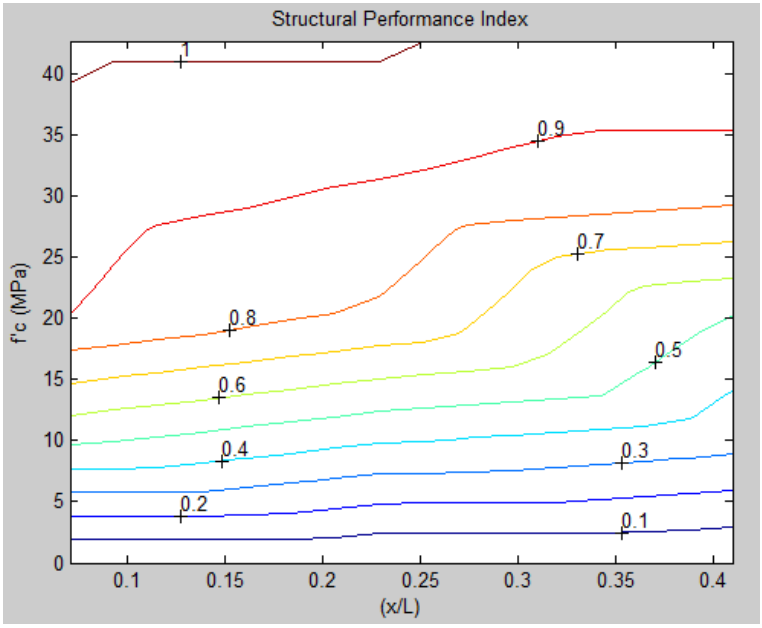

Figure 6-16 behavior of 32mm rebar under localized low f'c in 2D

6.3 Proposed generalized approach

Before developing a generalized empirical model, several assumptions were used in the flexural analysis of localized low strength reinforced concrete beams:

- Plane sections before loading remain plane after loading.
- Tensile strength of concrete is neglected.
- Bond between the concrete and steel reinforcement is simulated according to CEB-FIP model 2010.
- The original flexural strength of the structural member is assumed to be the designed nominal strength moment calculated based on ACI code
- Defective concrete is considered to be 500mm long at both sides because this model is empirical model and the honeycombing length in paper are assumed to be 500mm long.
- The load is assumed to be applied 400mm away from the center of the beams for both sides.
- The localized low strength concrete at problem volume is assumed to be a constant.
- The section of the RC beam is assumed to be rectangular

To propose a generalized practical model for the beams with localized concrete defects, all these data needed to be presented in a uniform method. Three important parameters are used here, as shown below.

6.3.1 Relative defective concrete position (x/L)

This parameter is defined the same as the one mentioned before. It is the ratio of distance from center of localized poor concrete to the support end.

6.3.2 Generalized structural performance index number

Generalized structural performance index number is defined by

$$GSPI = \frac{P_{localized}}{P_{ACI}} \tag{6.1}$$

The targeted structural member is assumed to have sufficient development length that the reinforcement and yield before the concrete crush. In this case, the predicted ultimate load P_{ACI} can be computed based on nominal moment from ACI equation

$$M_n = A_s F_y \times \left(d - \frac{a}{2} \right) \tag{6.2}$$

Where

F_y = the yielding strength of reinforcement

d= effective depth of the reinforced concrete

a=depth of equivalent rectangular stress block

Using equilibrium in Figure 6-17, applied force P can be obtained as $P=M_n$.

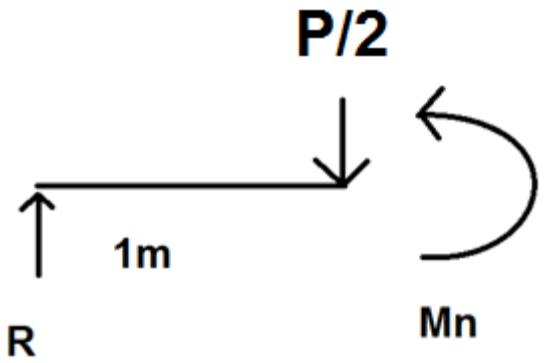

Figure 6-17 Simplified analytical model for all cases

For cases with 16mm rebar, the reference nominal moment is defined,

$$a_{16} = \frac{A_s \cdot f_y}{0.85 \cdot f'_c \cdot b} = 37.798mm$$

$$P_{ACI16} = 2 \times M_n = A_s \cdot f_y \cdot \left(d - \frac{a}{2} \right) = 105.402kN$$

For cases with 25mm rebar, the reference nominal moment is defined,

$$a_{25} = \frac{A_s \cdot f_y}{0.85 \cdot f'_c \cdot b} = 92.281mm$$

$$P_{ACI25} = 2 \times M_n = A_s \cdot f_y \cdot \left(d - \frac{a}{2} \right) = 229.958kN$$

For cases with 32mm rebar, the reference nominal moment is defined,

$$a_{25} = \frac{A_s \cdot f_y}{0.85 \cdot f'_c \cdot b} = 151.193mm$$

$$P_{ACI32} = 2 \times M_n = A_s \cdot f_y \cdot \left(d - \frac{a}{2} \right) = 328.27kN$$

6.3.3 Development sufficiency (L_{pd}/L'_d)

L_{pd}= provided development length, for beams subjected to concentrated load, the provided length is from the support to where the applied load is. for beams subjected to uniform load, the provided development length is half the beam.

L'_d = modified localized development length after the equations in ACI318M for beams which subjected to localized concrete degradation.

For the No. 19 and smaller deformed bars,

$$L'_d = \sum_i^n \Phi_i \frac{L_i}{L} \times \left(\frac{f_y}{2.1\sqrt{f'_{ci}}}\right) \times d_b \quad (6.3)$$

For the No. 22 and bigger deformed bars,

$$L'_d = \sum_i^n \Phi_i \frac{L_i}{L} \times \left(\frac{f_y}{1.7\sqrt{f'_{ci}}}\right) \times d_b \quad (6.4)$$

Where, Φ is location related factor, for concrete defect occurs in bond sensitive region, Φ=1.2 {from (x/L) to 0.167(x/L)}, for concrete defect occurs in shear sensitive region, Φ=1.05{from 0.133(x/L) to 0.333(x/L)}, for concrete defect occurs in bending sensitive region Φ=1{from 0.333(x/L) to 0.5(x/L)}.

L_i = the length of i^{th} segment of beam

f'_{ci} = the localized strength for i^{th} concrete

L = total span length

d_b= the diameter of the tensile reinforcement

Applying eqn(6.3) and eqn (6.4) , a uniform data can be achieved as listed in Table 6-4and Table 6-5.

Table 6-4 Localized development length

16mm (provided development length =1000mm)				
Required development length (L'd)		Relative defective concrete position (x/L)		
		0.41	0.232	0.071
Localized concrete strength f'c (MPa)	42.7	596.98	607.64	631.09
	30	638.13	650.85	670.60
	20	695.30	710.87	725.48
	10	824.34	846.37	849.36
	0	0.00	0.00	0.00
25mm (provided development length =1000mm)				

Required development length (L'd)		Relative defective concrete position (x/L)		
		0.41	0.232	0.071
Localized concrete strength f'c (MPa)	42.7	1152.25	1172.83	1218.09
	30	1231.69	1256.24	1294.35
	20	1342.03	1372.09	1400.28
	10	1591.09	1633.61	1639.38
	0	0	0	0
32mm (provided development length =1000mm)				
Required development length (L'd)		Relative defective concrete position (x/L)		
		0.41	0.232	0.071
Localized concrete strength f'c (MPa)	42.7	1474.88	1501.22	1559.16
	30	1576.56	1607.98	1656.77
	20	1717.80	1756.28	1792.36
	10	2036.60	2091.02	2098.41
	0	0	0	0

Table 6-5 Uniform ratio of load distance to development

16mm (provided development length =1000mm)				
Development Sufficiency (Lpd/L'd)		Relative defective concrete position (x/L)		
		0.41	0.232	0.071
Localized concrete strength f'c (MPa)	42.7	1.675	1.646	1.585
	30	1.567	1.536	1.491
	20	1.438	1.407	1.378
	10	1.213	1.182	1.177
	0	0.000	0.00	0.00
25mm (provided development length =1000mm)				
Development Sufficiency (Lpd/L'd)		Relative defective concrete position (x/L)		
		0.41	0.232	0.071
Localized concrete strength f'c (MPa)	42.7	0.87	0.85	0.82
	30	0.81	0.80	0.77
	20	0.75	0.73	0.71

	10	0.63	0.61	0.61
	0	0	0	0
32mm (provided development length =1000mm)				
Development Sufficiency (Lpd/L'd)		Relative defective concrete position (x/L)		
		0.41	0.232	0.071
Localized concrete strength f'c (MPa)	42.7	0.68	0.67	0.64
	30	0.63	0.62	0.60
	20	0.58	0.57	0.56
	10	0.49	0.48	0.48
	0	0	0	0

Table 6-6 Existing sampling data after manipulation

Relative defect position (x/L)	Development sufficiency ratio ($L_{pd}L/L'_d$)	localized concrete strength f'c (MPa)	Generalized structural performance index
0.410	1.675	42.7	0.989
0.410	1.567	30.0	0.960
0.410	1.438	20.0	0.833
0.410	1.213	10.0	0.509
0.410	0.000	0.0	0.000
0.232	1.646	42.7	0.989
0.232	1.536	30.0	0.969
0.232	1.407	20.0	0.911
0.232	1.182	10.0	0.572
0.232	0.000	0.0	0.000
0.071	1.585	42.7	0.989
0.071	1.491	30.0	0.985
0.071	1.378	20.0	0.985
0.071	1.177	10.0	0.686
0.071	0.000	0.0	0.000
0.410	0.868	42.7	0.778
0.410	0.812	30.0	0.700
0.410	0.745	20.0	0.414
0.410	0.628	10.0	0.265
0.410	0.000	0.0	0.000

0.232	0.853	42.7	0.778
0.232	0.796	30.0	0.728
0.232	0.729	20.0	0.501
0.232	0.612	10.0	0.295
0.232	0.000	0.0	0.000
0.071	0.821	42.7	0.778
0.071	0.773	30.0	0.757
0.071	0.714	20.0	0.561
0.071	0.610	10.0	0.442
0.071	0.000	0.0	0.000
0.410	0.678	42.7	0.595
0.410	0.634	30.0	0.492
0.410	0.582	20.0	0.291
0.410	0.491	10.0	0.201
0.410	0.000	0.0	0.000
0.232	0.666	42.7	0.595
0.232	0.622	30.0	0.528
0.232	0.569	20.0	0.465
0.232	0.478	10.0	0.243
0.232	0.000	0.0	0.000
0.071	0.641	42.7	0.595
0.071	0.604	30.0	0.559
0.071	0.558	20.0	0.535
0.071	0.477	10.0	0.311
0.071	0.000	0.0	0.000

All 30 finite element analysis solutions calculated and discussed before are processed in Table 6-6 plus some boundary condition data through the four defined parameters. They are plotted in Figure 6-18.

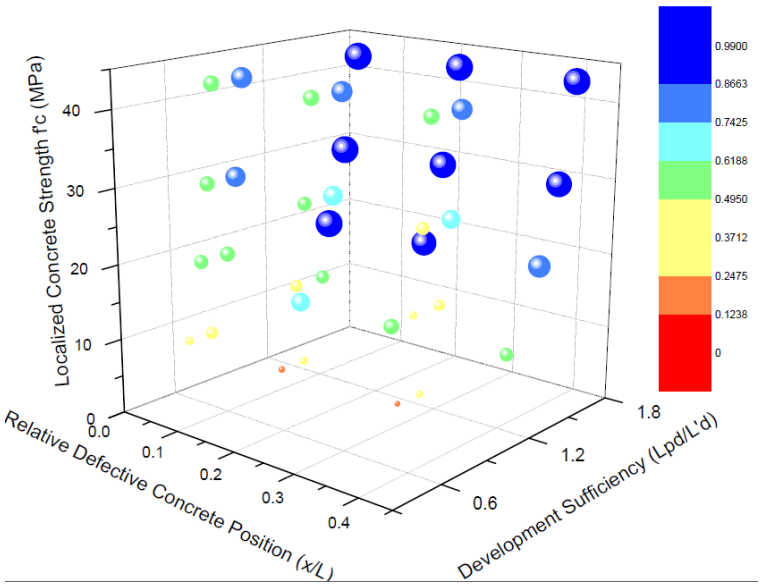

Figure 6-18 Existing generalized model sample

The bubble size and color are scaled according to the global structural performance index number in Table 6-6.

Then these existing samples will be used to generate an expanded generalized practical mode for RC members subjected to localized low strength concrete. A modification of Shepard's method is used here to do the 3-D interpolation job. The algorithm is described as below:

A function constructs a smooth function Q(x,y,z) which interpolates a set of m scattered data points (x_r,y_r,z_r,f_r) for r=1,2,…m, using a modification of Shepard's method, and then evaluates the interpolant at the set of selected points (u_r,v_r,w_r), as well as its first partial derivatives. The surface is continuous and has continuous first partial derivatives.

$$Q(x,y,z,) = \frac{\sum w_r(x,y,z) \times q_r}{\sum w_r(x,y,z)} \tag{6.5}$$

Where $q_r = f_{r,} w_r (x, y, z) = \frac{1}{d^2_r}$, $d^2_r = (x - x_r)^2 + (y - y_r)^2 + (z - z_r)^2$

After the 3-D interpolation is done, a generalized practical model produced from existing data can be set up. The empirical mode can be visually presented in Figure 6-19. The bubble size and color are scaled according to the global structural performance index number after linear interpolation. Samples of the generalized practical model are listed in Figure 6-20, Figure 6-21 and Figure 6-22.

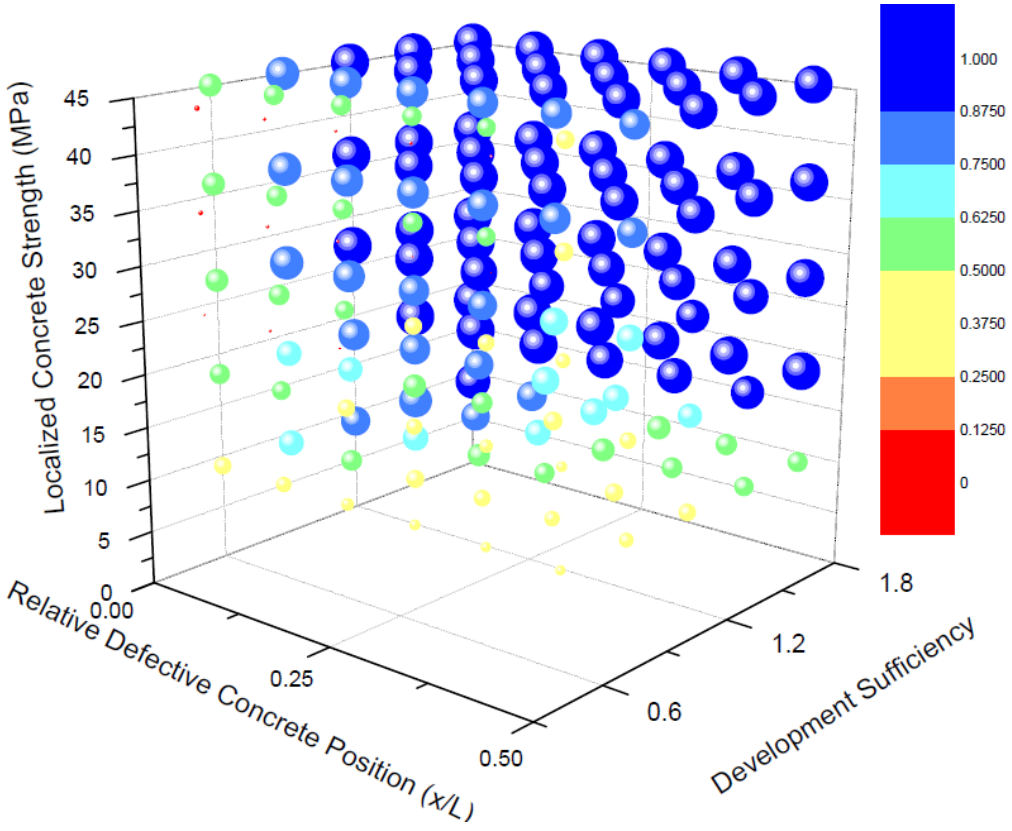

Figure 6-19 Generalized practical model

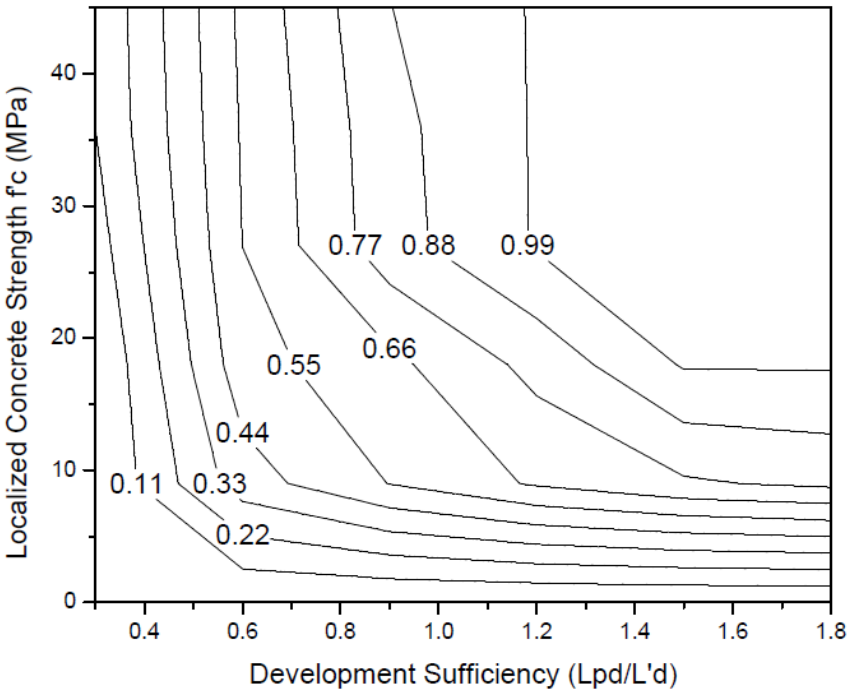

Figure 6-20 Slice of practical model when (x/L) =0.09

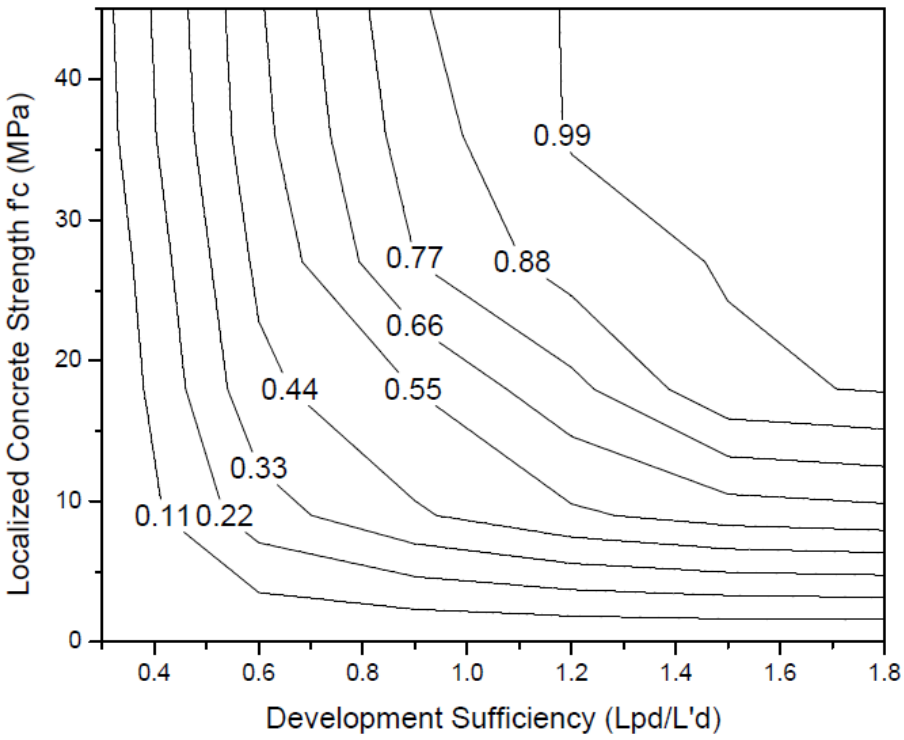

Figure 6-21 Slice of practical model when (x/L) =0.27

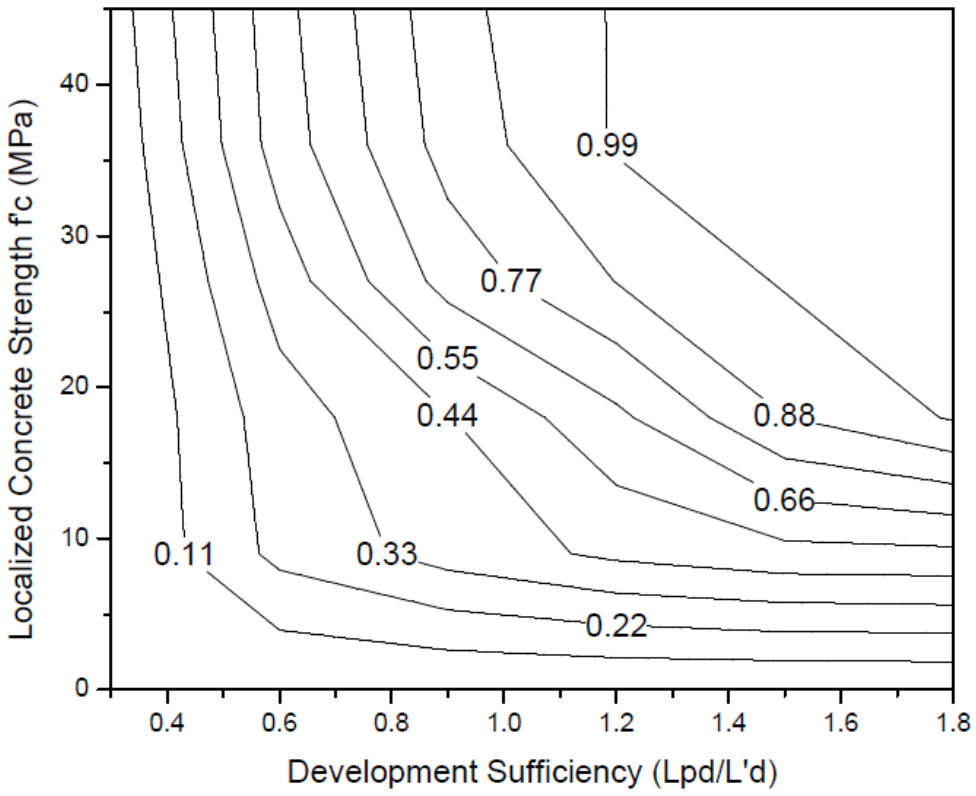

Figure 6-22 Slice of practical model when (x/L) =0.45

6.4 Assessment procedure for RC beams with low f'c

With the generalized empirical model abstracted from finite element experiment, it is feasible to assess the structural performance for the structural member needed to be evaluated.

1) Measure the distance from the center of the honeycombing concrete to the beam's support end. (x/L). The relative defect position (x/L) should be taken as the center of the damaged concrete.

2) Rebound hammer test to obtain the localized concrete strength f'c.

3) Get the reinforcement information and calculate the development sufficiency.

4)

a. Using the structural performance chart provided in the paper (range from Figure 6-20 to Figure 6-22). And do a linear interpolation from these generalized structural performance charts to get the generalized structural performance index for the inspected members.

b. Or constructing own structural performance index chart with respect to the structural member for the localized concrete problem based on experiment and the generalized approach discussed in previous sections. Once the structural performance chart is constructed, follow linear interpolation in step (4.a)

5) Read the GSPI from the chart directly or using linear interpolation, and calculate the remaining flexural capacity by multiplying the GSPI value by the original flexural strength based on ACI code.

Chapter 7 CONCLUSIONS AND RECOMMENDATIONS FOR FUTURE WORK

7.1 Summary and Conclusions

This study introduces a finite element modeling method to simulate the flexural strength of real concrete which is subjected to a localized defect like honeycombing. Two verification programs were used to calibrate the accuracy of the finite elements model. The solutions of finite element model in macroscopic and microscopic both match the experiment result well, which also proof the accuracy of the program. Then the material properties of finite element model were changed to simulate the localized concrete physical behavior in real world. The responses of 30 beams in many aspects were carefully analyzed.

In general, if a reinforced beam is strong and long enough to prevent the structural member fail in bond, the middle portion of the beam is the most critical region. When the localized concrete defect occurs in the bending zone of reinforced concrete beams, the reduction of flexural strength for that beam is the largest.

The data of all finite element beams were collected and a generalized structural performance assessment approach was proposed in the paper and can be used to predict the performance of RC beams considering the localized low strength concrete problems. It could work for both concentrated and distributed load. The generalized structural performance charts provided based on linear interpolation can be used to predict the reduction effect numerically. However, this model is still an empirical model based on existing data. Proposing a uniform formula to describe structural performance index behavior is very difficult, because many factors could affect the result of the chart.

In conclusion, the basic behavior with respect to the change of flexural strength of RC beams under localized concrete degradation is present and well matches the solutions. With the generalized structural performance index model, we could predict the fundamental behavior of a partially inferior concrete structural member, and the potential structural brittle failure, which is the most dangerous situation.

7.2 Recommendations for Future Research

Experiment validation

As only experiments of ordinary reference beams can be found, experiment cost and time, the FEM solutions have no chance to compare with a beam having localized low strength concrete problem. Future research can set up an experiment program to testify the FEM results with localized low strength concrete problem by following steps:

1. Constructing beams having the same dimensions, reinforcement and problem concrete the same as those cases in FEM.

2. Conducting experiments and get the results of these experiments.

3. Compare the experiments results with the FEM results.

4. If the experiment results get close to the FEM results, then the proposed assessment approach in the paper is verified

Other possible research

The load applied in this model is monotonic loading. The behavior of the deteriorated concrete under repeated loadings is still unknown.

The actual behavior of these concrete damaged concrete under severe seismic shaking are still unknown.

Predict the maximum midspan deflection and maximum impact load, which aids as an important performance index to evaluate the damage levels of RC beams when subjected to impact loadings.

AS sufficient amount of stirrups has been provided in this analysis, no shear failure occurs in the analysis. Future research could explore the shear failure.

In this paper, the RC beam was divided roughly based on the load response. A more accurate division for the RC beam regarding to the sensitivity for bending moment, shear force and bond force.

In this paper, only the longitudinal bond strength between steel and concrete have been considered, the transvers bond strength are assumed to be fully bonded, so a model including bond behavior can be added to the model in future research.

Only the most affected parameters are being analyzed in this paper whereas others are ignored, next research can investigate those parameters effect.

Only cases with concentrated load are being analyzed here, uniform load should be considered in future research.

Since the strength of the concrete are assumed in this paper due to lack of experimental data on relationship between concrete defects and concrete strength, future research can focus on setting up a numerical approach to assess the concrete strength under different situations.

In field, the honeycombing or other defected concrete is a continuous deteriorated model, but the problem is simplified as a discrete deteriorated model with

localized low strength concrete, so future research could build a continuous damaged concrete model.

The expected bond resistance for a localized low strength concrete is calculated based on CEB-FIP 2010 model. However, the real bond stress for a localized low strength concrete need to be investigated in details in the future.

Localized low strength concrete may have three different kinds of failure modes, flexural failure due to premature concrete crushing, flexural after the reinforcement has yielded, or bond failure. The critical point for these failure modes are very difficult to estimated due to the complex mechanism and heterogeneous material. Future research can investigate the critical turning point from one failure mode to the other.

Constructing a uniform structural performance index chart is very difficult. There are many coefficients that could affect the structural performance chart, and the mechanism of different failure also contributes to the complexity of making a structural performance index chart. Those factors that could affect this chart need more research before conclusion can be drawn.

In the generalized practical model, there is an expected fixed critical surface, which separates the flexural failure controlled by compression, flexural failure controlled by tension, and bond failure modes.

REFERENCES

Abrishami, Homayoun H., and Denis Mitchell. "Simulation of uniform bond stress." ACI materials Journal 89.2 (1992).

American Concrete Institution. **The Contractor's Guide to Quality Concrete Construction - Third Edition** (ACI-ASCC-1-2005). N.p.: 2005, n.d. Print.

ANSYS® Academic Research, Release 14.0, Help System, Theory Reference, ANSYS, Inc.

"ASCE | 2013 Report Card for America's Infrastructure." ASCE | 2013 Report Card for America's Infrastructure. N.p., n.d. Web. 03 Feb. 2014.

Barzegar-Jamshidi, Fariborz, and William C. Schnobrich. Nonlinear finite element analysis of reinforced concrete under short term monotonic loading. University of Illinois Engineering Experiment Station. College of Engineering. University of Illinois at Urbana-Champaign., 1986.

Bažant, Z. P., and Arthur H. Nilson. *State-of-the-art Report on Finite Element Analysis of Reinforced Concrete*. New York, NY: American Society of Civil Engineers, 1982. Print.

Braverman, J.I., Miller, C.A, Ellingwood, B.R., Naus, D.J., Hofmayer, C.H., Bezler, P., and Chang, T.Y.. “STRUCTURAL PERFORMANCE OF DEGRADED REINFORCED CONCRETE MEMBERS.” N. p., 2001.

Bresler, Boris, and Alex C. Scordelis. "Shear strength of reinforced concrete beams." ACI Journal Proceedings. Vol. 60. No. 1. ACI, 1963.

Bond and Development of Straight Reinforcing Bars in Tension(ACI 408R-03). Farmington Hills, MI: American Concrete Institute, 2003. Print.

"Bond Under Cyclic Loads (ACI 408.2R-92 R2005)." - American Concrete Institute / 01-Jan-1992 / 32 Pages. N.p., n.d. Web. 07 Mar. 2014.

Building Code Requirements for Structural Concrete (ACI 318-08) and Commentary. Farmington Hills, MI: American Concrete Institute, 2008. Print.

Building Code Requirements for Structural Concrete (ACI 318M-11) and Commentary. Farmington Hills, MI: American Concrete Institute, 2011. Print.

CEB-FIP Model Code 2010 fib Model Code for Concrete Structures 2010. Document Competence Center Siegmar Kästl e.K., Germany, 2010.

Chana, P. S. "Investigation of the mechanism of shear failure of reinforced concrete beams." Magazine of Concrete Research 39.141 (1987): 196-204.

Chen, Wai-Fah. "Chapter 1 - Introduction". **Plasticity in Reinforced Concrete**. J. Ross Publishing, © 2007. Books24x7. Web. Mar. 3, 2014.

Comité Euro-International du Beton (CEB) (1978). CEB-FIP Model Code of Concrete Structures. Bulletind'Information 124/125E, Paris, France.

"Guide to Concrete Repair." U.S. Department of the Interior | Bureau of Reclamation | Technical Service Center, 1996. Web.

C. Hsu, Thomas T., and Y. L Mo. "Chapter 9 - Finite Element Modeling of Frames and Walls". Unified Theory of Concrete Structures. John Wiley & Sons, © 2010. Books24x7. Web. Mar. 13, 2014.

Chen, F.W., 1982. “Plasticity in reinforced concrete”. McGraw-Hill, New York.

Darwin, David, and Ebenezer K. Graham. "Effect of deformation height and spacing on bond strength of reinforcing bars." ACI Structural Journal 90.6 (1993).

Desayi, Prakash, and S. Krishnan. "Equation for the stress-strain curve of concrete." ACI Journal Proceedings. Vol. 61. No. 3. ACI, 1964.

Eligehausen, Rolf, Egor P. Popov, and Vitelmo V. Bertero. "Local Bond Stress-slip Relationships of Deformed Bars under Generalized Excitations." The Earthquake Engineering Online Archive. National Science Foundation, Oct. 1983. Web.

Filippou, F. C., and A. Saritas. "A beam finite element for shear-critical RC beams." ACI Special Publication 237 (2006).

Gan, Youai. "Bond Stress and Slip Modeling in Nonlinear Finite Element Analysis of Reinforced Concrete Structures." University of Toronto's Research Repository. University of Toronto, 2000. Web.

Gilbert, R. Ian, and Robert F. Warner. "Tension stiffening in reinforced concrete slabs." Journal of the structural division 104.12 (1978): 1885-1900.

Gregori, J. Navarro, P. Miguel Sosa, M.a. Fernández Prada, and Filip C. Filippou. "A 3D Numerical Model for Reinforced and Prestressed Concrete Elements Subjected

to Combined Axial, Bending, Shear and Torsion Loading." Engineering Structures 29.12 (2007): 3404-419. Print.

Goto, Yukimasa. "Cracks formed in concrete around deformed tension bars." ACI Journal Proceedings. Vol. 68. No. 4. ACI, 1971.

Harajli, Mohamed H., Bilal S. Hamad, and Ahmad A. Rteil. "Effect of Confinement on Bond Strength between Steel Bars and Concrete." Structural Journal 101.5 (2004): 595-603. Print.

Hasegawa, T. "Numerical study of mechanism of diagonal tension failure in reinforced concrete beams." Fracture Mechanics of Concrete Structures (2004): 391-398.

Hasegawa, T. "Rebar bond slip in diagonal tension failure of reinforced concrete beams." Fracture Mechanics concrete and of Concrete Structures (2010). Print

Hognestad, E. (1951). "A Study of Combined Bending and Axial Load in Reinforced Concrete Members". University of Illinois Engineering Experiment Station, Bulletin Series No. 399, Bulletin No. 1.

Identification and Control of Visible Effects of Consolidation on Formed Concrete Surfaces(ACI 309.2R-98). Farmington Hills, MI: American Concrete Institute, 1998. Print.

Jain, Satish C., and John B. Kennedy. "Yield criterion for reinforced concrete slabs." Journal of the Structural Division 100.3 (1974): 631-644.

Jendele , Libor, and Jan Cervenka. "Finite element modelling of reinforcement with bond." Computers & structures 84.28 (2006): 1780-1791.

Karsan, I. Demir, and James O. Jirsa. "Behavior of concrete under compressive loadings." Journal of the Structural Division (1969).

Keuser, Manfred, and Gerhard Mehlhorn. "Finite element models for bond problems." Journal of Structural Engineering 113.10 (1987): 2160-2173.

Khalfallah, S. "MODELING OF BOND FOR PULL-OUT TESTS." Building Research Journal 56.1 (2008).

Kim, Sang Hun, and Riyad S. Aboutaha. "Ductility of Carbon Fiber-reinforced Polymer (CFRP) Strengthened Reinforced Concrete Beams: Experimental Investigation." Steel and Composite Structures 4.5 (2004): 333-53. Print.

K. J. Willam and E. D. Warnke. "Constitutive Model for the Triaxial Behavior of Concrete". Proceedings, International Association for Bridge and Structural Engineering. Vol. 19. ISMES. Bergamo, Italy. p. 174. 1975.

Kohnehpooshi, O., J. Noorzaei, M. S. Jaafar, A. A. Abdulrazeg, and M. R Saifulnaz Raizal. "3D Numerical Models for Reinforced Concrete Components." IOP Conference Series: Materials Science and Engineering 17 (2011): 012036. Print.

Kotsovos, M. D., and Newman, J. B., 1977. “Behavior of concrete under multiaxial stress”. ACI, 74(9), 443-444.

Kupfer, Helmut, Hubert K. Hilsdorf, and Hubert Rusch. "Behavior of concrete under biaxial stresses." ACI Journal proceedings. Vol. 66. No. 8. ACI, 1969.

Kwak, Hyo-Gyoung, and Filip C. Filippou. "Finite Element Analysis of Reinforced Concrete Structures Under Monotonic Loads." The Earthquake Engineering Online Archive. California Department of Transportation, Nov. 1990. Web.

Kwak, H.g., and F.c. Filippou. "Nonlinear FE Analysis of Structures under Monotonic Loads." Computers & Structures 65.1 (1997): 1-16. Print.

Lowes, Laura Nicole. Finite element modeling of reinforced concrete beam-column bridge connections. Diss. University of California, 1999.

Lundgren, Karin. Three-dimensional modelling of bond in reinforced concrete theoretical model, experiments and applications. Diss. Chalmers University of Technology, 1999.

Lutz, Leroy A., and Peter Gergely. "Mechanics of bond and slip of deformed bars in concrete." ACI Journal Proceedings. Vol. 64. No. 11. ACI, 1967.

Macgregor, James G, and James K. Wight. Reinforced Concrete: Mechanics and Design. Singapore: Pearson/Prentice Hall, 2006.

Mains, Robert M. "Measurement of the distribution of tensile and bond stresses along reinforcing bars." ACI Journal Proceedings. Vol. 48. No. 11. ACI, 1951.

Mirza, S. M., and Houde, J., 1979. "Study of Bond-Slip Relationships in Reinforced Concrete", AC1 Joumal, Vol. 76, No. 1, January, pp. 19- 46.

Montoya, Esneyder. "Modeling of confined concrete." Master of Applied Science thesis, University of Toronto (2000).

Mordini, Andrea. "Three-Dimensional Numerical Modeling of Reinforced Concrete Behavior." University of Parma, Mar. 2006. Web.

Naito, Clay J., Jack P. Moehle, and Khalid M. Mosalam. Experimental and computational evaluation of reinforced concrete bridge beam-column connections for seismic performance. No. PEER 2001/08. 2001.

Ngo, D. and Scordelis, A.C., 1967. “Finite element analysis of reinforced concrete beams”. Journal of ACI, 64(3), 152-163.

Nilson, Arthur H. "Nonlinear analysis of reinforced concrete by the finite element method." ACI Journal Proceedings. Vol. 65. No. 9. ACI, 1968.

Nilson, Arthur H. "Internal measurement of bond slip." ACI Journal Proceedings. Vol. 69. No. 7. ACI, 1972.

Ožbolt, Joško, Steffen Lettow, and Ivica Kožar. "Discrete bond element for 3D finite element analysis of reinforced concrete structures." Proceedings of the 3rd International Symposium: Bond in Concrete-from research to standards. Budapest: University of Technology and Economics. 2002.

Pauw, Adrian. Static Modulus of Elasticity of Concrete as Affected by Density. Columbia: University of Missouri, 1960. Print.

Peterson, P. E., 1981. “Crack growth and development of fracture zones in plain concrete and similar materials”. Rep. No. TVBM-11-6, Division of Building Materials, University of Lund, Lund, Sweden.

Podgorniak-Stanik, Bogdan A. "The Influence of Concrete Strength, Distribution of Logitudinal Reinforcement, Amount of Transverse Reinforcement and Member Size on Shear Strength of Reinforced Concrete Members." Library and Archives Canada. University of Toronto, 1998. Web.

POPOVICS, SANDOR. "A Review of Stress-Strain Relationships for Concrete." ACI JOURNAL 67.14 (1970): 243-48. Web.

Rashid, Y.r. "Ultimate Strength Analysis of Prestressed Concrete Pressure Vessels." Nuclear Engineering and Design 7.4 (1968): 334-44. Print.

Reddiar, Madhu Karthik Murugesan. Stress-Strain Model of Unconfined and Confined Concrete and Stress-Block Parameters. Diss. Texas A&M University, 2009.

Scott, B.D.,Park, R. and Priestley, M.J.N. (1982) 'Stress—Strain Behavior of Concrete Confined by Overlapping Hoops at Low and High Strain Rates,' ACI Journal, 13–27.

Shafaie, J., A. Hosseini, and M. S. Marefat. “3d finite element modelling of bond-slip between rebar and concrete in pull-out test”. Proc. of The Third International Conference on Concrete and Development, Iran, Tehran, I.R. N.p., 2009. Web.

Sin, Lim Hwee, Wee Tiong Huan, Md Rafiqul Islam, and Md Abul Mansur. "Reinforced Lightweight Concrete Beams in Flexure." ACI Structural Journal S01 108 (2011): n. pag. Print.

Taqieddin, Ziad N. "ELASTO-PLASTIC AND DAMAGE MODELING OF REINFORCED CONCRETE." Louisiana State University, Aug. 2008. Web.

Thomas, Job, and Ananth Ramaswamy. "Nonlinear analysis of shear dominant prestressed concrete beams using ANSYS." International ANSYS Conference Proceedings. 2006.

APPENDICES

Appendix A Concrete Material Data

- Concrete Strength 42.7MPa

$$f'_c := 42.7 \qquad f''_c := 0.9 \cdot f'_c = 38.43$$

$$E_c := 4700 \cdot \sqrt{f'_c} = 30712.261 \qquad \varepsilon_0 := 1.8 \cdot \frac{f''_c}{E_c} = 0.002252$$

$$f_c(\varepsilon_c) := f''_c \cdot \left(\frac{2 \cdot \varepsilon_c}{\varepsilon_0} - \left(\frac{\varepsilon_c}{\varepsilon_0} \right)^2 \right)$$

$$f_c(0.0003) = 9.556 \qquad f_c(0.0006) = 17.748$$
$$f_c(0.0009) = 24.576 \qquad f_c(0.0012) = 30.041$$

$$f_c(0.0015) = 34.142 \qquad f_c(0.0018) = 36.88$$
$$f_c(0.0021) = 38.254 \qquad f_c(\varepsilon_0) = 38.43$$

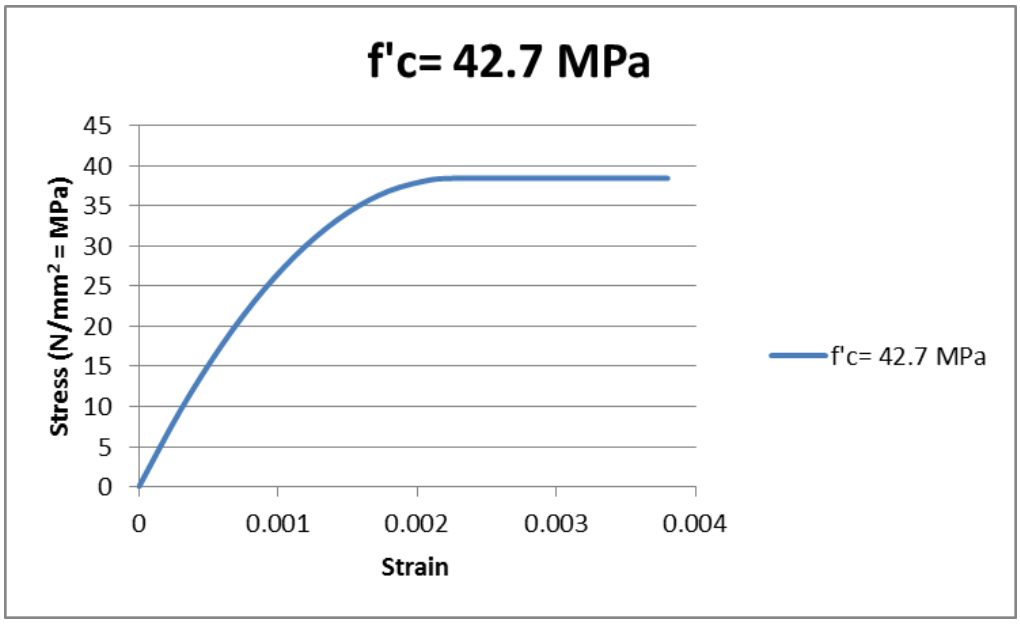

Figure A-1 Stress Strain relationship for 42.7 MPa concrete

- Concrete Strength 37MPa

$$f'_c := 37 \qquad f''_c := 0.9 \cdot f'_c = 33.3$$

$$E_c := 4700 \cdot \sqrt{f'_c} = 28588.984 \qquad \varepsilon_0 := 1.8 \cdot \frac{f''_c}{E_c} = 0.002097$$

$$f_c(\varepsilon_c) := f''_c \cdot \left(\frac{2 \cdot \varepsilon_c}{\varepsilon_0} - \left(\frac{\varepsilon_c}{\varepsilon_0} \right)^2 \right)$$

$$f_c(0.0006) = 16.332$$
$$f_c(0.0009) = 22.453$$
$$f_c(0.0012) = 27.21$$
$$f_c(0.0015) = 30.604$$
$$f_c(0.0018) = 32.634$$
$$f_c(\varepsilon_0) = 33.3$$

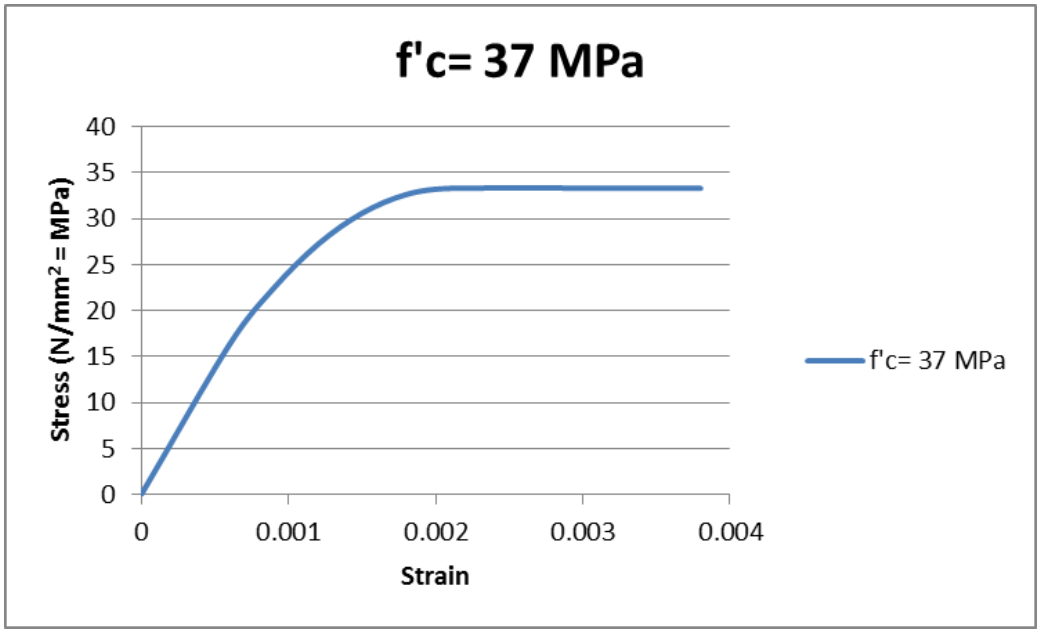

Figure A-2 Stress Strain relationship for 37 MPa concrete

- Concrete Strength 30MPa

$$f'_c := 30 \qquad f''_c := 0.9 \cdot f'_c = 27$$

$$E_c := 4700 \cdot \sqrt{f'_c} = 25742.96 \qquad \varepsilon_0 := 1.8 \cdot \frac{f''_c}{E_c} = 0.001888$$

$$f_c(\varepsilon_c) := f''_c \cdot \left(\frac{2 \cdot \varepsilon_c}{\varepsilon_0} - \left(\frac{\varepsilon_c}{\varepsilon_0} \right)^2 \right)$$

$$f_c(0.0005) = 12.408 \qquad f_c(0.00075) = 17.191$$
$$f_c(0.0010) = 21.028 \qquad f_c(0.00125) = 23.917$$
$$f_c(0.0015) = 25.86 \qquad f_c(0.00175) = 26.856$$
$$f_c(\varepsilon_0) = 27$$

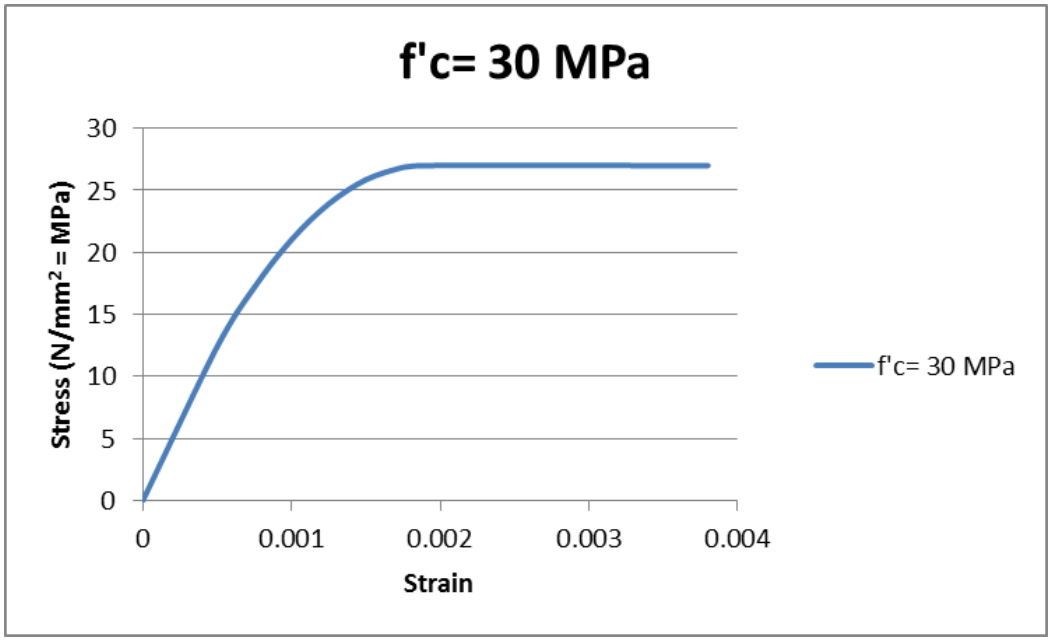

Figure A-3 Stress Strain relationship for 30 MPa concrete

- Concrete Strength 20MPa

$$f'_c := 20 \qquad f''_c := 0.9 \cdot f'_c = 18$$

$$E_c := 4700 \cdot \sqrt{f'_c} = 21019.039 \qquad \varepsilon_0 := 1.8 \cdot \frac{f''_c}{E_c} = 0.001541$$

$$f_c(\varepsilon_c) := f''_c \cdot \left(\frac{2 \cdot \varepsilon_c}{\varepsilon_0} - \left(\frac{\varepsilon_c}{\varepsilon_0} \right)^2 \right)$$

$$f_c(0.0004) = 8.13 \qquad f_c(0.0006) = 11.286$$
$$f_c(0.0008) = 13.835 \qquad f_c(0.0010) = 15.779$$
$$f_c(0.0012) = 17.117$$
$$f_c(\varepsilon_0) = 18$$

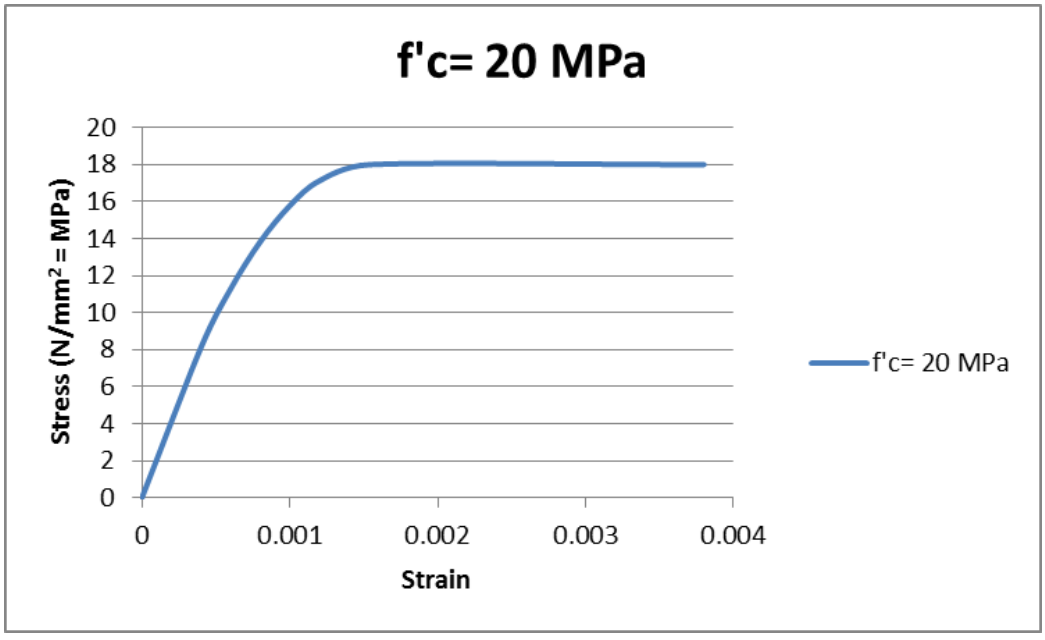

Figure A-4 Stress Strain relationship for 20 MPa concrete

- Concrete Strength 10MPa

$$f'_c := 10 \qquad f''_c := 0.9 \cdot f'_c = 9$$

$$E_c := 4700 \cdot \sqrt{f'_c} = 14862.705 \qquad \varepsilon_0 := 1.8 \cdot \frac{f''_c}{E_c} = 0.00109$$

$$f_c(\varepsilon_c) := f''_c \cdot \left(\frac{2 \cdot \varepsilon_c}{\varepsilon_0} - \left(\frac{\varepsilon_c}{\varepsilon_0} \right)^2 \right)$$

$$f_c(0.0003) = 4.272 \qquad f_c(0.00045) = 5.897$$

$$f_c(0.0006) = 7.181 \qquad f_c(0.00075) = 8.124$$

$$f_c(0.0009) = 8.727 \qquad f_c(\varepsilon_0) = 9$$

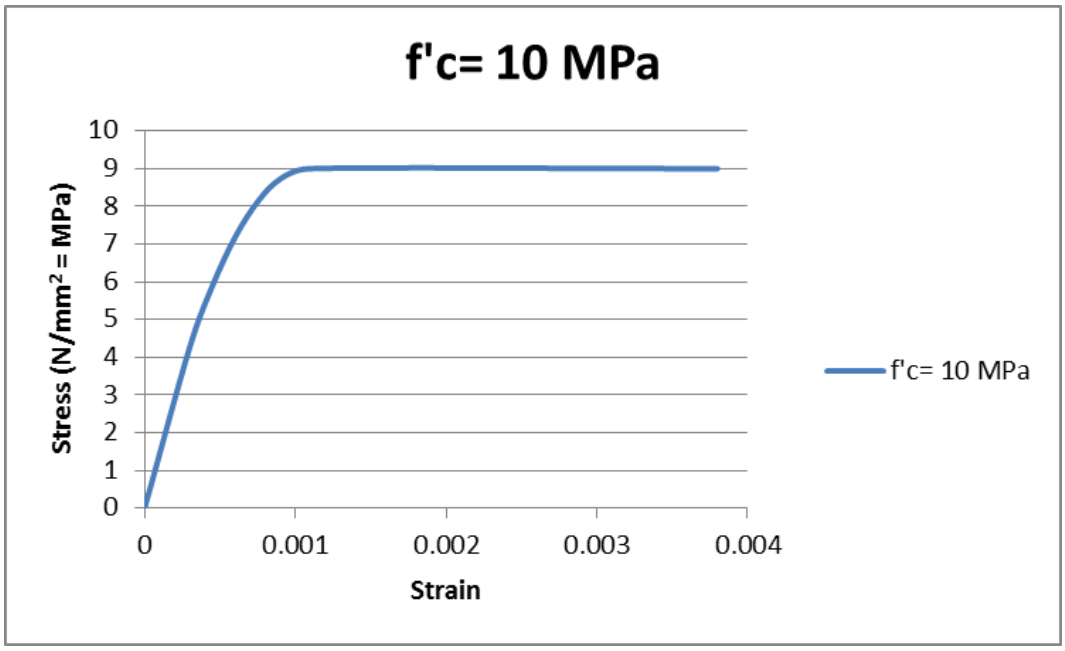

Figure A-5 Stress Strain relationship for 10 MPa concrete

Appendix B Steel Material Data

- Reinforcement size 10mm

$$A_s = \left(\frac{10}{2}\right)^2 \times \pi = 78.5\ \text{mm}^2$$

E_s = 185 GPa σ_y = 550 MPa

$$\varepsilon_y = \frac{\sigma_y}{E_s} = \frac{550}{185000} = 0.00297297$$

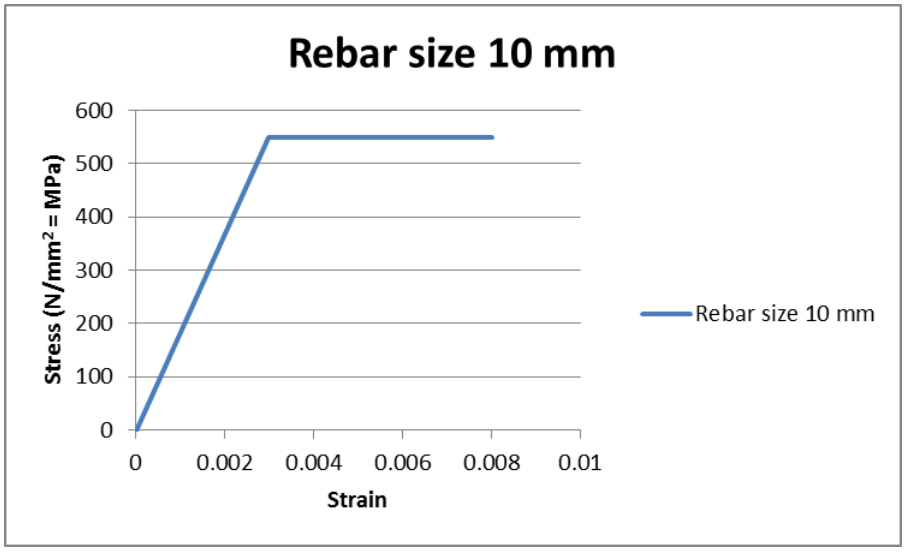

Figure B-1 Stress Strain relationship for 10mm rebar

- Reinforcement size 16mm

$$A_s = \left(\frac{16}{2}\right)^2 \times \pi = 200.96\ \text{mm}^2$$

E_s = 183 GPa σ_y = 512 MPa

$$\varepsilon_y = \frac{\sigma_y}{E_s} = \frac{512}{183000} = 0.0027978$$

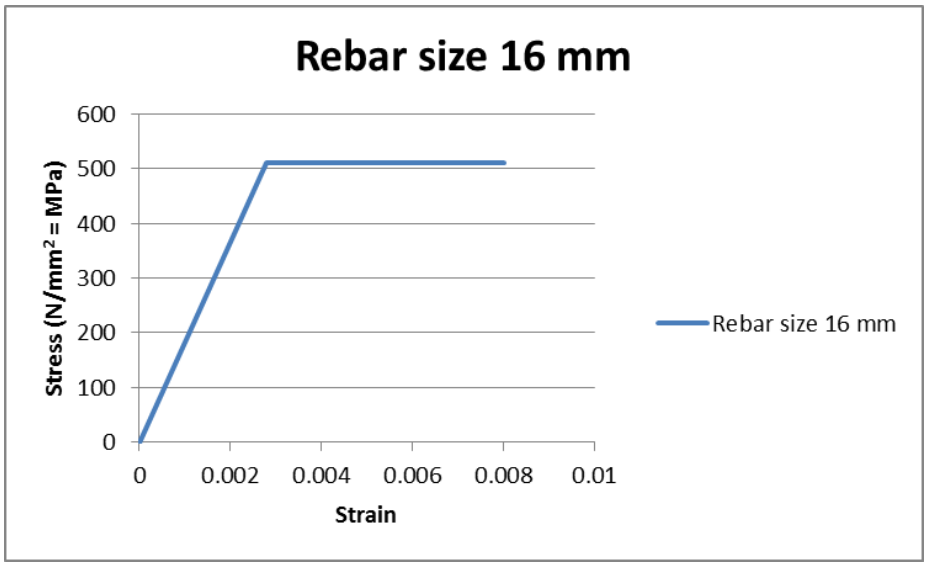

Figure B-2 Stress Strain relationship for 16mm rebar

- Reinforcement size 25mm

$$A_s = \left(\frac{25}{2}\right)^2 \times \pi = 490.625\,\text{mm}^2$$

E_s = 183 GPa σ_y = 512 MPa

$$\varepsilon_y = \frac{\sigma_y}{E_s} = \frac{512}{183000} = 0.0027978$$

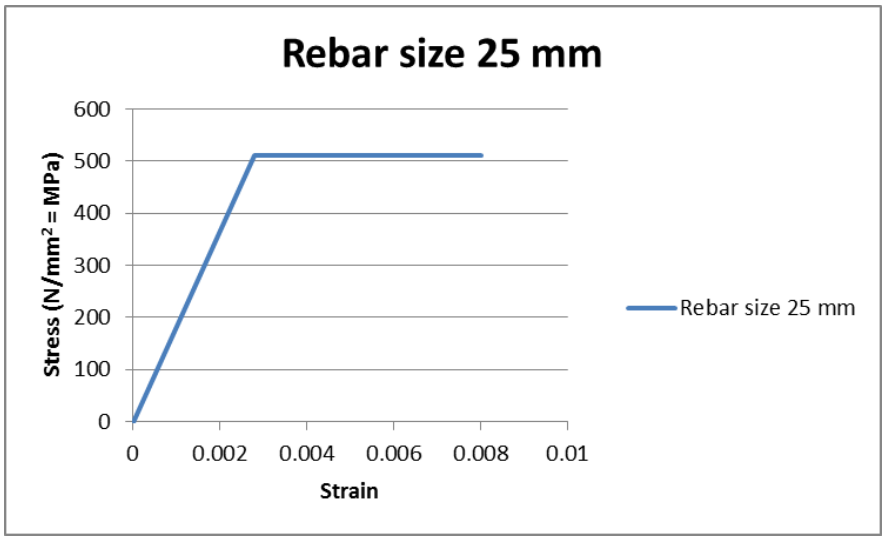

Figure B-3 Stress Strain relationship for 25mm rebar

- Reinforcement size 32mm

$$A_s = \left(\frac{32}{2}\right)^2 \times \pi = 803.84\,\text{mm}^2$$

E_s = 183 GPa σ_y = 512 MPa

$$\varepsilon_y = \frac{\sigma_y}{E_s} = \frac{512}{183000} = 0.0027978$$

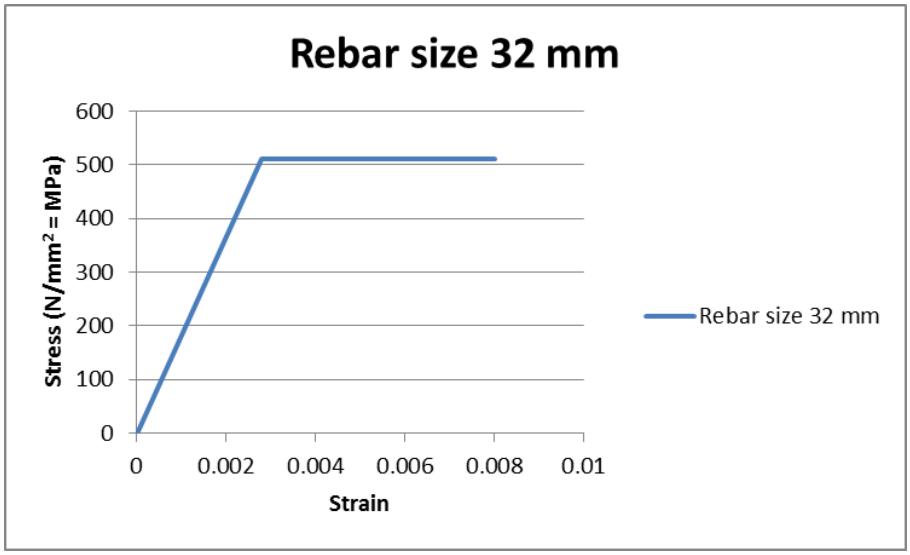

Figure B-4 Stress Strain relationship for 32mm rebar

- Reinforcement size 20M (d=19.5 mm)

$$A_s = \left(\frac{19.5}{2}\right)^2 \times \pi = 298.5\,\text{mm}^2$$

E_s = 200 GPa σ_y = 483 MPa

$$\varepsilon_y = \frac{\sigma_y}{E_s} = \frac{483}{200000} = 0.002415$$

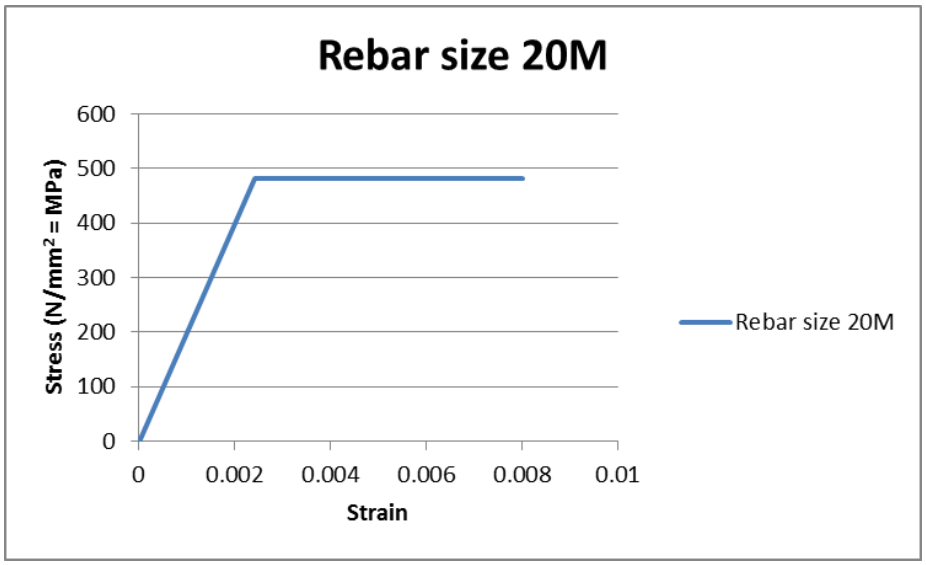

Figure B-5 Stress Strain relationship for 20M rebar

- Reinforcement size 25M (d=25.2 mm)

$$A_s = \left(\frac{25.2}{2}\right)^2 \times \pi = 498.5\,\text{mm}^2$$

E_s = 185 GPa σ_y = 490 MPa

$$\varepsilon_y = \frac{\sigma_y}{E_s} = \frac{490}{200000} = 0.00245$$

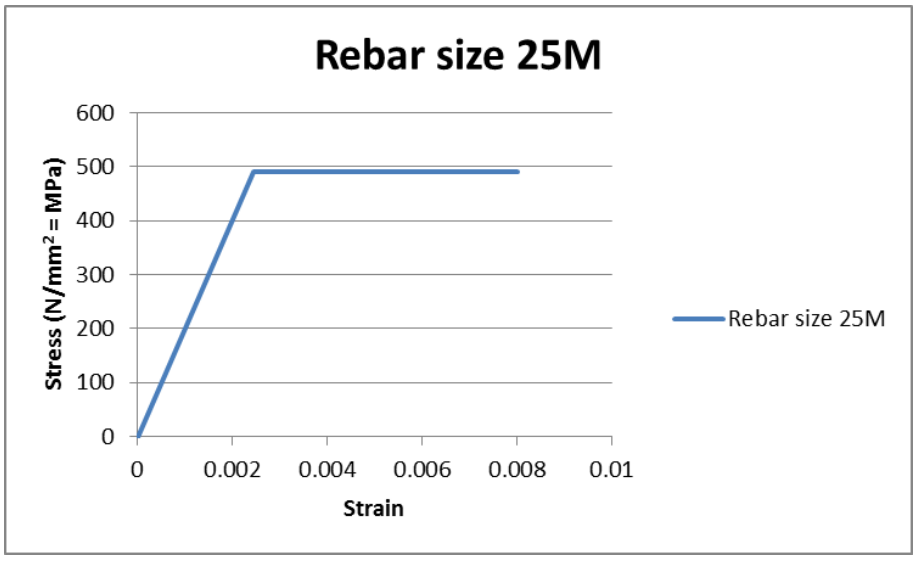

Figure B-6 Stress Strain relationship for 25M rebar

Appendix C Spring Load Displacement Data

- Spring of 10mm rebar and 10MPa concrete

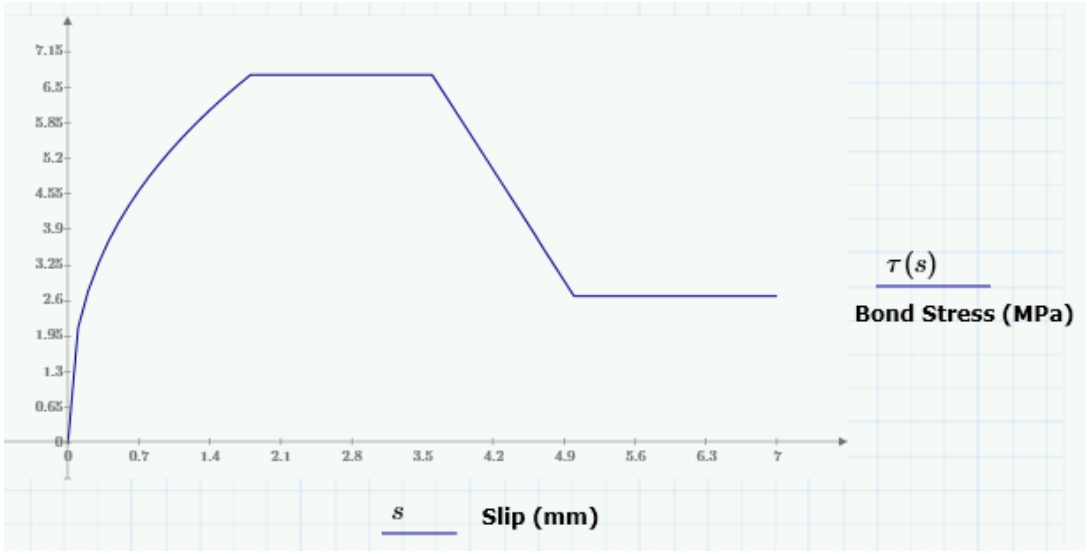

Figure C-1 spring stress strain relationships for 10mm rebar and f'c=10MPa

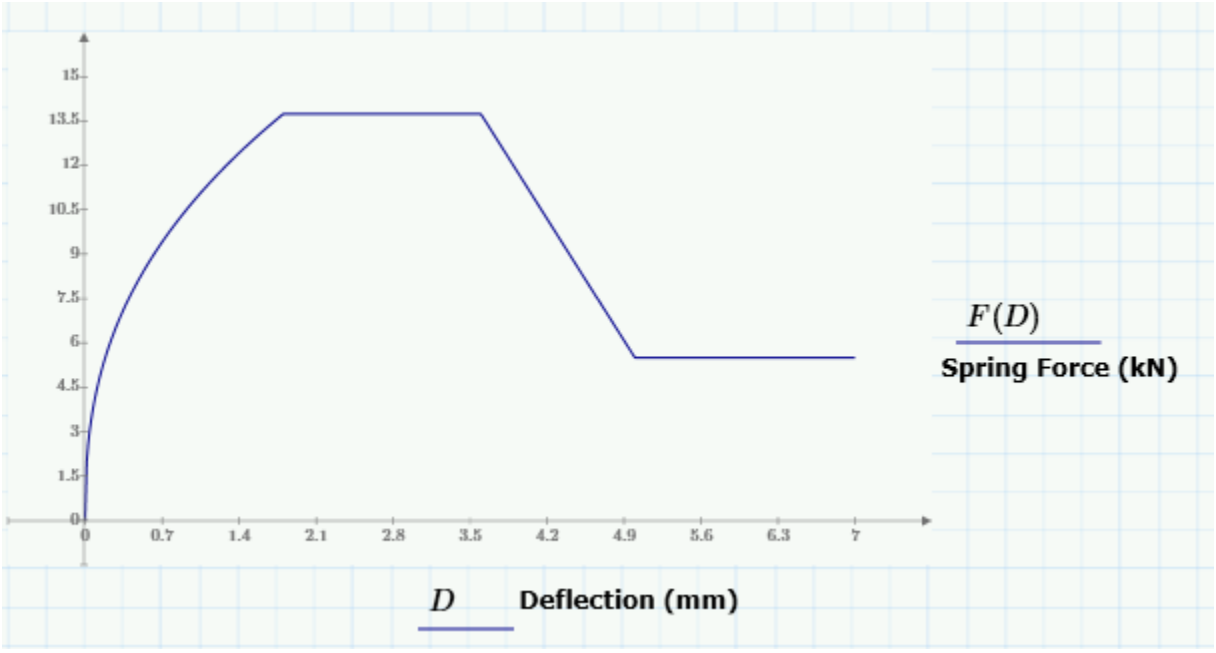

Figure C-2 spring load displacement relationships for 10mm rebar and f'c=10MPa

- Spring of 10mm rebar and 20MPa concrete

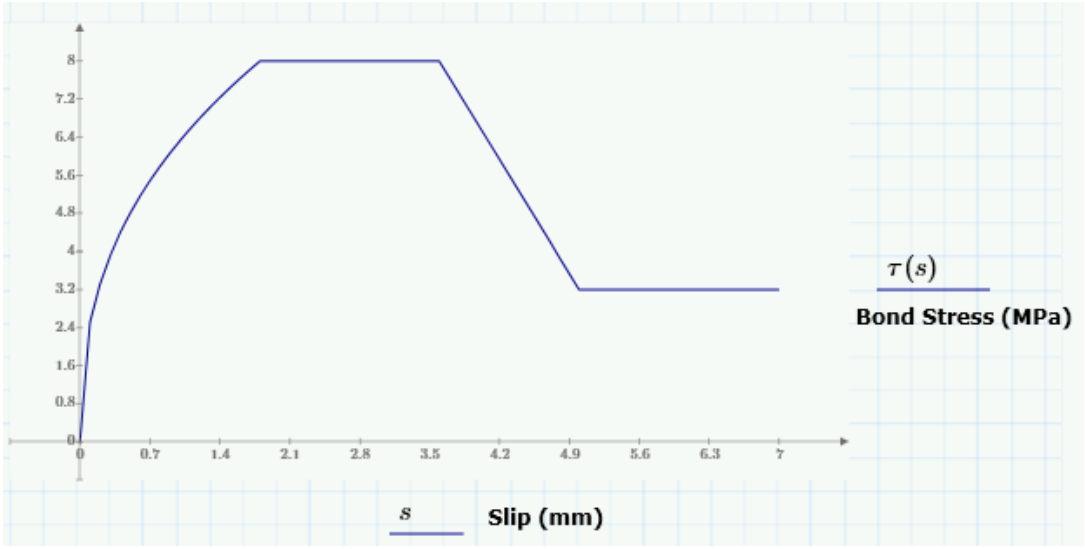

Figure C-3 spring stress strain relationships for 10mm rebar and f'c=20MPa

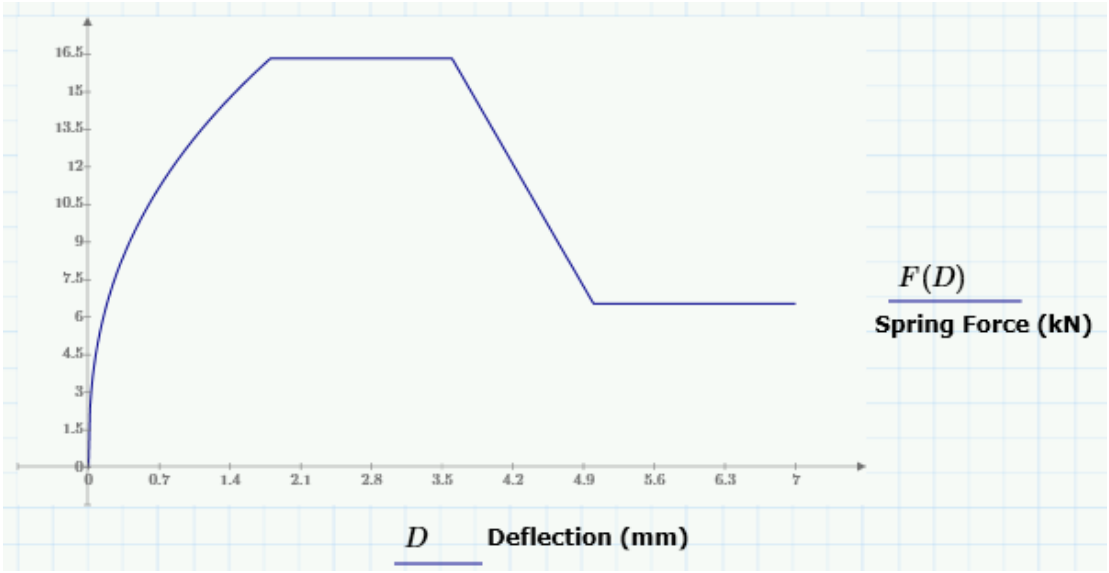

Figure C-4 spring load displacement relationships for 10mm rebar and f'c=20MPa

- Spring of 10mm rebar and 30MPa concrete

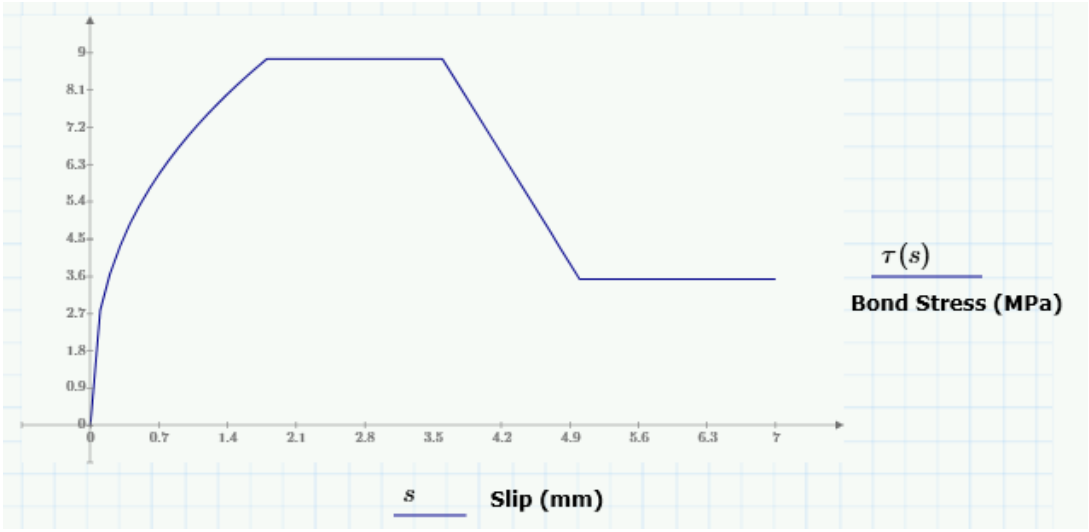

Figure C-5 spring stress strain relationships for 10mm rebar and f'c=30MPa

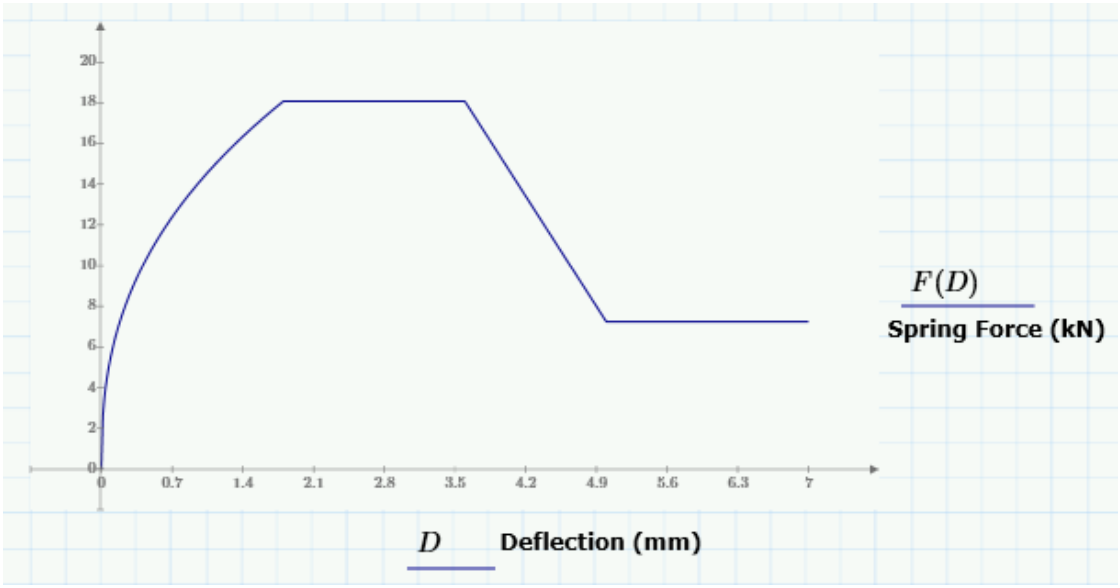

Figure C-6 spring load displacement relationships for 10mm rebar and f'c=30MPa

- Spring of 10mm rebar and 42.7MPa concrete

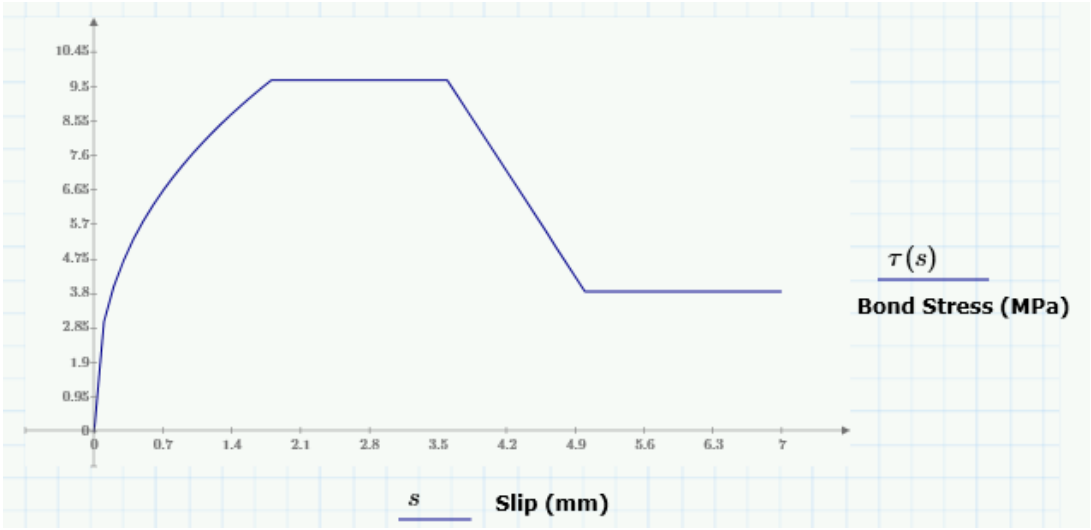

Figure C-7 spring stress strain relationships for 10mm rebar and f'c=42.7MPa

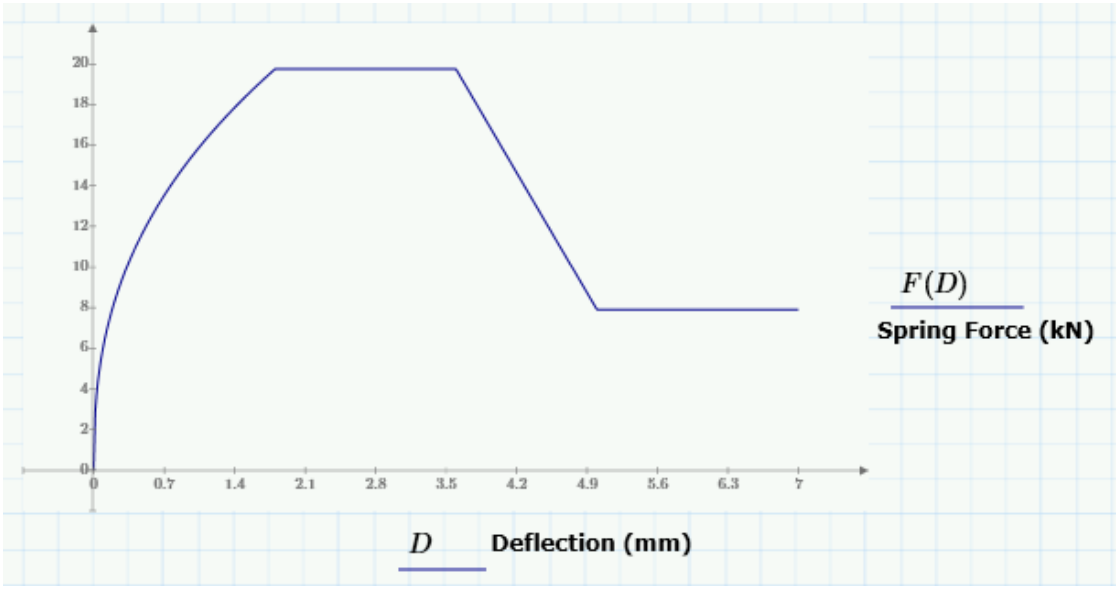

Figure C-8 spring load displacement relationships for 10mm rebar and f'c=42.7MPa

- Spring of 16mm rebar and 10MPa concrete

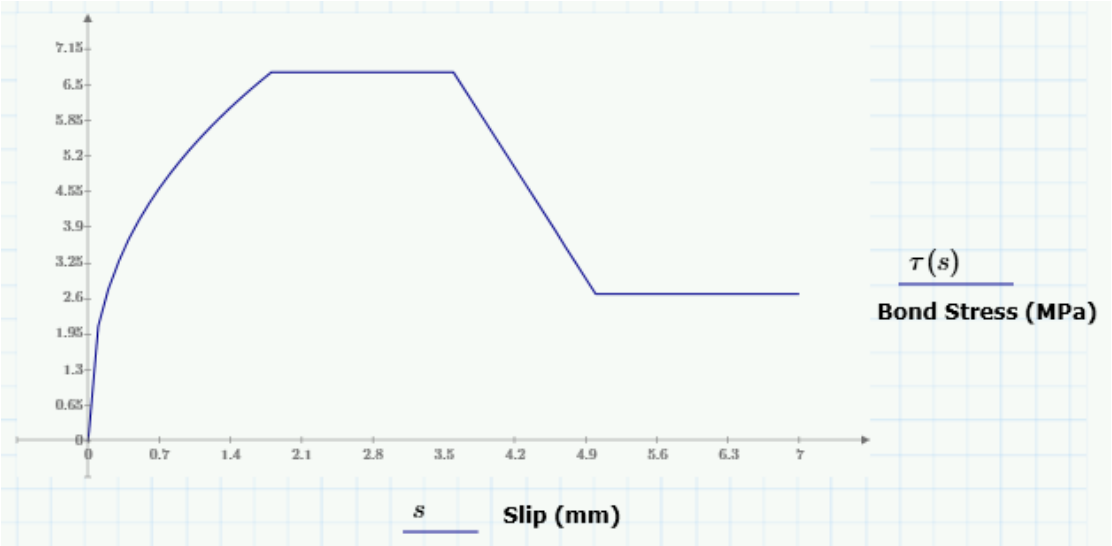

Figure C-9 spring stress strain relationships for 16mm rebar and f'c=10MPa

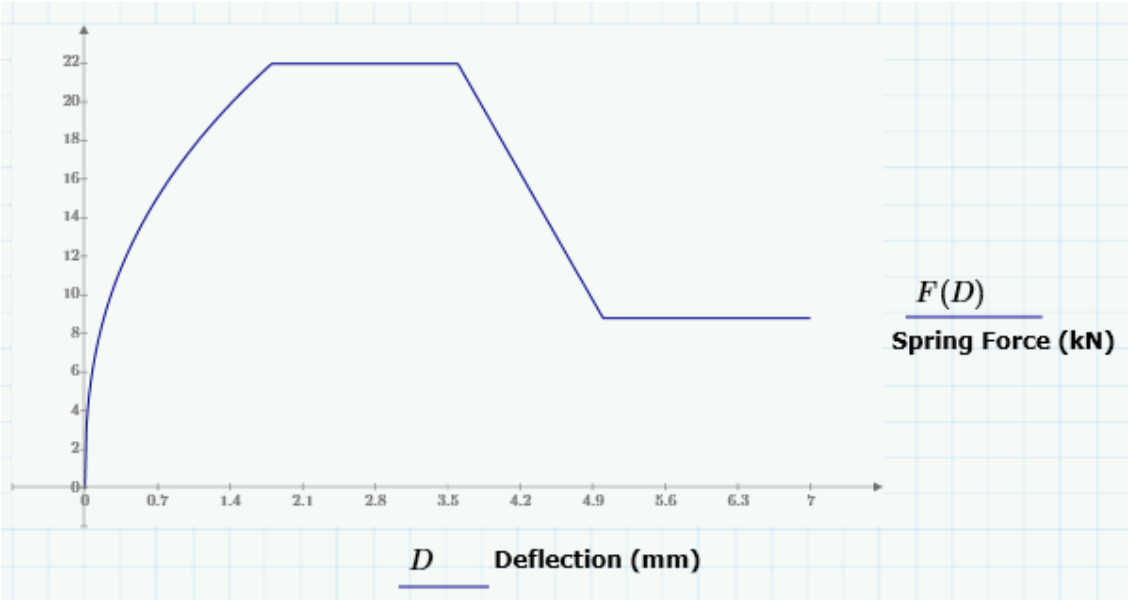

Figure C-10 spring load displacement relationships for 16mm rebar and f'c=10MPa

- Spring of 16mm rebar and 20MPa concrete

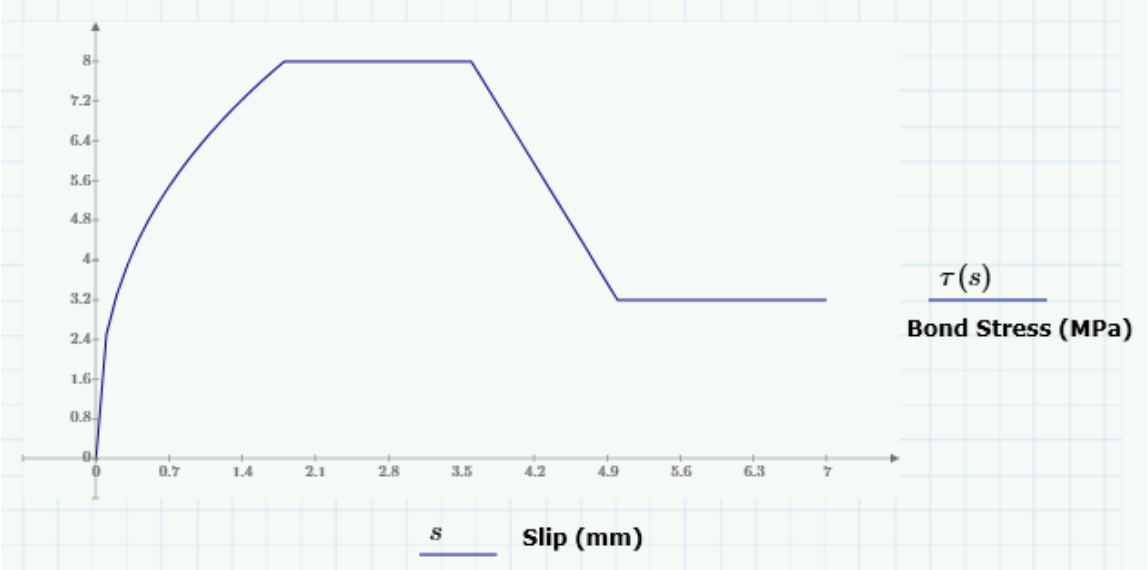

Figure C-11 spring stress strain relationships for 16mm rebar and f'c=20MPa

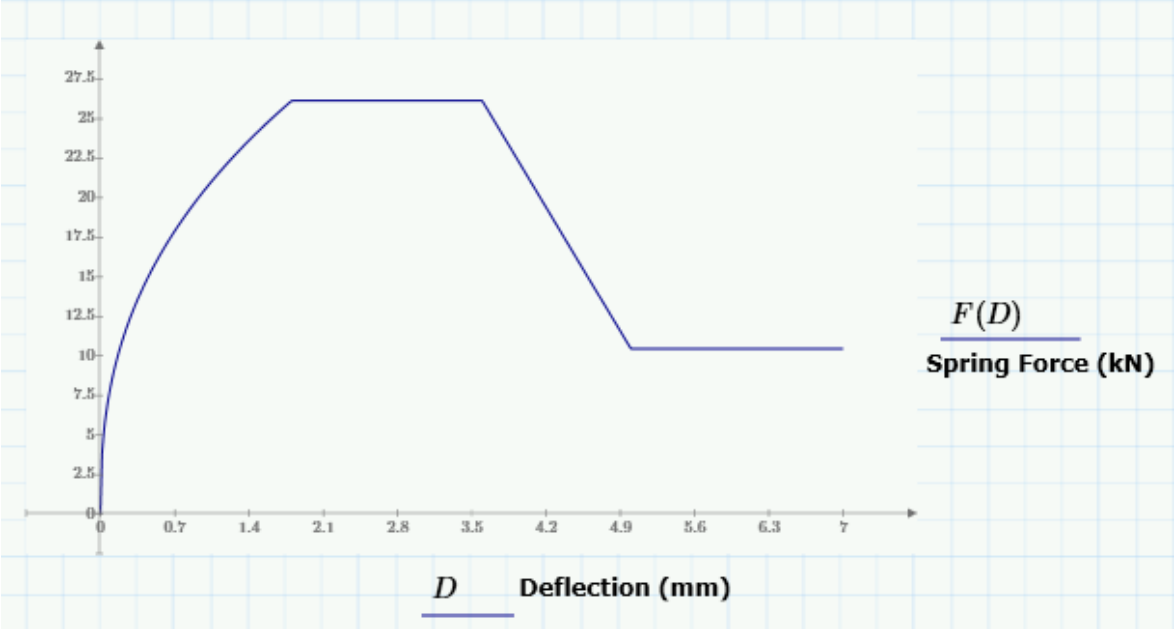

Figure C-12 spring load displacement relationships for 16mm rebar and f'c=20MPa

- Spring of 16mm rebar and 30MPa concrete

Figure C-13 spring stress strain relationships for 16mm rebar and f'c=30MPa

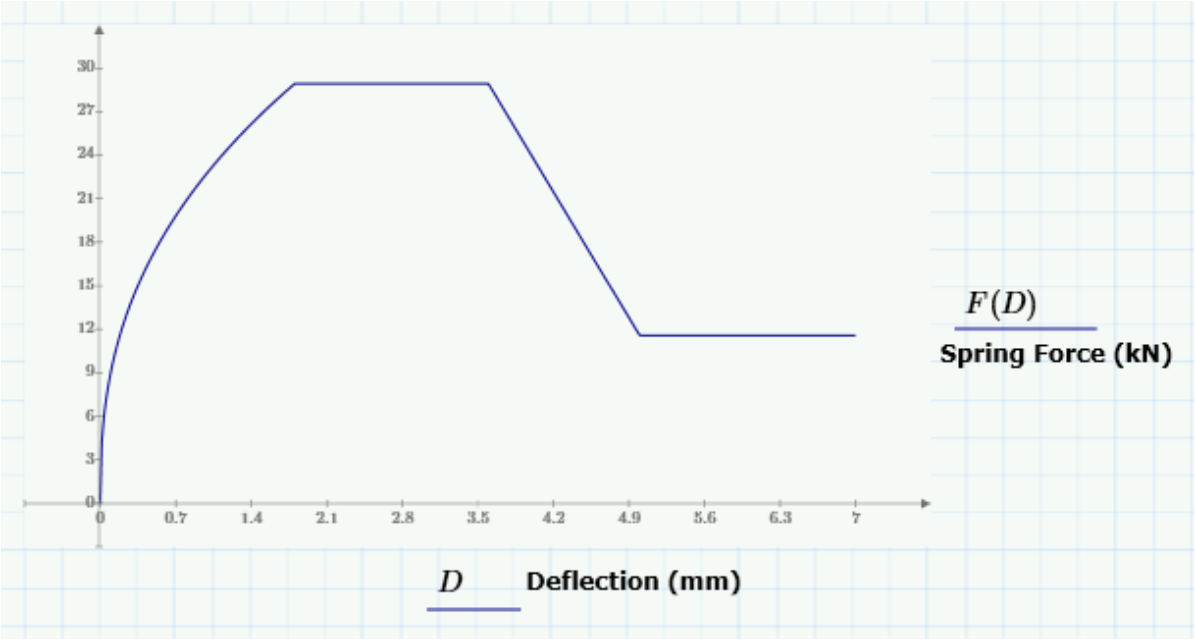

Figure C-14 spring load displacement relationships for 16mm rebar and f'c=30MPa

- Spring of 16mm rebar and 42.7MPa concrete

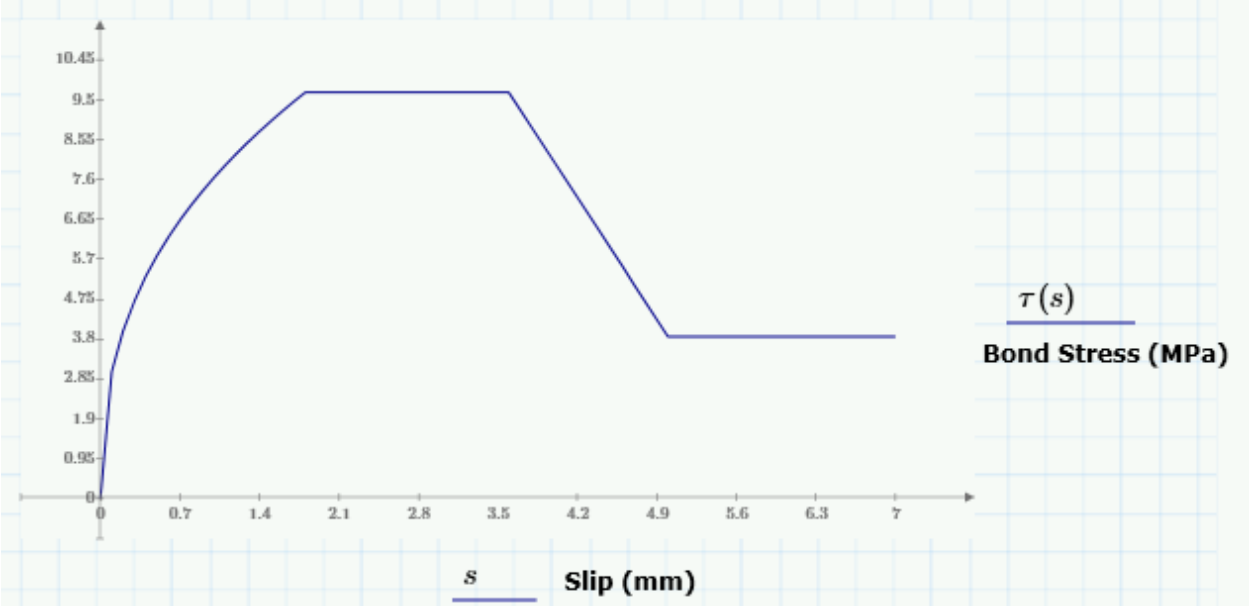

Figure C-15 spring stress strain relationships for 16mm rebar and f'c=42.7MPa

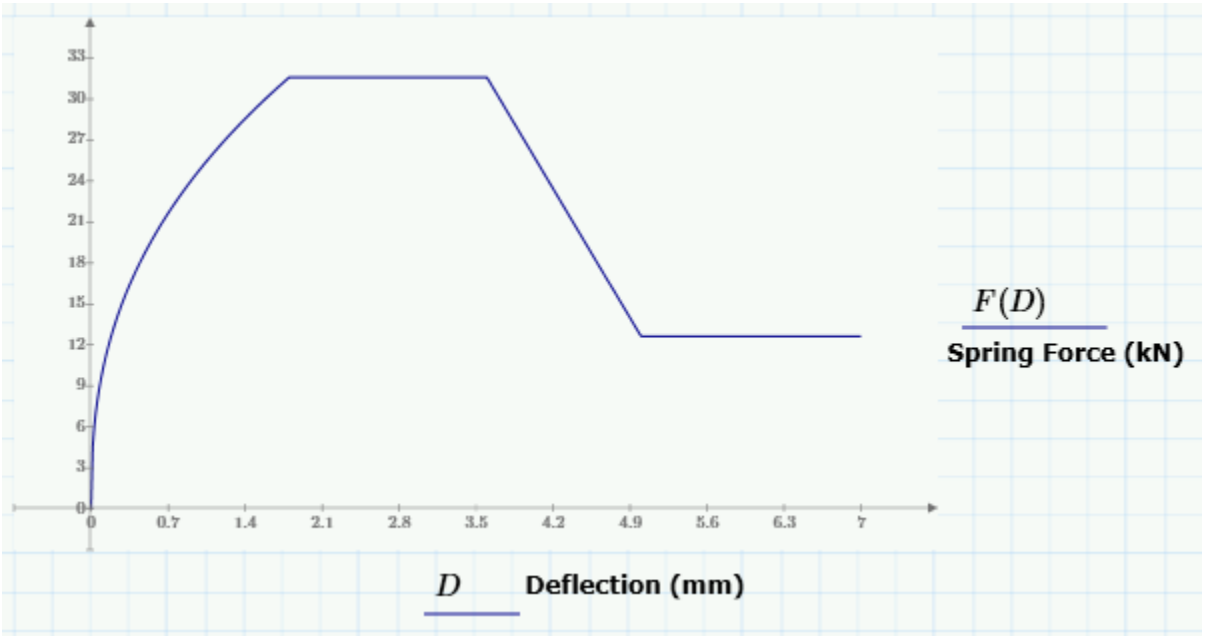

Figure C-16 spring load displacement relationships for 16mm rebar and f'c=42.7MPa

- Spring of 25mm rebar and 10MPa concrete

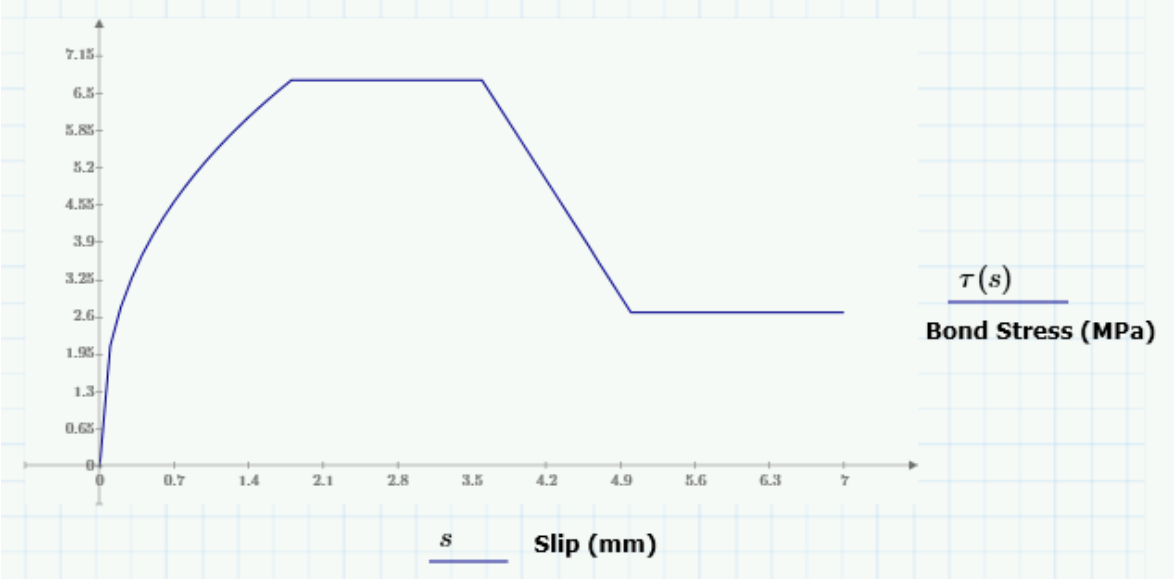

Figure C-17 spring stress strain relationships for 25mm rebar and f'c=10MPa

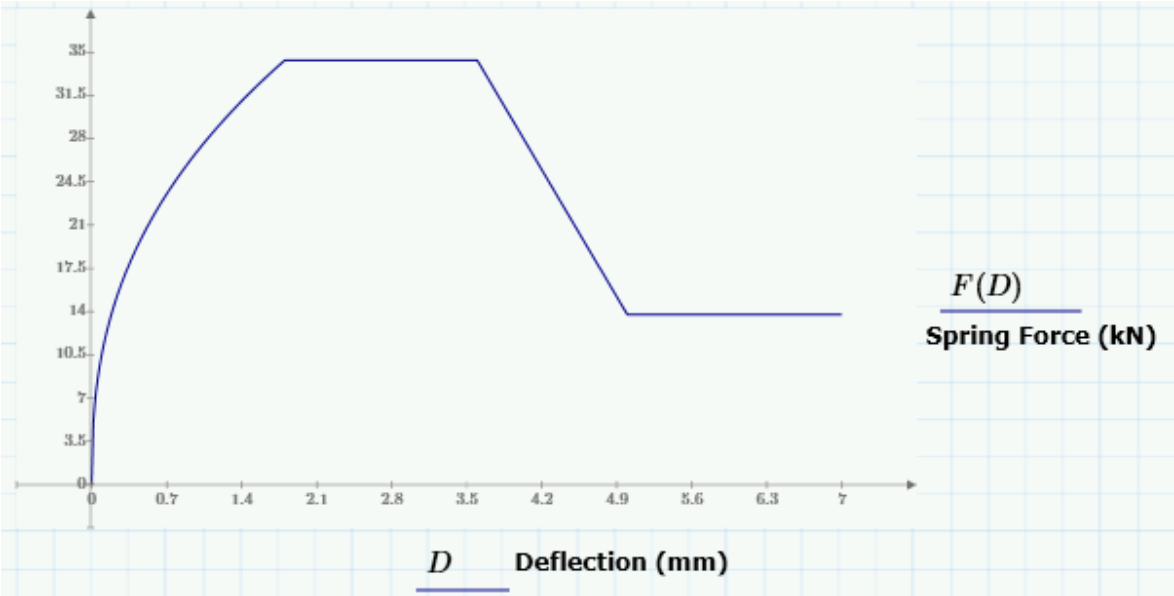

Figure C-18 spring load displacement relationships for 25mm rebar and f'c=10MPa

- Spring of 25mm rebar and 20MPa concrete

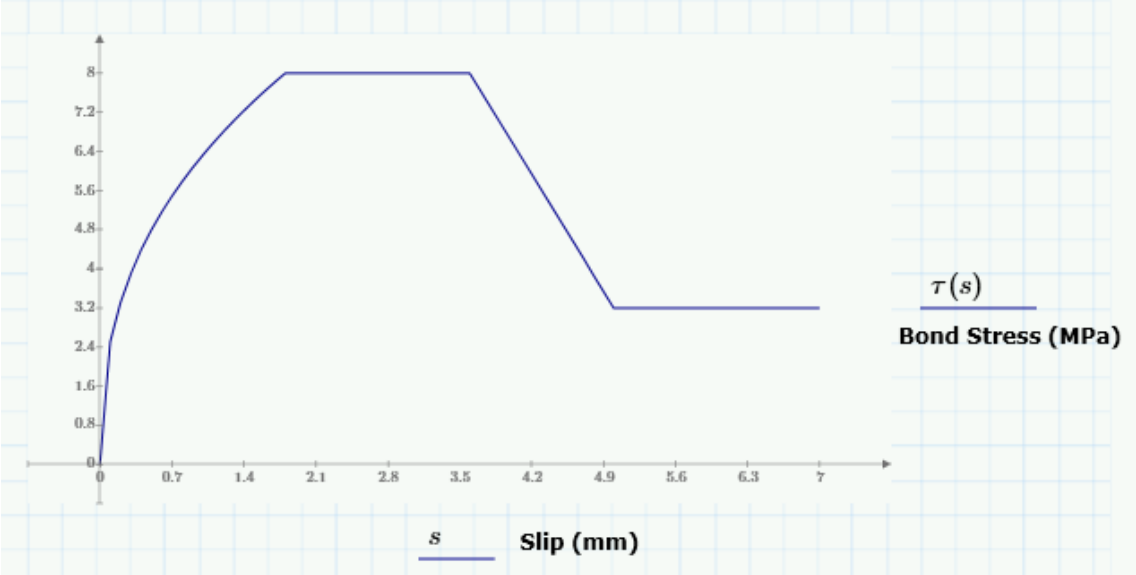

Figure C-19 spring stress strain relationships for 25mm rebar and f'c=20MPa

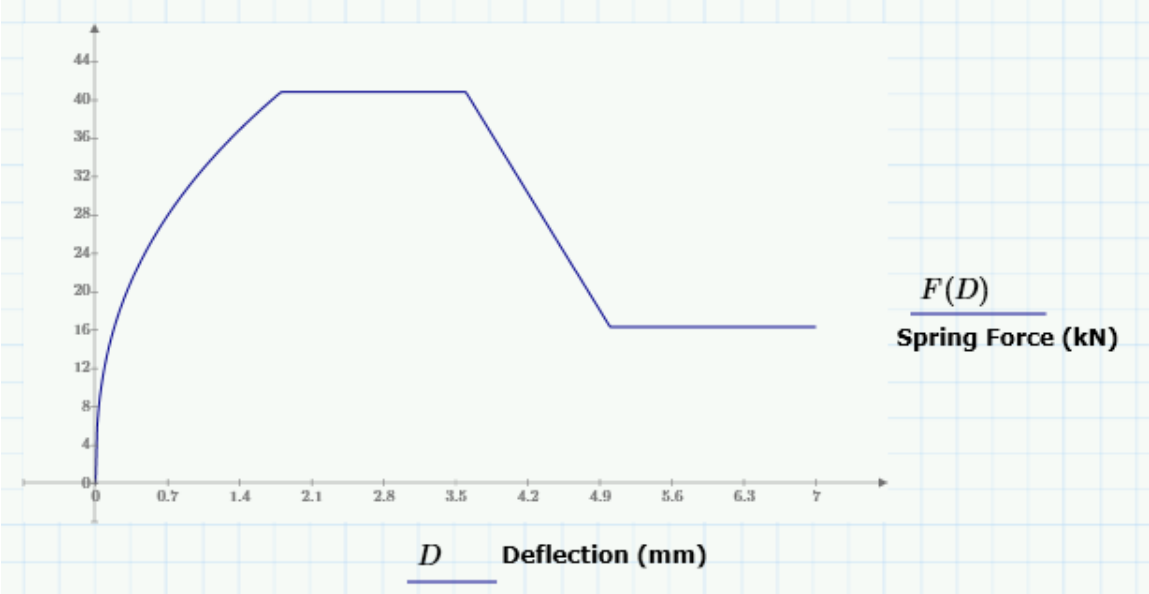

Figure C-20 spring load displacement relationships for 25mm rebar and f'c=20MPa

- Spring of 25mm rebar and 30MPa concrete

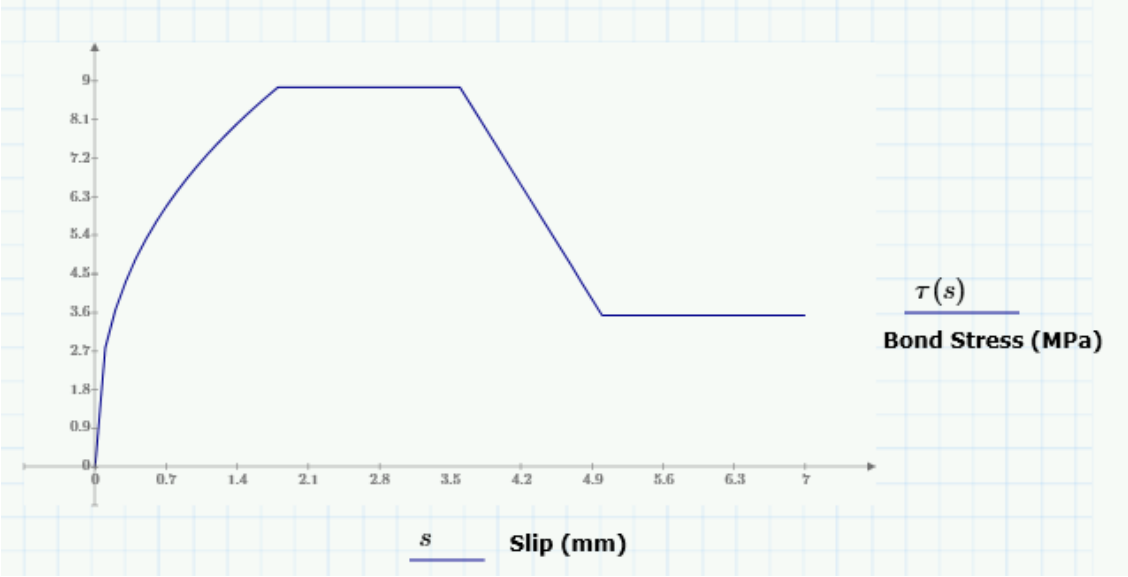

Figure C-21 spring stress strain relationships for 25mm rebar and f'c=30MPa

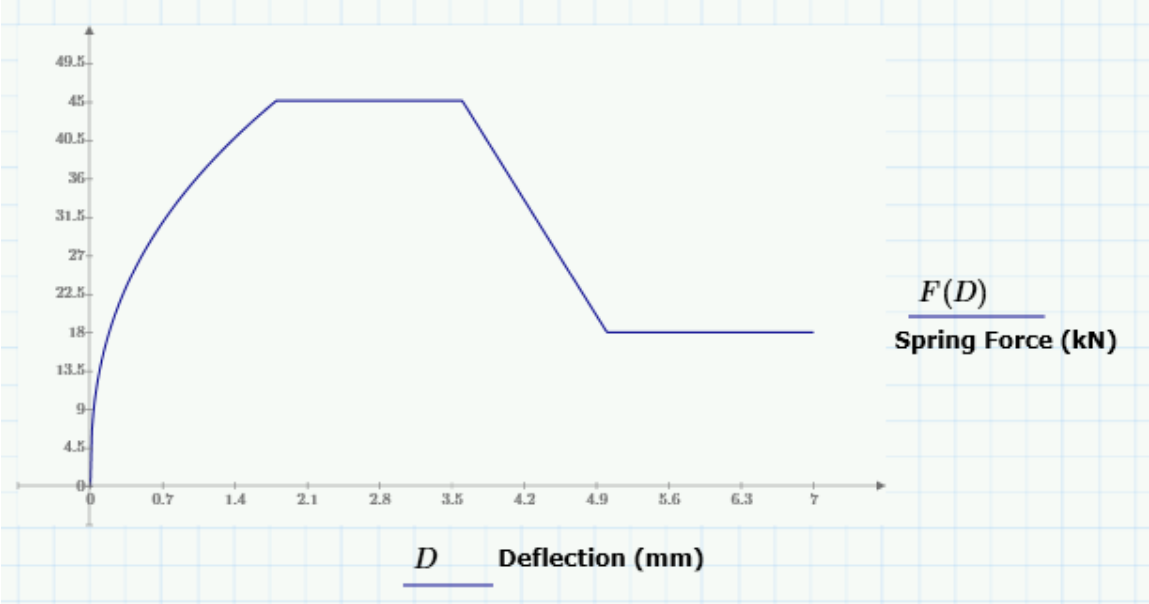

Figure C-22 spring load displacement relationships for 25mm rebar and f'c=30MPa

- Spring of 25mm rebar and 42.7MPa concrete

Figure C-23 spring stress strain relationships for 25mm rebar and f'c=42.7MPa

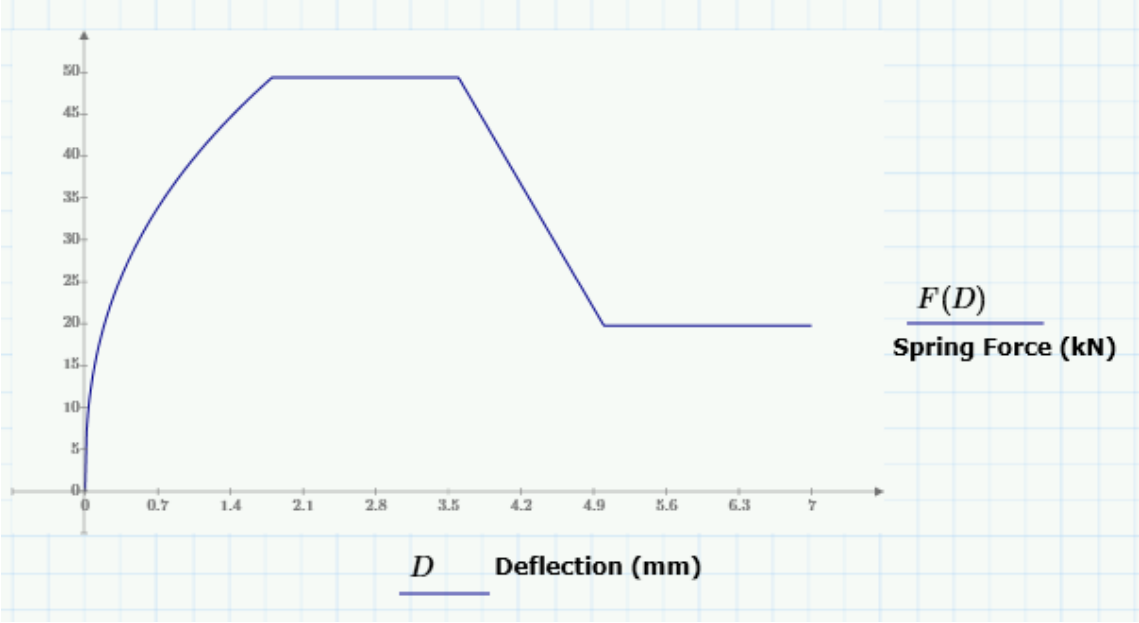

Figure C-24 spring load displacement relationships for 25mm rebar and f'c=42.7MPa

- Spring of 32mm rebar and 10MPa concrete

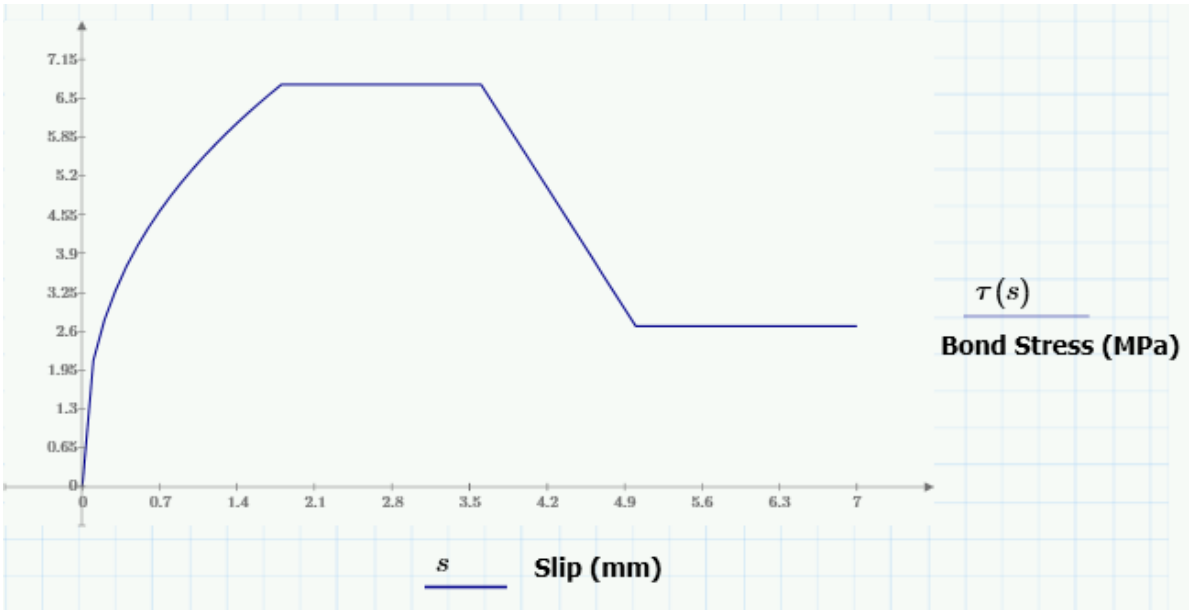

Figure C-25 spring stress strain relationships for 32mm rebar and f'c=10MPa

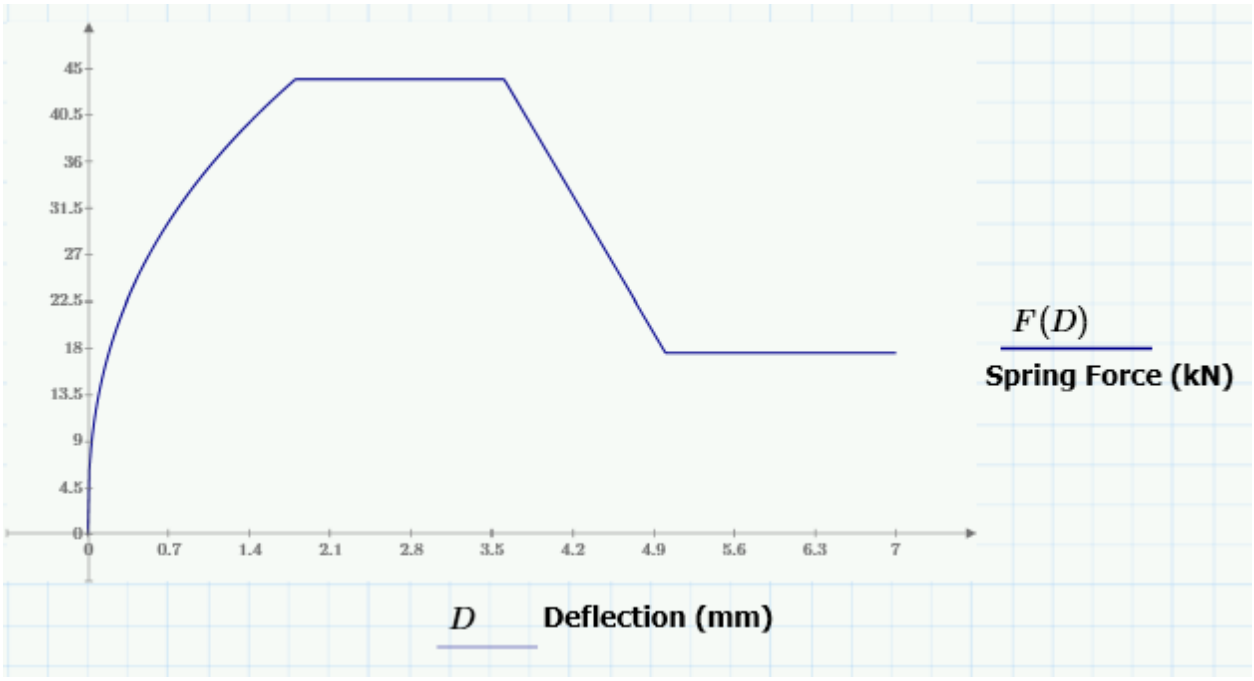

Figure C-26 spring load displacement relationships for 32mm rebar and f'c=10MPa

- Spring of 32mm rebar and 20MPa concrete

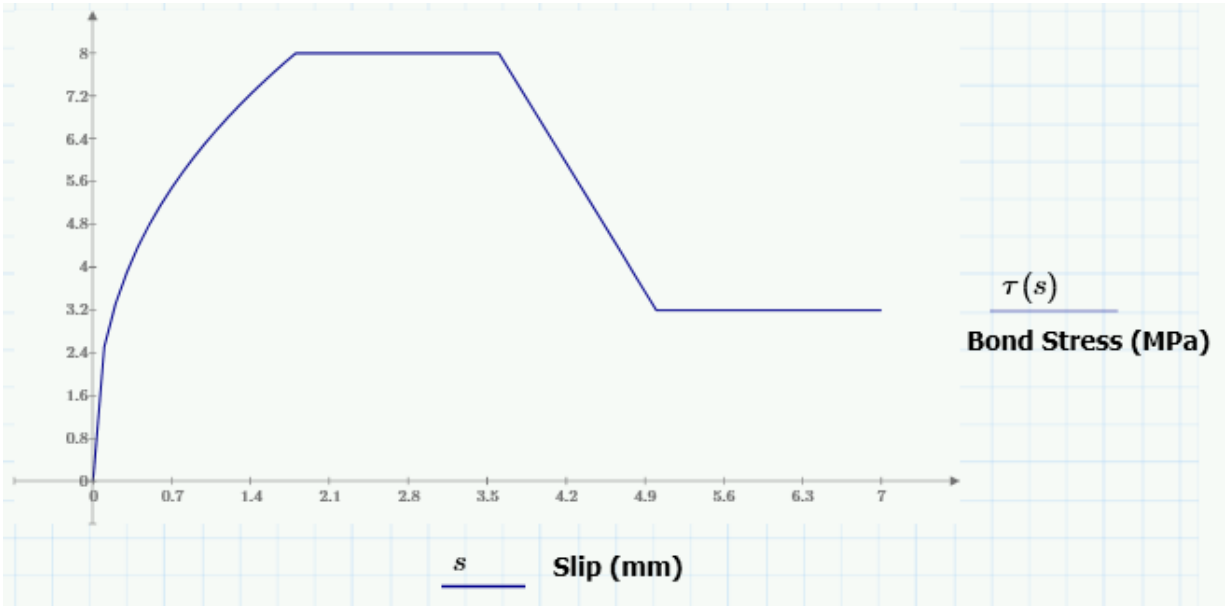

Figure C-27 spring stress strain relationships for 32mm rebar and f'c=20MPa

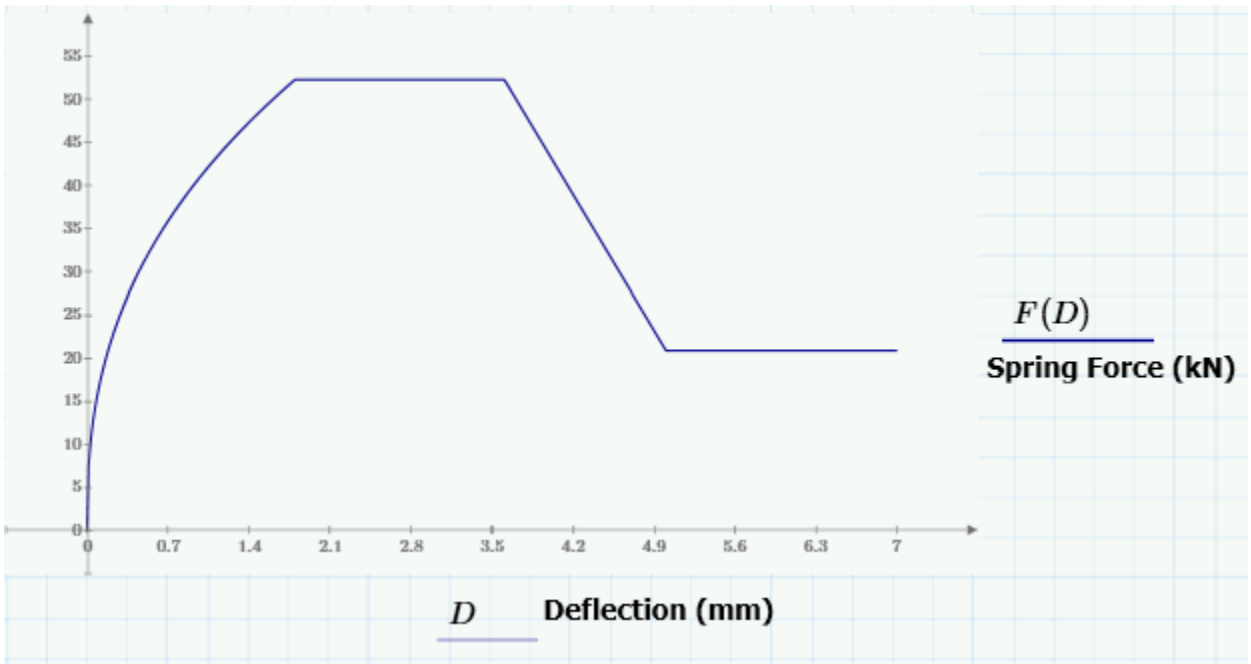

Figure C-28 spring load displacement relationships for 32mm rebar and f'c=20MPa

- Spring of 32mm rebar and 30MPa concrete

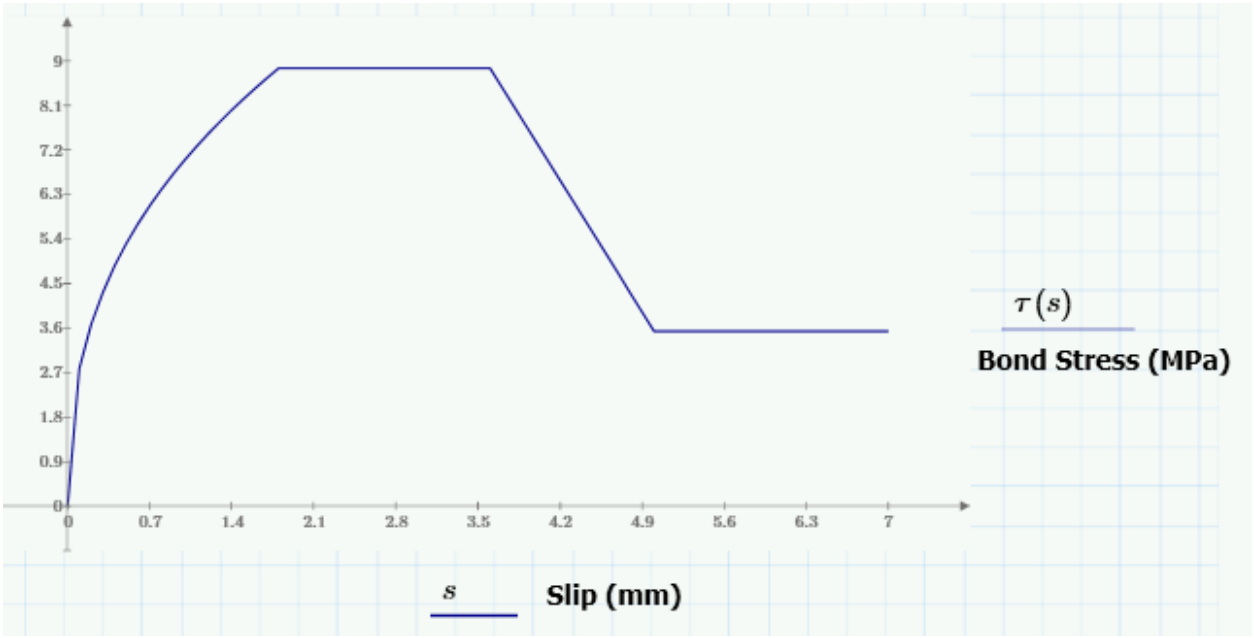

Figure C-29 spring stress strain relationships for 32mm rebar and f'c=30MPa

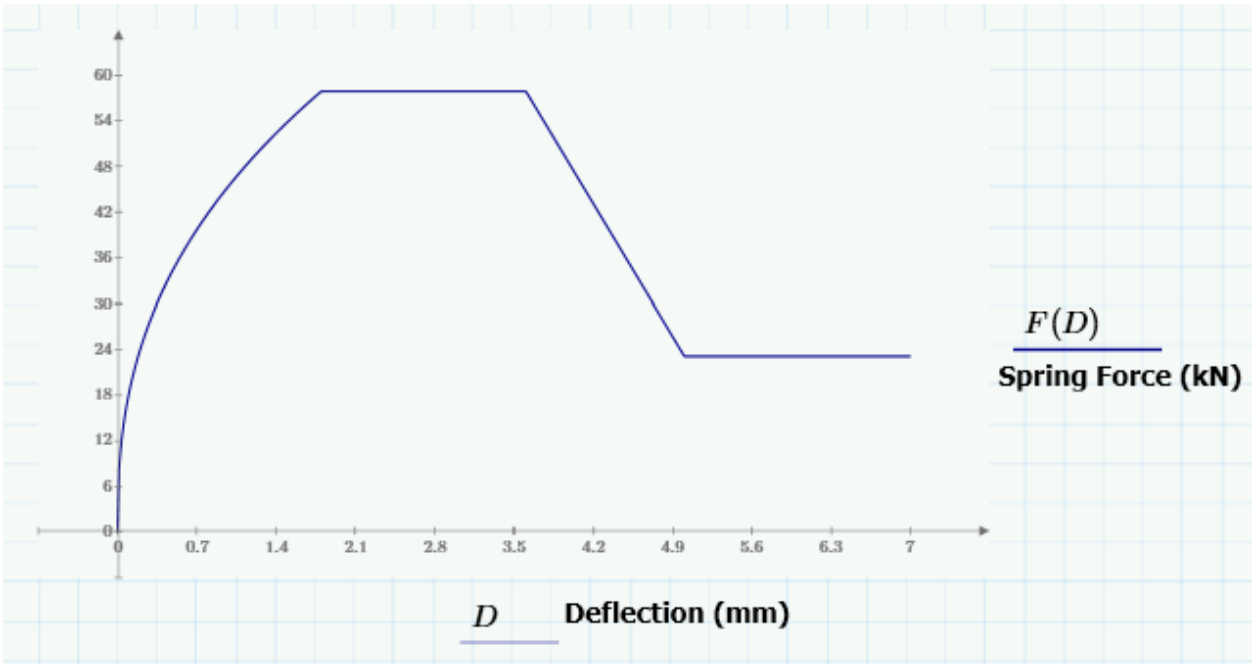

Figure C-30 spring load displacement relationships for 32mm rebar and f'c=30MPa

- Spring of 32mm rebar and 42.7MPa concrete

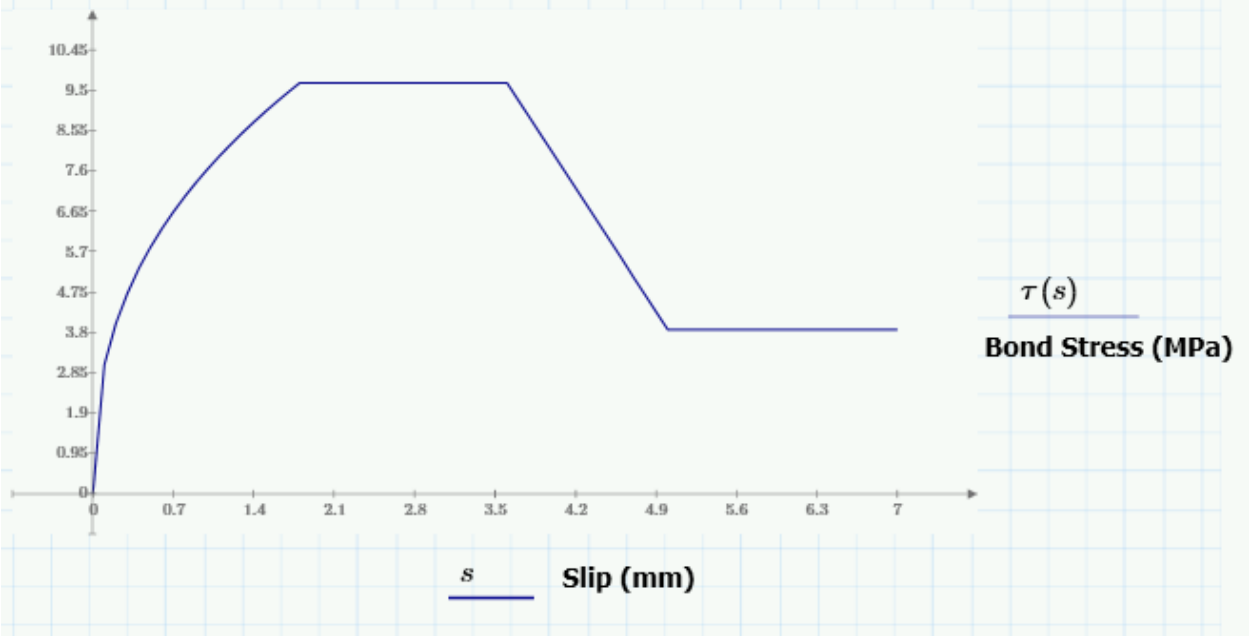

Figure C-31 spring stress strain relationships for 32mm rebar and f'c=42.7MPa

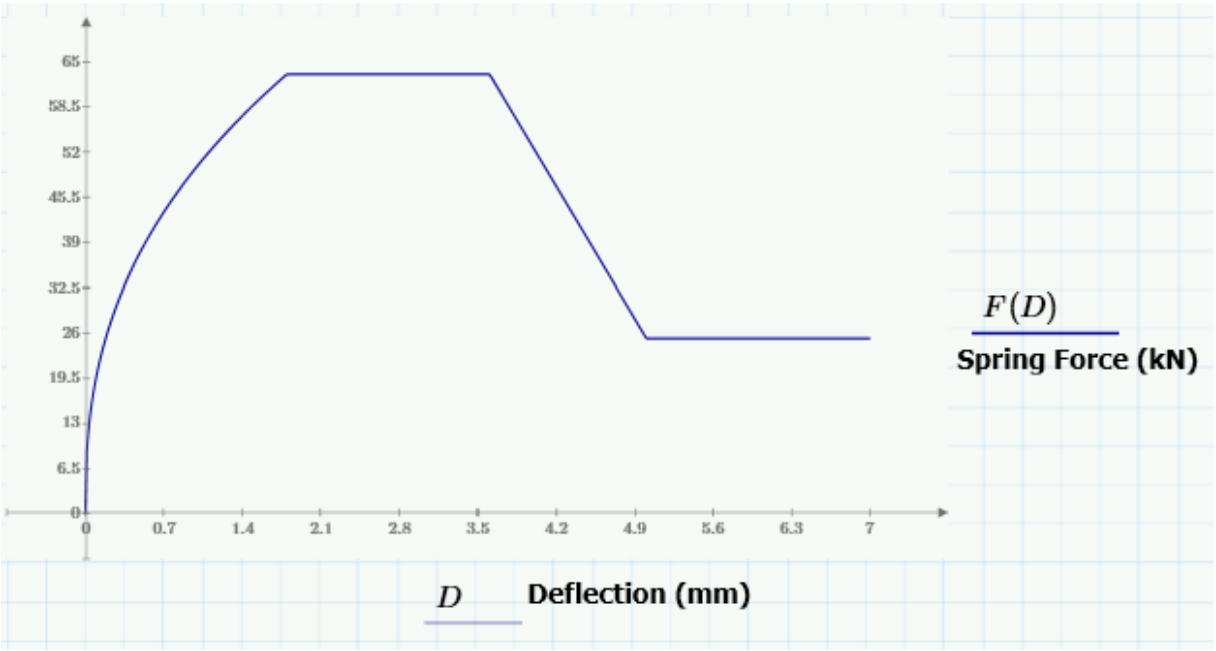

Figure C-32 spring load displacement relationships for 32mm rebar and f'c=42.7MPa

- Spring of 20M rebar and 37MPa concrete

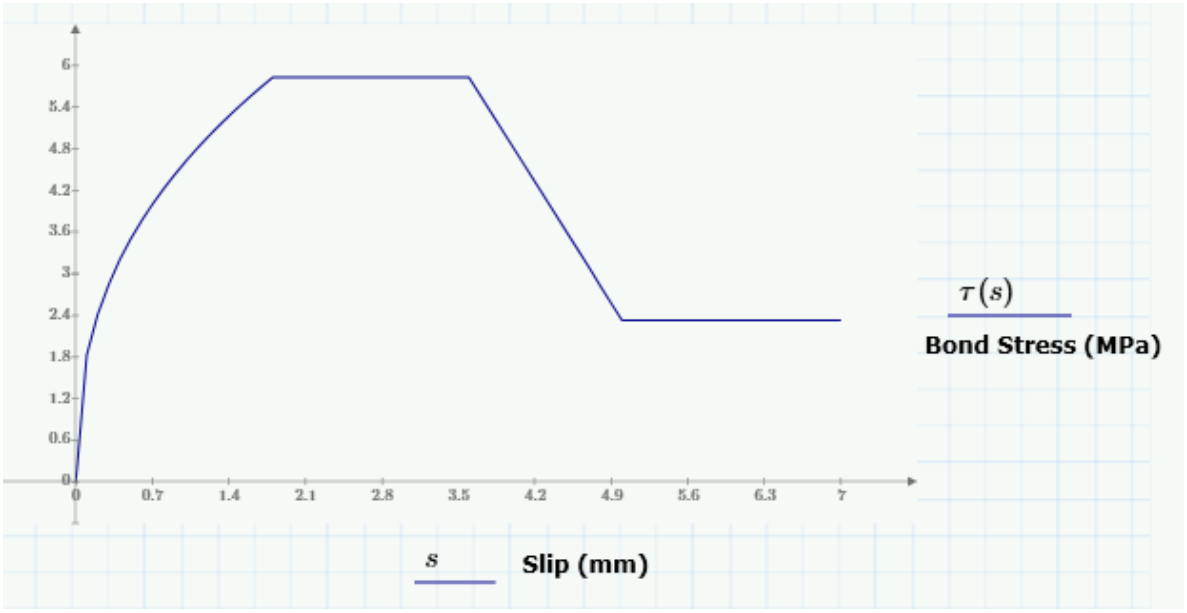

Figure C-33 spring stress strain relationships for 20M rebar and f'c=37MPa

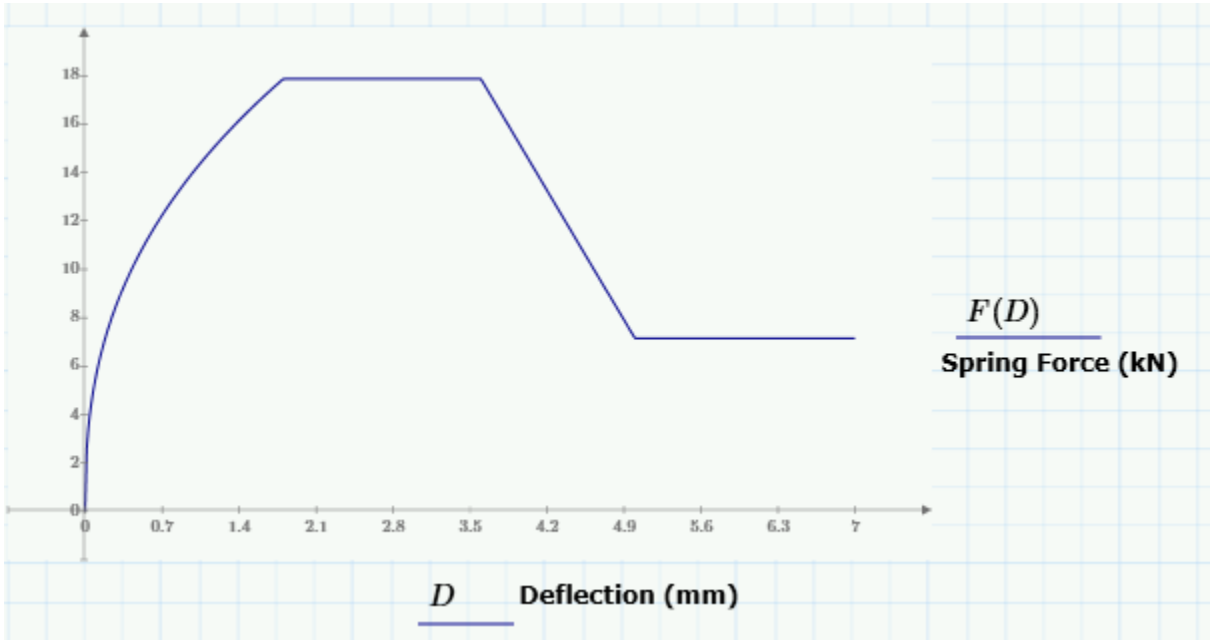

Figure C-34 spring load displacement relationships for 20M rebar and f'c=37MPa

- Spring of 25M rebar and 37MPa concrete

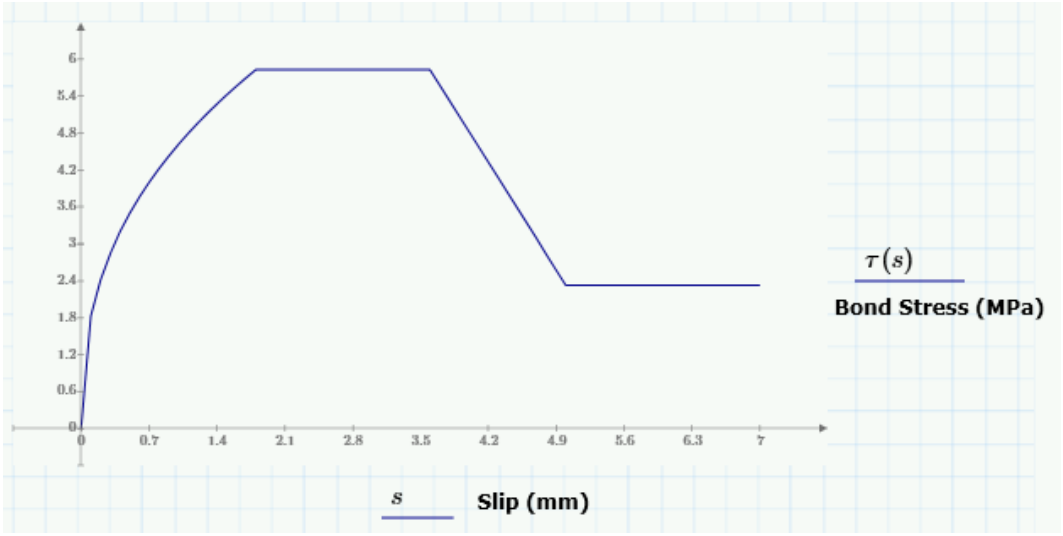

Figure C-35 spring stress strain relationships for 25M rebar and f'c=37MPa

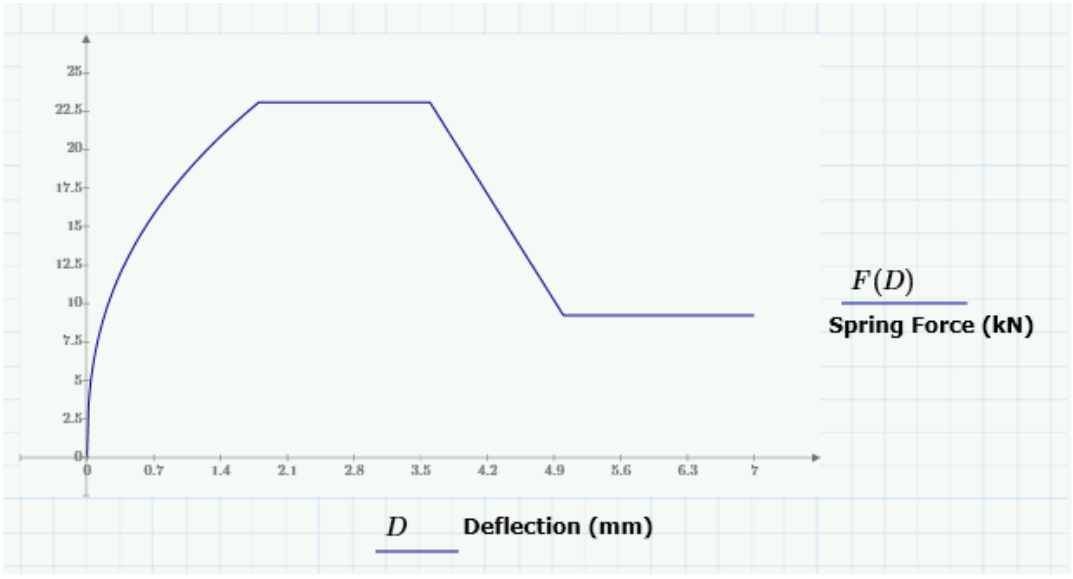

Figure C-36 spring load displacement relationships for 25M rebar and f'c=37MPa

Appendix D Finite Element Analysis Solution

Table D-1 Details of case 16-0

Case Name	Bottom Reinforcement	Honeycombing Location	Strength of Concrete(MPa)	Ultimate Load (kN)	Ultimate Deflection(mm)	Failure Mode
16-0	16mm	None	42.7	104.2137	17.334	

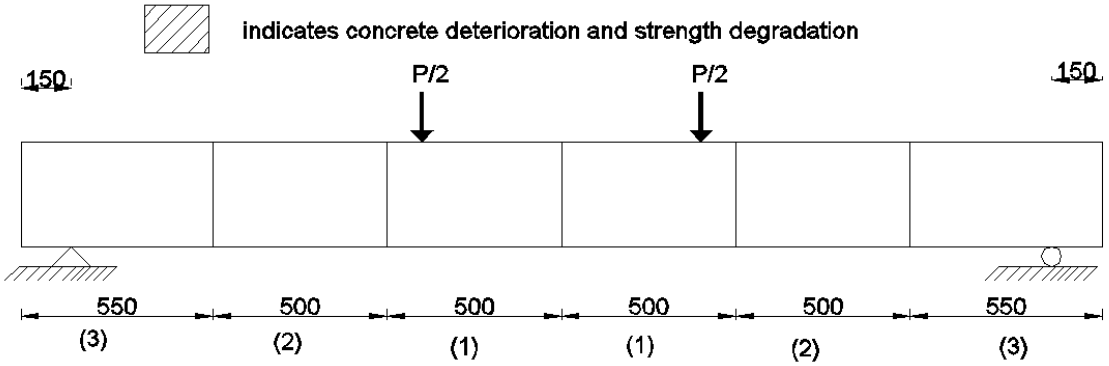

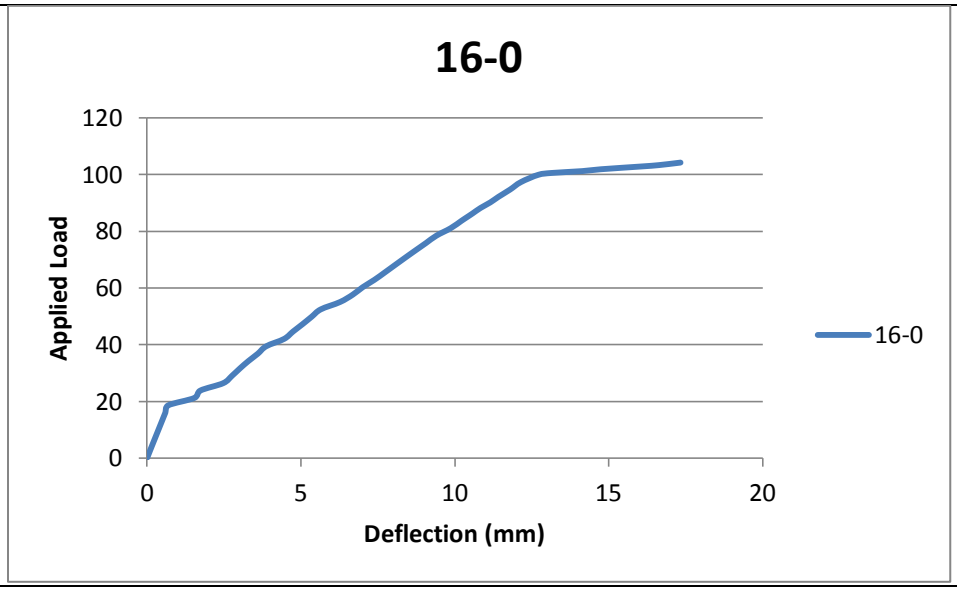

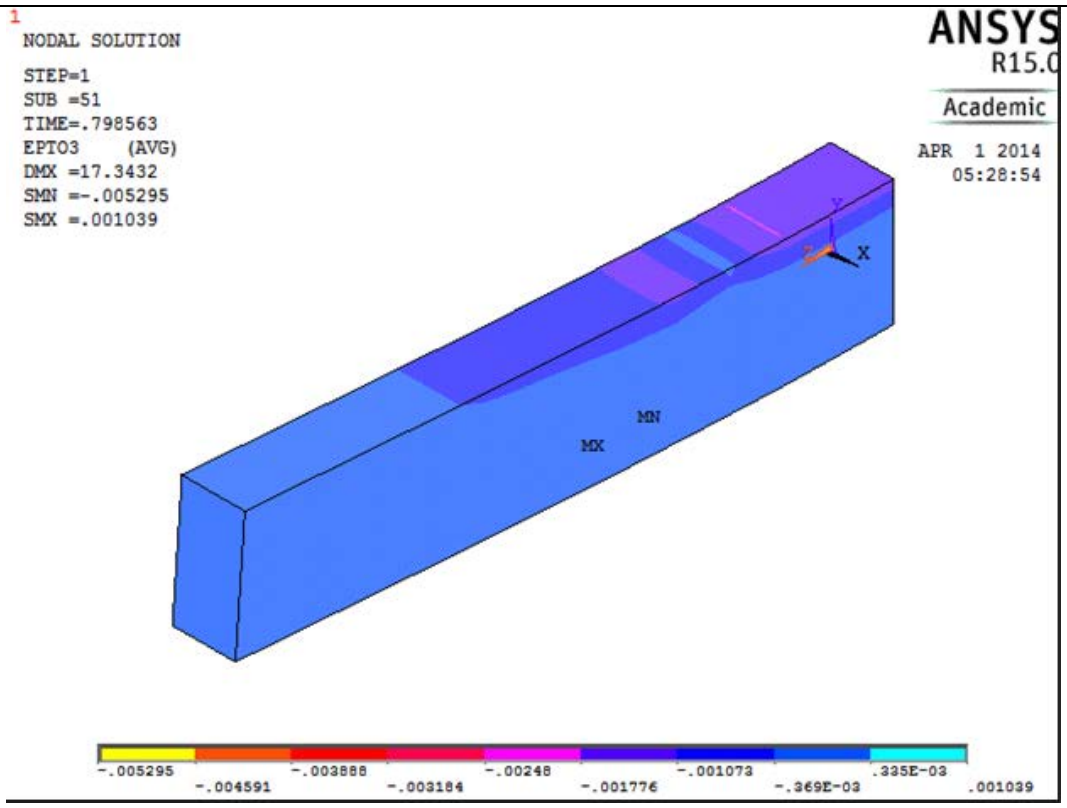

Figure D-1 Nodal solution – 3rd principal total mechanical strain for 16-0

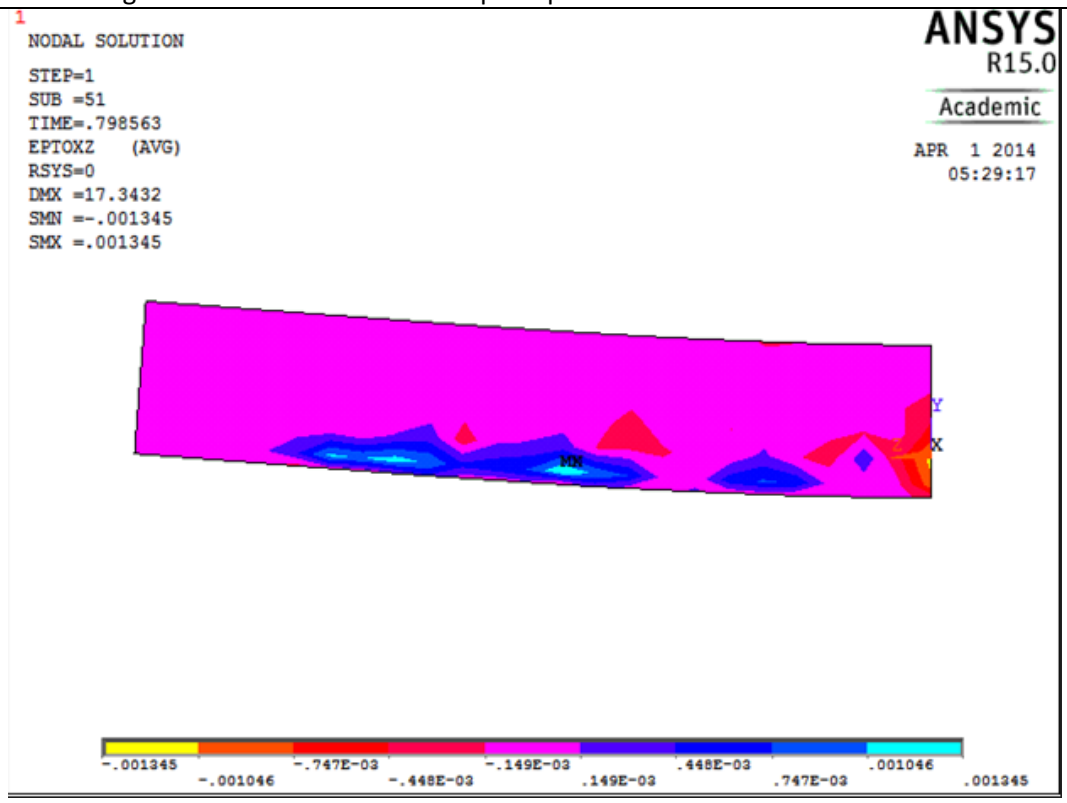

Figure D-2 Nodal Solution XZ shear total mechanical strain for 16-0

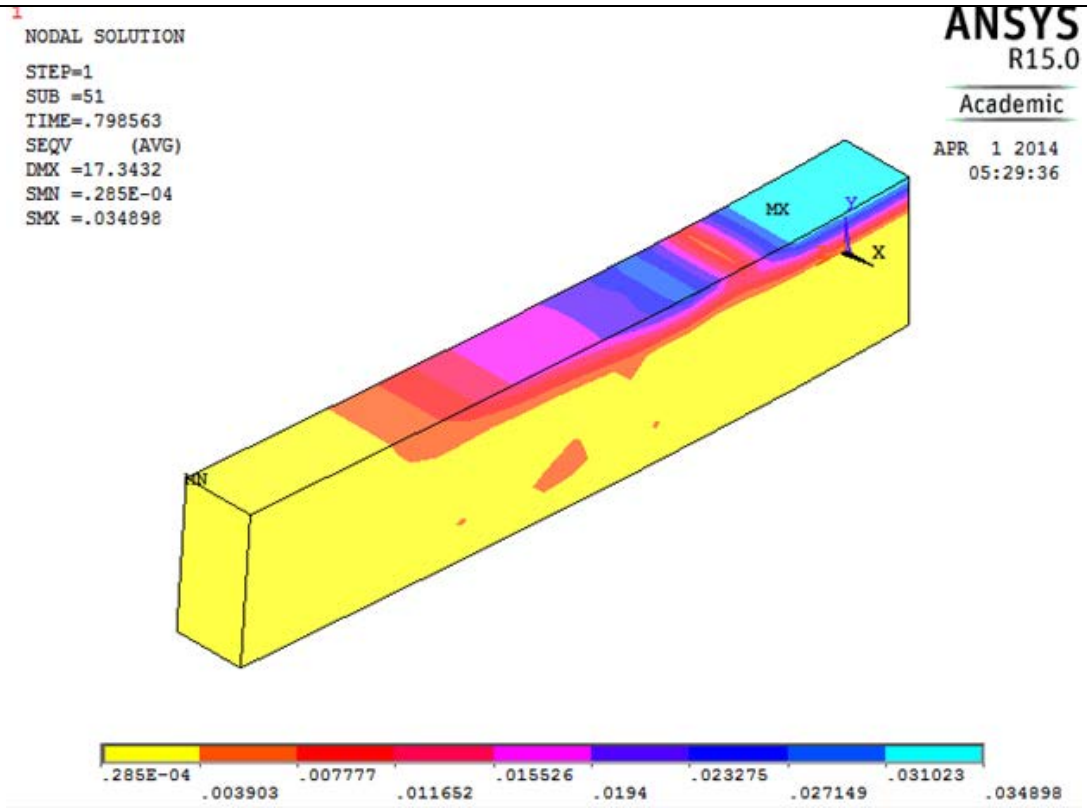

Figure D-3 Nodal Solution -Von Mises Stress of 16-0

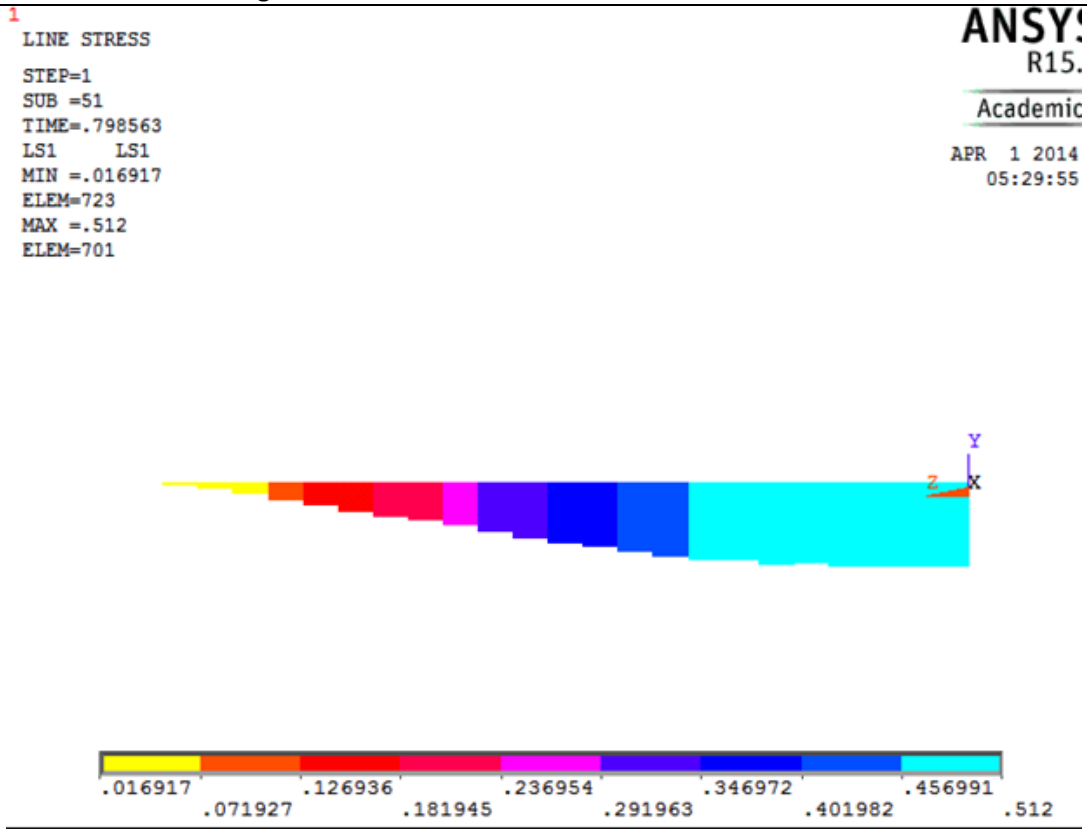

Figure D-4 Reinforcement Stress for 16-0

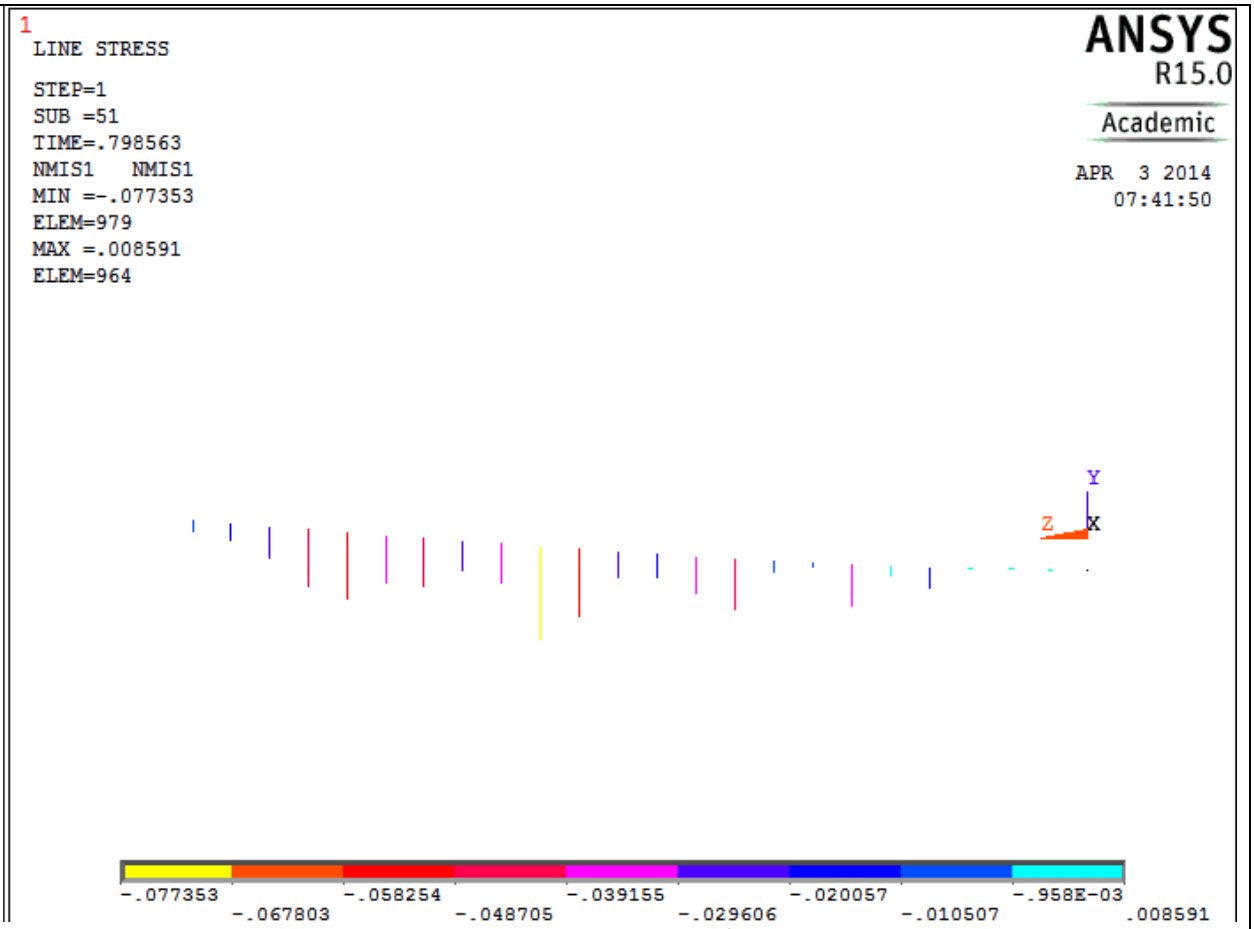

Figure D-5 Spring Stretch for 16-0

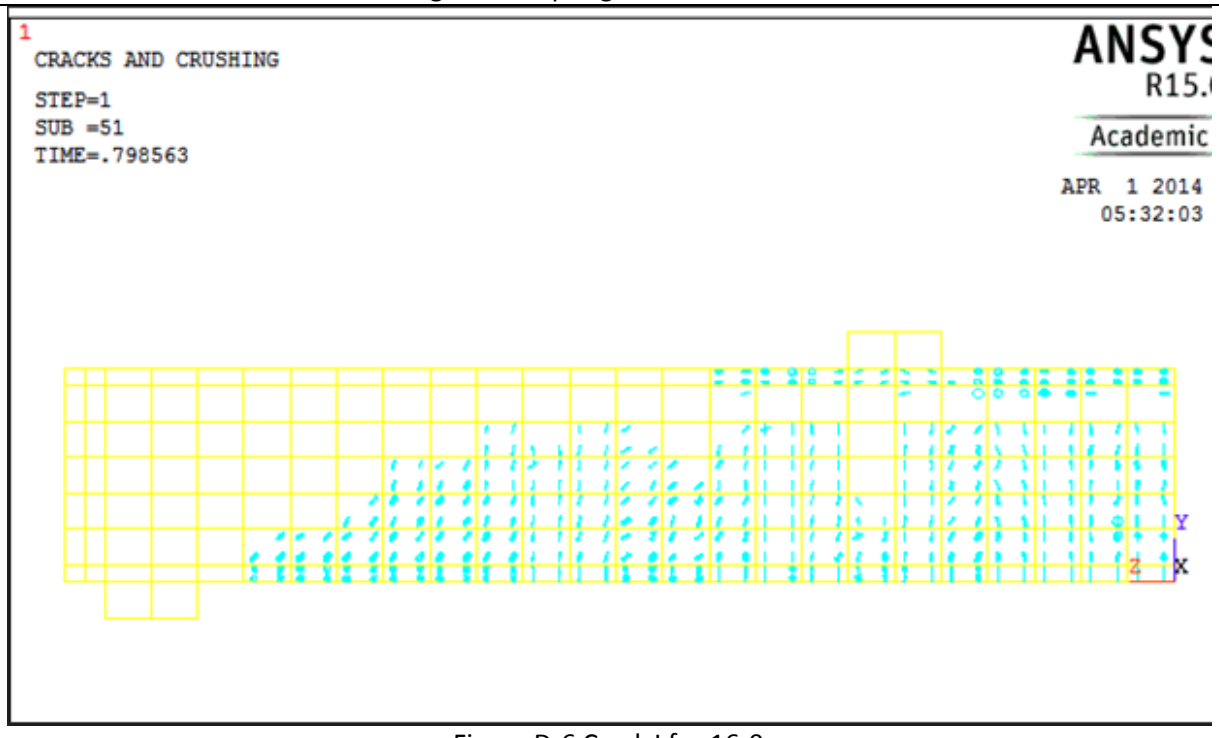

Figure D-6 Crack I for 16-0

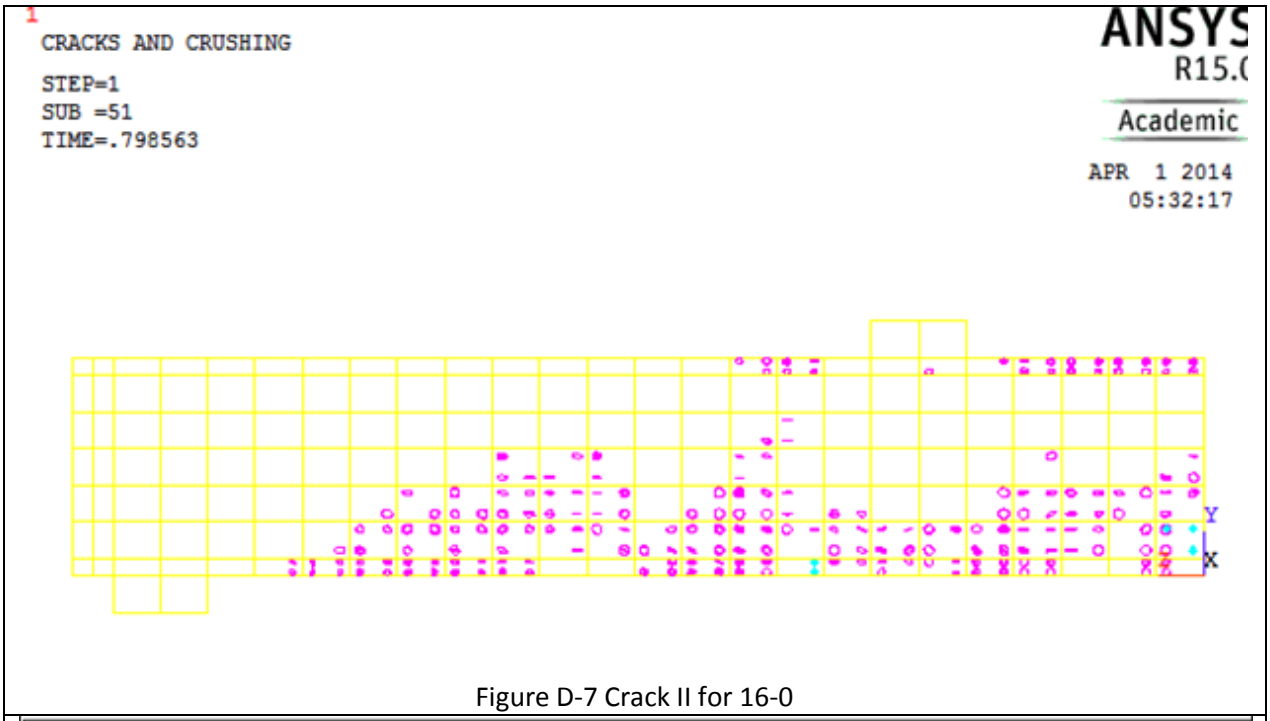

Figure D-7 Crack II for 16-0

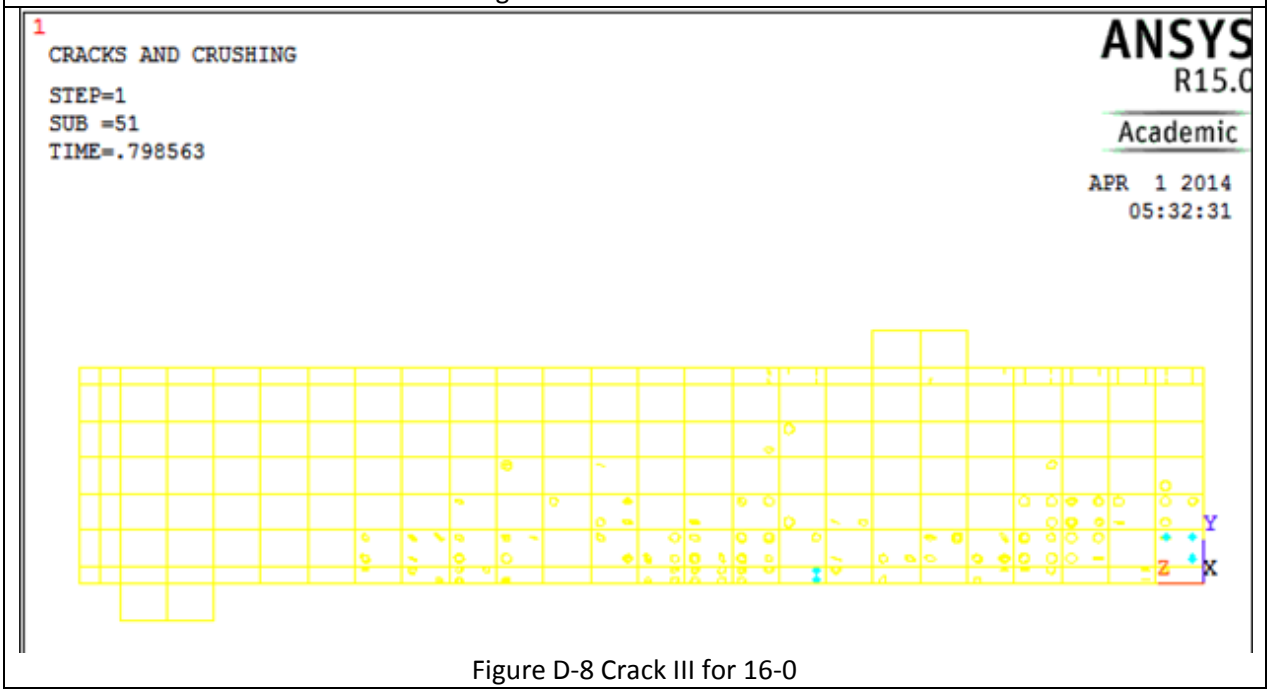

Figure D-8 Crack III for 16-0

Table D-2 Details of case 16-1-10

Case Name	Bottom Reinforcement	Honeycombing Location	Strength of Concrete(MPa)	Ultimate Load (kN)	Ultimate Deflection(mm)	Failure Mode
16-1-10	16mm	1	10	53.6185	8.3638	

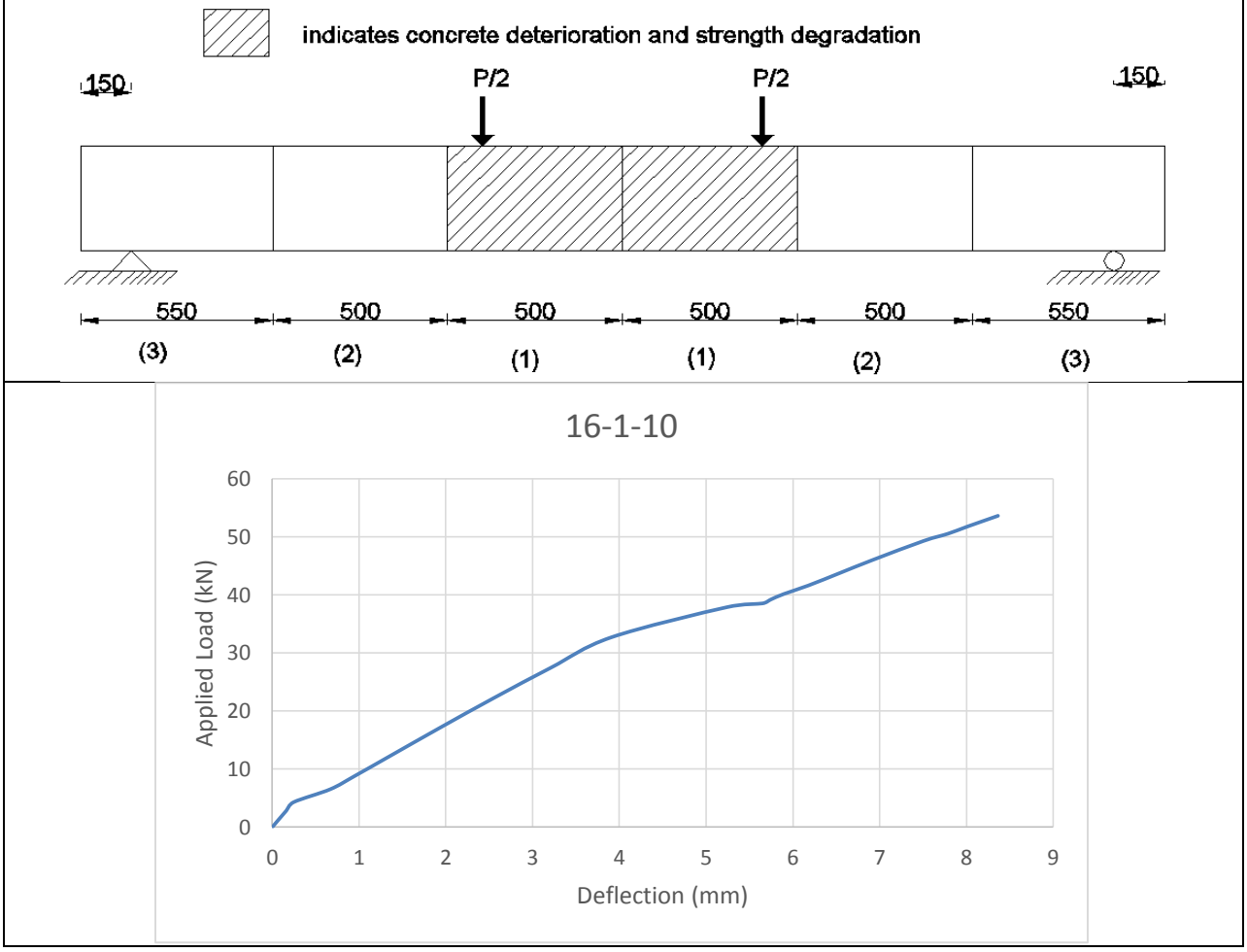

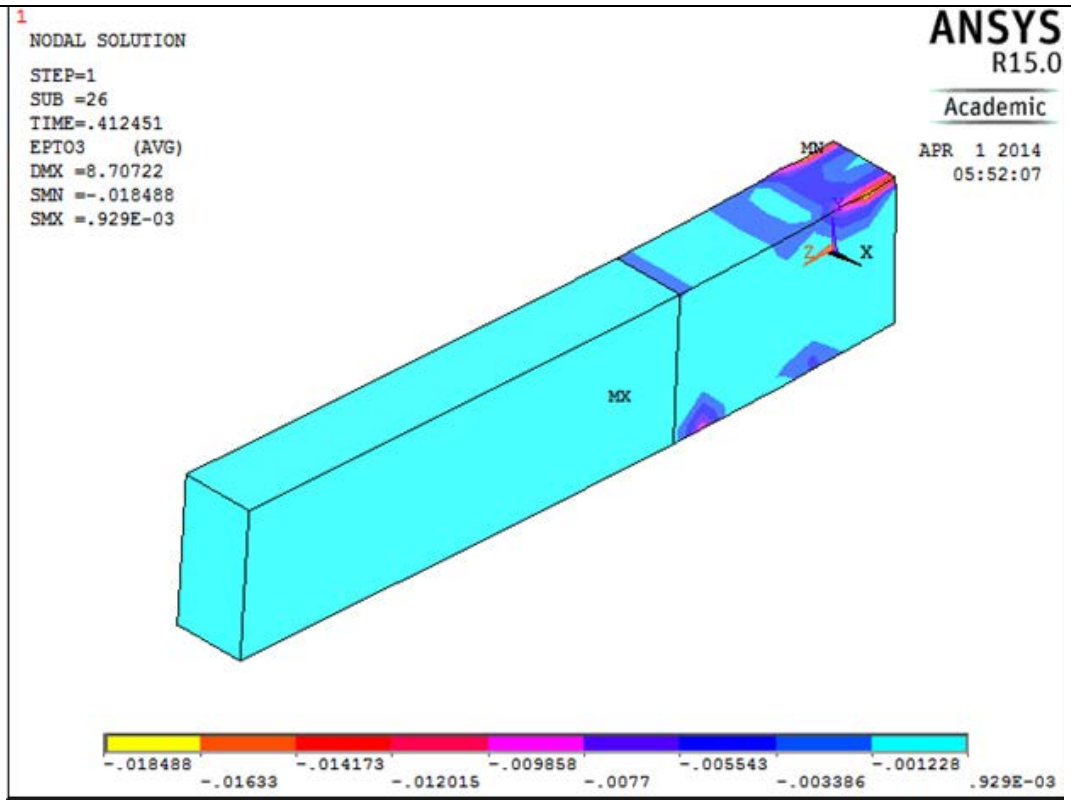

Figure D-9 Nodal solution – 3rd principal total mechanical strain for 16-1-10

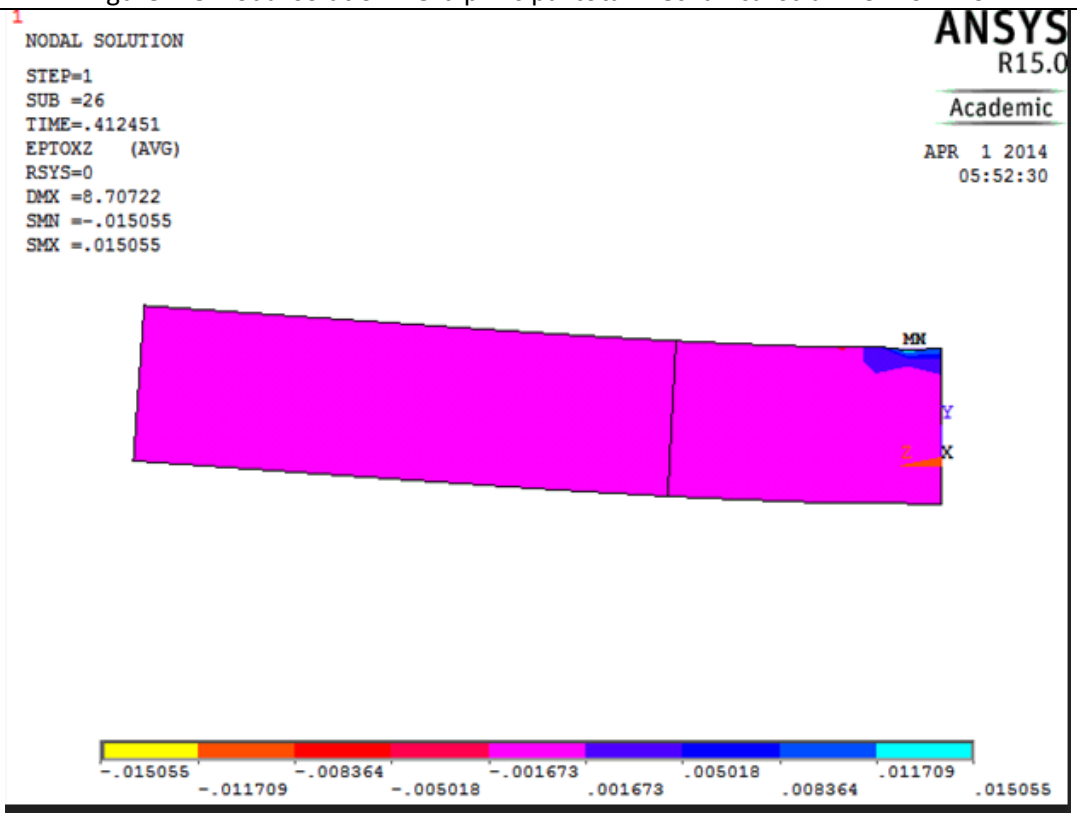

Figure D-10 Nodal Solution XZ shear total mechanical strain for 16-1-10

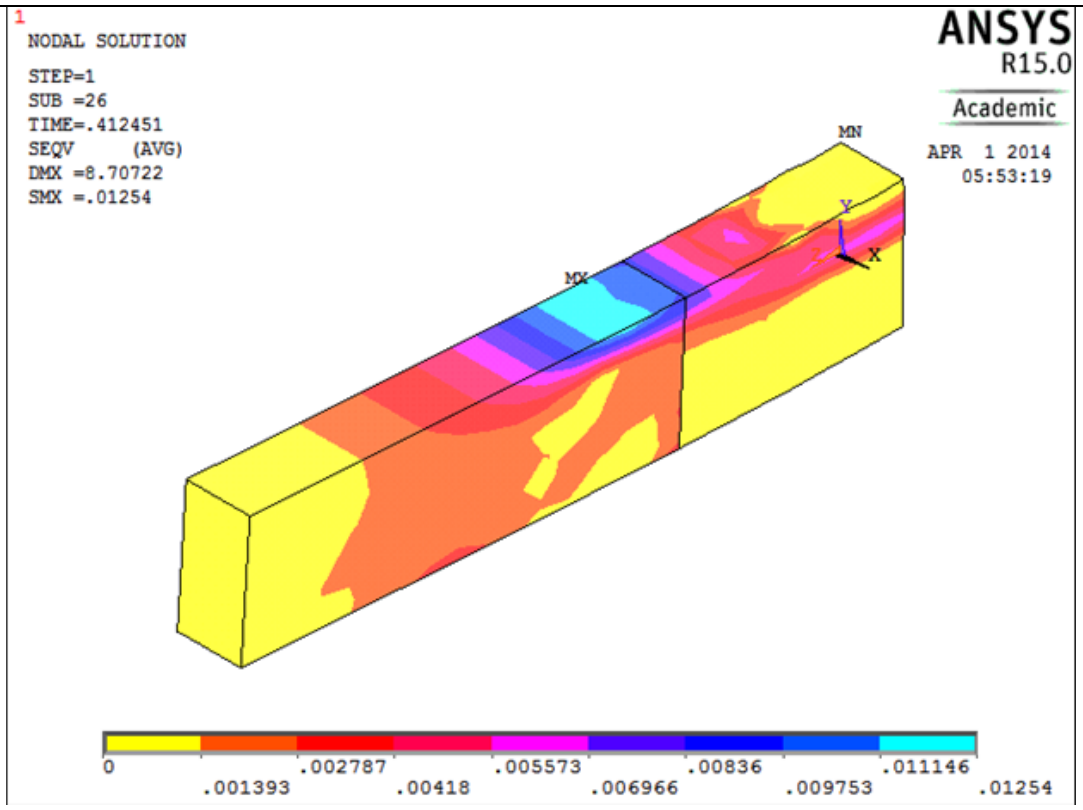

Figure D-11 Nodal Solution -Von Mises Stress for 16-1-10

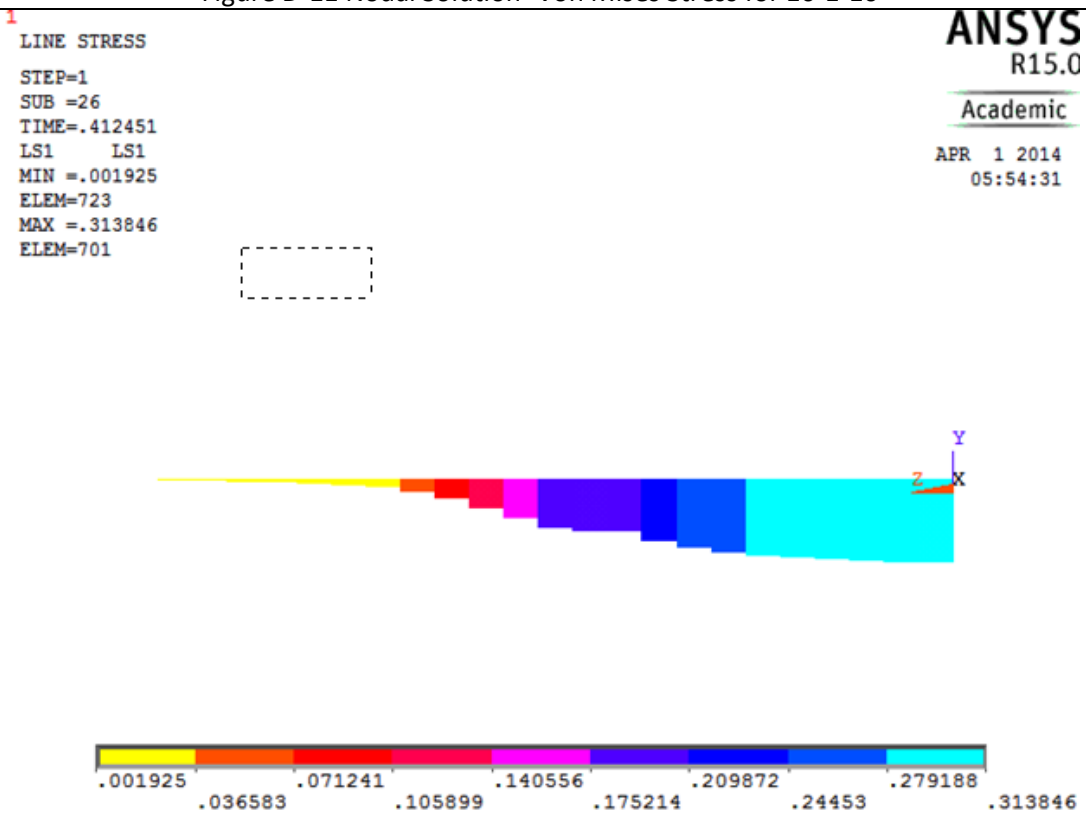

Figure D-12 Reinforcement Stress for 16-1-10

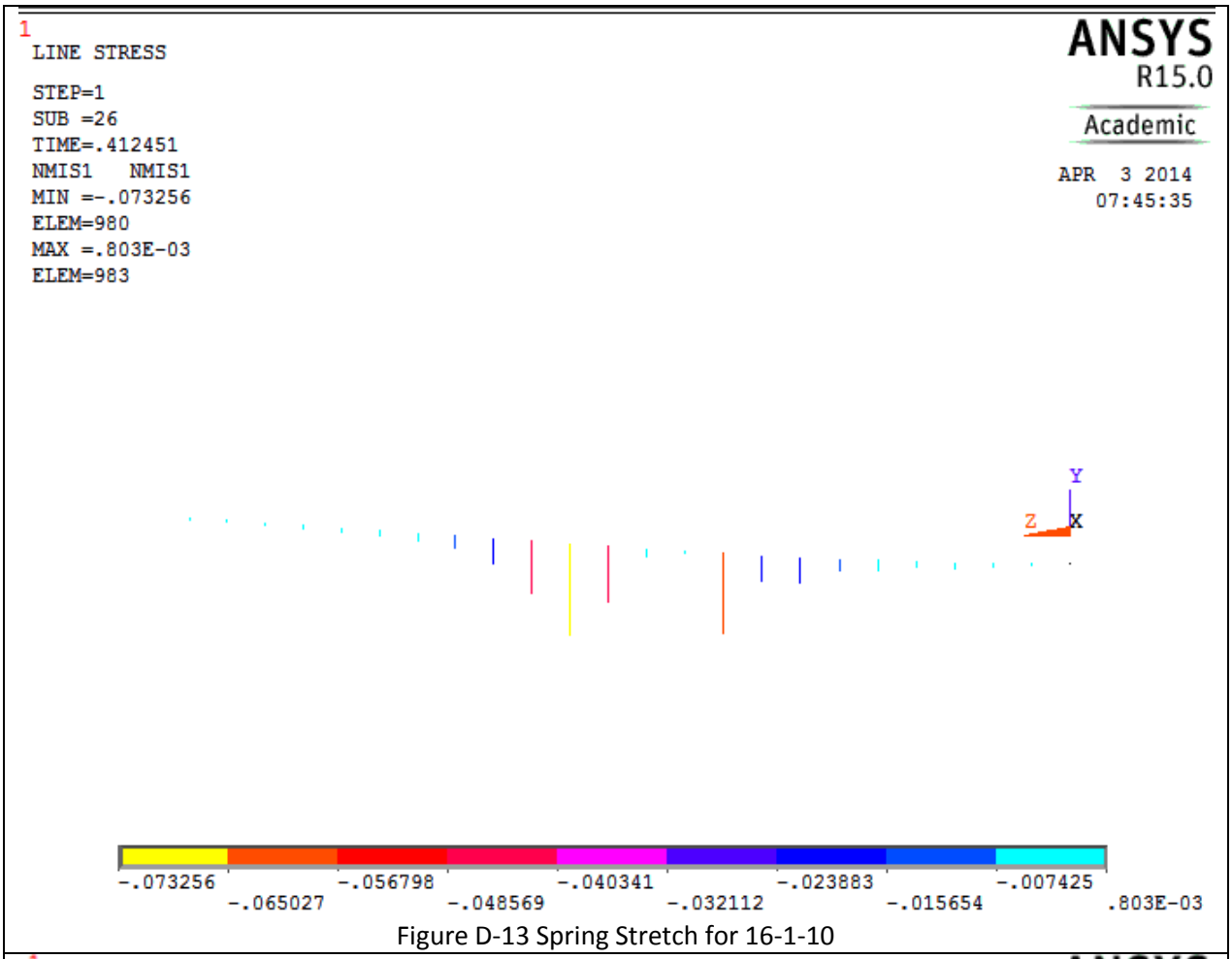

Figure D-13 Spring Stretch for 16-1-10

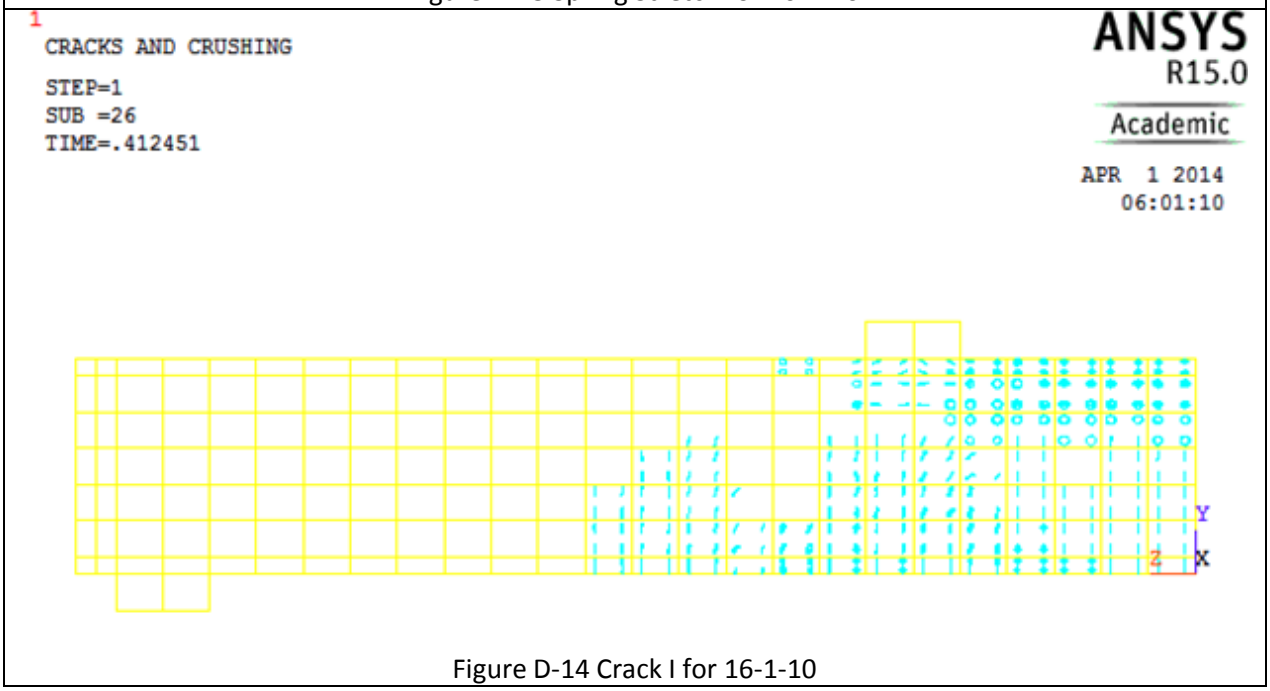

Figure D-14 Crack I for 16-1-10

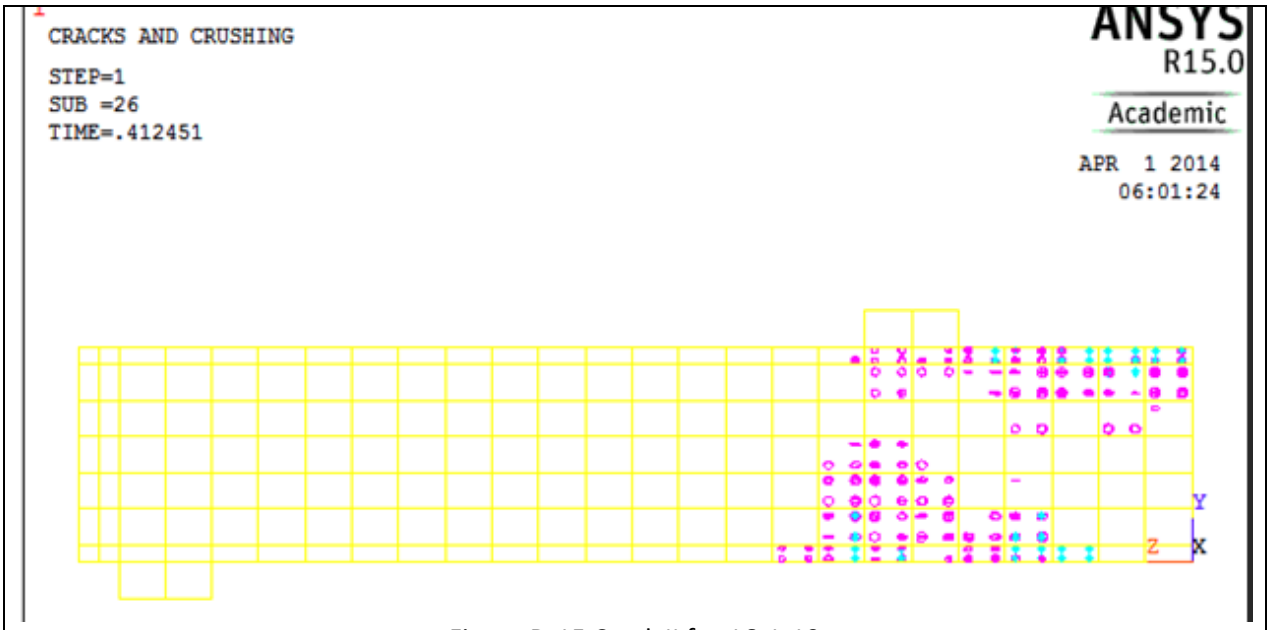

Figure D-15 Crack II for 16-1-10

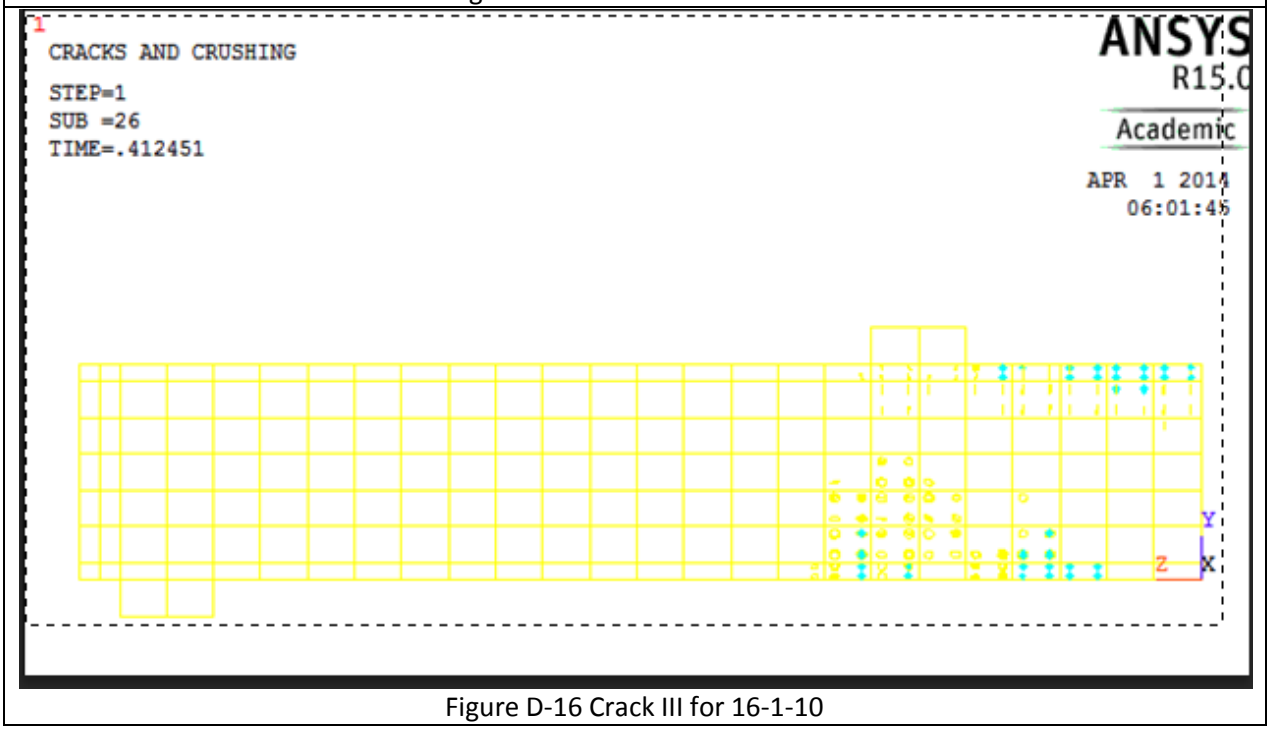

Figure D-16 Crack III for 16-1-10

Table D-3 Details of case 16-1-20

Case Name	Bottom Reinforcement	Honeycombing Location	Strength of Concrete(MPa)	Ultimate Load (kN)	Ultimate Deflection(mm)	Failure Mode
16-1-20	16mm	1	20	87.7643	12.3896	

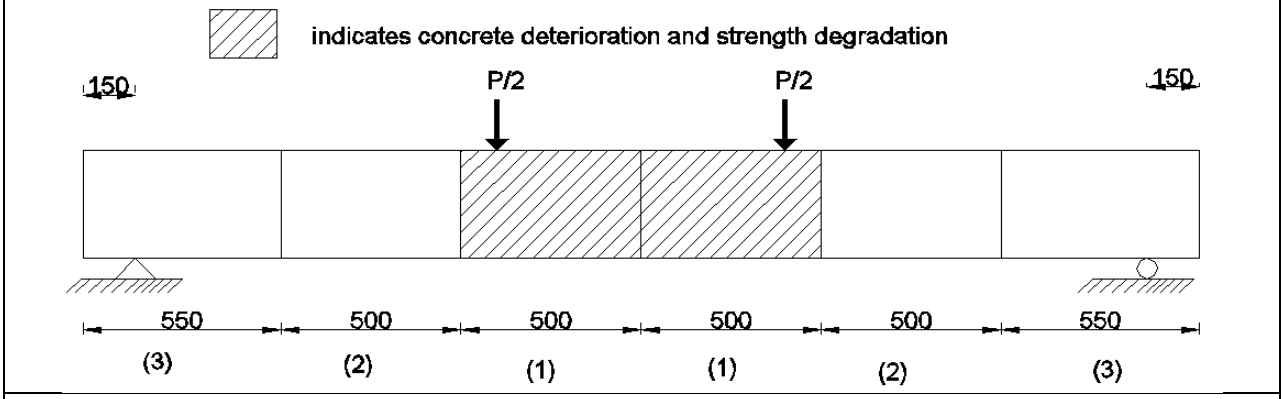

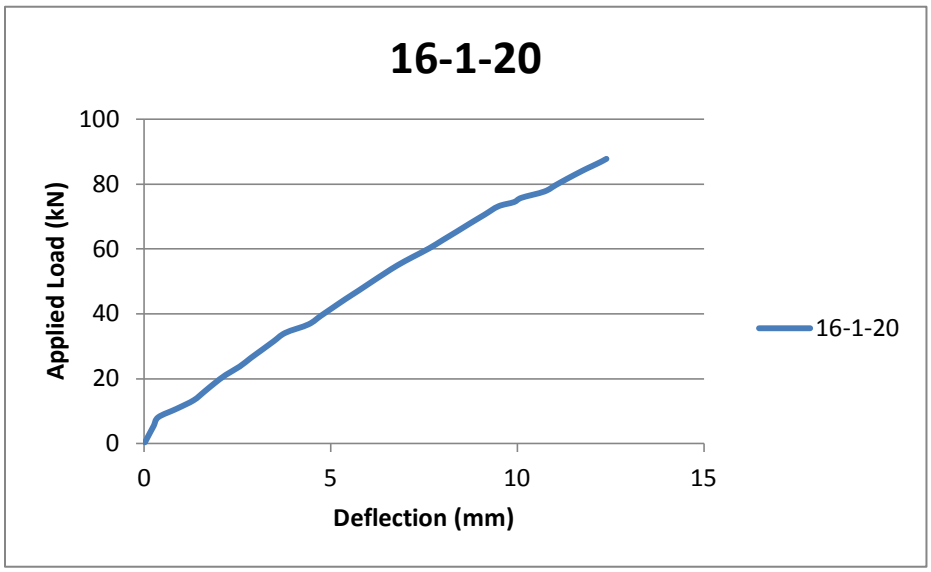

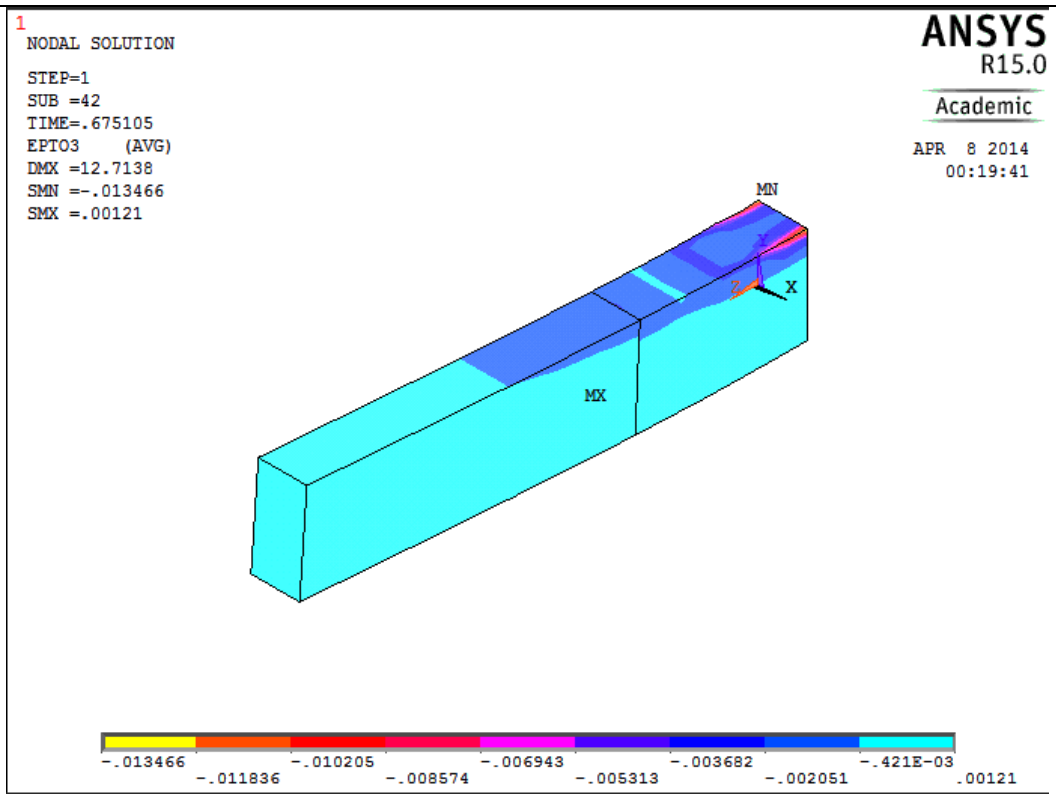

Figure D-17 Nodal solution – 3rd principal total mechanical strain for 16-1-20

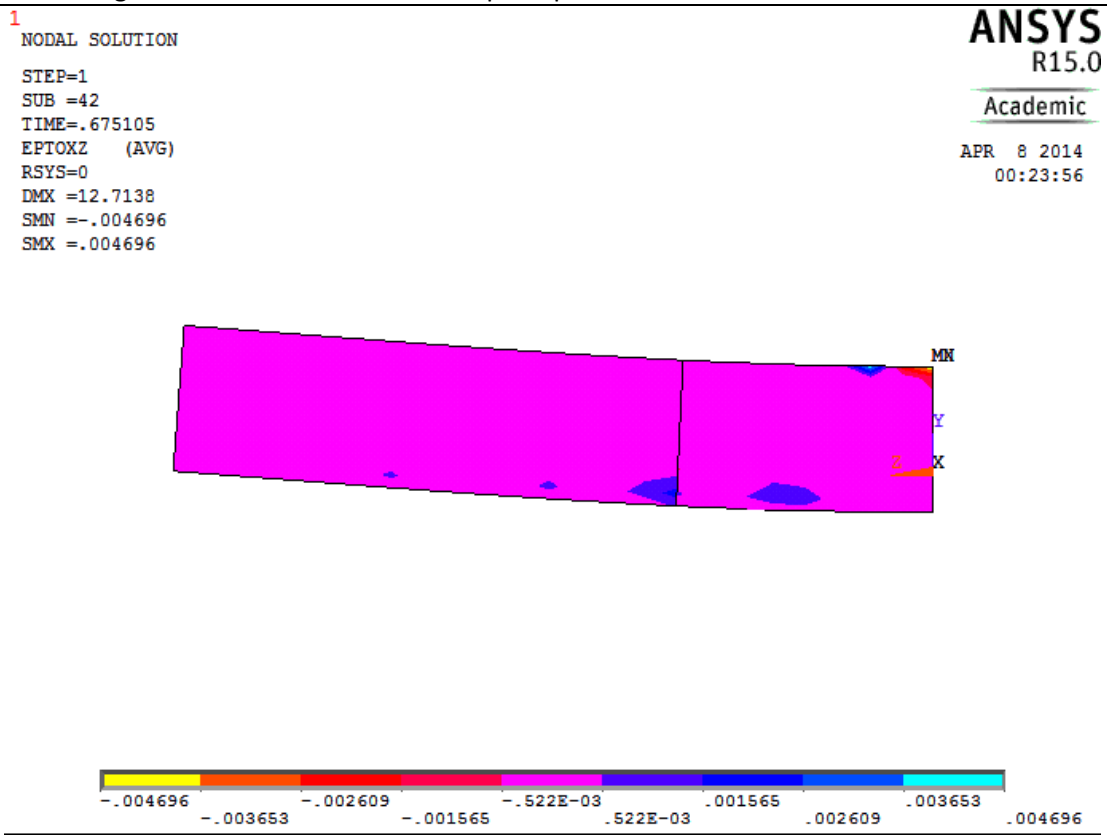

Figure D-18 Nodal Solution XZ shear total mechanical strain for 16-1-20

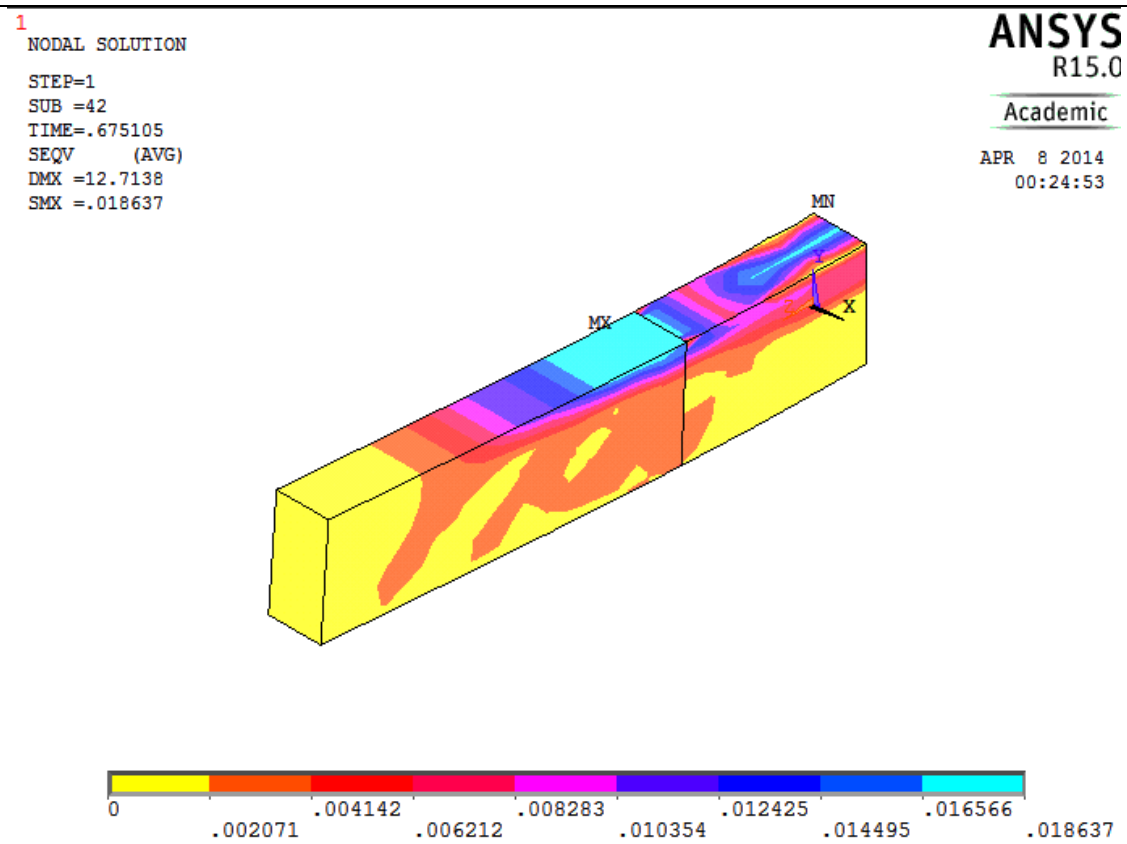

Figure D-19 Nodal Solution -Von Mises Stress for 16-1-20

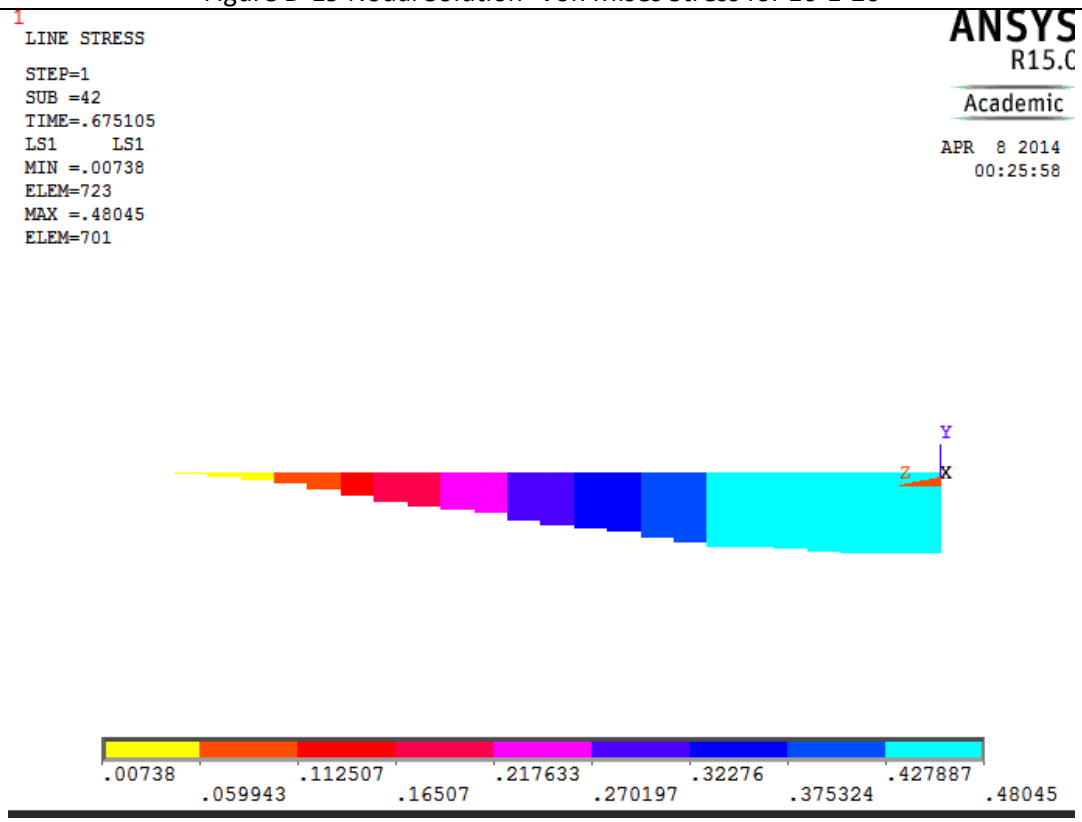

Figure D-20 Reinforcement Stress for 16-1-20

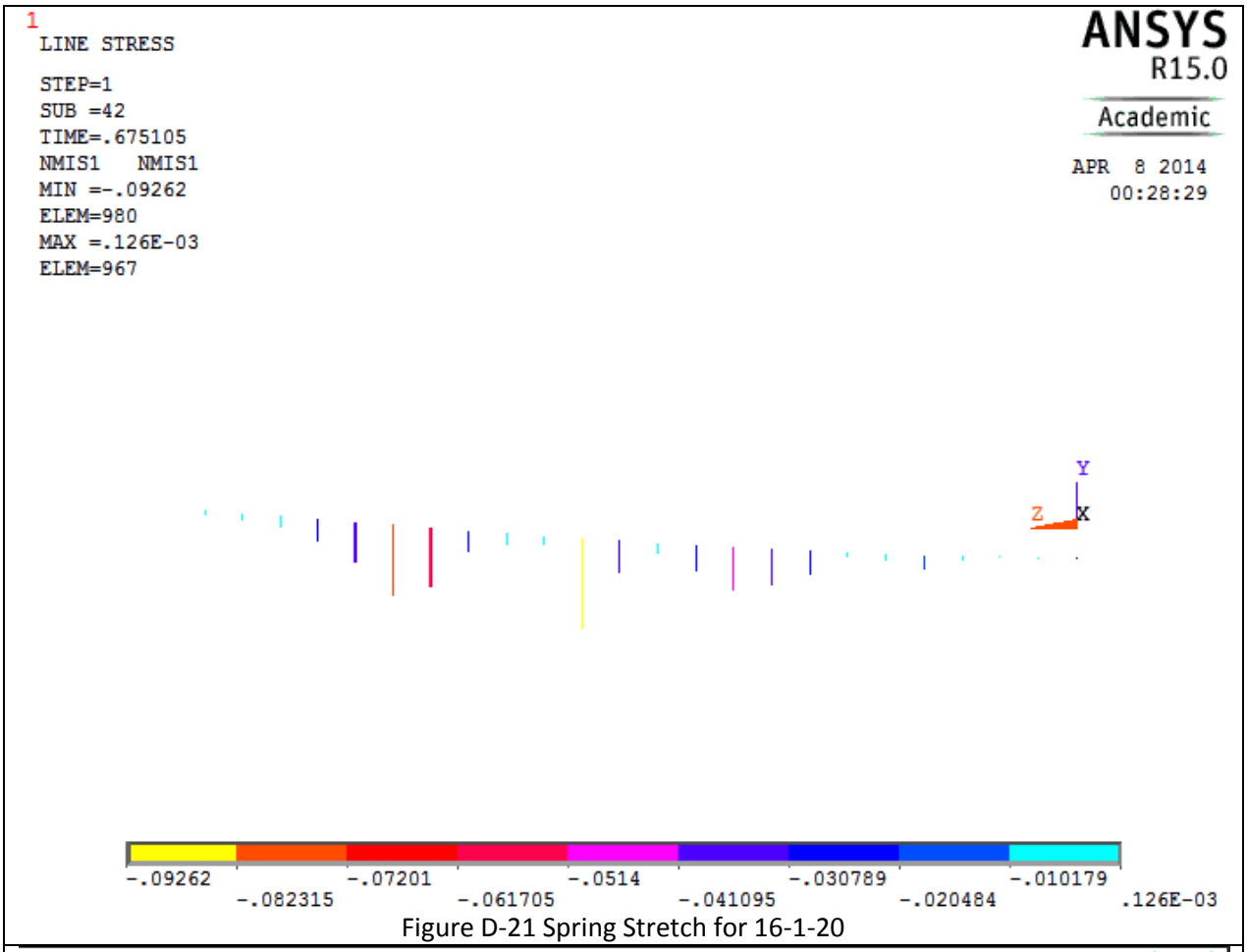

Figure D-21 Spring Stretch for 16-1-20

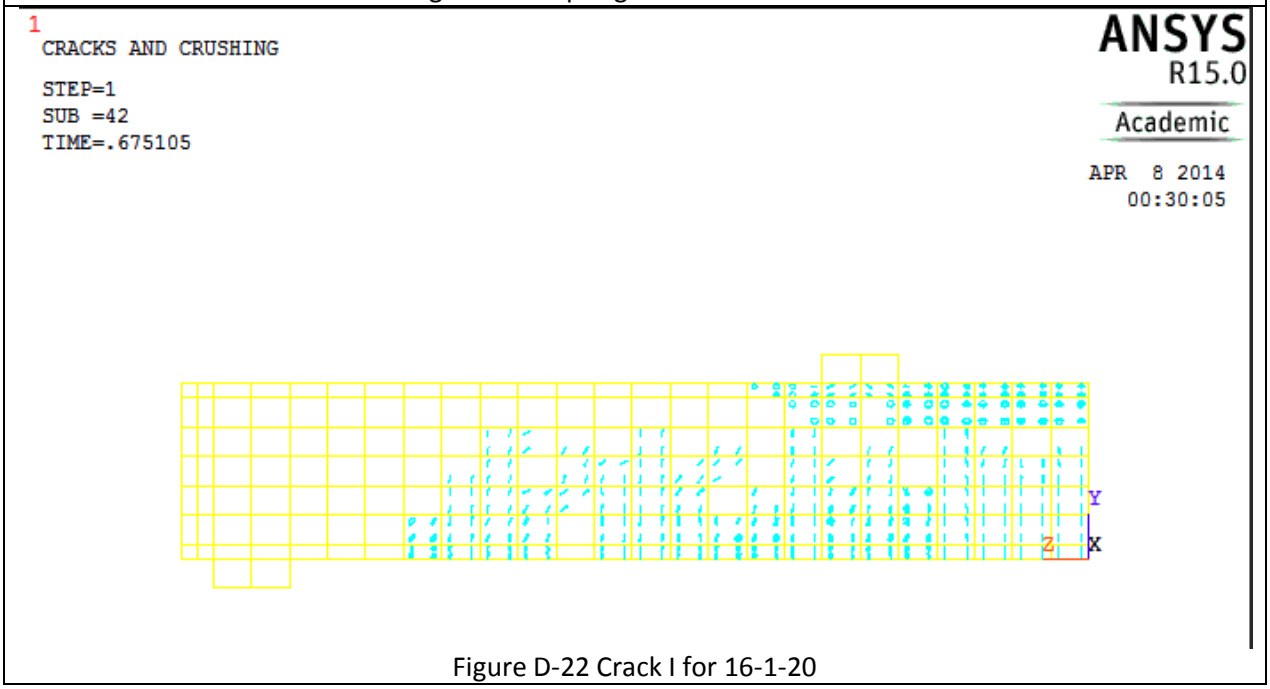

Figure D-22 Crack I for 16-1-20

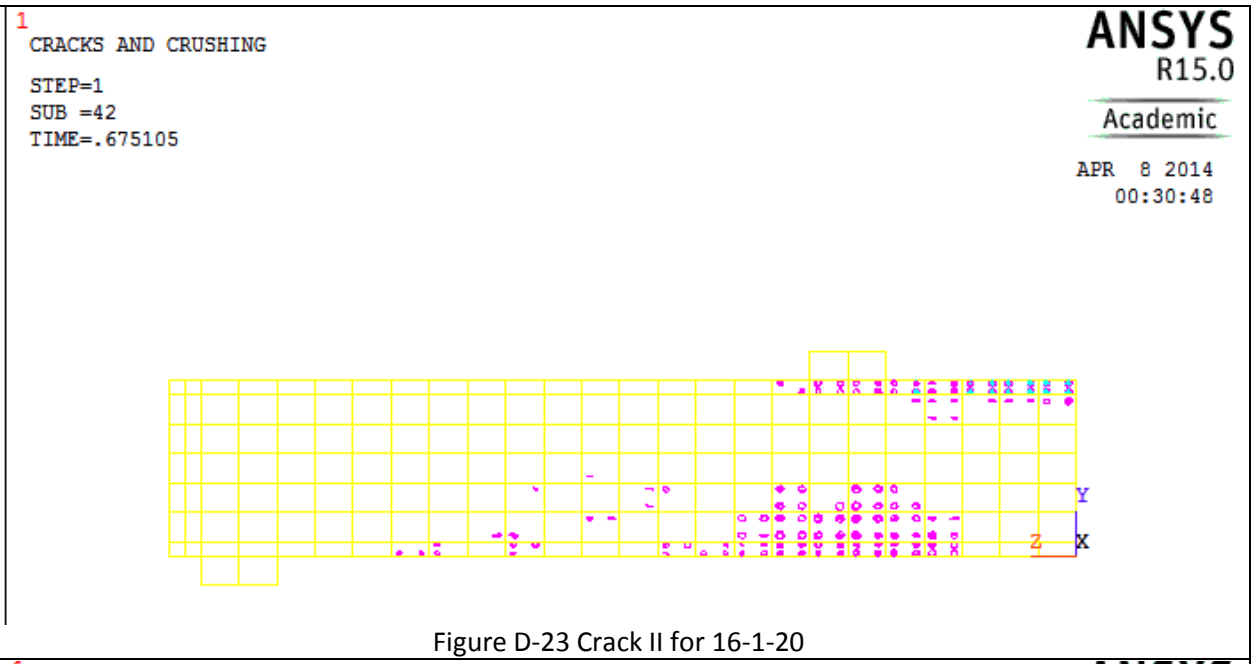

Figure D-23 Crack II for 16-1-20

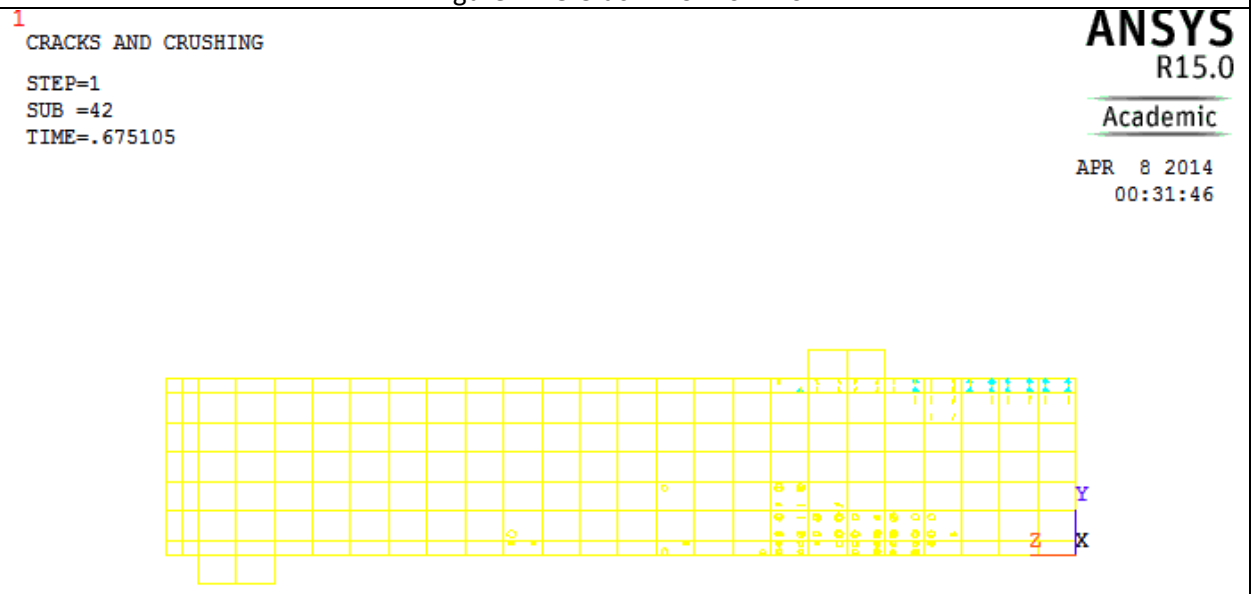

Figure D-24 Crack III for 16-1-20

Table D-4 Details of case 16-1-30

Case Name	Bottom Reinforcement	Honeycombing Location	Strength of Concrete(MPa)	Ultimate Load (kN)	Ultimate Deflection(mm)	Failure Mode
16-1-30	16mm	1	30	101.231	20.2826	

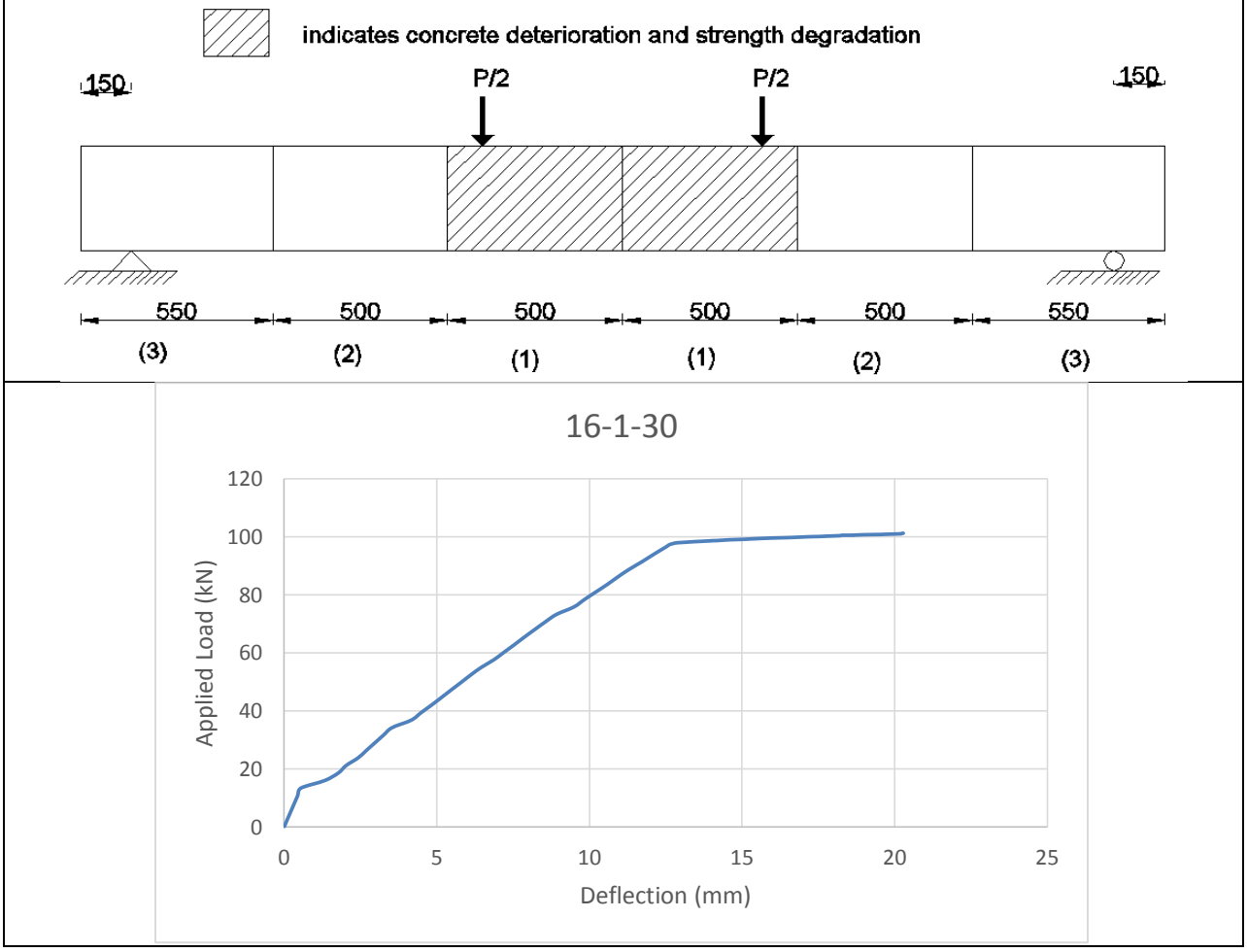

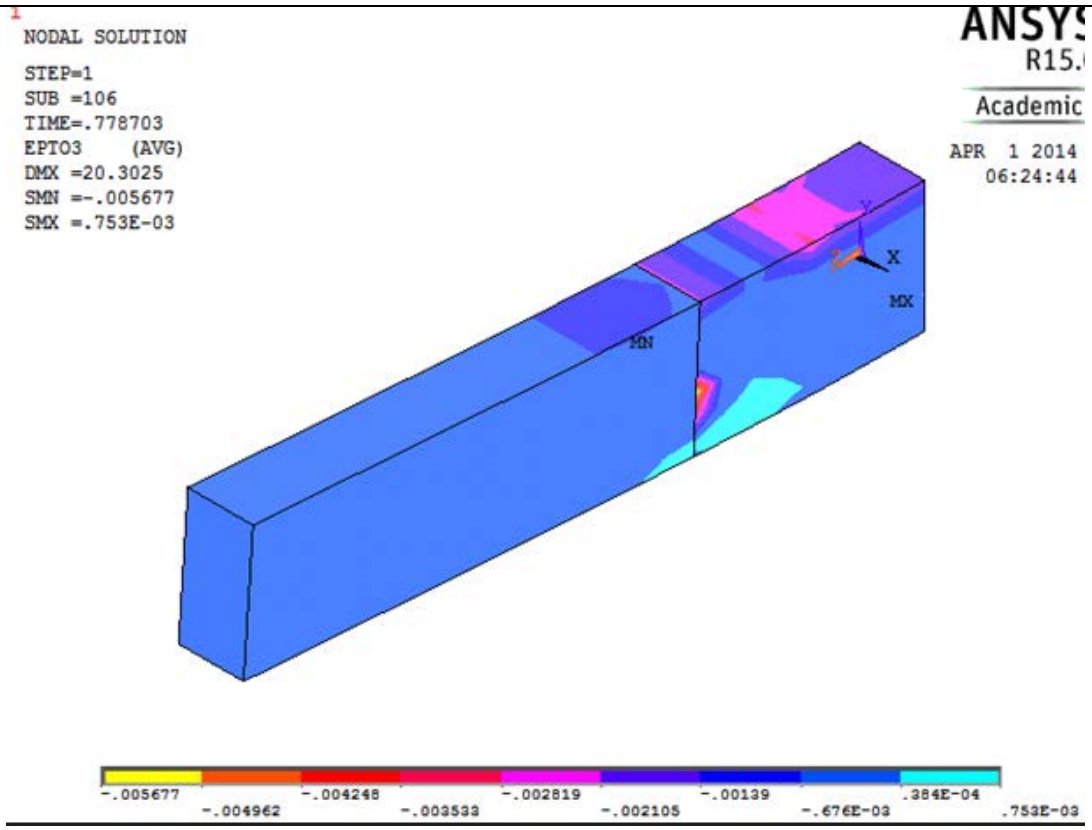

Figure D-25 Nodal solution – 3rd principal total mechanical strain for 16-1-30

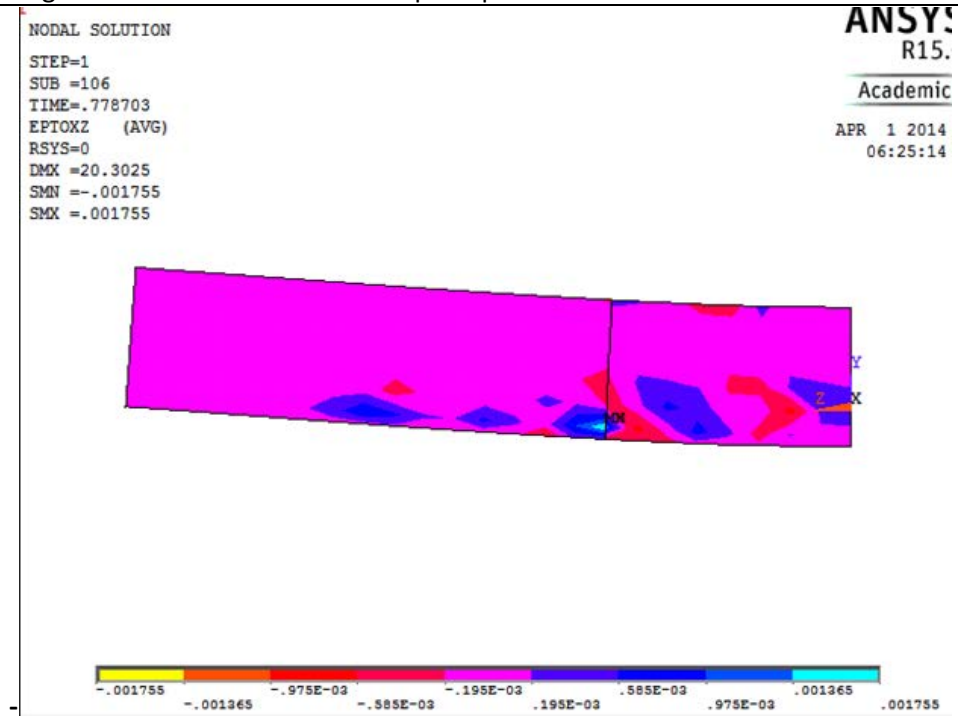

Figure D-26 Nodal Solution XZ shear total mechanical strain for 16-1-30

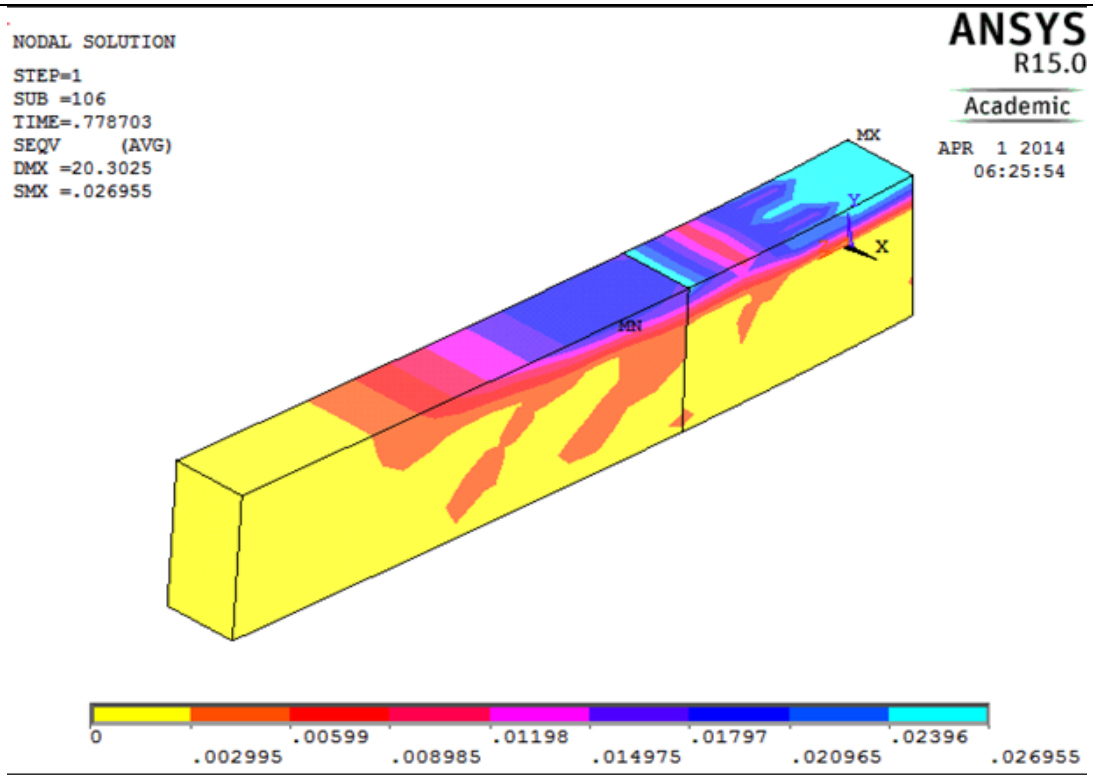

Figure D-27 Nodal Solution -Von Mises Stress for 16-1-30

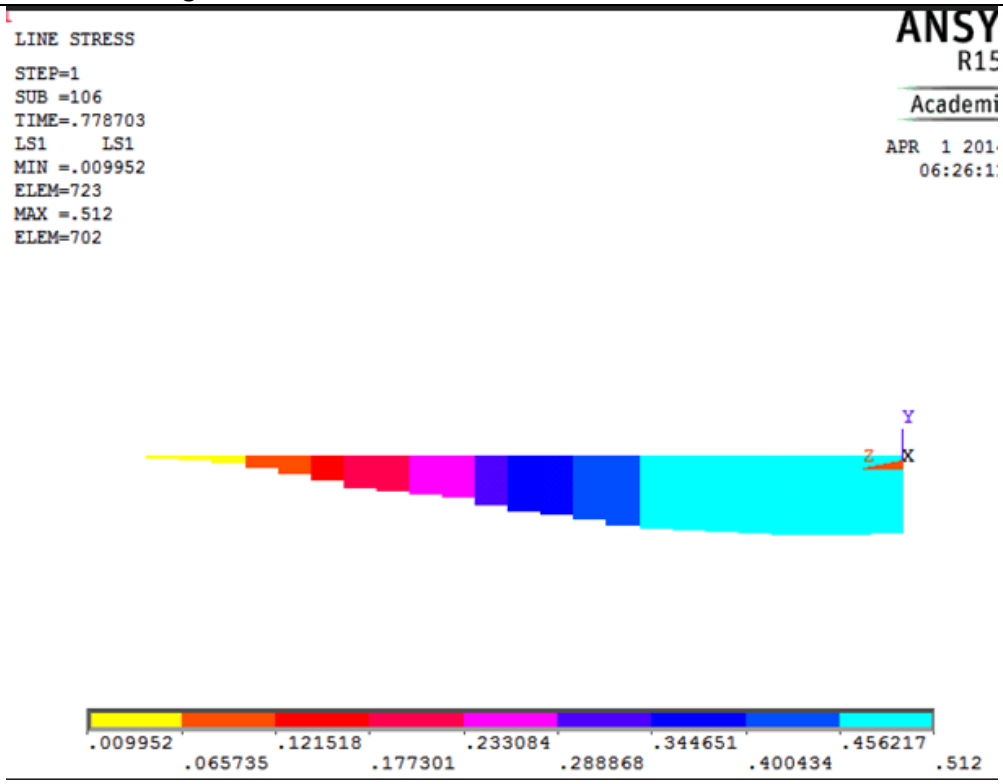

Figure D-28 Reinforcement Stress for 16-1-30

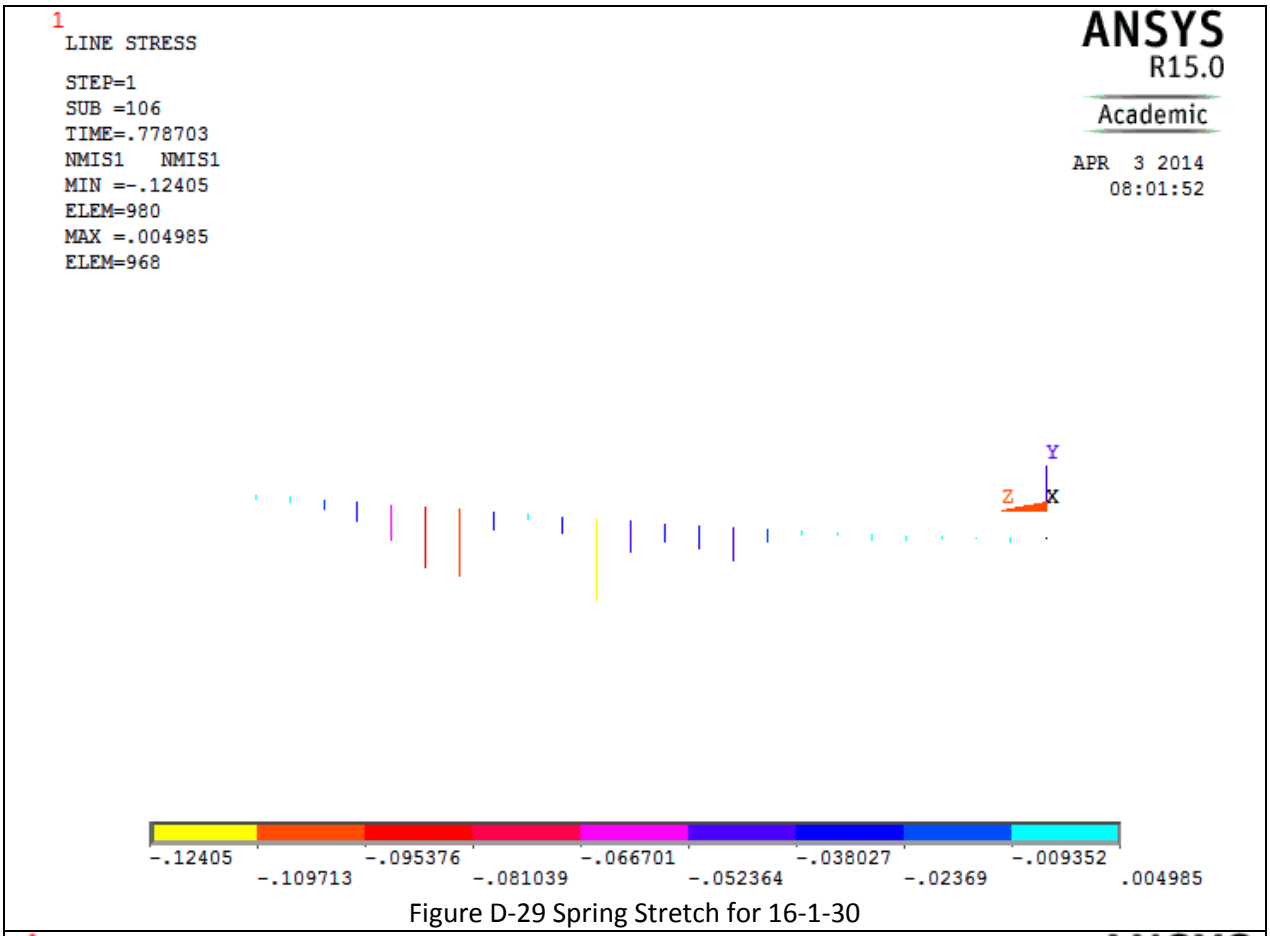

Figure D-29 Spring Stretch for 16-1-30

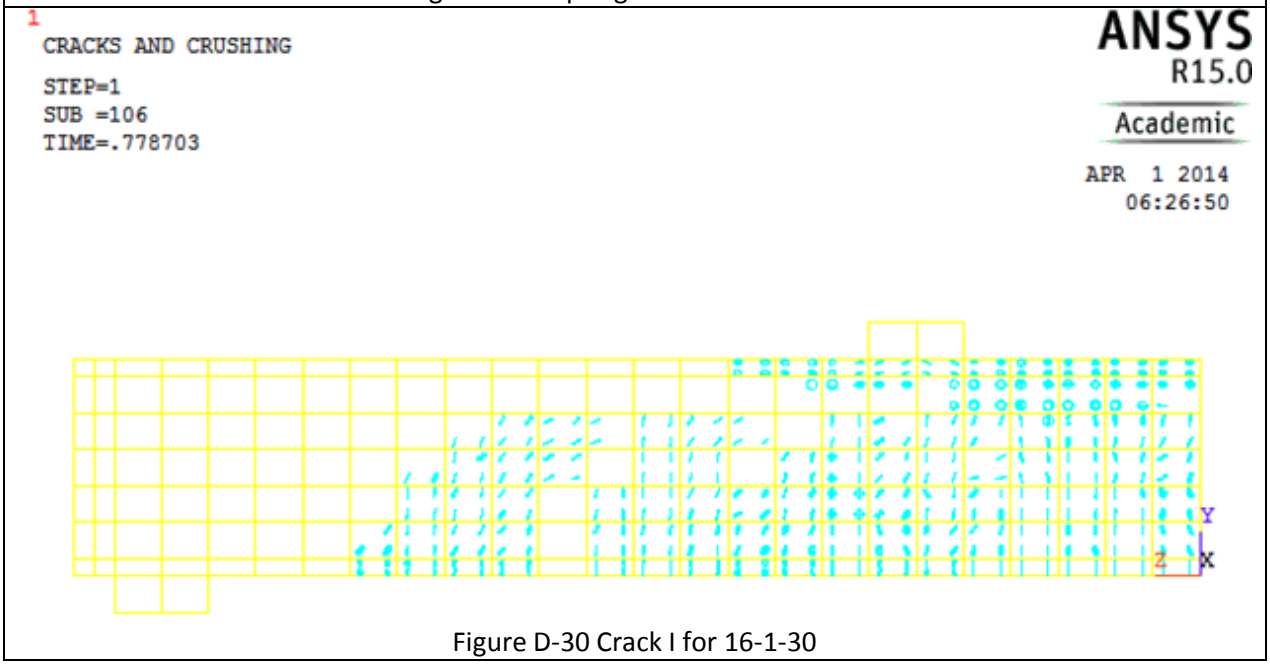

Figure D-30 Crack I for 16-1-30

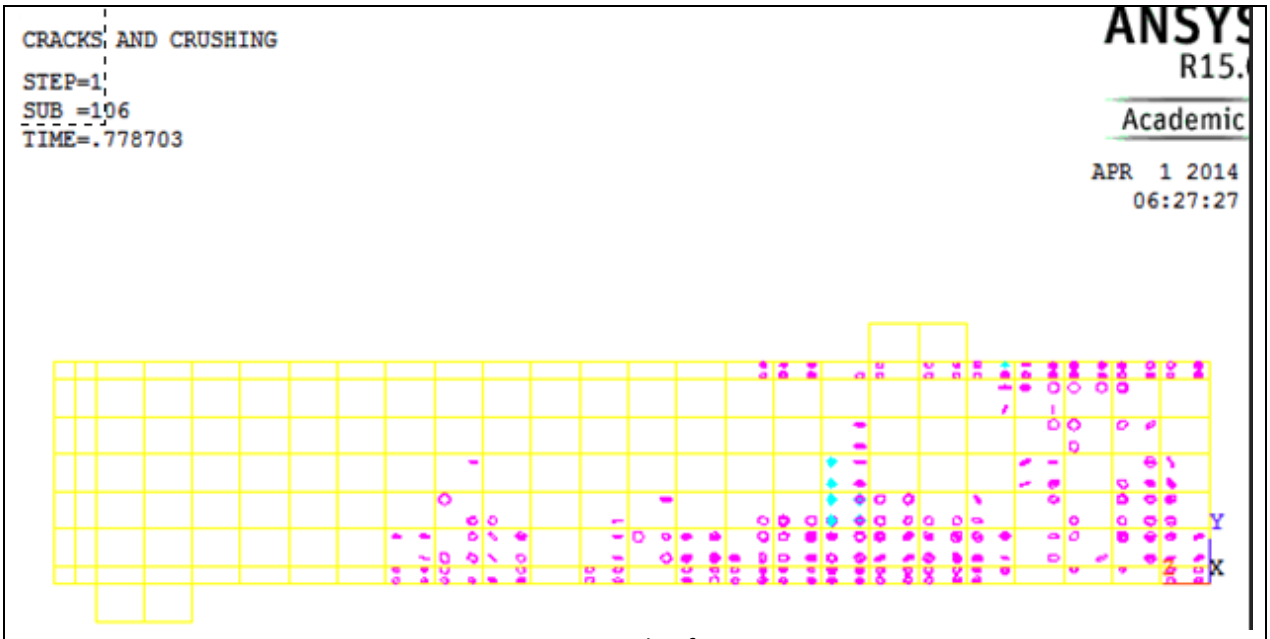

Figure D-31 Crack II for 16-1-30

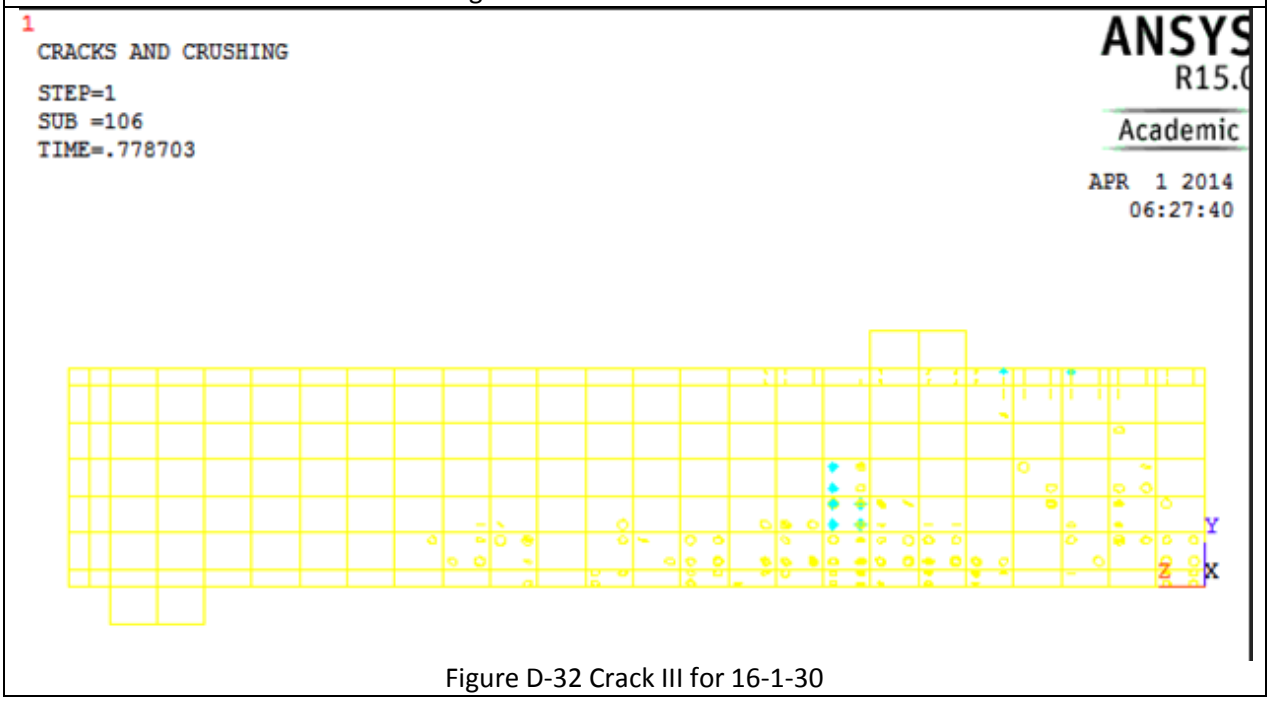

Figure D-32 Crack III for 16-1-30

Table D-5 Details of case 16-2-10

Case Name	Bottom Reinforcement	Honeycombing Location	Strength of Concrete(MPa)	Ultimate Load (kN)	Ultimate Deflection(mm)	Failure Mode
16-2-10	16mm	2	10	60.2628	8.42473	

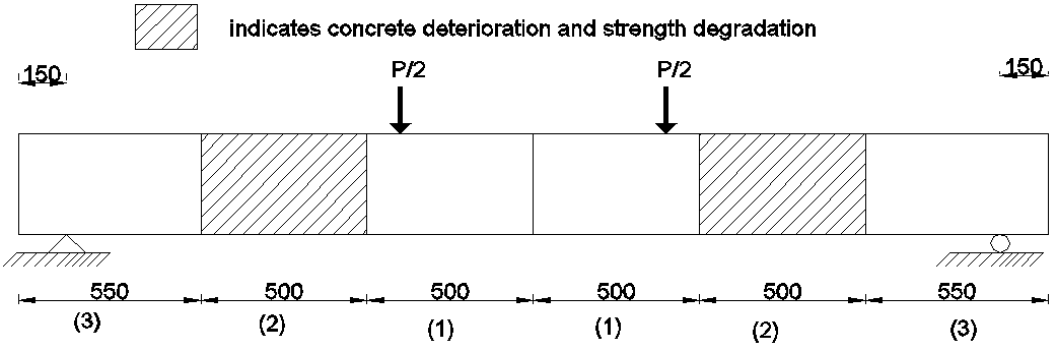

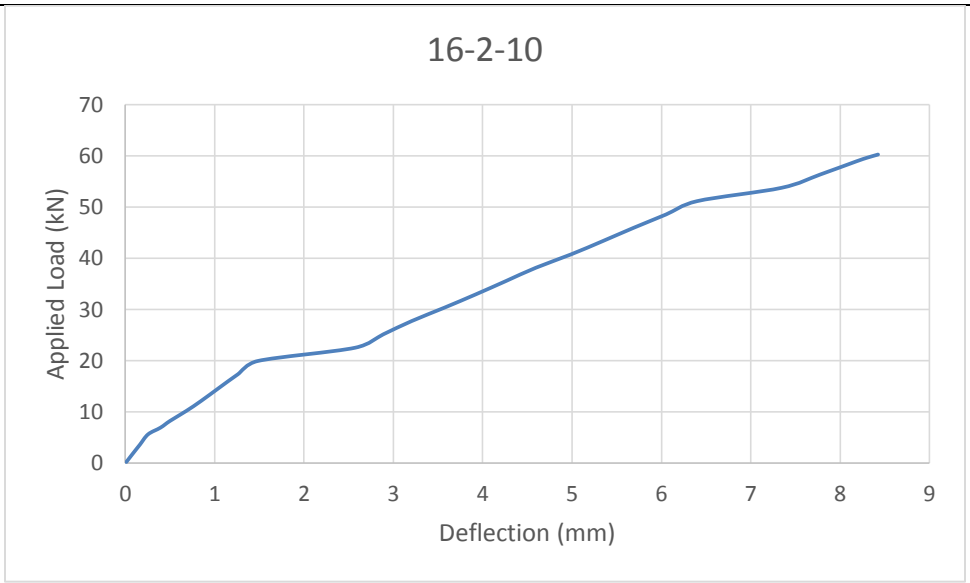

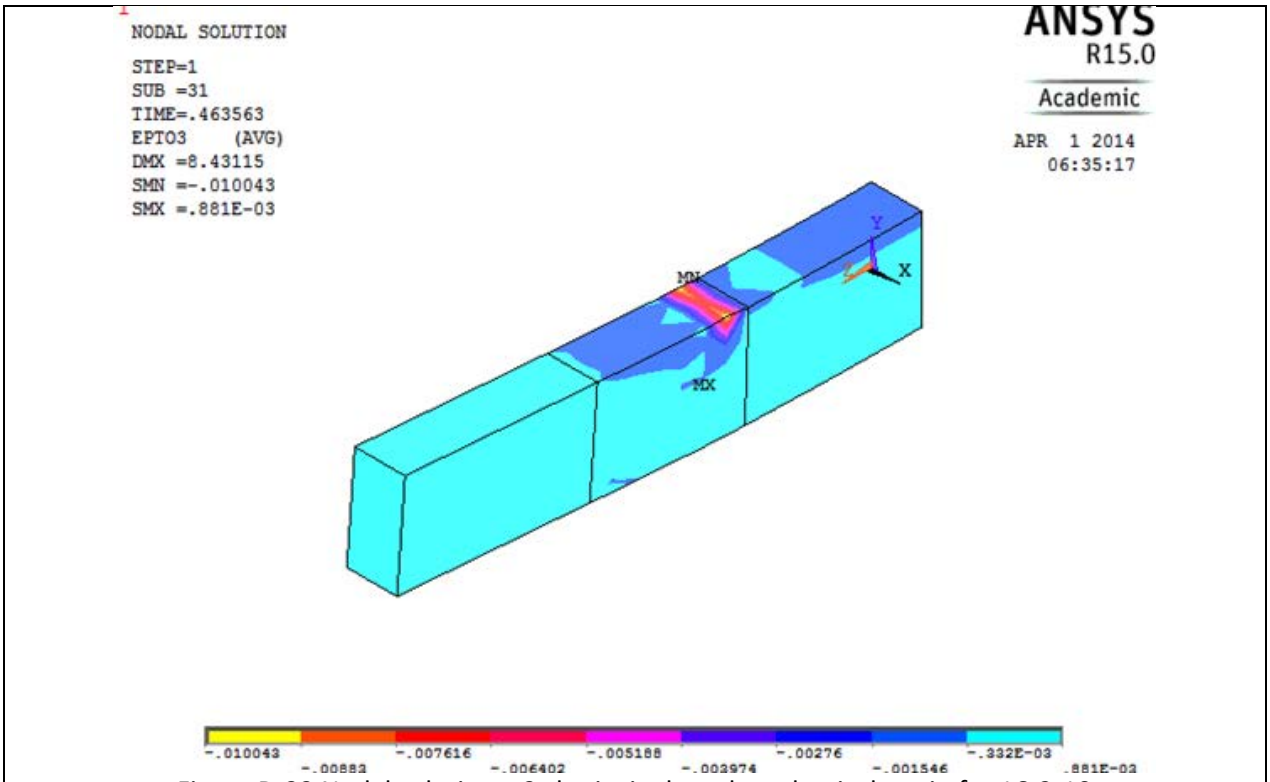

Figure D-33 Nodal solution – 3rd principal total mechanical strain for 16-2-10

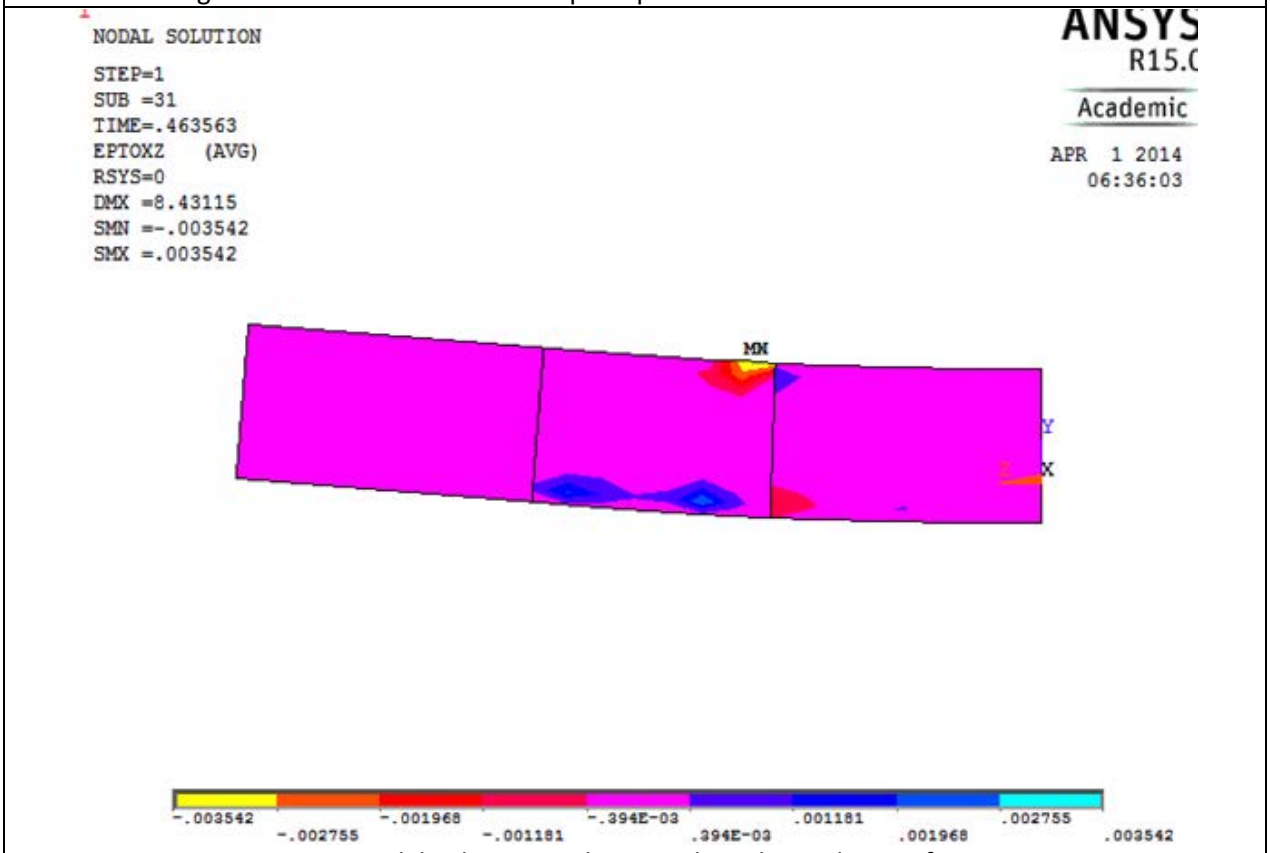

Figure D-34 Nodal Solution XZ shear total mechanical strain for 16-2-10

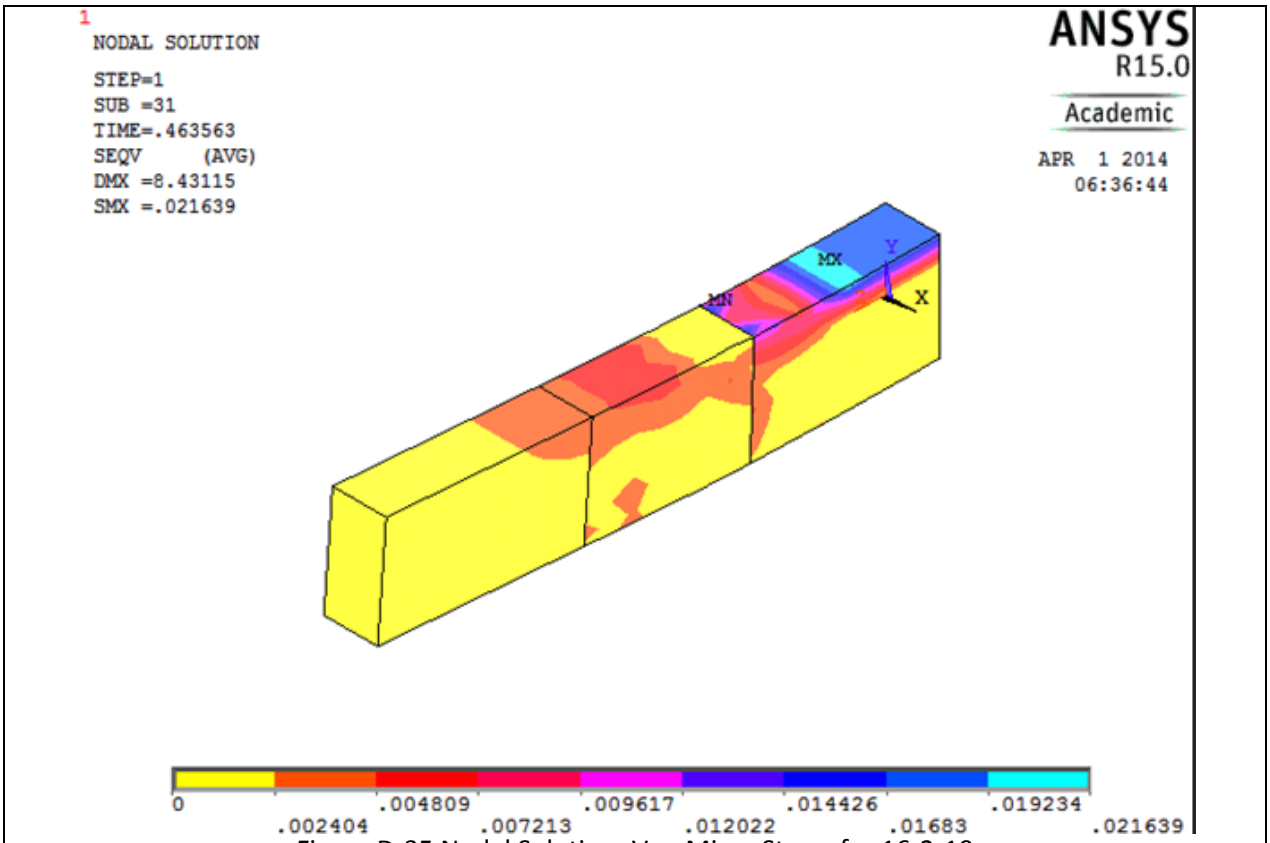

Figure D-35 Nodal Solution -Von Mises Stress for 16-2-10

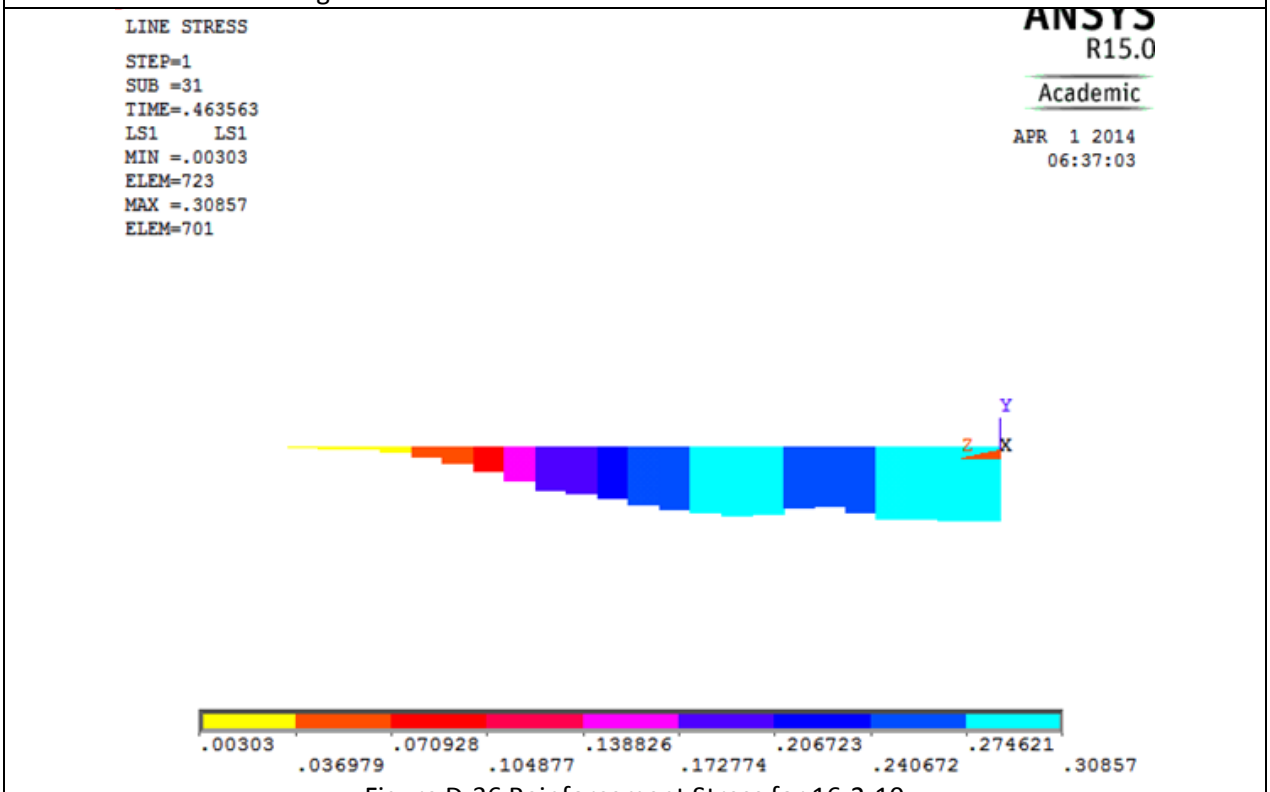

Figure D-36 Reinforcement Stress for 16-2-10

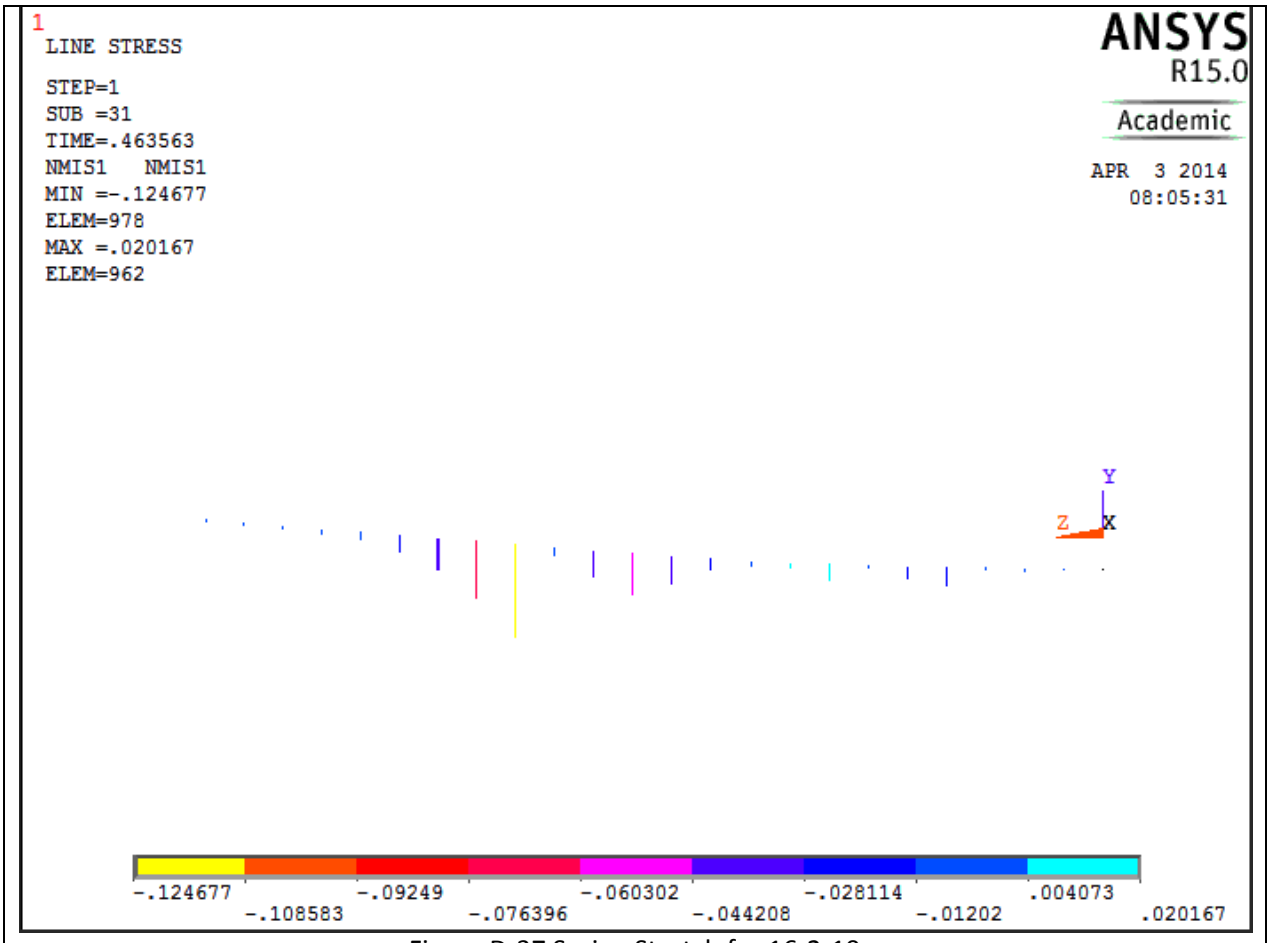

Figure D-37 Spring Stretch for 16-2-10

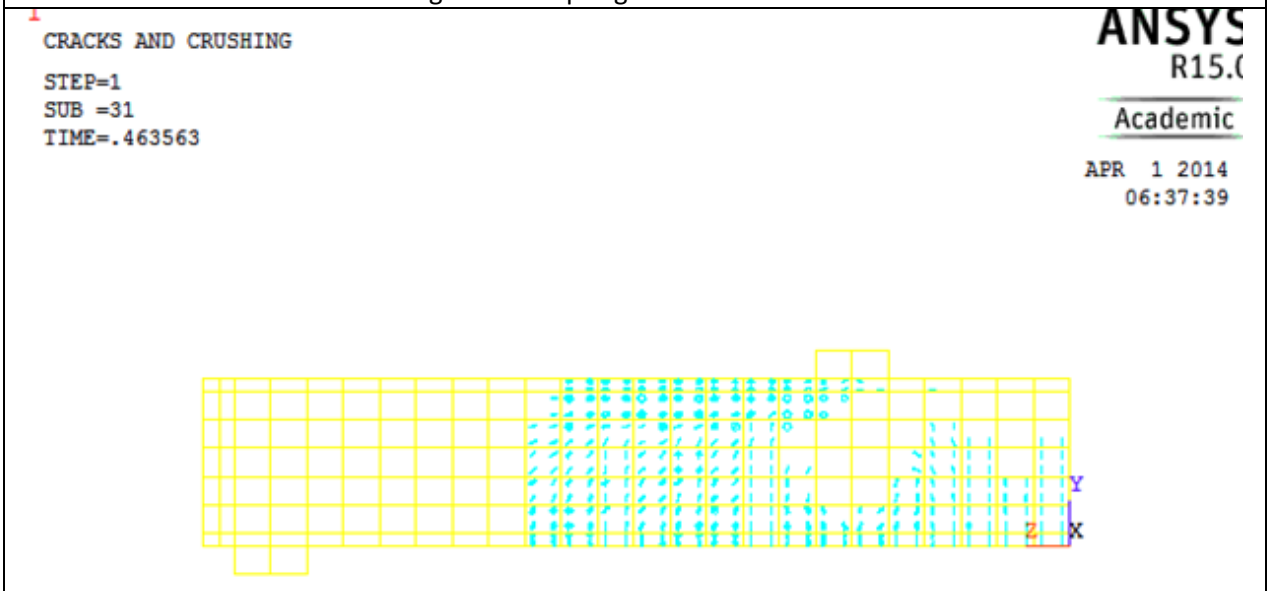

Figure D-38 Crack I for 16-2-10

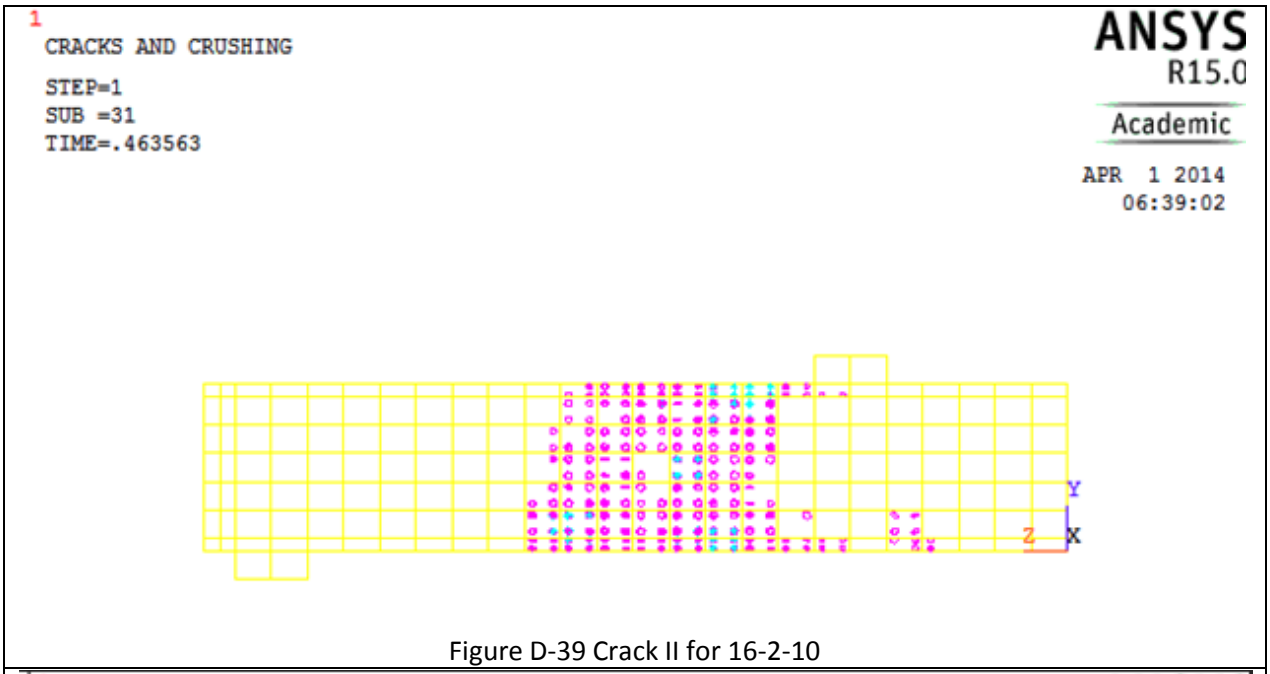

Figure D-39 Crack II for 16-2-10

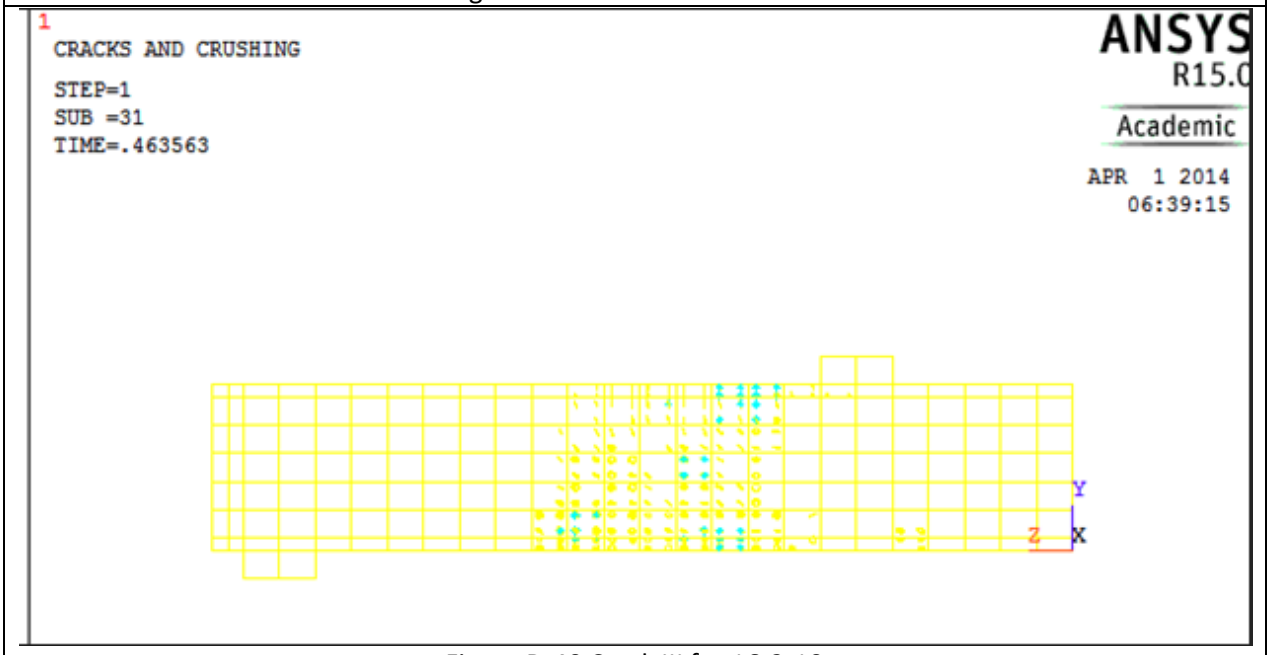

Figure D-40 Crack III for 16-2-10

Table D-6 Details of case 16-2-20

Case Name	Bottom Reinforcement	Honeycombing Location	Strength of Concrete(MPa)	Ultimate Load (kN)	Ultimate Deflection(mm)	Failure Mode
16-2-20	16mm	2	20	95.9725	12.5958	

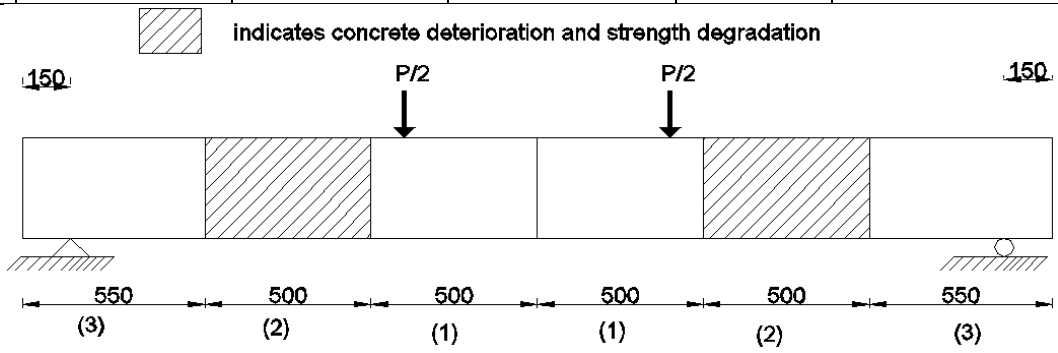

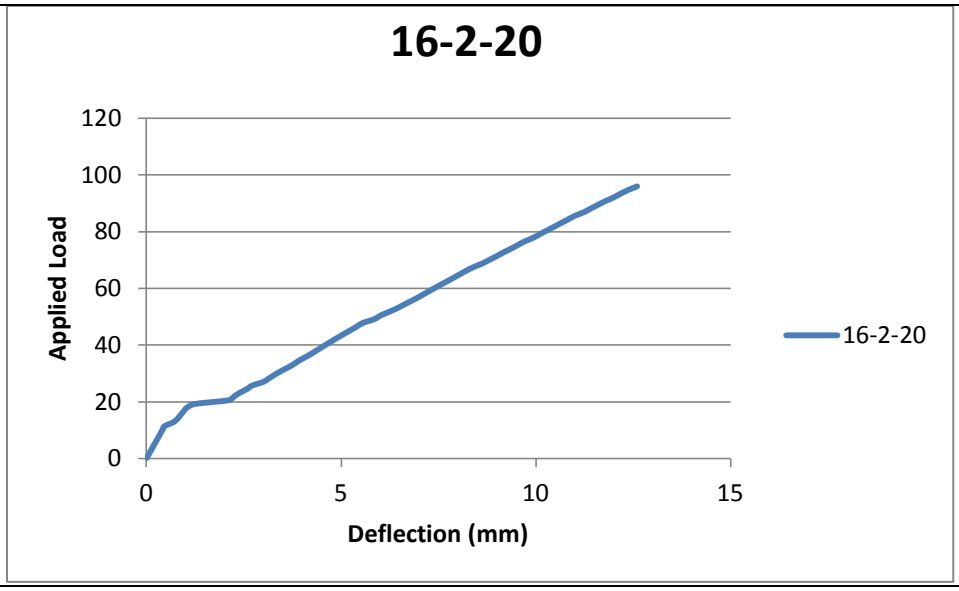

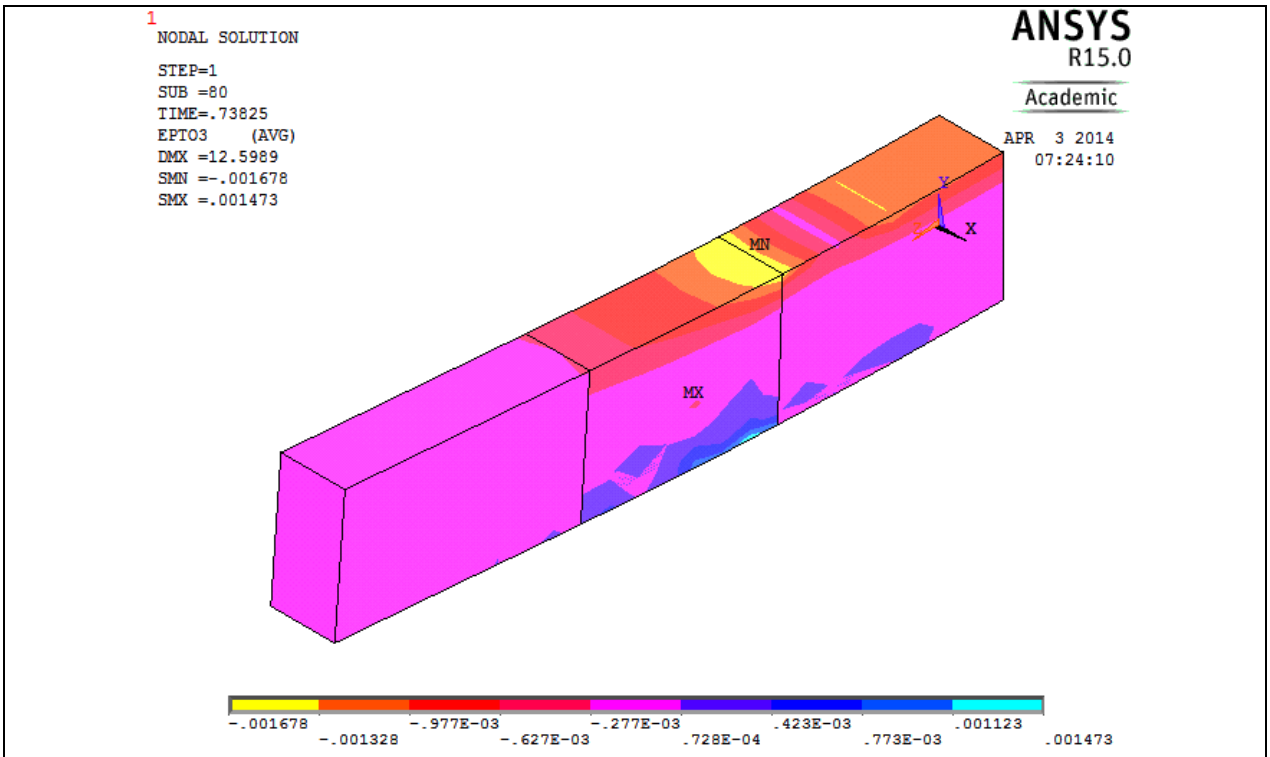

Figure D-41 Nodal solution – 3rd principal total mechanical strain for 16-2-20

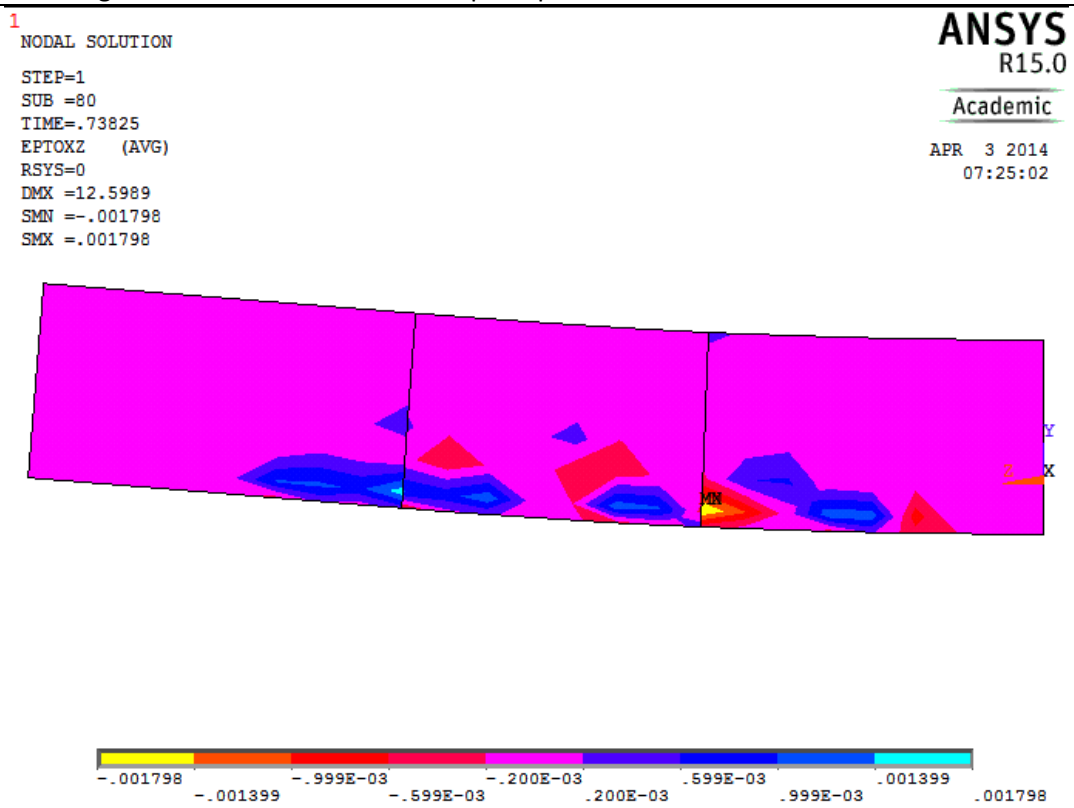

Figure D-42 Nodal Solution XZ shear total mechanical strain for 16-2-20

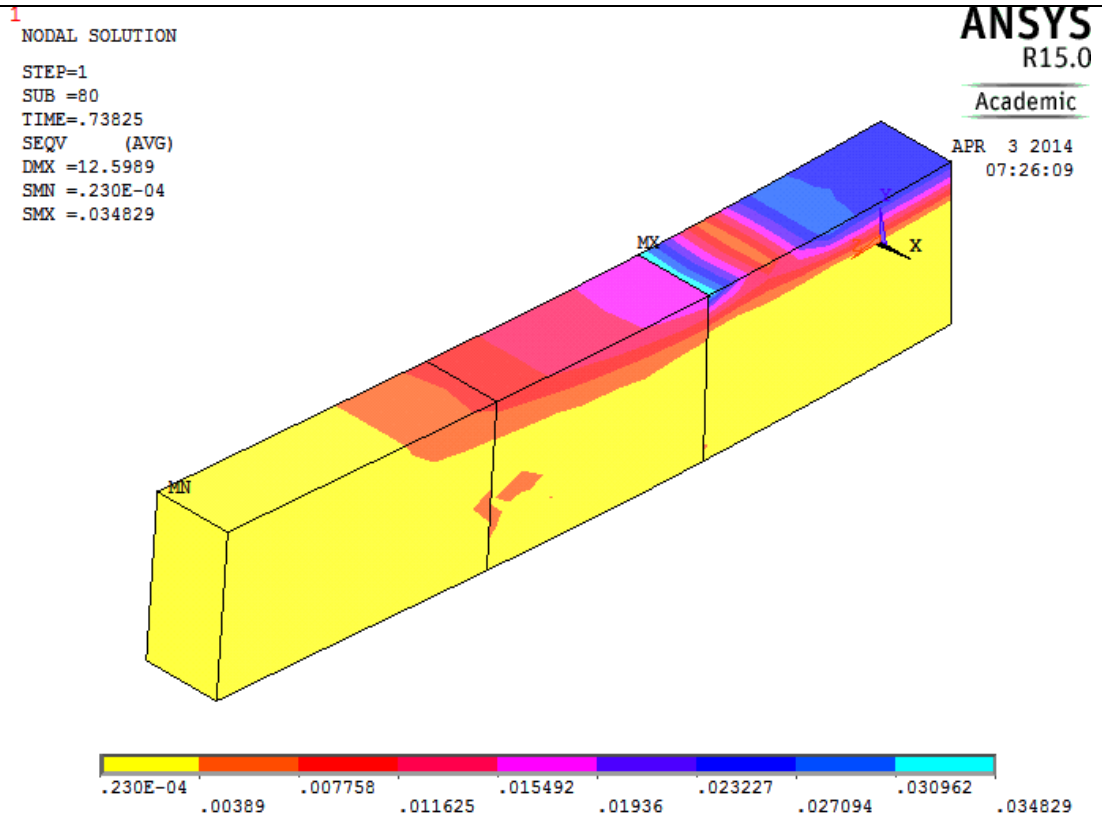

Figure D-43 Nodal Solution -Von Mises Stress for 16-2-20

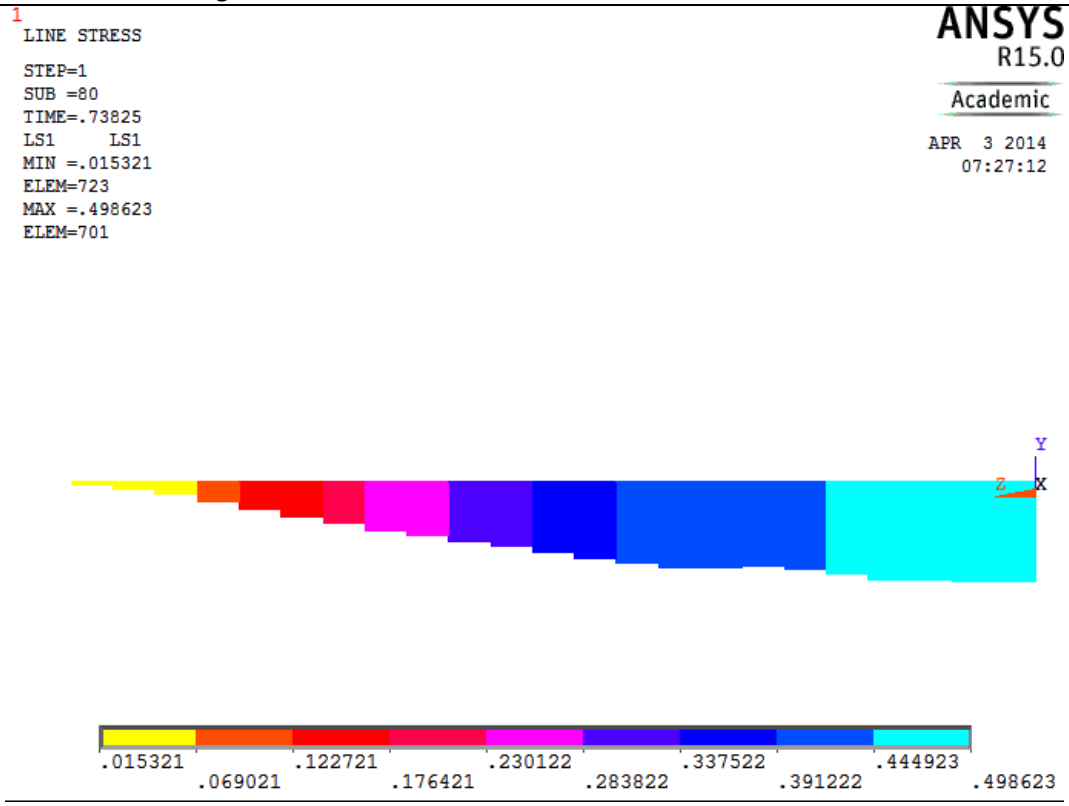

Figure D-44 Reinforcement Stress for 16-2-20

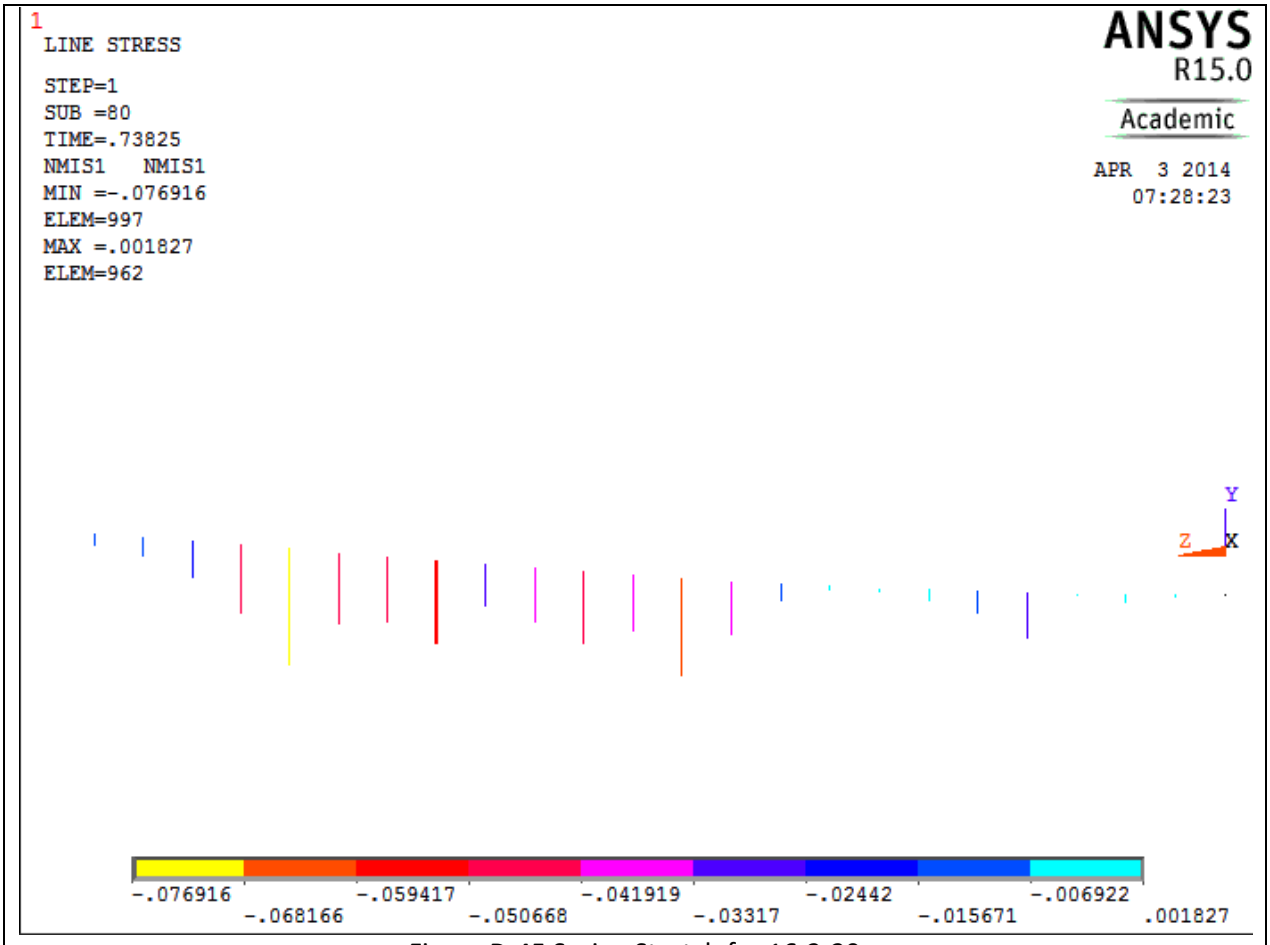

Figure D-45 Spring Stretch for 16-2-20

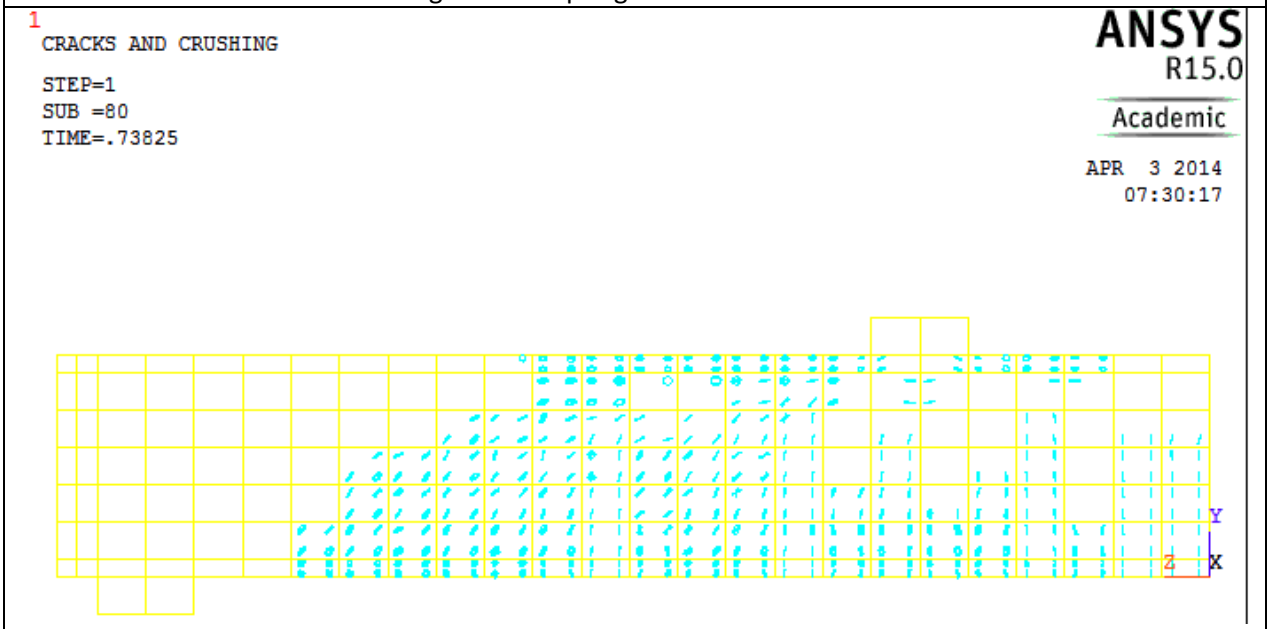

Figure D-46 Crack I for 16-2-20

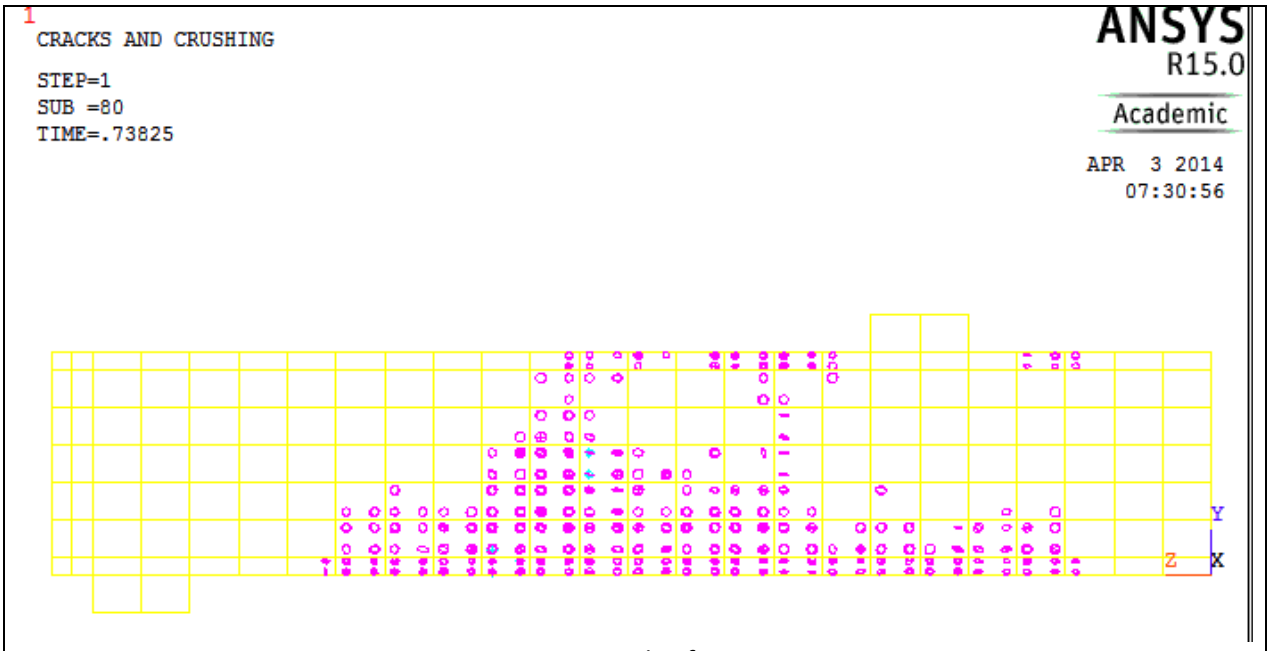

Figure D-47 Crack II for 16-2-20

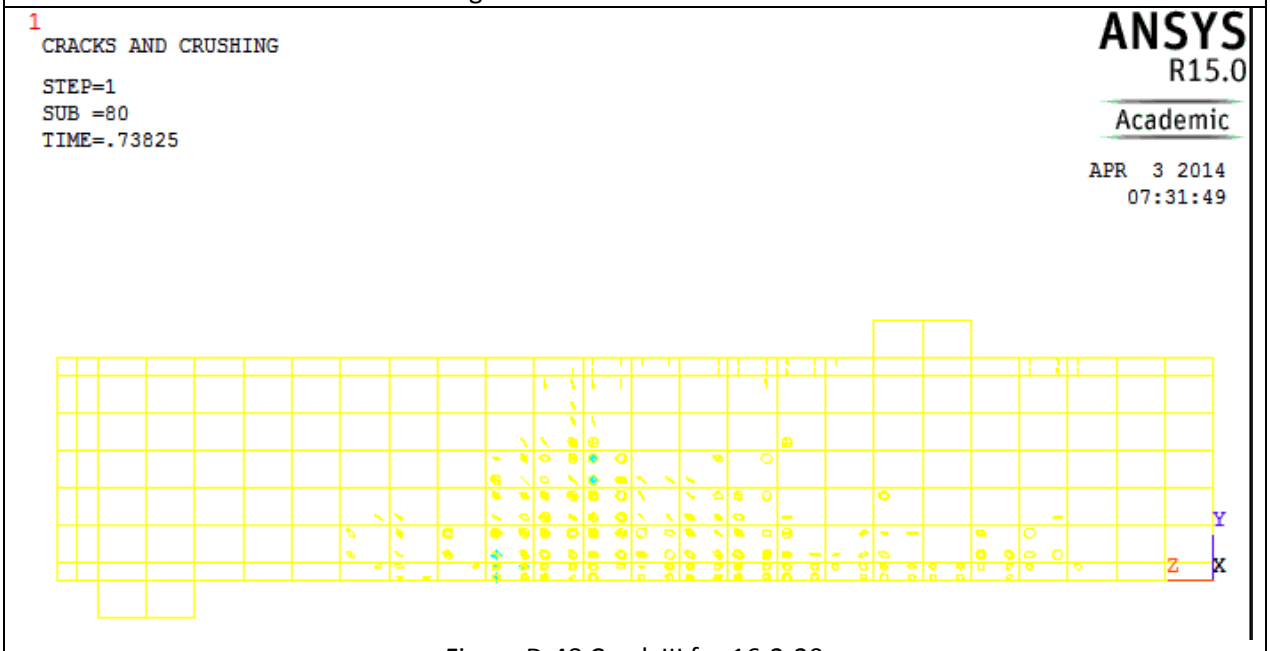

Figure D-48 Crack III for 16-2-20

Table D-7 Details of case 16-2-30

Case Name	Bottom Reinforcement	Honeycombing Location	Strength of Concrete(MPa)	Ultimate Load (kN)	Ultimate Deflection(mm)	Failure Mode
16-2-30	16mm	2	30	102.1683	24.7973	

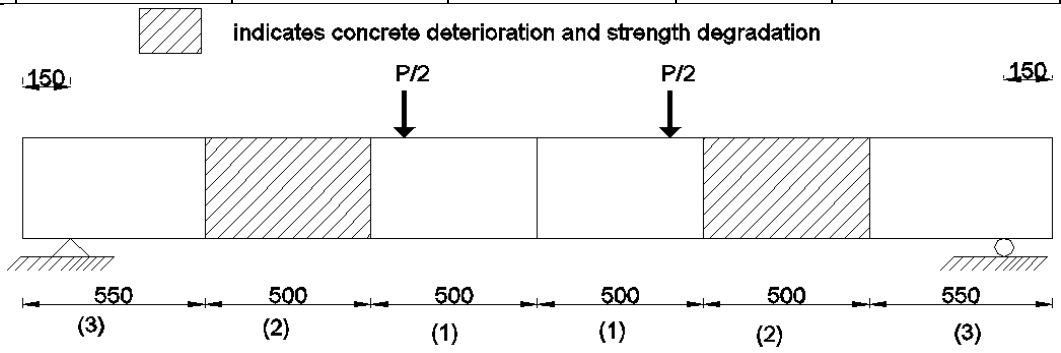

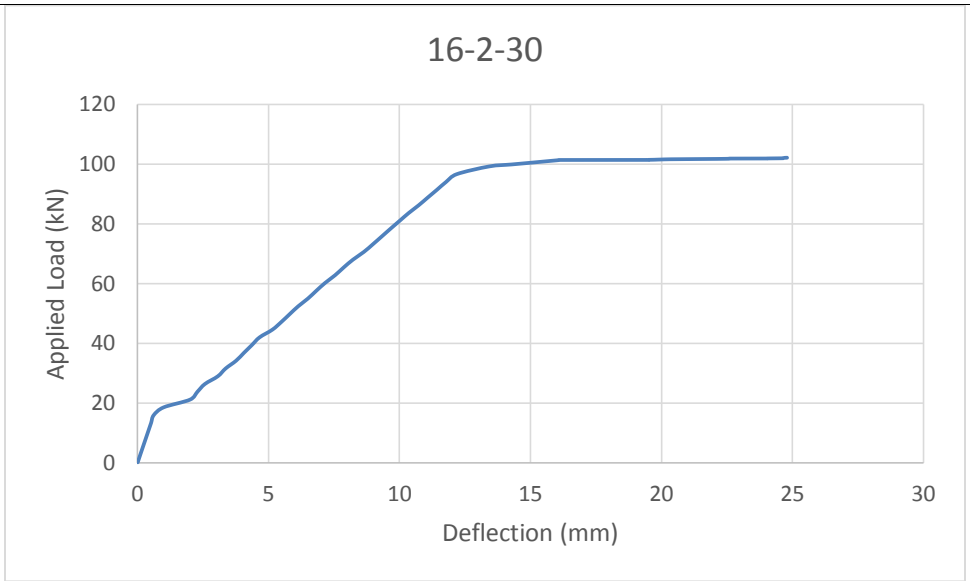

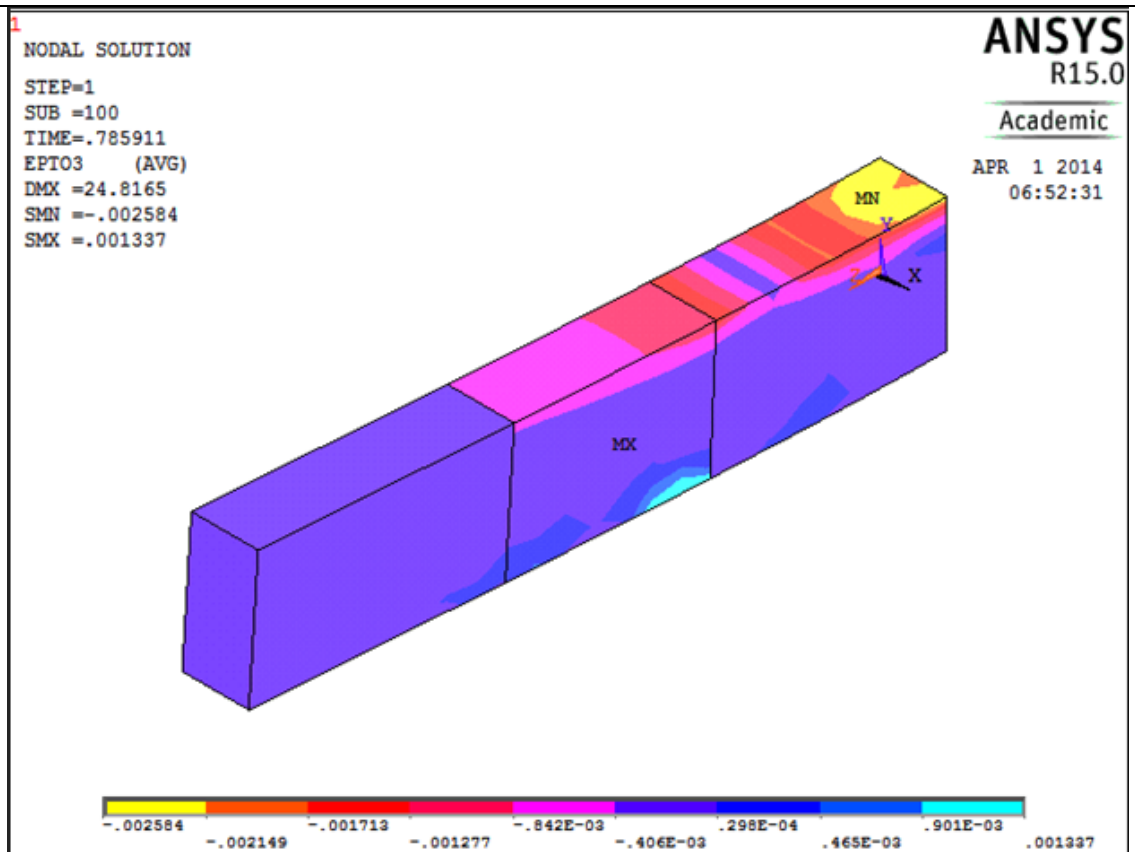

Figure D-49 Nodal solution – 3rd principal total mechanical strain for 16-2-30

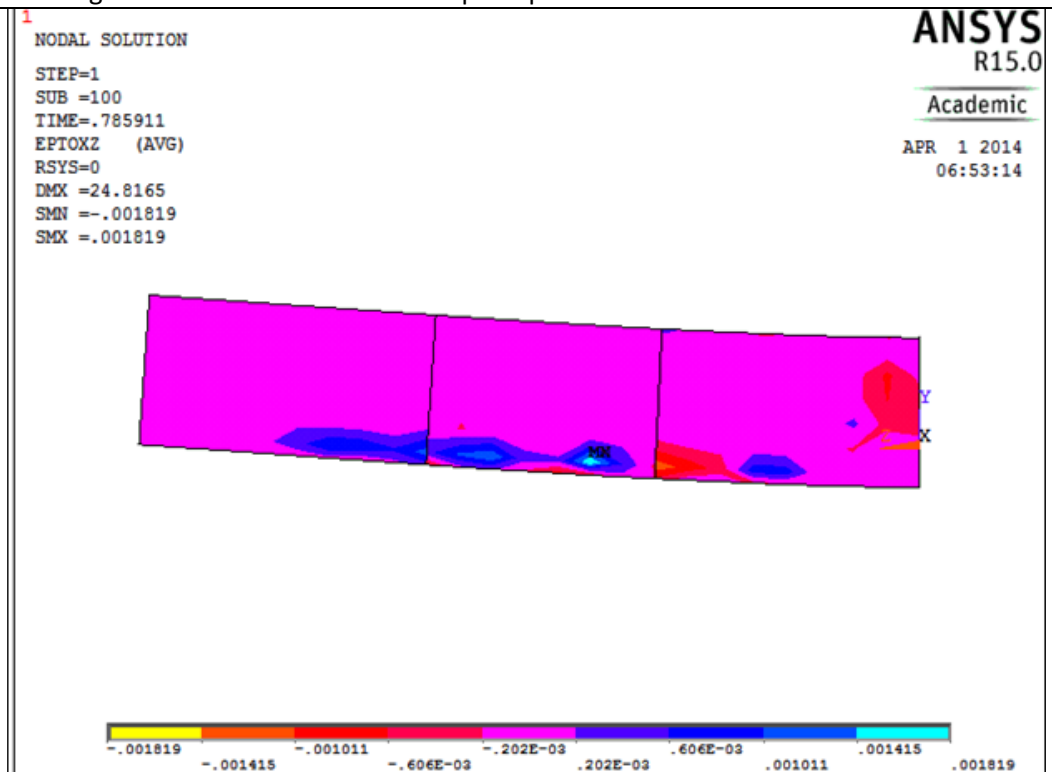

Figure D-50 Nodal Solution XZ shear total mechanical strain for 16-2-30

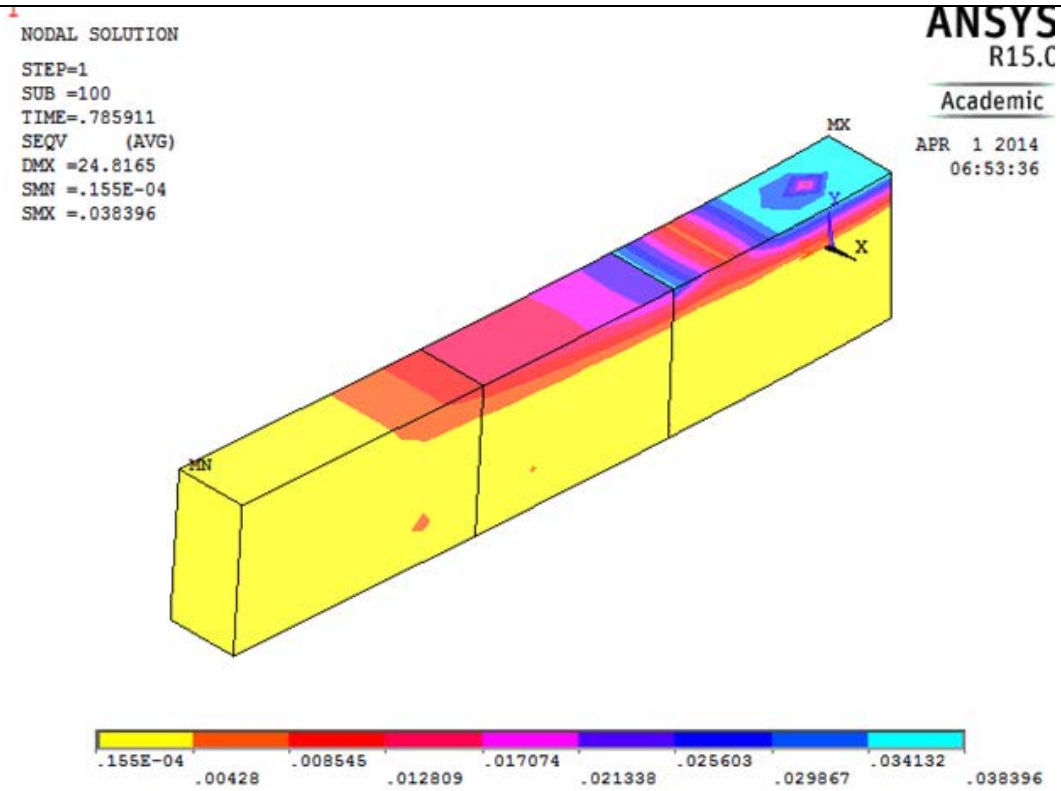

Figure D-51 Nodal Solution -Von Mises Stress for 16-2-30

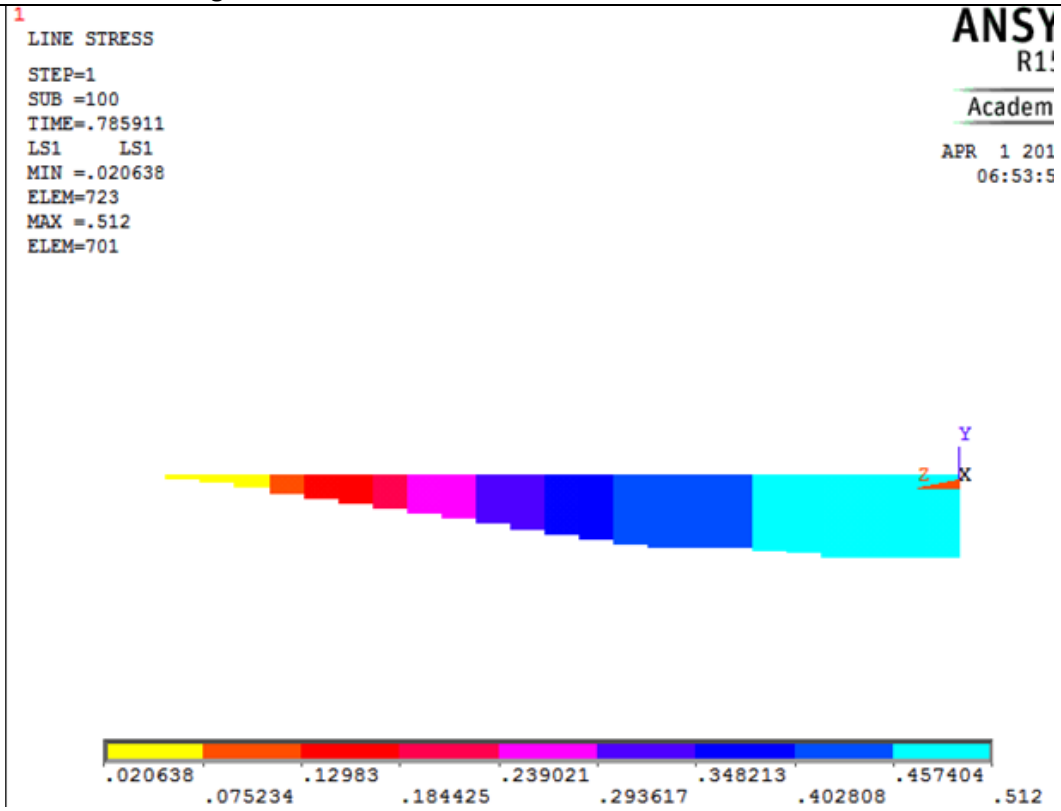

Figure D-52 Reinforcement Stress for 16-2-30

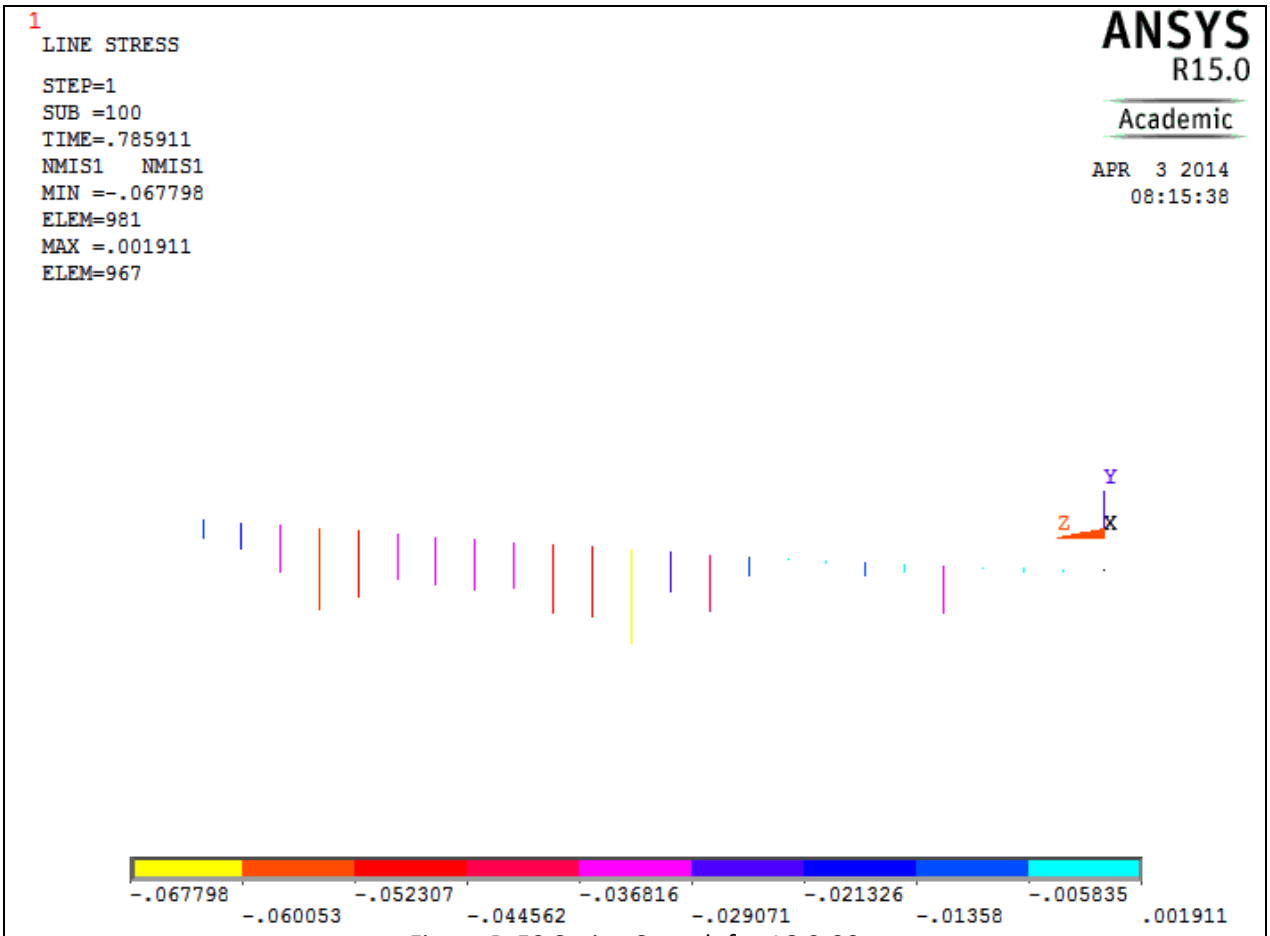

Figure D-53 Spring Stretch for 16-2-30

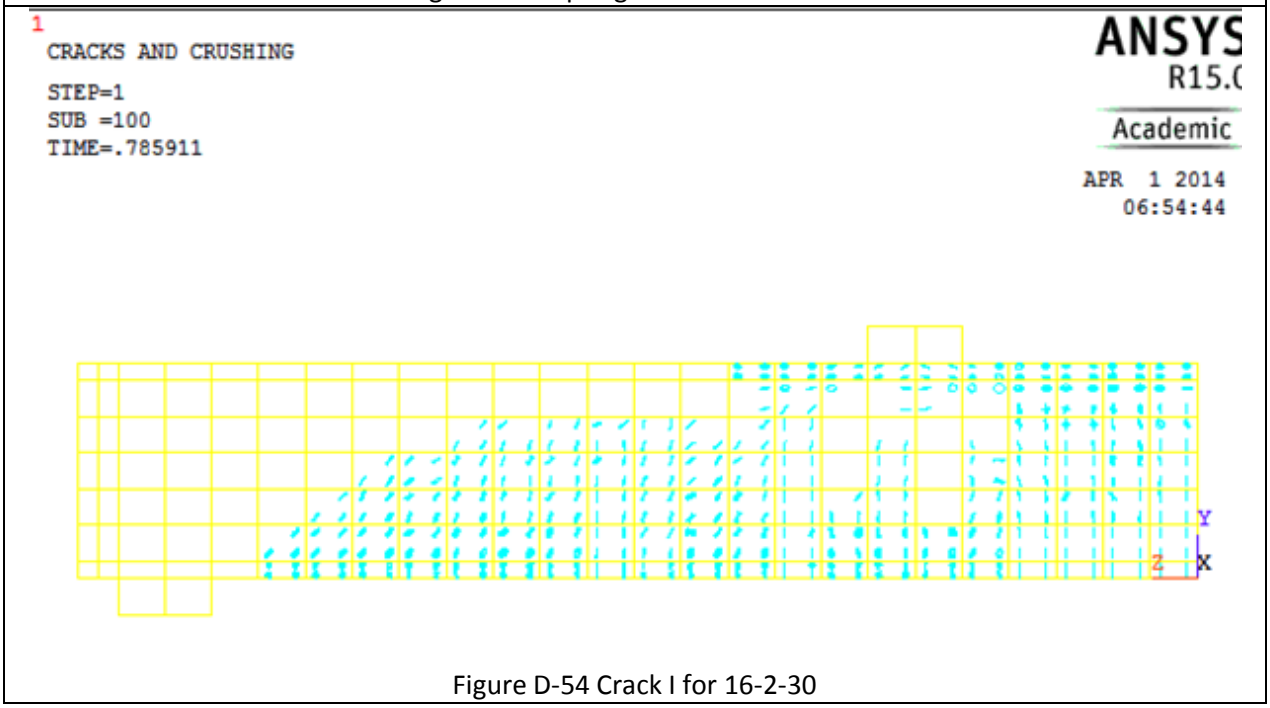

Figure D-54 Crack I for 16-2-30

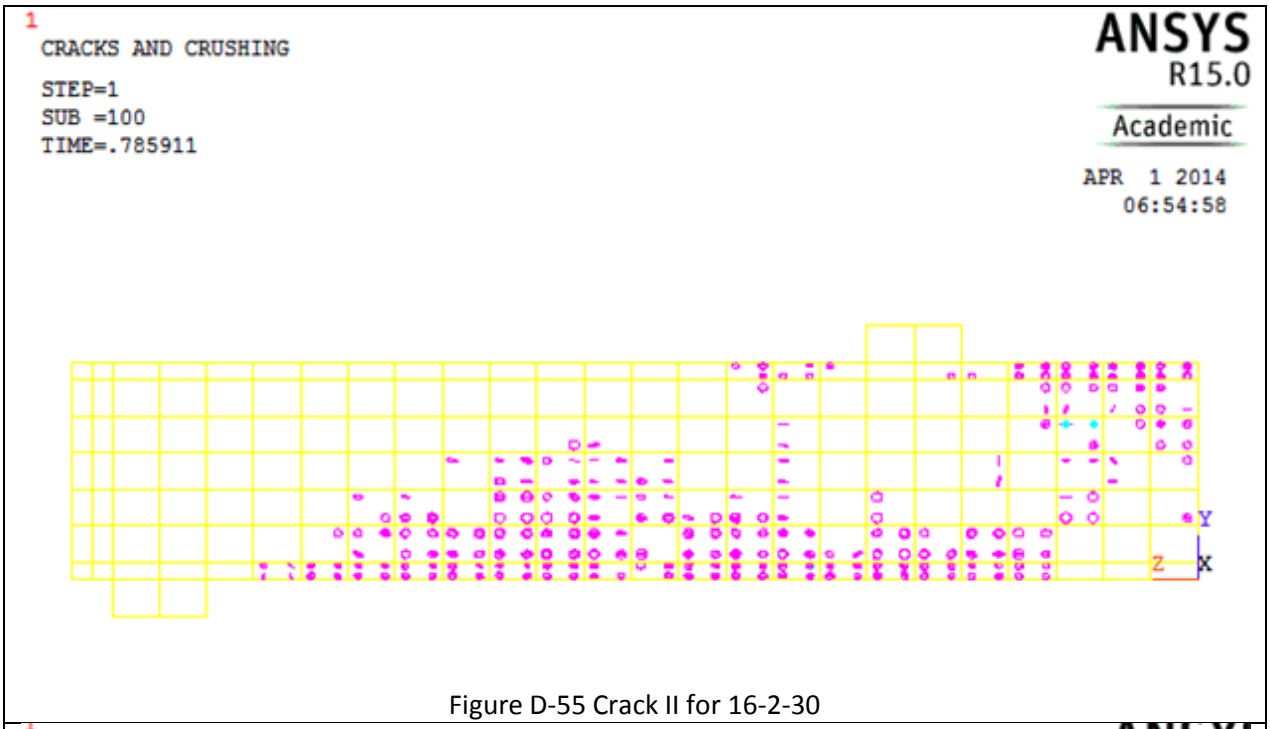

Figure D-55 Crack II for 16-2-30

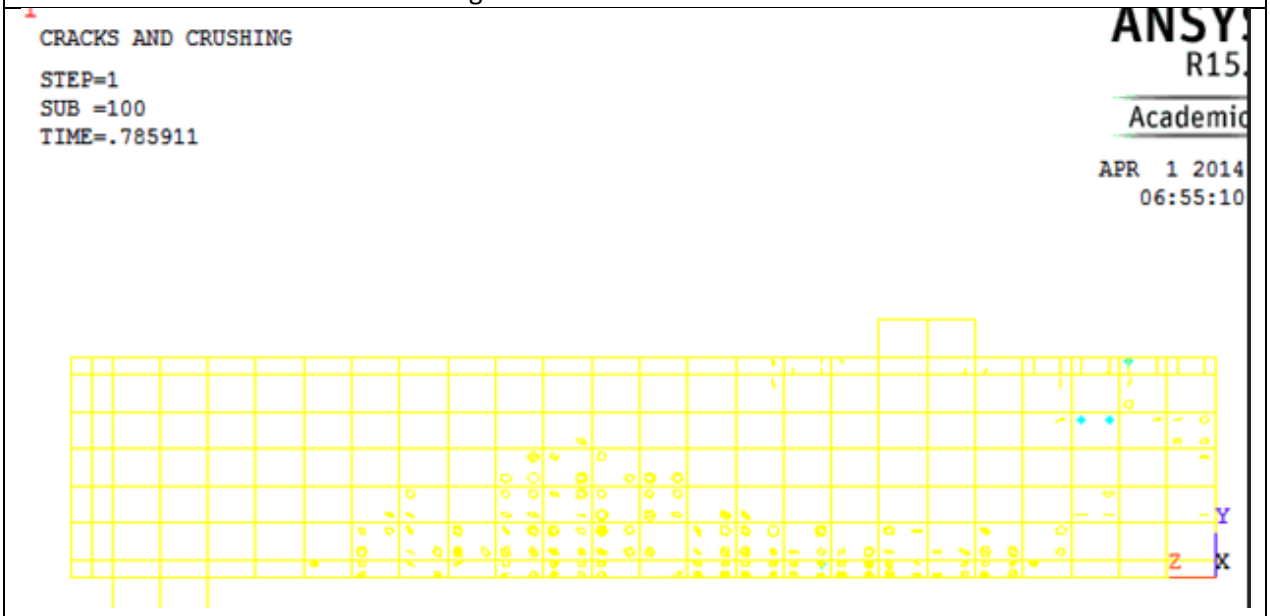

Figure D-56 Crack III for 16-2-30

Table D-8 Details of case 16-3-10

Case Name	Bottom Reinforcement	Honeycombing Location	Strength of Concrete(MPa)	Ultimate Load (kN)	Ultimate Deflection(mm)	Failure Mode
16-3-10	16mm	3	10	72.2657	8.97666	

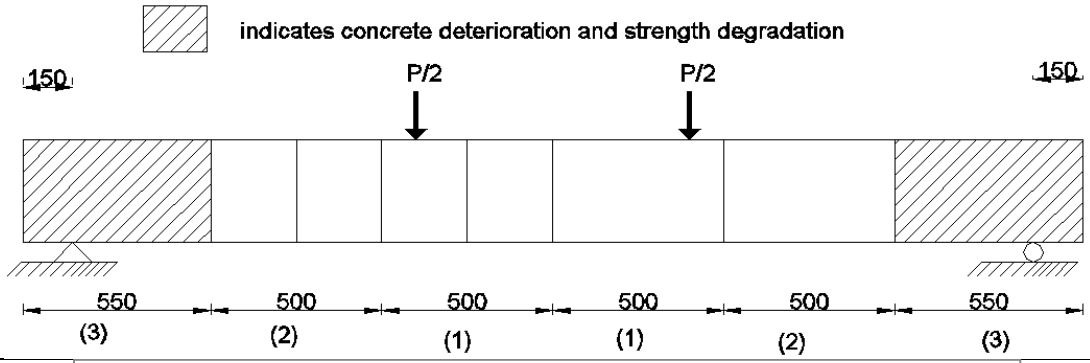

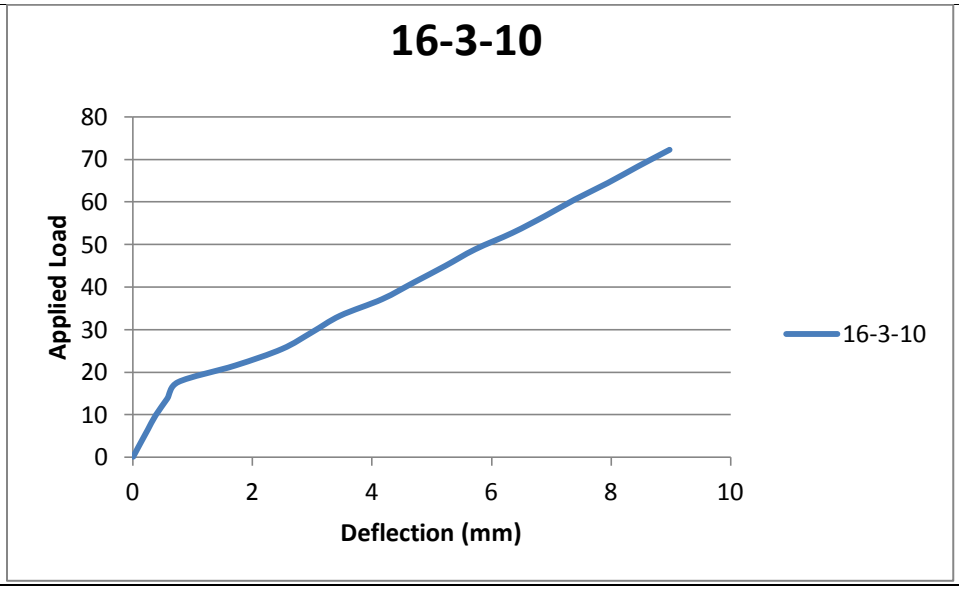

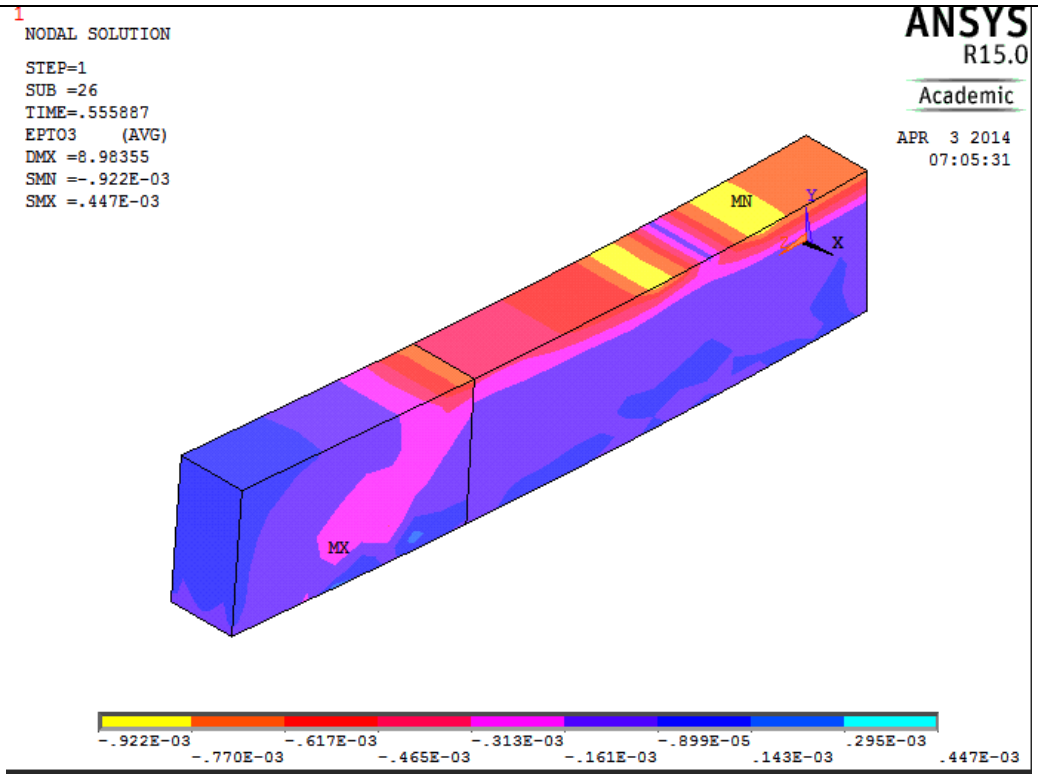

Figure D-57 Nodal solution – 3rd principal total mechanical strain for 16-3-10

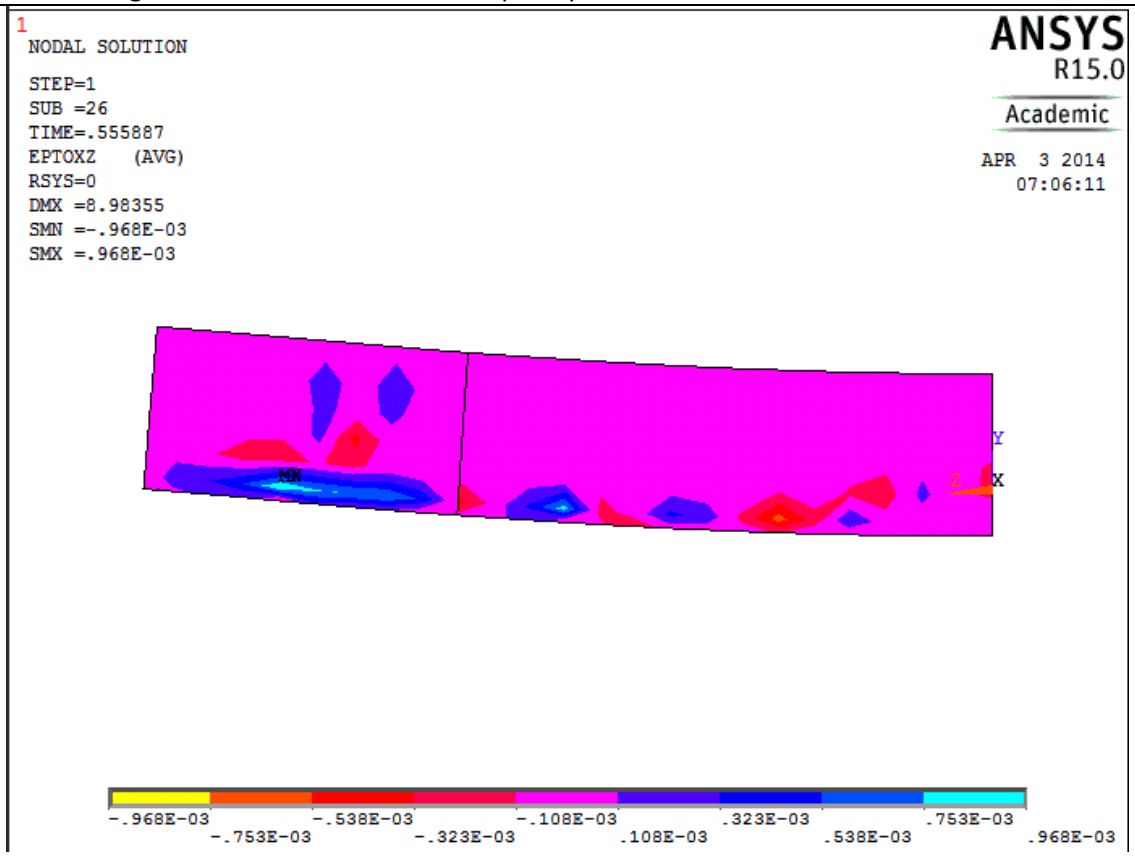

Figure D-58 Nodal Solution XZ shear total mechanical strain for 16-3-10

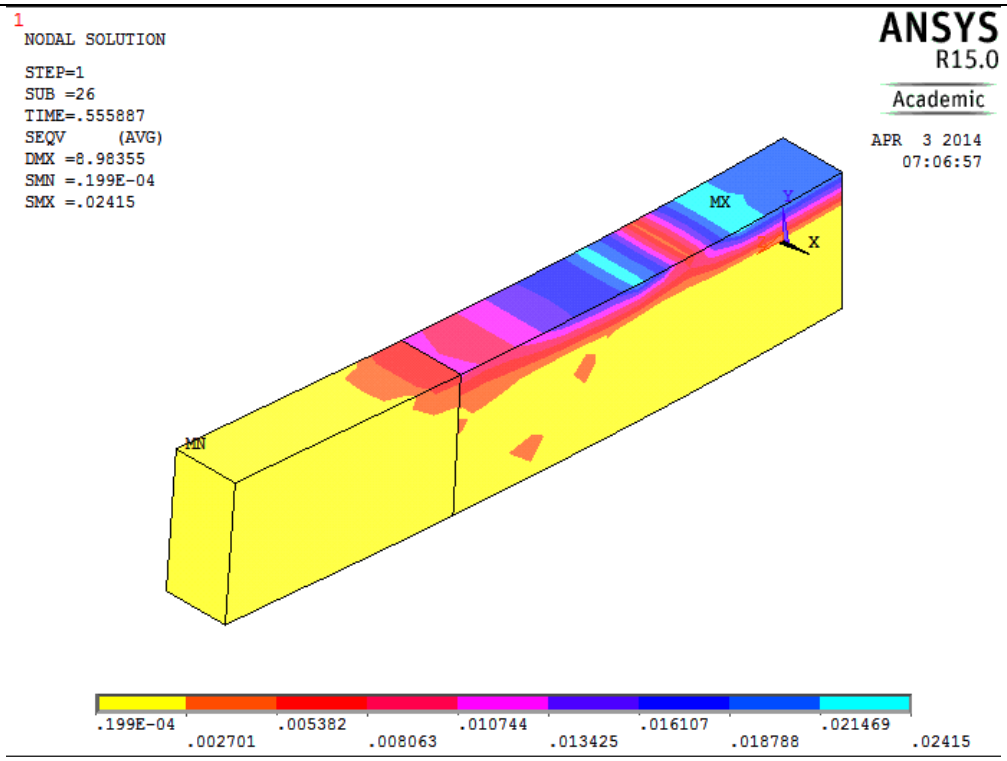

Figure D-59 Nodal Solution -Von Mises Stress for 16-3-10

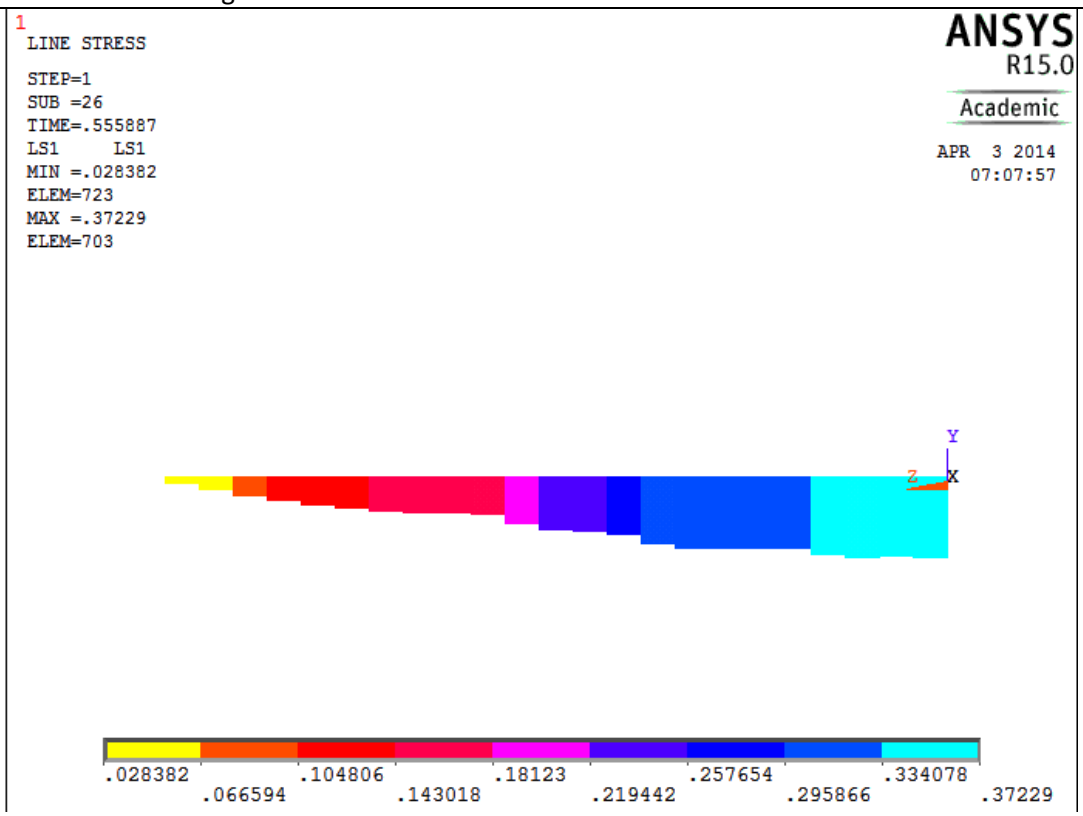

Figure D-60 Reinforcement Stress for 16-3-10

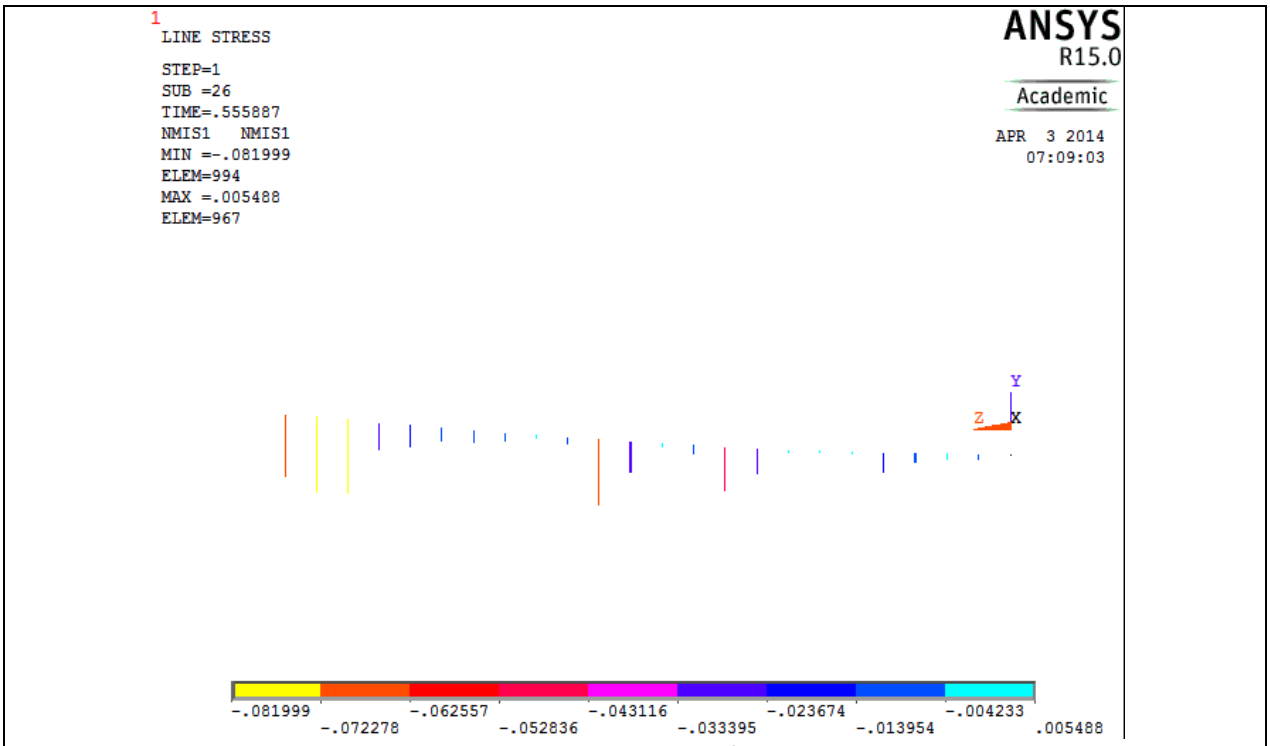

Figure D-61 Spring Stretch for 16-3-10

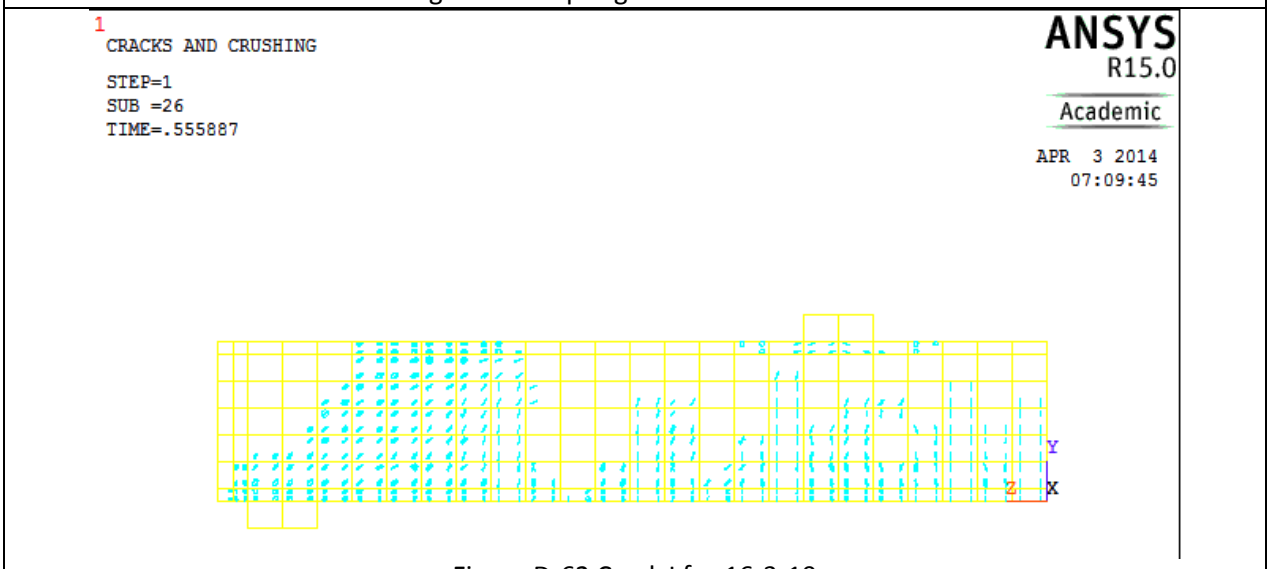

Figure D-62 Crack I for 16-3-10

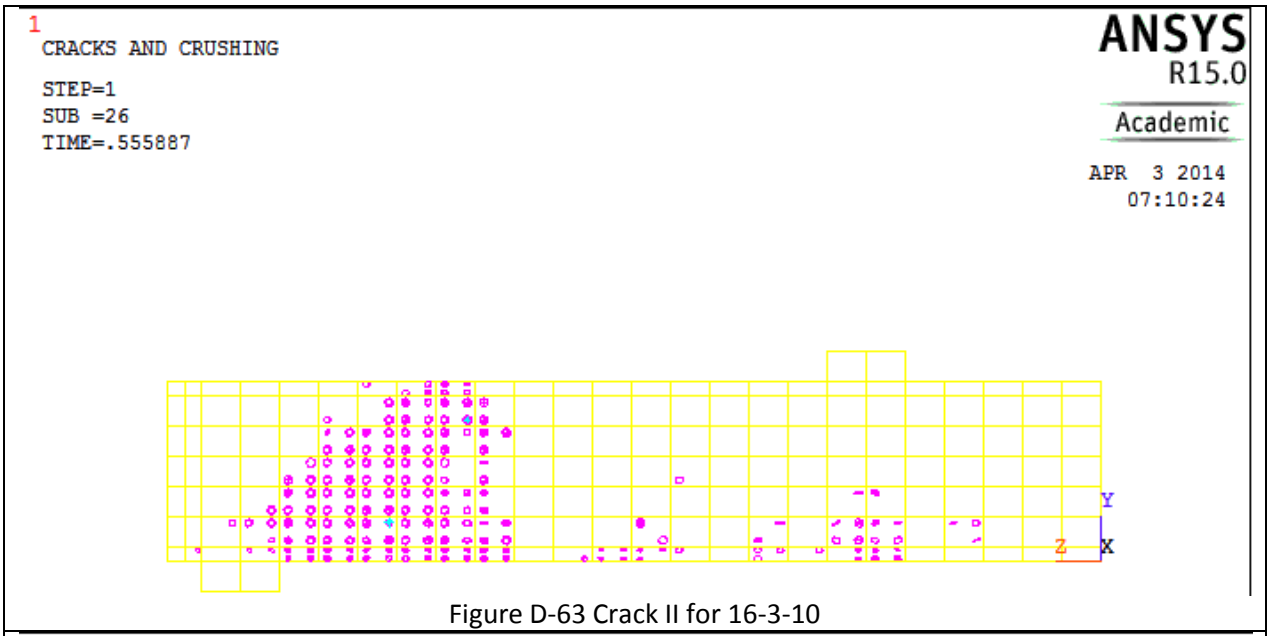

Figure D-63 Crack II for 16-3-10

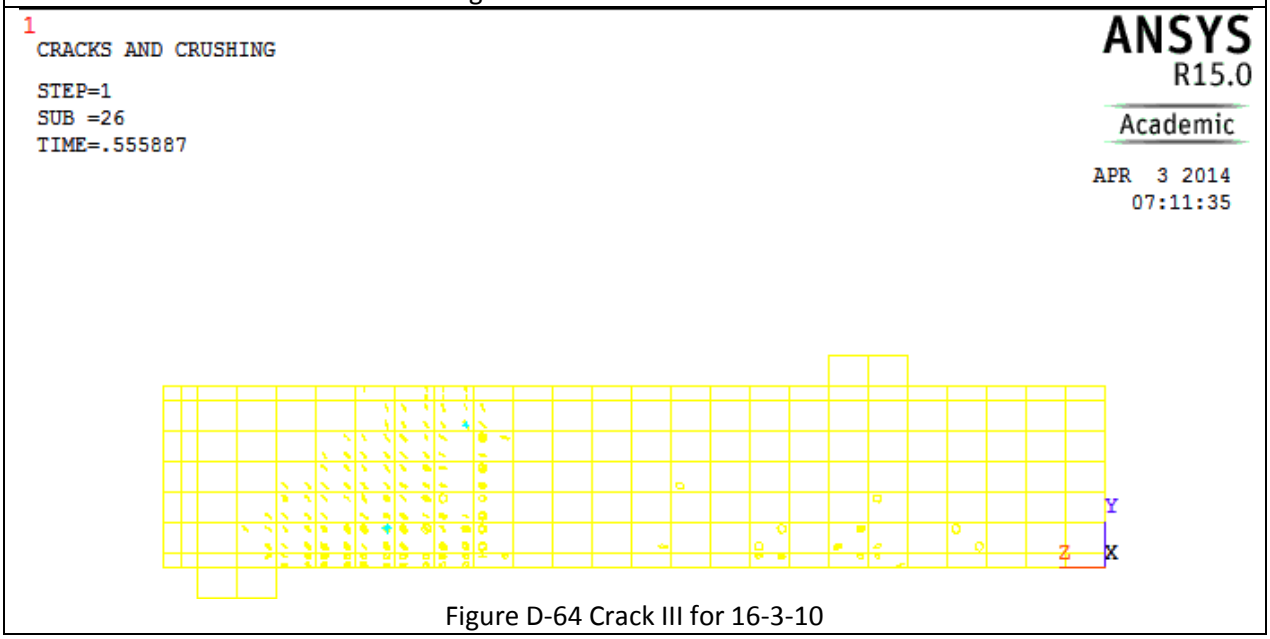

Figure D-64 Crack III for 16-3-10

Table D-9 Details of case 16-3-20

Case Name	Bottom Reinforcement	Honeycombing Location	Strength of Concrete(MPa)	Ultimate Load (kN)	Ultimate Deflection(mm)	Failure Mode
16-3-20	16mm	3	20	103.8102	18.9709	

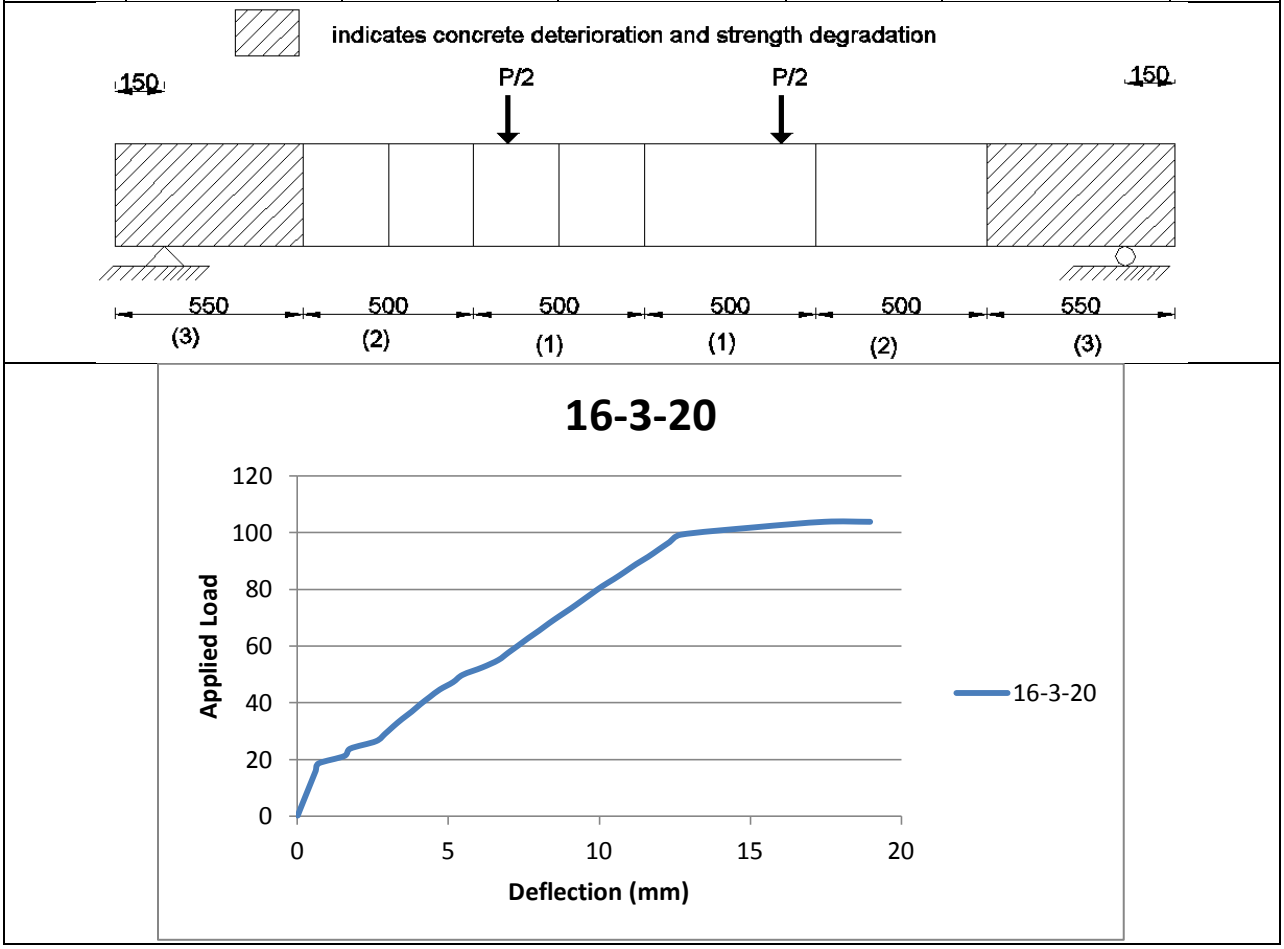

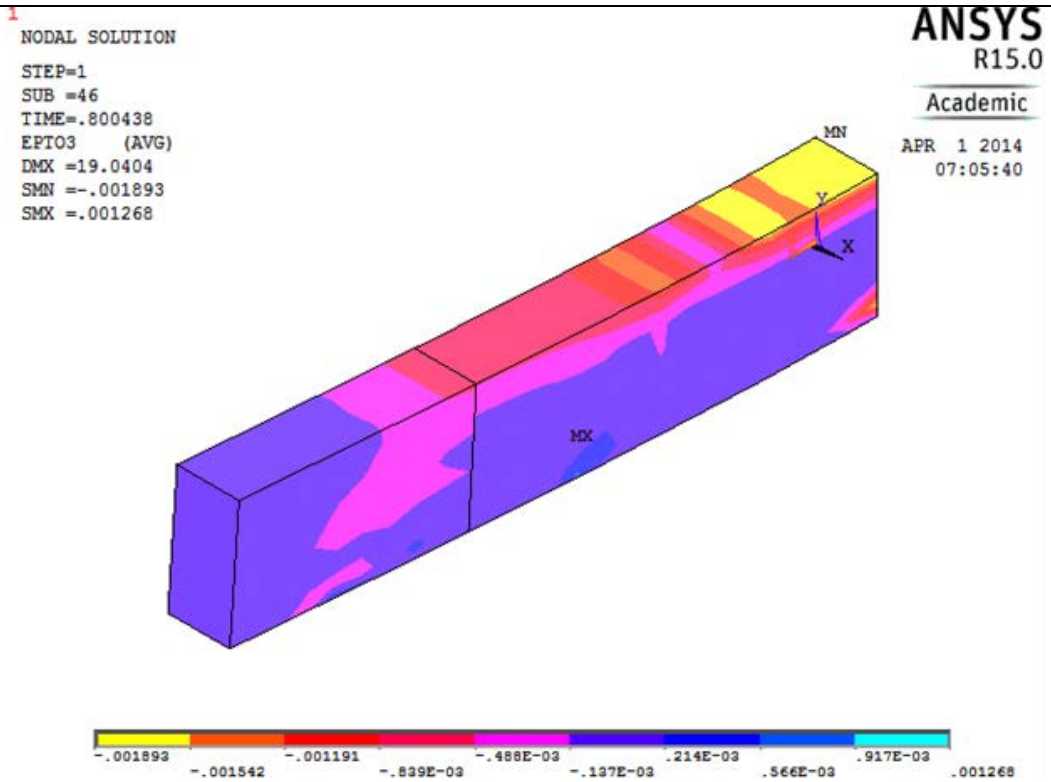

Figure D-65 Nodal solution – 3rd principal total mechanical strain for 16-3-20

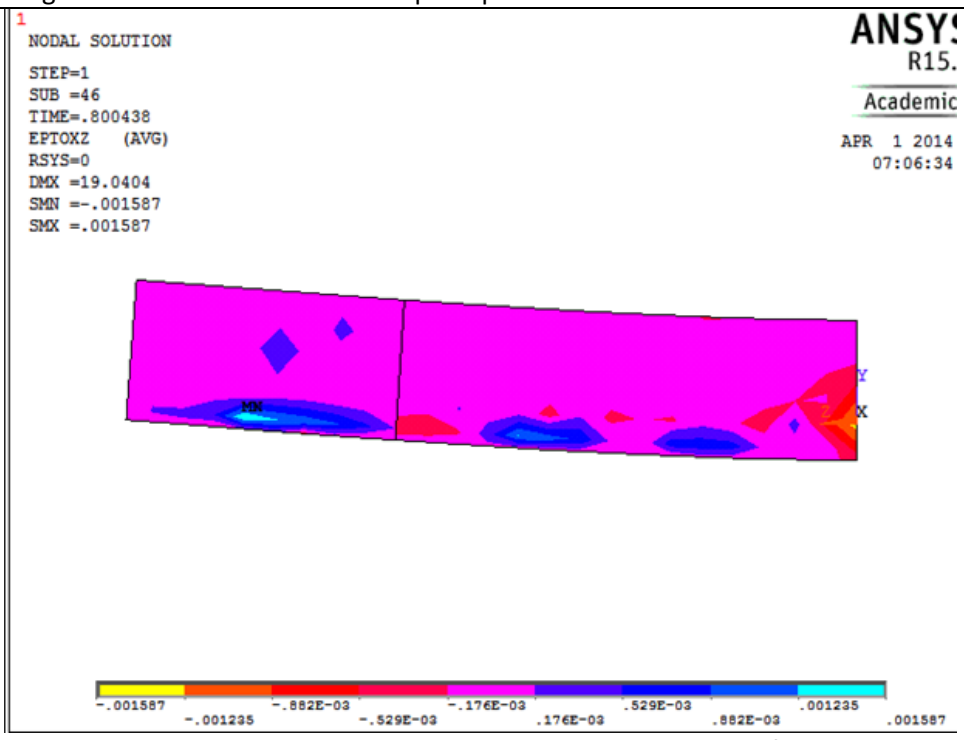

Figure D-66 Nodal Solution XZ shear total mechanical strain for 16-3-20

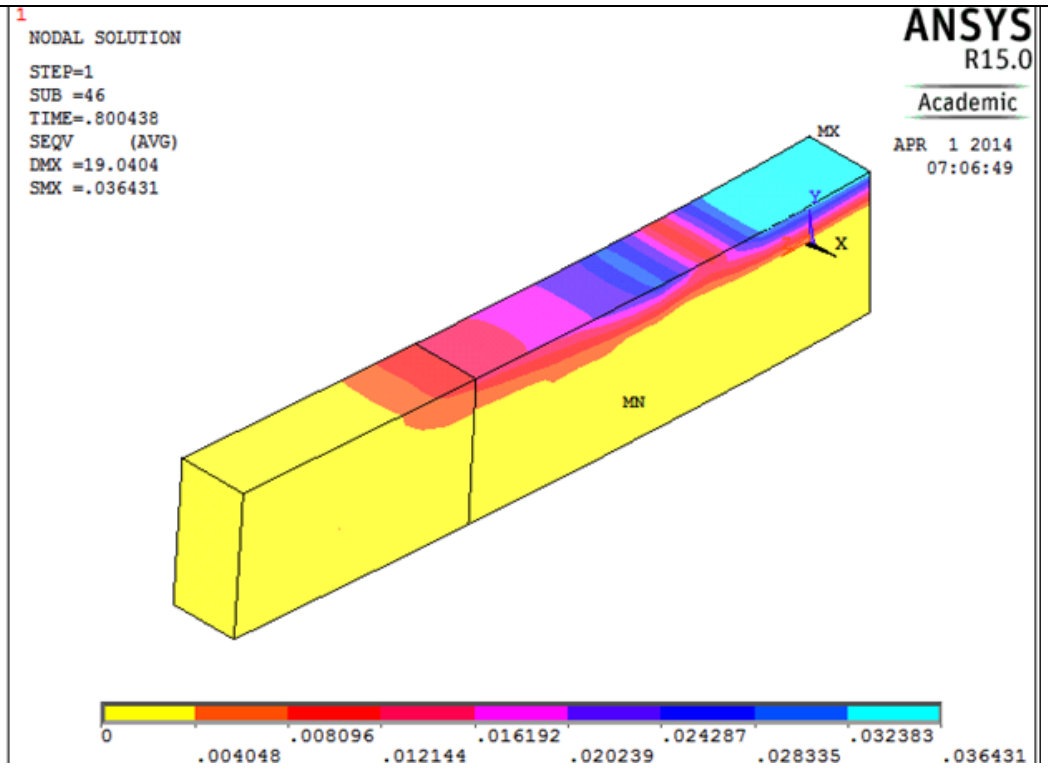

Figure D-67 Nodal Solution -Von Mises Stress for 16-3-20

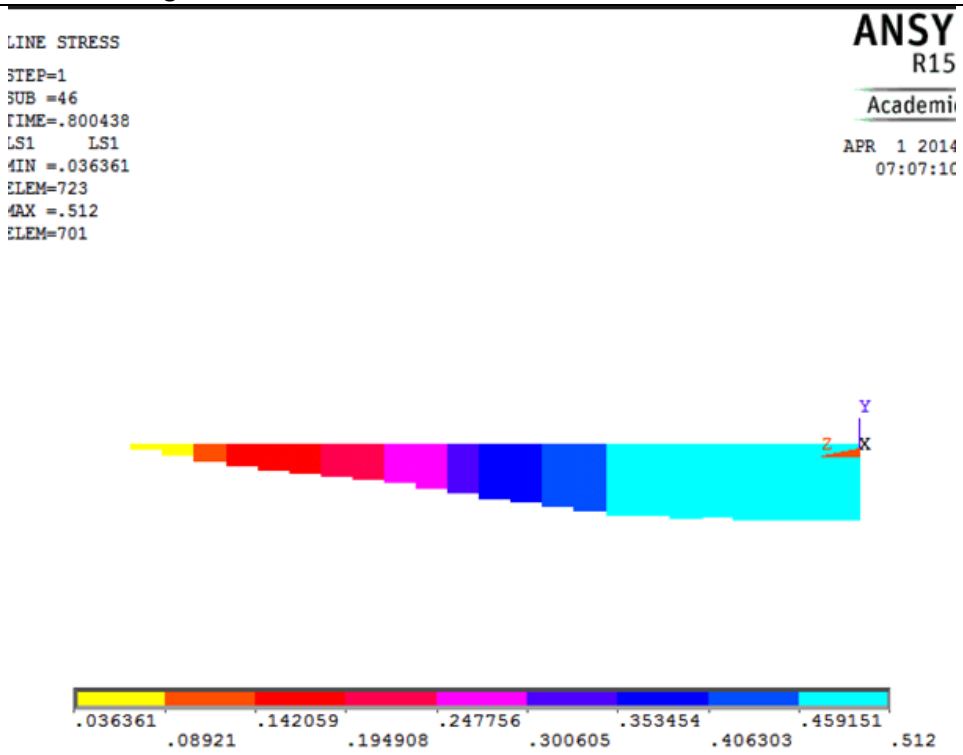

Figure D-68 Reinforcement Stress for 16-3-20

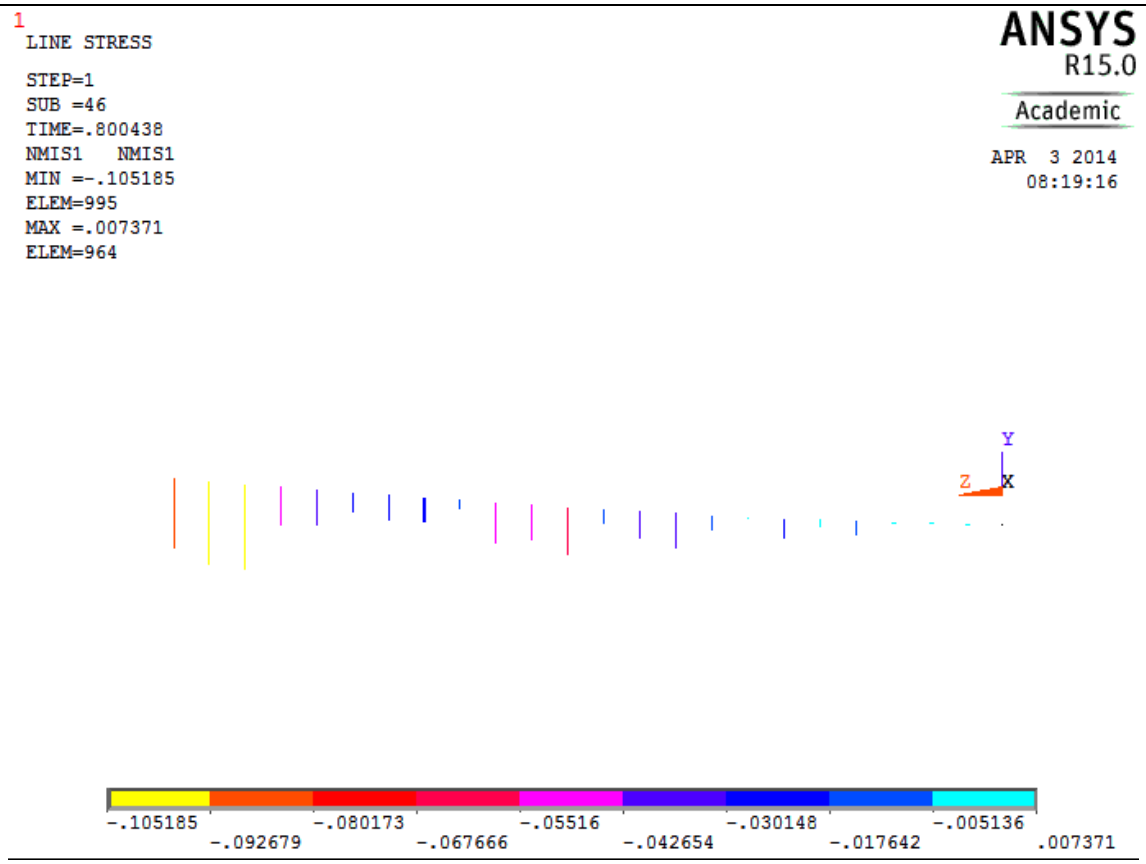

Figure D-69 Spring Stretch for 16-3-20

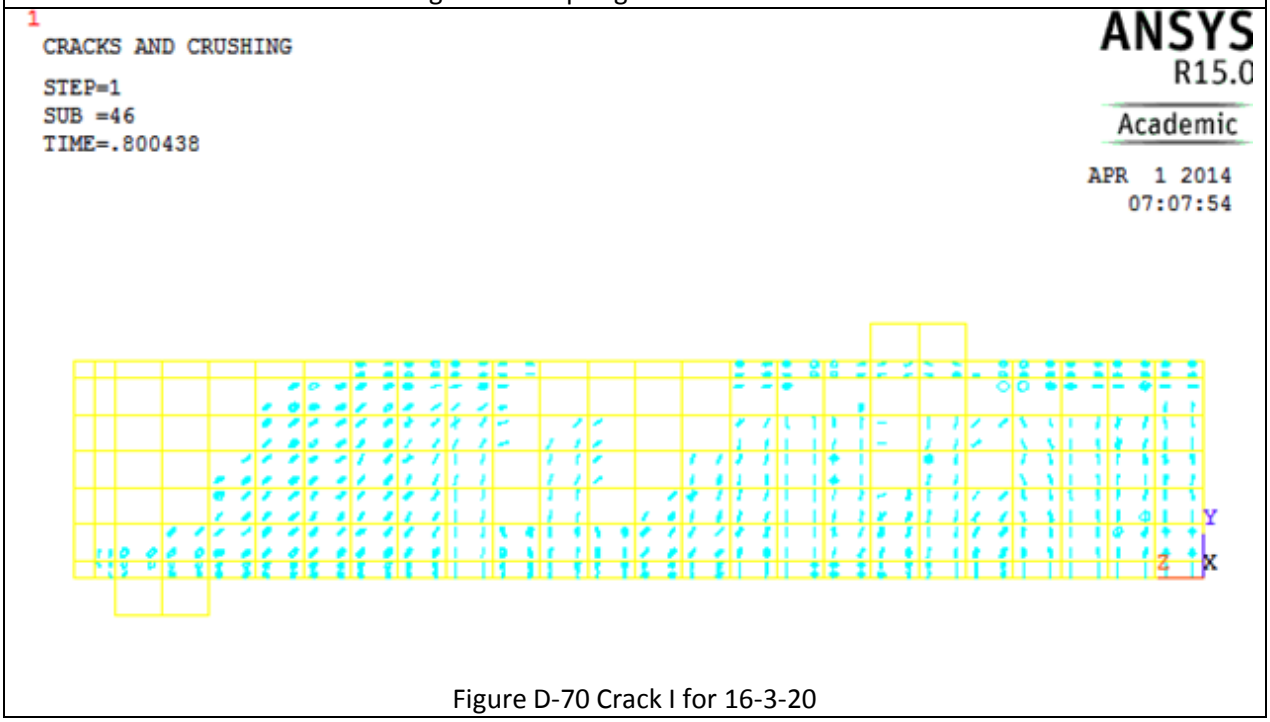

Figure D-70 Crack I for 16-3-20

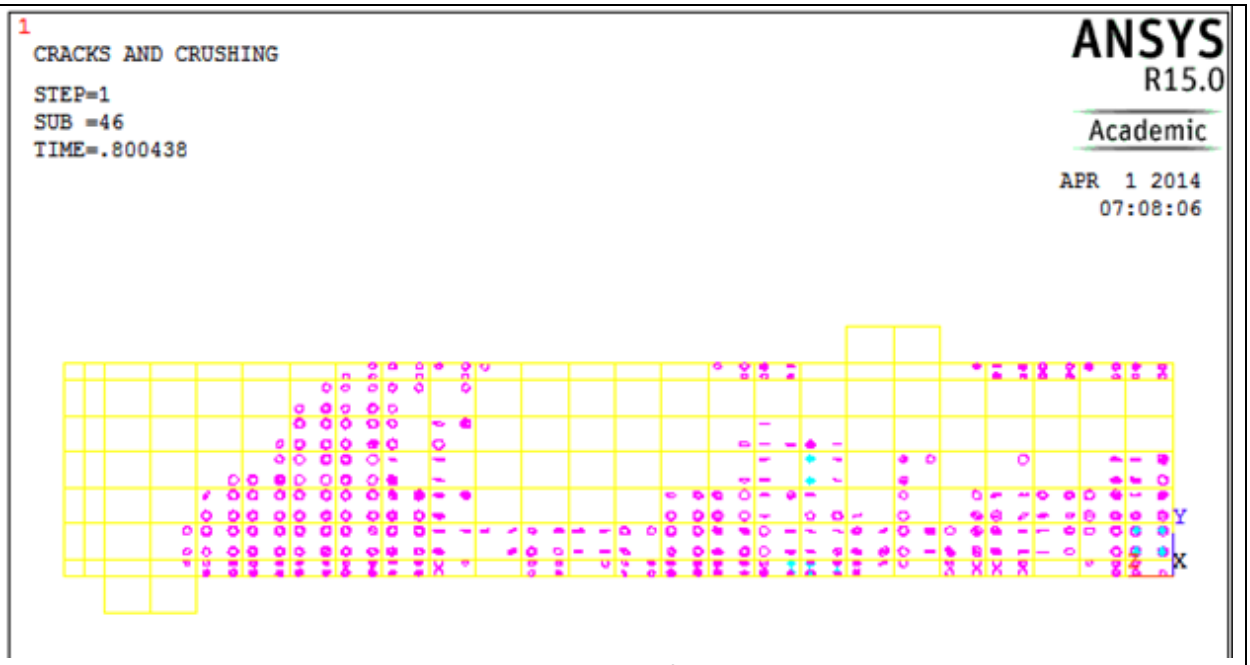

Figure D-71 Crack II for 16-3-20

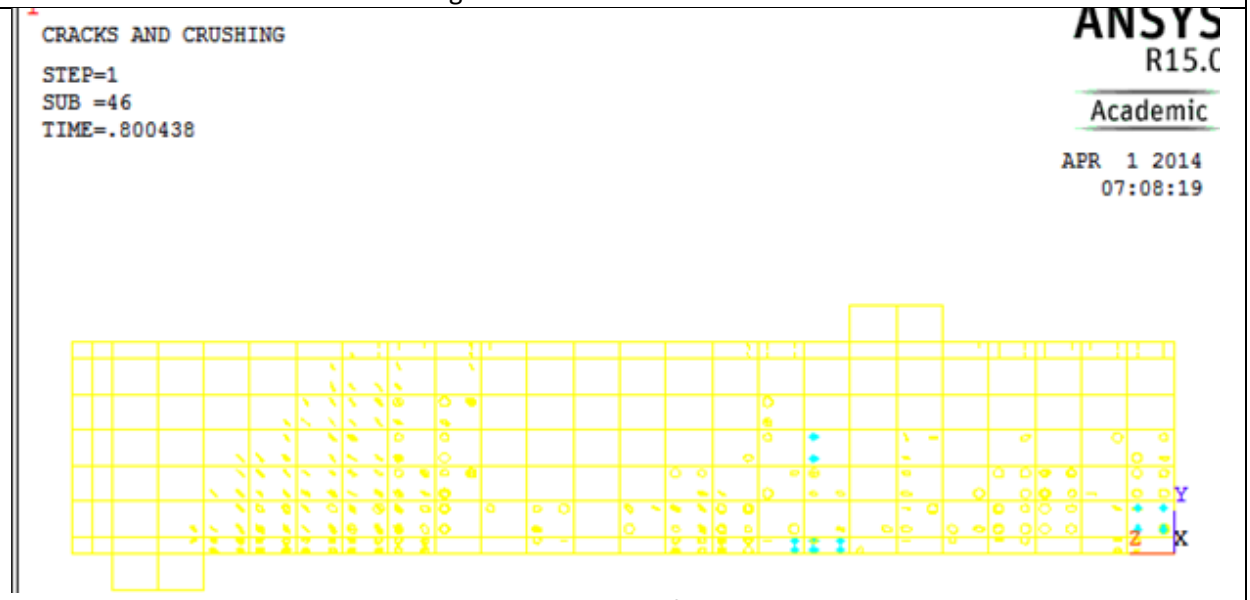

Figure D-72 Crack III for 16-3-20

Table D-10 Details of case 16-3-30

Case Name	Bottom Reinforcement	Honeycombing Location	Strength of Concrete(MPa)	Ultimate Load (kN)	Ultimate Deflection(mm)	Failure Mode
16-3-30	16mm	3	30	103.8193	18.0242	

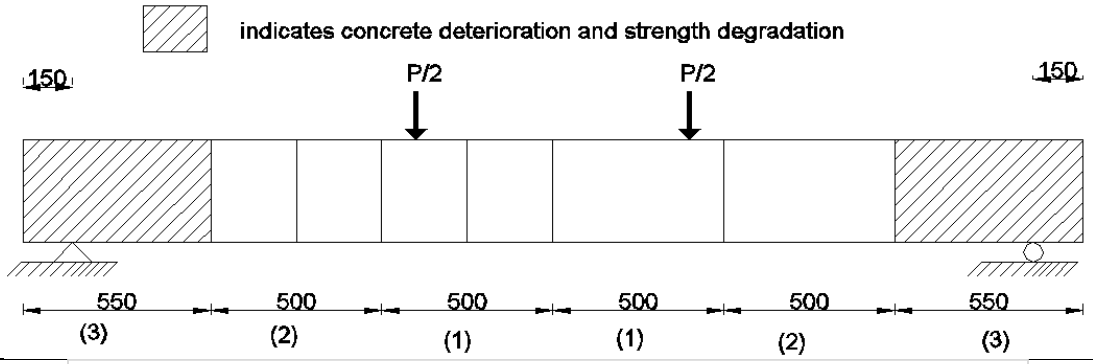

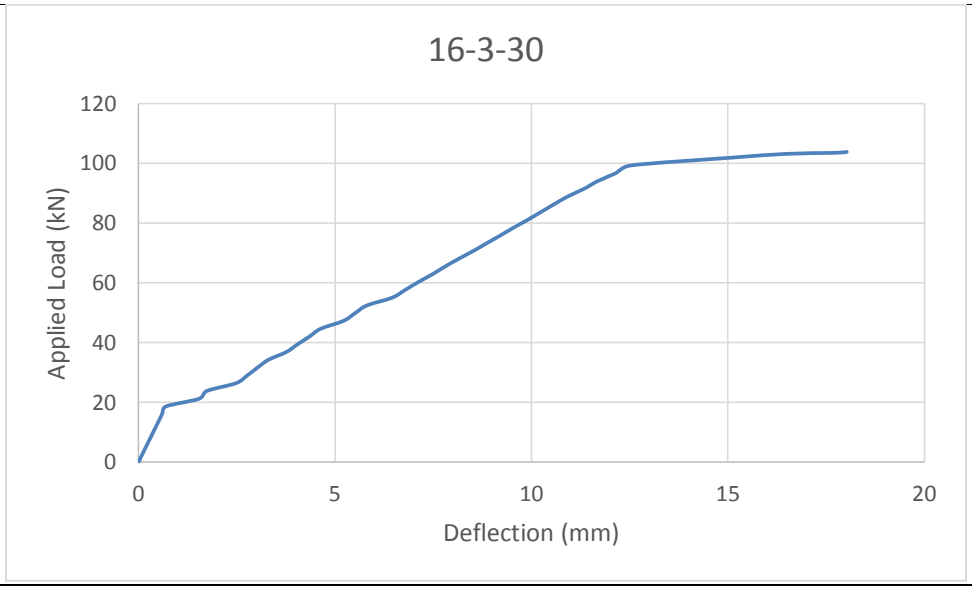

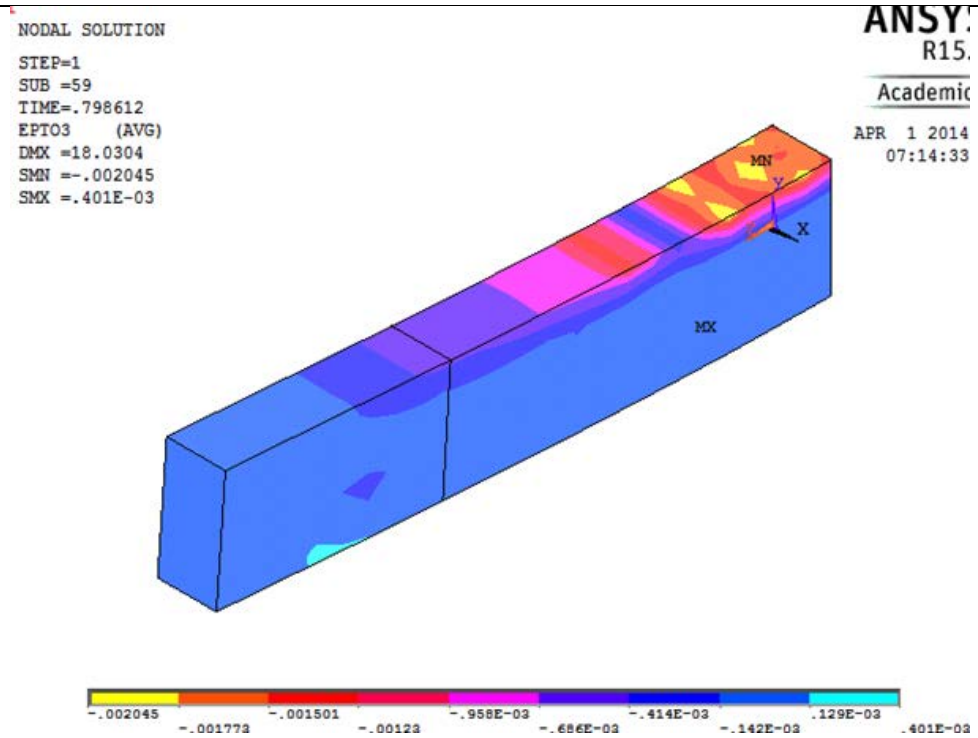

Figure D-73 Nodal solution – 3rd principal total mechanical strain for 16-3-30

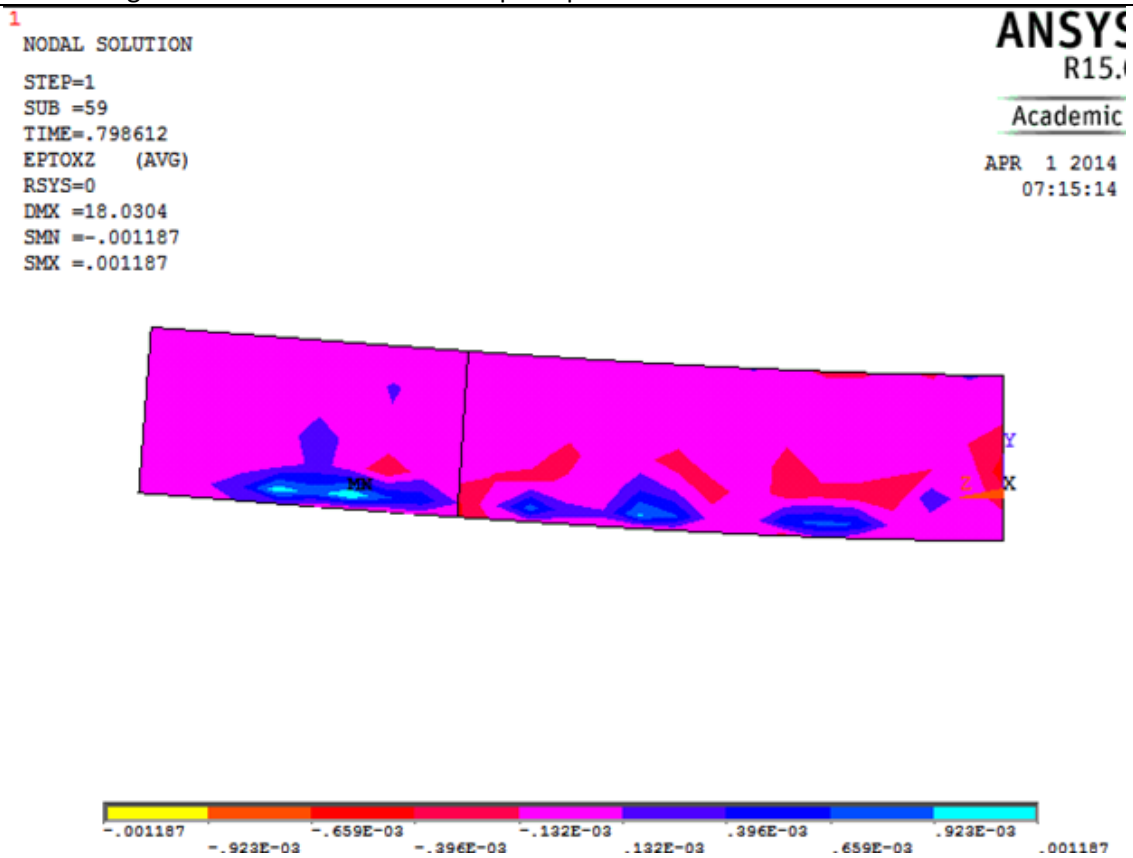

Figure D-74 Nodal Solution XZ shear total mechanical strain for 16-3-30

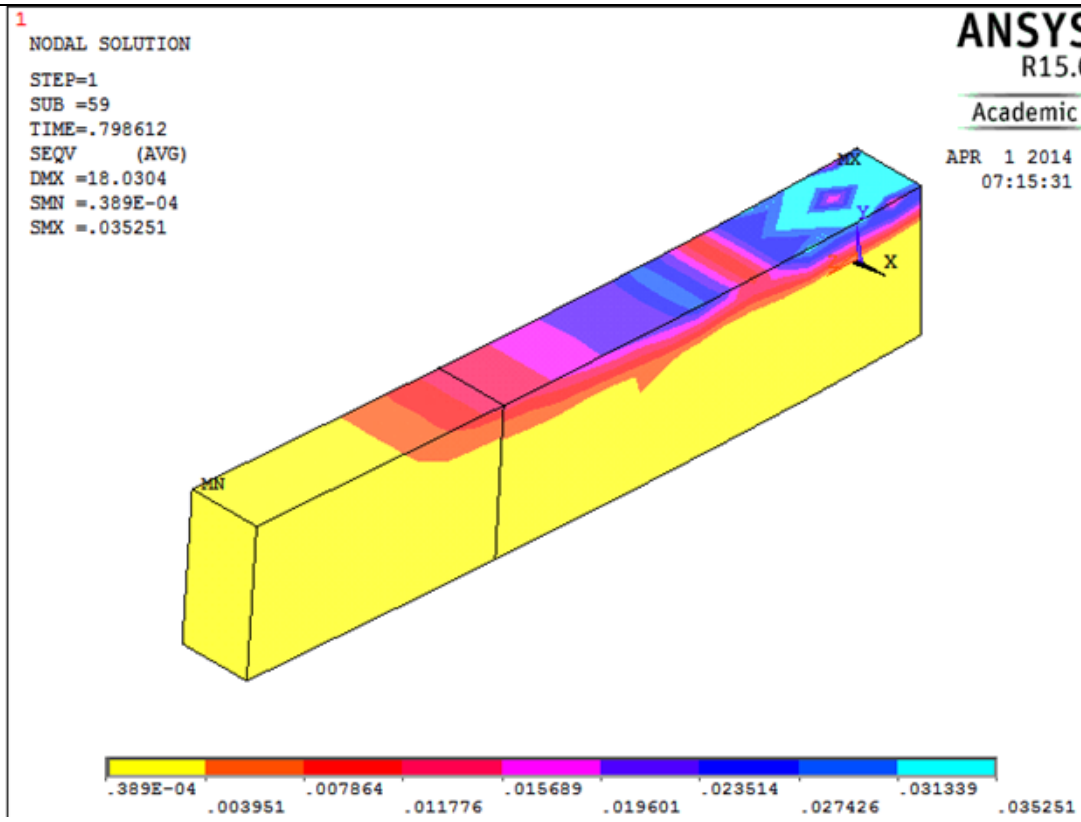

Figure D-75 Nodal Solution -Von Mises Stress for 16-3-30

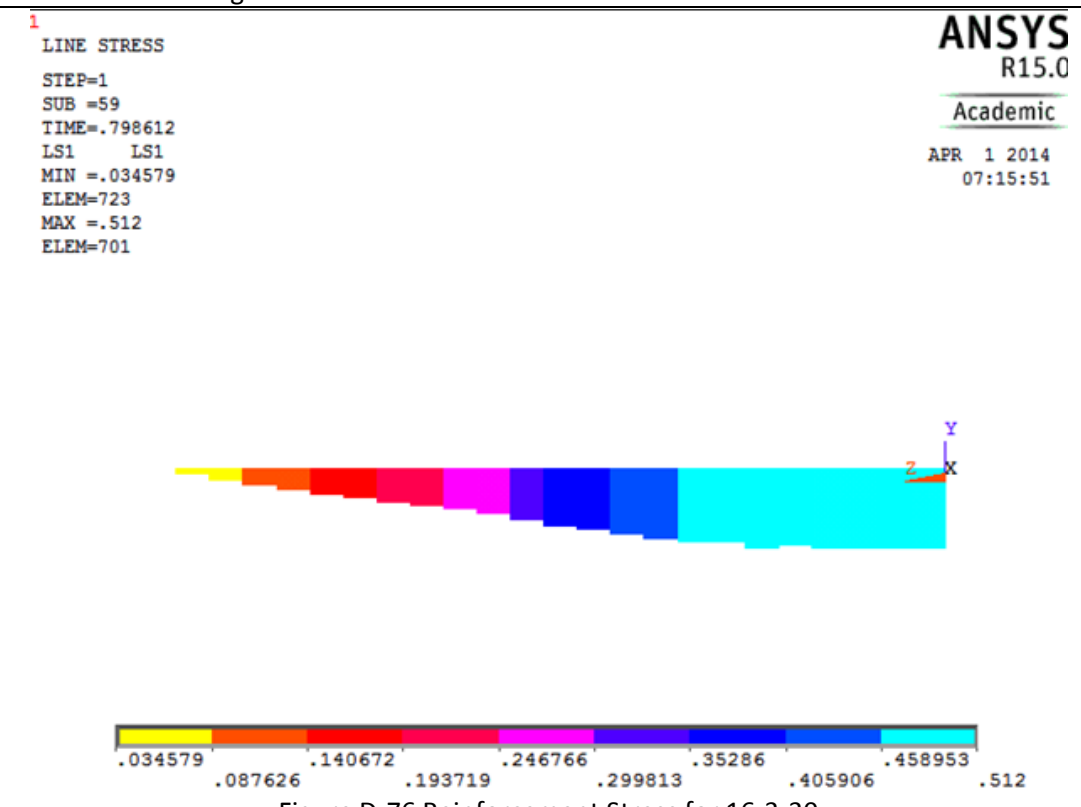

Figure D-76 Reinforcement Stress for 16-3-30

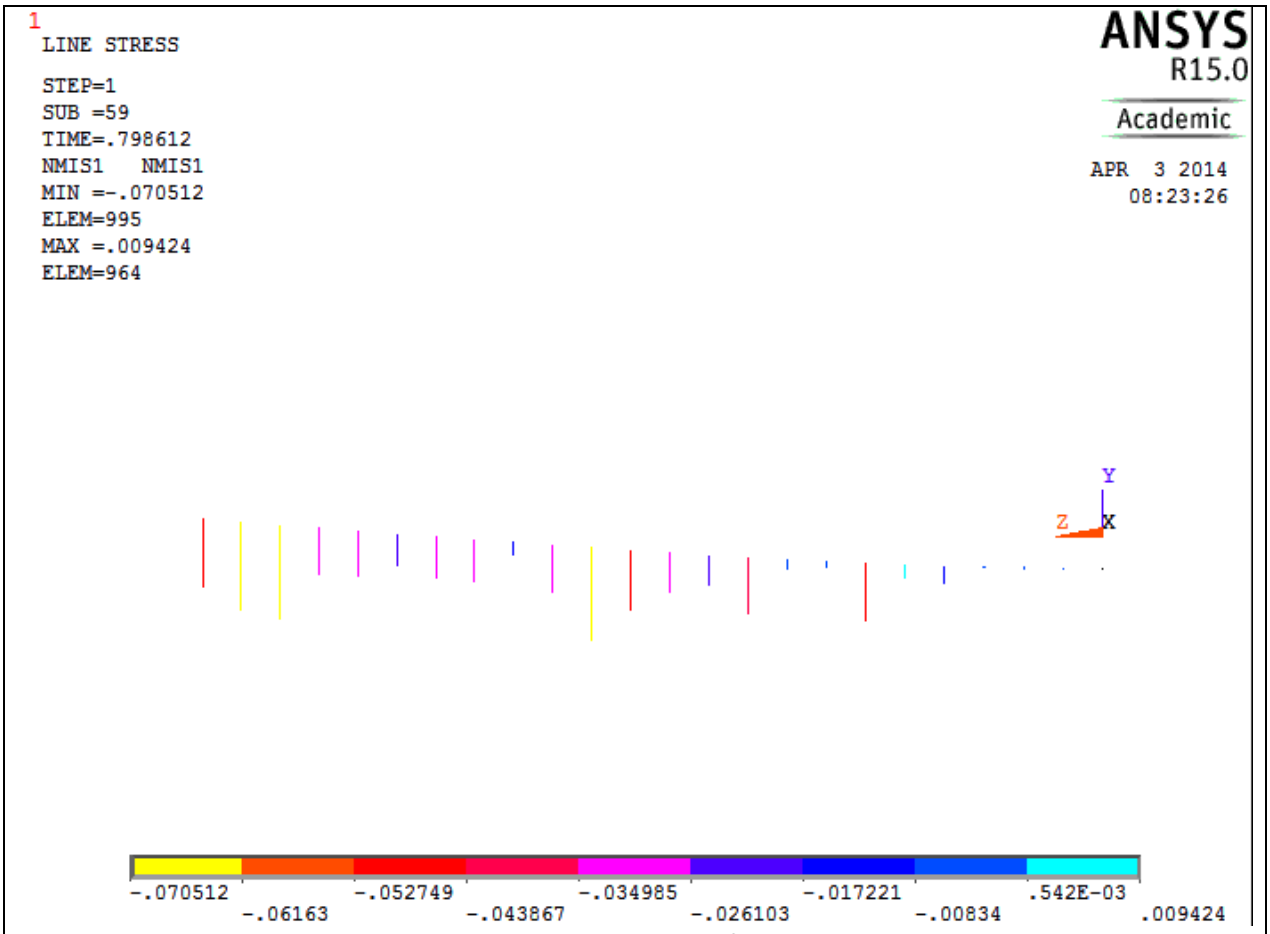

Figure D-77 Spring Stretch for 16-3-30

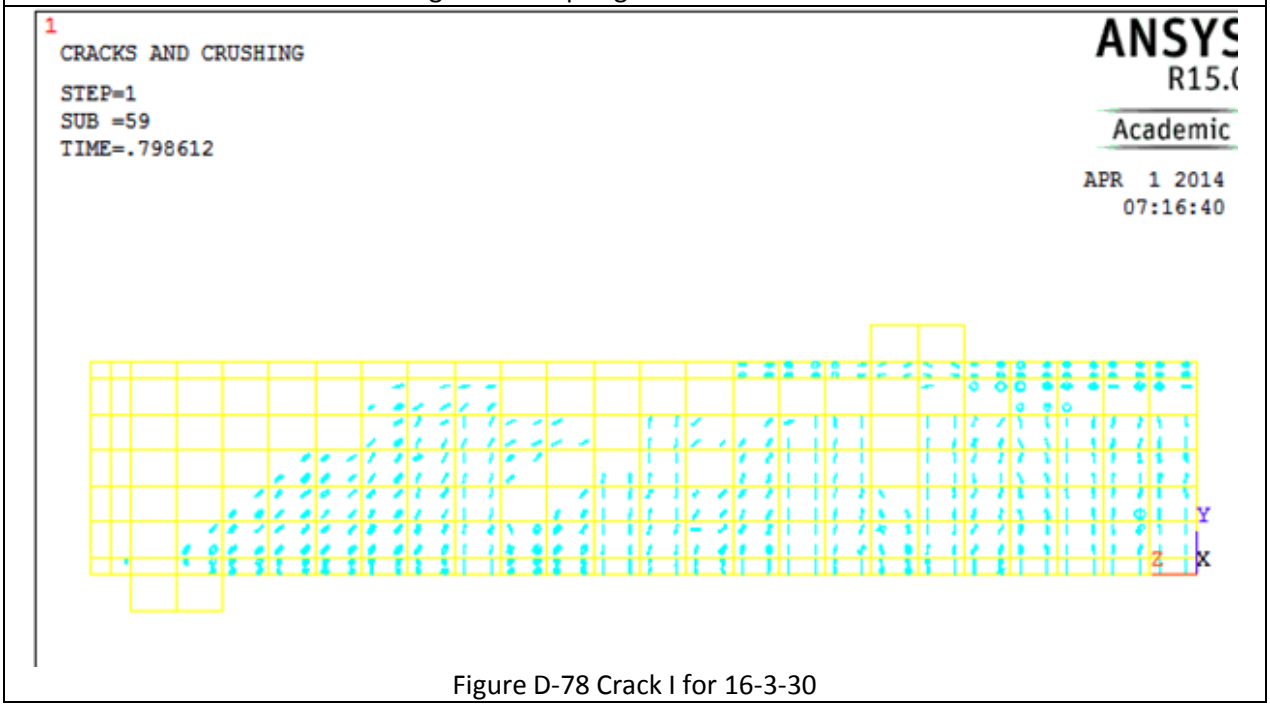

Figure D-78 Crack I for 16-3-30

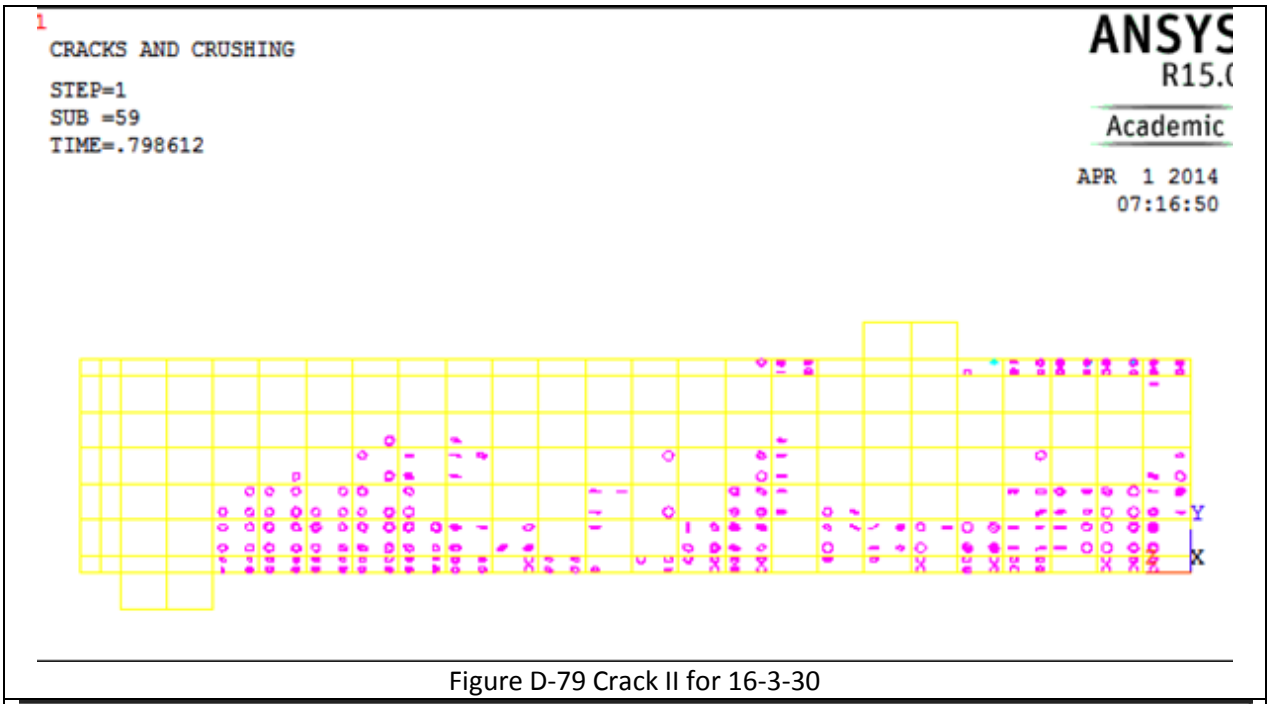

Figure D-79 Crack II for 16-3-30

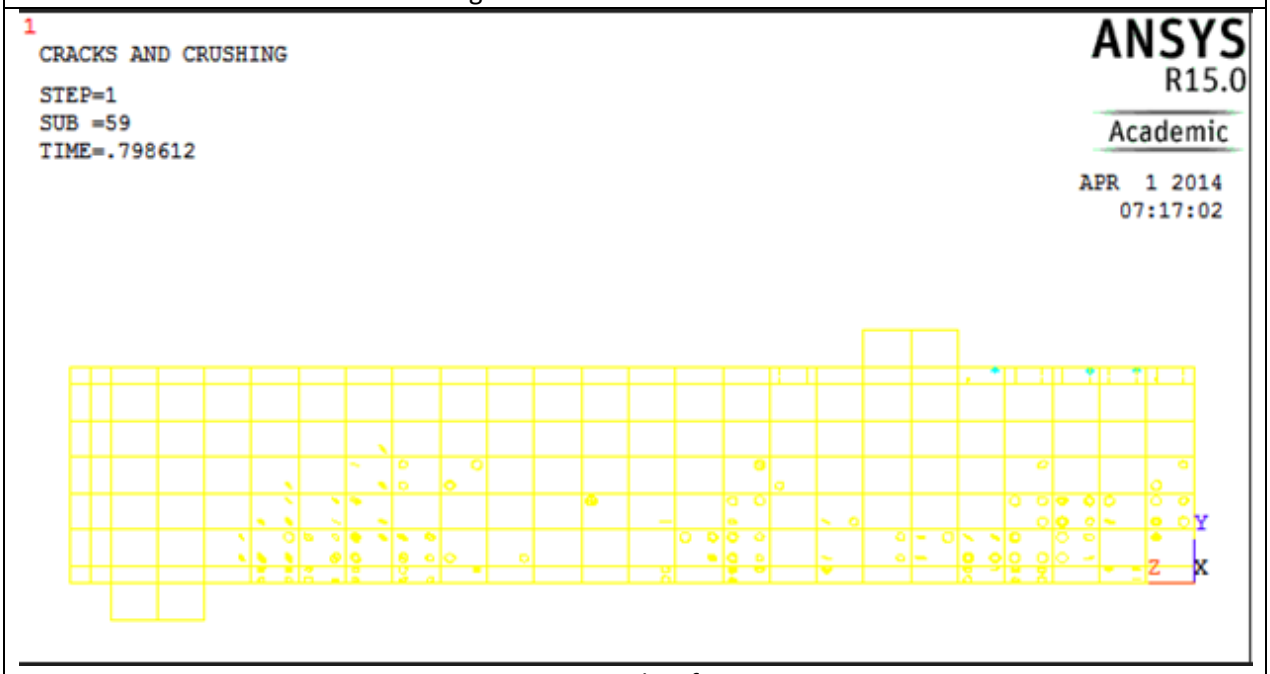

Figure D-80 Crack III for 16-3-30

Table D-11 Details of case 25-0

Case Name	Bottom Reinforcement	Honeycombing Location	Strength of Concrete(MPa)	Ultimate Load (kN)	Ultimate Deflection(mm)	Failure Mode
25-0	25mm	None	42.7	178.915	12.9172	

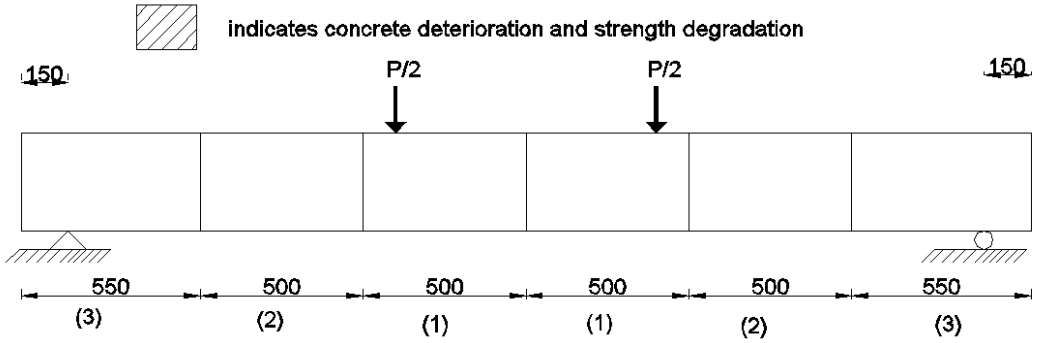

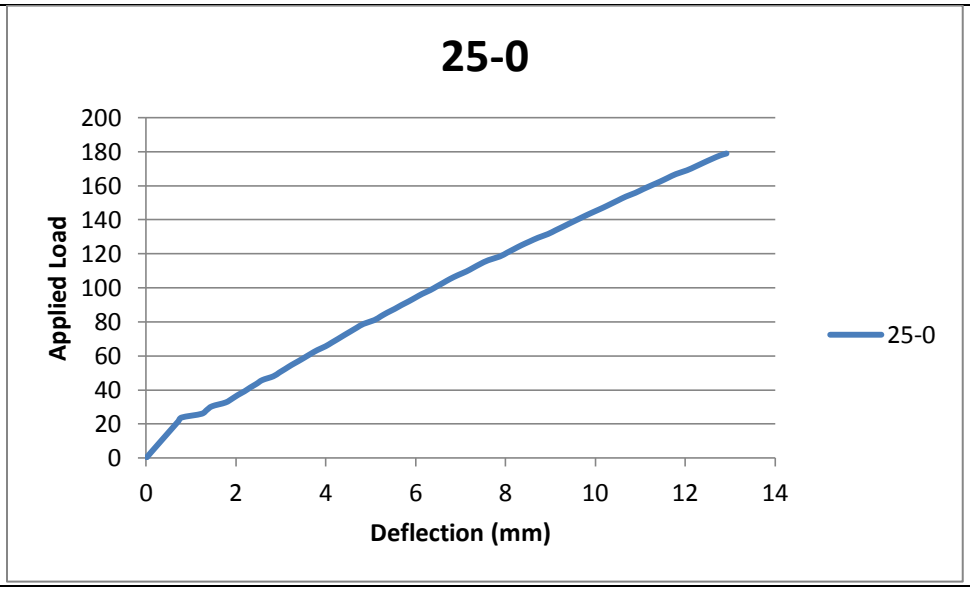

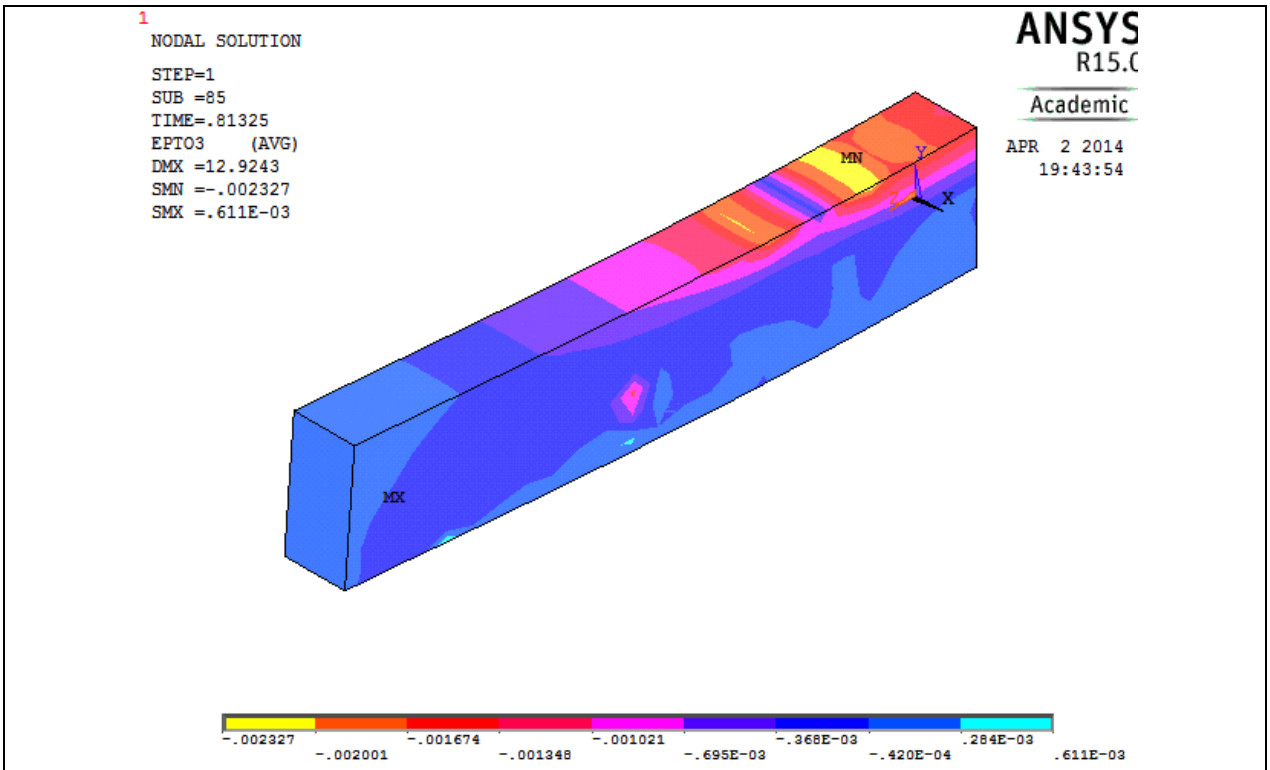

Figure D-81 Nodal solution – 3rd principal total mechanical strain for 25-0

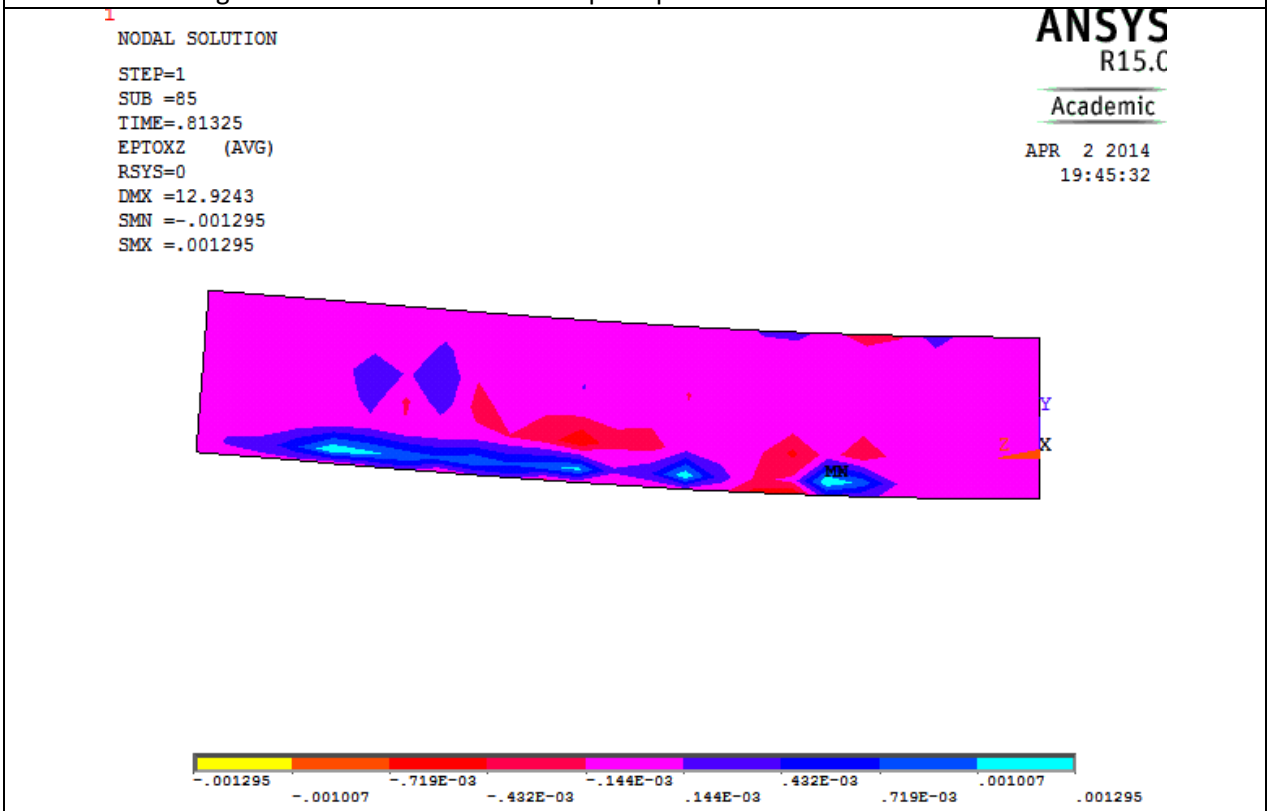

Figure D-82 Nodal Solution XZ shear total mechanical strain for 25-0

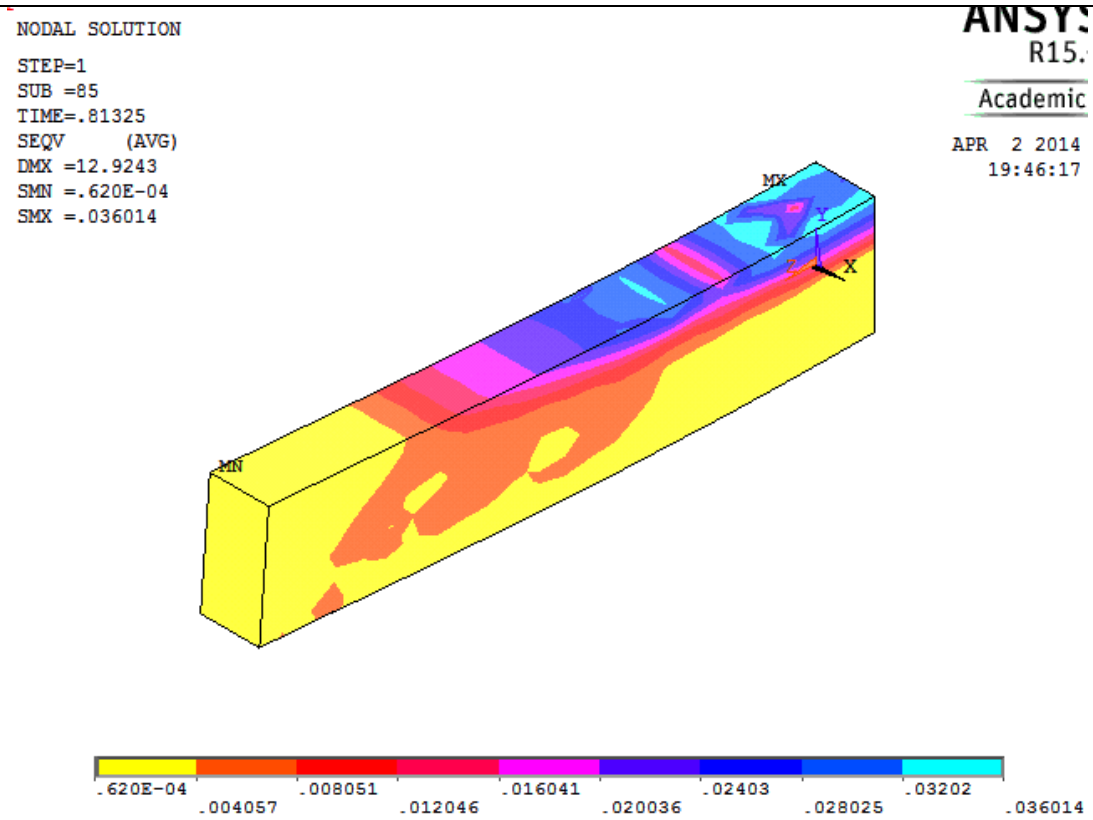

Figure D-83 Nodal Solution -Von Mises Stress for 25-0

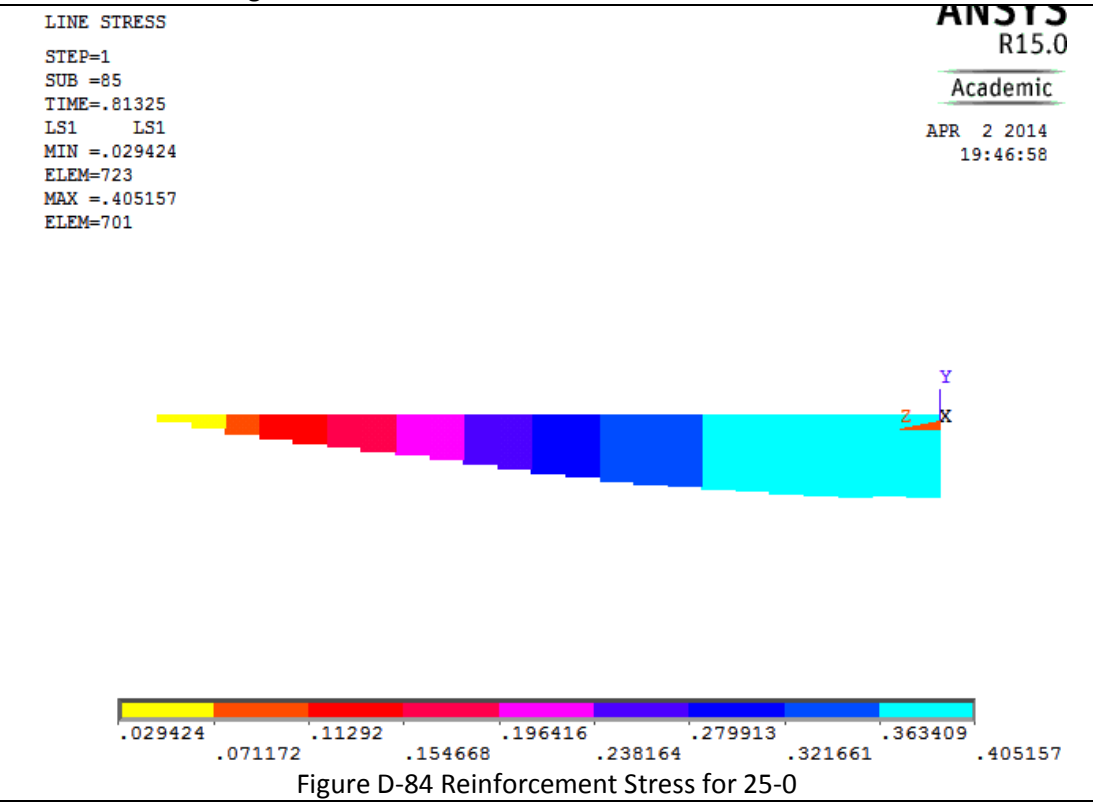

Figure D-84 Reinforcement Stress for 25-0

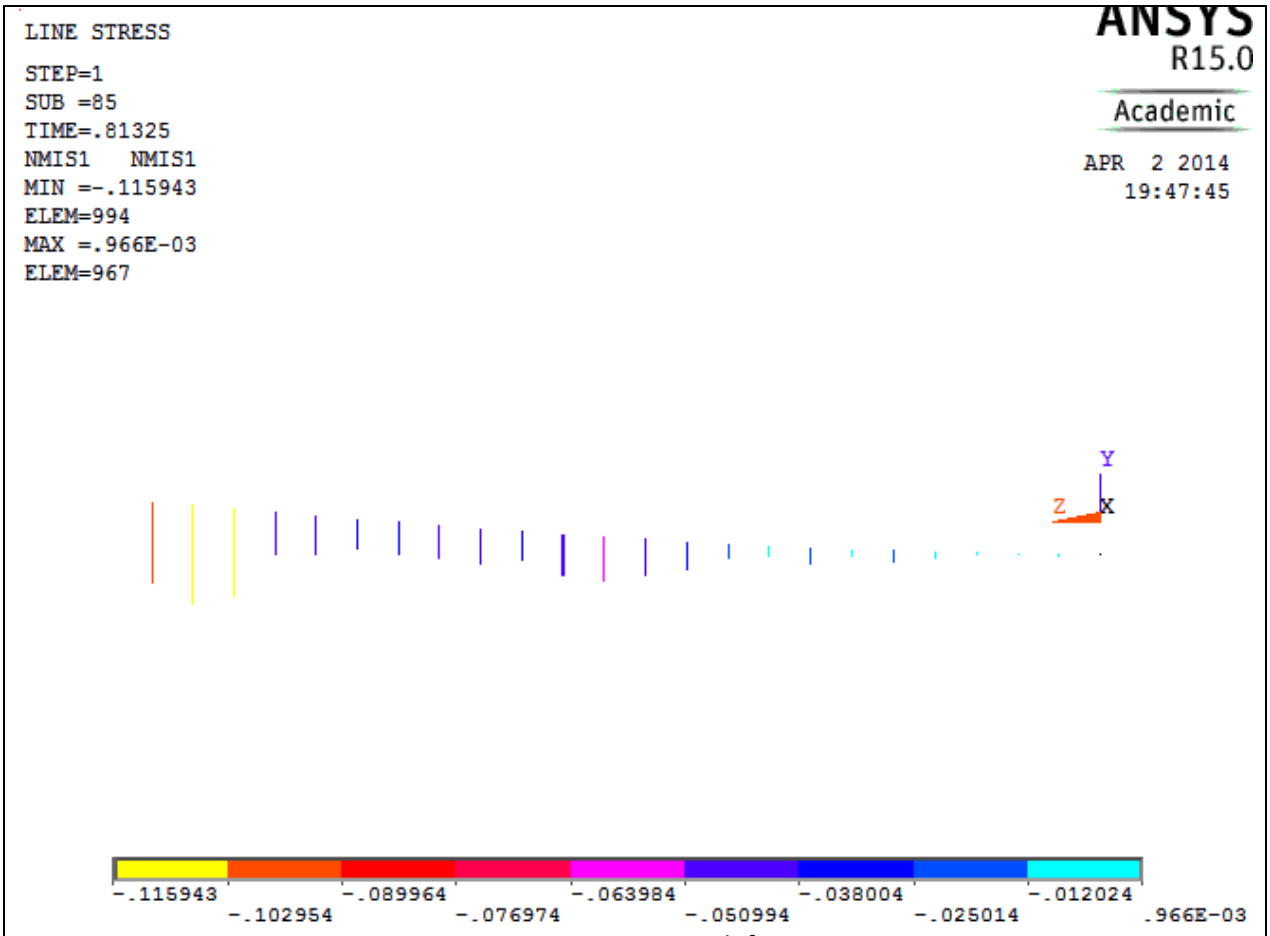

Figure D-85 Spring Stretch for 25-0

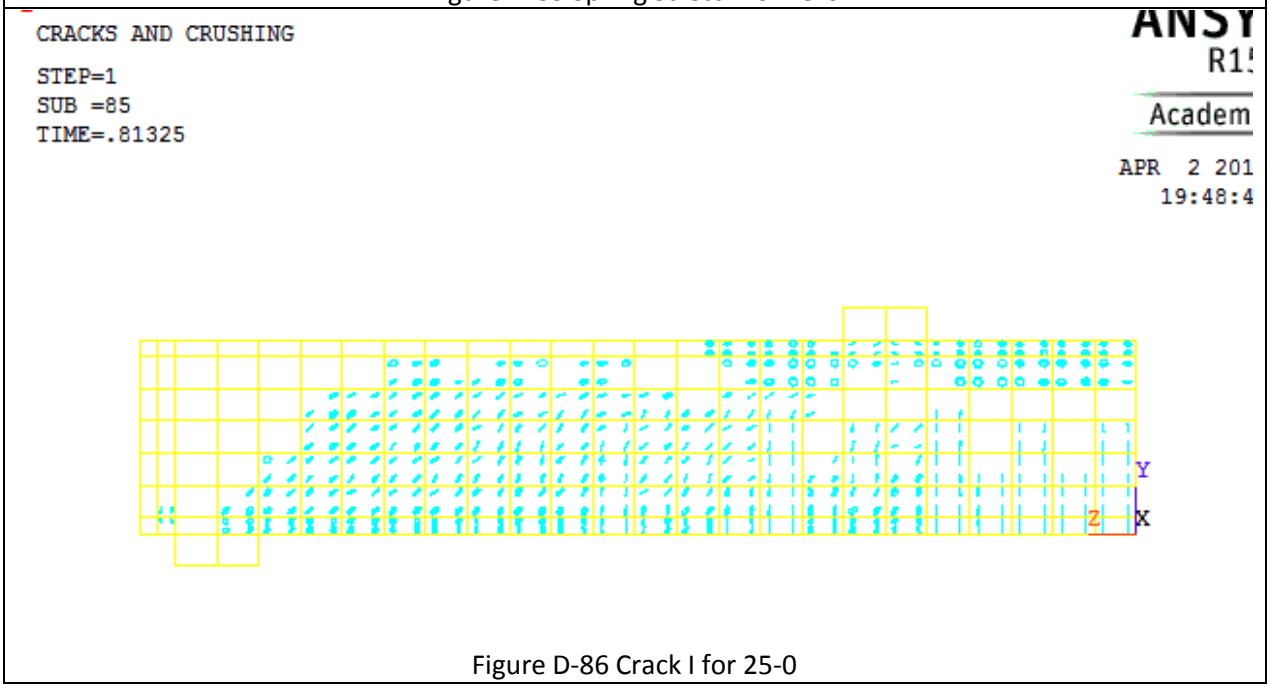

Figure D-86 Crack I for 25-0

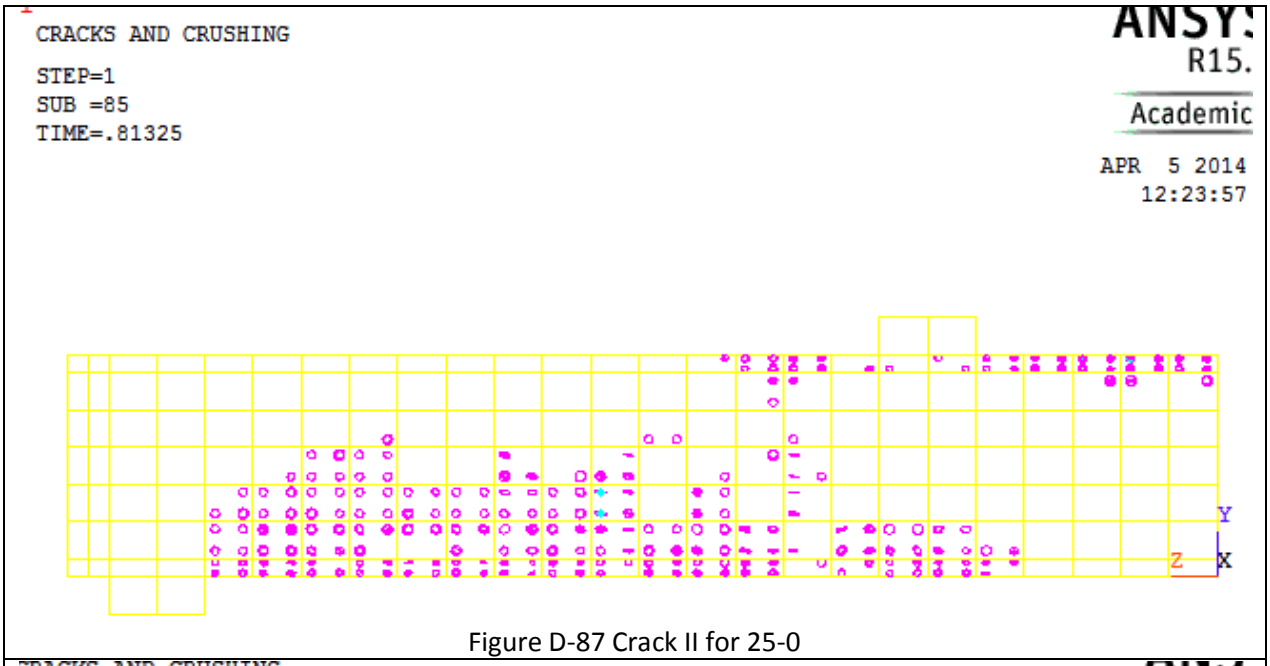

Figure D-87 Crack II for 25-0

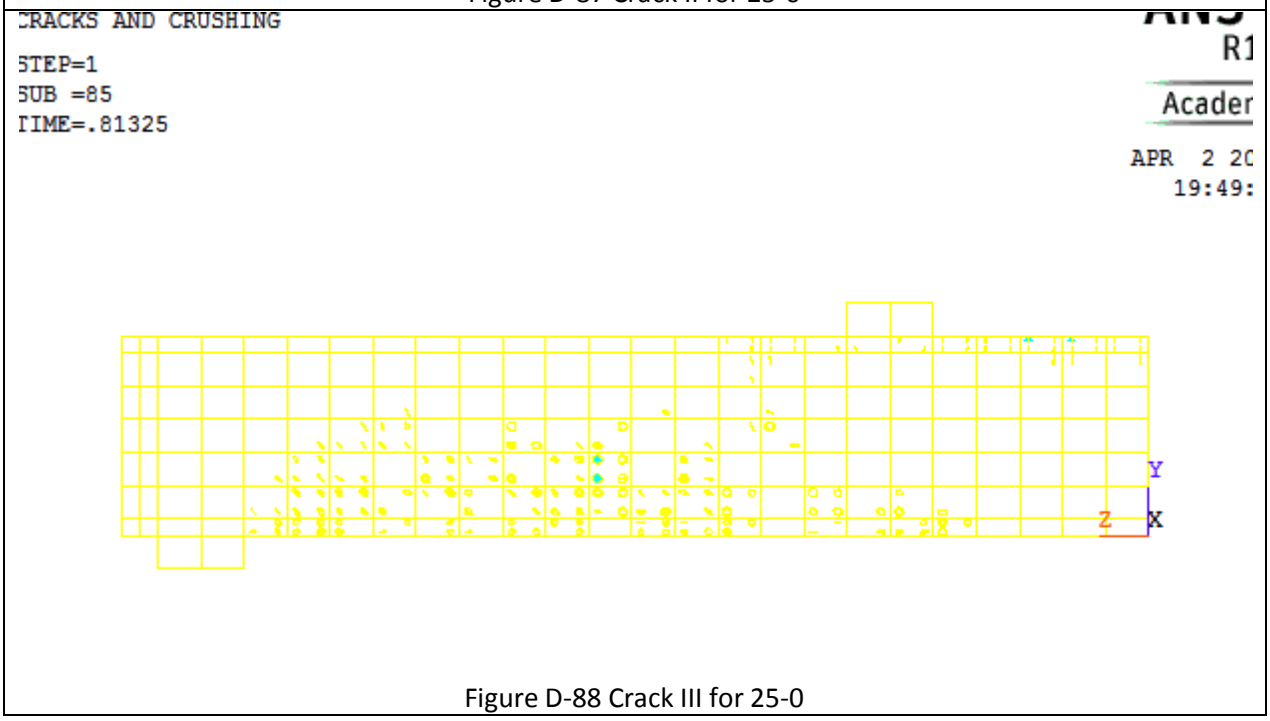

Figure D-88 Crack III for 25-0

Table D-12 Details of case 25-1-10

Case Name	Bottom Reinforcement	Honeycombing Location	Strength of Concrete(MPa)	Ultimate Load (kN)	Ultimate Deflection(mm)	Failure Mode
25-1-10	25mm	1	10	60.94	4.96507	

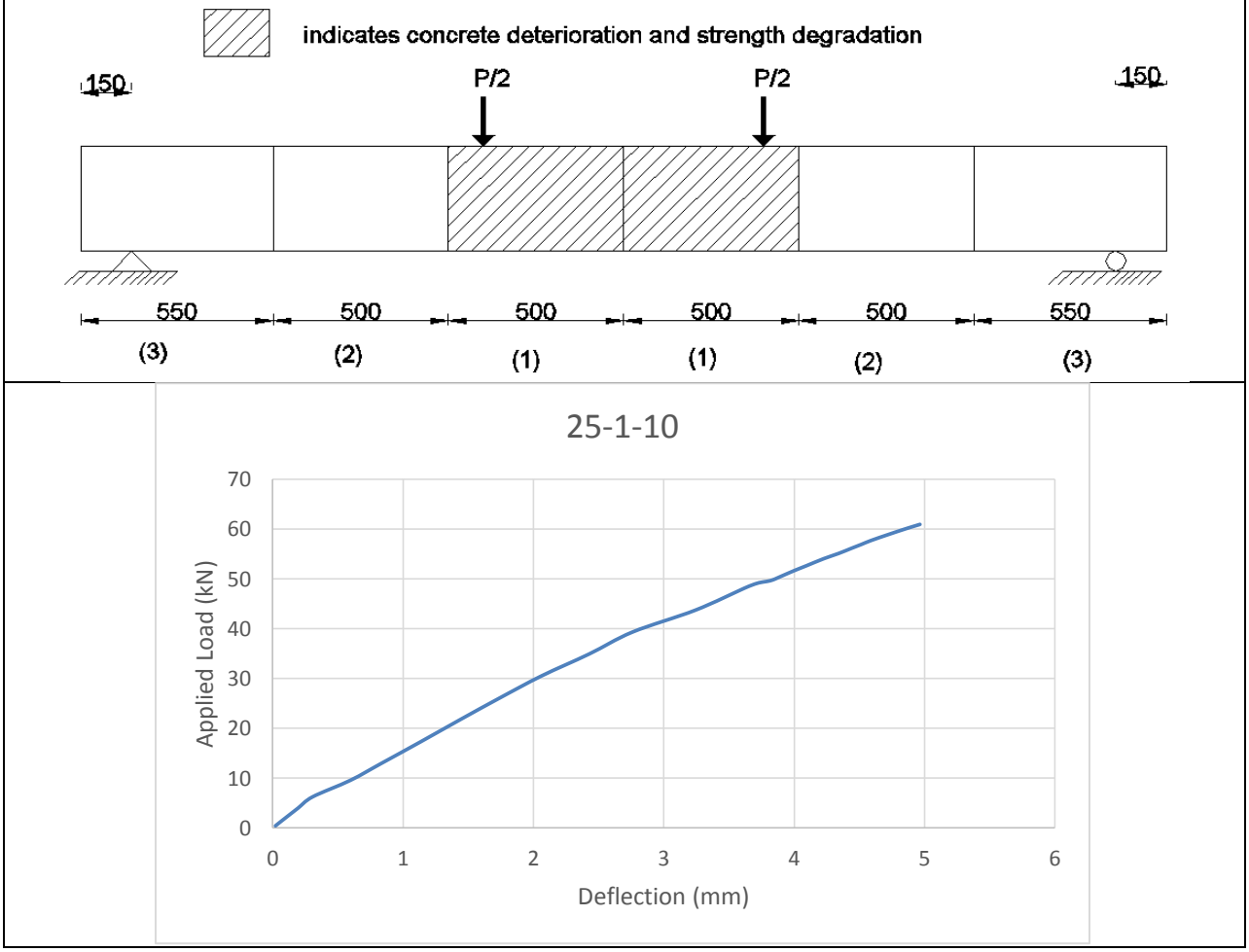

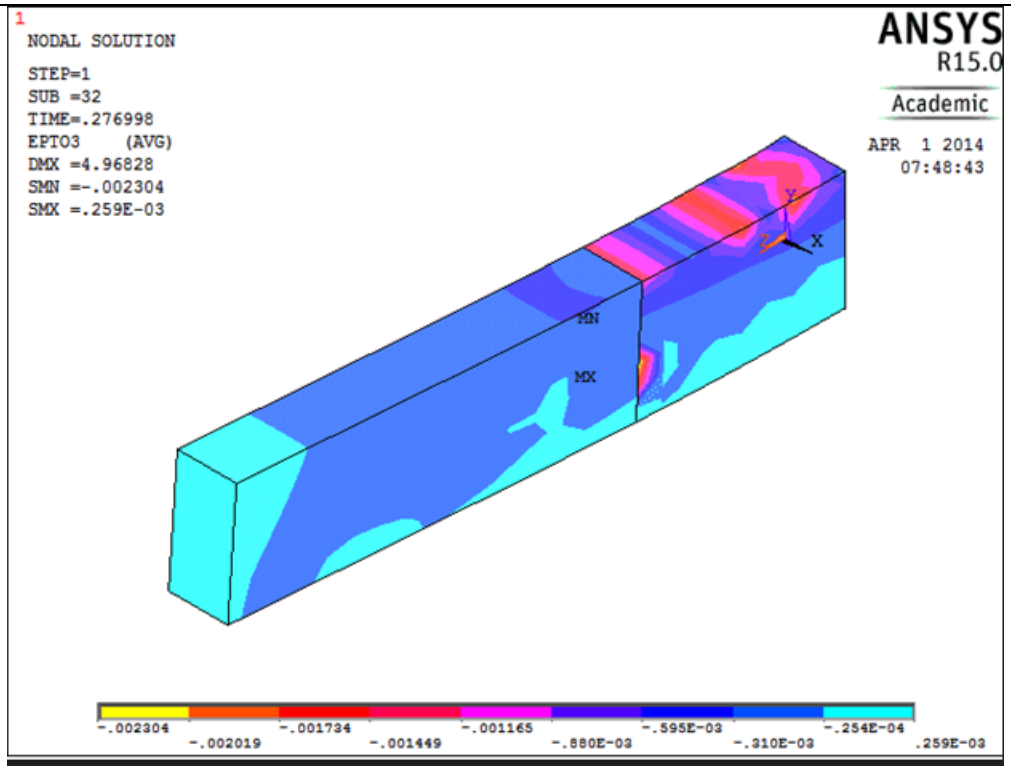

Figure D-89 Nodal solution – 3rd principal total mechanical strain for 25-1-10

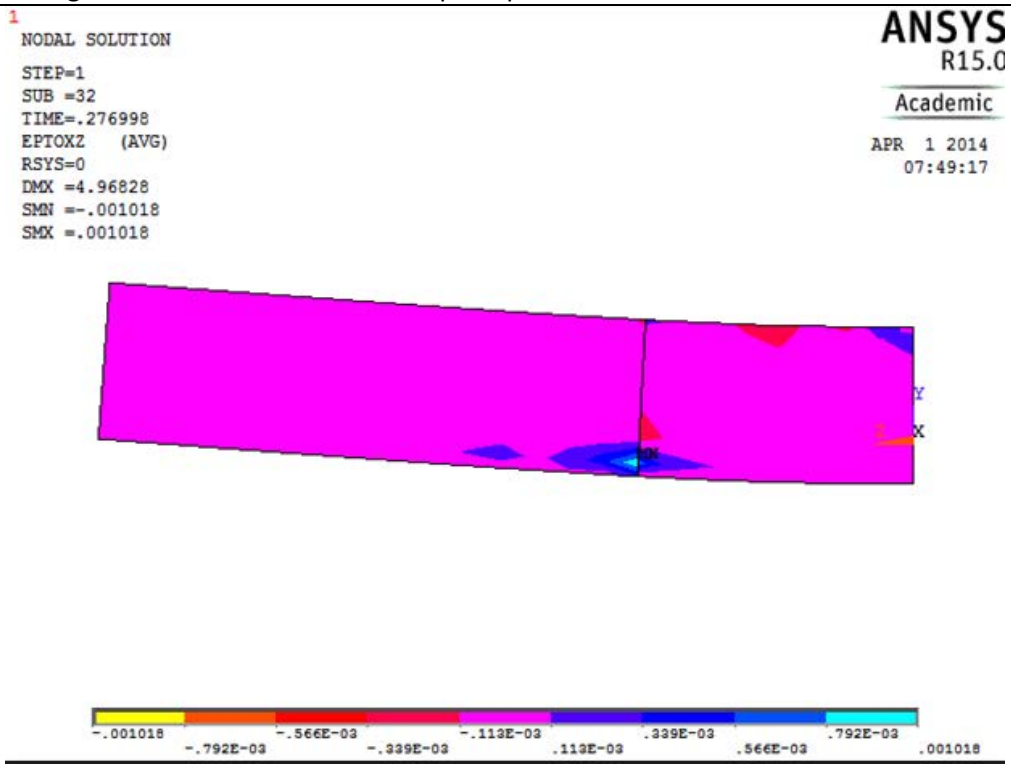

Figure D-90 Nodal Solution XZ shear total mechanical strain for 25-1-10

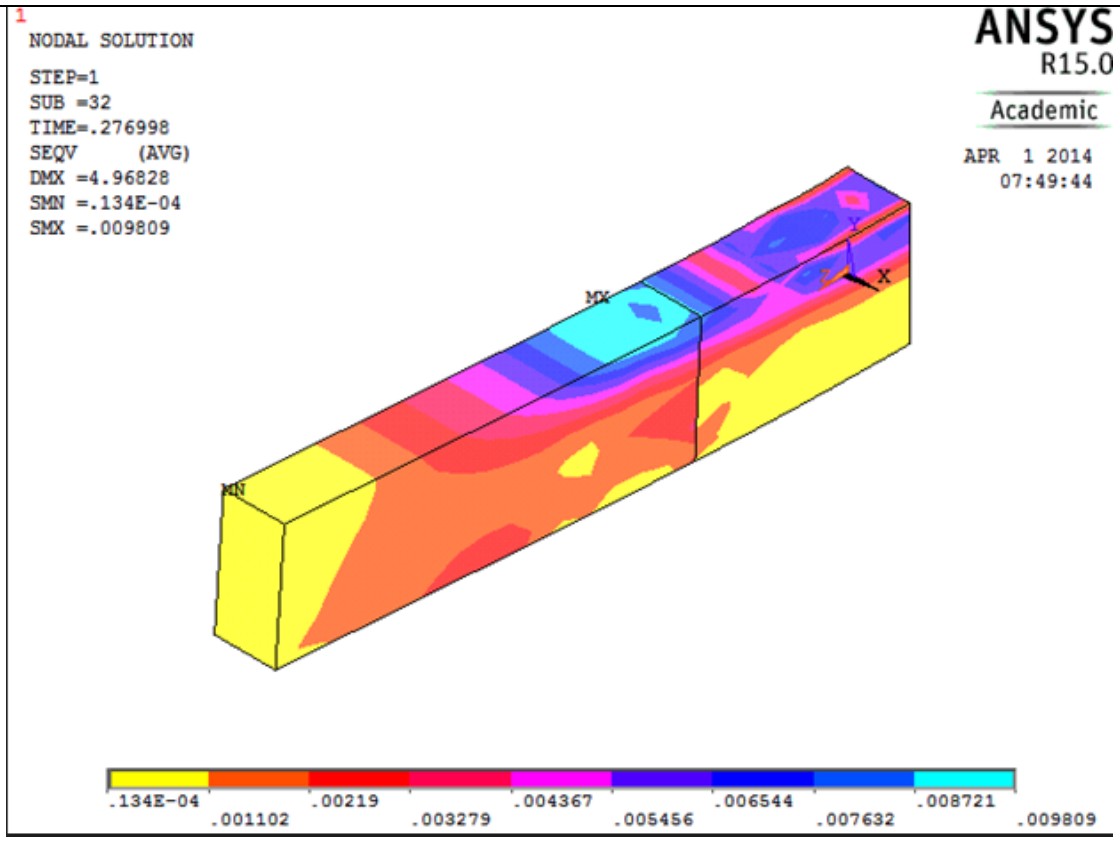

Figure D-91 Nodal Solution -Von Mises Stress for 25-1-10

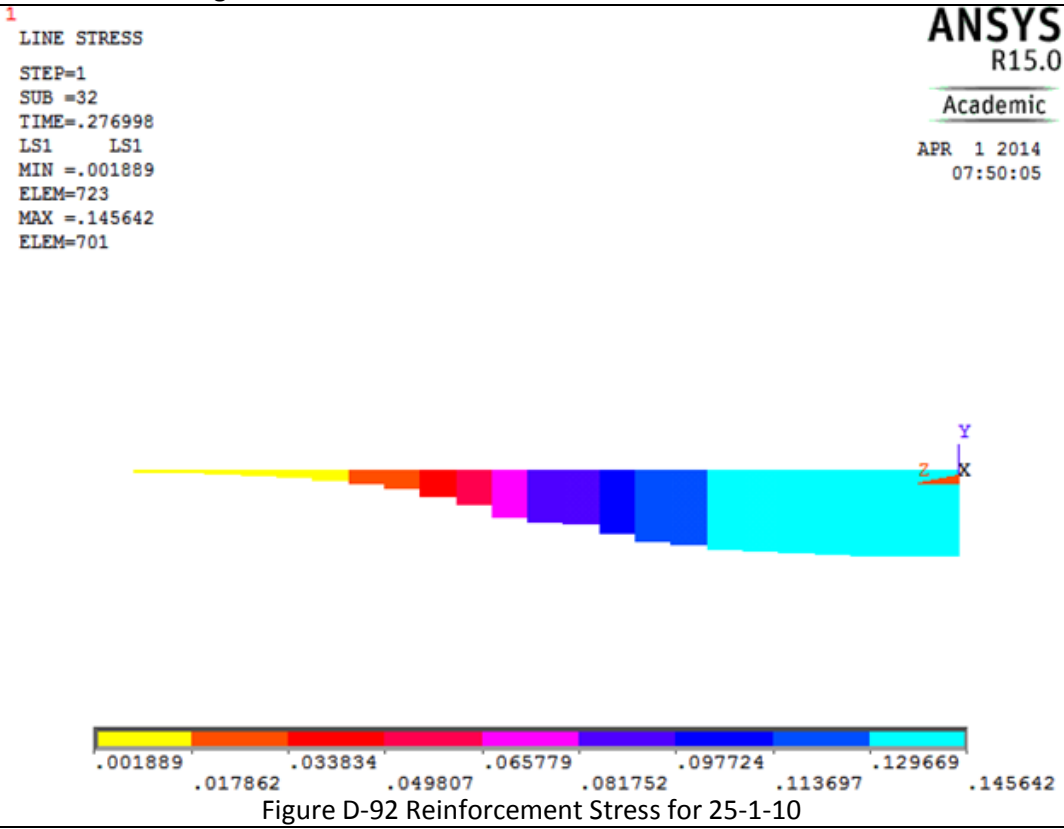

Figure D-92 Reinforcement Stress for 25-1-10

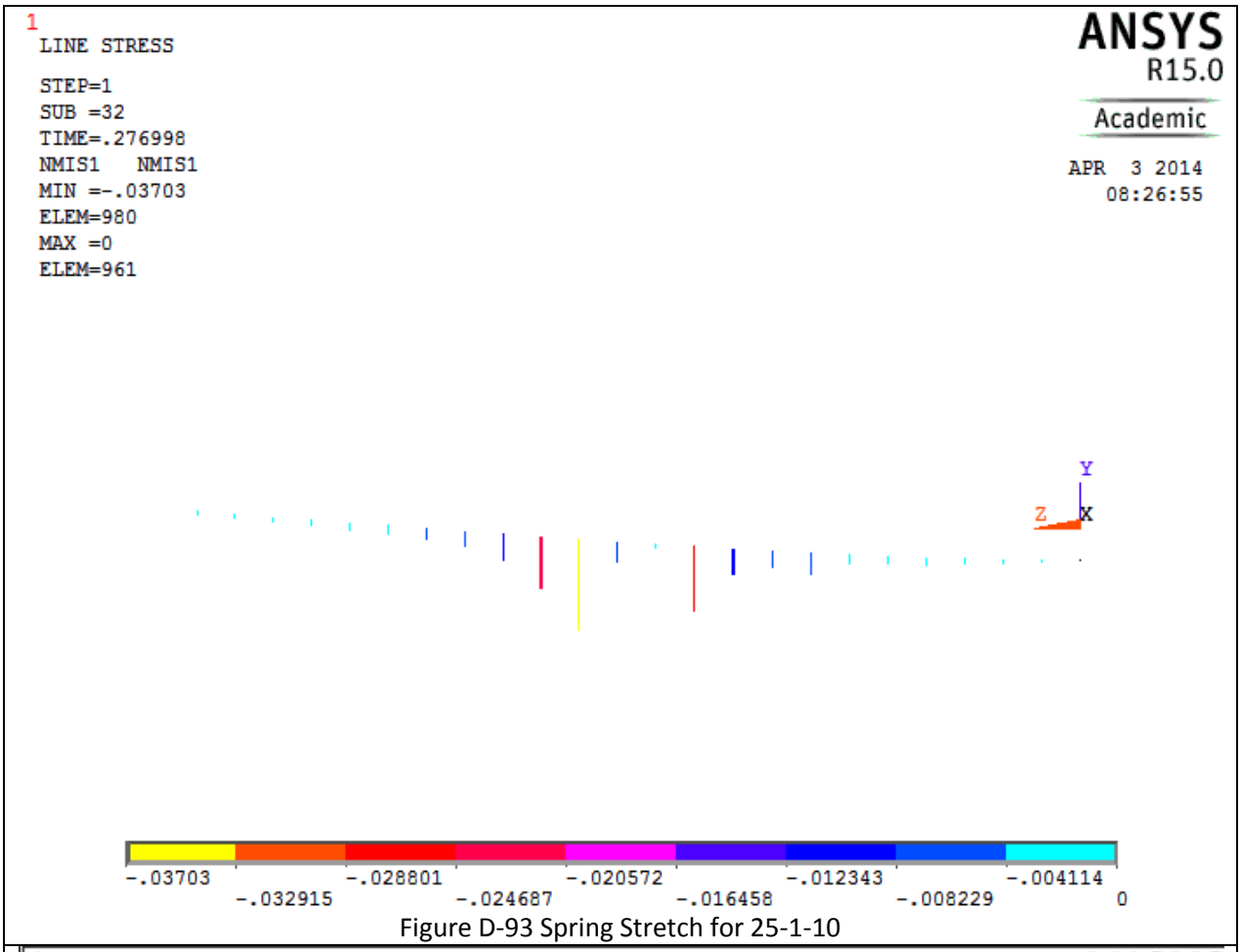

Figure D-93 Spring Stretch for 25-1-10

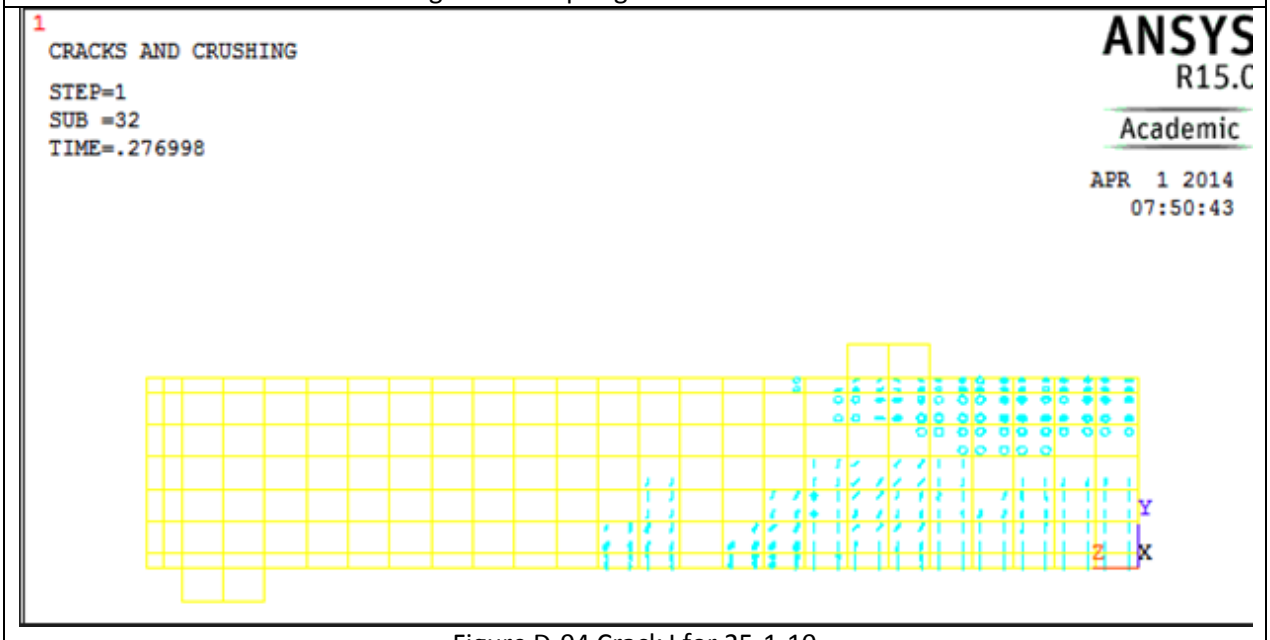

Figure D-94 Crack I for 25-1-10

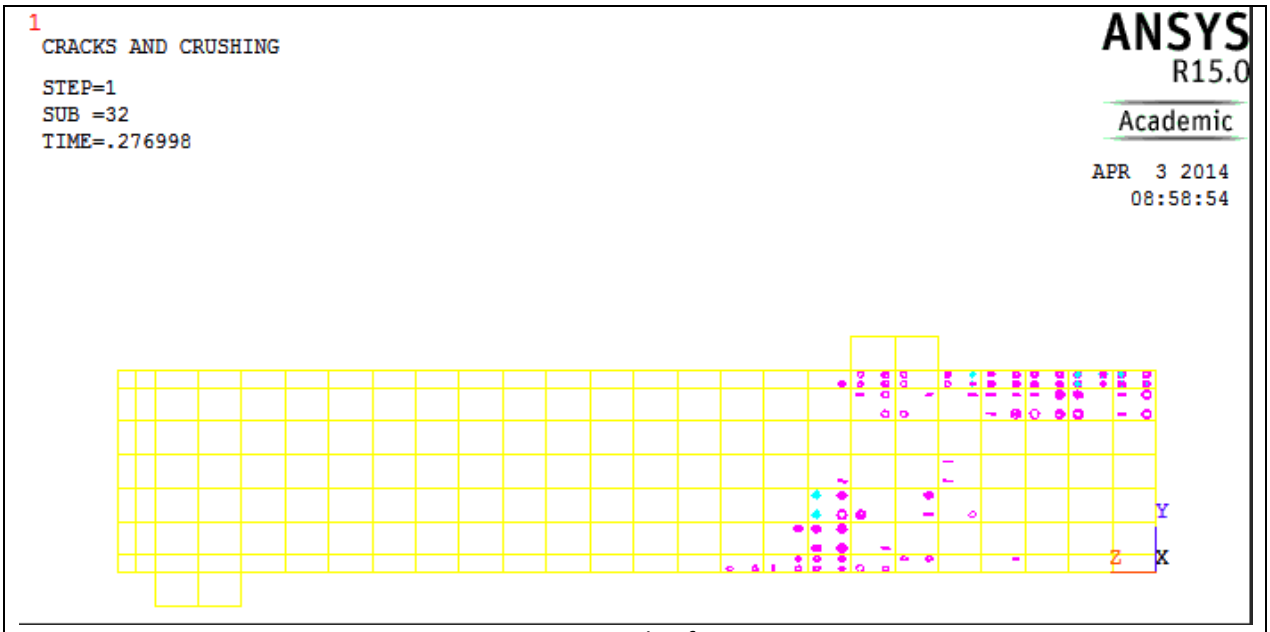

Figure D-95 Crack II for 25-1-10

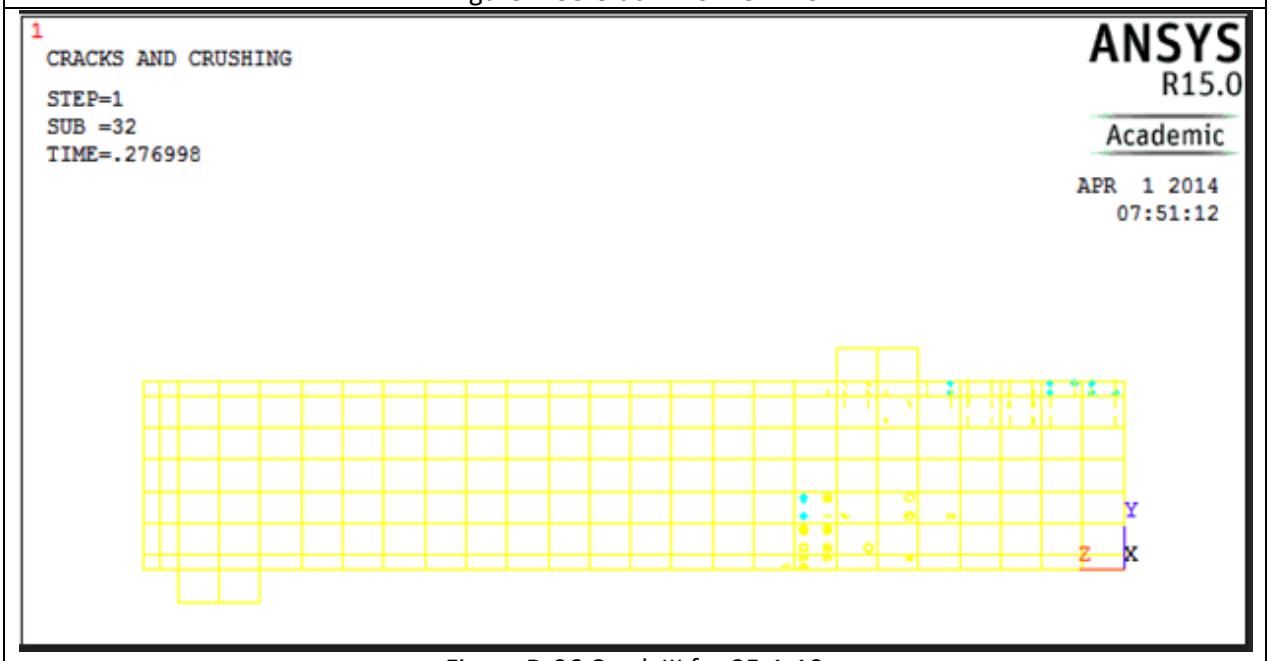

Figure D-96 Crack III for 25-1-10

Table D-13 Details of case 25-1-20

Case Name	Bottom Reinforcement	Honeycombing Location	Strength of Concrete(MPa)	Ultimate Load (kN)	Ultimate Deflection(mm)	Failure Mode
25-1-20	25mm	1	20	95.183	7.06836	

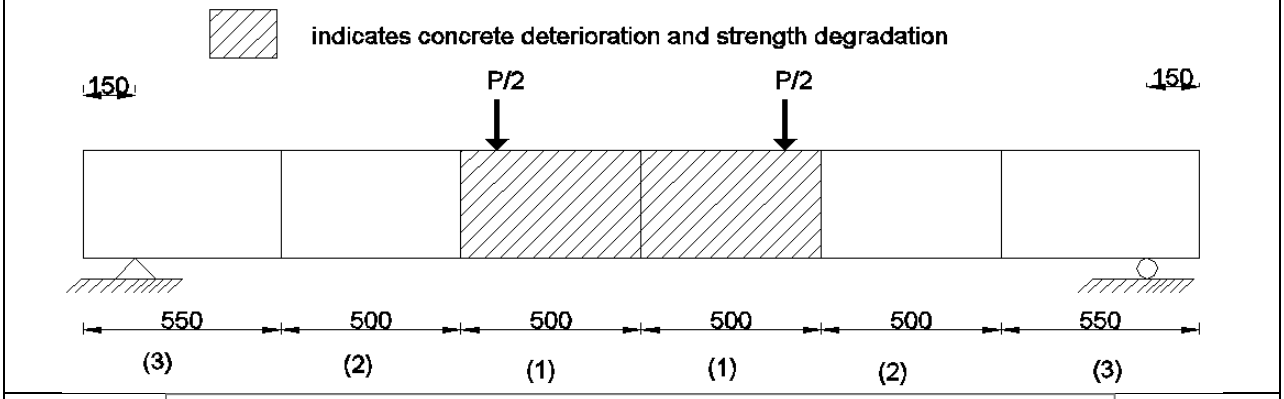

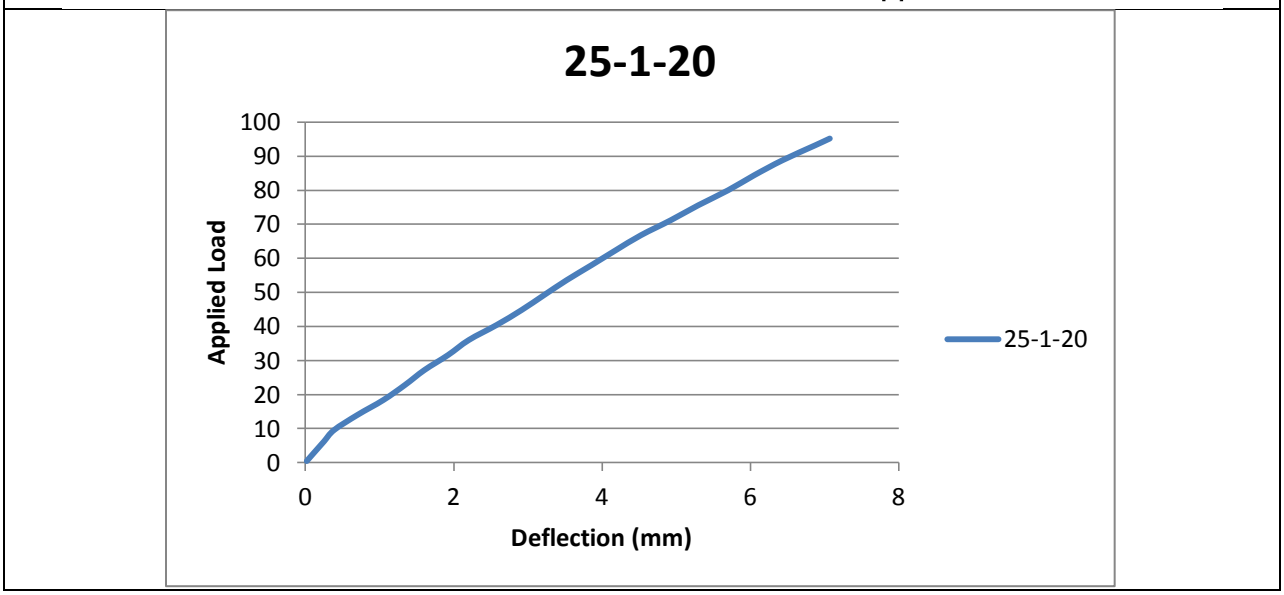

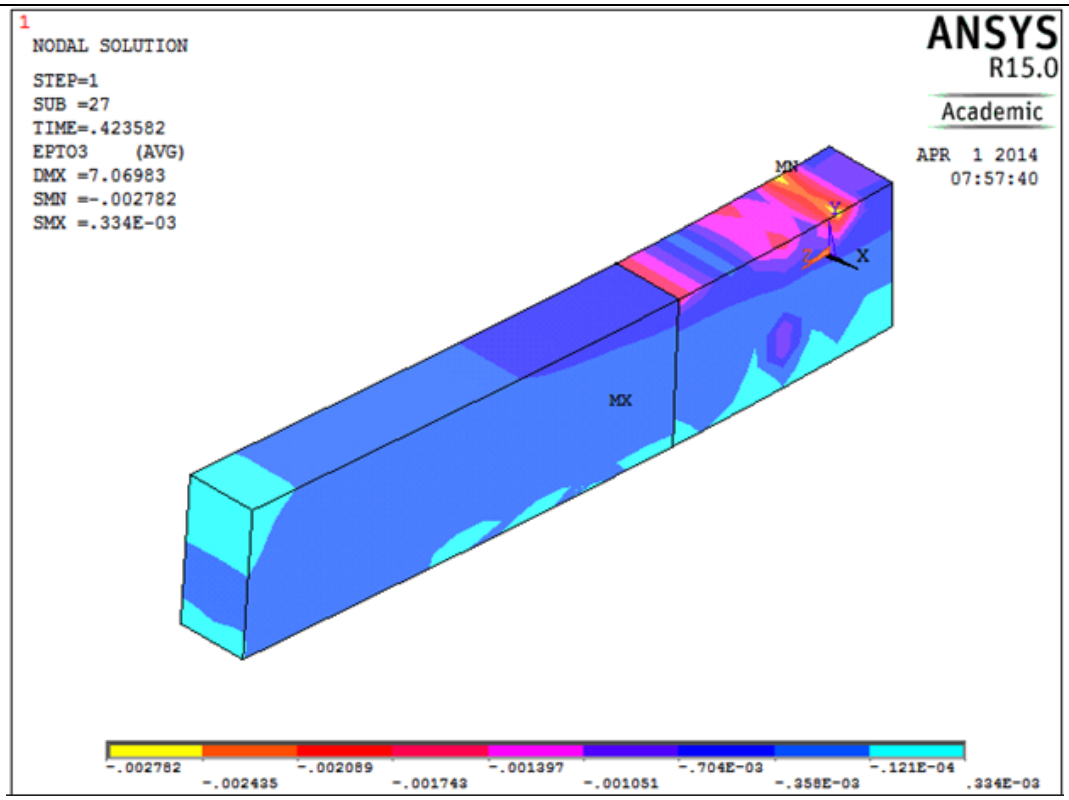

Figure D-97 Nodal solution – 3rd principal total mechanical strain for 25-1-20

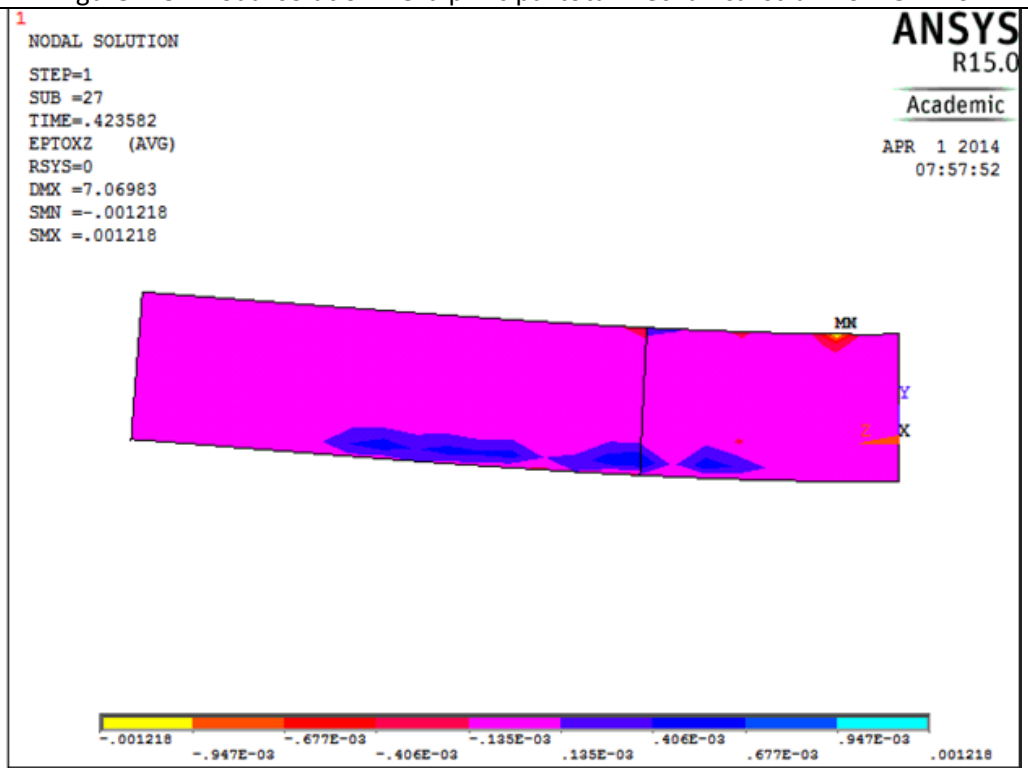

Figure D-98 Nodal Solution XZ shear total mechanical strain for 25-1-20

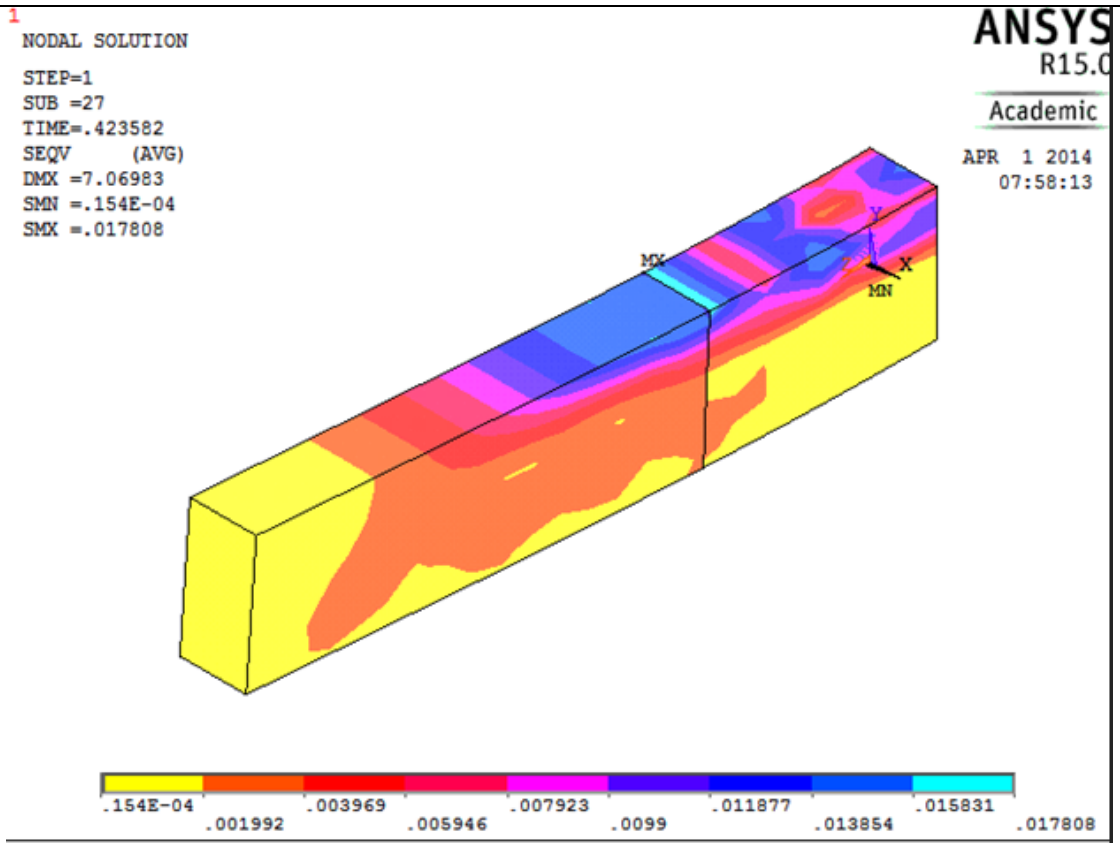

Figure D-99 Nodal Solution -Von Mises Stress for 25-1-20

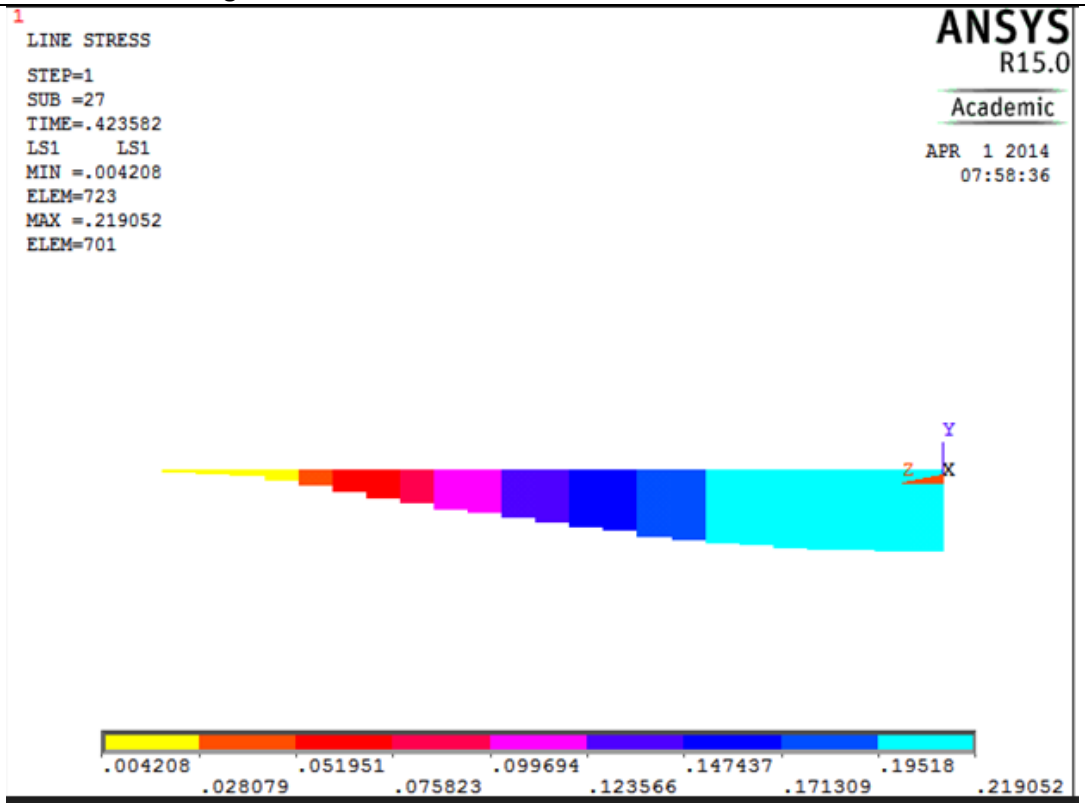

Figure D-100 Reinforcement Stress for 25-1-20

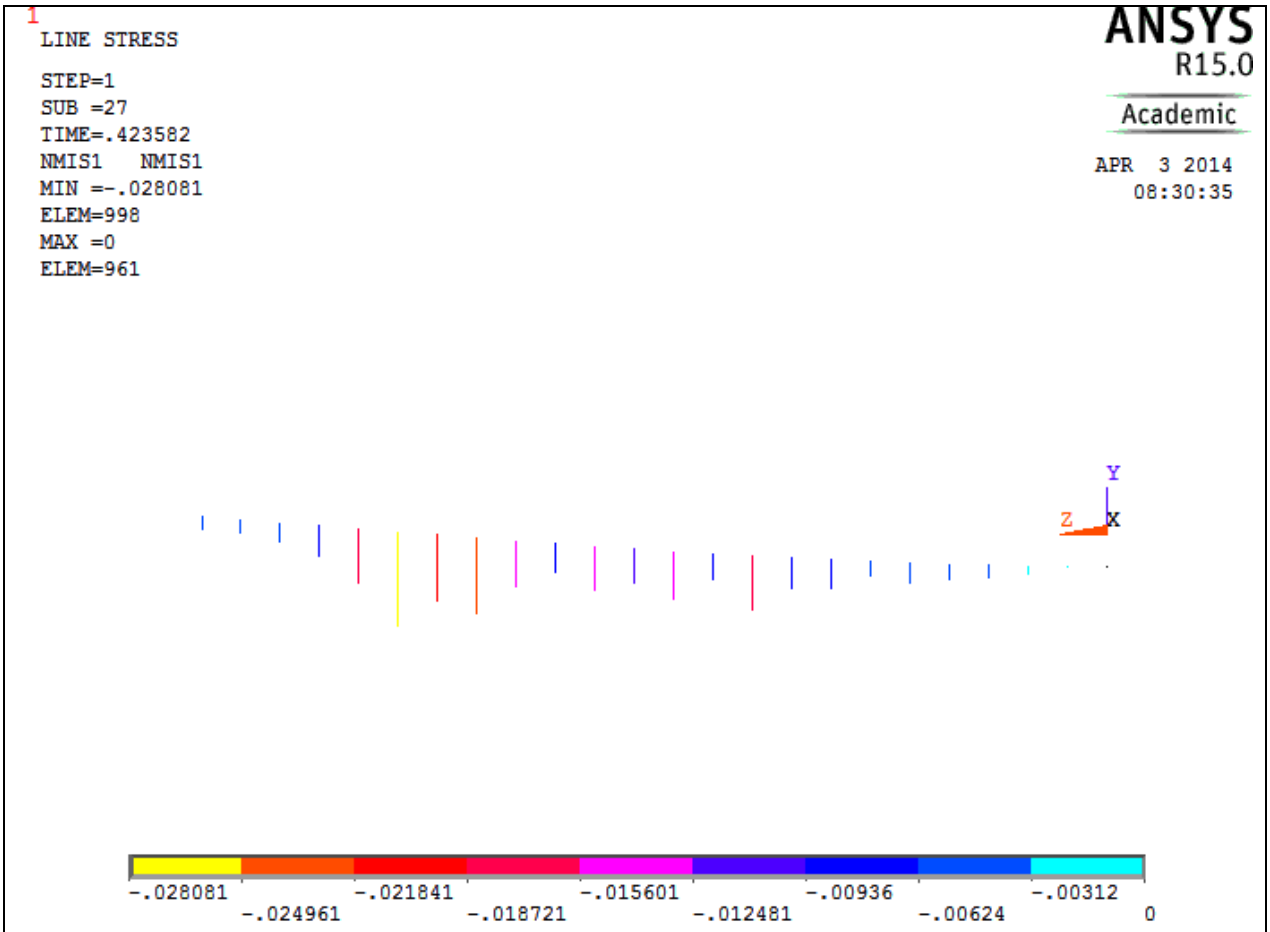

Figure D-101 Spring Stretch for 25-1-20

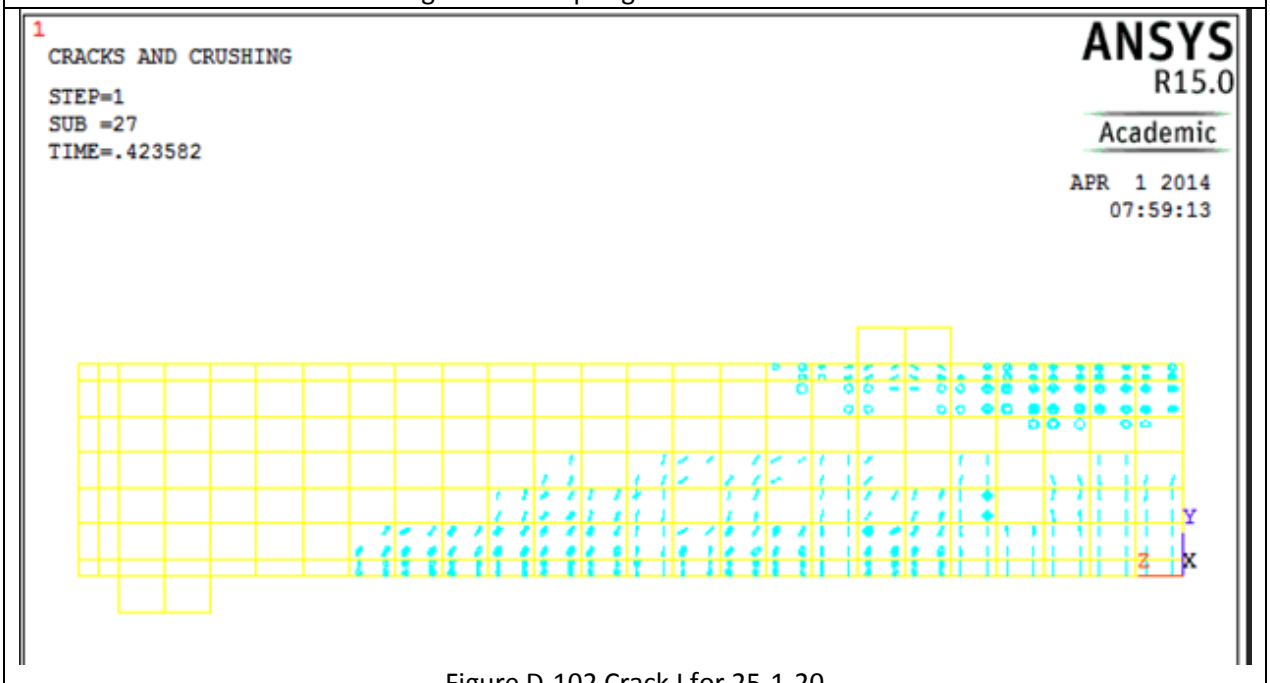

Figure D-102 Crack I for 25-1-20

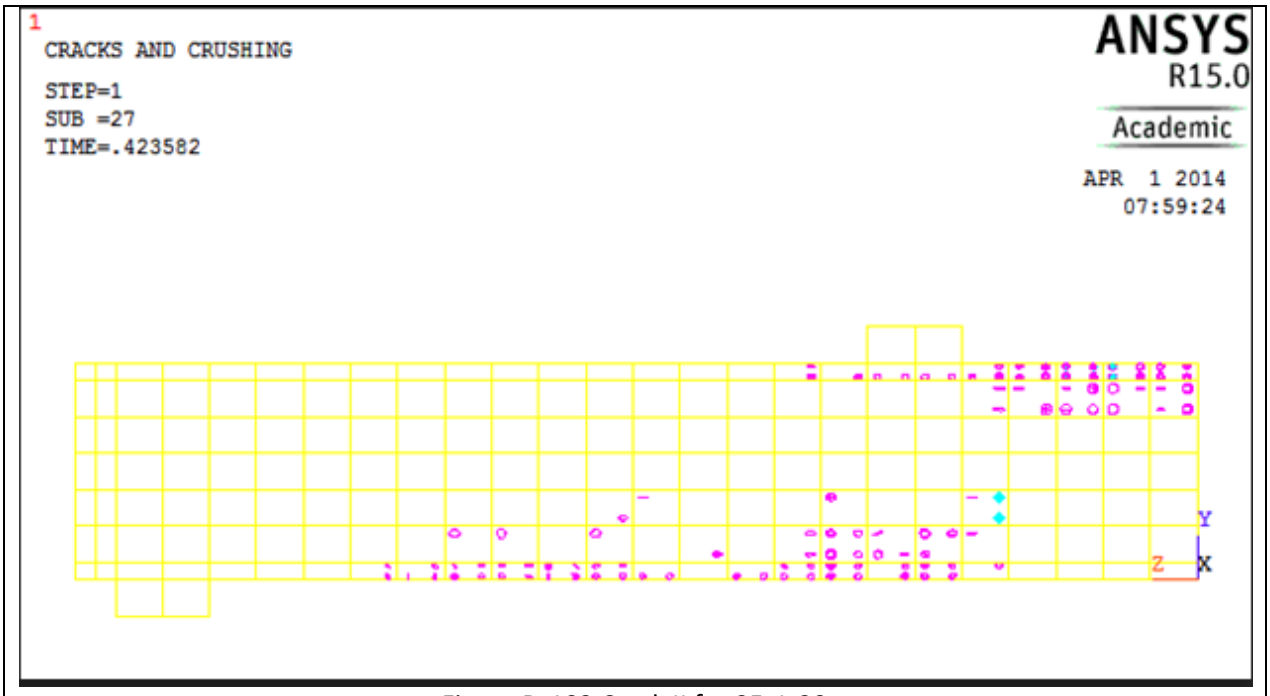

Figure D-103 Crack II for 25-1-20

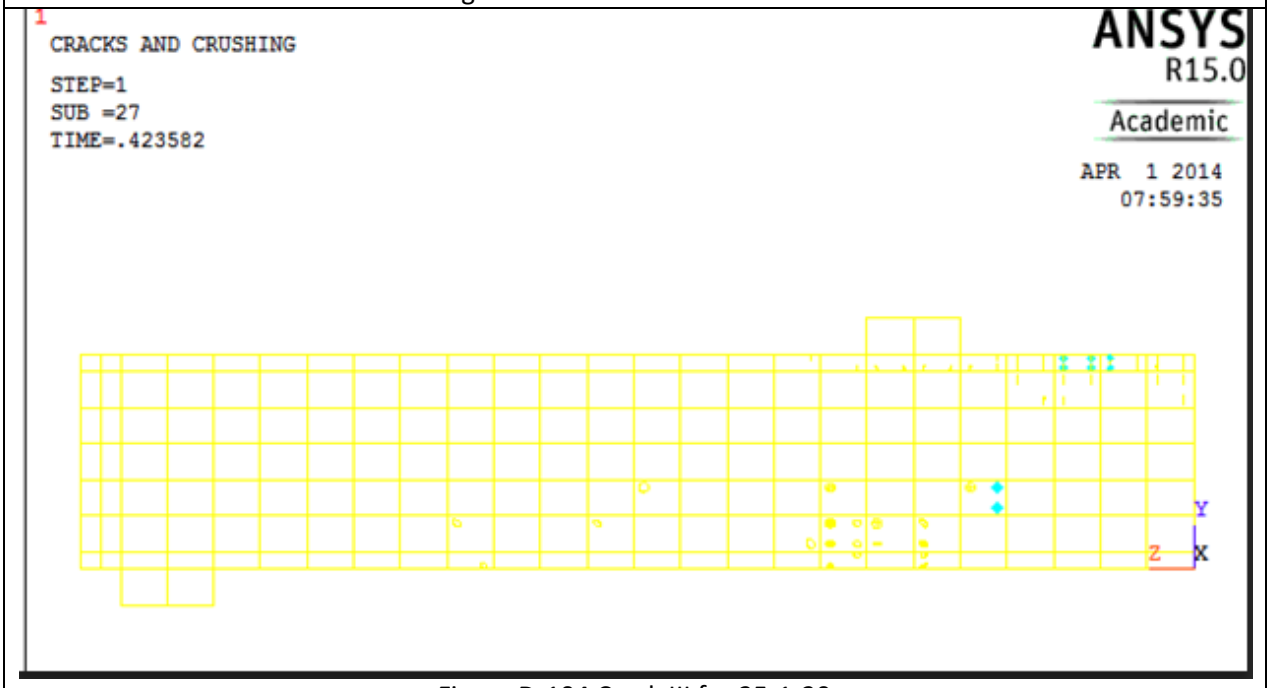

Figure D-104 Crack III for 25-1-20

Table D-14 Details of case 25-1-30

Case Name	Bottom Reinforcement	Honeycombing Location	Strength of Concrete(MPa)	Ultimate Load (kN)	Ultimate Deflection(mm)	Failure Mode
25-1-30	25mm	1	30	161.0334	12.3898	

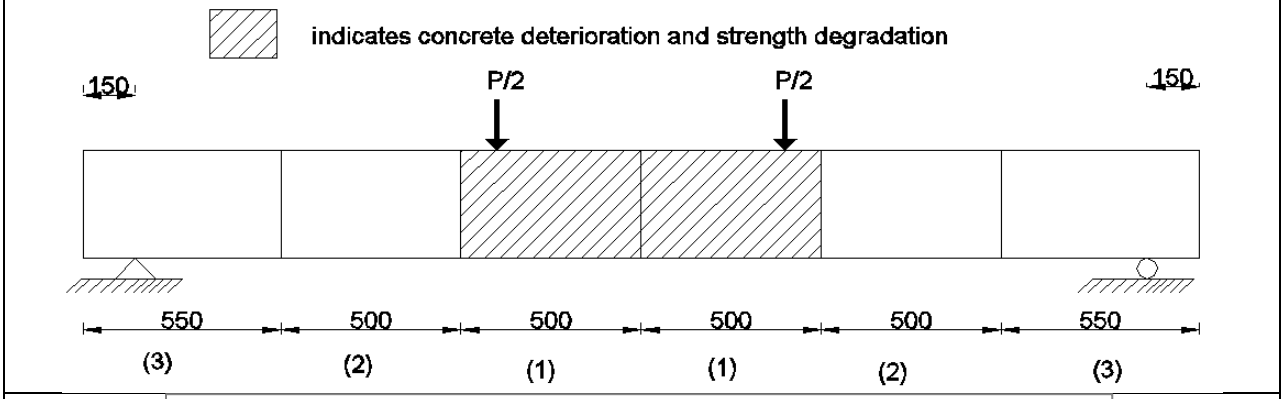

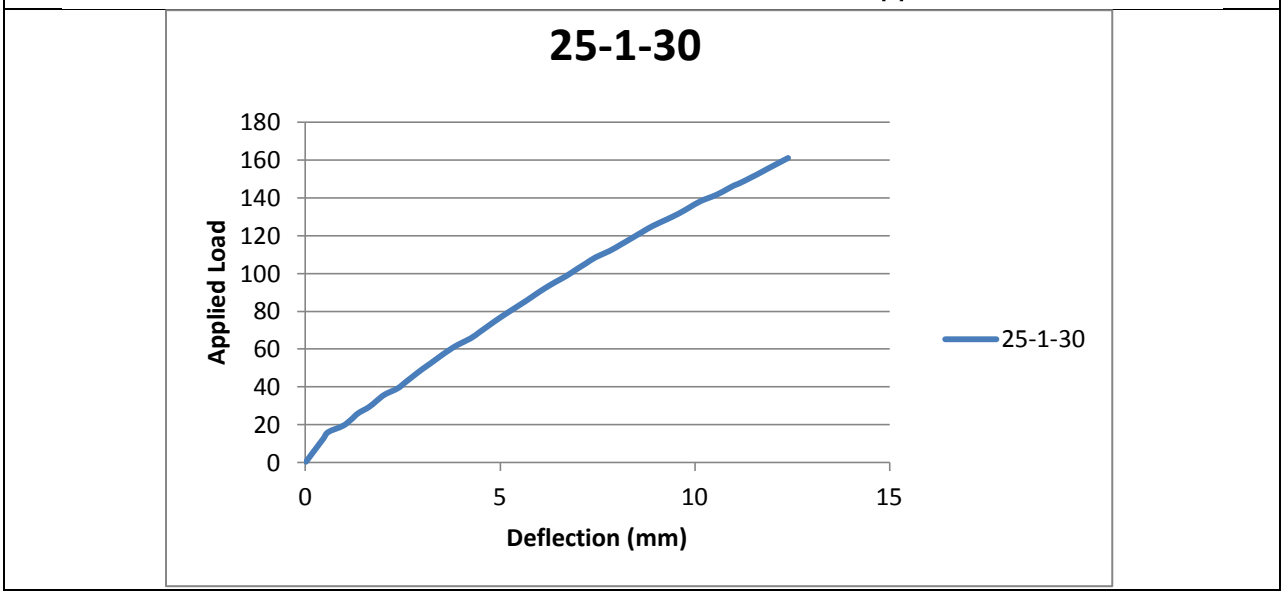

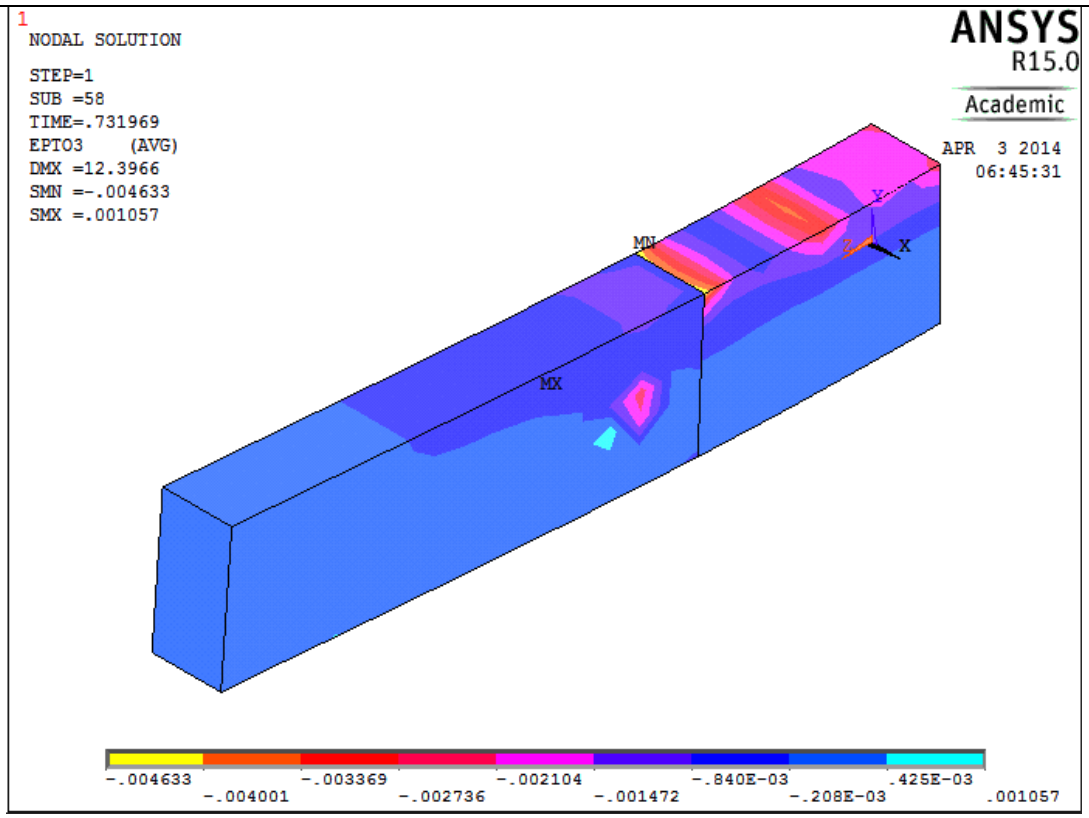

Figure D-105 Nodal solution – 3rd principal total mechanical strain

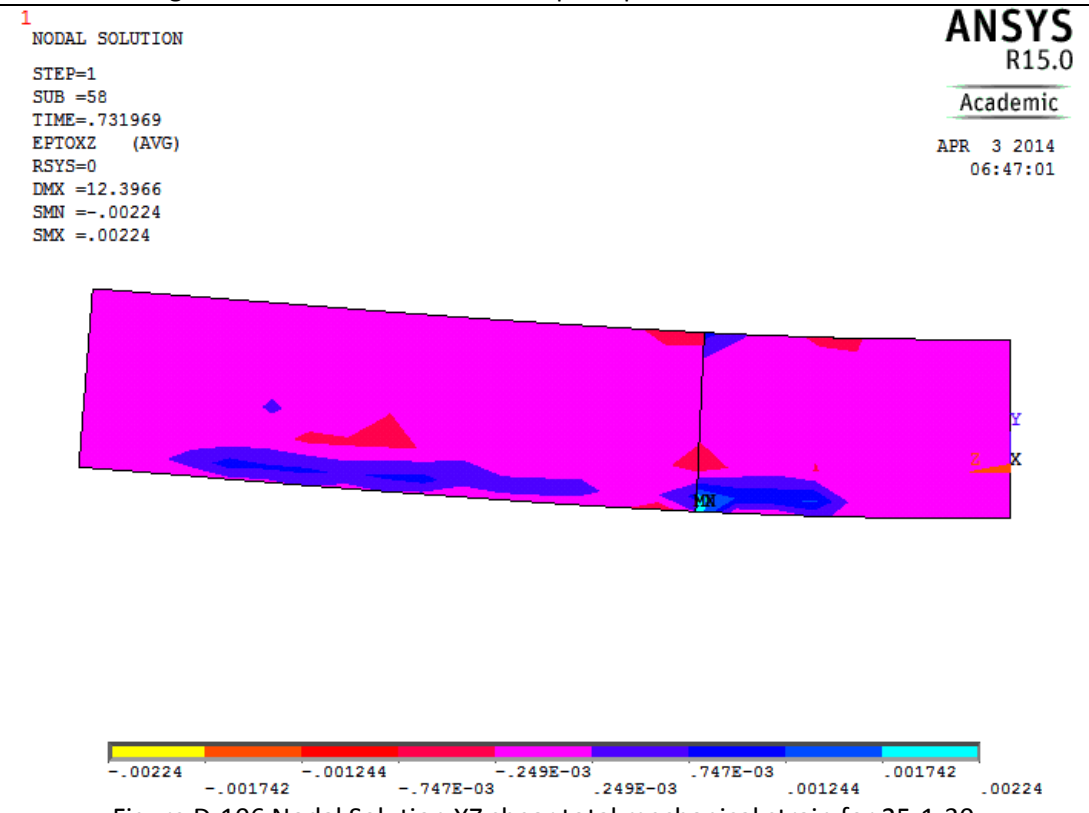

Figure D-106 Nodal Solution XZ shear total mechanical strain for 25-1-30

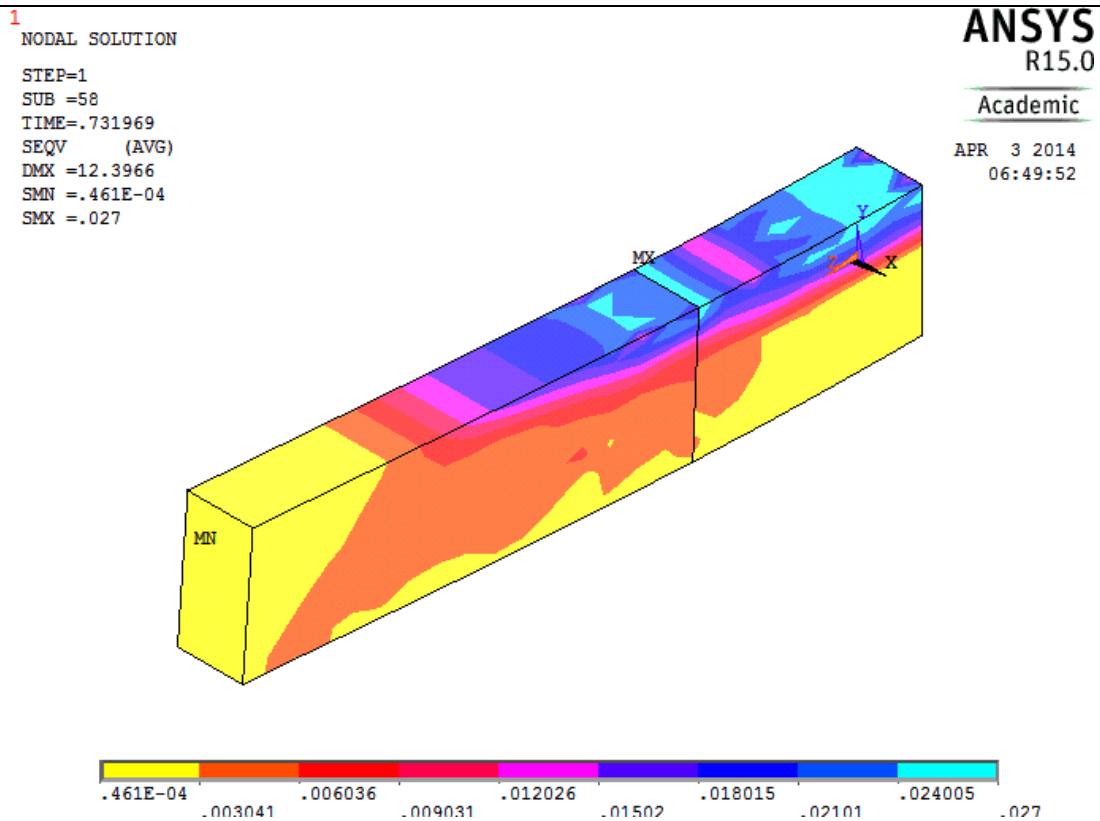

Figure D-107 Nodal Solution -Von Mises Stress for 25-1-30

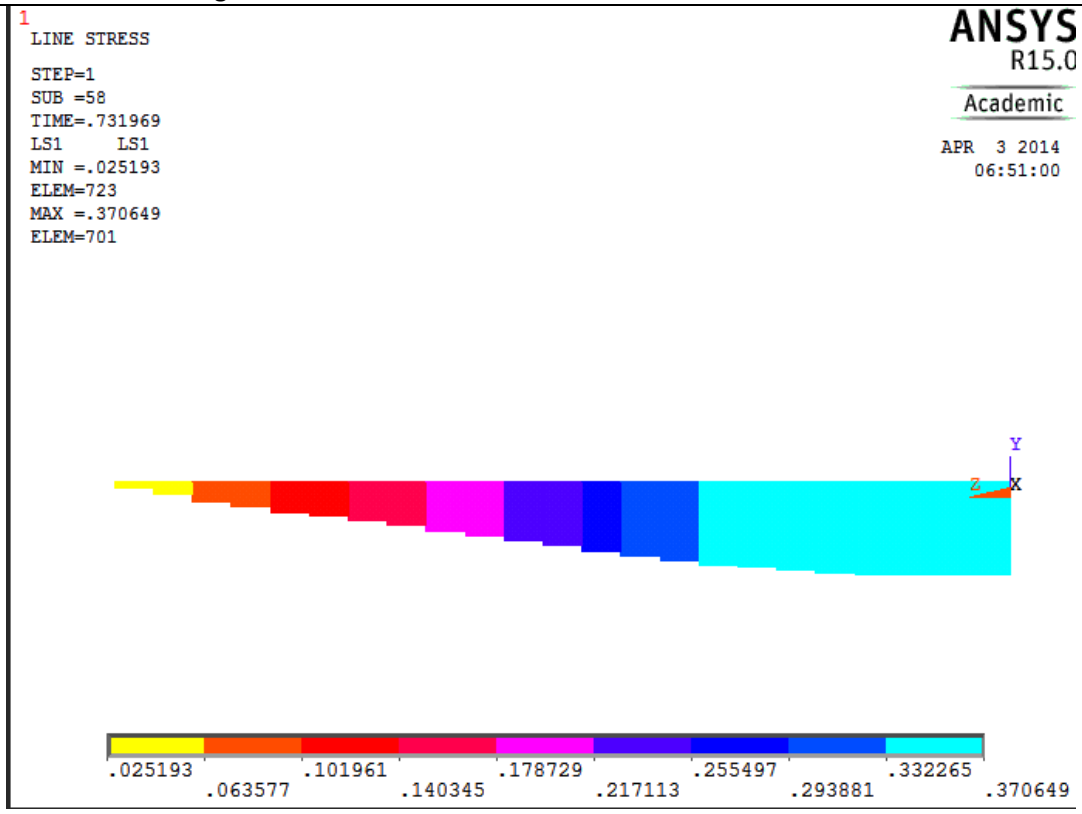

Figure D-108 Reinforcement Stress for 25-1-30

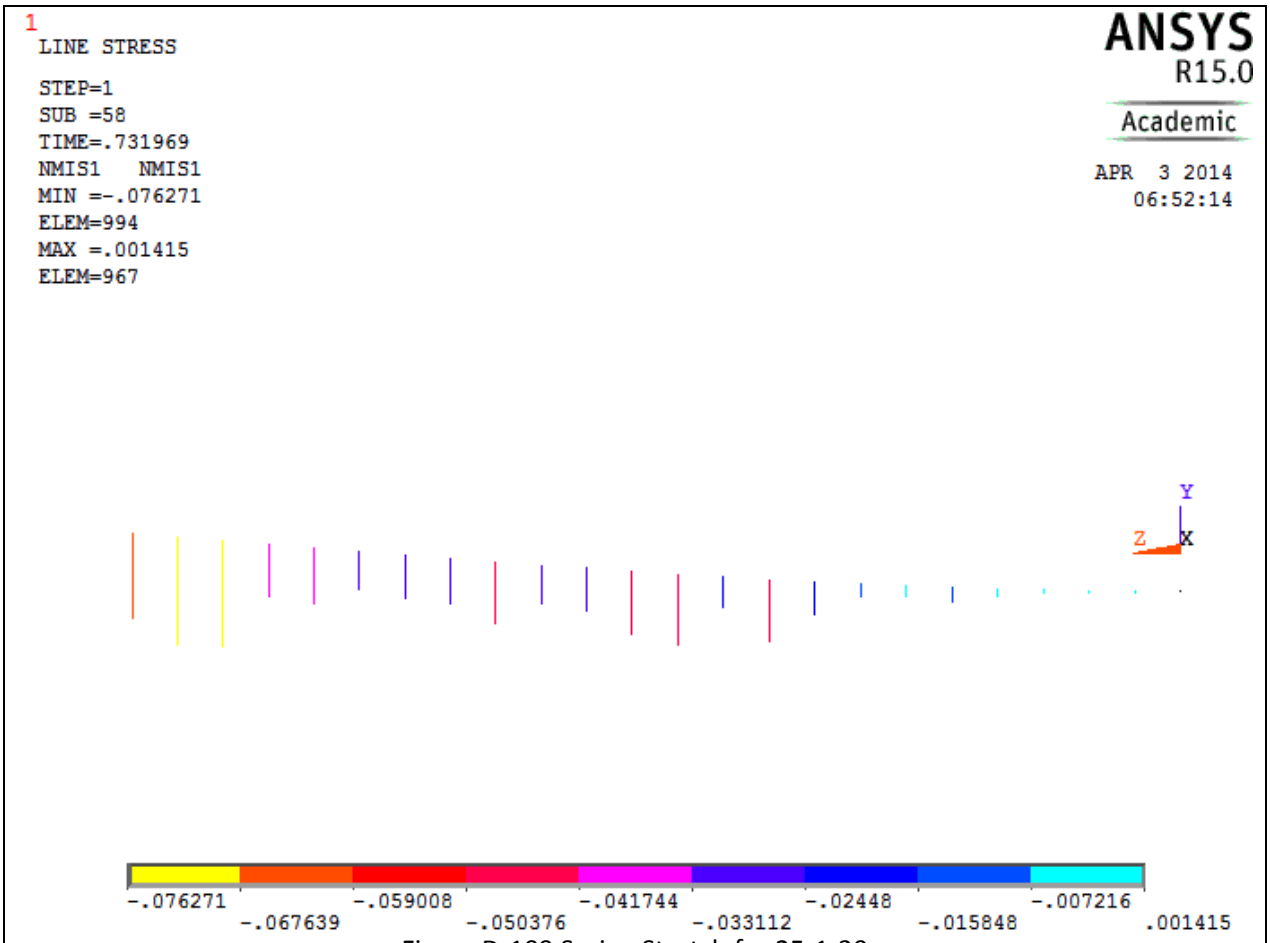

Figure D-109 Spring Stretch for 25-1-30

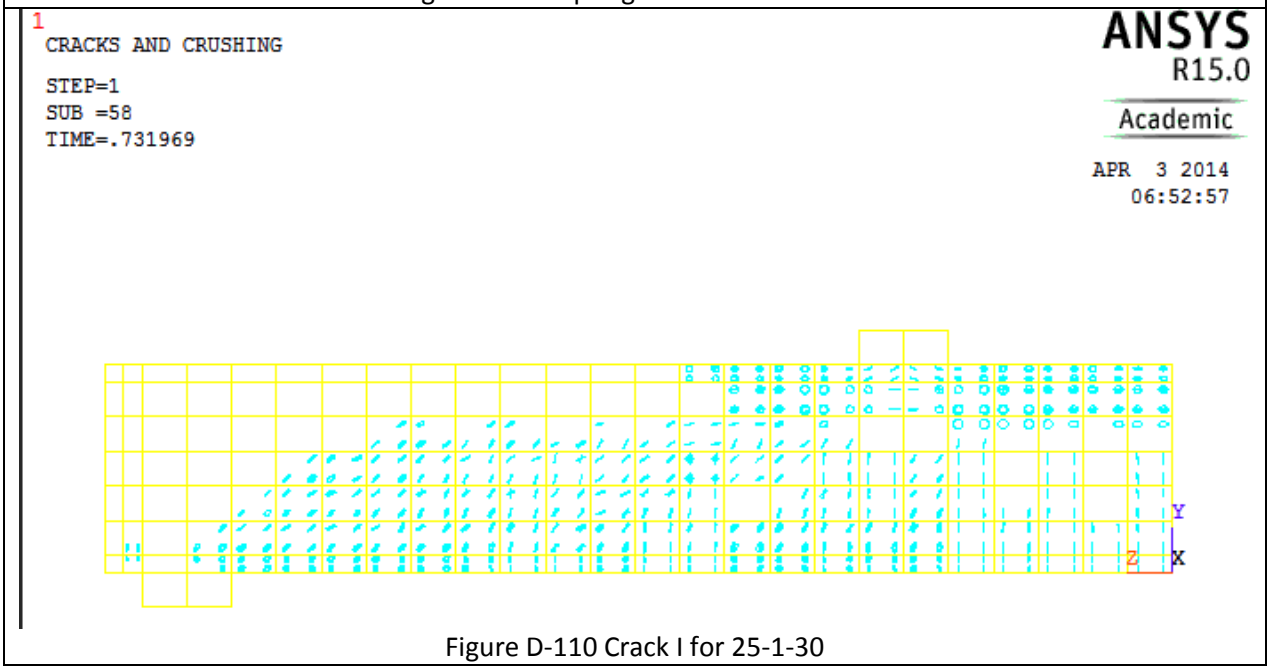

Figure D-110 Crack I for 25-1-30

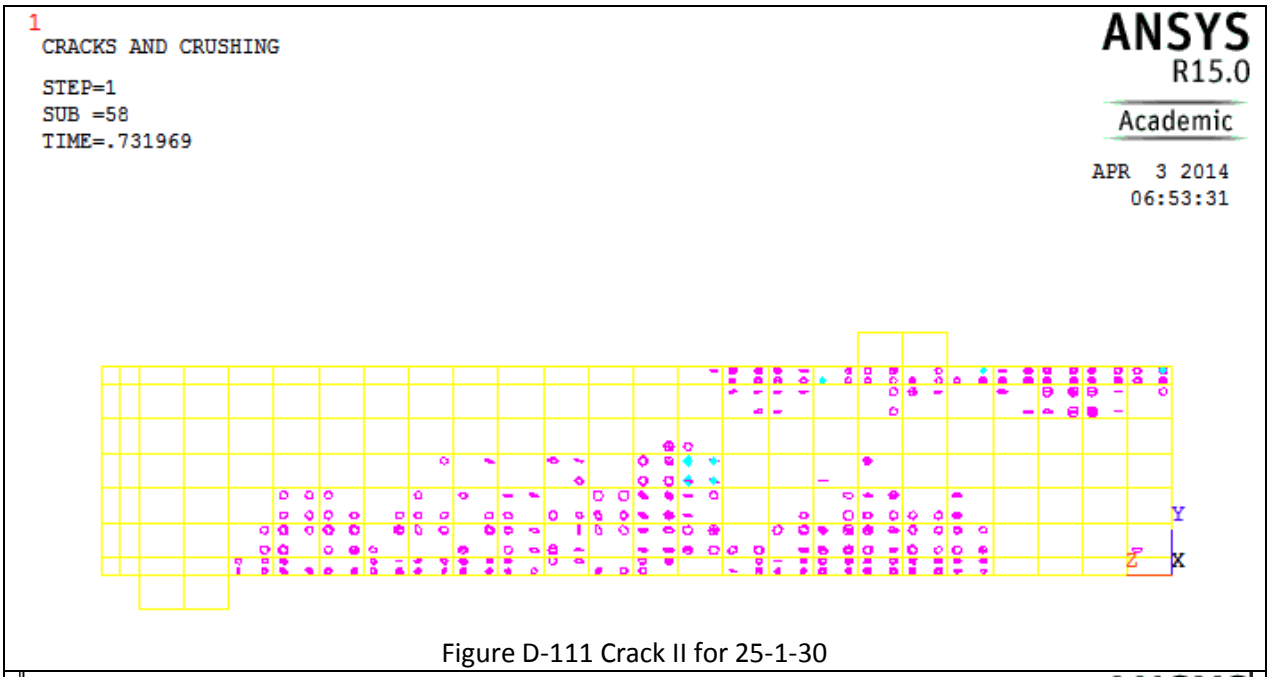

Figure D-111 Crack II for 25-1-30

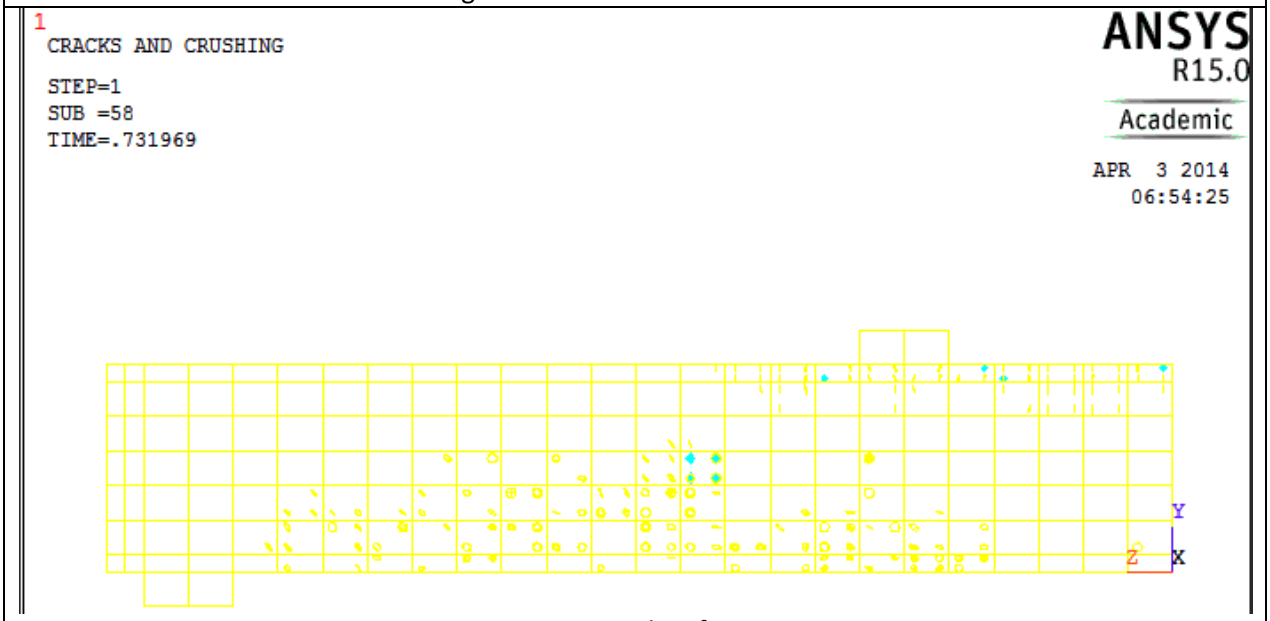

Figure D-112 Crack III for 25-1-30

Table D-15 Details of case 25-2-10

Case Name	Bottom Reinforcement	Honeycombing Location	Strength of Concrete(MPa)	Ultimate Load (kN)	Ultimate Deflection(mm)	Failure Mode
25-2-10	25mm	2	10	67.925	5.30364	

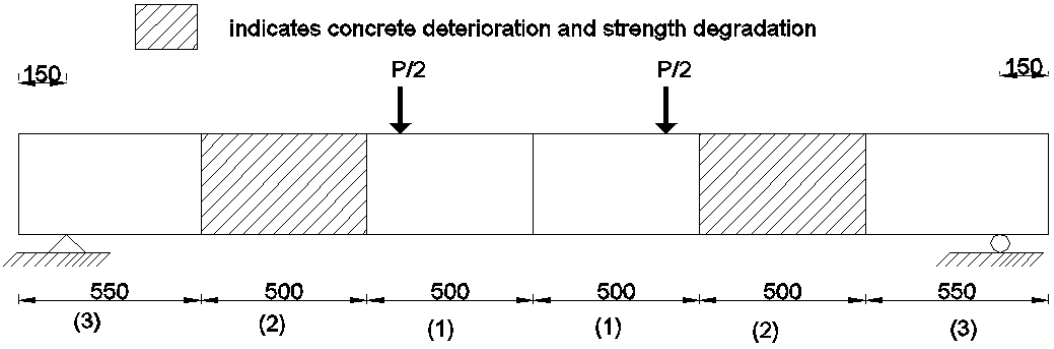

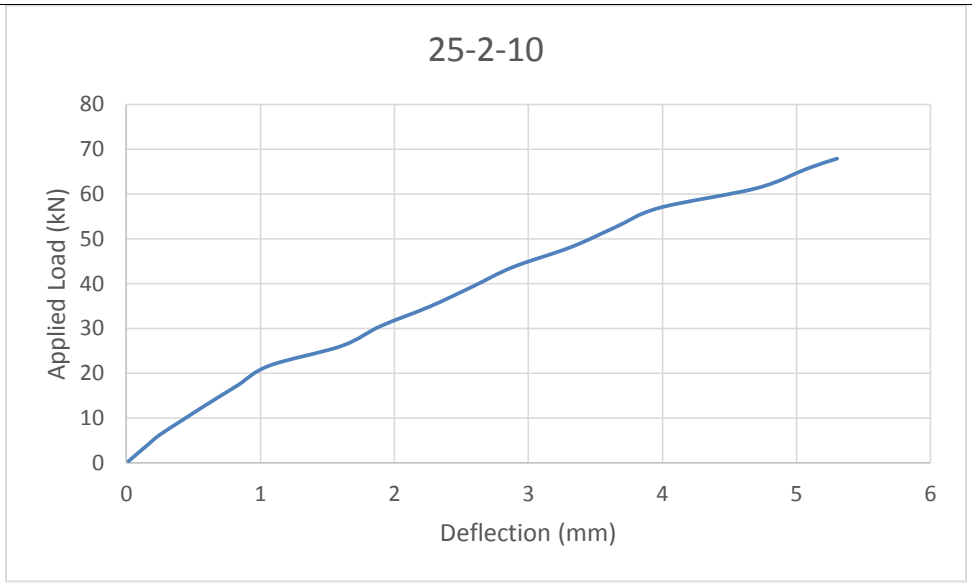

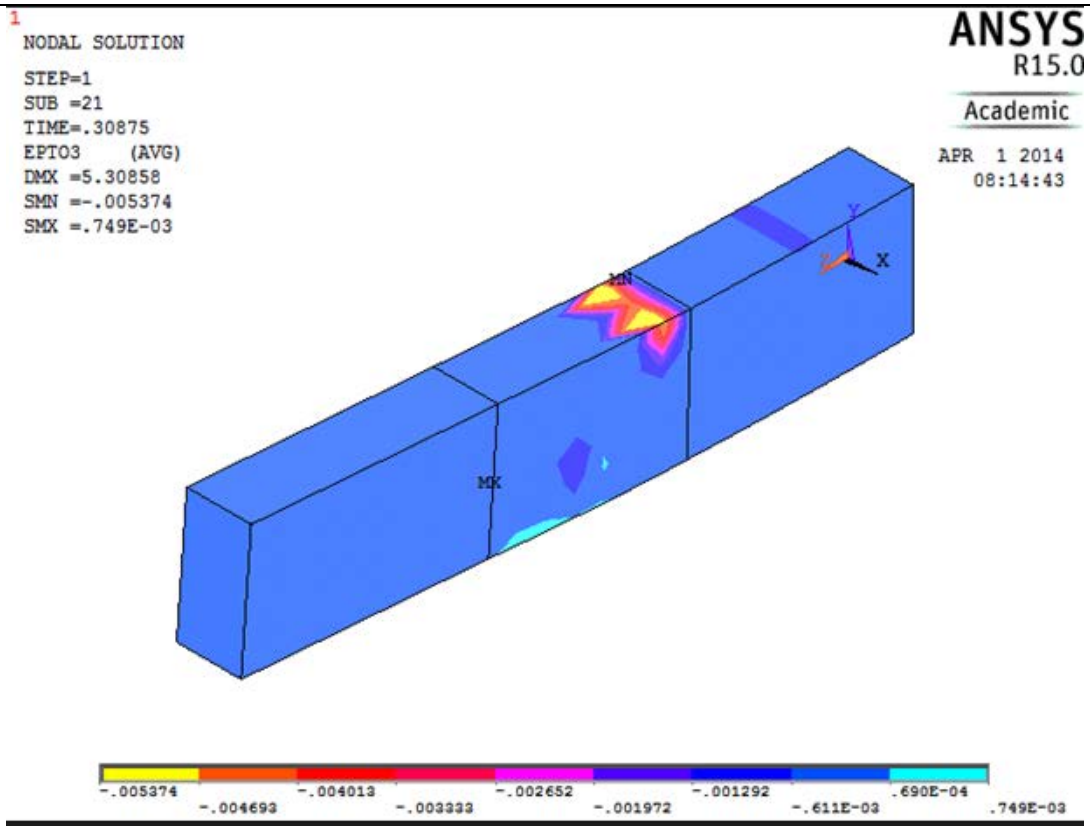

Figure D-113 Nodal solution – 3rd principal total mechanical strain for 25-2-10

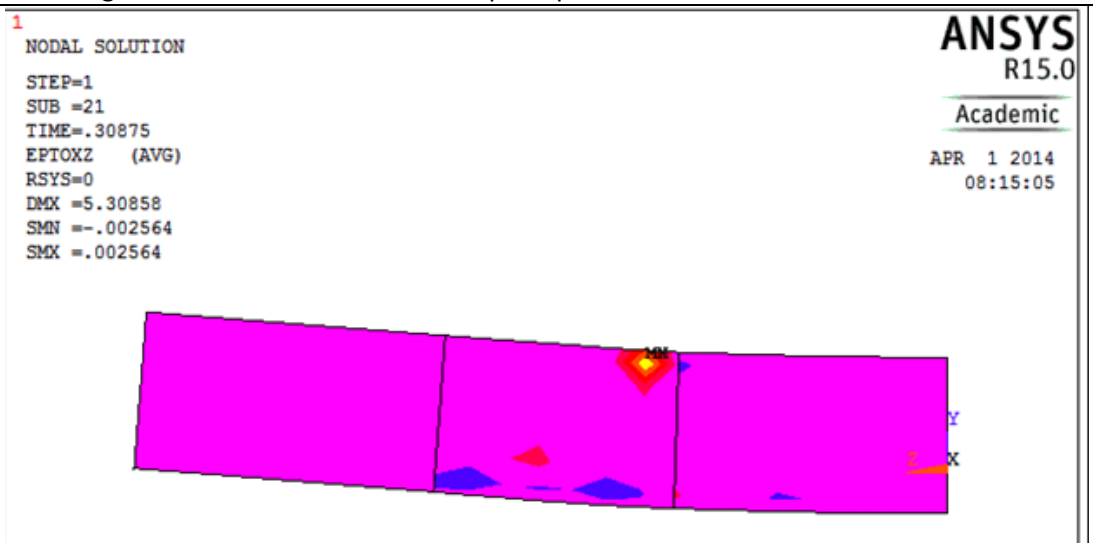

Figure D-114 Nodal Solution XZ shear total mechanical strain for 25-2-10

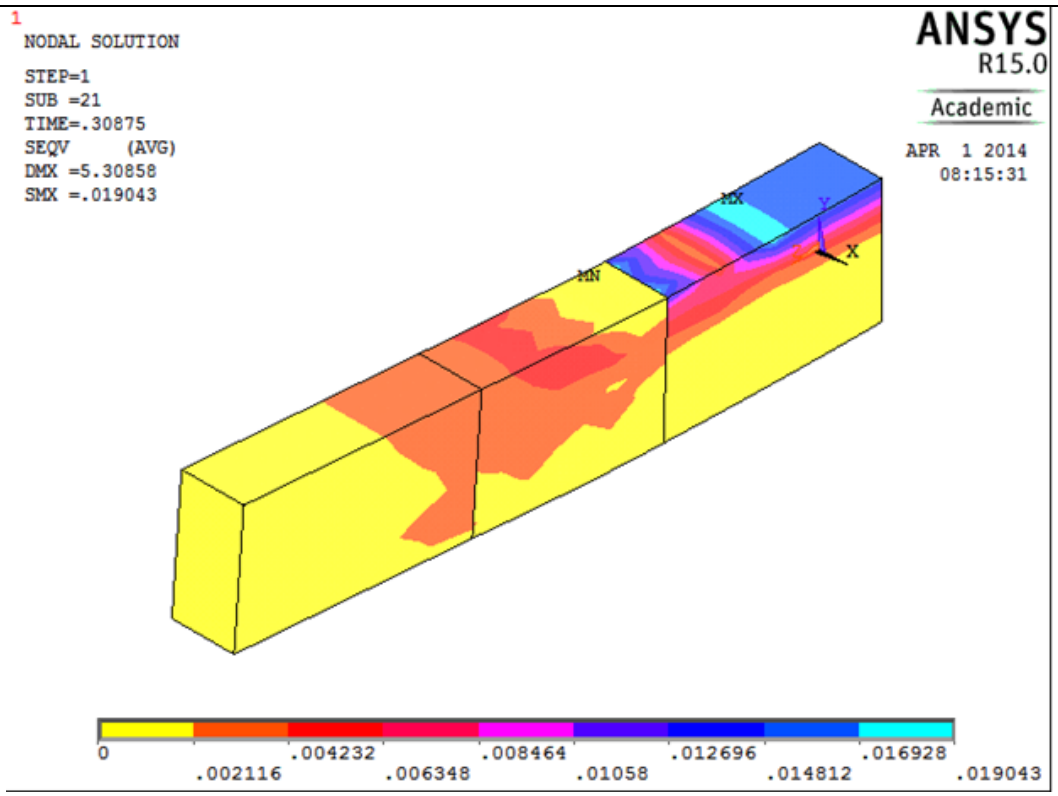

Figure D-115 Nodal Solution -Von Mises Stress for 25-2-10

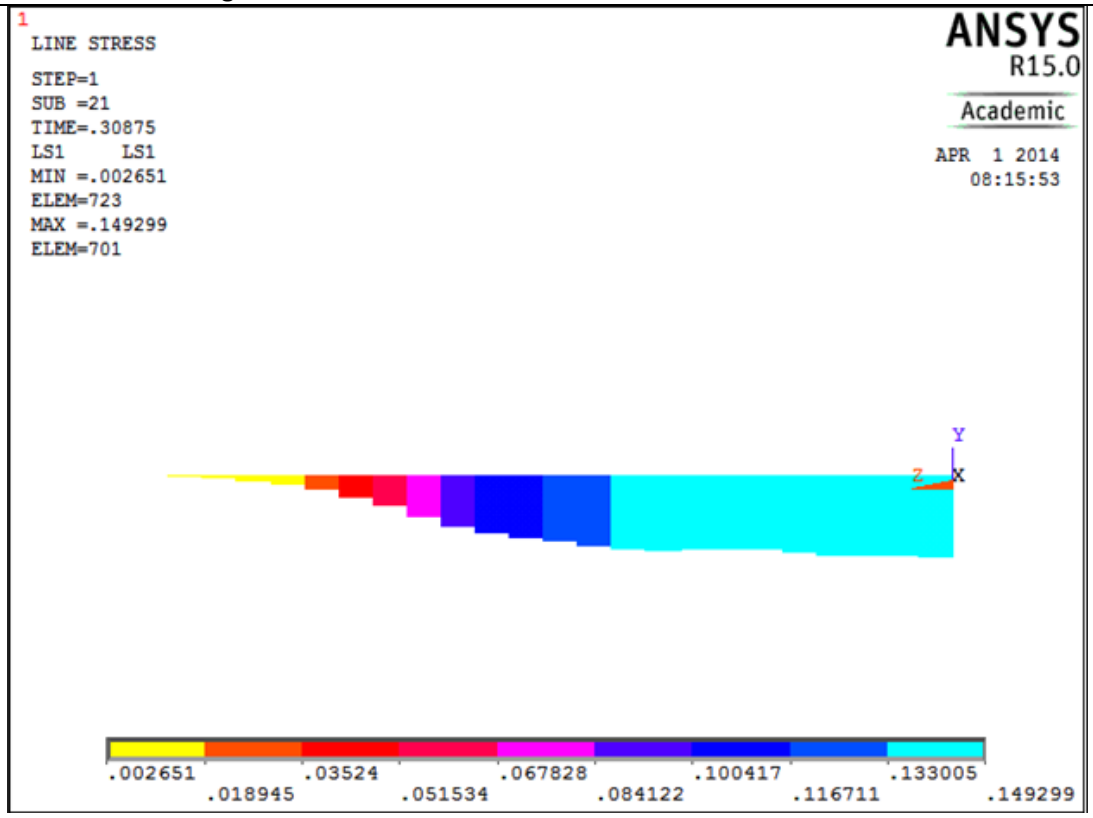

Figure D-116 Reinforcement Stress for 25-2-10

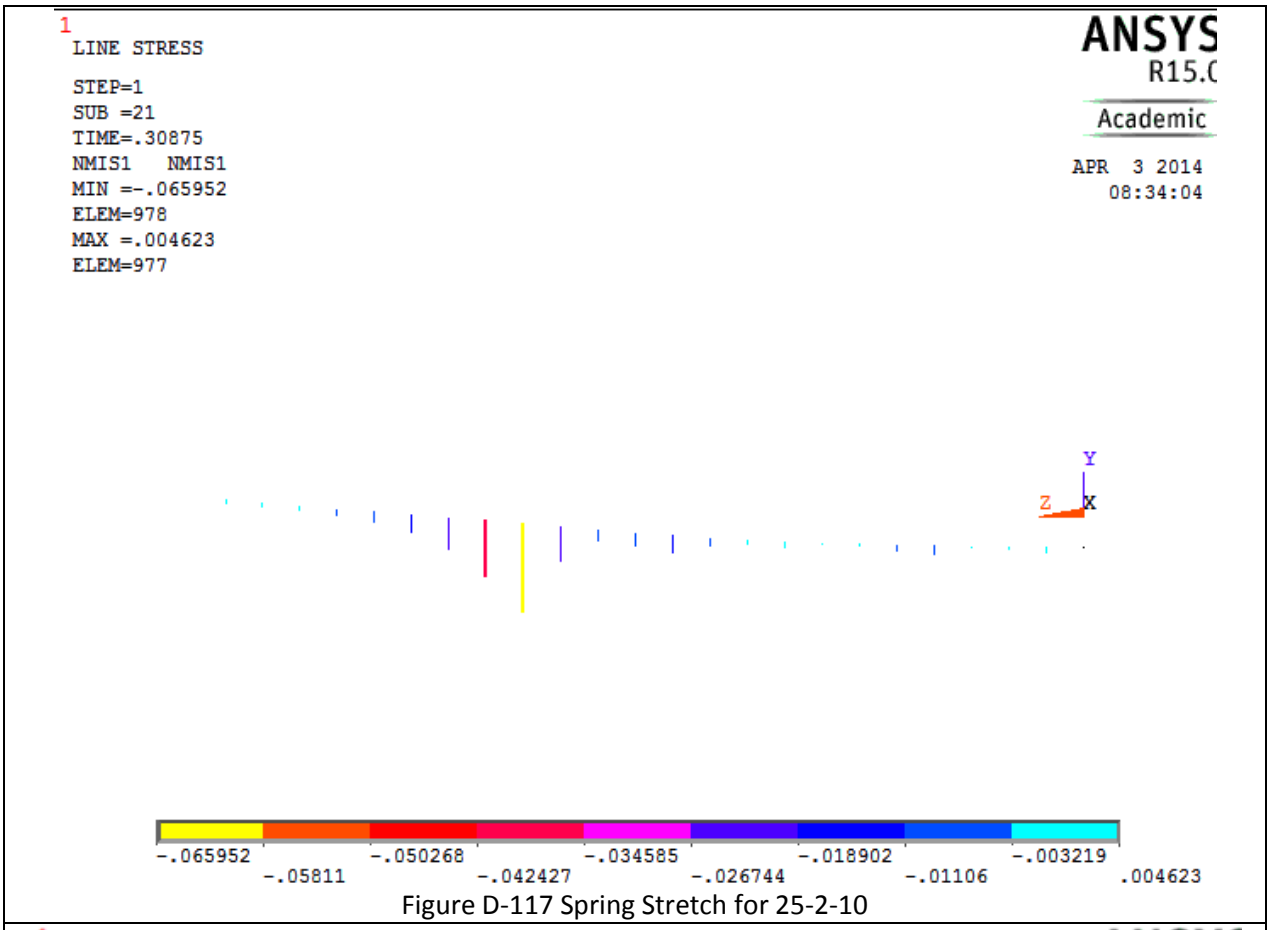

Figure D-117 Spring Stretch for 25-2-10

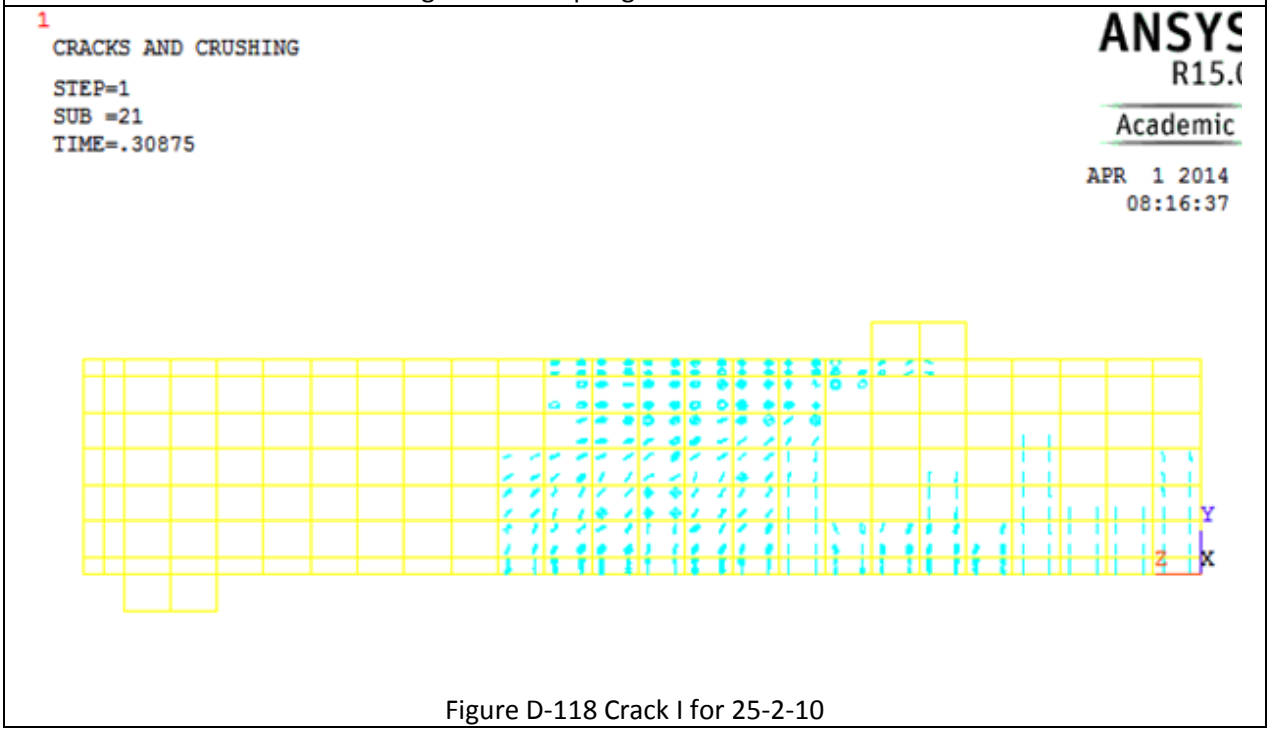

Figure D-118 Crack I for 25-2-10

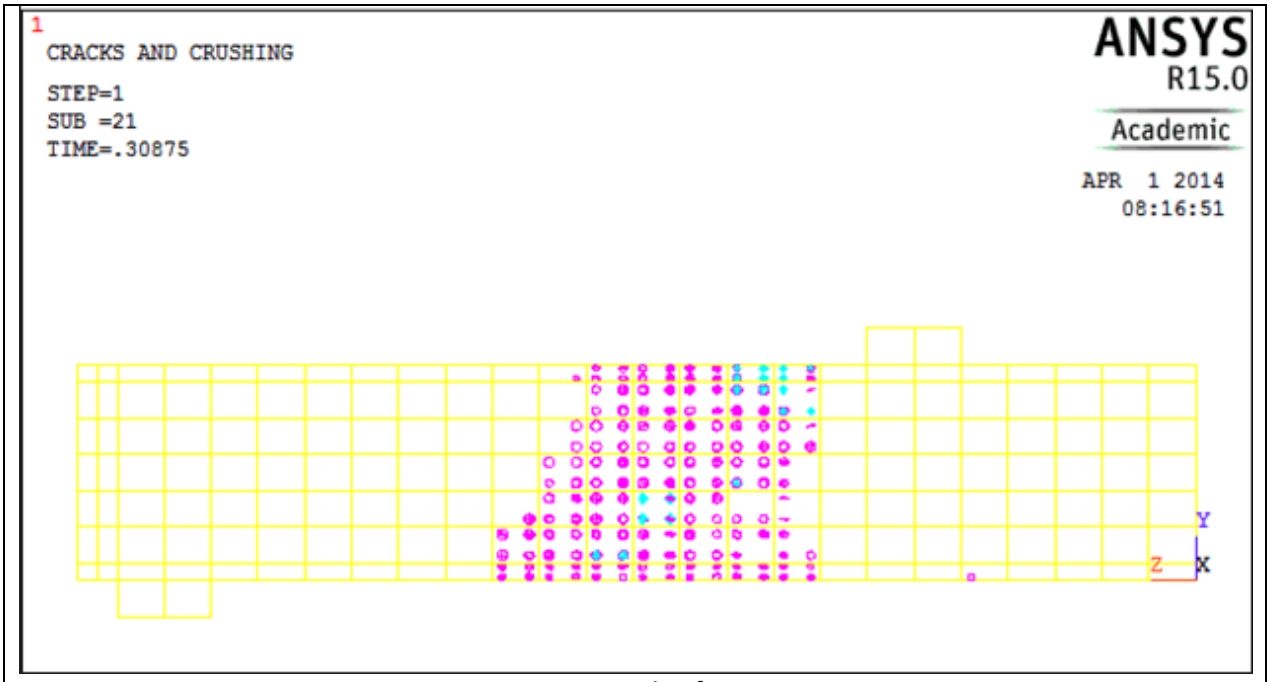

Figure D-119 Crack II for 25-2-10

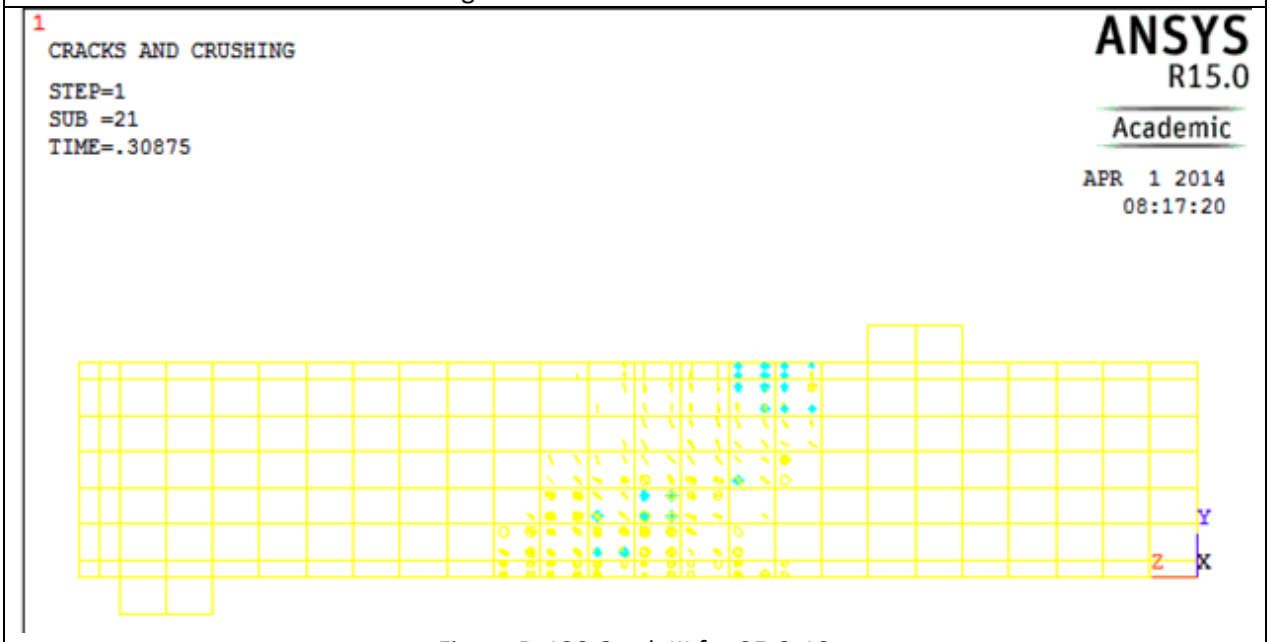

Figure D-120 Crack III for 25-2-10

Table D-16 Details of case 25-2-20

Case Name	Bottom Reinforcement	Honeycombing Location	Strength of Concrete(MPa)	Ultimate Load (kN)	Ultimate Deflection(mm)	Failure Mode
25-2-20	25mm	2	20	115.1458	8.22183	

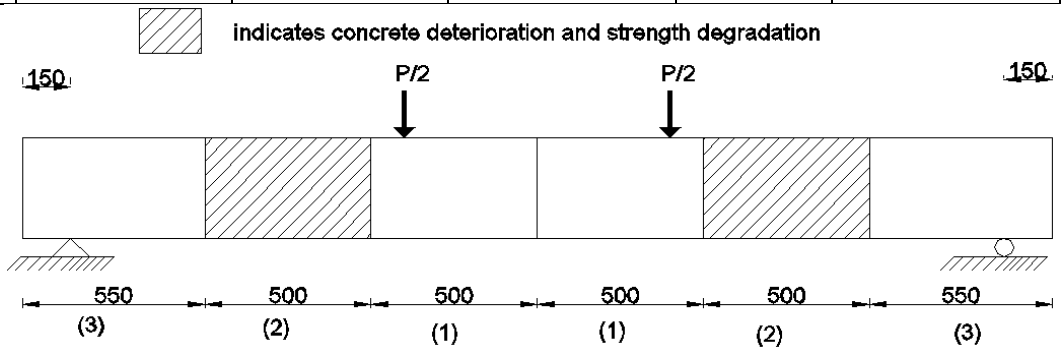

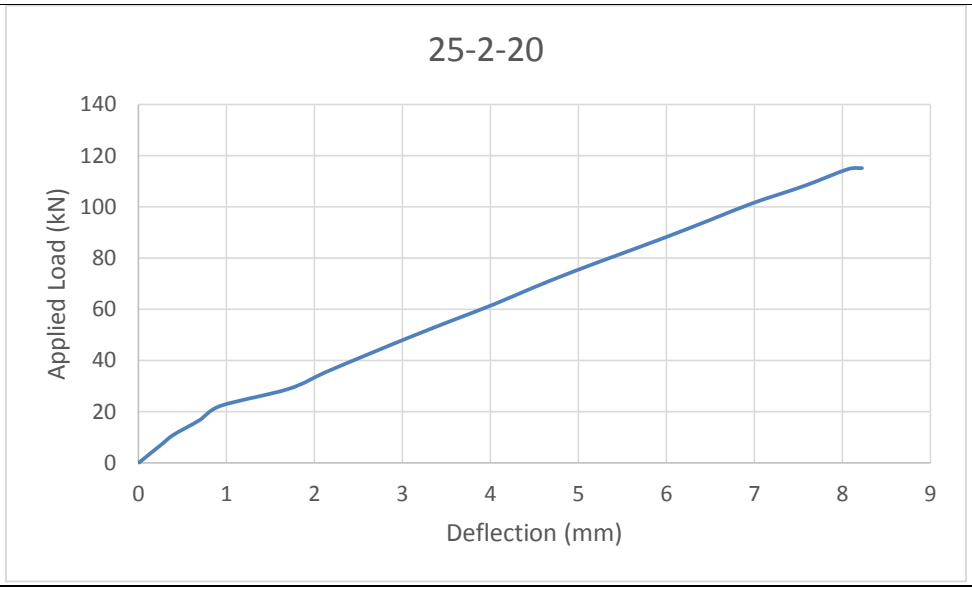

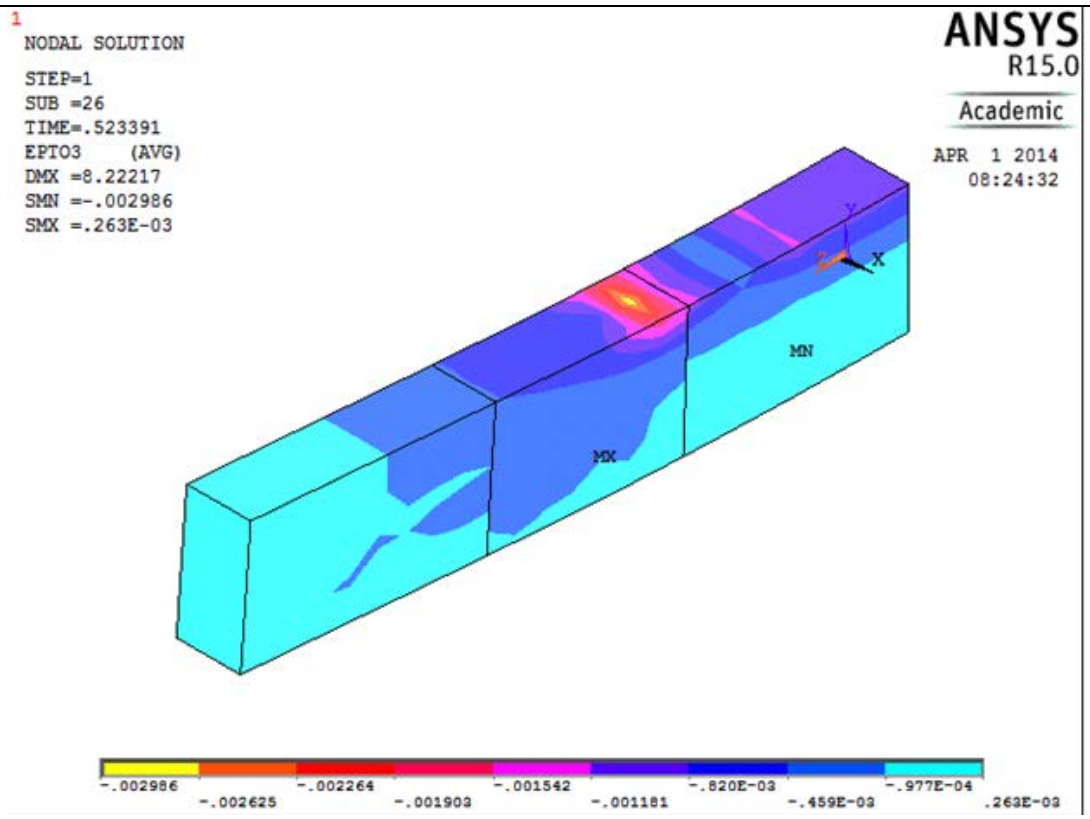

Figure D-121 Nodal solution – 3rd principal total mechanical strain for 25-2-20

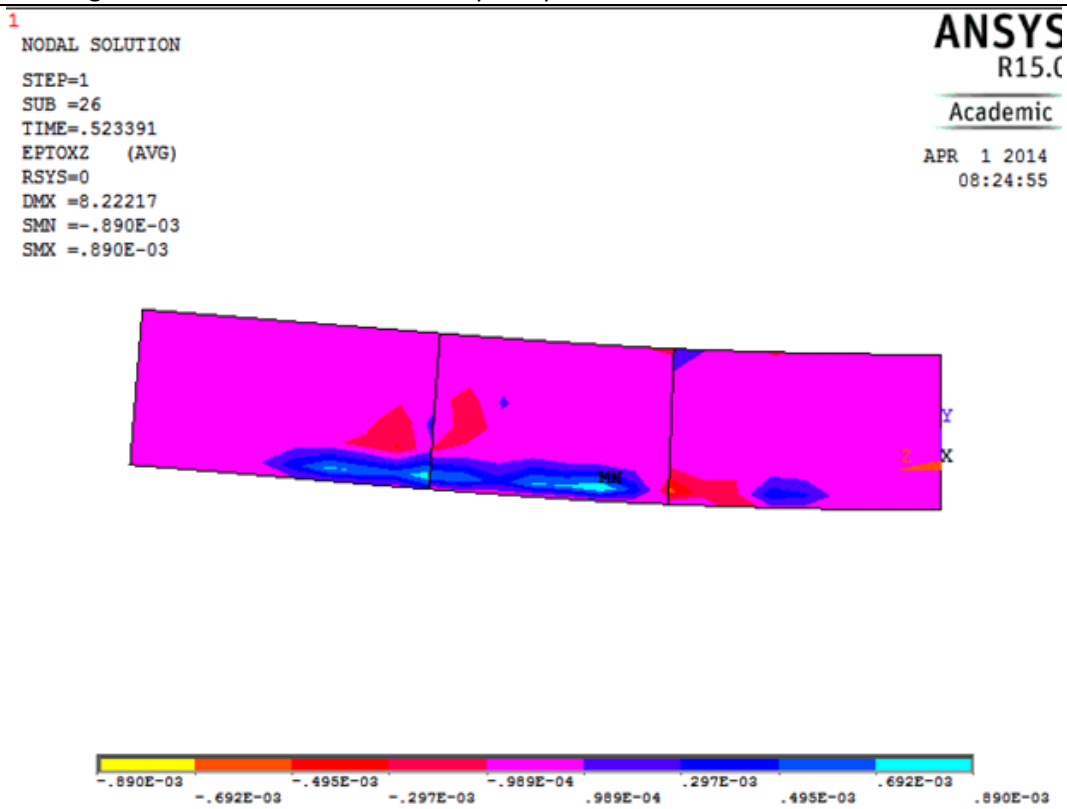

Figure D-122 Nodal Solution XZ shear total mechanical strain for 25-2-20

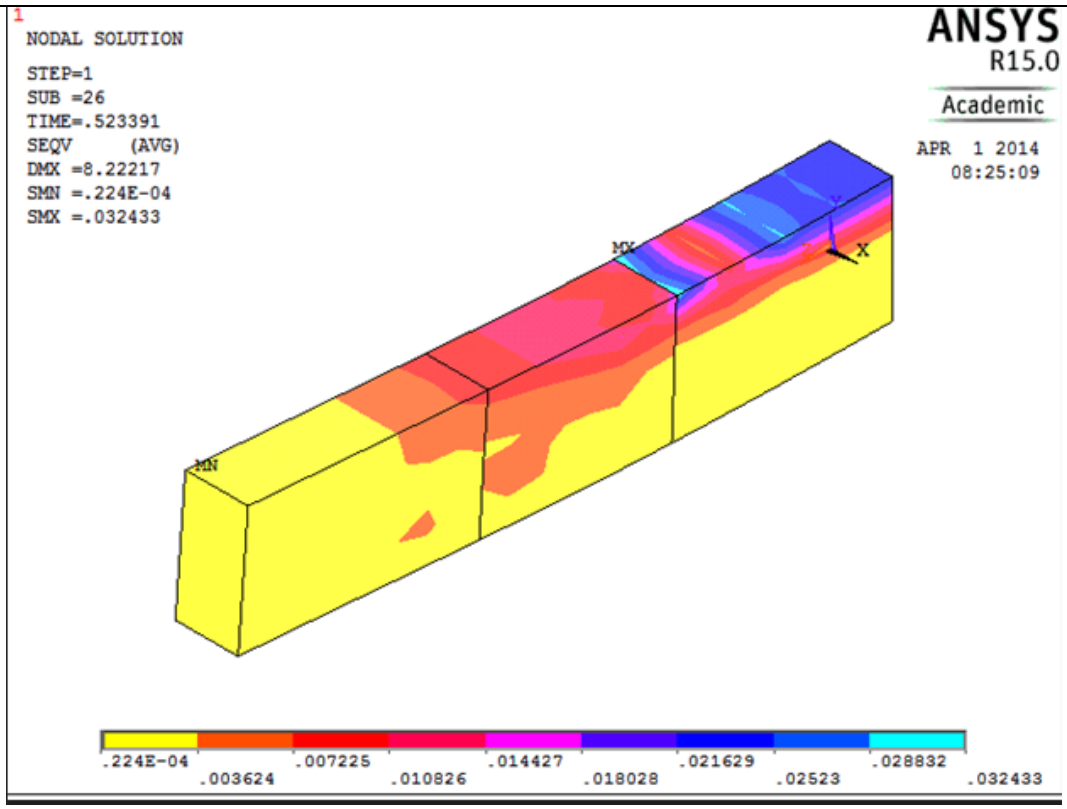

Figure D-123 Nodal Solution -Von Mises Stress for 25-2-20

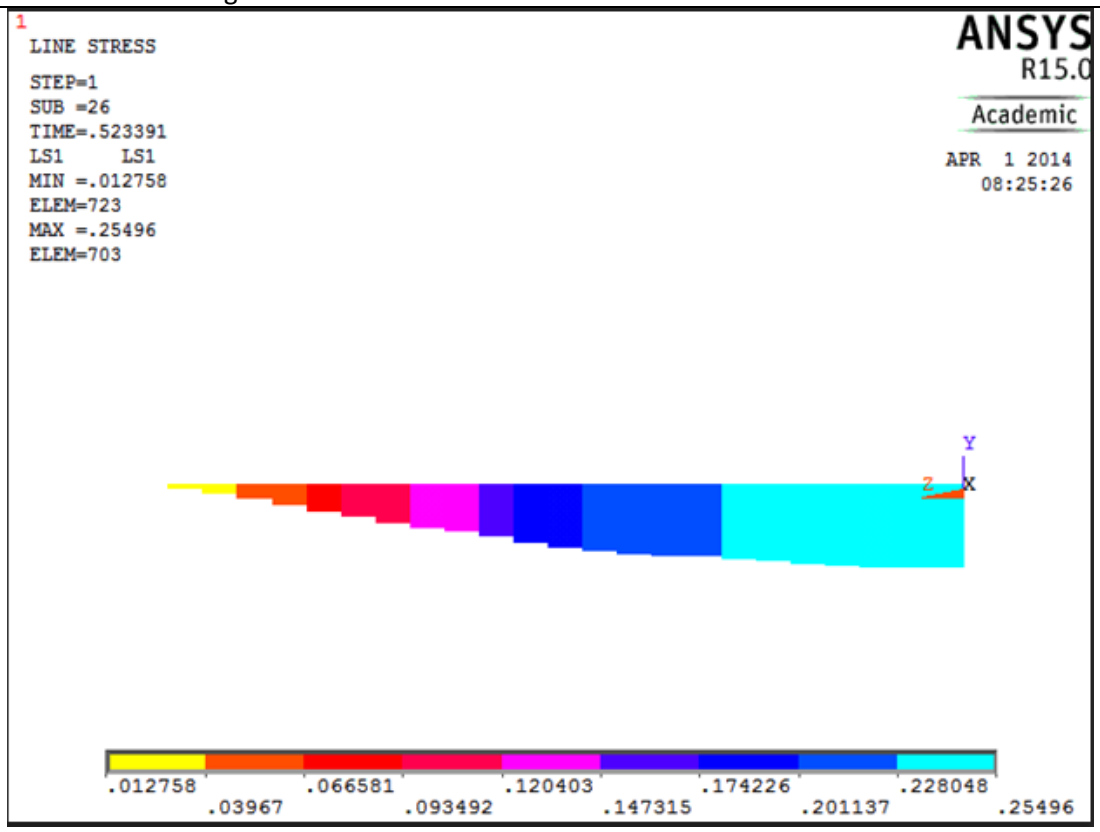

Figure D-124 Reinforcement Stress for 25-2-20

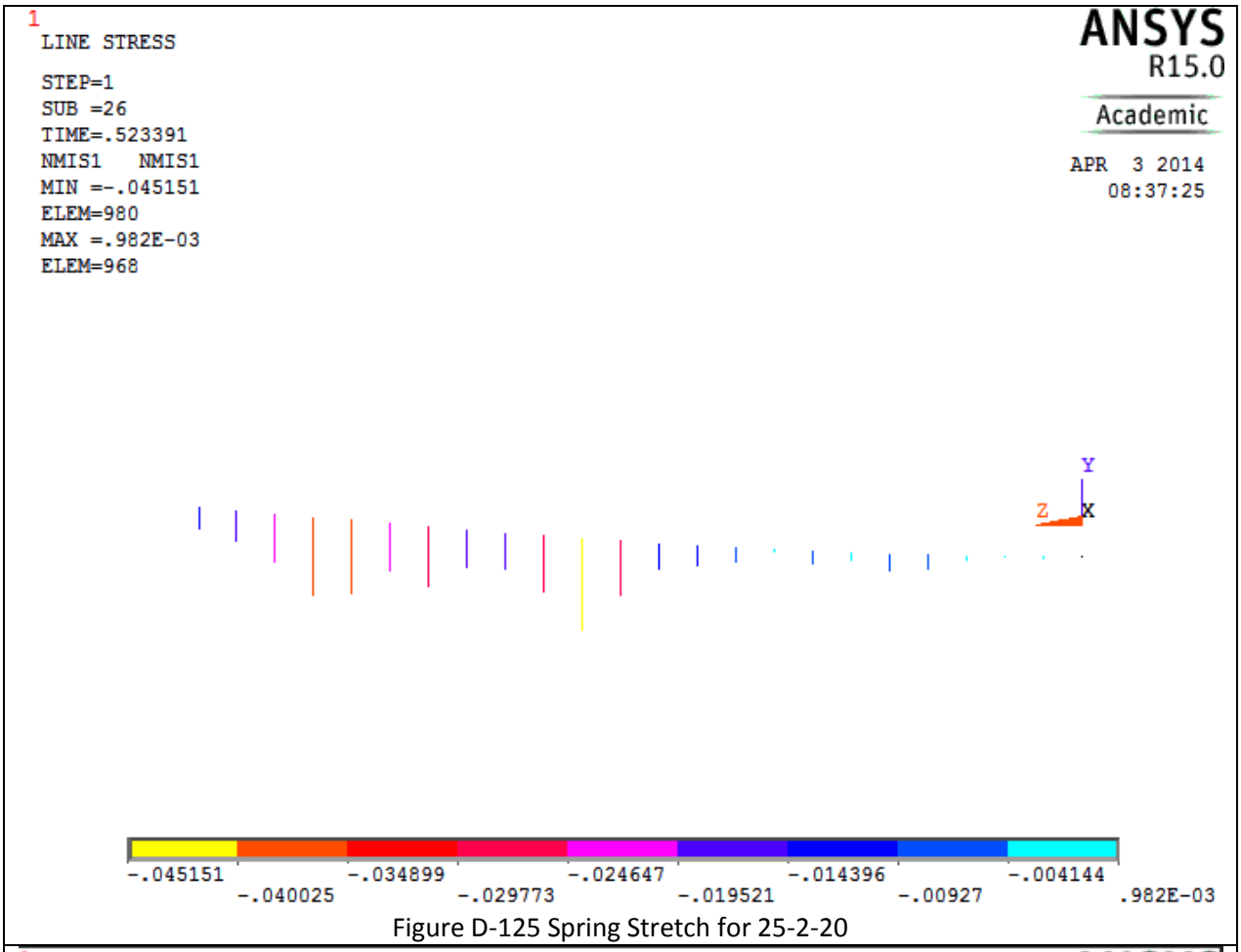

Figure D-125 Spring Stretch for 25-2-20

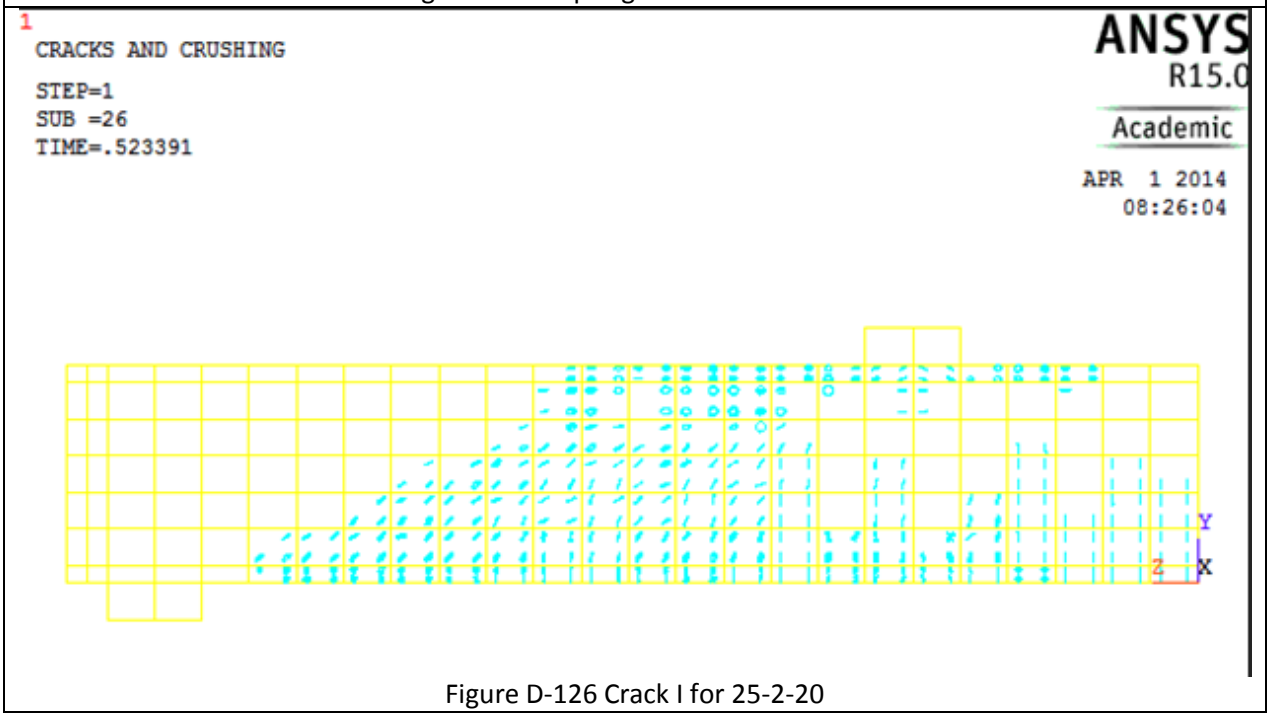

Figure D-126 Crack I for 25-2-20

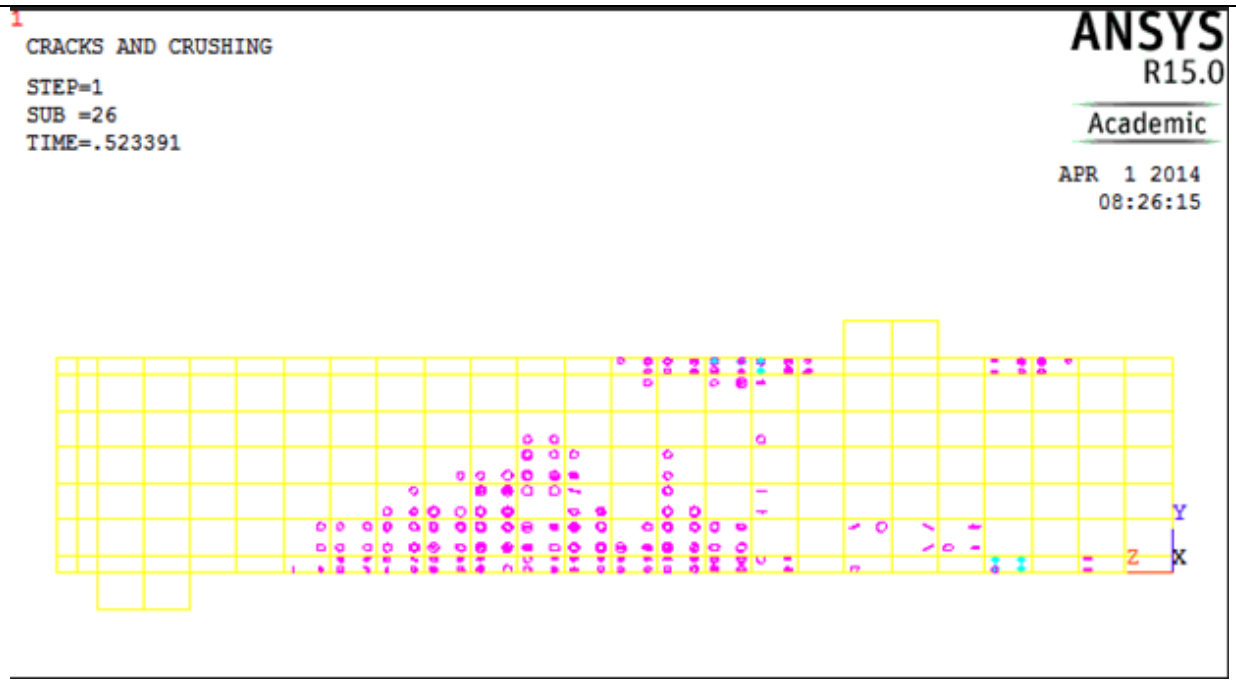

Figure D-127 Crack II for 25-2-20

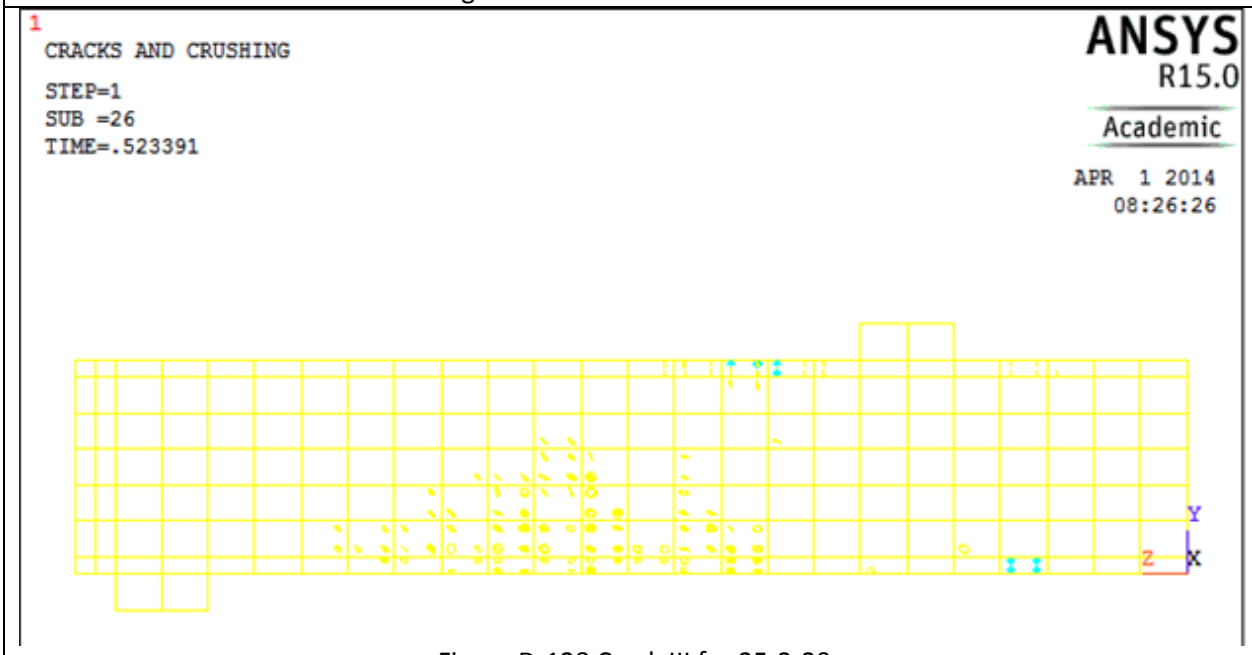

Figure D-128 Crack III for 25-2-20

Table D-17 Details of case 25-2-30

Case Name	Bottom Reinforcement	Honeycombing Location	Strength of Concrete(MPa)	Ultimate Load (kN)	Ultimate Deflection(mm)	Failure Mode
25-2-30	25mm	2	30	167.365	12.2062	

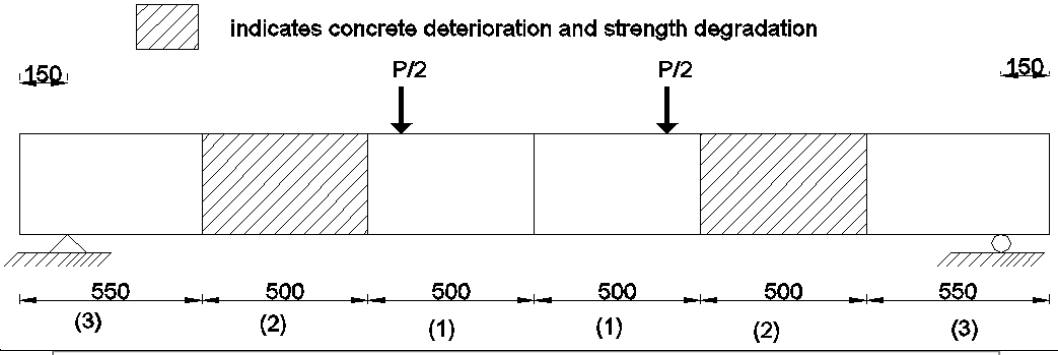

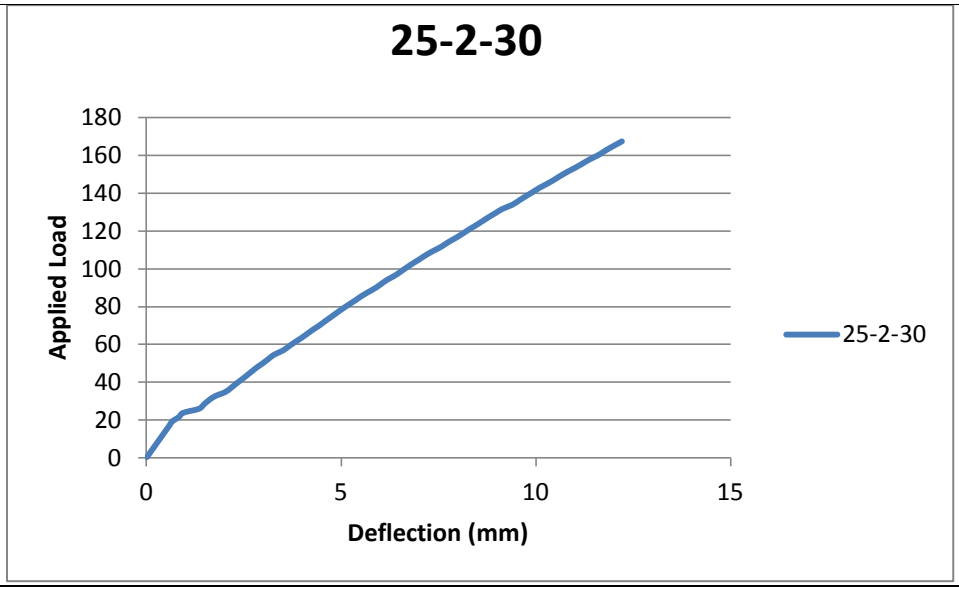

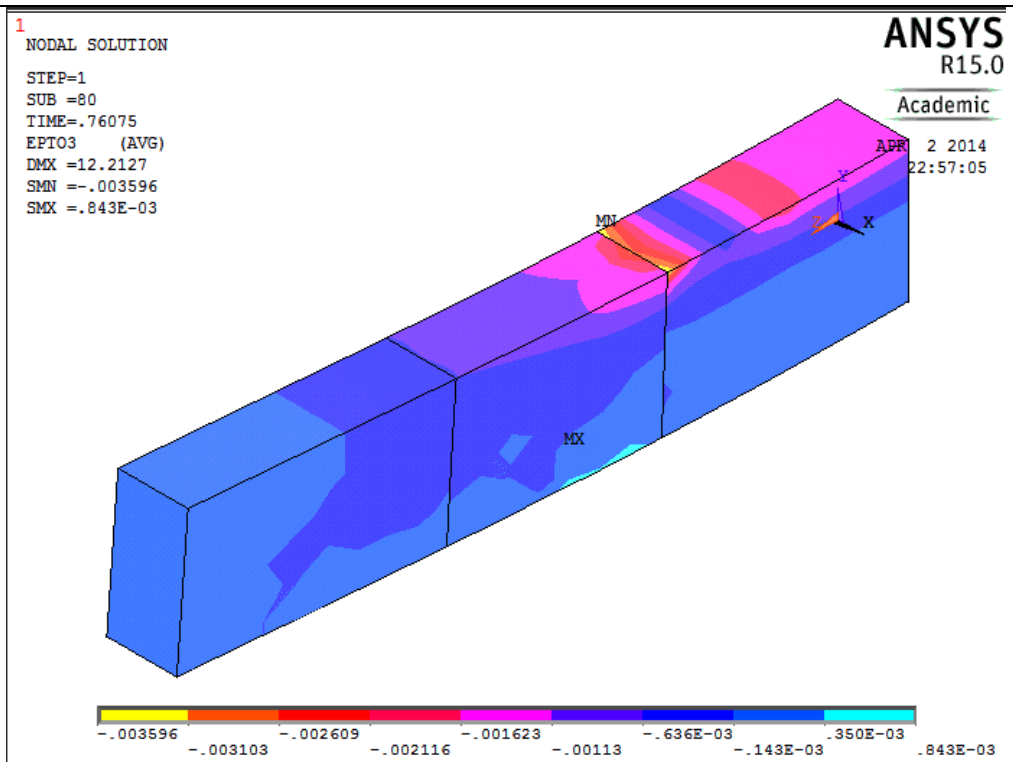

Figure D-129 Nodal solution – 3rd principal total mechanical strain for 25-2-30

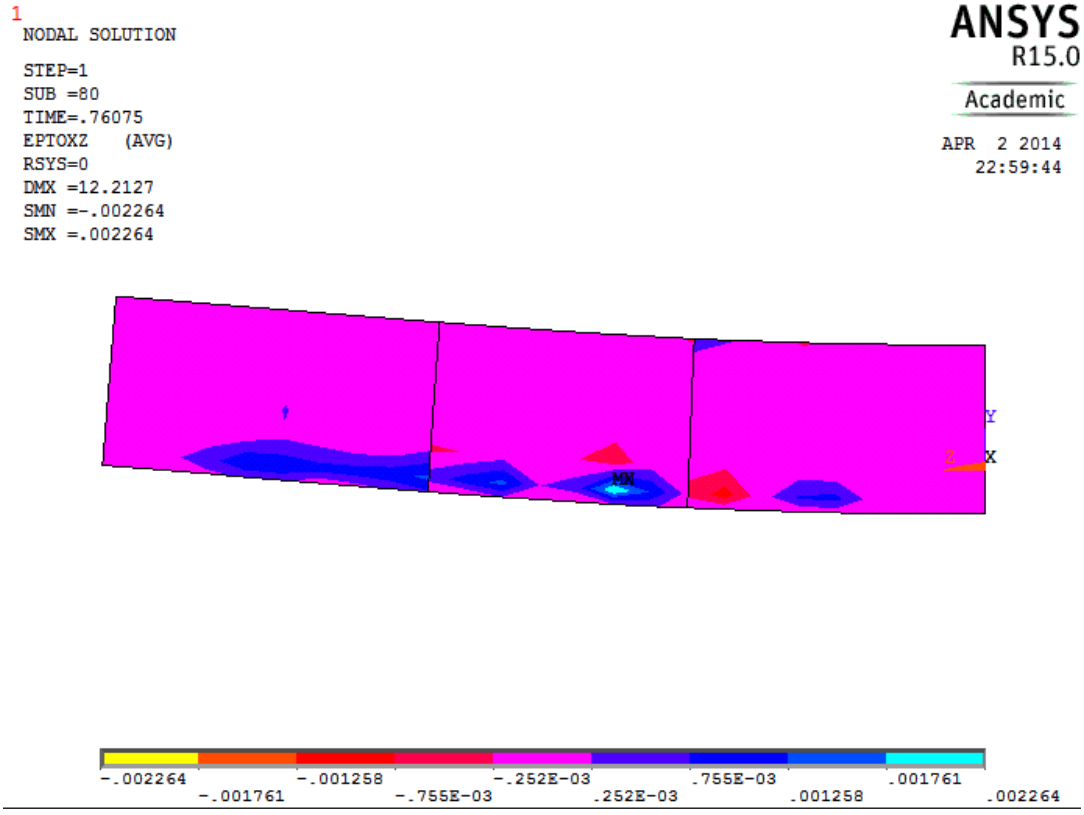

Figure D-130 Nodal Solution XZ shear total mechanical strain for 25-2-30

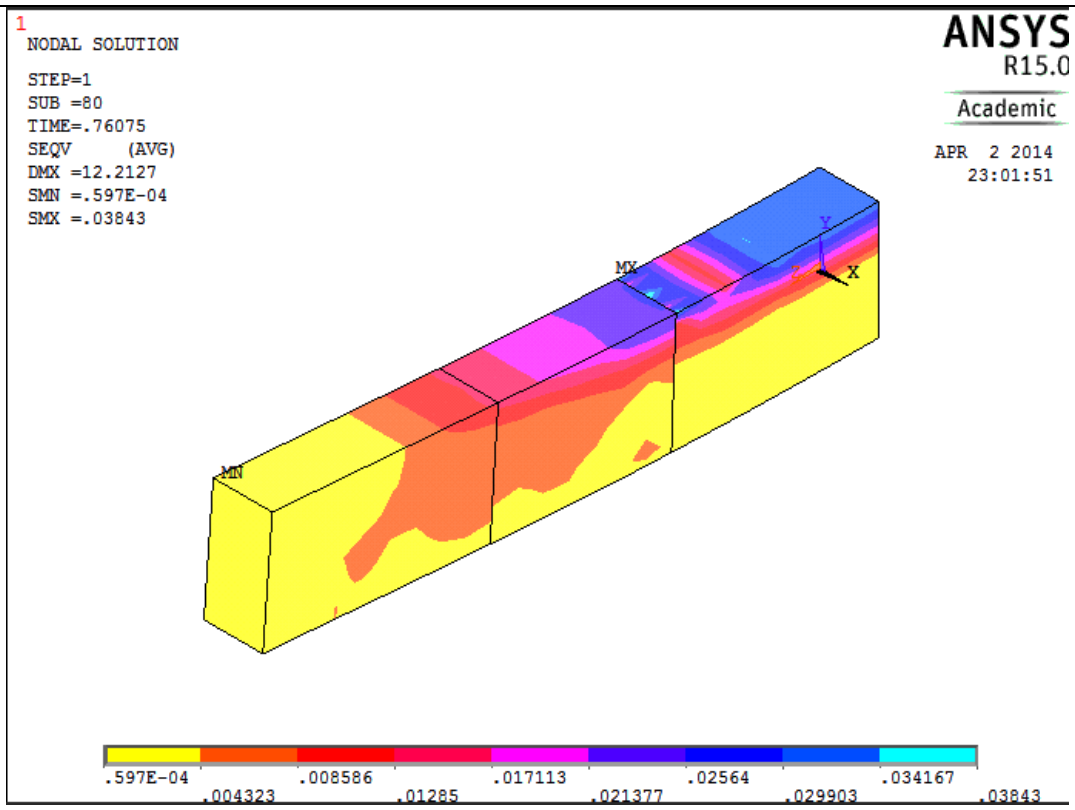

Figure D-131 Nodal Solution -Von Mises Stress for 25-2-30

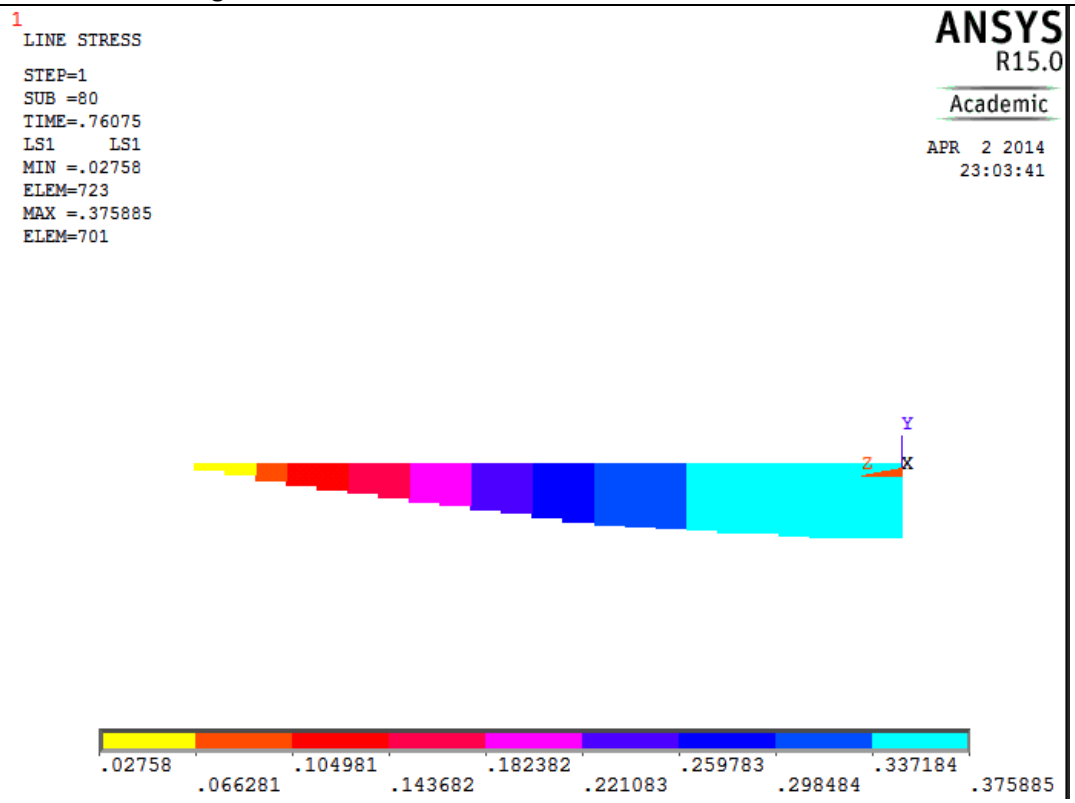

Figure D-132 Reinforcement Stress for 25-2-30

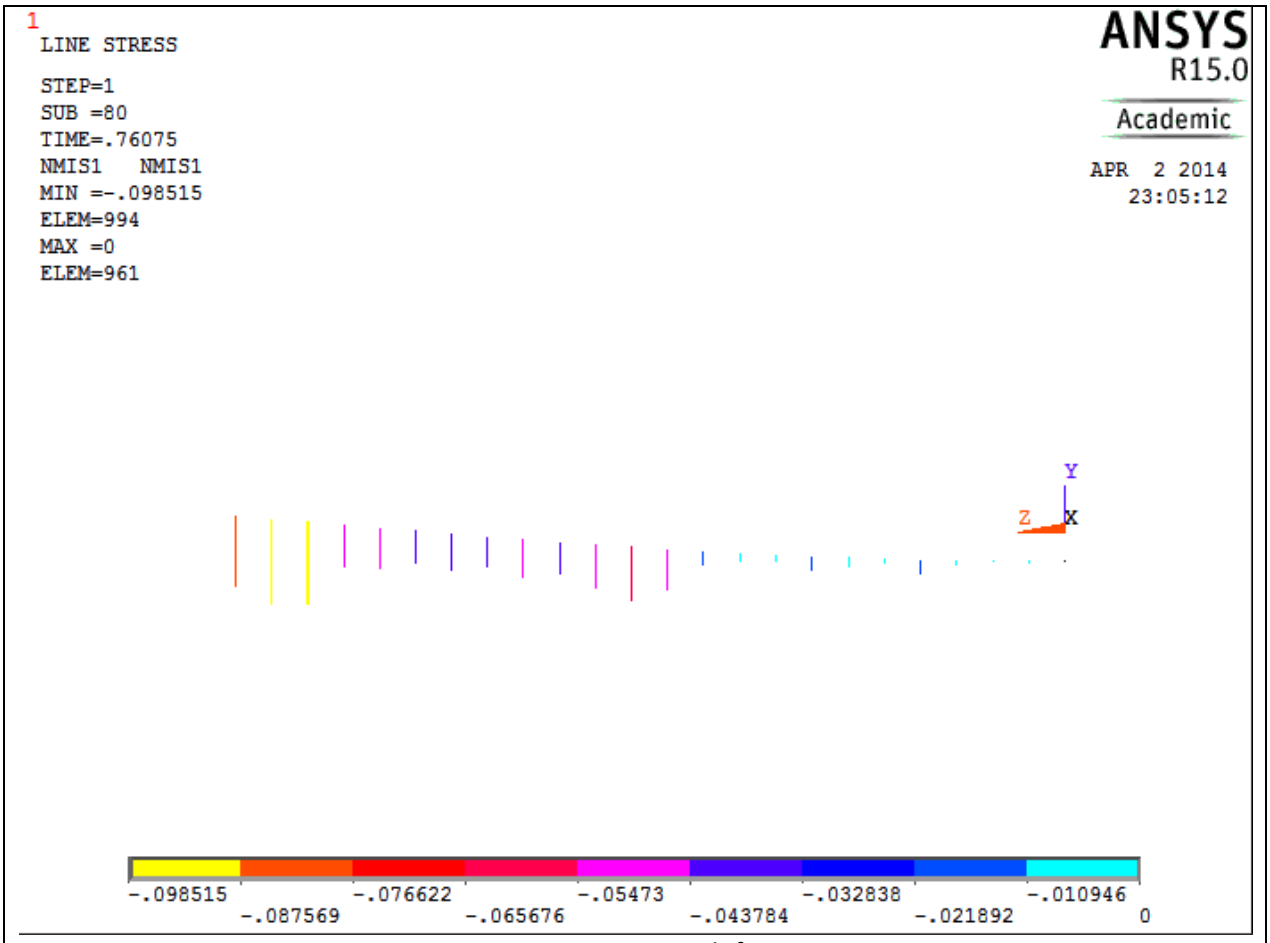

Figure D-133 Spring Stretch for 25-2-30

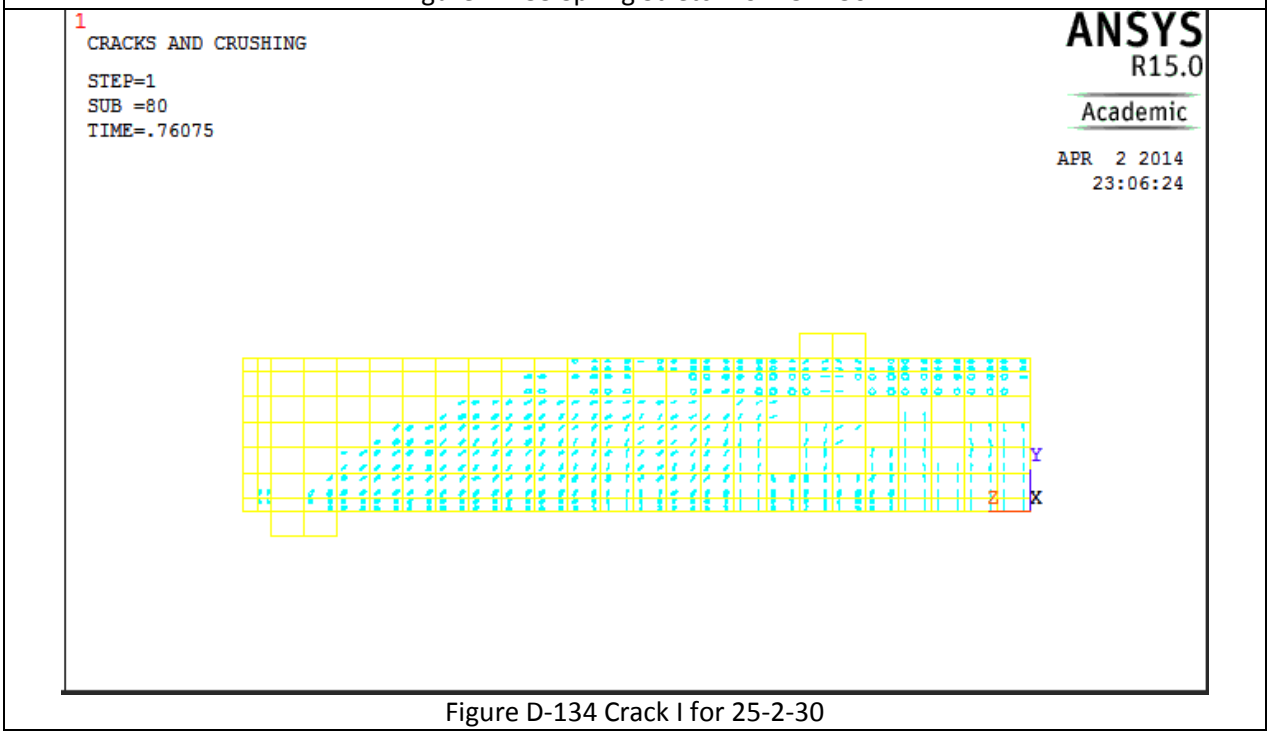

Figure D-134 Crack I for 25-2-30

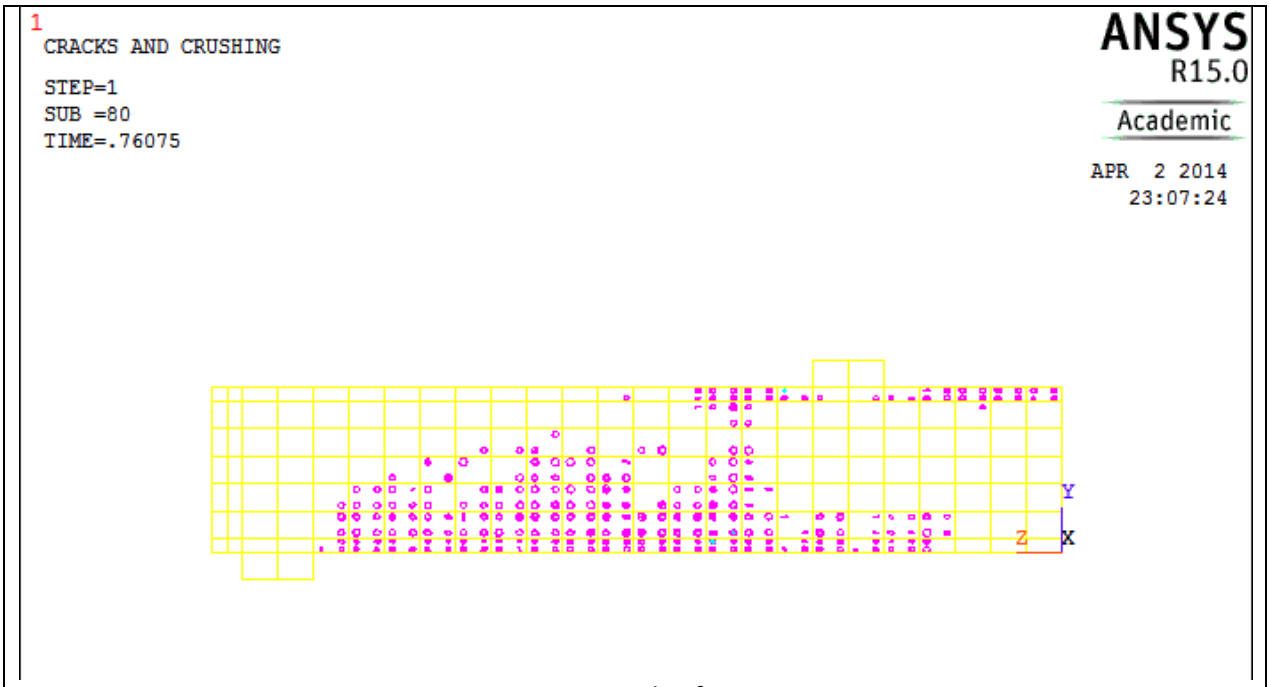

Figure D-135 Crack II for 25-2-30

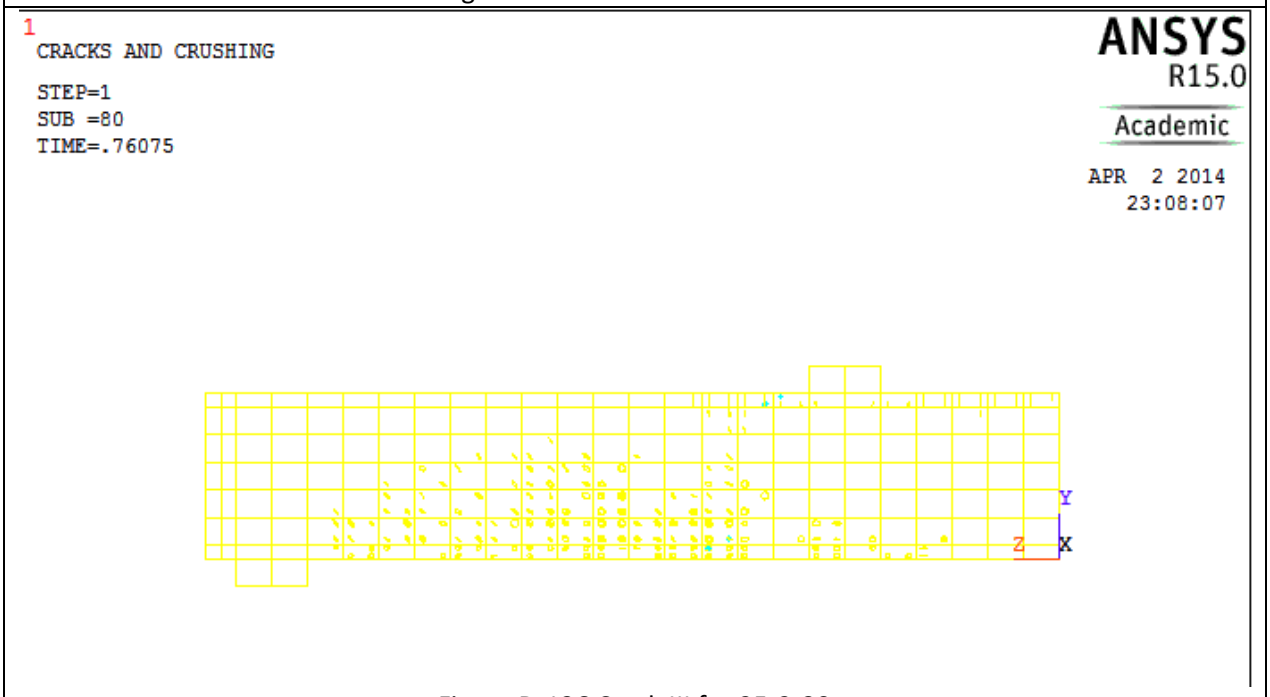

Figure D-136 Crack III for 25-2-30

Table D-18 Details of case 25-3-10

Case Name	Bottom Reinforcement	Honeycombing Location	Strength of Concrete(MPa)	Ultimate Load (kN)	Ultimate Deflection(mm)	Failure Mode
25-3-10	25mm	3	10	101.565	7.25606	

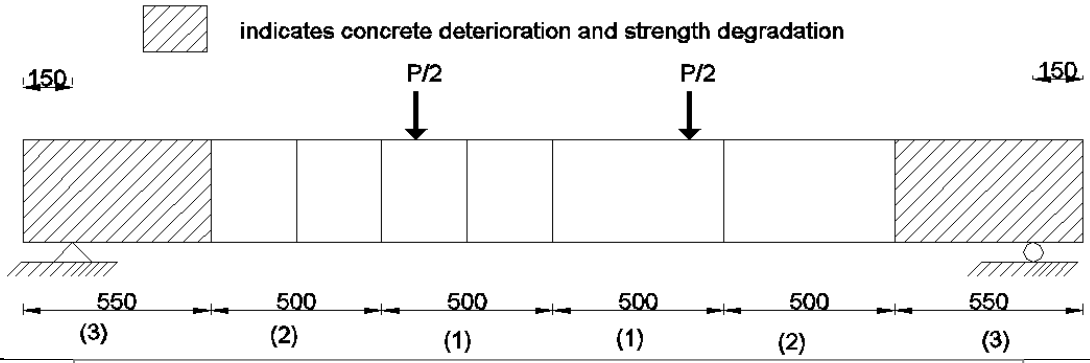

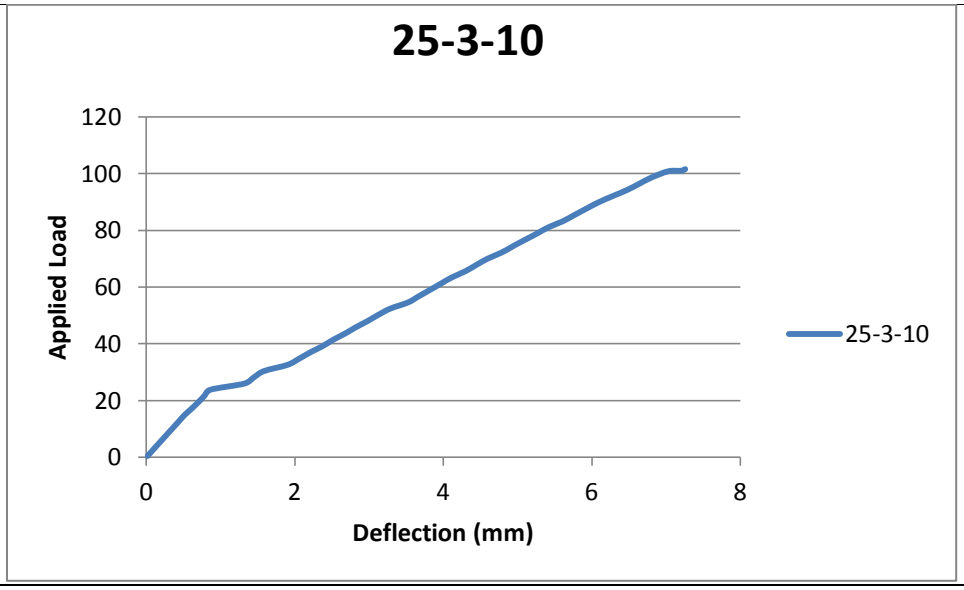

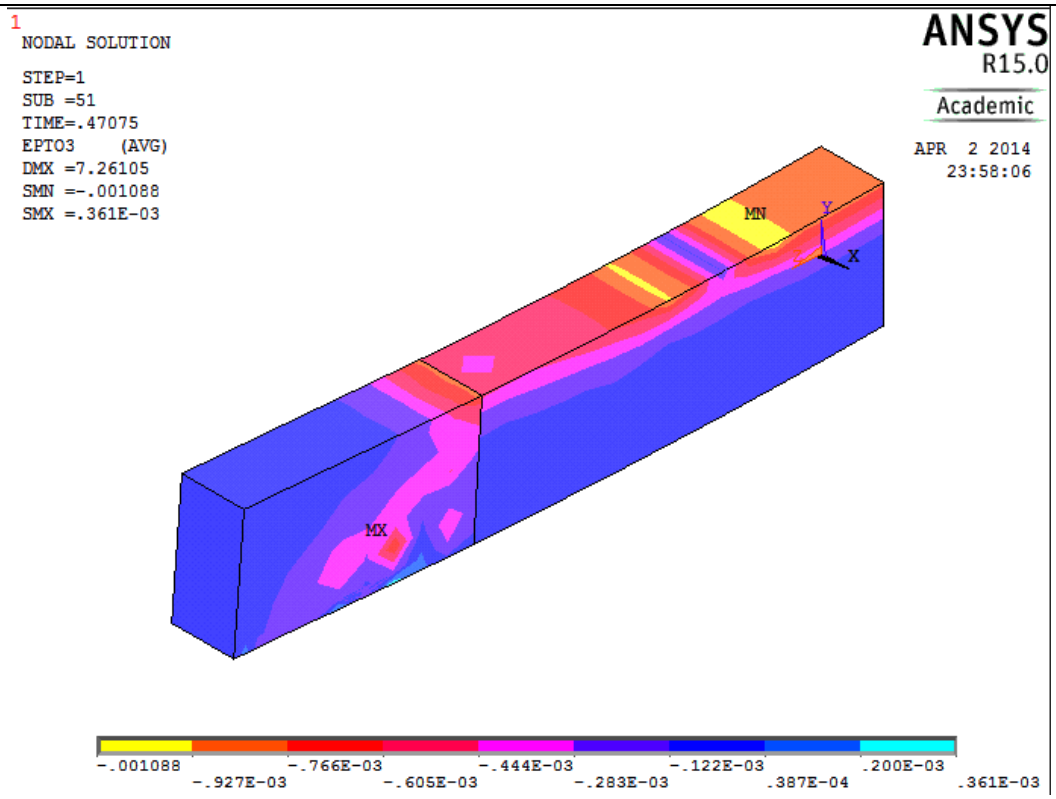

Figure D-137 Nodal solution – 3rd principal total mechanical strain for 25-3-10

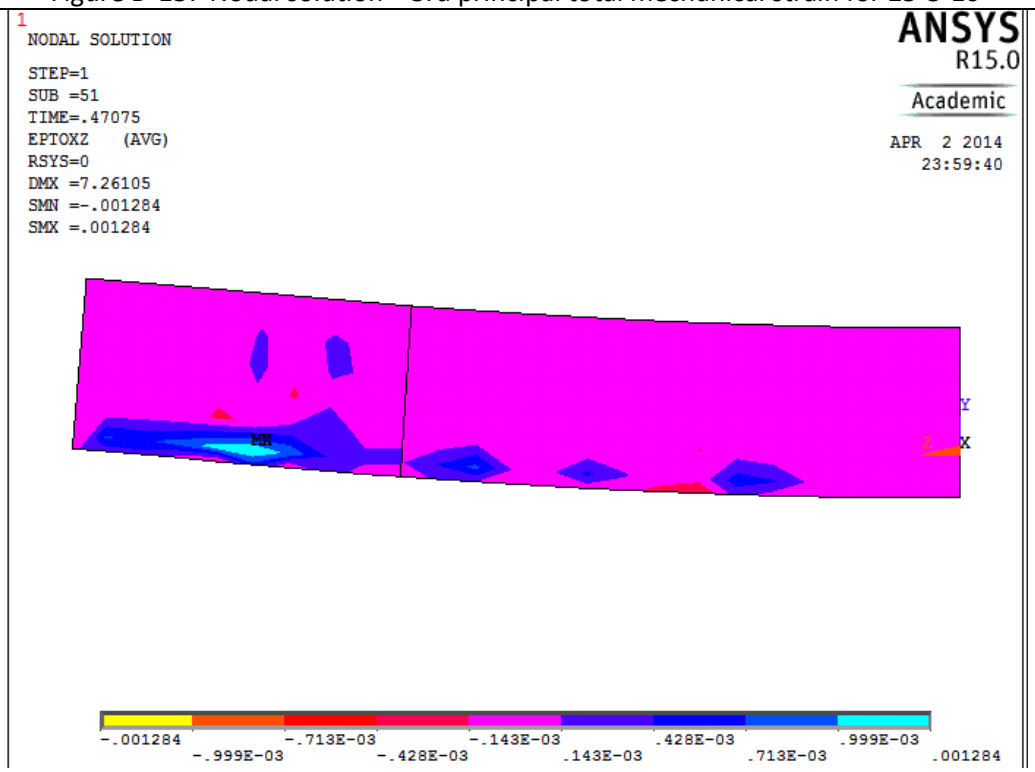

Figure D-138 Nodal Solution XZ shear total mechanical strain for 25-3-10

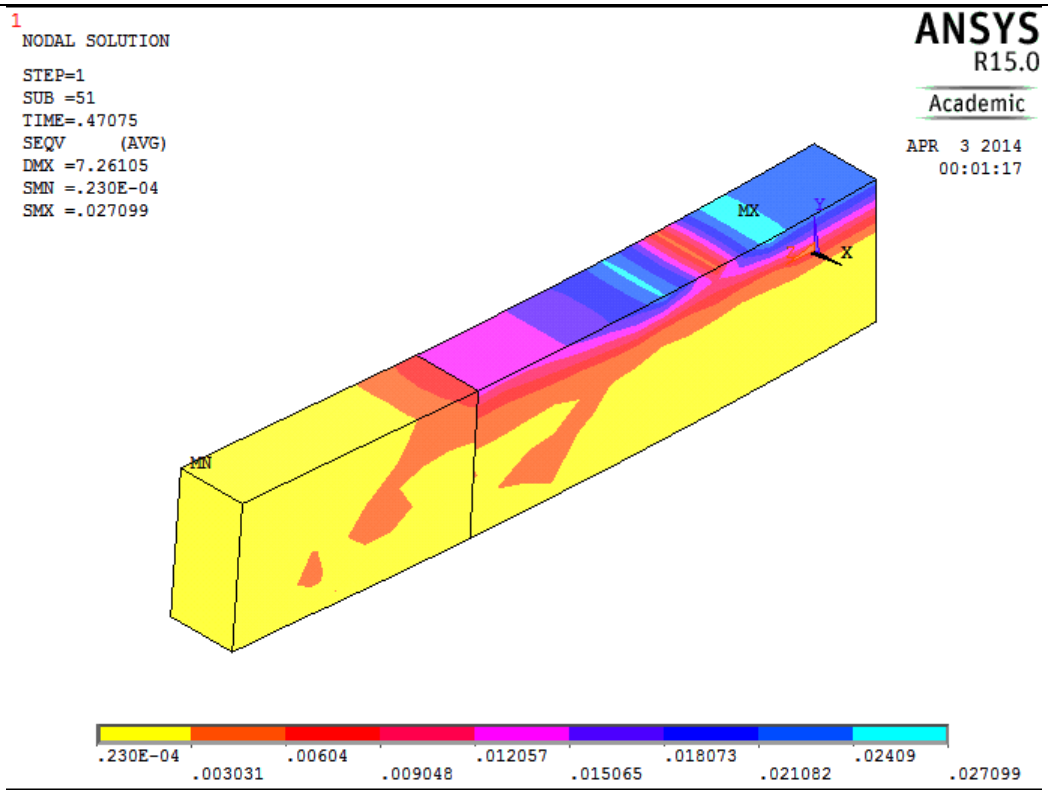

Figure D-139 Nodal Solution -Von Mises Stress for 25-3-10

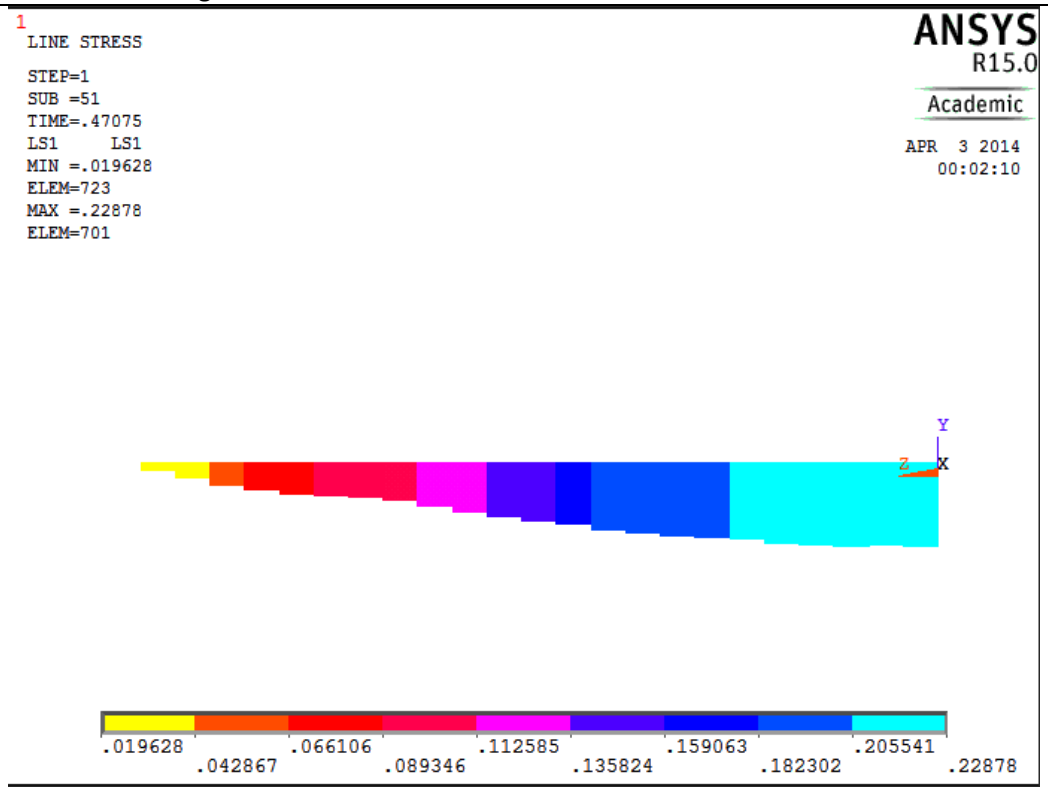

Figure D-140 Reinforcement Stress for 25-3-10

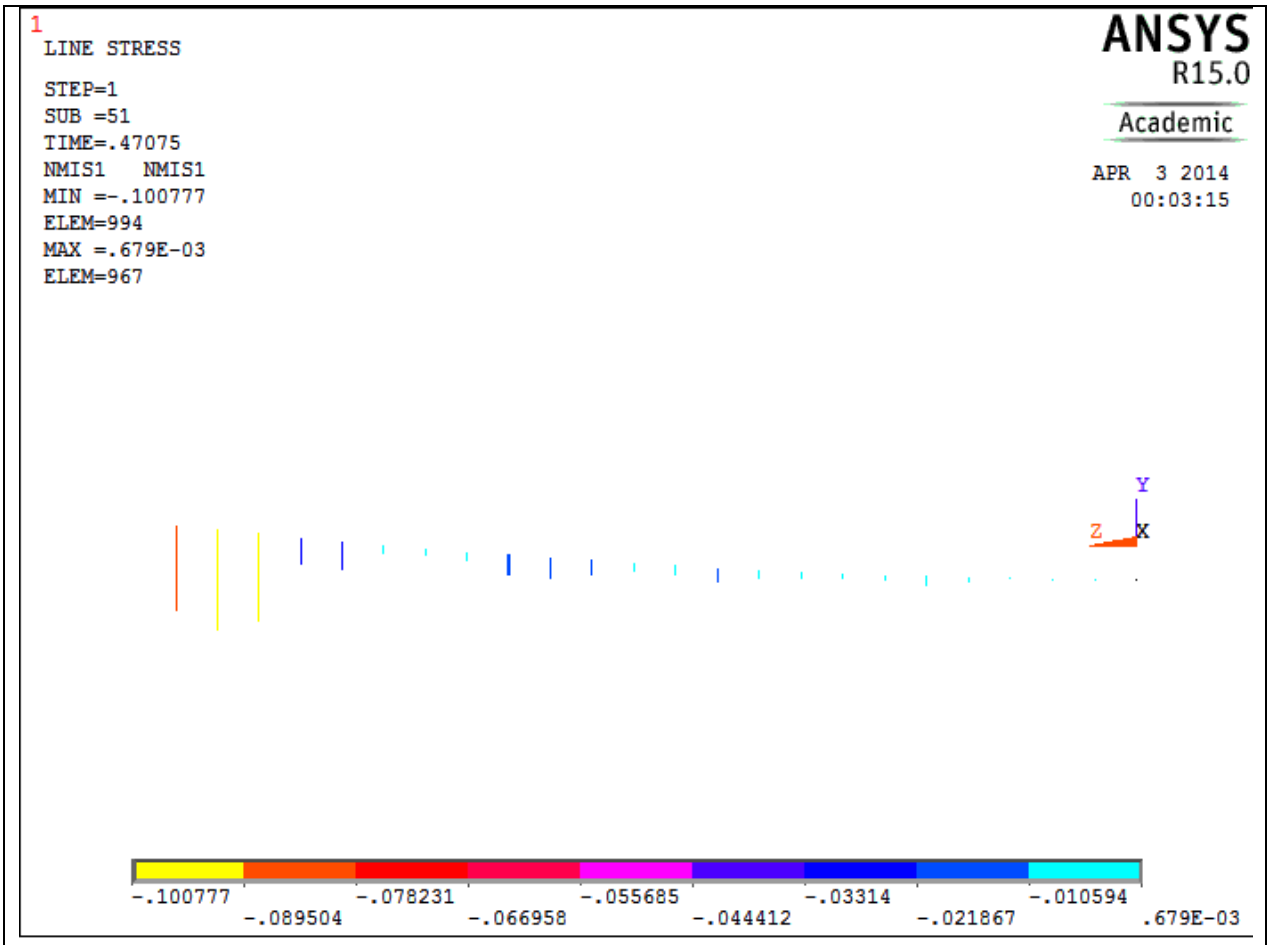

Figure D-141 Spring Stretch for 25-3-10

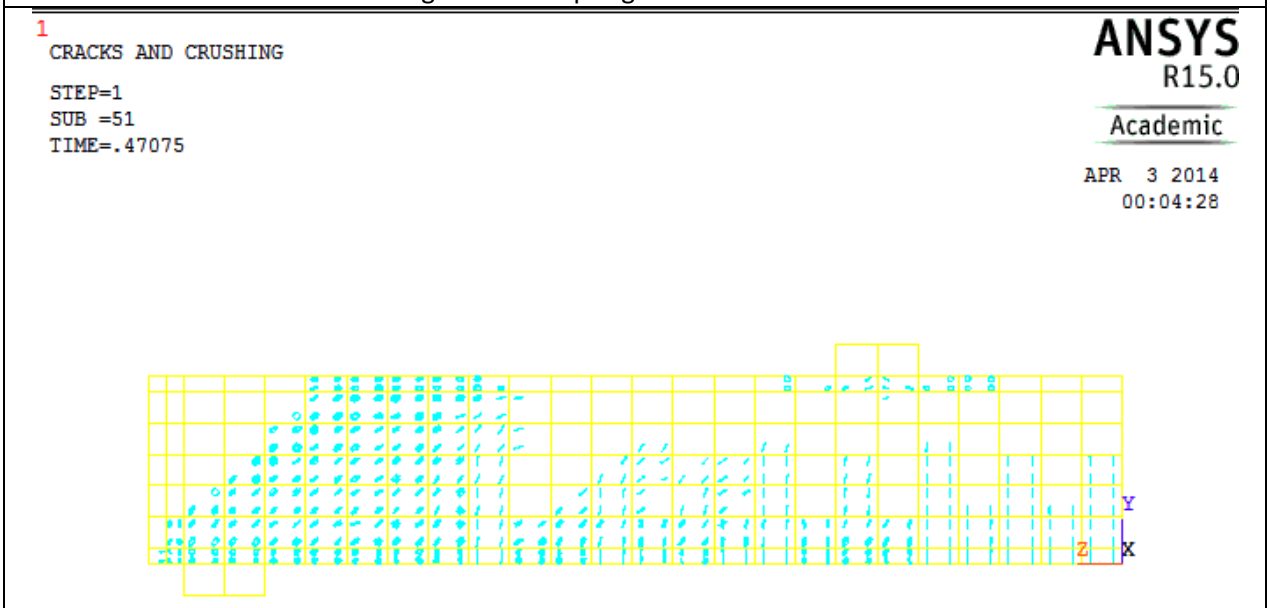

Figure D-142 Crack I for 25-3-10

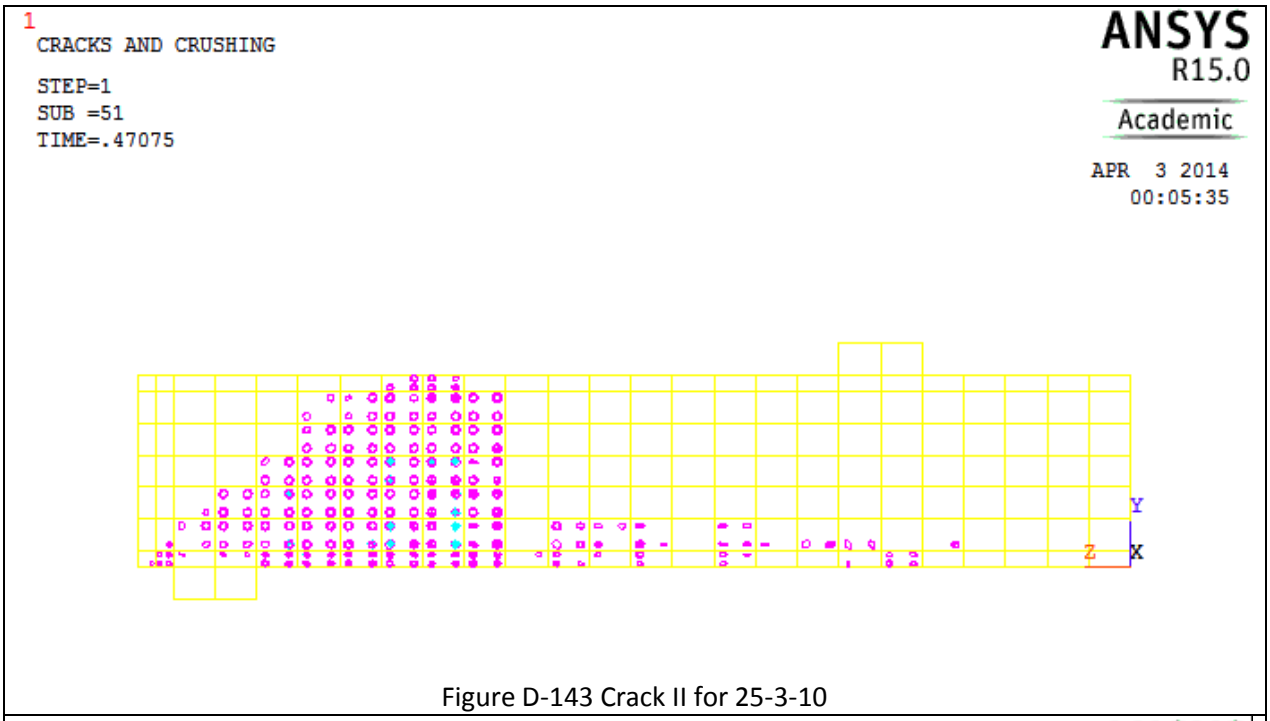

Figure D-143 Crack II for 25-3-10

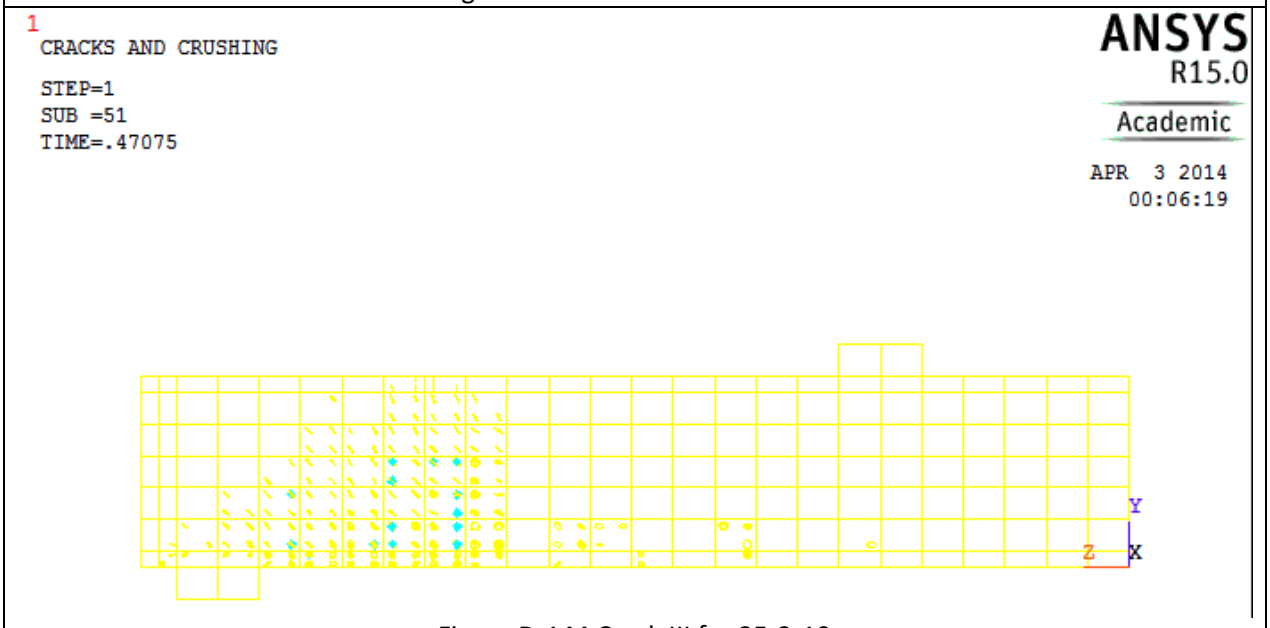

Figure D-144 Crack III for 25-3-10

Table D-19 Details of case 25-3-20

Case Name	Bottom Reinforcement	Honeycombing Location	Strength of Concrete(MPa)	Ultimate Load (kN)	Ultimate Deflection(mm)	Failure Mode
25-3-20	25mm	3	20	128.8958	9.05594	

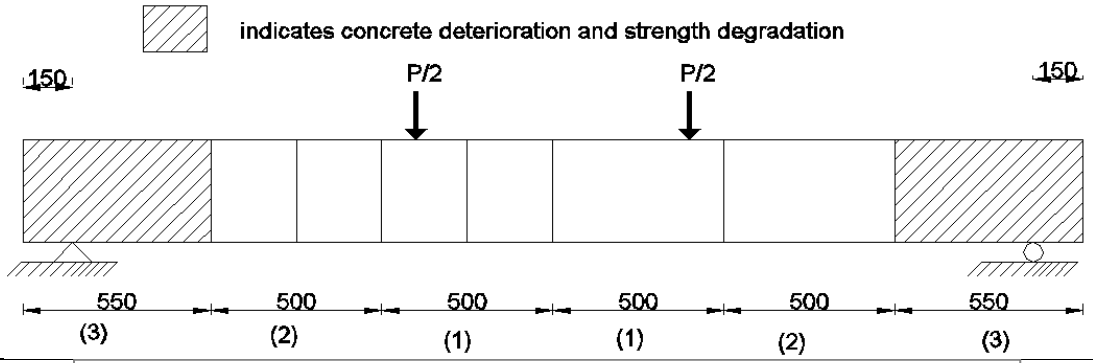

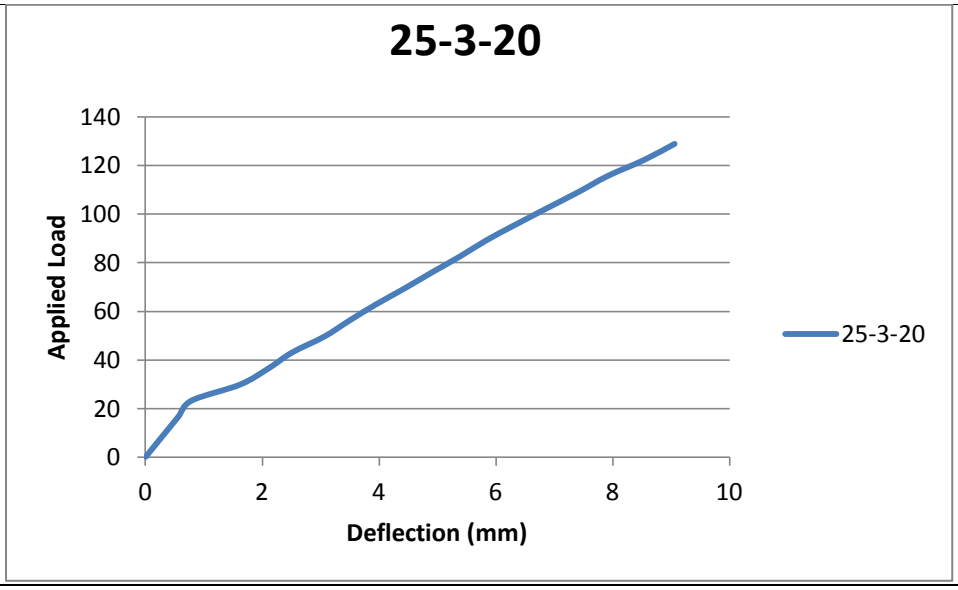

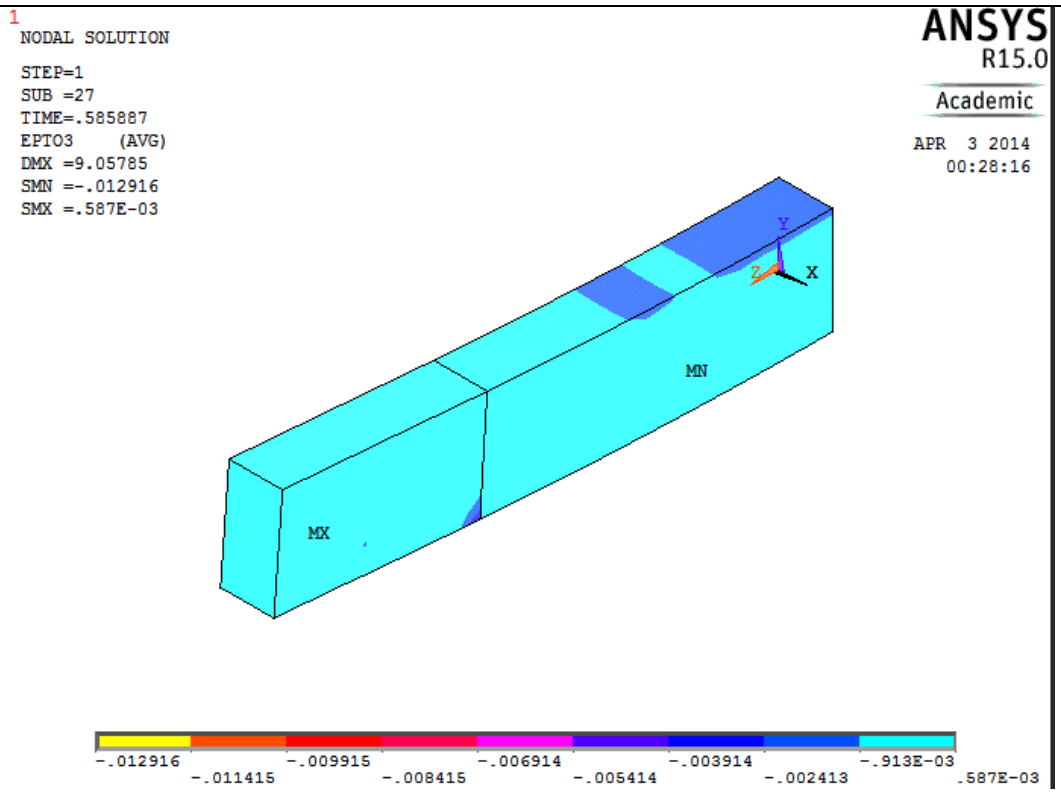

Figure D-145 Nodal solution – 3rd principal total mechanical strain for 25-3-20

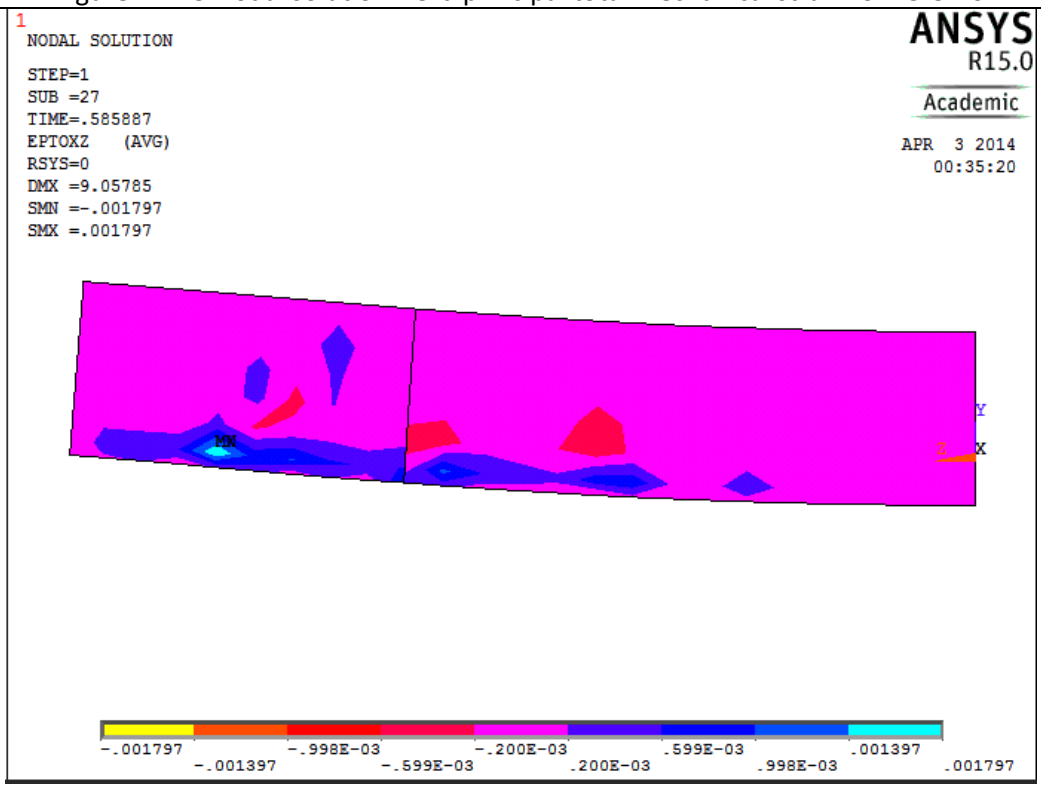

Figure D-146 Nodal Solution XZ shear total mechanical strain for 25-3-20

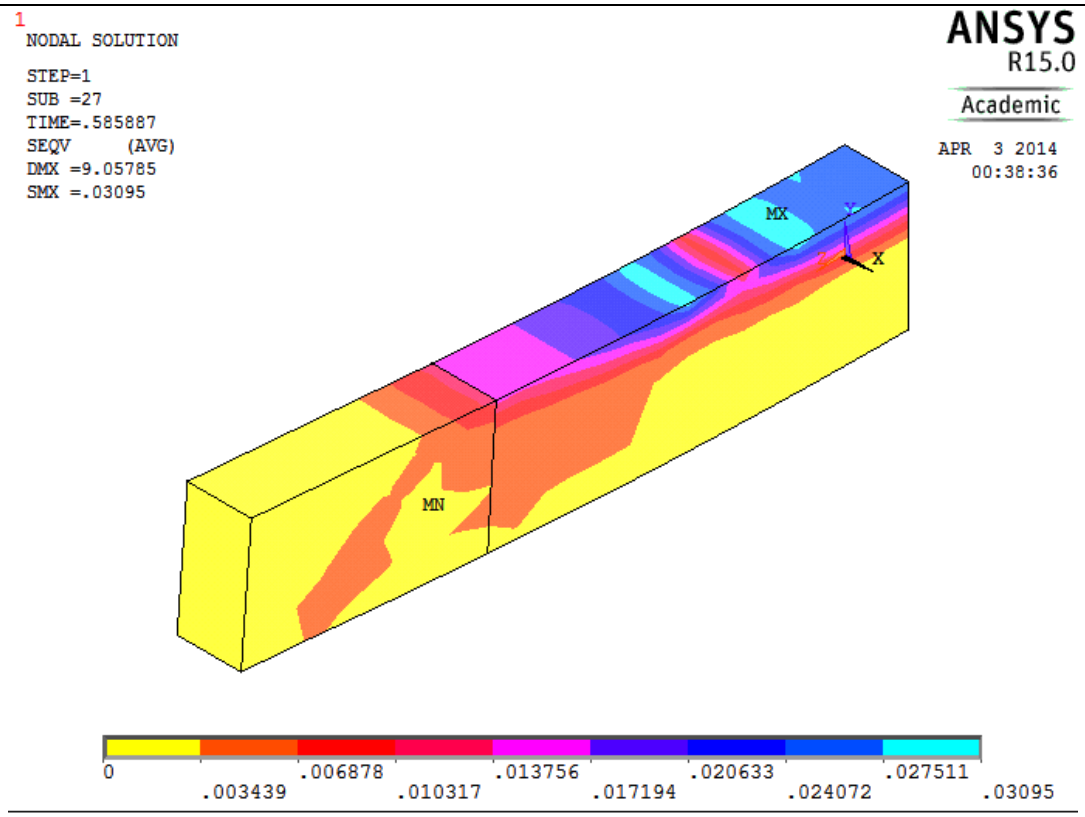

Figure D-147 Nodal Solution -Von Mises Stress for 25-3-20

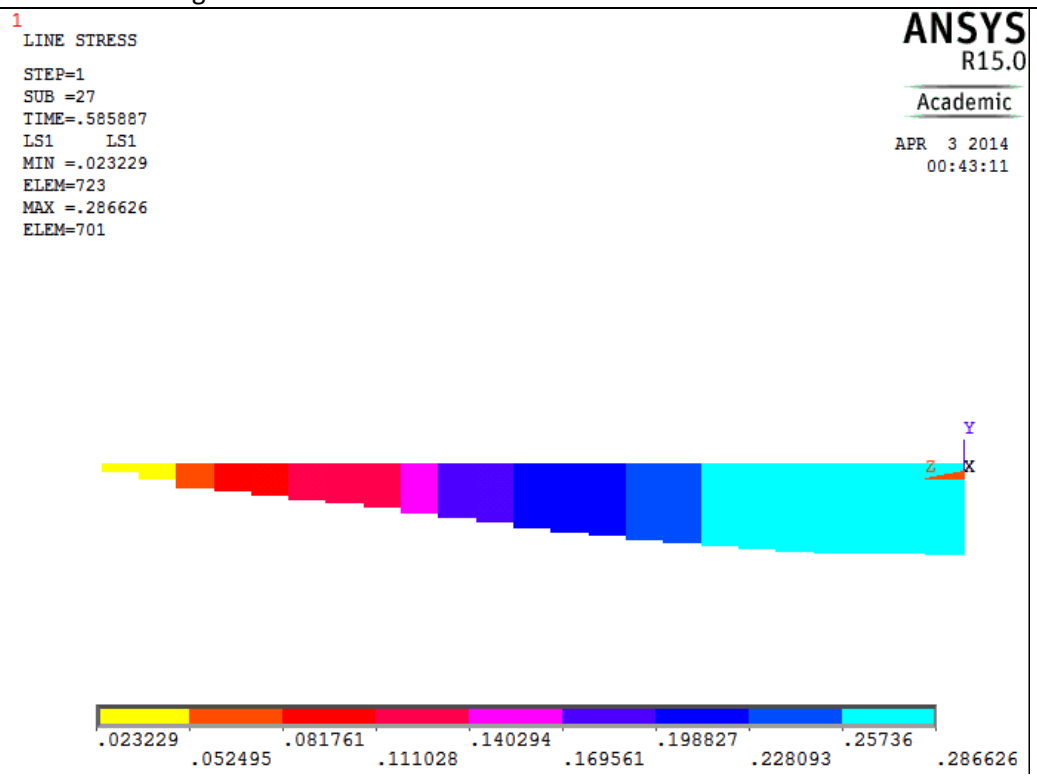

Figure D-148 Reinforcement Stress for 25-3-20

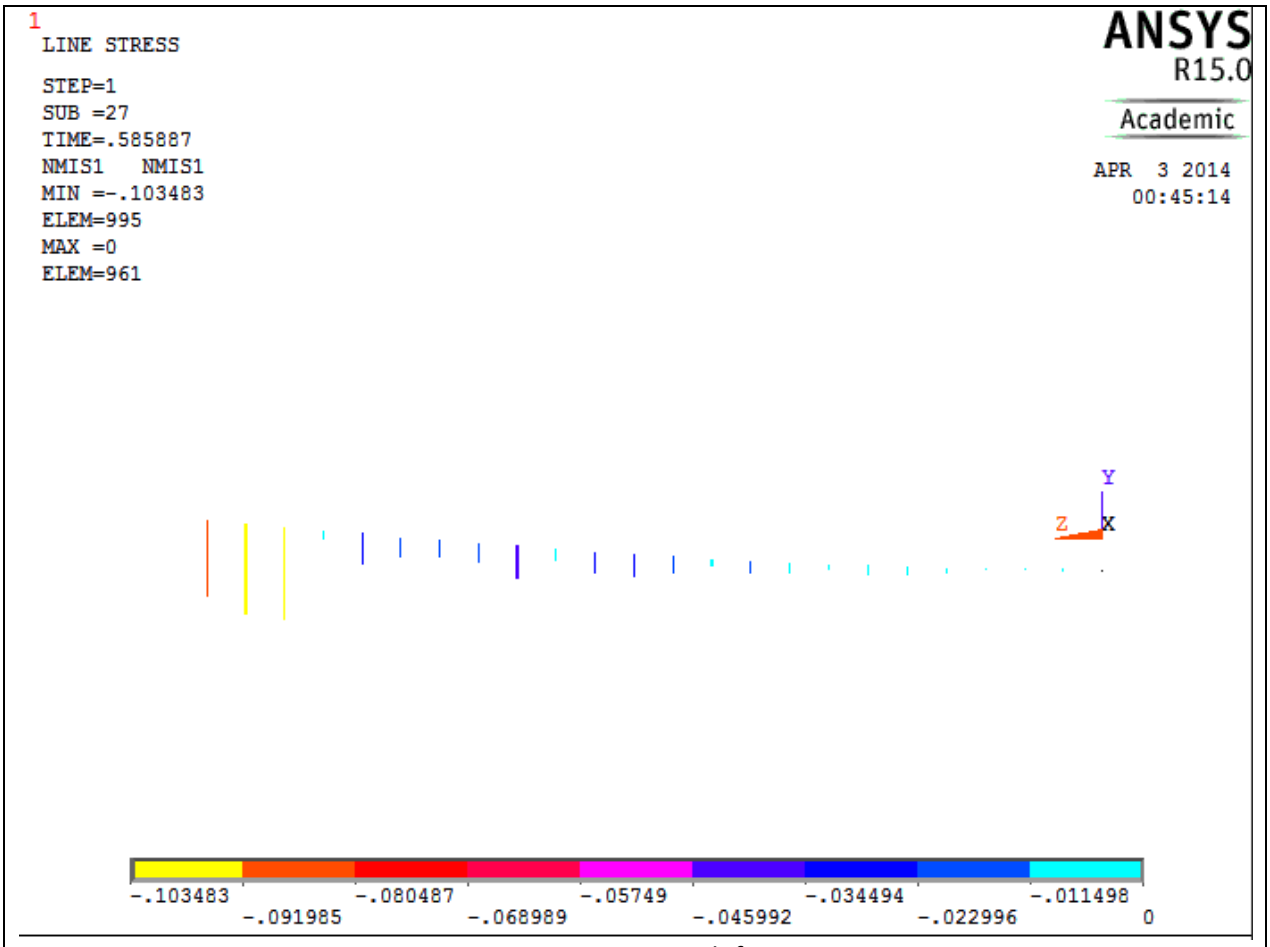

Figure D-149 Spring Stretch for 25-3-20

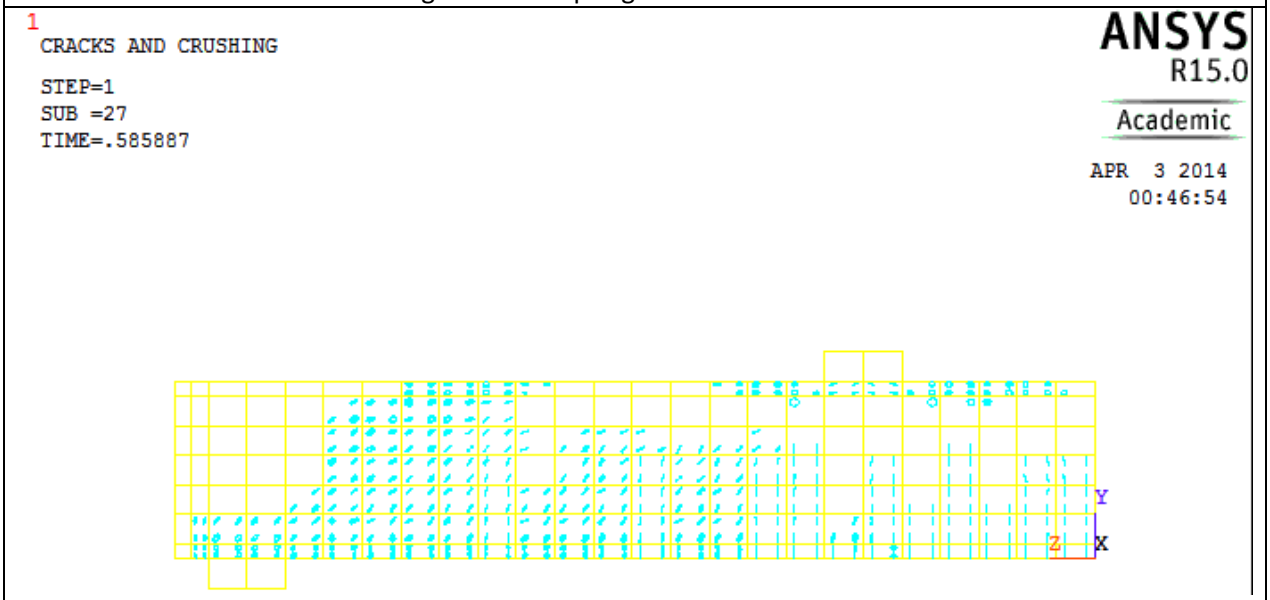

Figure D-150 Crack I for 25-3-20

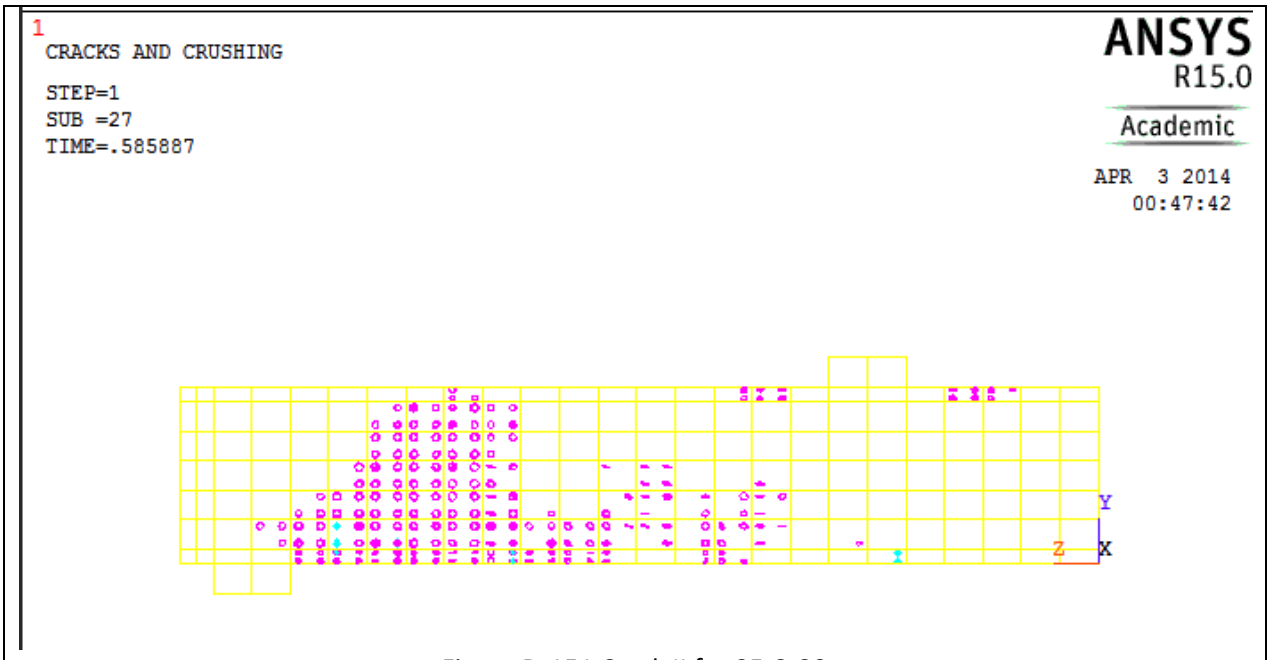

Figure D-151 Crack II for 25-3-20

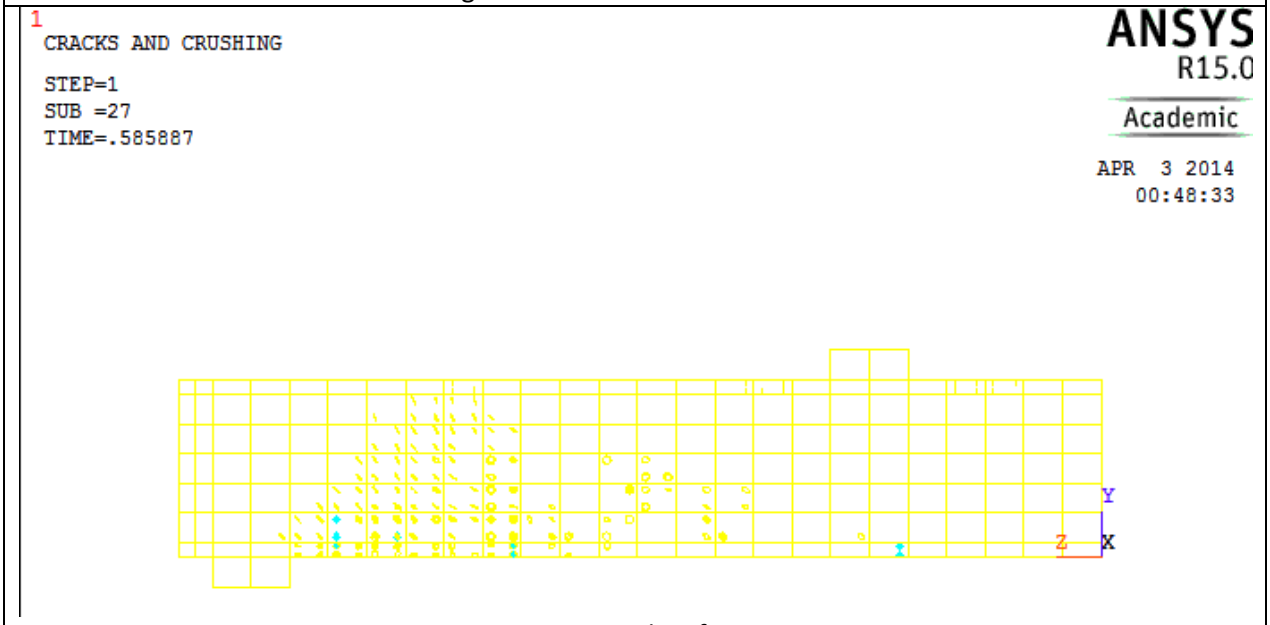

Figure D-152 Crack III for 25-3-20

Table D-20 Details of case 25-3-30

Case Name	Bottom Reinforcement	Honeycombing Location	Strength of Concrete(MPa)	Ultimate Load (kN)	Ultimate Deflection(mm)	Failure Mode
25-3-30	25mm	3	30	173.9848	12.8042	

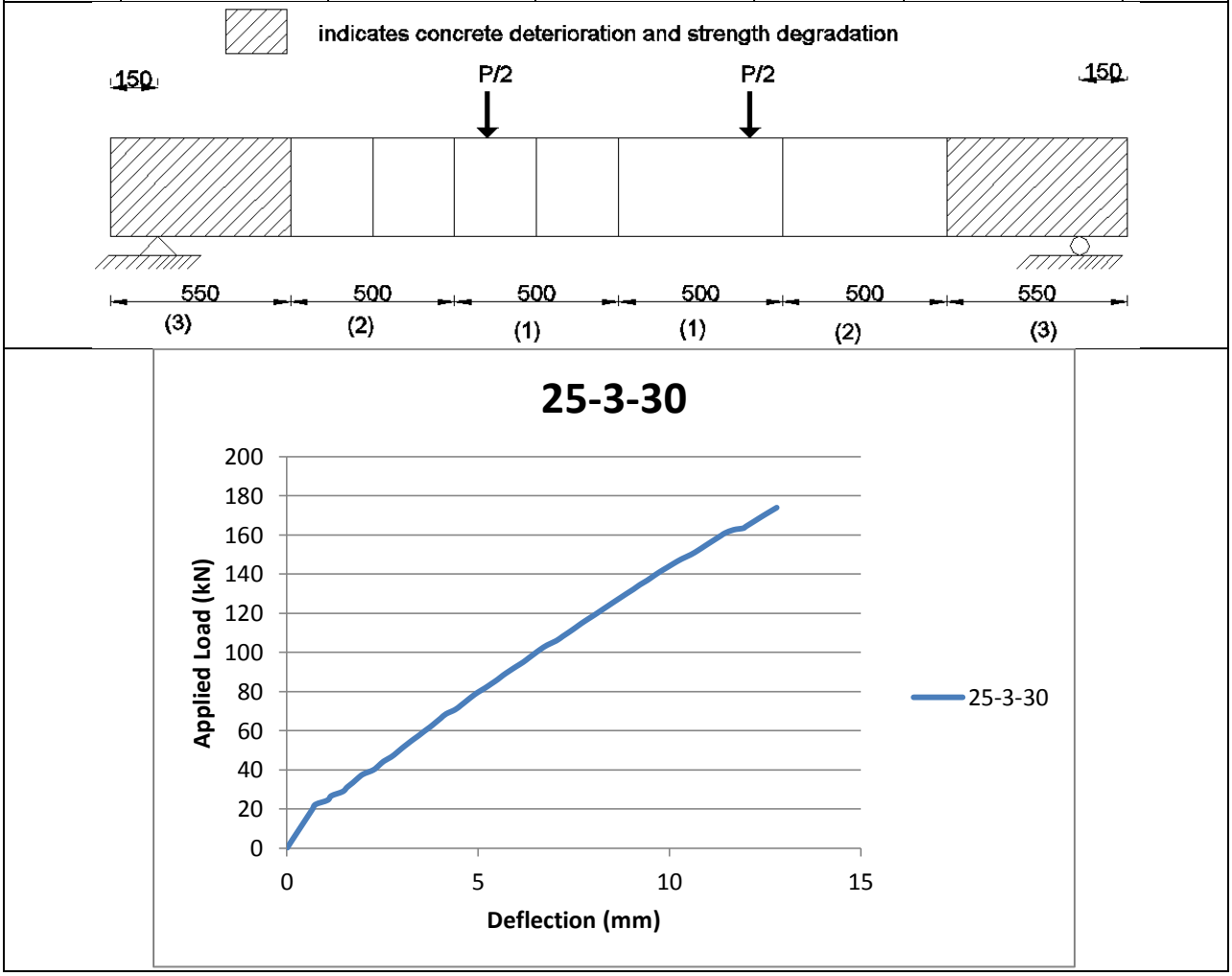

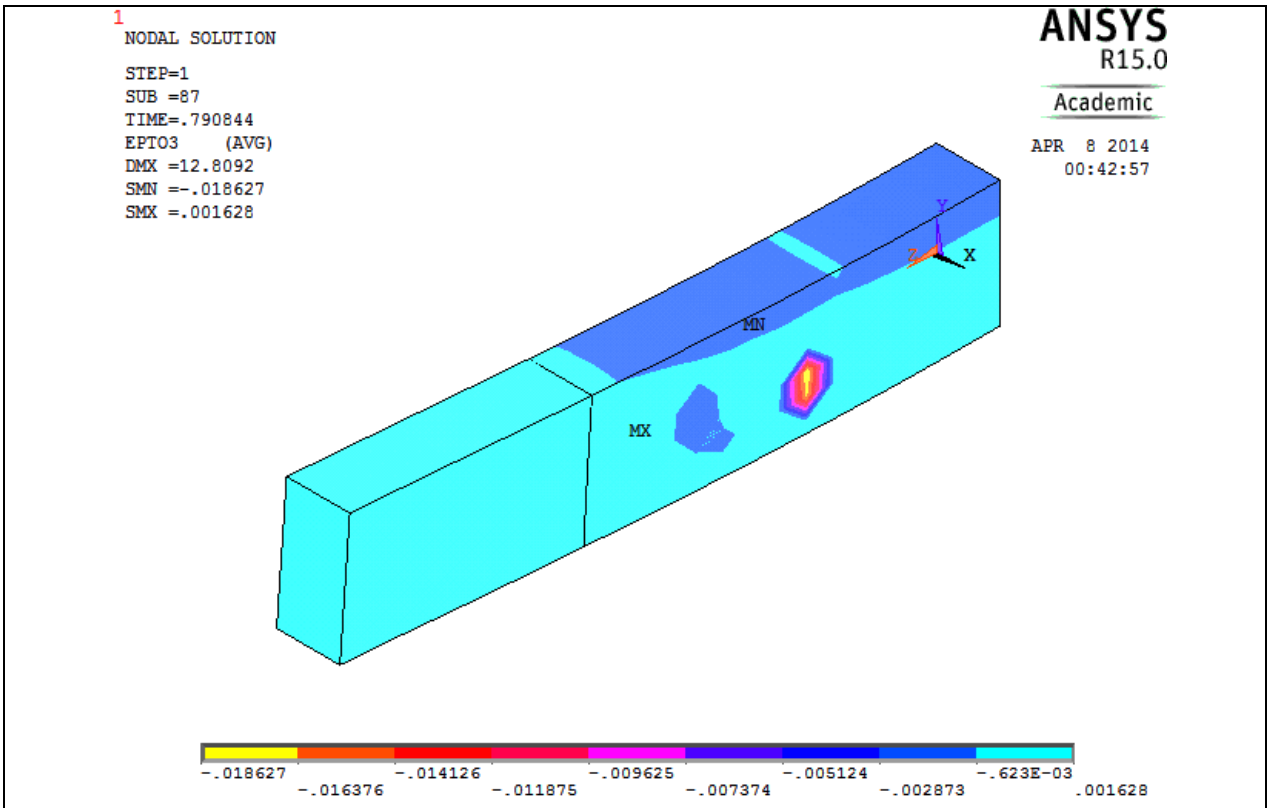

Figure D-153 Nodal solution – 3rd principal total mechanical strain for 25-3-30

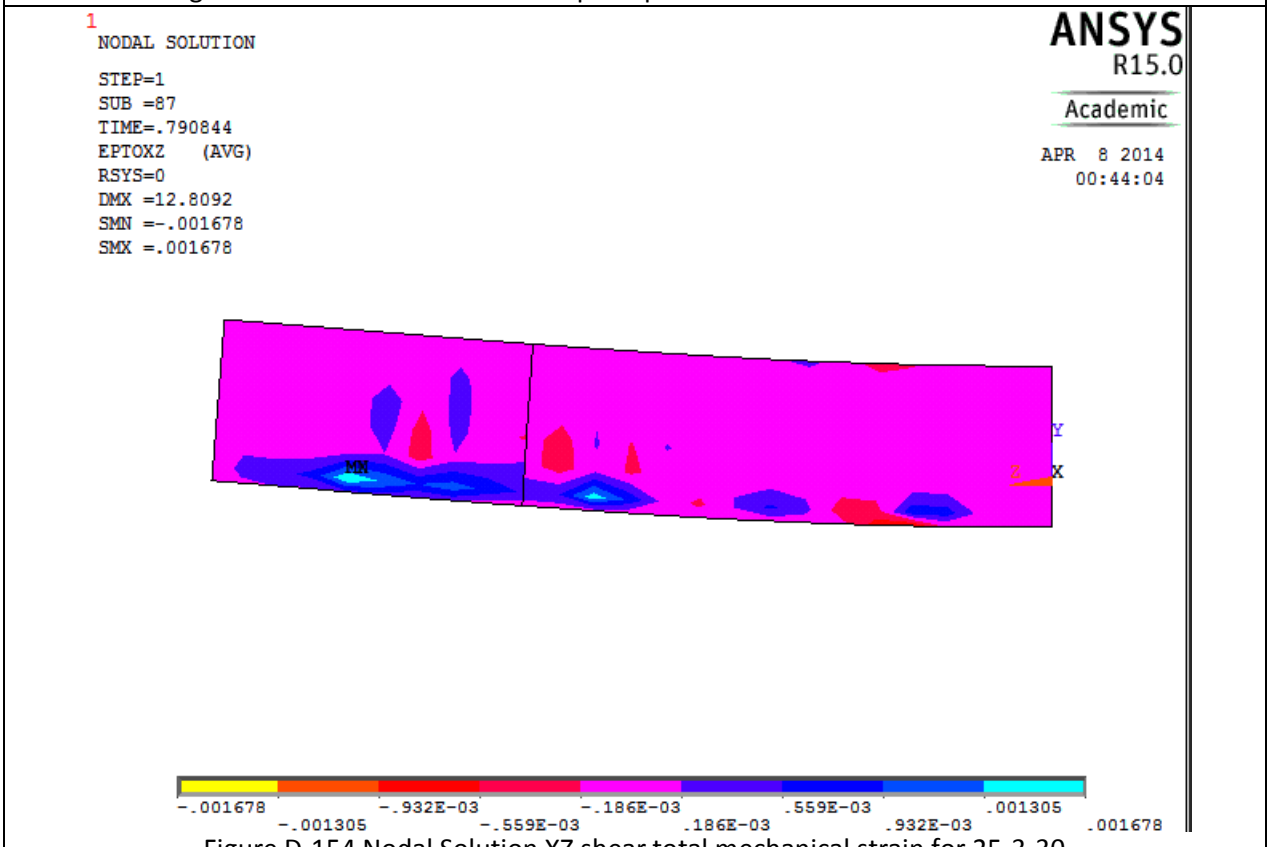

Figure D-154 Nodal Solution XZ shear total mechanical strain for 25-3-30

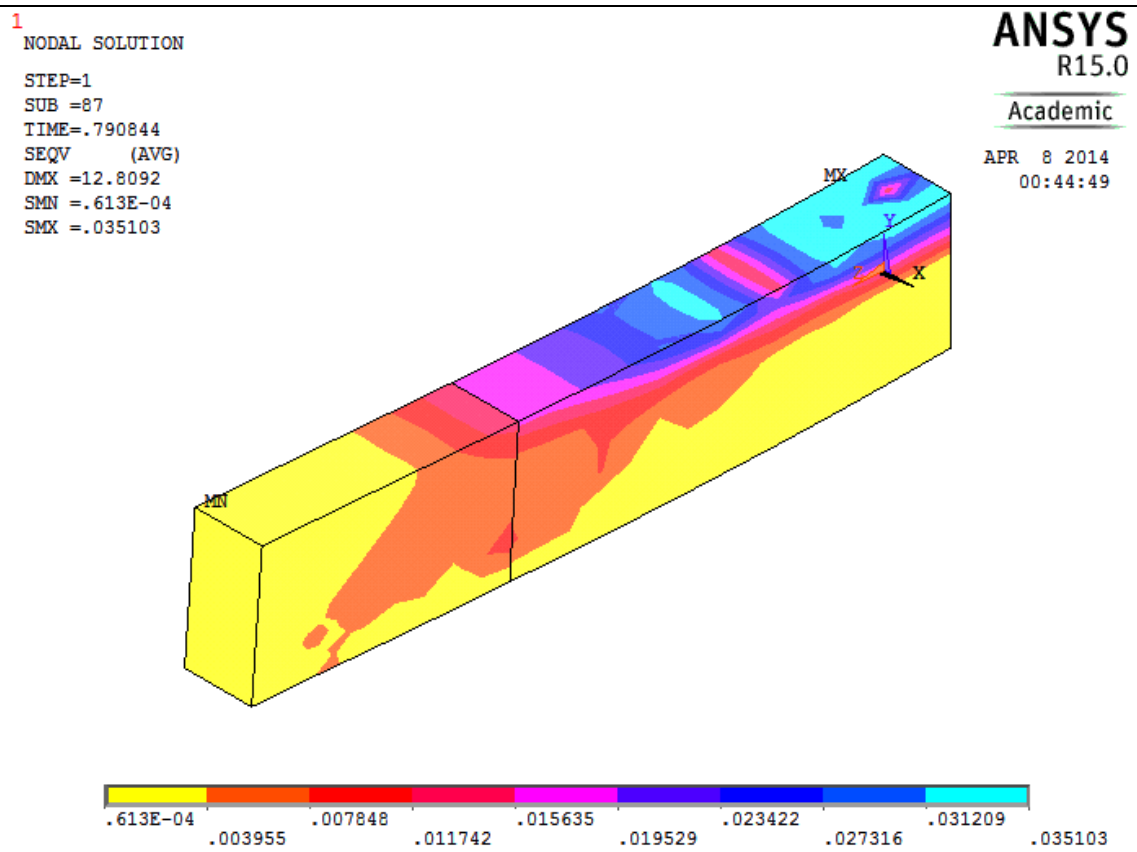

Figure D-155 Nodal Solution -Von Mises Stress for 25-3-30

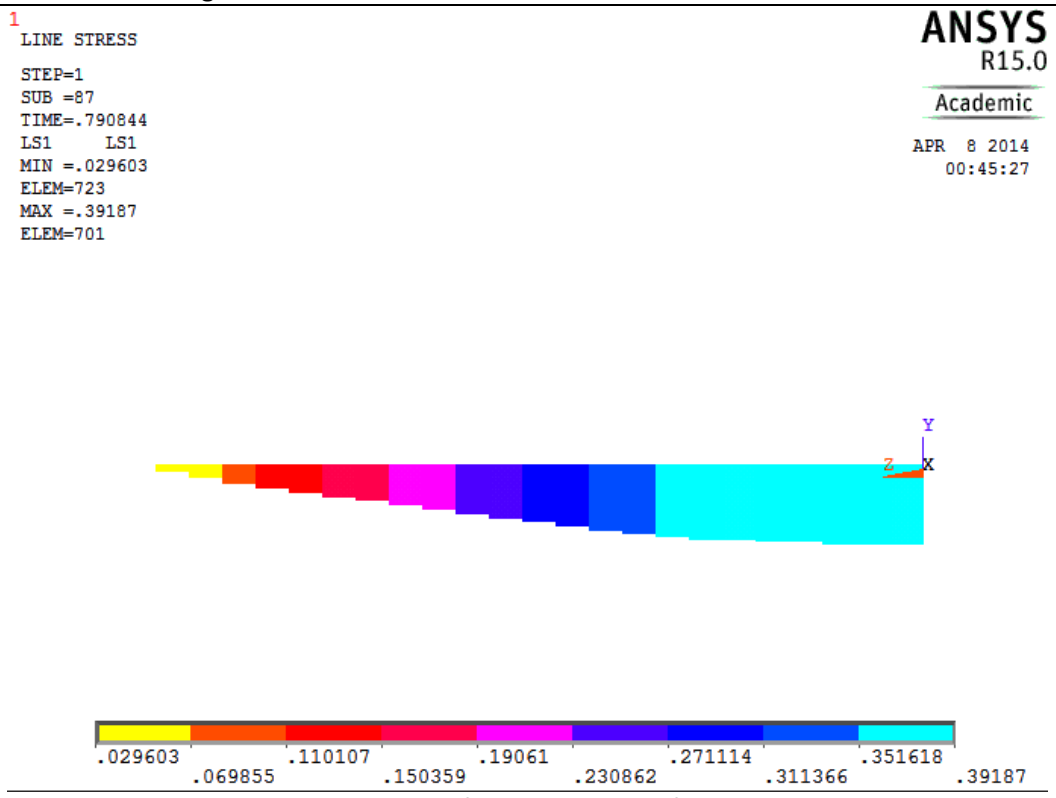

Figure D-156 Reinforcement Stress for 25-3-30

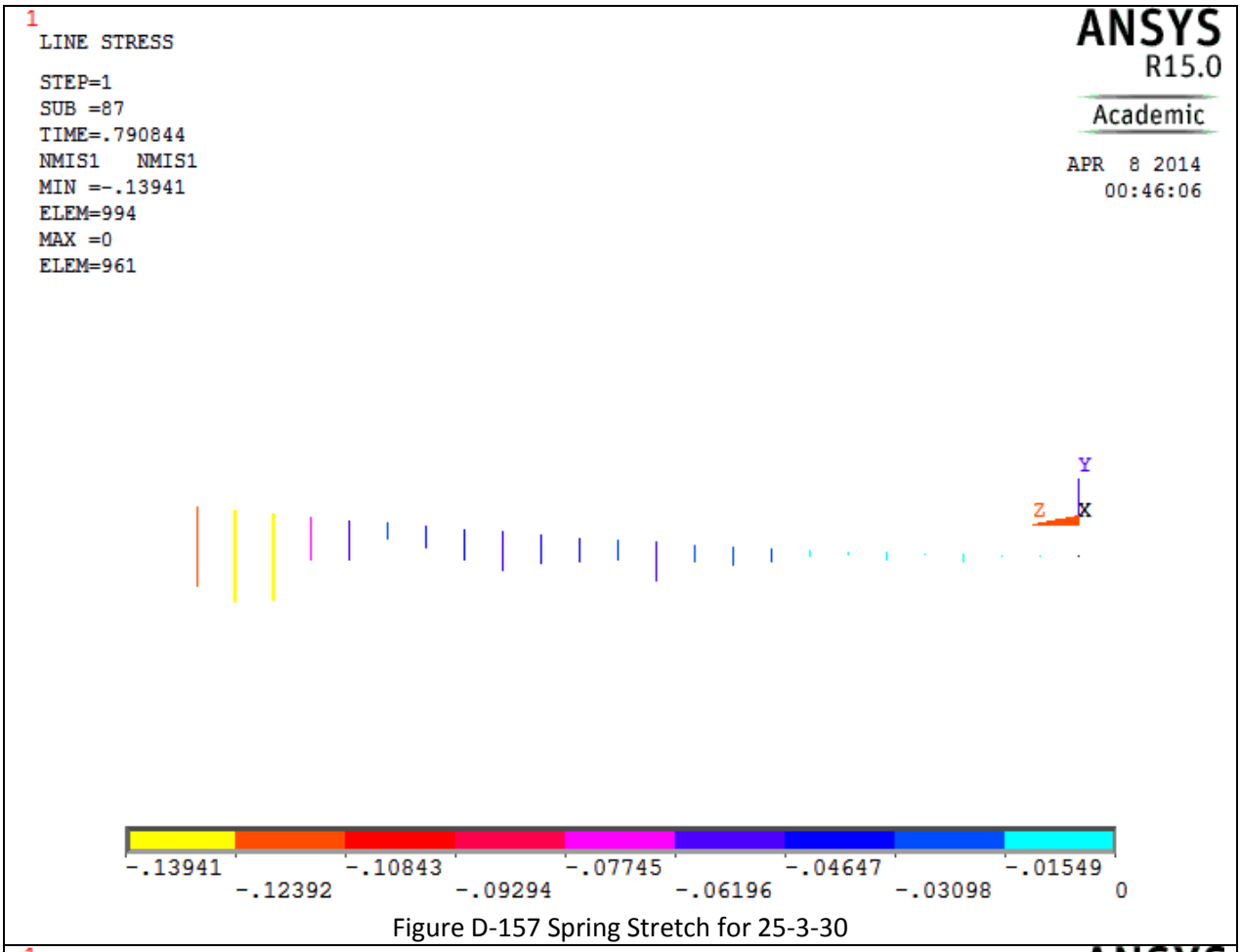

Figure D-157 Spring Stretch for 25-3-30

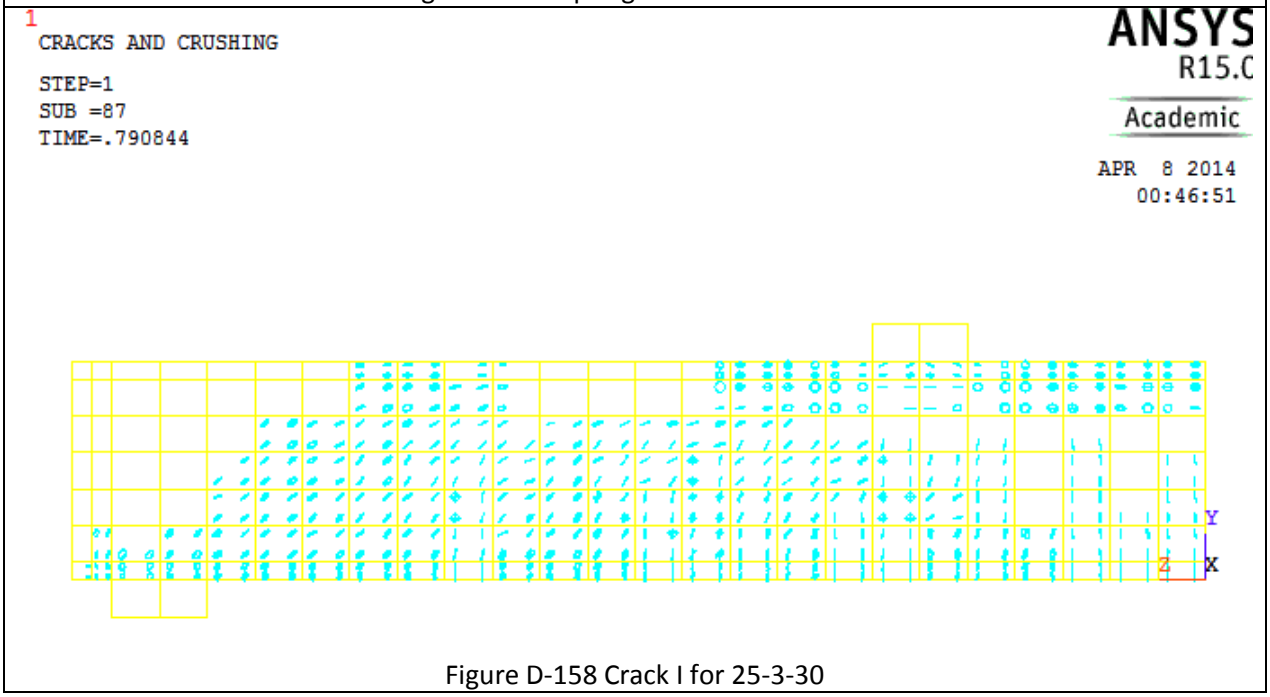

Figure D-158 Crack I for 25-3-30

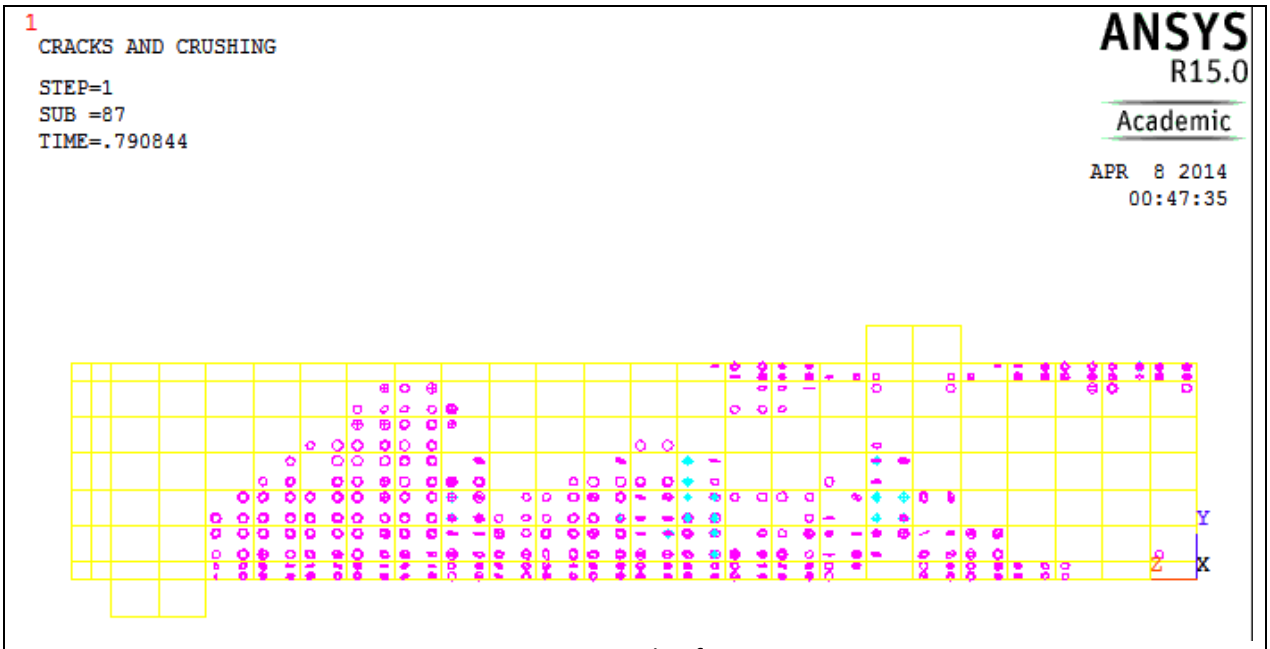

Figure D-159 Crack II for 25-3-30

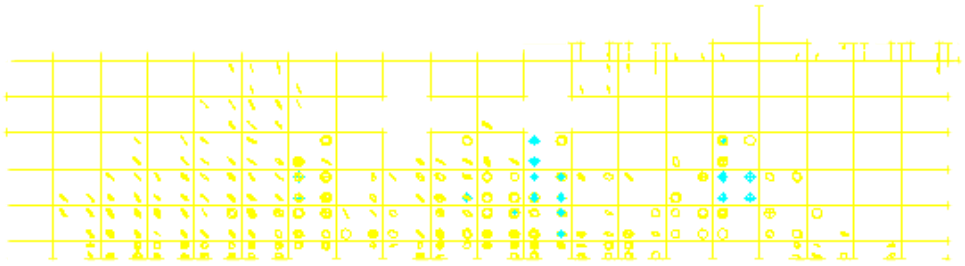

Figure D-160 Crack III for 25-3-30

Table D-21 Details of case 32-0

Case Name	Bottom Reinforcement	Honeycombing Location	Strength of Concrete(MPa)	Ultimate Load (kN)	Ultimate Deflection(mm)	Failure Mode
32-0	32mm	None	42.7	195.415	10.4612	

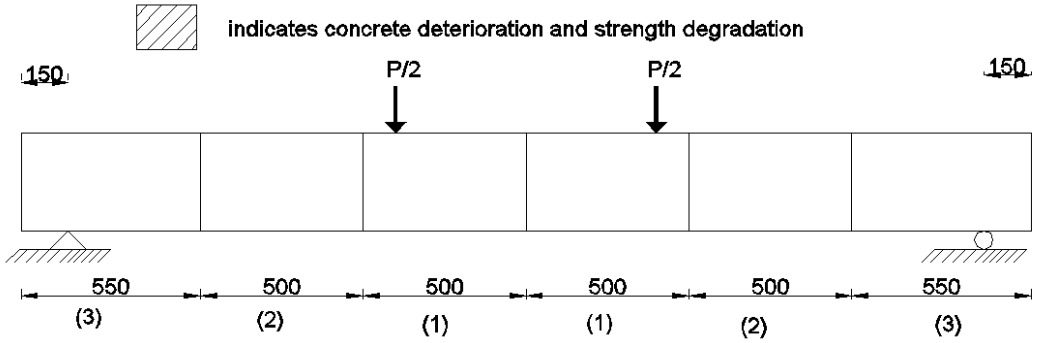

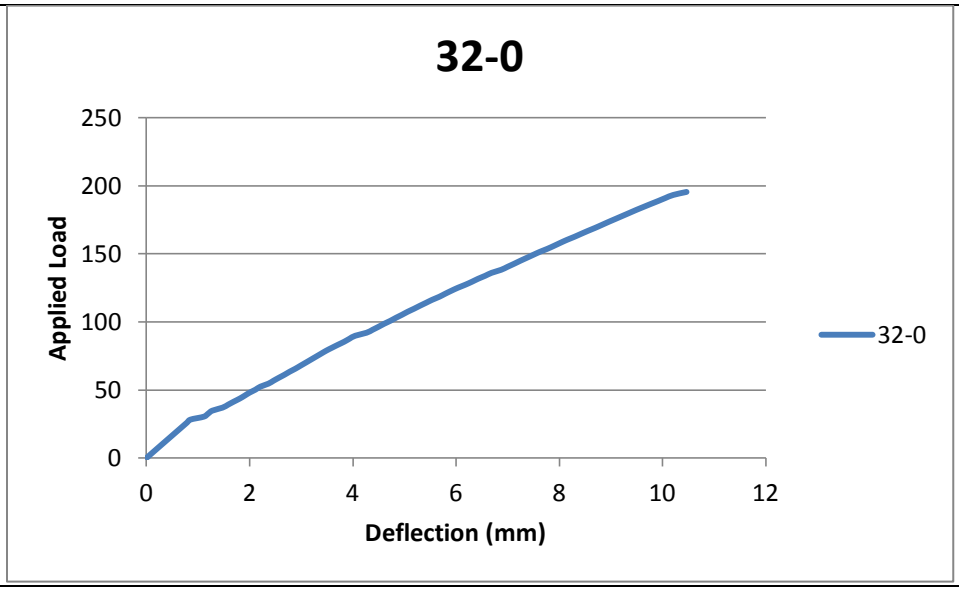

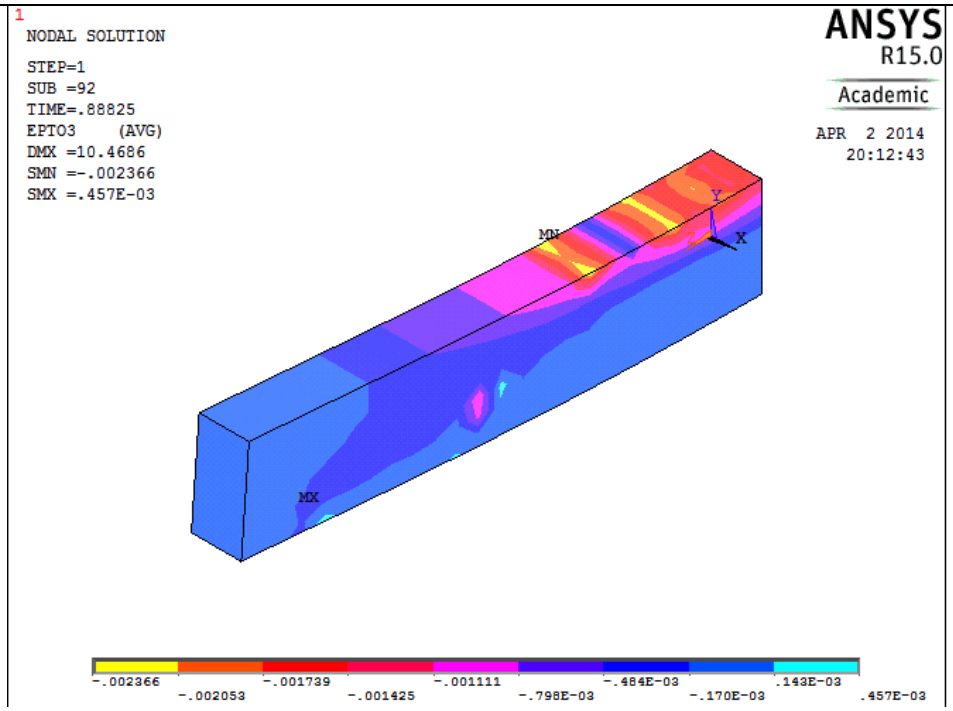

Figure D-161 Nodal solution – 3rd principal total mechanical strain for 32-0

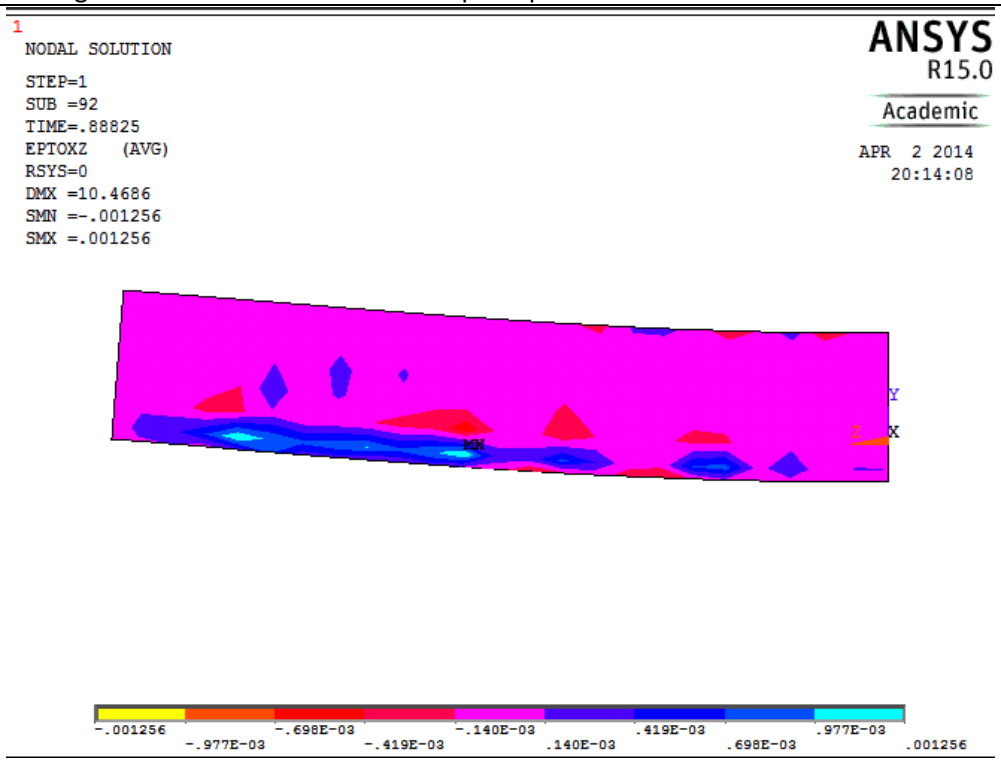

Figure D-162 Nodal Solution XZ shear total mechanical strain for 32-0

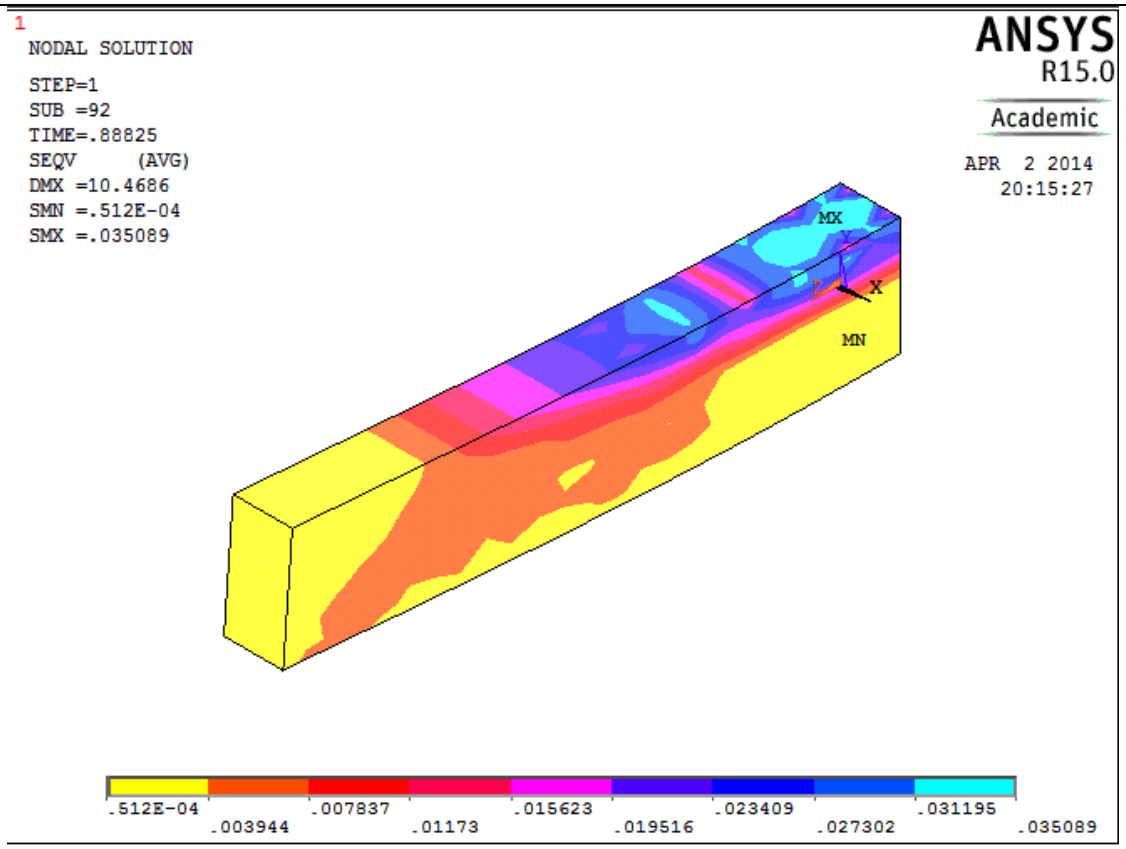

Figure D-163 Nodal Solution -Von Mises Stress for 32-0

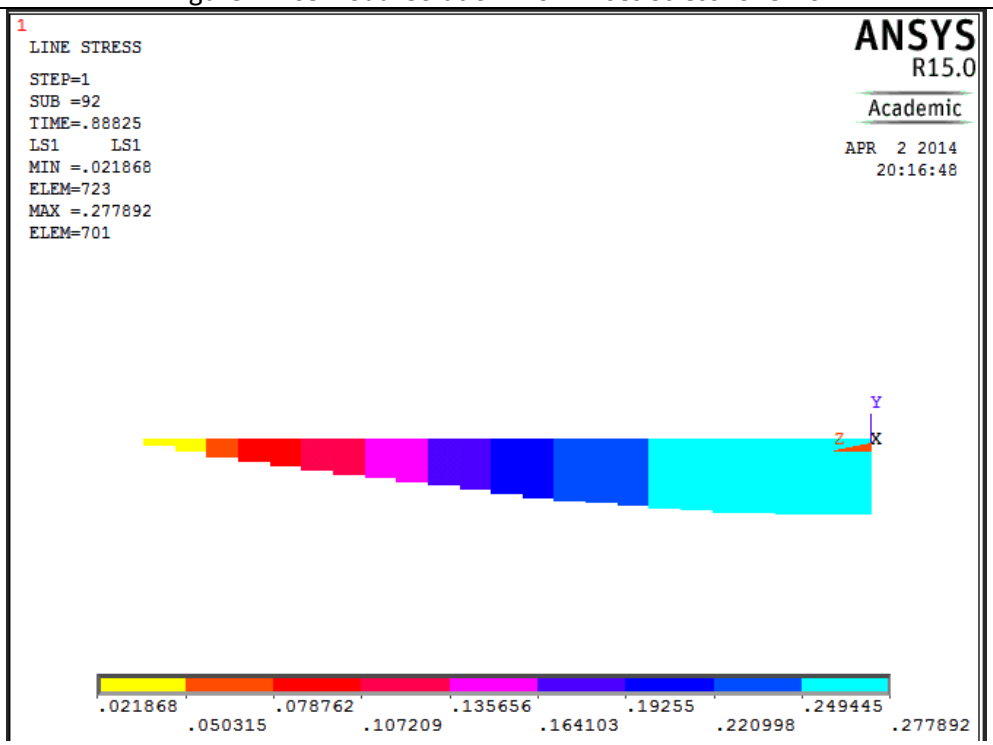

Figure D-164 Reinforcement Stress for 32-0

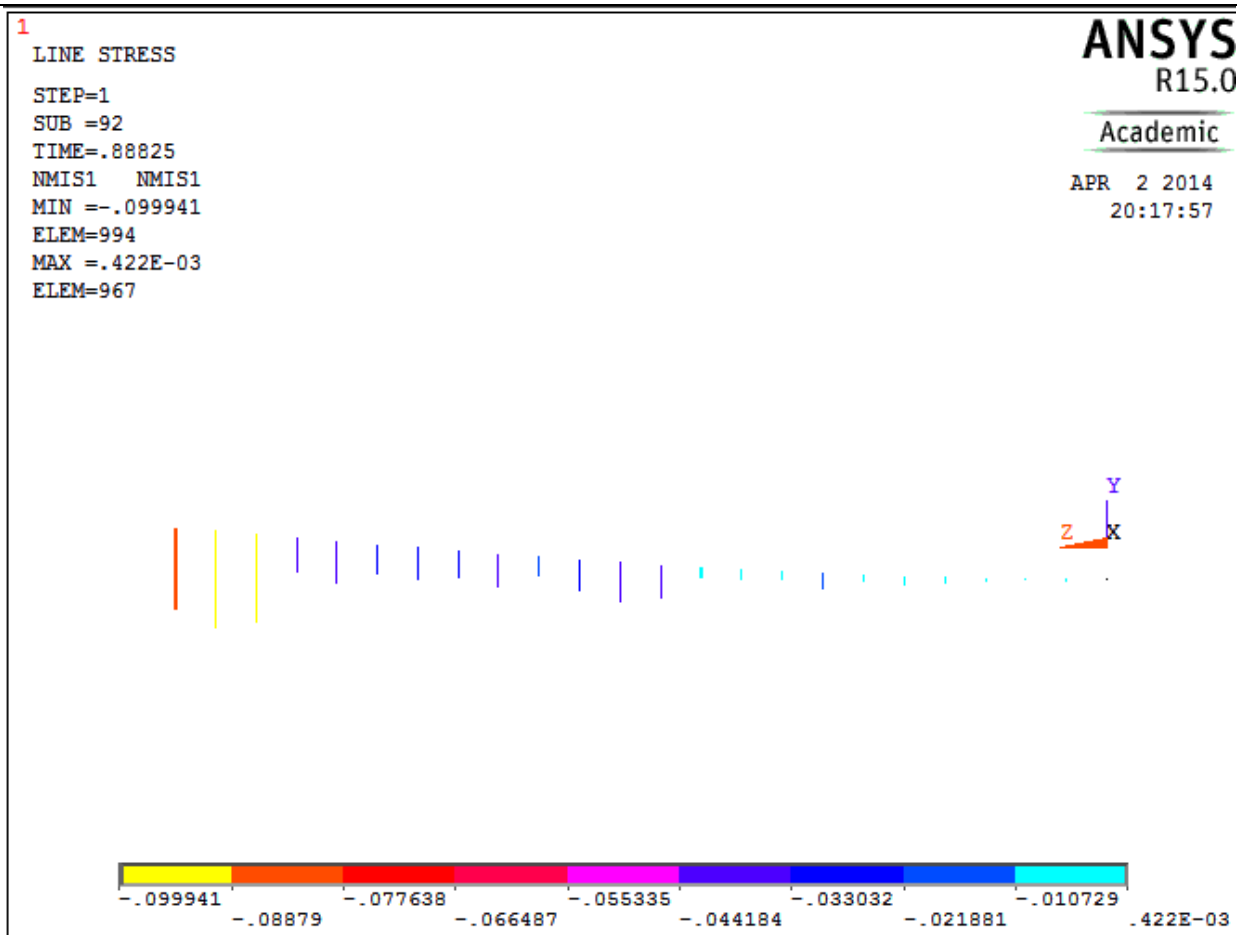

Figure D-165 Spring Stretch for 32-0

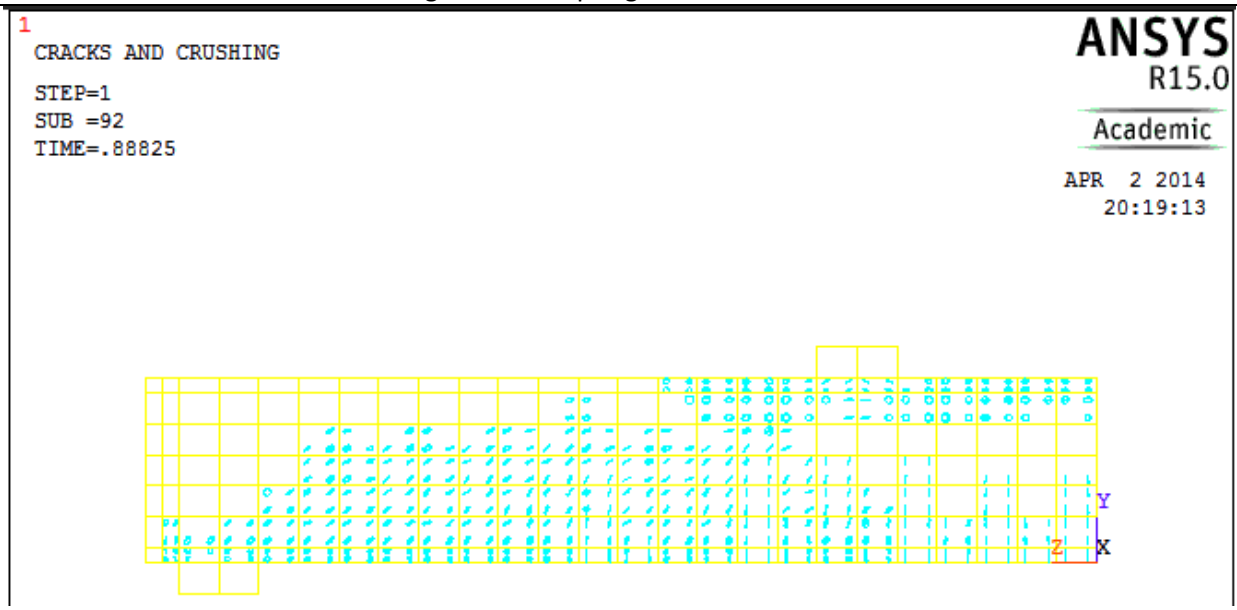

Figure D-166 Crack I for 32-0

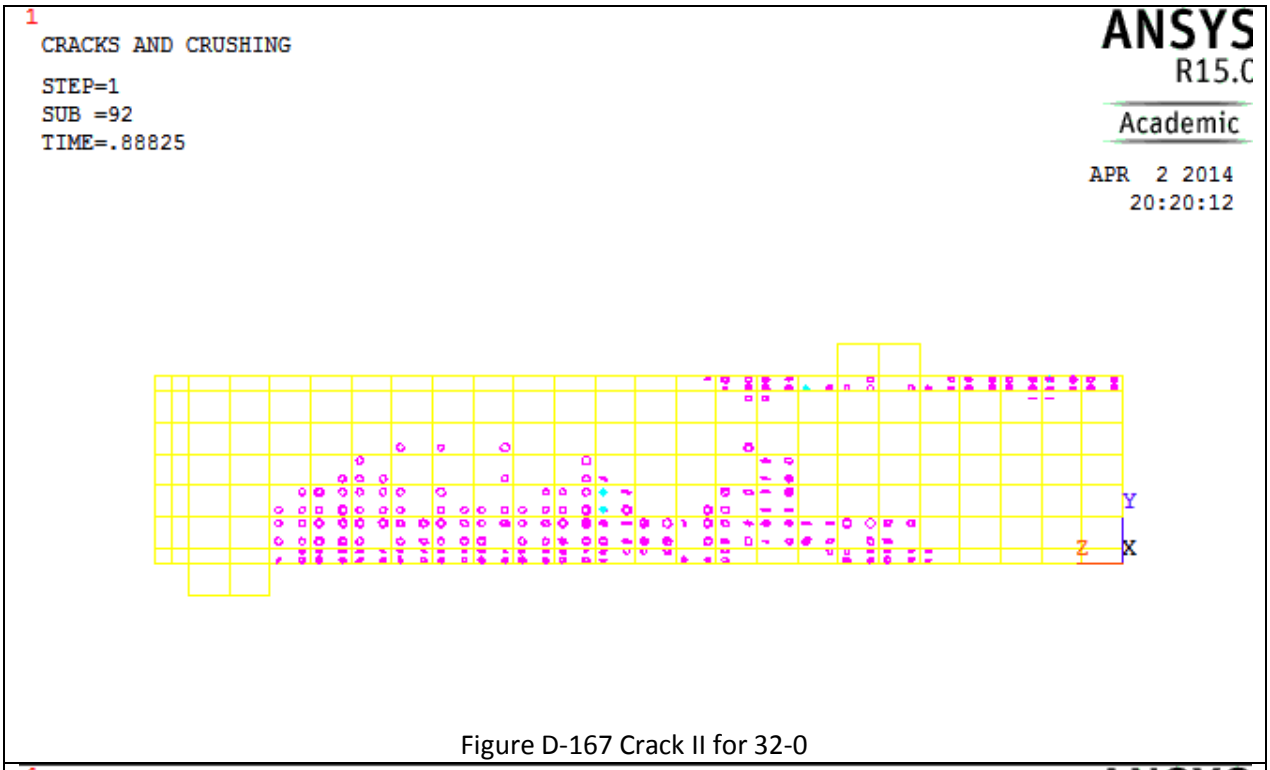

Figure D-167 Crack II for 32-0

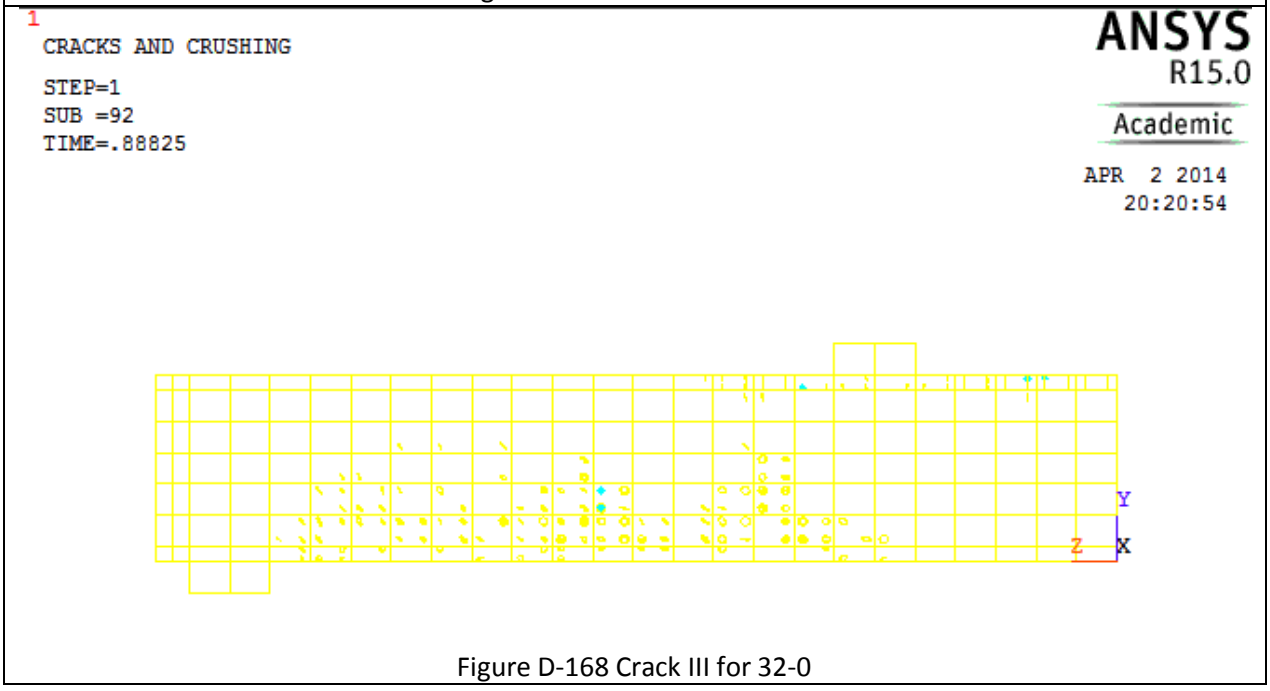

Figure D-168 Crack III for 32-0

Table D-22 Details of case 32-1-10

Case Name	Bottom Reinforcement	Honeycombing Location	Strength of Concrete(MPa)	Ultimate Load (kN)	Ultimate Deflection(mm)	Failure Mode
32-1-10	32mm	1	10	66.0484	4.19115	

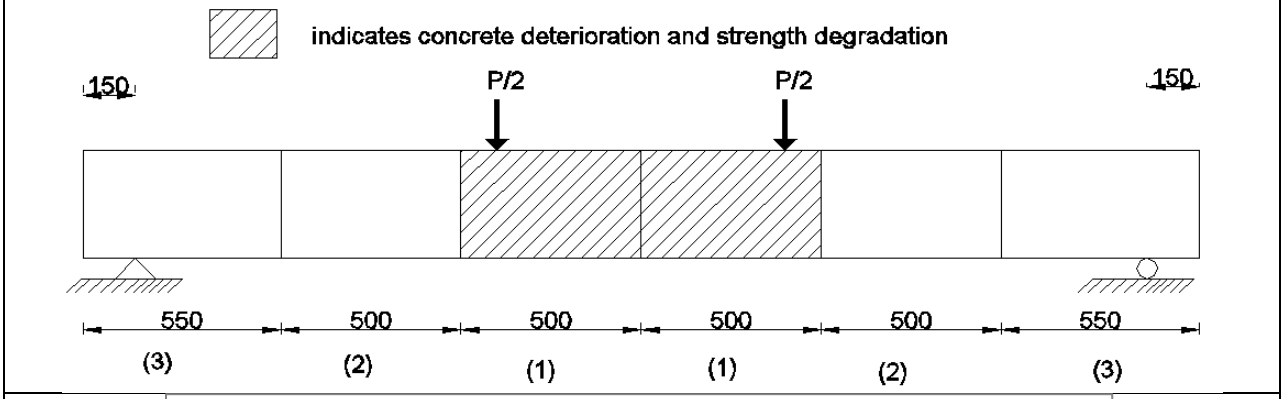

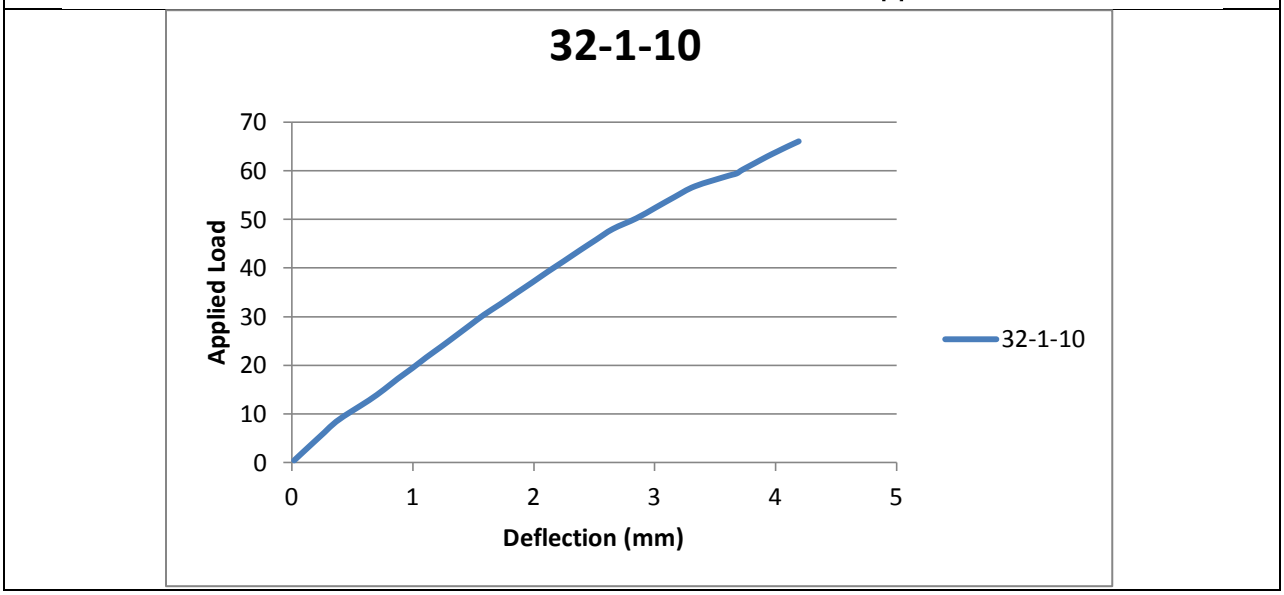

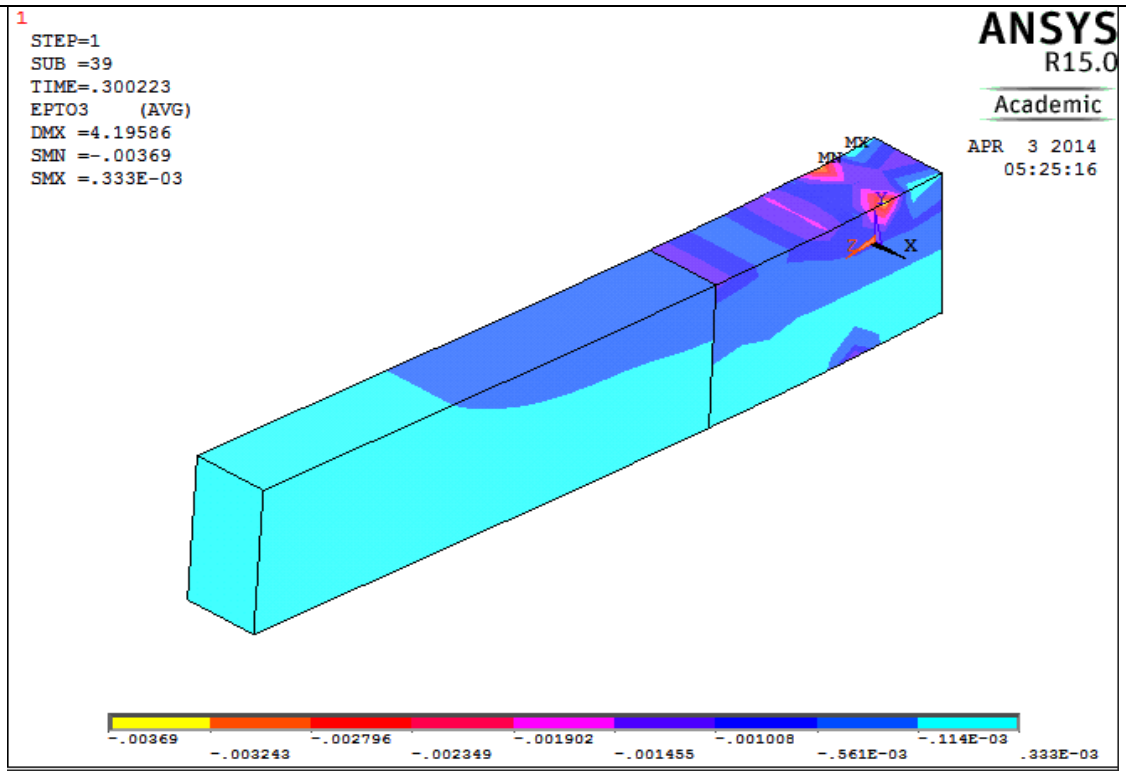

Figure D-169 Nodal solution – 3rd principal total mechanical strain for 32-1-10

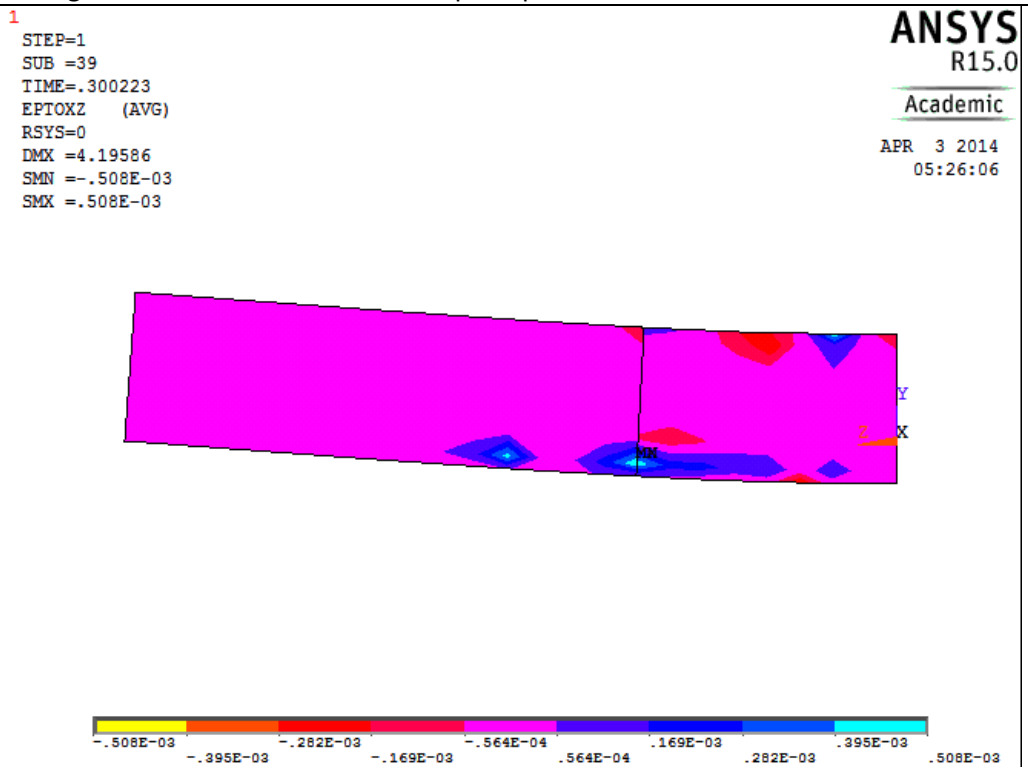

Figure D-170 Nodal Solution XZ shear total mechanical strain for 32-1-10

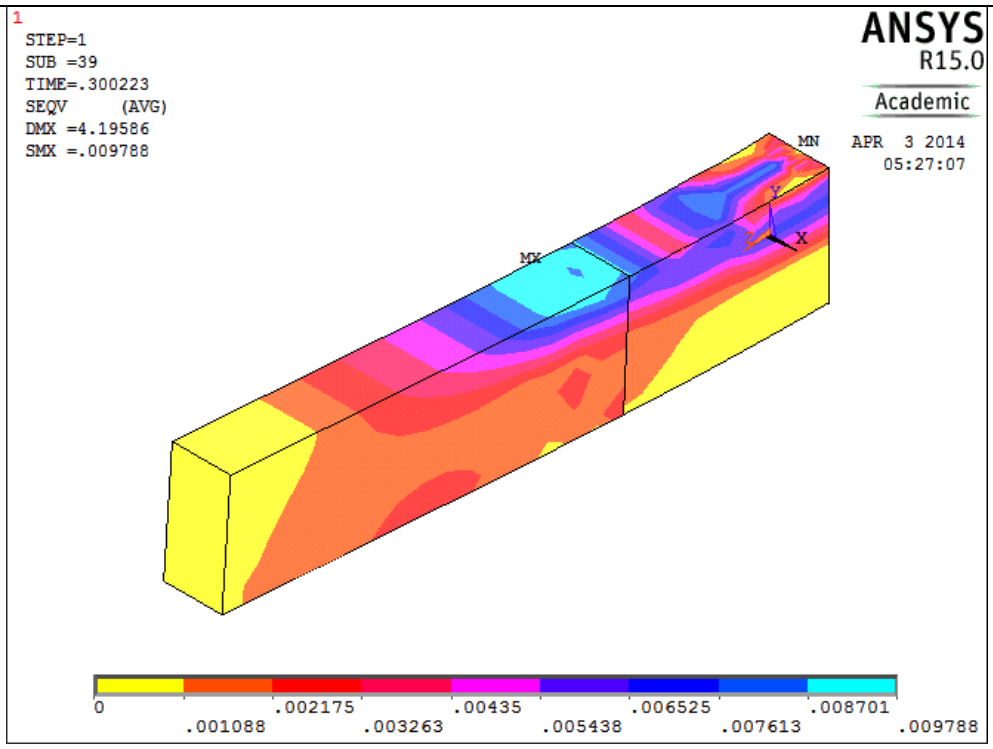

Figure D-171 Nodal Solution -Von Mises Stress for 32-1-10

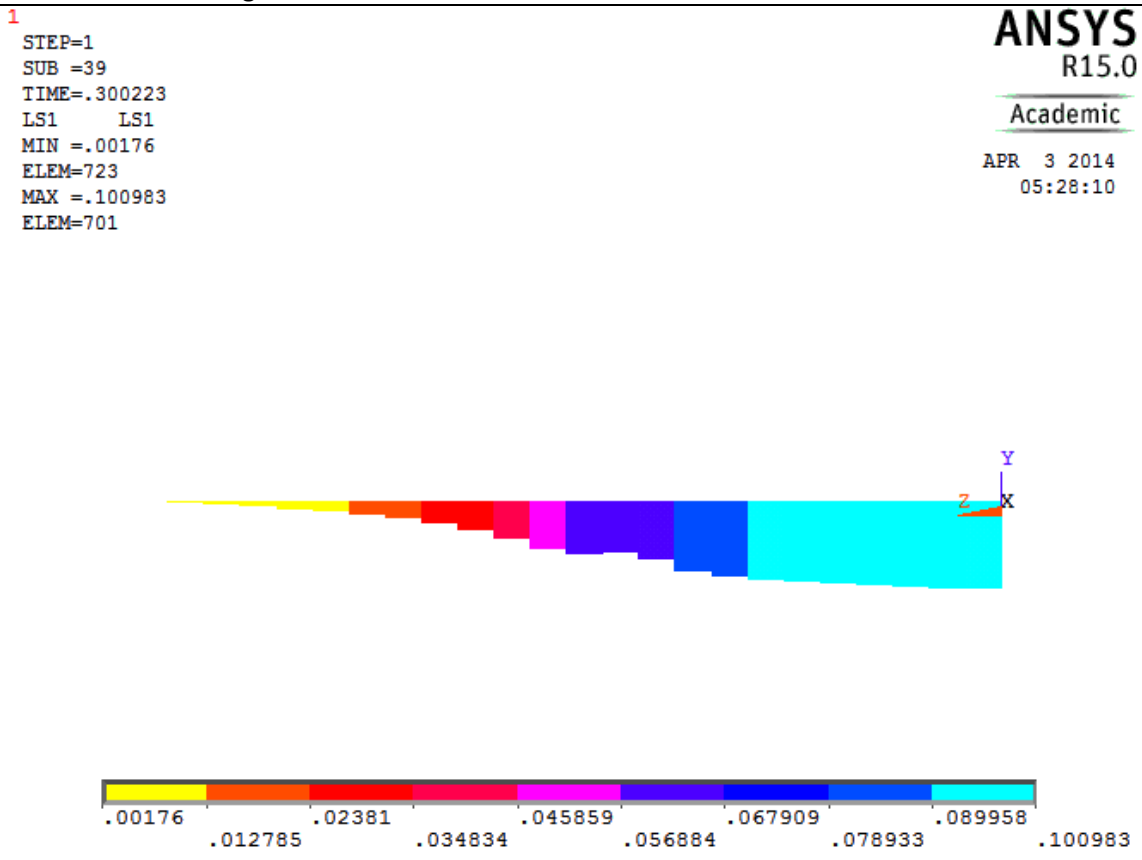

Figure D-172 Reinforcement Stress for 32-1-10

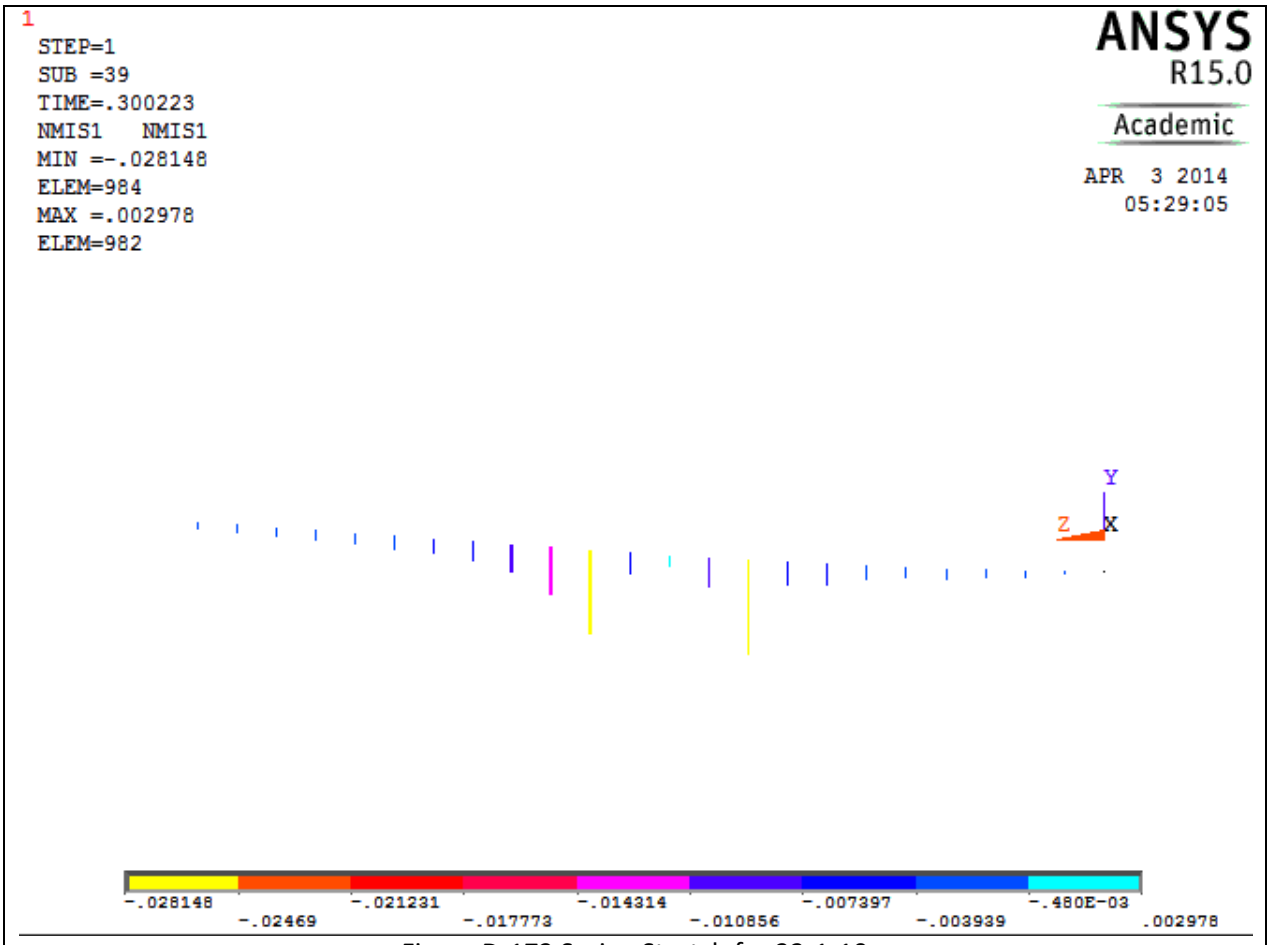

Figure D-173 Spring Stretch for 32-1-10

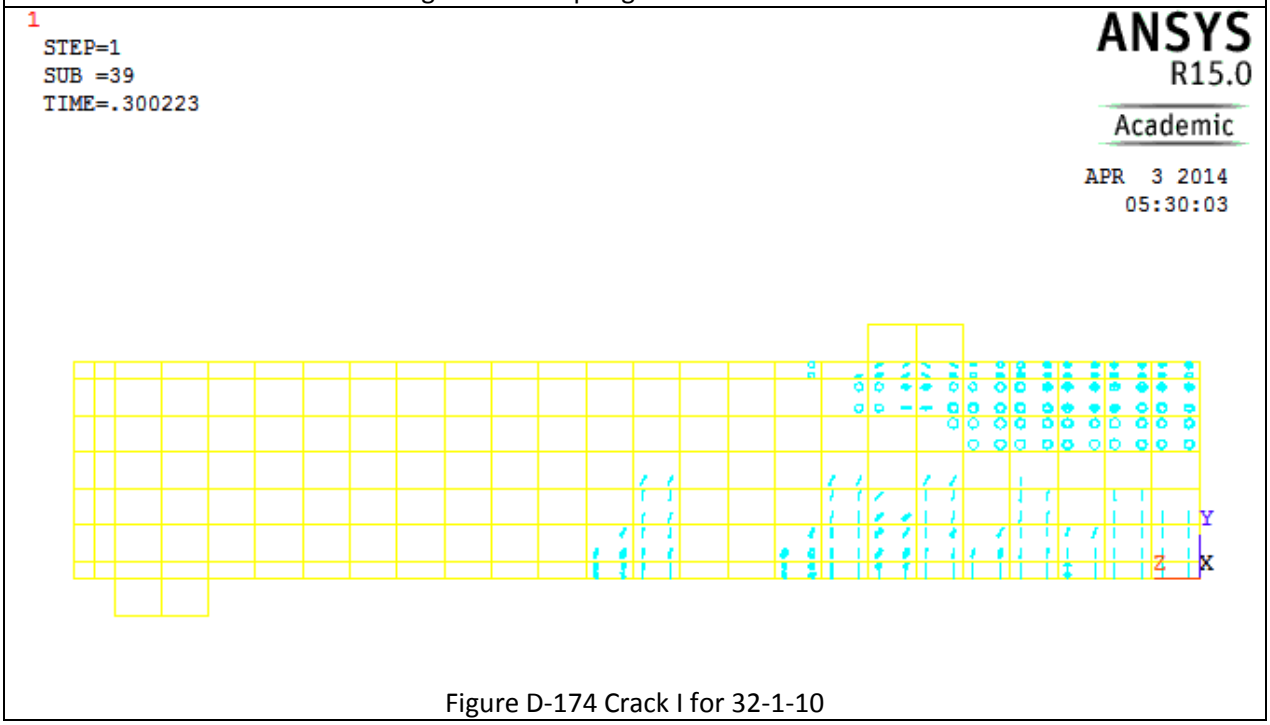

Figure D-174 Crack I for 32-1-10

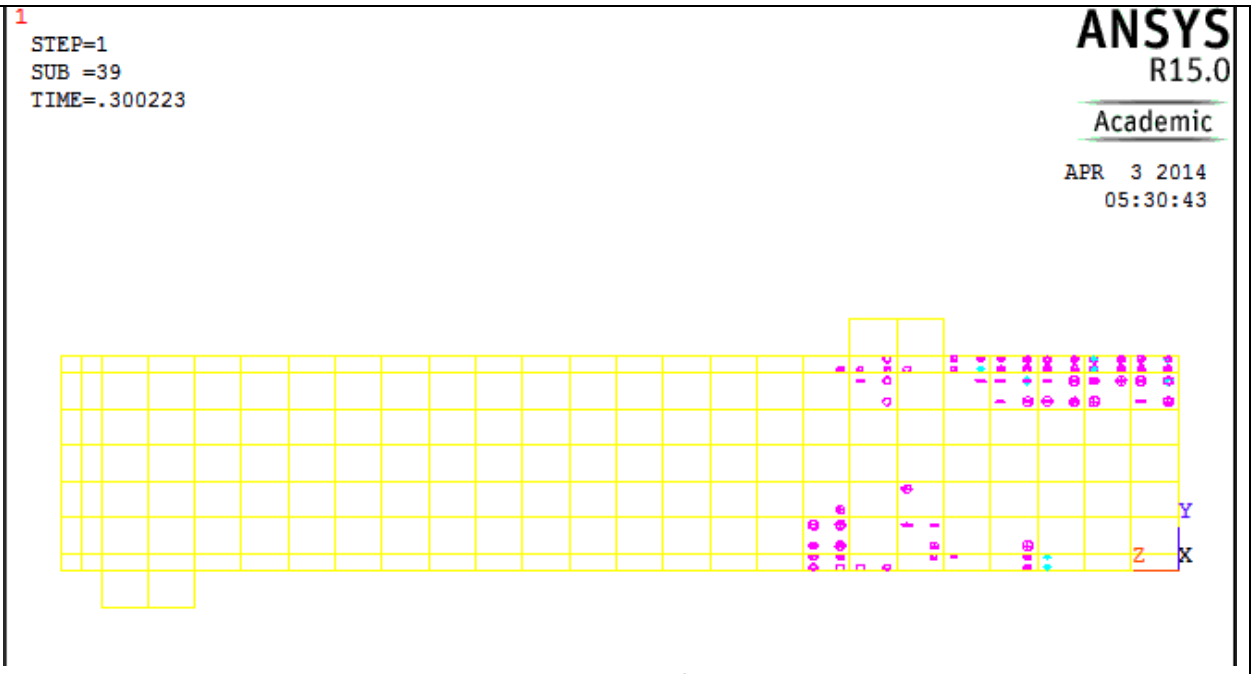

Figure D-175 Crack II for 32-1-10

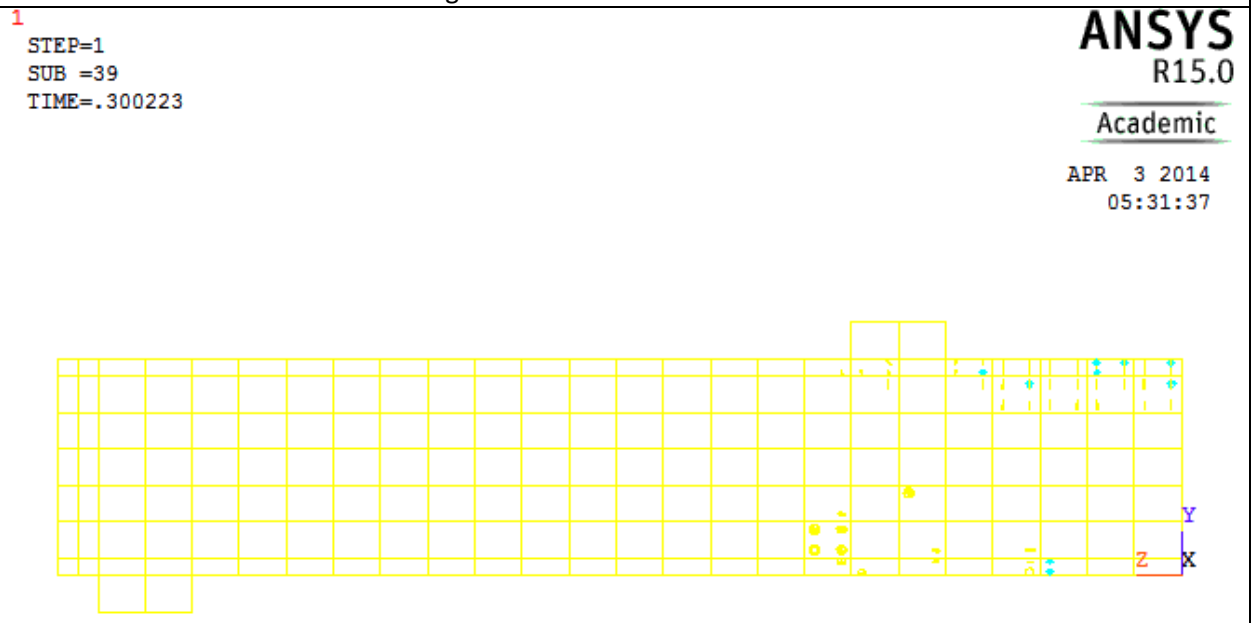

Figure D-176 Crack III for 32-1-10

Table D-23 Details of case 32-1-20

Case Name	Bottom Reinforcement	Honeycombing Location	Strength of Concrete(MPa)	Ultimate Load (kN)	Ultimate Deflection(mm)	Failure Mode
32-1-20	32mm	1	20	95.6318	5.31877	

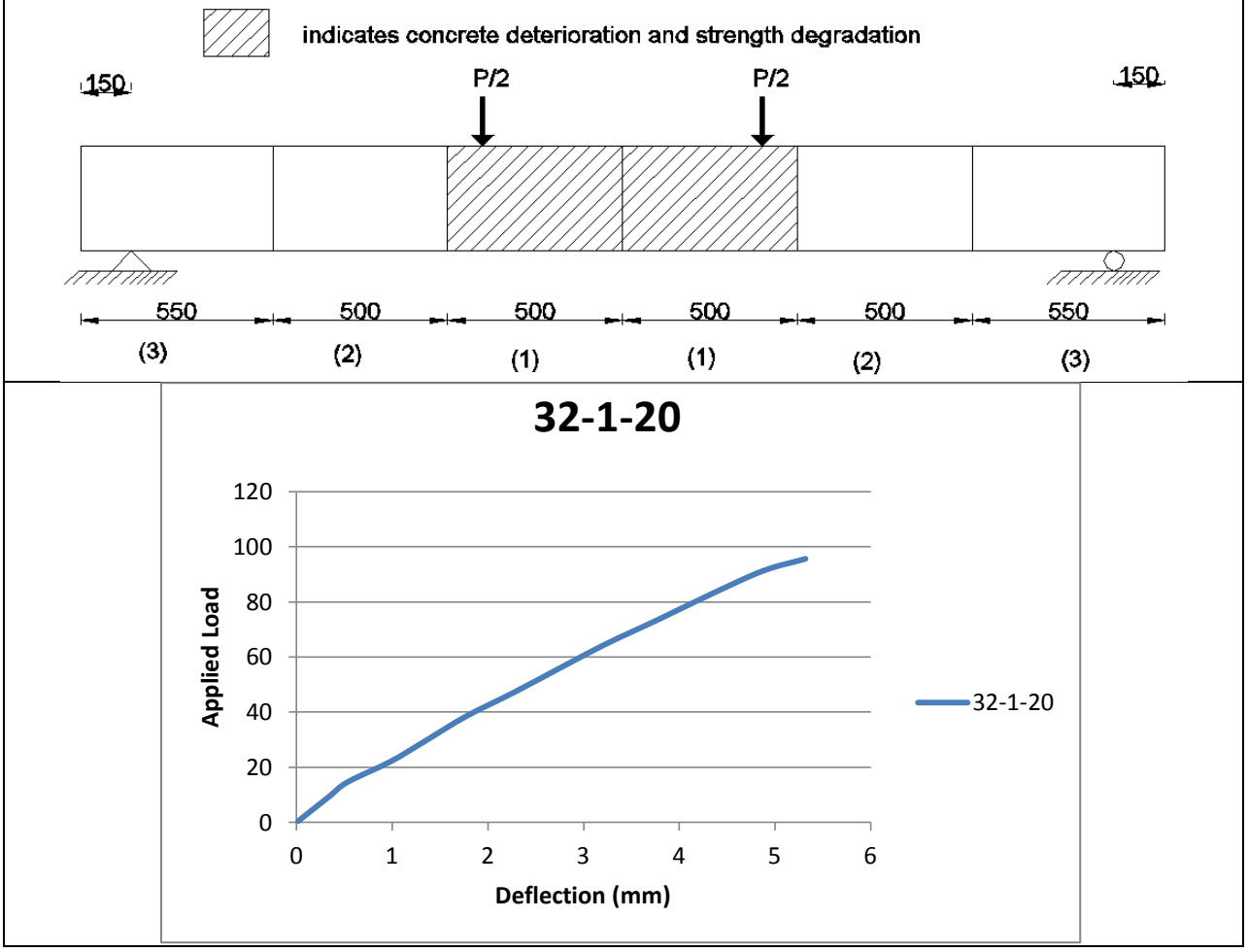

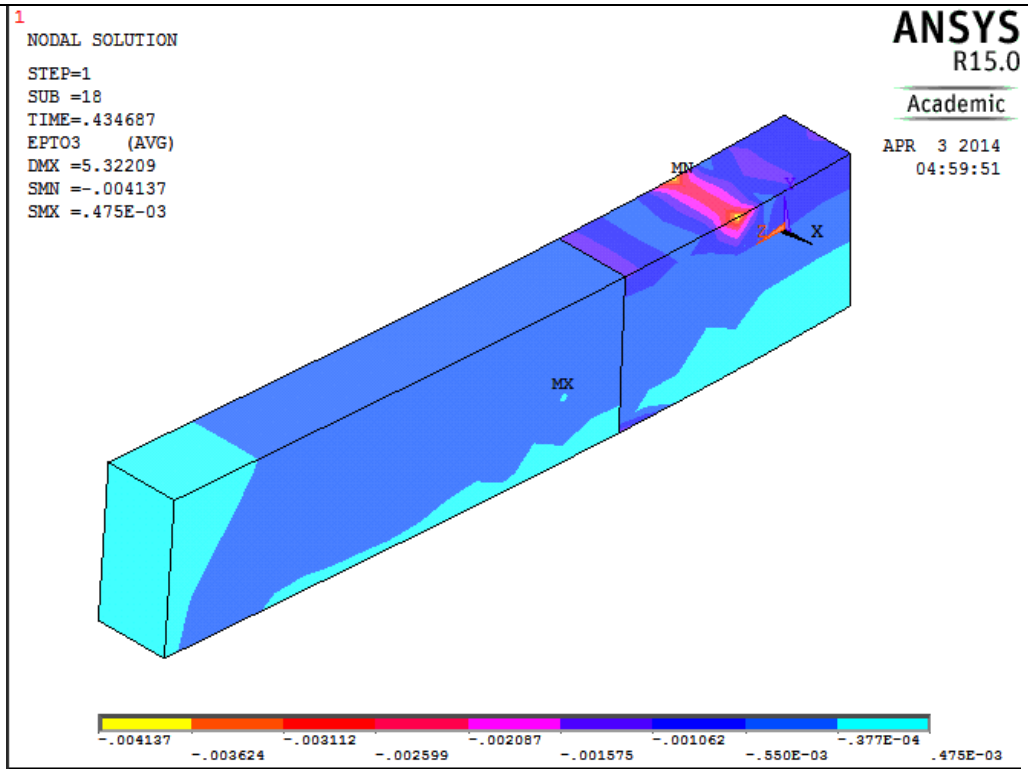

Figure D-177 Nodal solution – 3rd principal total mechanical strain for 32-1-20

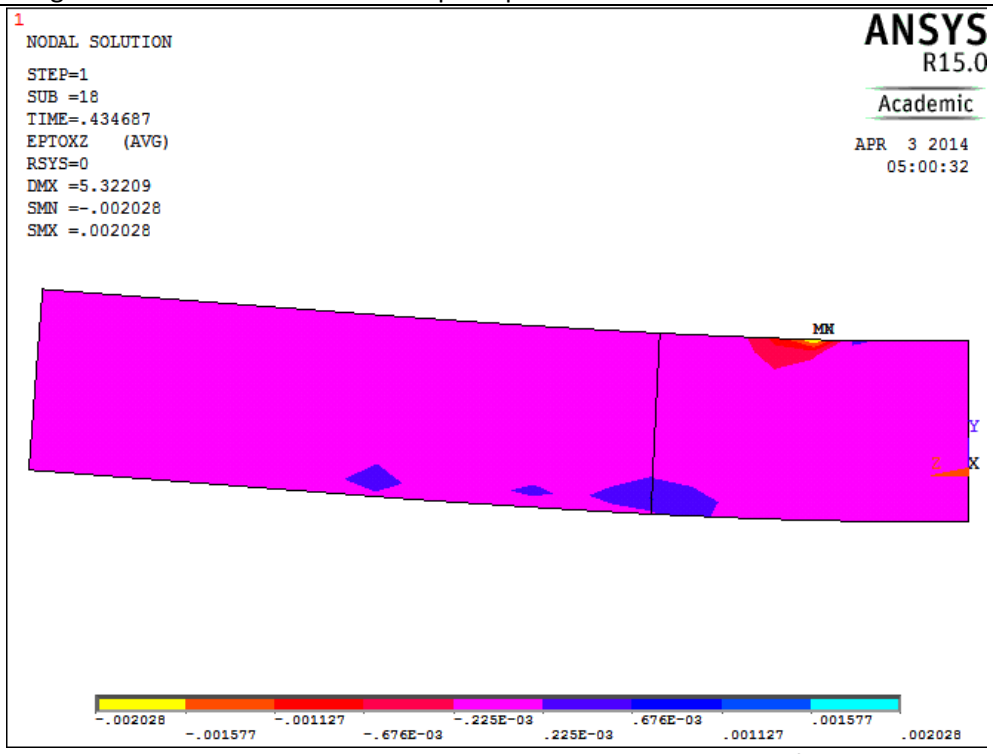

Figure D-178 Nodal Solution XZ shear total mechanical strain for 32-1-20

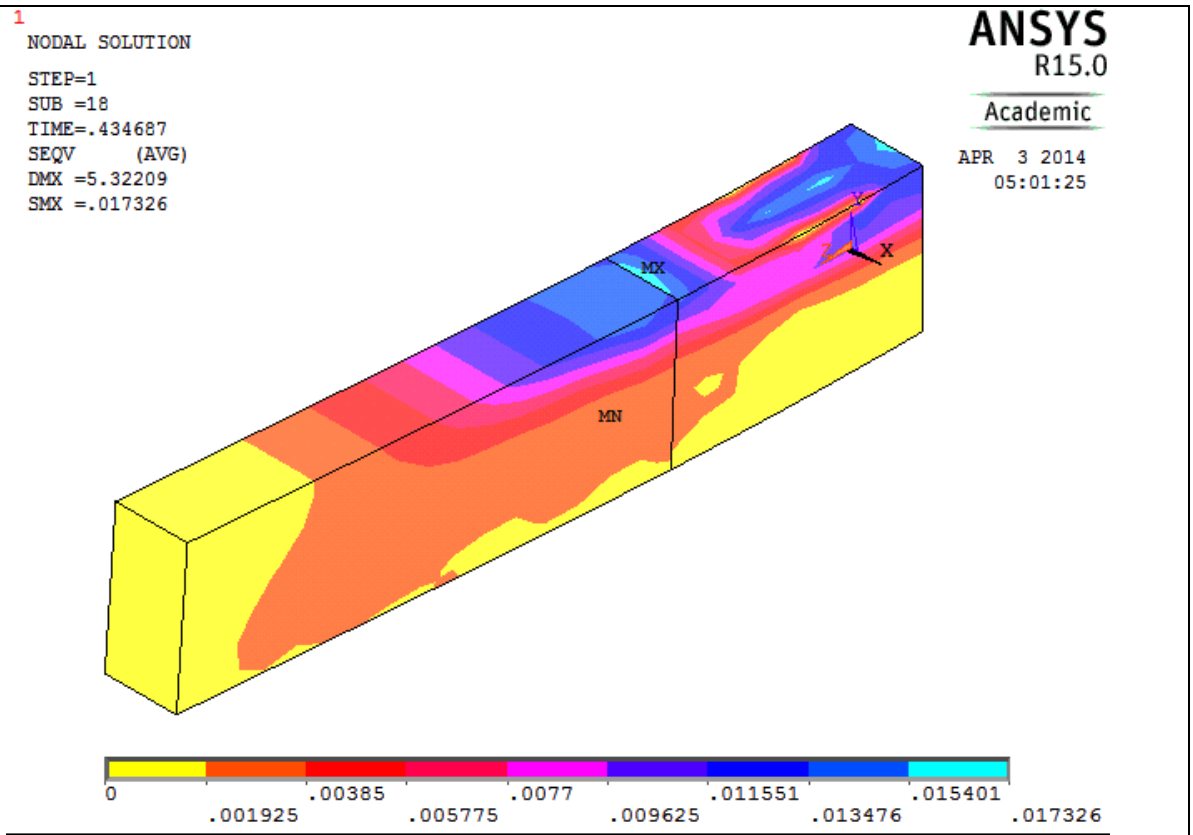

Figure D-179 Nodal Solution -Von Mises Stress for 32-1-20

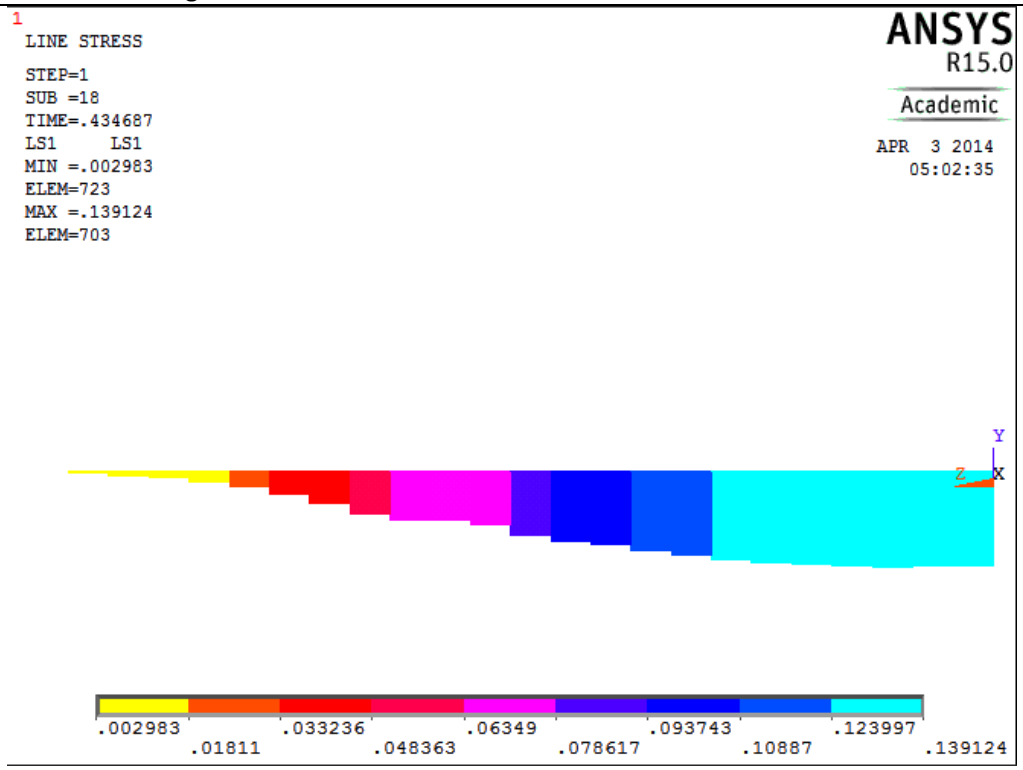

Figure D-180 Reinforcement Stress for 32-1-20

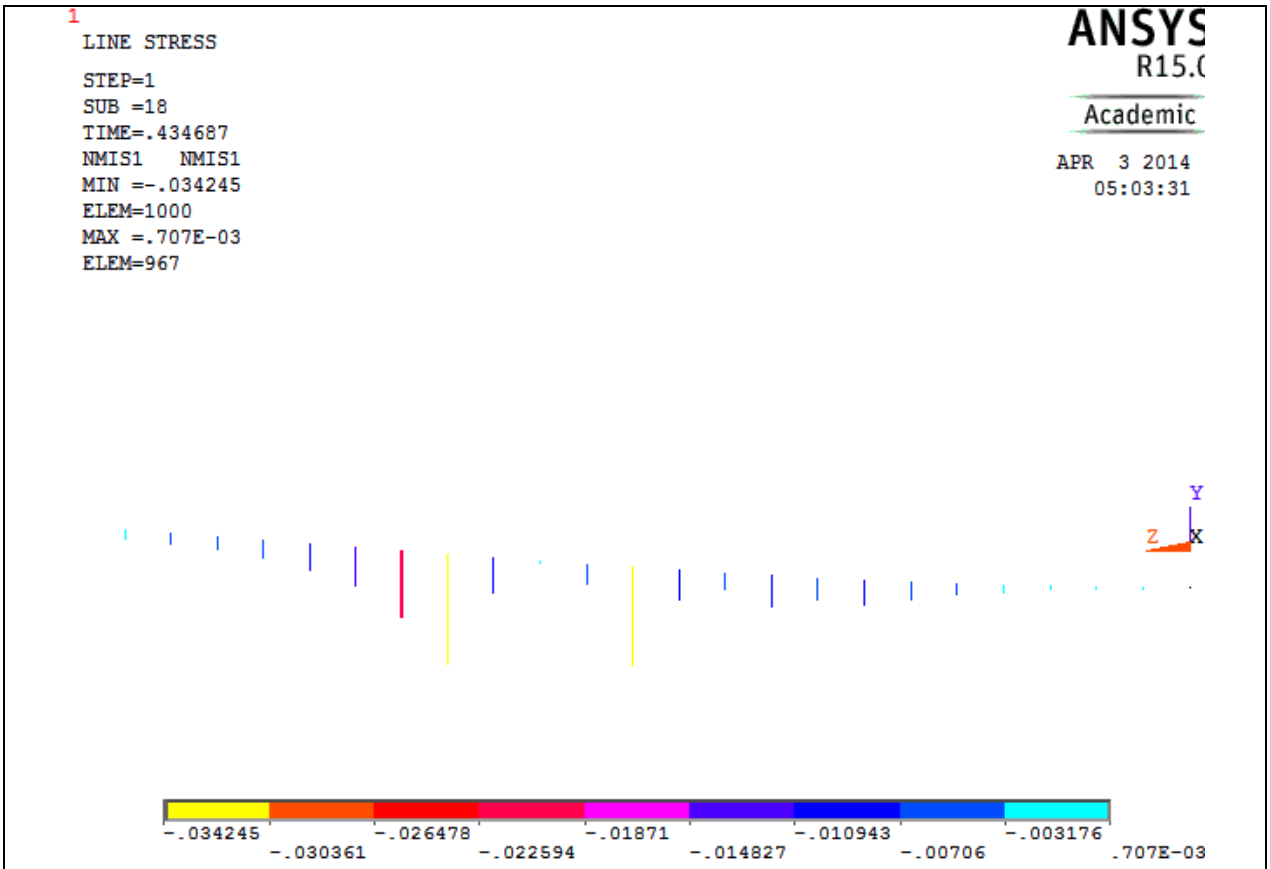

Figure D-181 Spring Stretch for 32-1-20

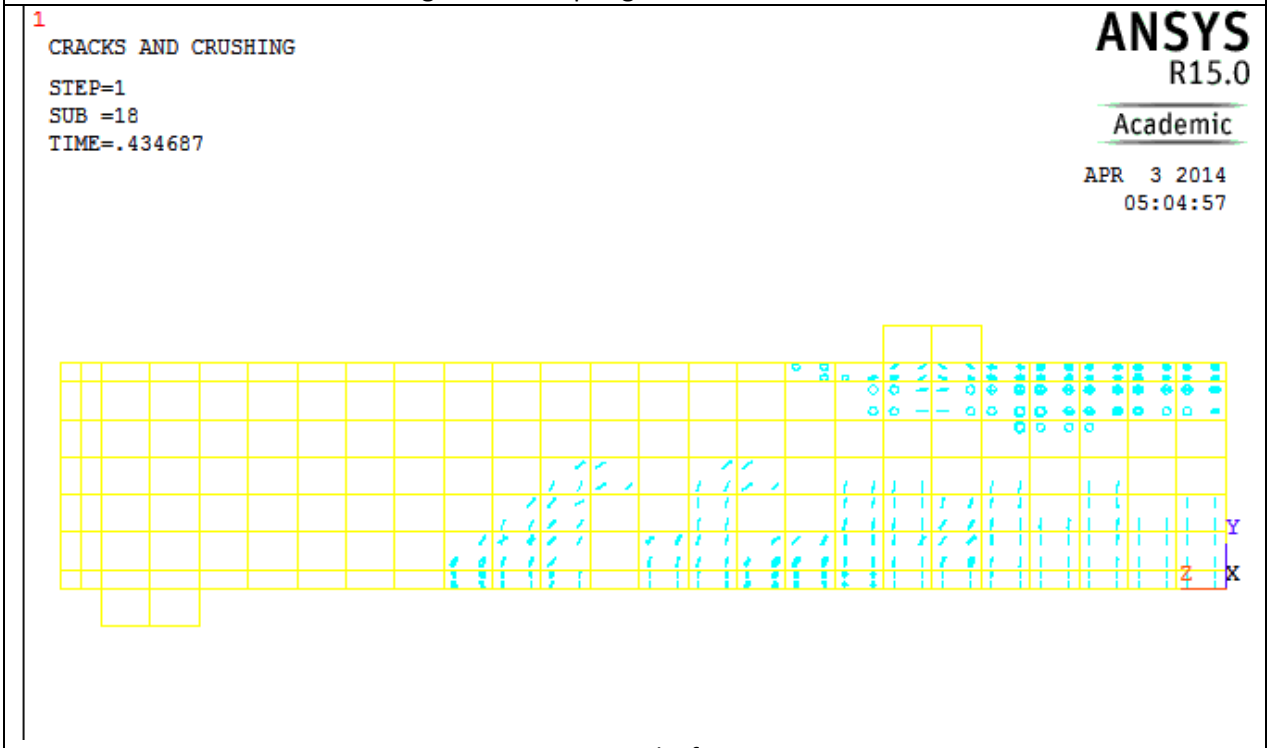

Figure D-182 Crack I for 32-1-20

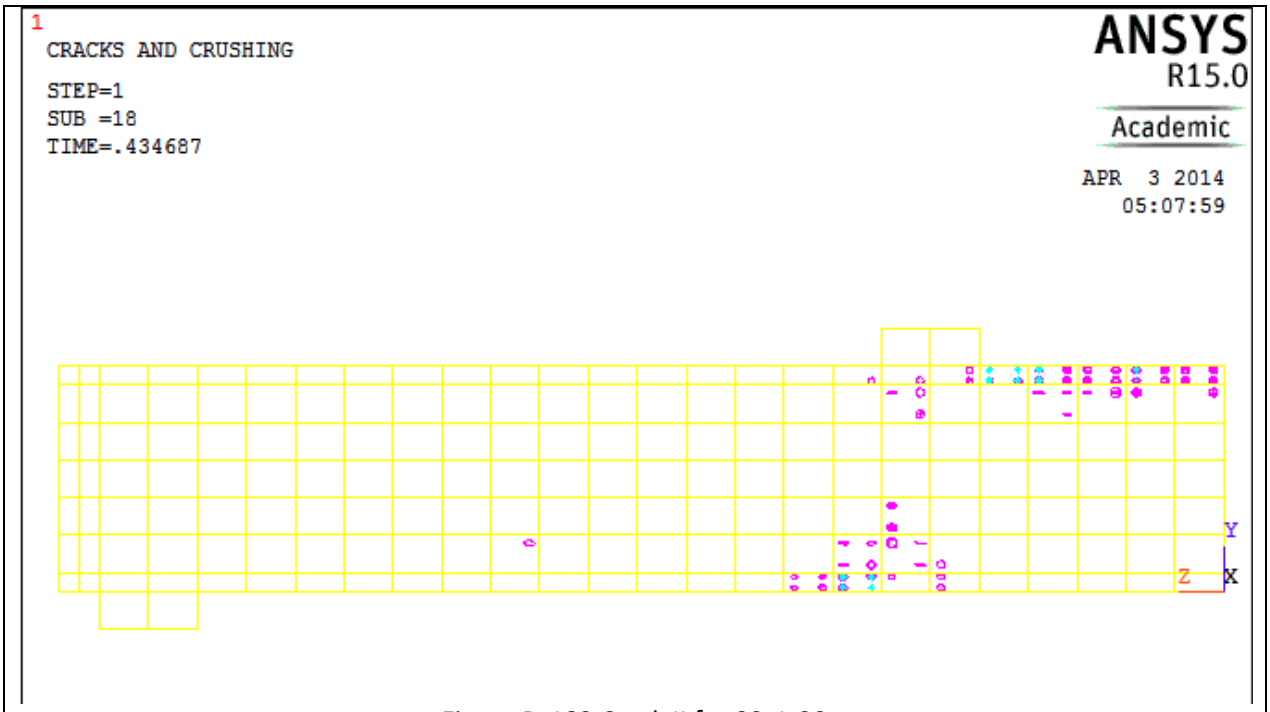

Figure D-183 Crack II for 32-1-20

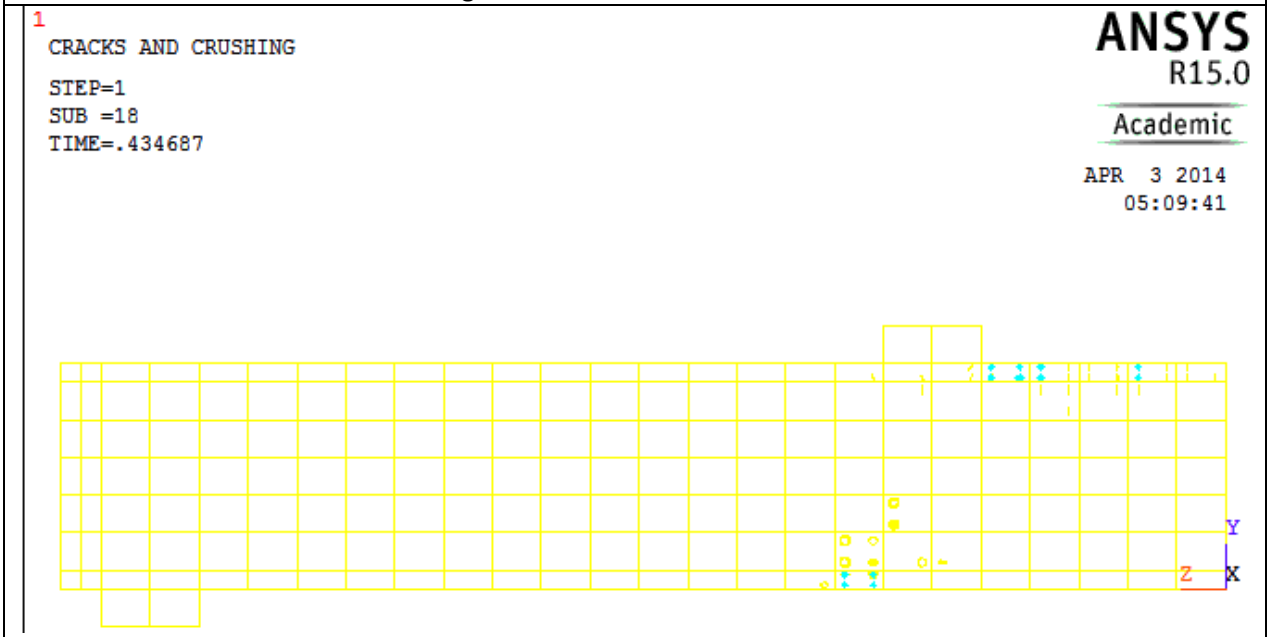

Figure D-184 Crack III for 32-1-20

Table D-24 Details of case 32-1-30

Case Name	Bottom Reinforcement	Honeycombing Location	Strength of Concrete(MPa)	Ultimate Load (kN)	Ultimate Deflection(mm)	Failure Mode
32-1-30	32mm	1	30	161.315	9.03126	

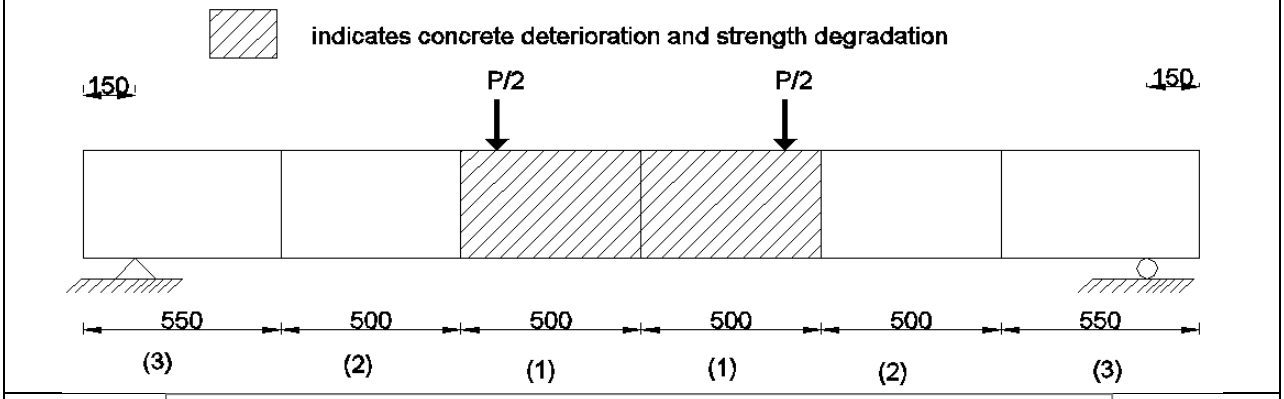

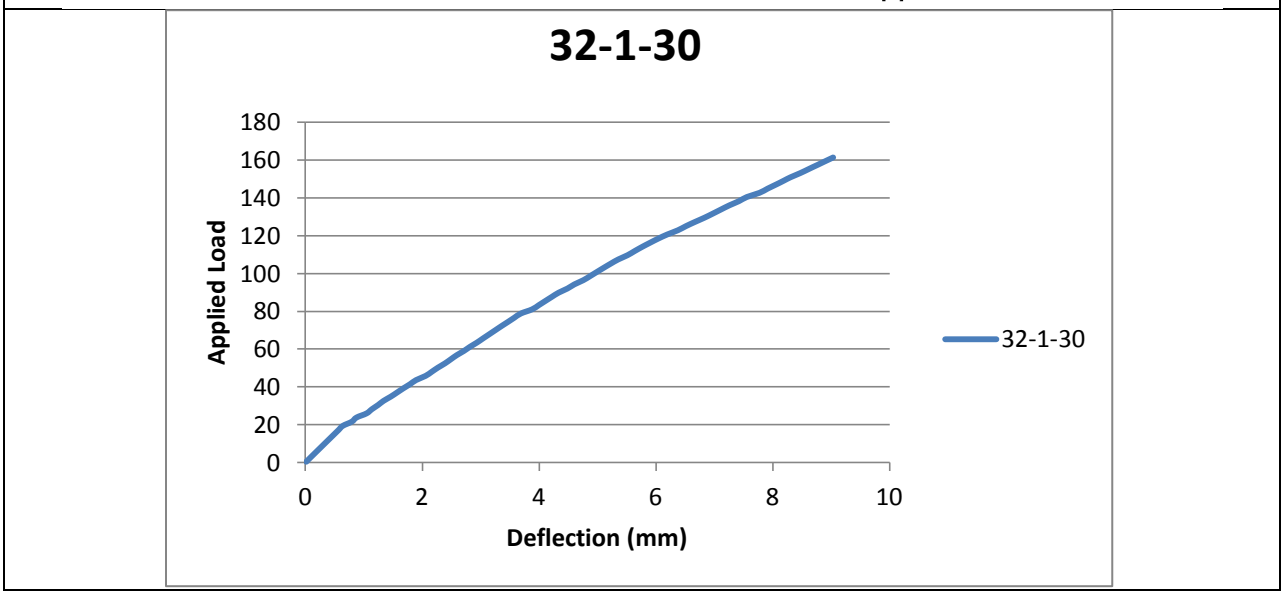

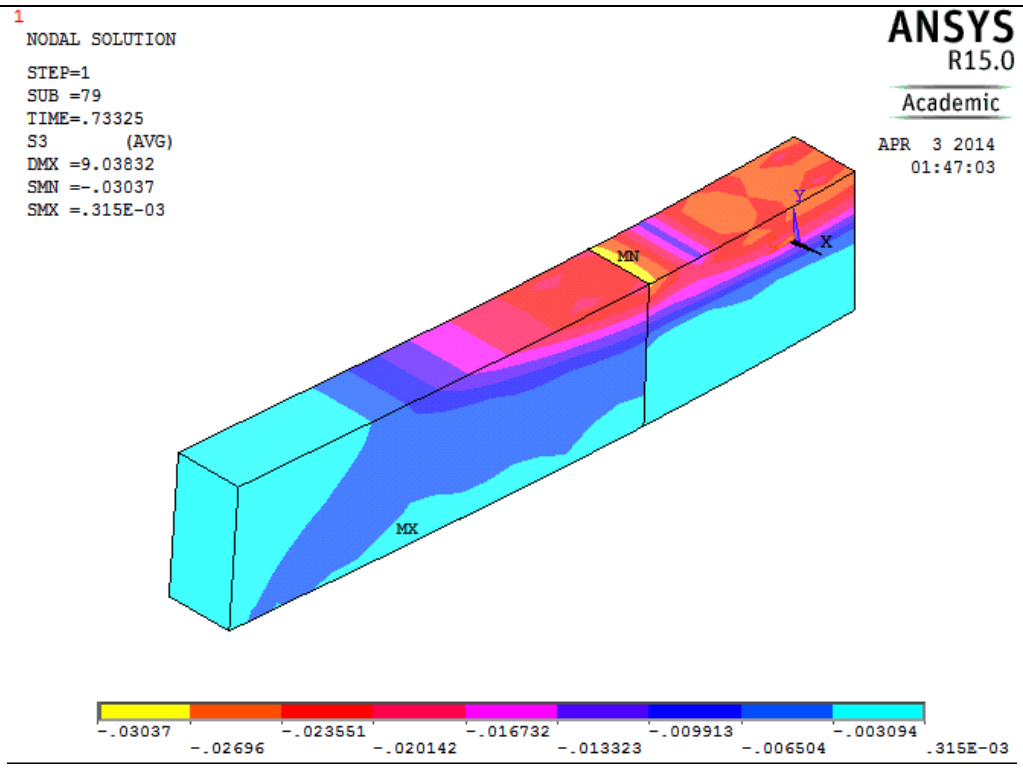

Figure D-185 Nodal solution – 3rd principal total mechanical strain for 32-1-30

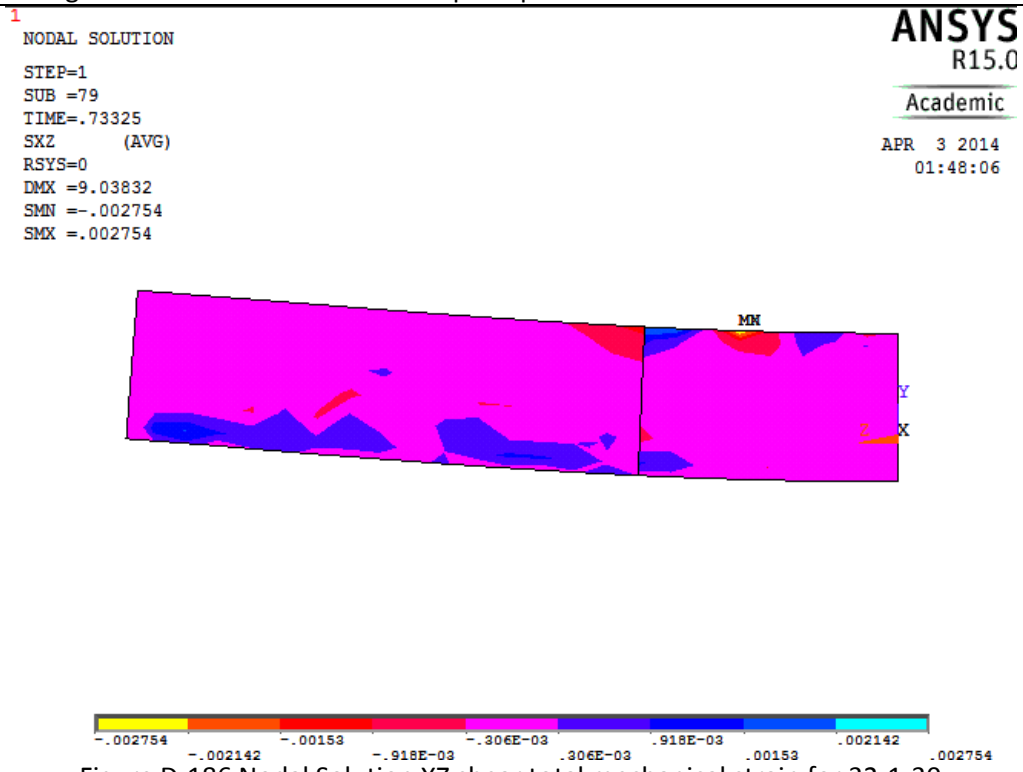

Figure D-186 Nodal Solution XZ shear total mechanical strain for 32-1-30

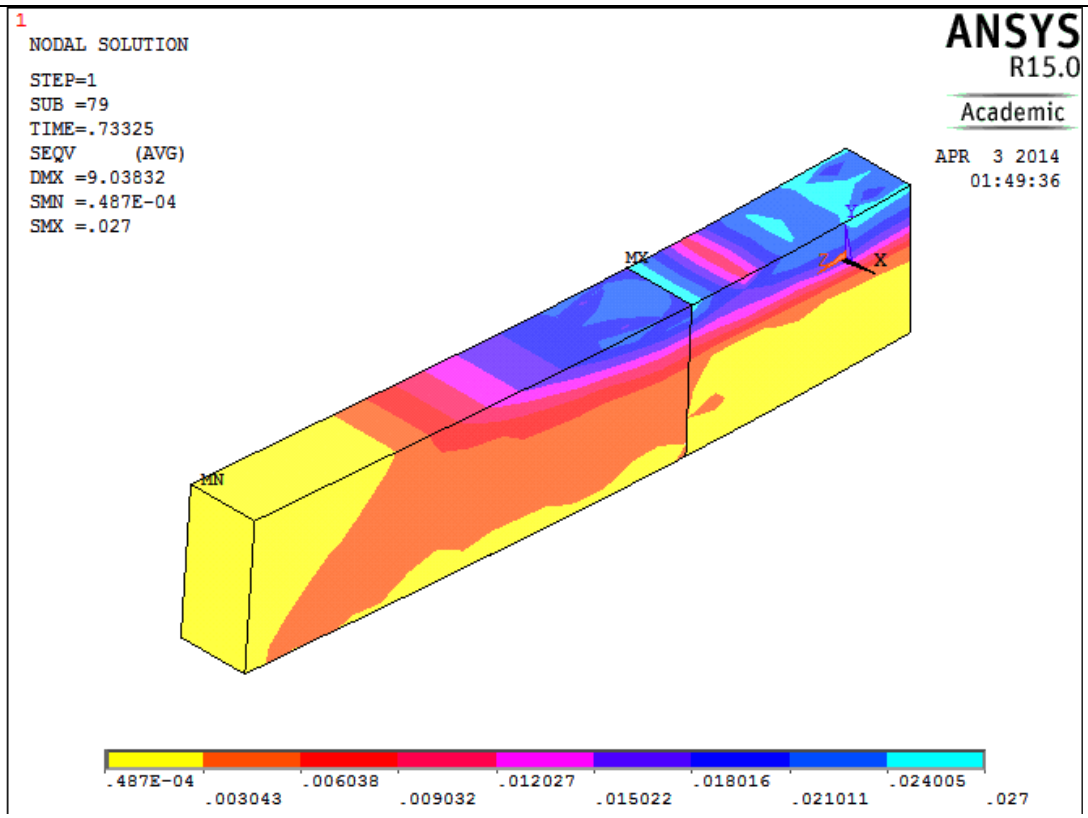

Figure D-187 Nodal Solution -Von Mises Stress for 32-1-30

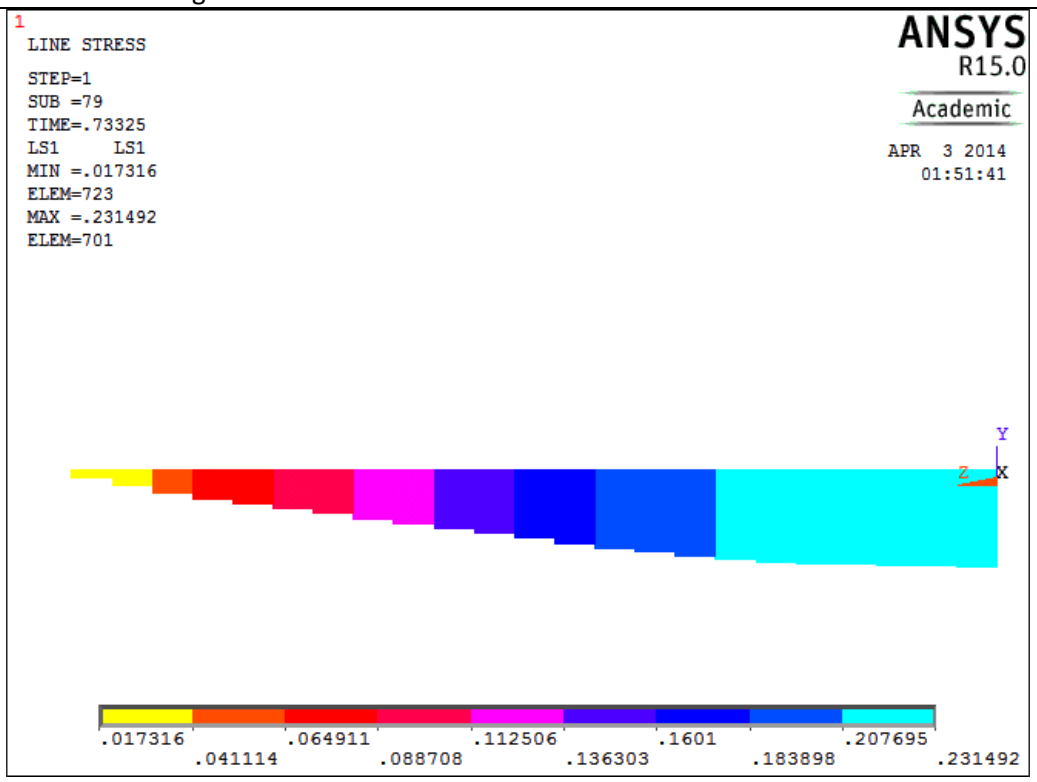

Figure D-188 Reinforcement Stress for 32-1-30

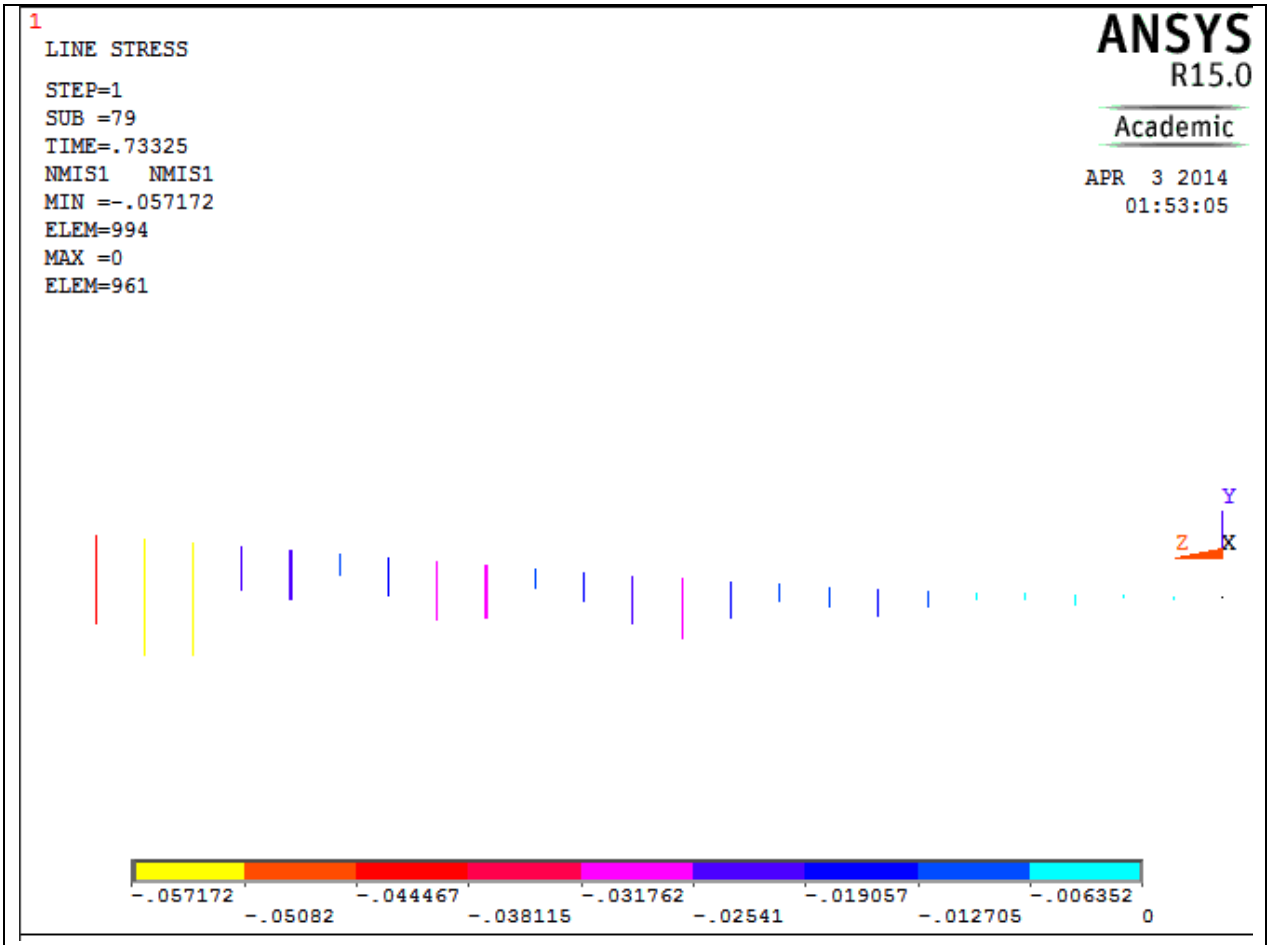

Figure D-189 Spring Stretch for 32-1-30

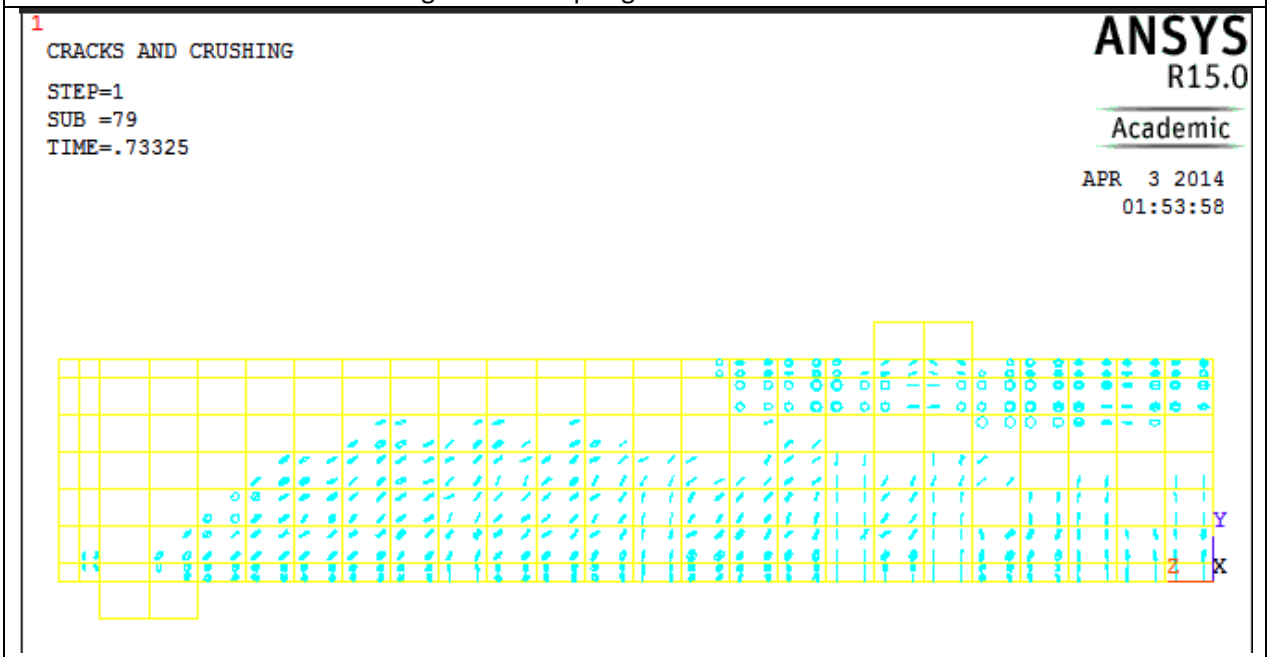

Figure D-190 Crack I for 32-1-30

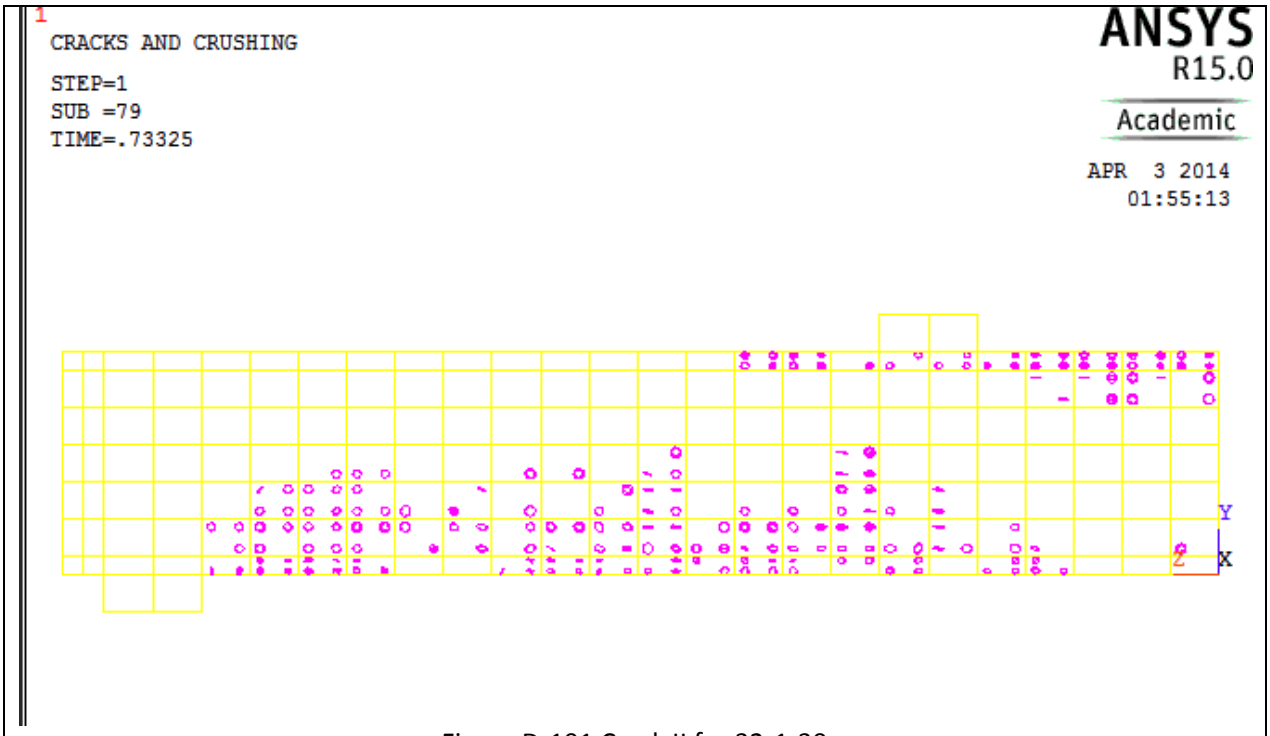

Figure D-191 Crack II for 32-1-30

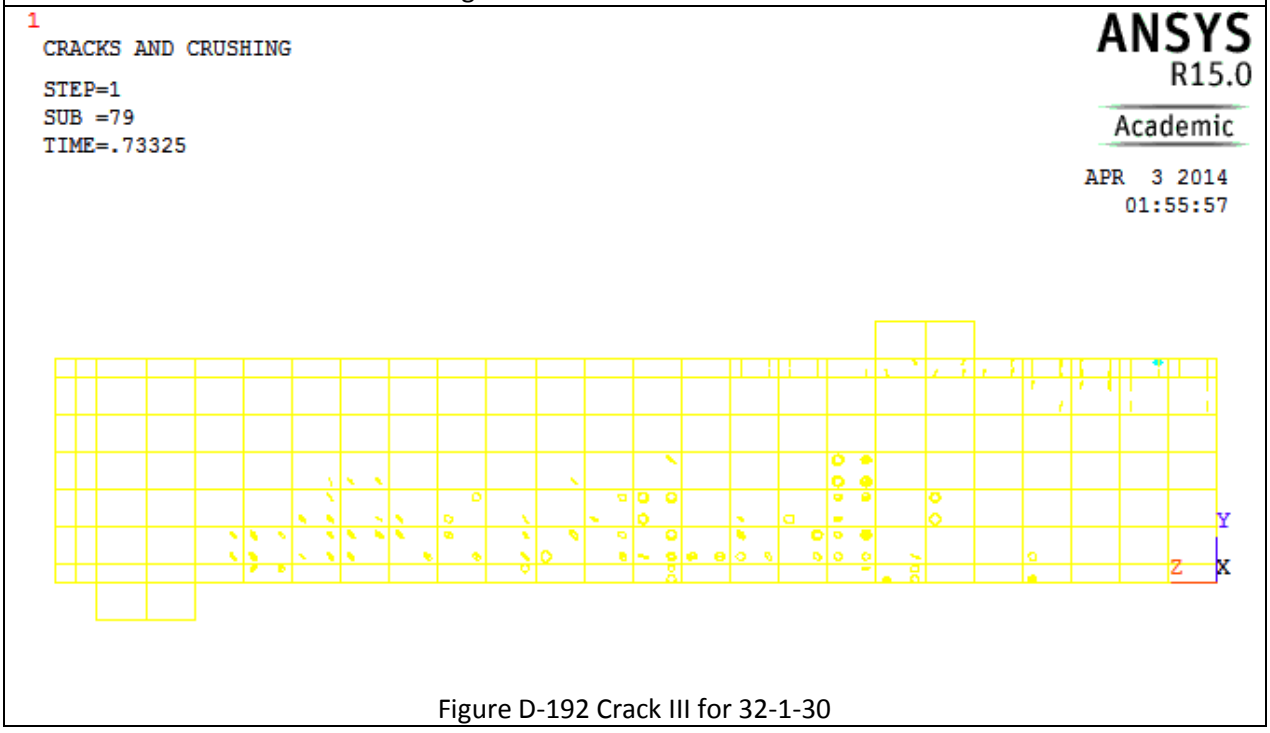

Figure D-192 Crack III for 32-1-30

Table D-25 Details of case 32-2-10

Case Name	Bottom Reinforcement	Honeycombing Location	Strength of Concrete(MPa)	Ultimate Load (kN)	Ultimate Deflection(mm)	Failure Mode
32-2-10	32mm	2	10	79.6875	4.85226	

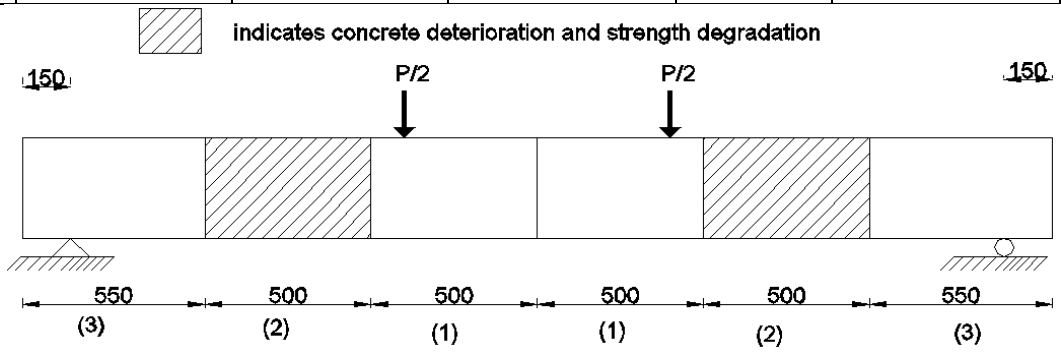

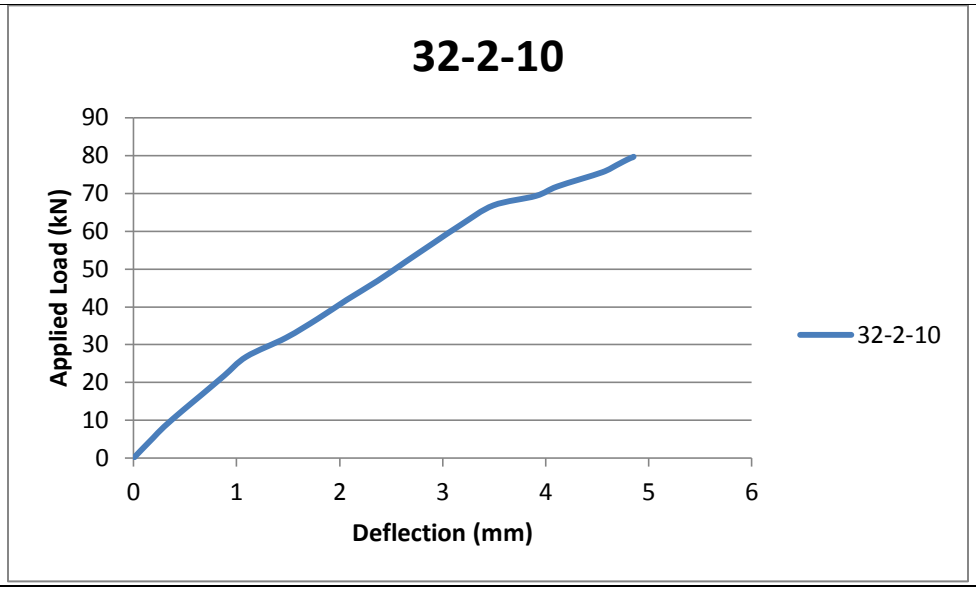

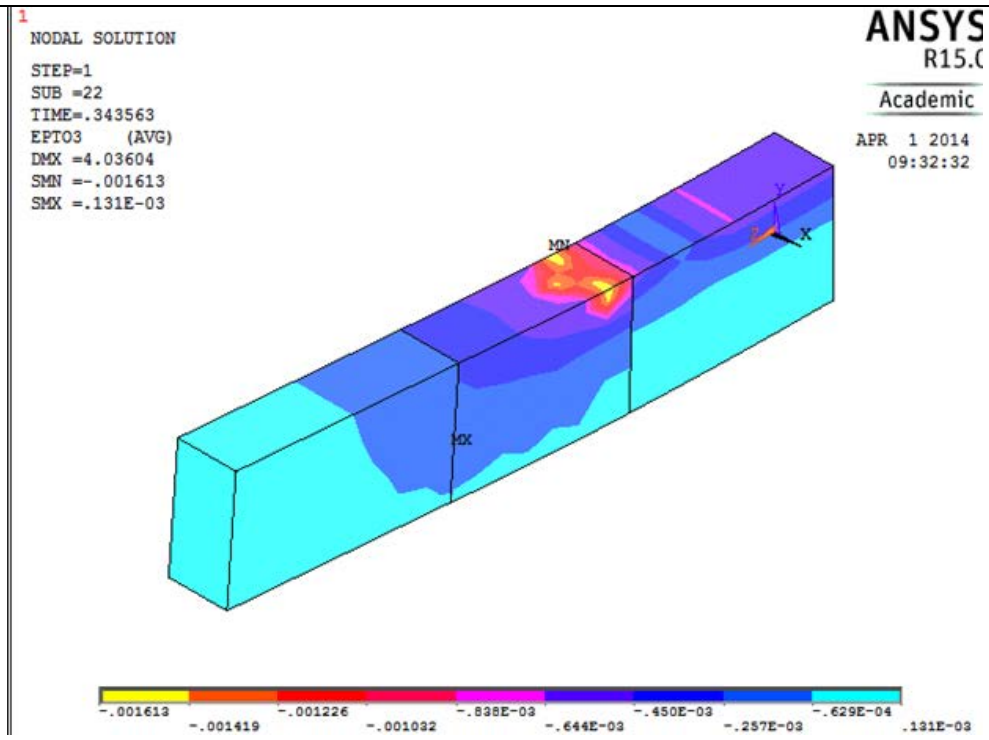

Figure D-193 Nodal solution – 3rd principal total mechanical strain for 32-2-10

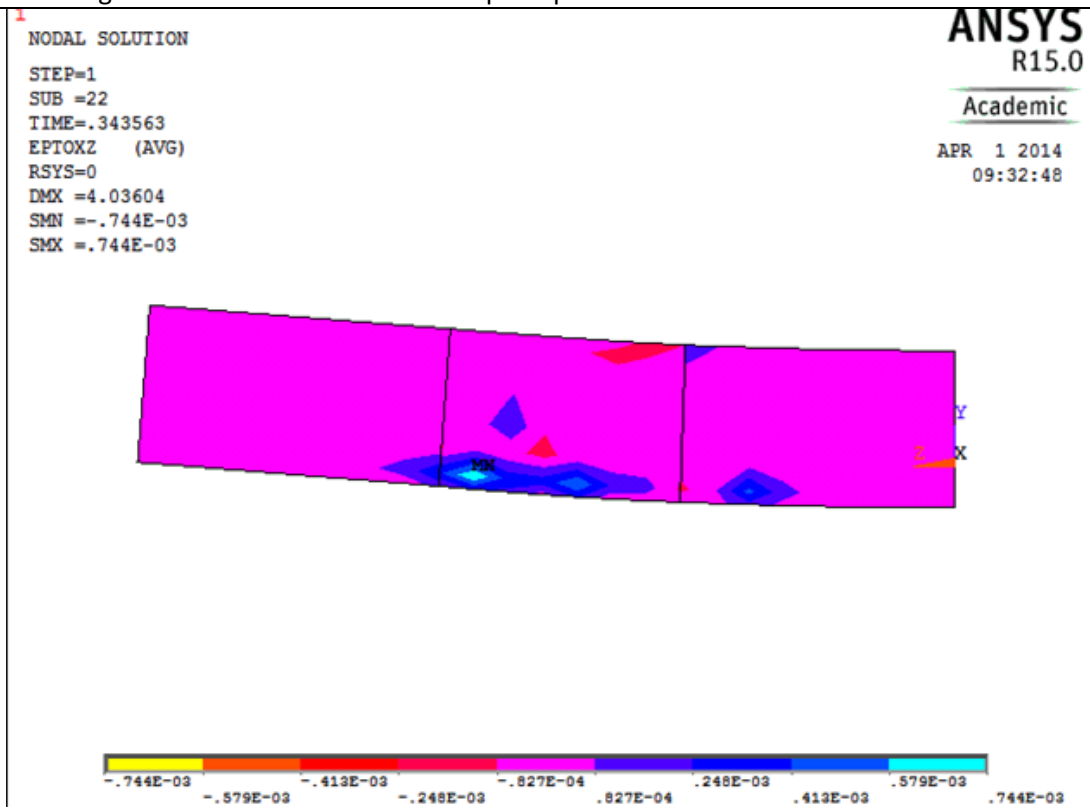

Figure D-194 Nodal Solution XZ shear total mechanical strain for 32-2-10

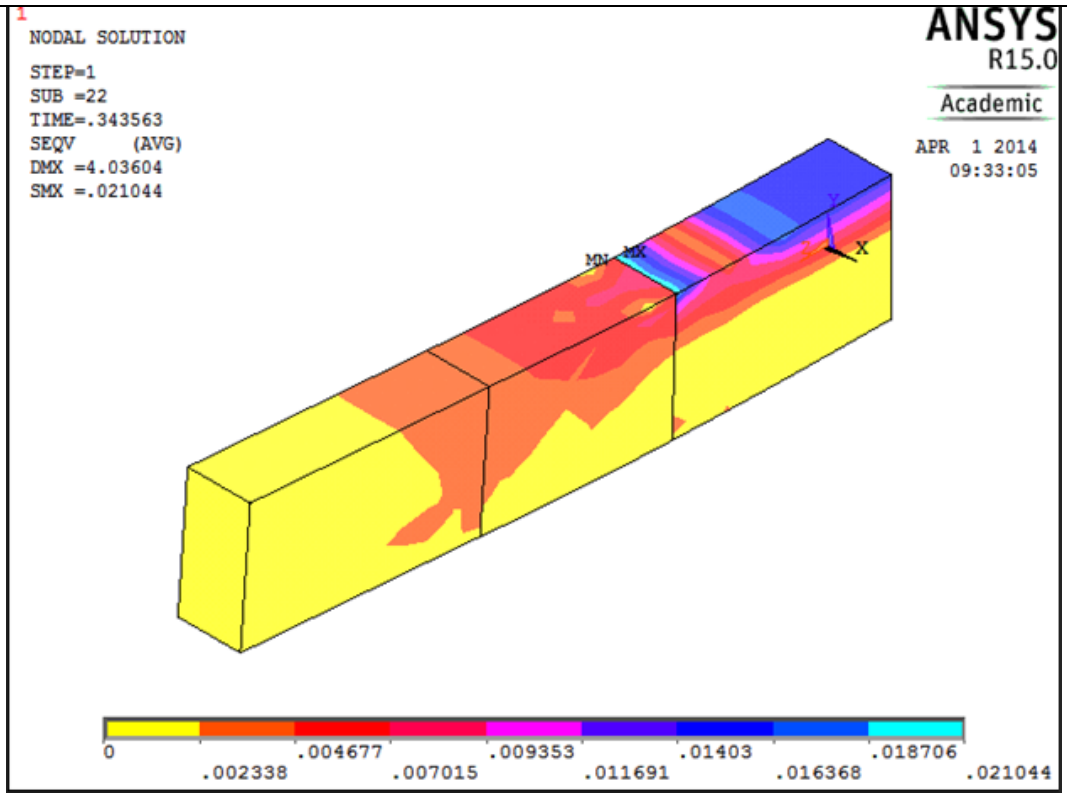

Figure D-195 Nodal Solution -Von Mises Stress for 32-2-10

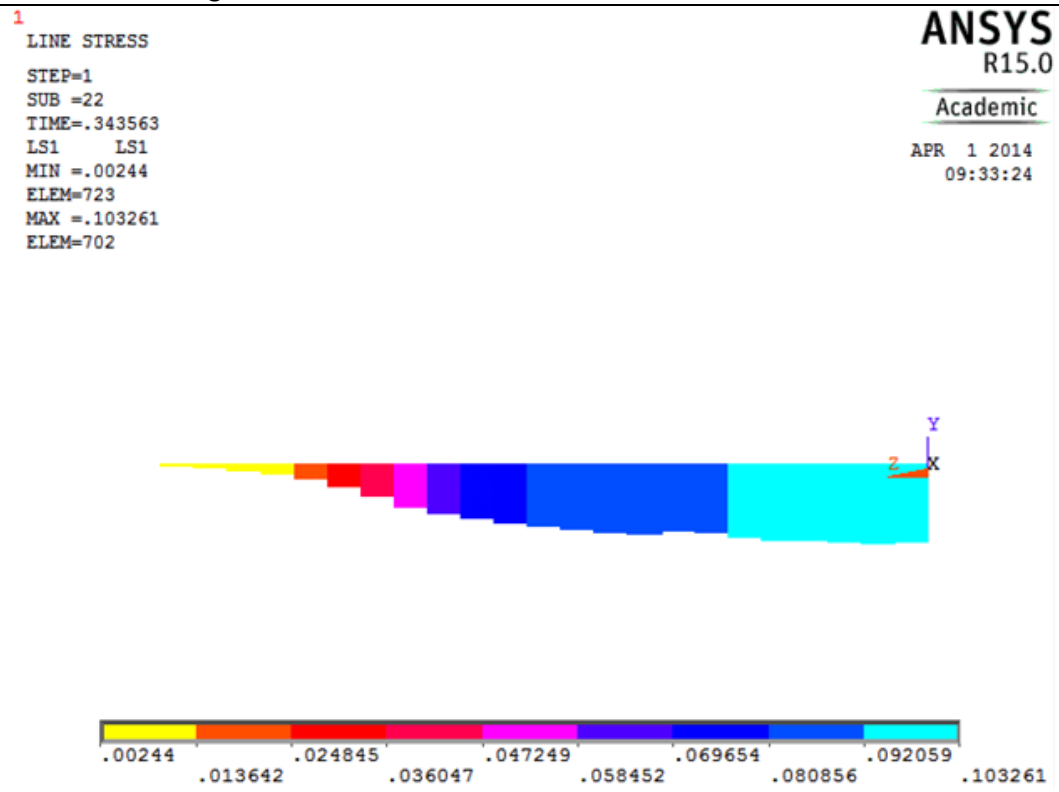

Figure D-196 Reinforcement Stress for 32-2-10

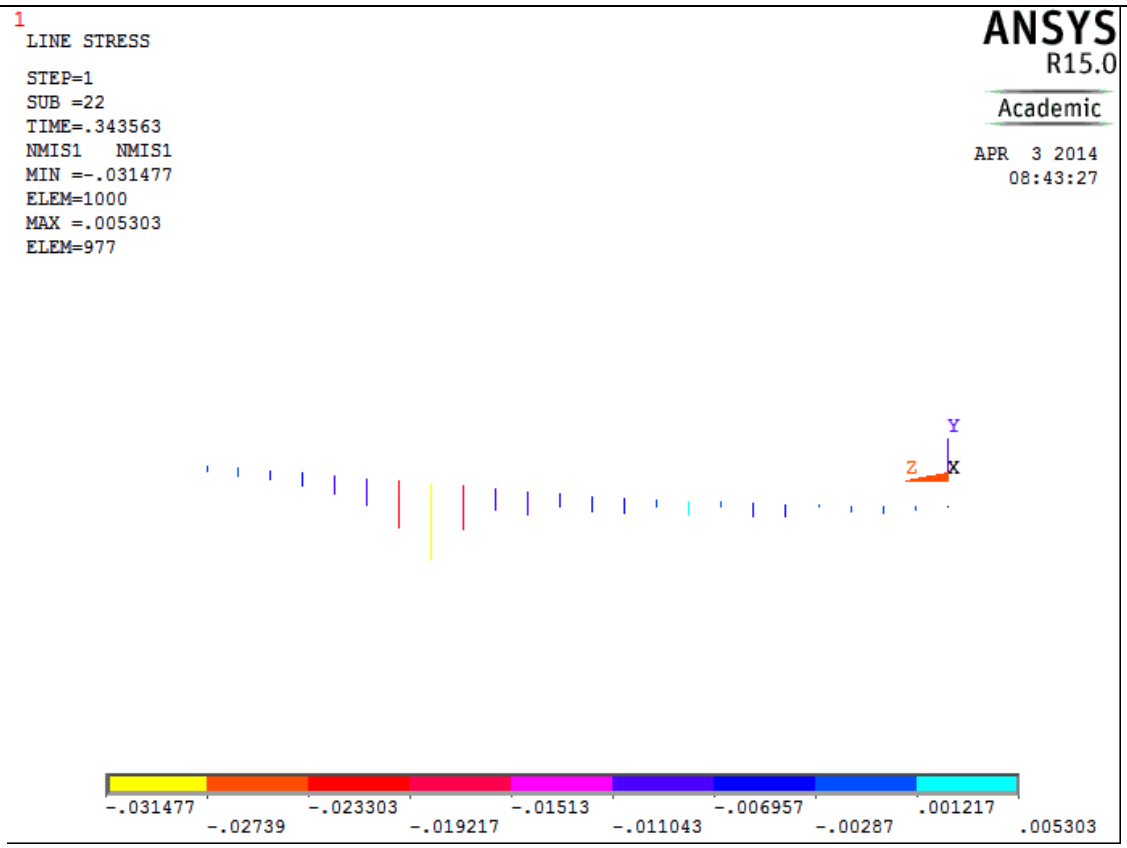

Figure D-197 Spring Stretch for 32-2-10

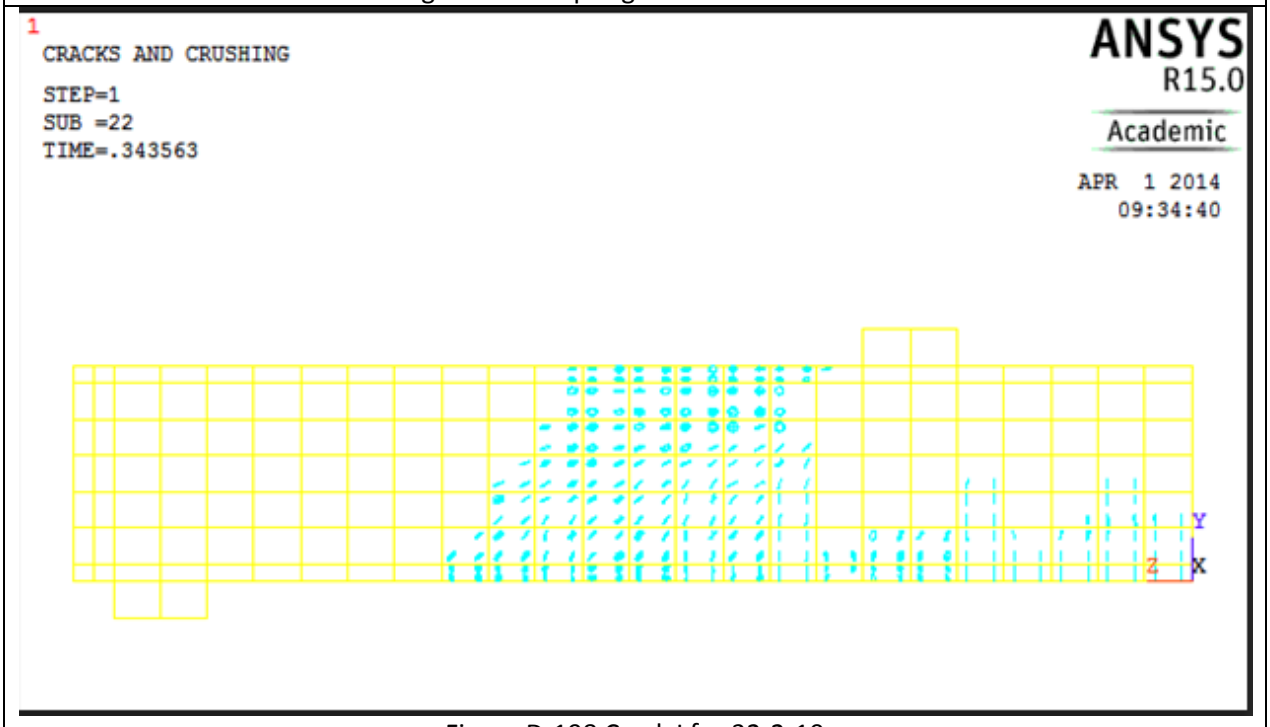

Figure D-198 Crack I for 32-2-10

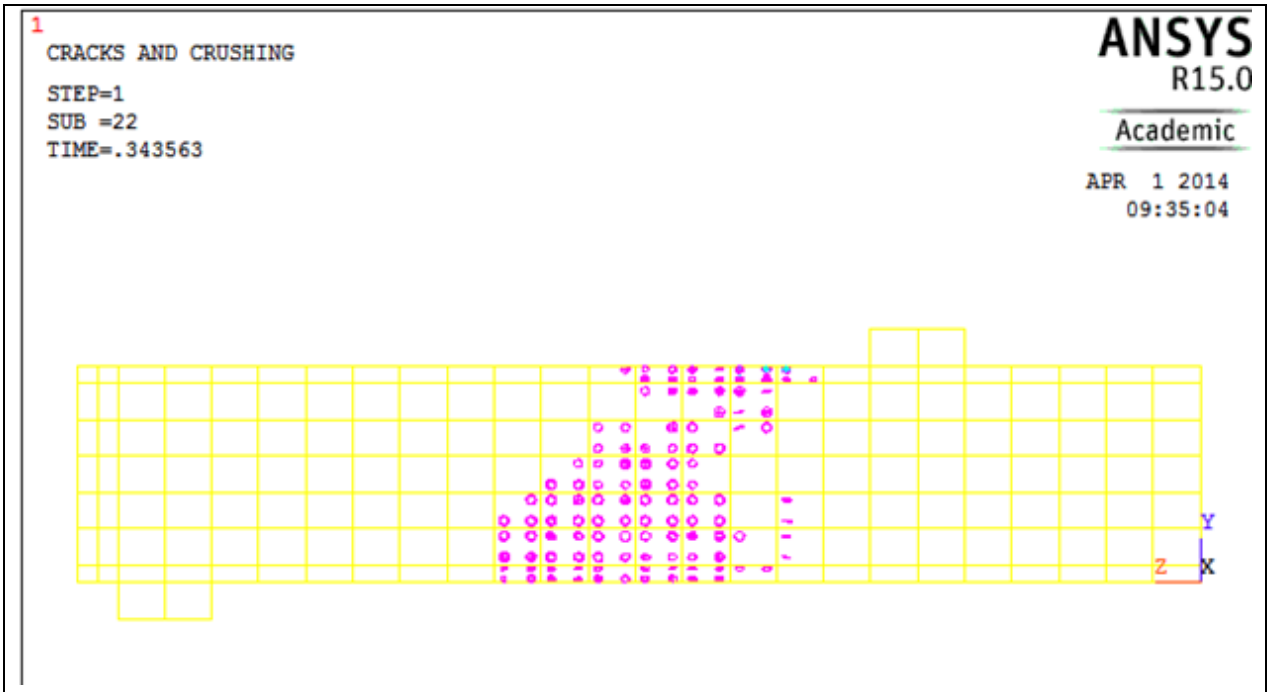

Figure D-199 Crack II for 32-2-10

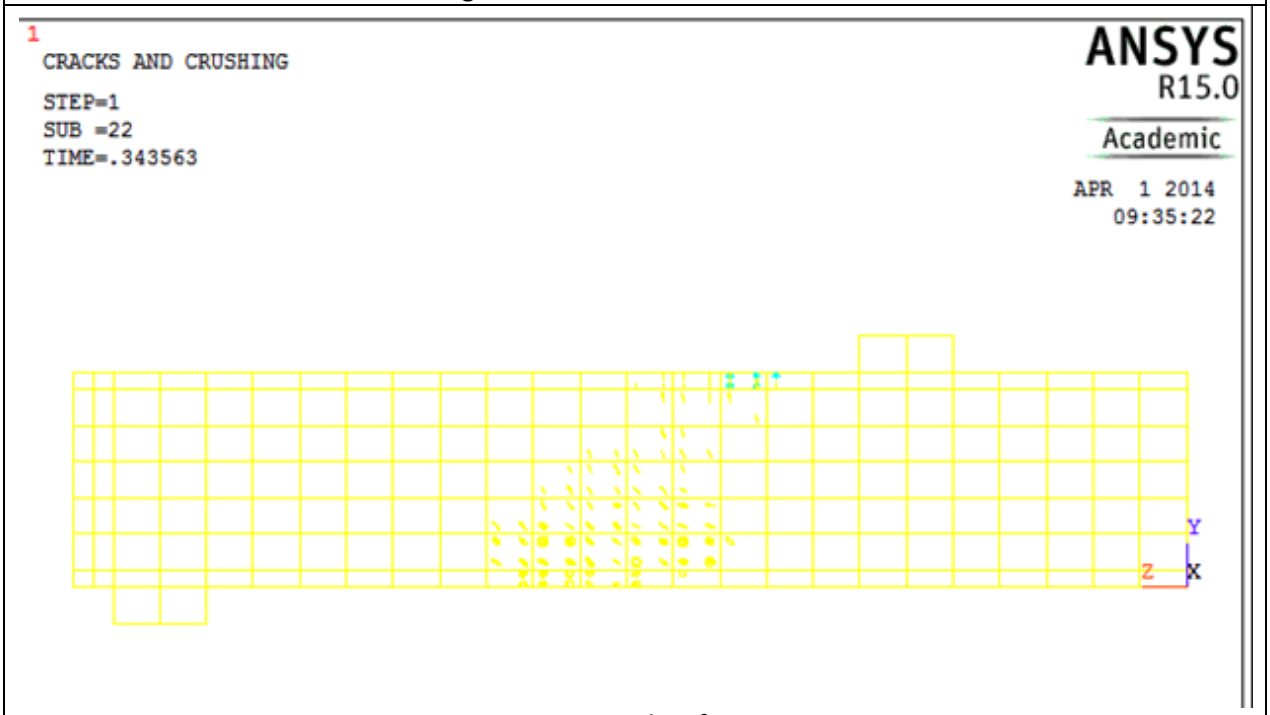

Figure D-200 Crack III for 32-2-10

Table D-26 Details of case 32-2-20

Case Name	Bottom Reinforcement	Honeycombing Location	Strength of Concrete(MPa)	Ultimate Load (kN)	Ultimate Deflection(mm)	Failure Mode
32-2-20	32mm	2	20	152.4842	8.48477	

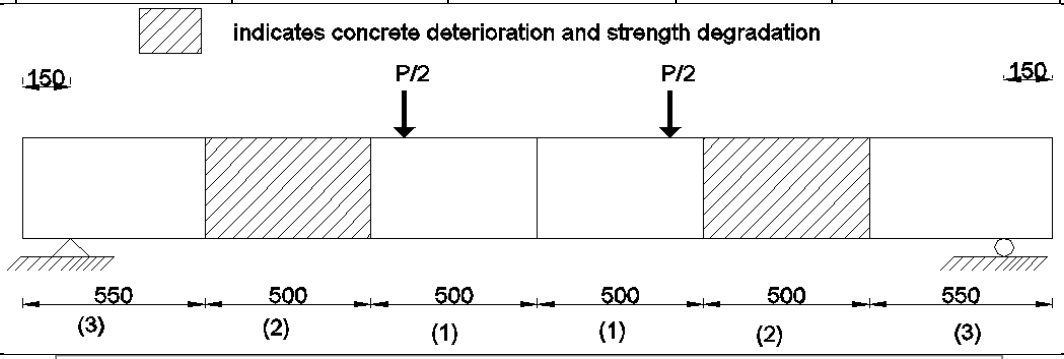

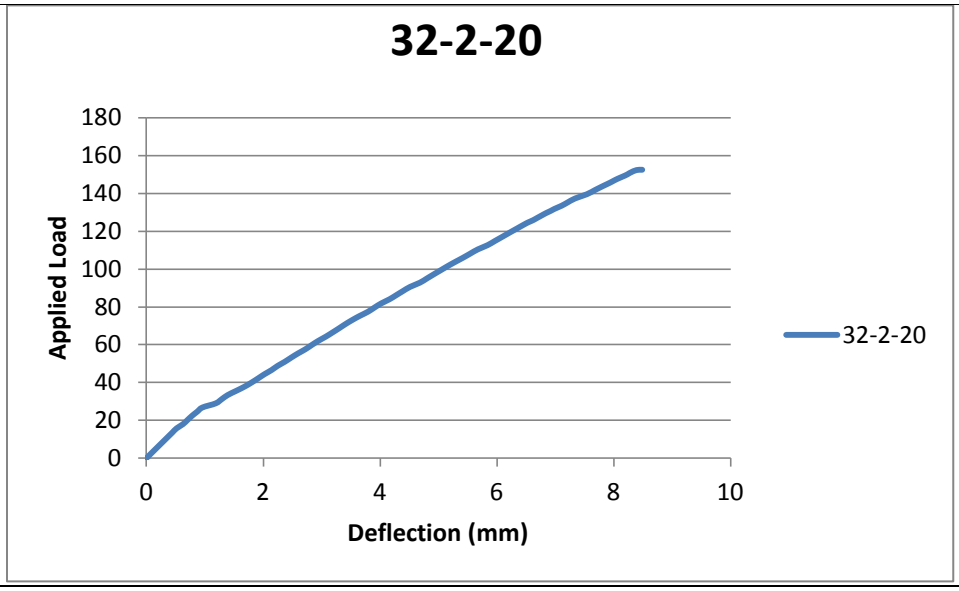

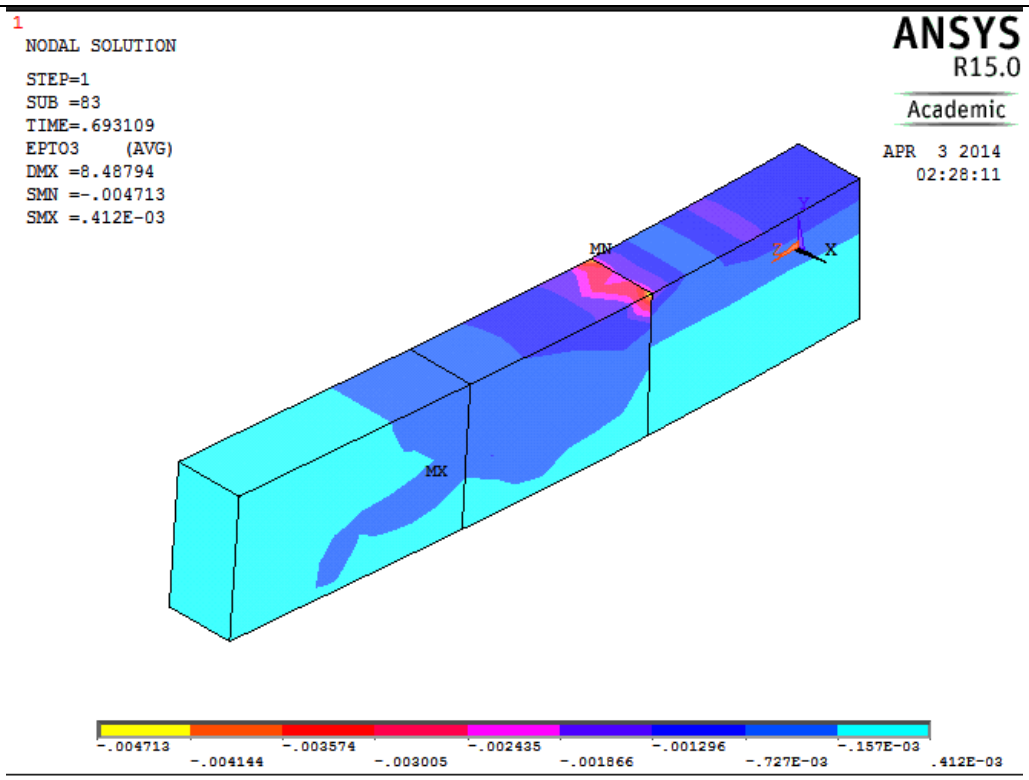

Figure D-201 Nodal solution – 3rd principal total mechanical strain for 32-2-20

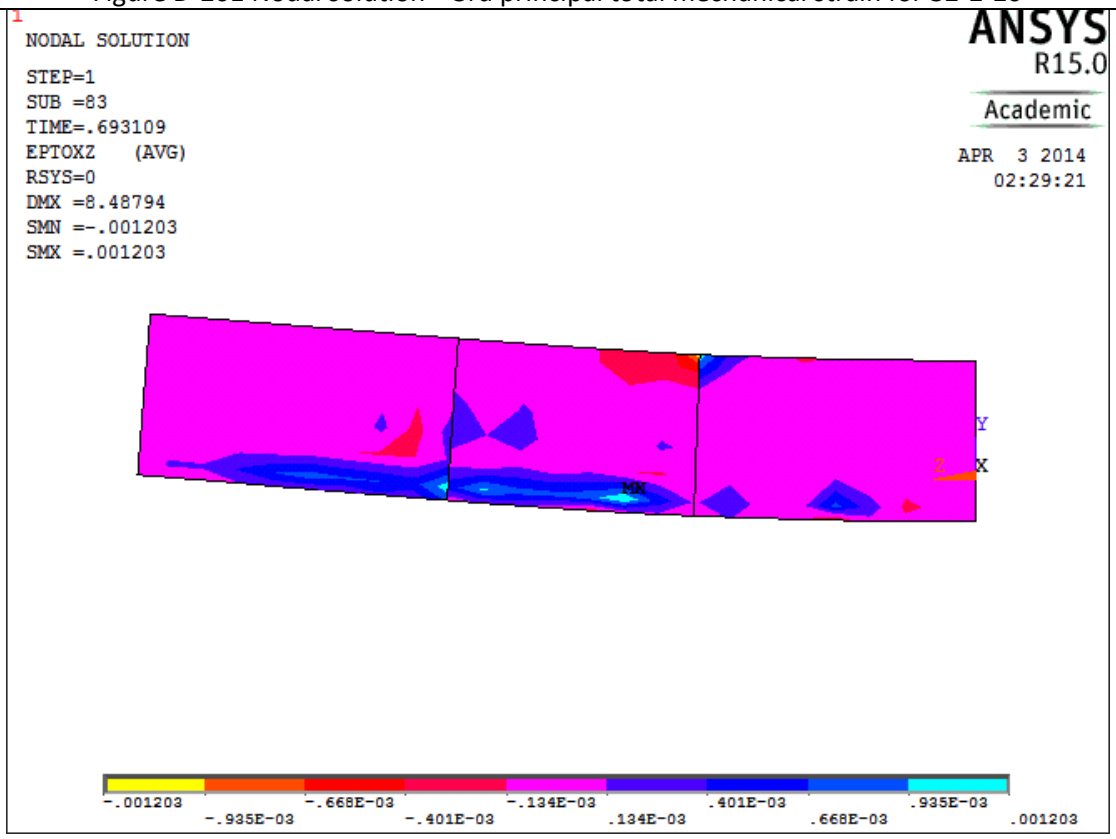

Figure D-202 Nodal Solution XZ shear total mechanical strain for 32-2-20

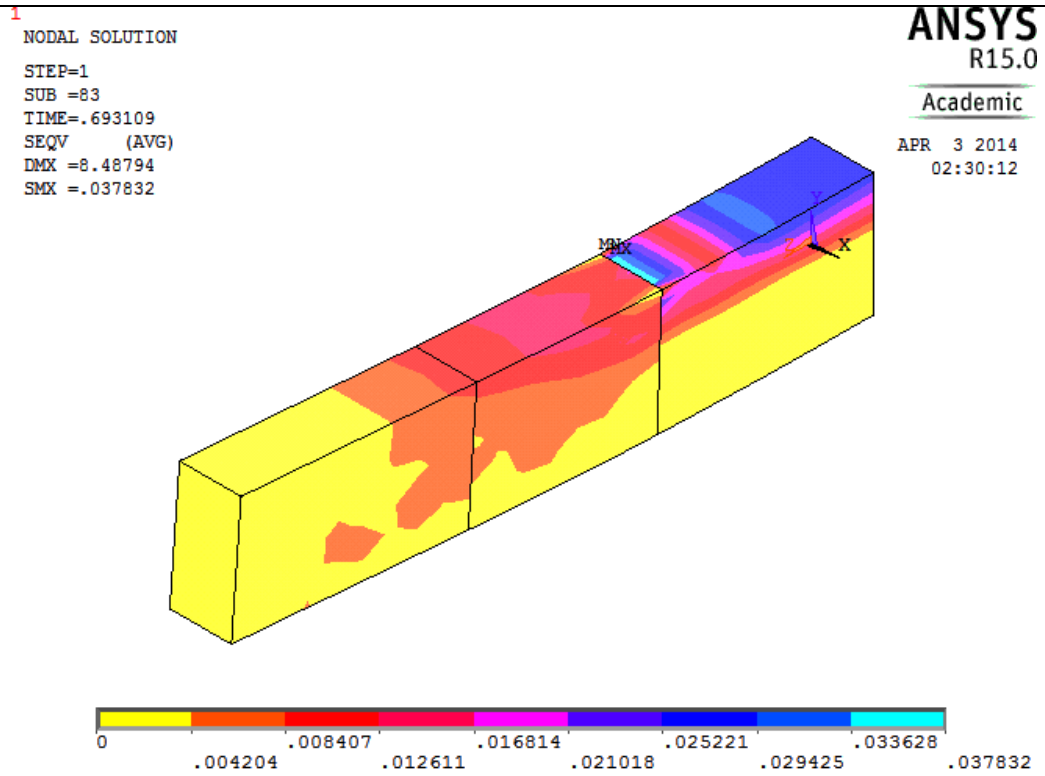

Figure D-203 Nodal Solution -Von Mises Stress for 32-2-20

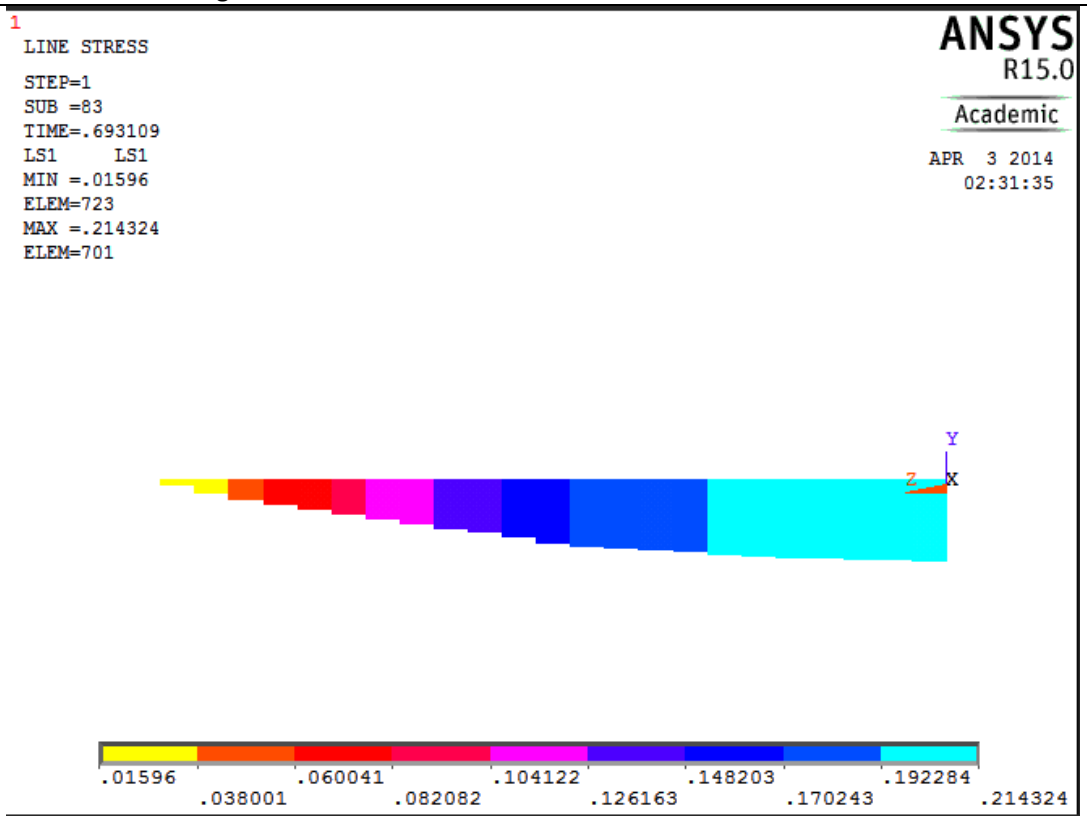

Figure D-204 Reinforcement Stress for 32-2-20

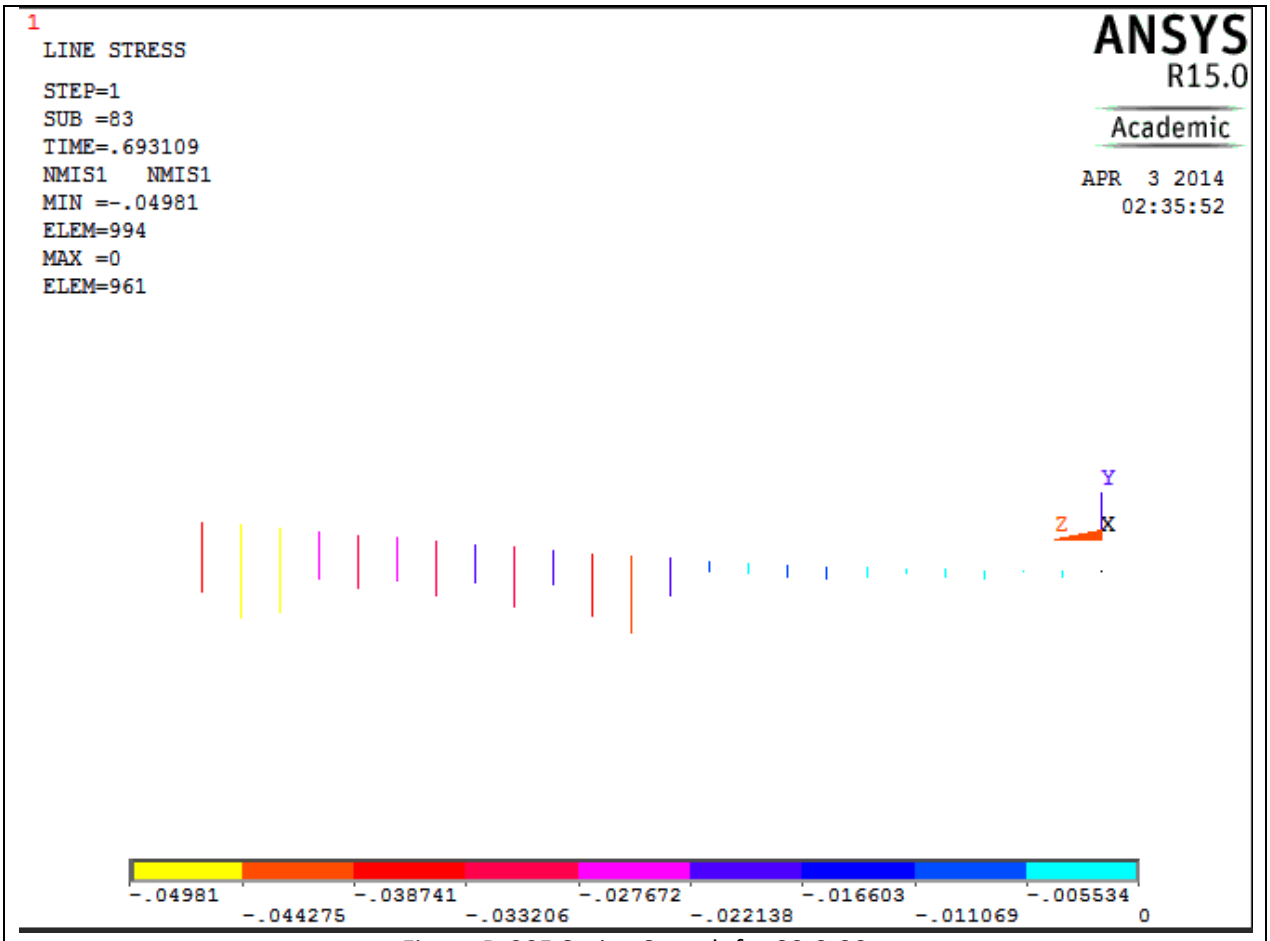

Figure D-205 Spring Stretch for 32-2-20

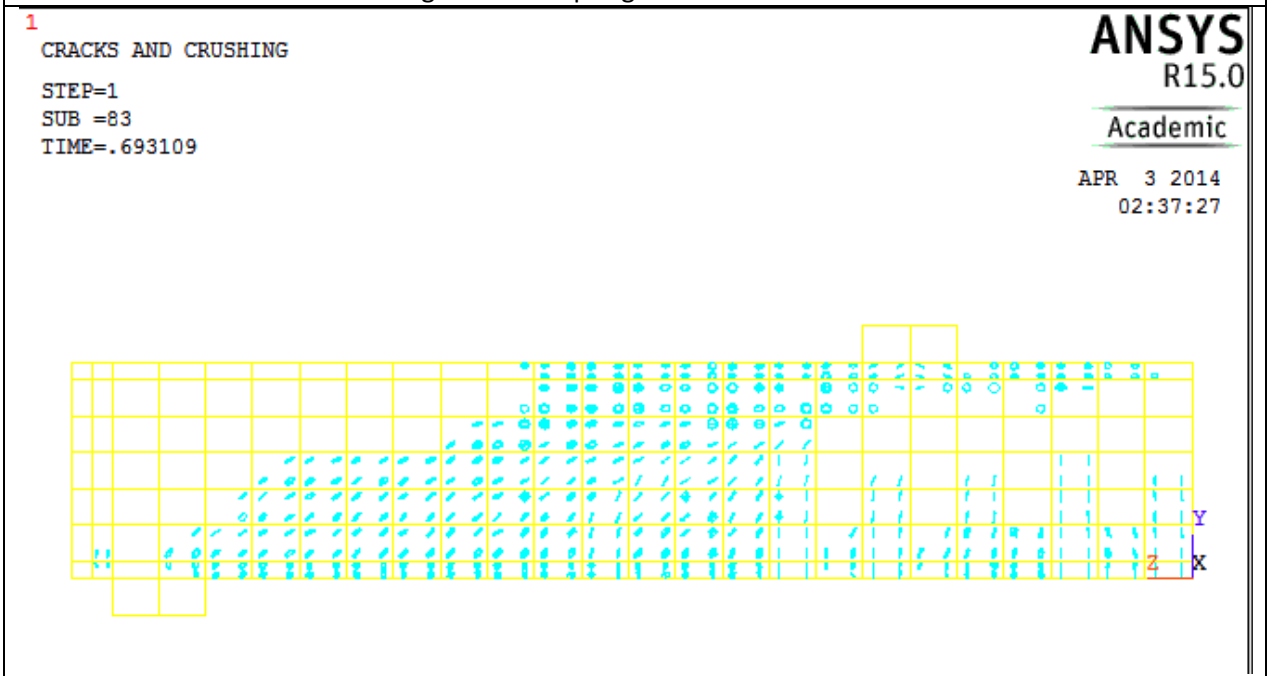

Figure D-206 Crack I for 32-2-20

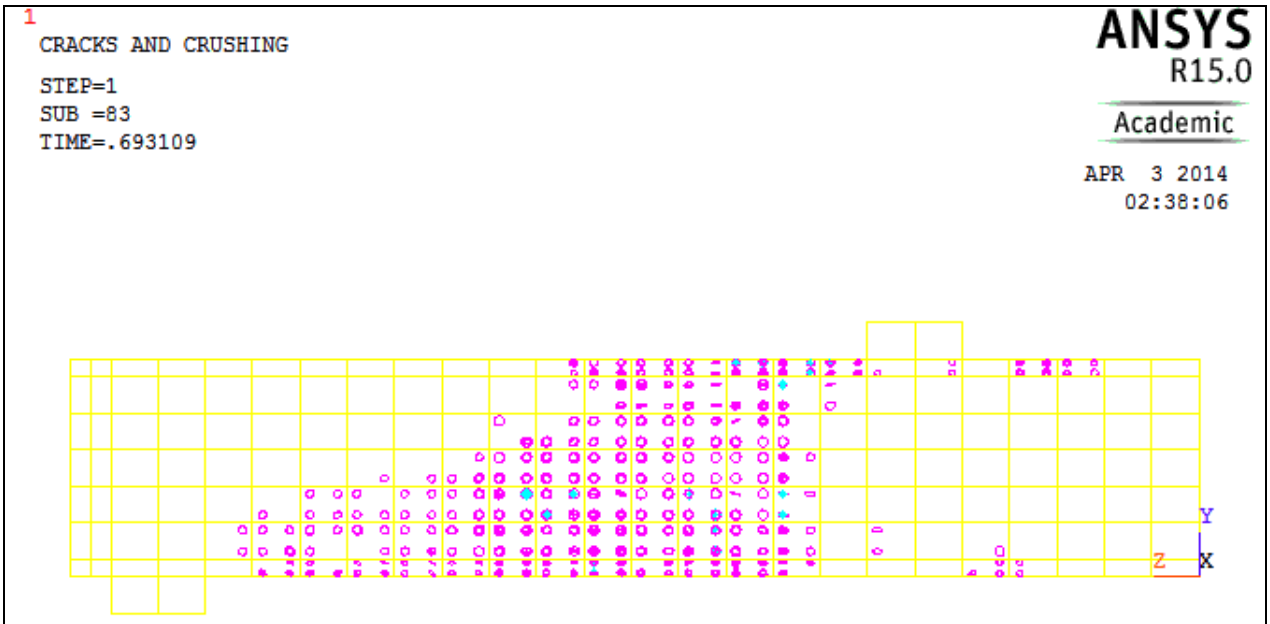

Figure D-207 Crack II for 32-2-20

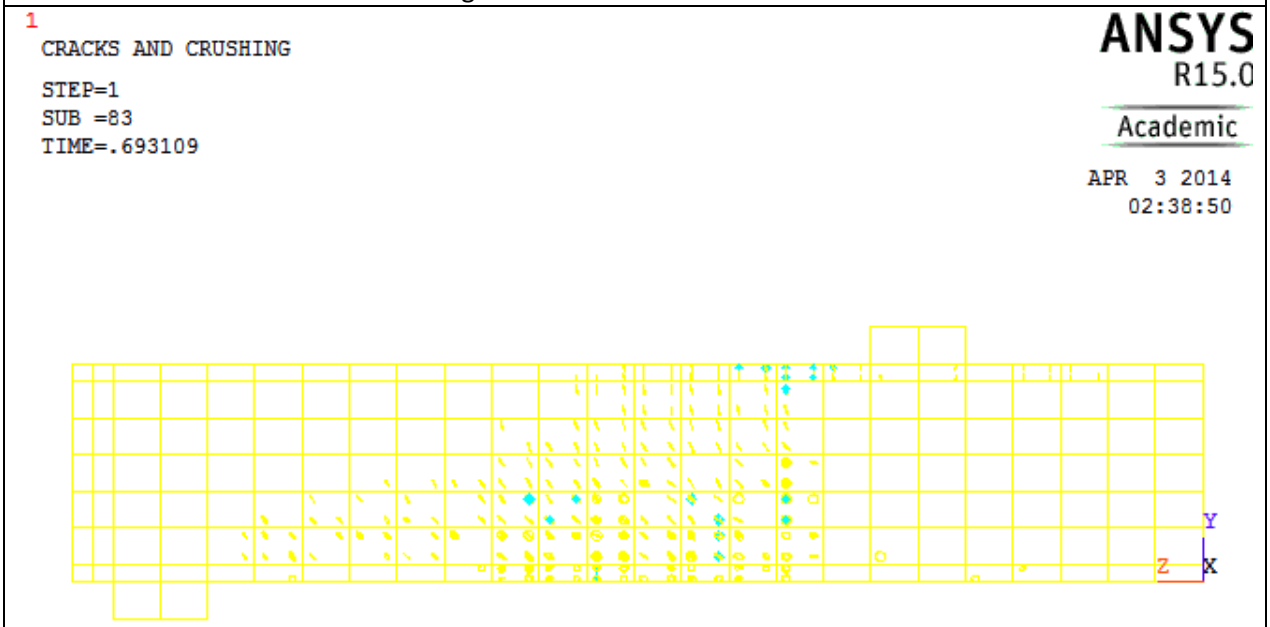

Figure D-208 Crack III for 32-2-20

Table D-27 Details of case 32-2-30

Case Name	Bottom Reinforcement	Honeycombing Location	Strength of Concrete(MPa)	Ultimate Load (kN)	Ultimate Deflection(mm)	Failure Mode
32-2-30	32mm	2	30	173.4458	9.4373	

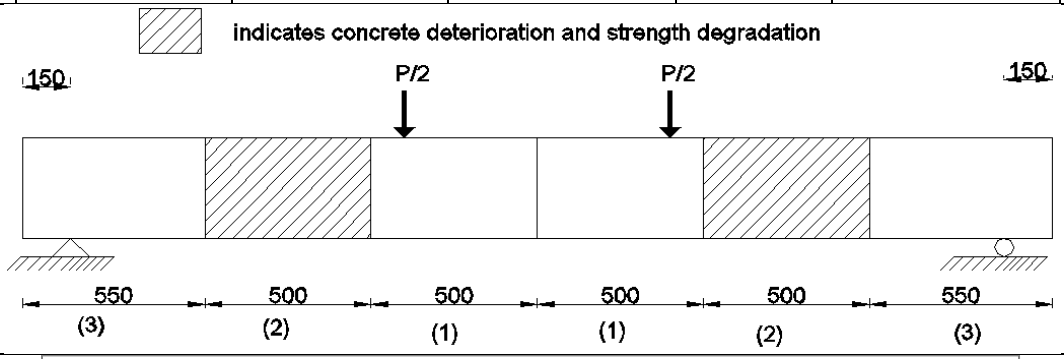

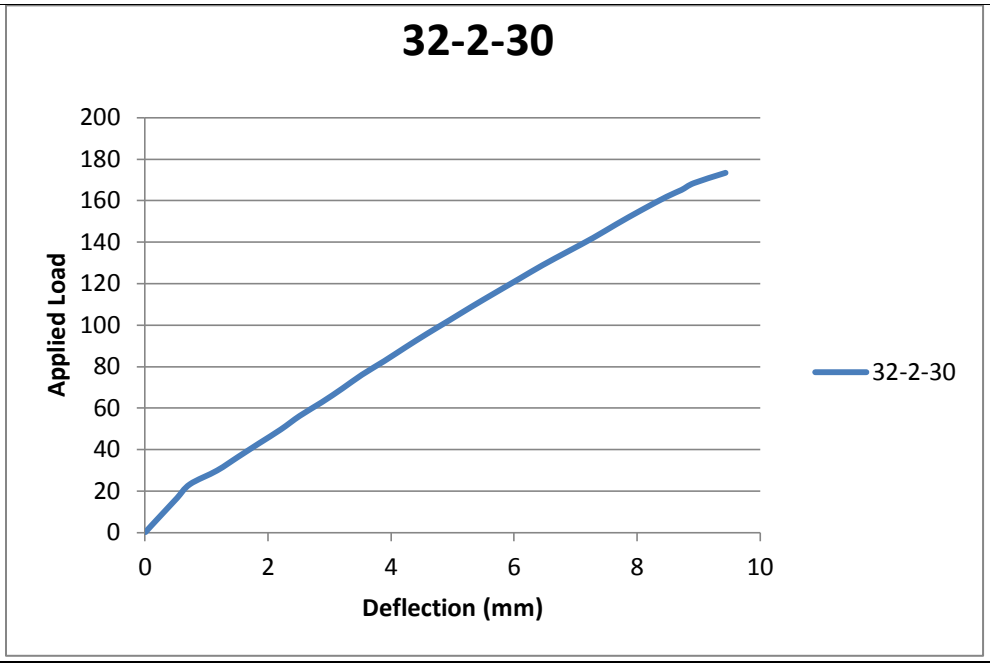

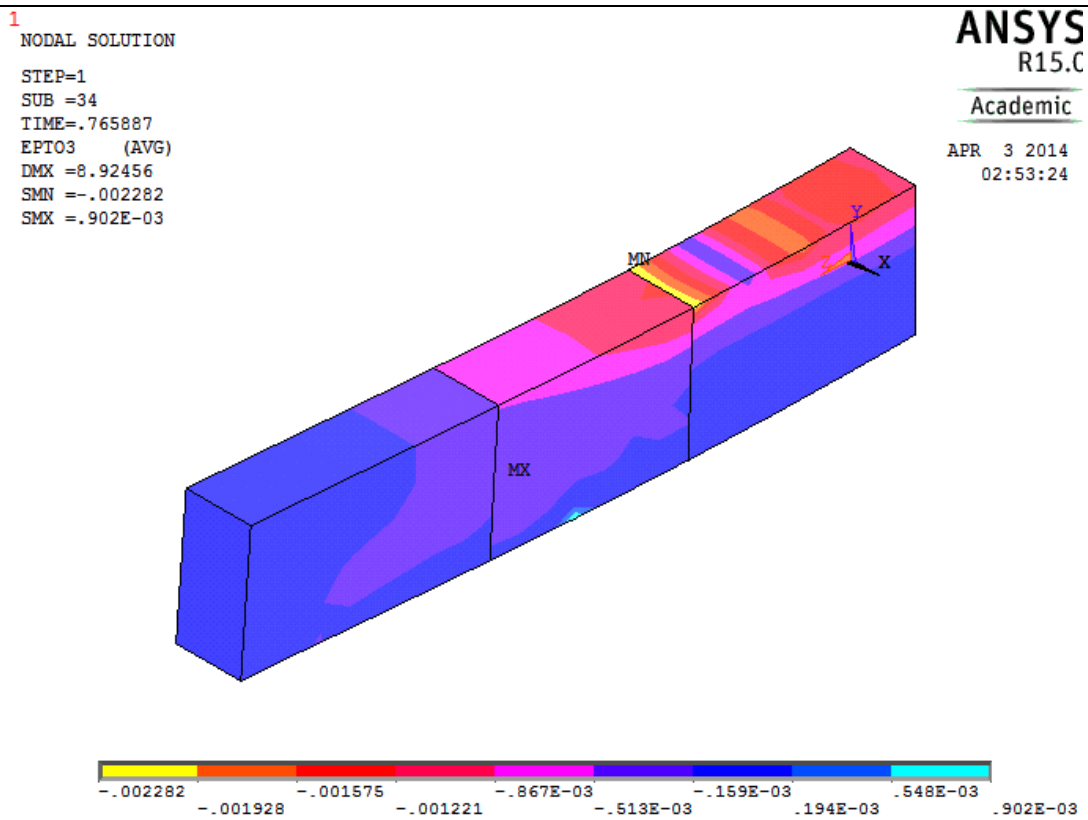

Figure D-209 Nodal solution – 3rd principal total mechanical strain for 32-2-30

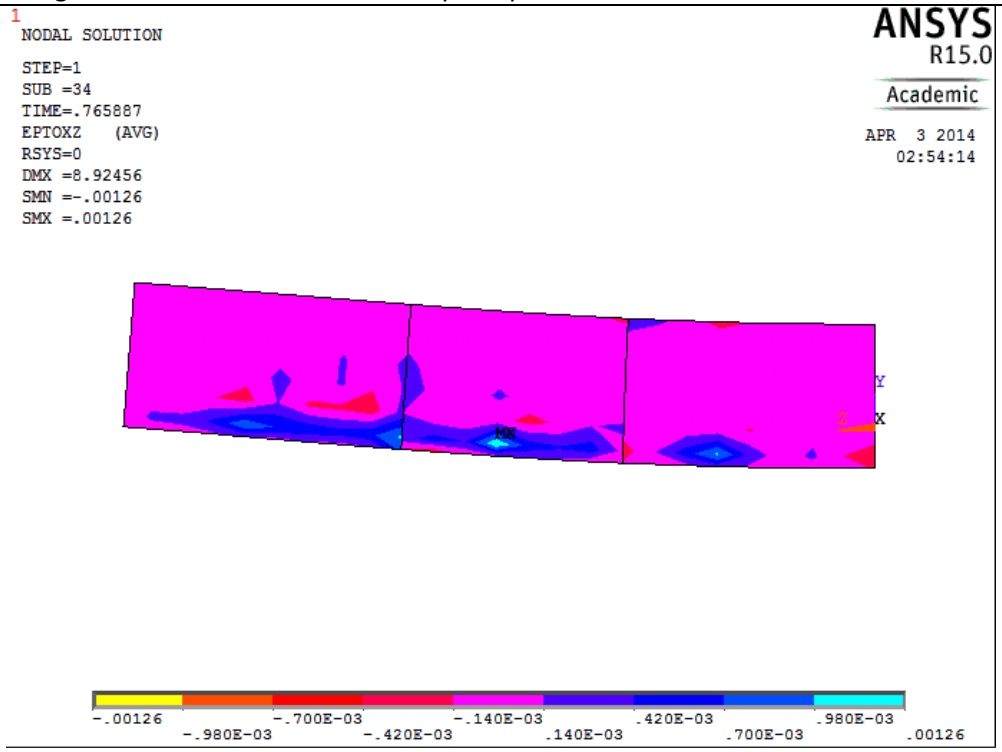

Figure D-210 Nodal Solution XZ shear total mechanical strain for 32-2-30

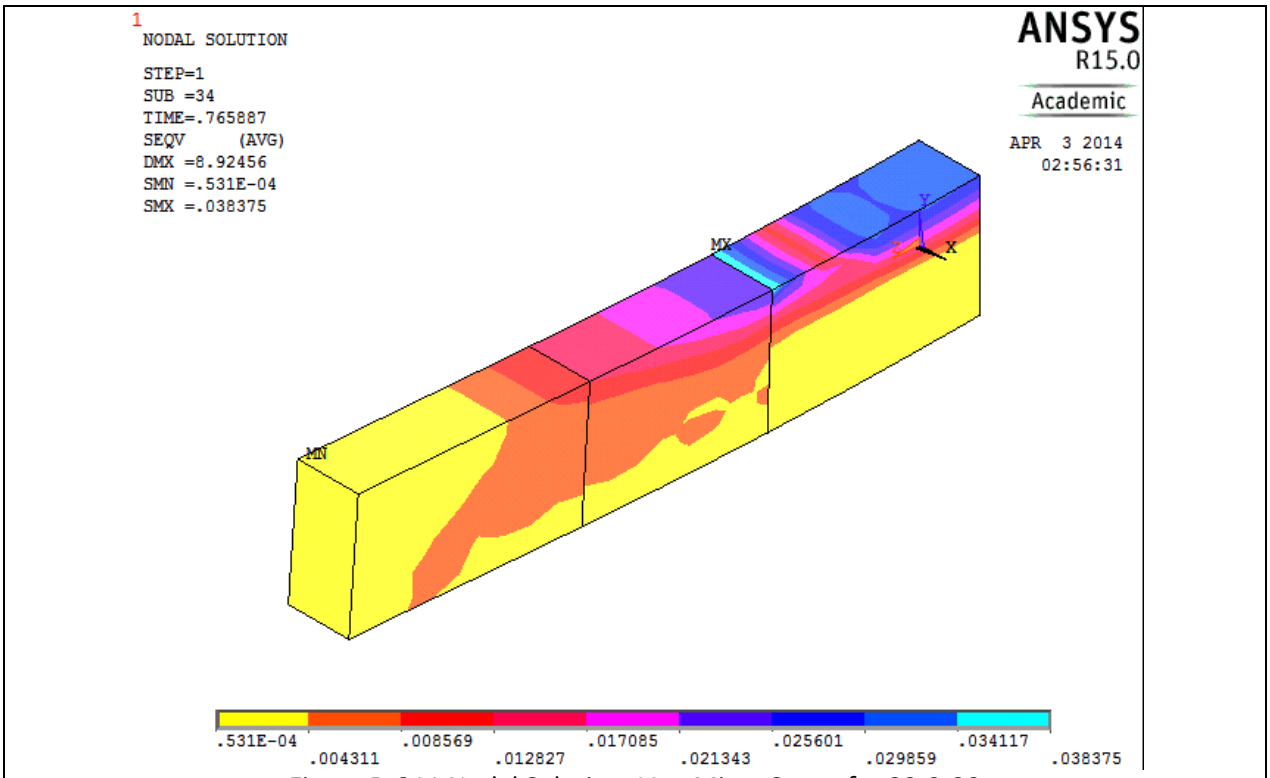

Figure D-211 Nodal Solution -Von Mises Stress for 32-2-30

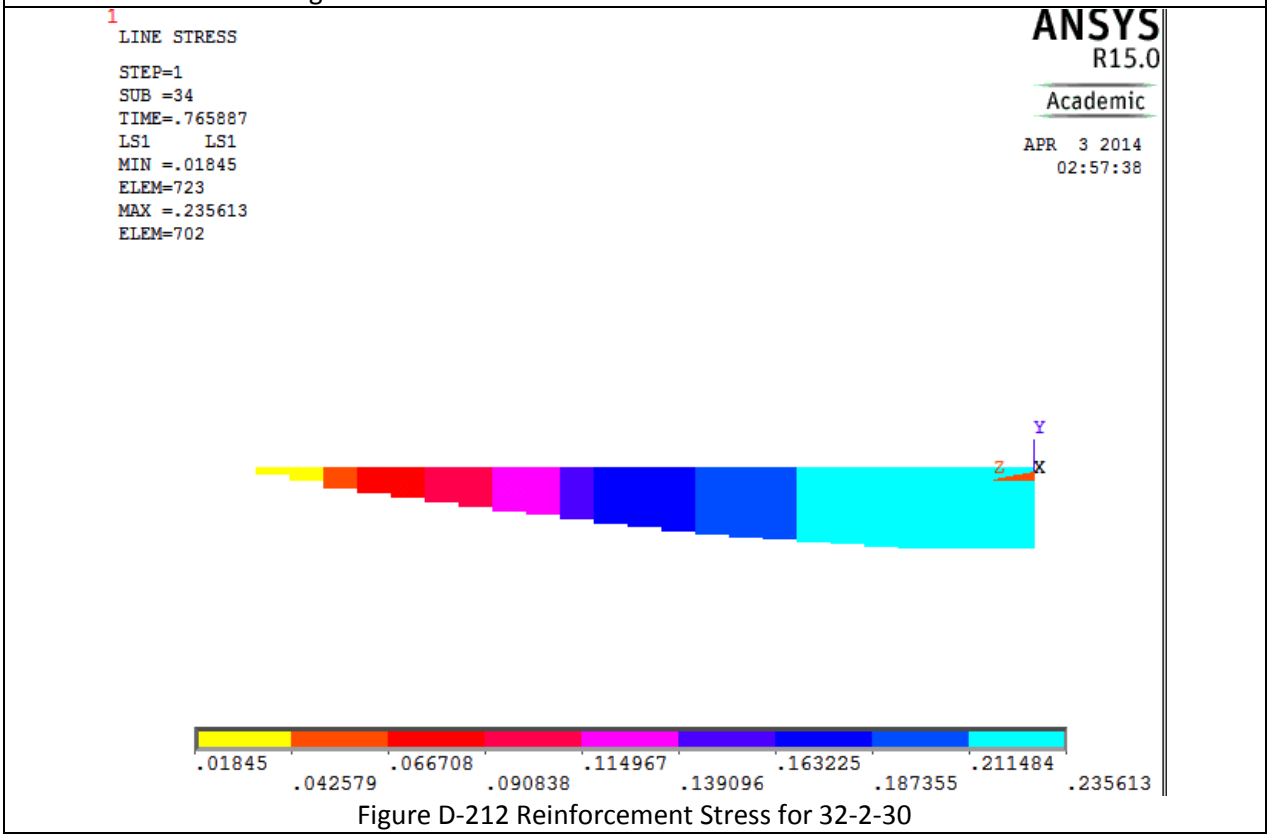

Figure D-212 Reinforcement Stress for 32-2-30

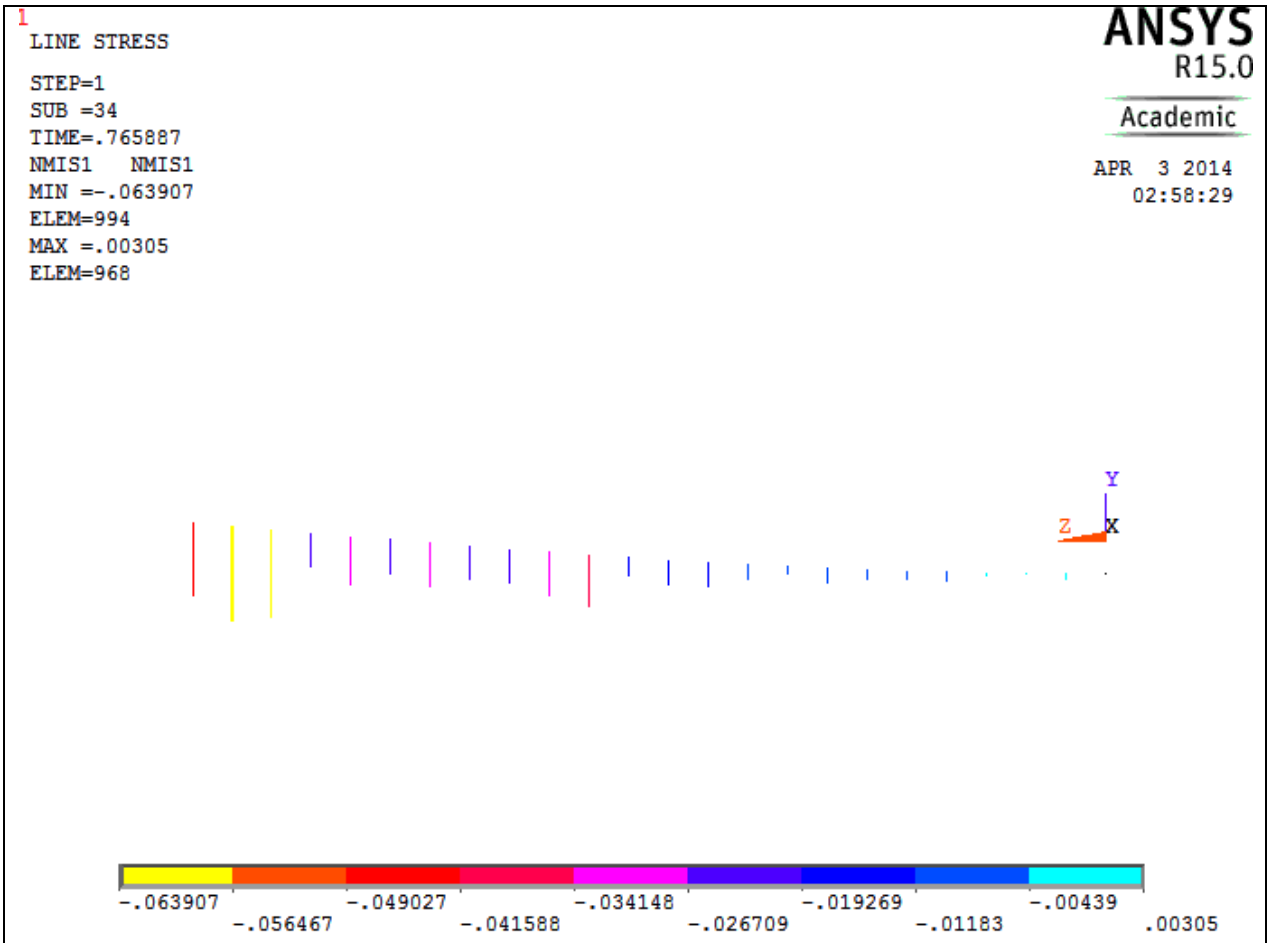

Figure D-213 Spring Stretch for 32-2-30

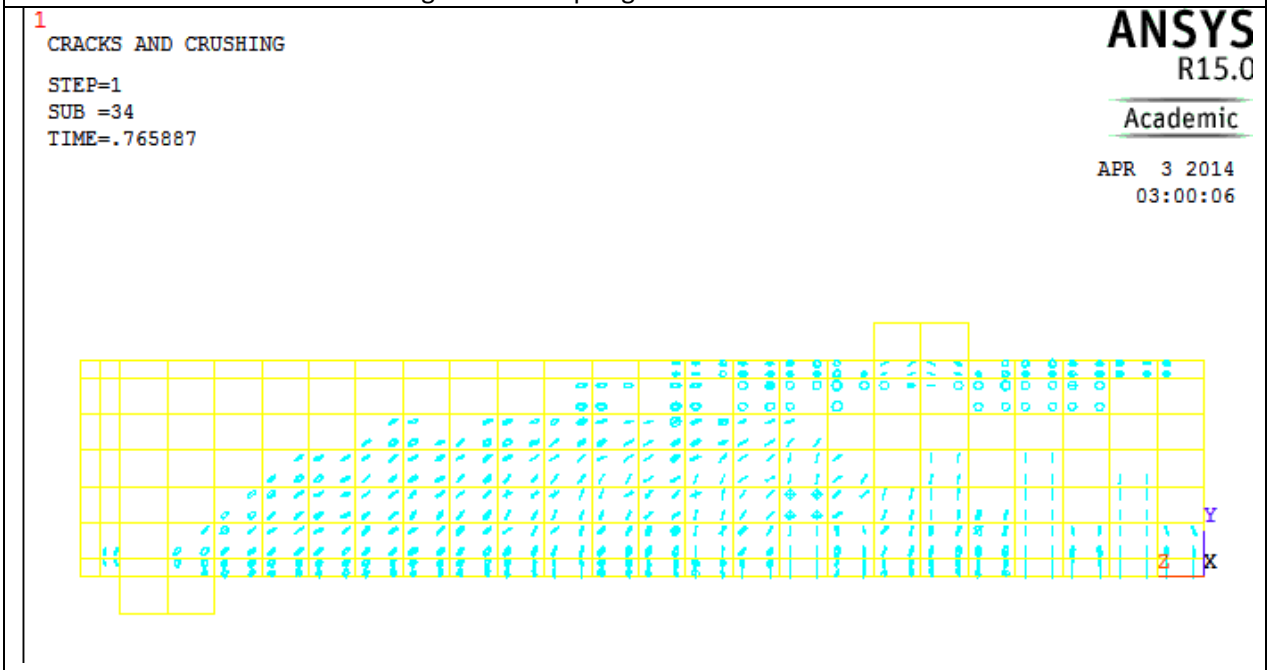

Figure D-214 Crack I for 32-2-30

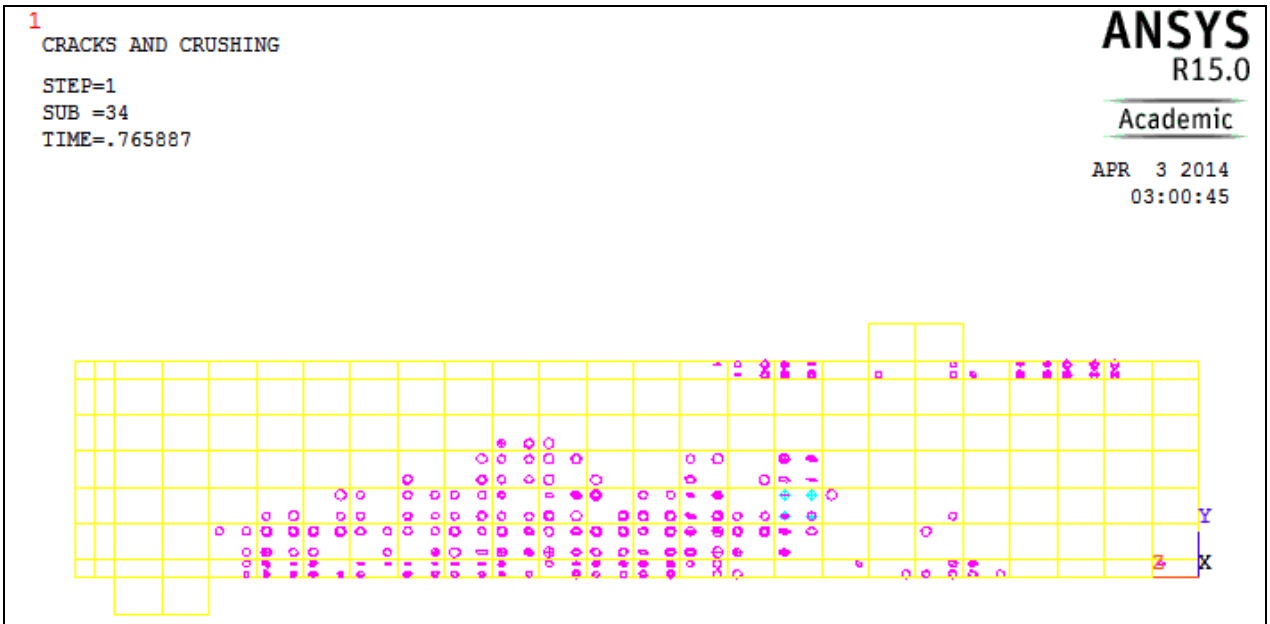

Figure D-215 Crack II for 32-2-30

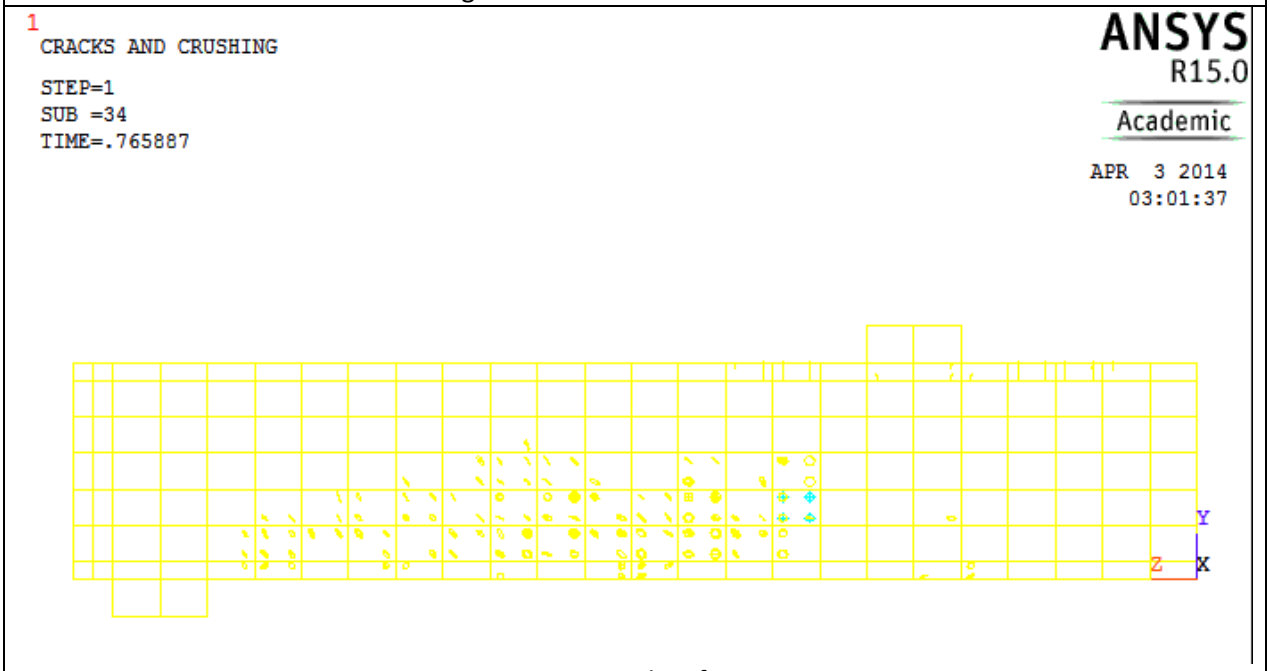

Figure D-216 Crack III for 32-2-30

Table D-28 Details of case 32-3-10

Case Name	Bottom Reinforcement	Honeycombing Location	Strength of Concrete(MPa)	Ultimate Load (kN)	Ultimate Deflection(mm)	Failure Mode
32-3-10	32mm	3	10	101.9832	5.17767	

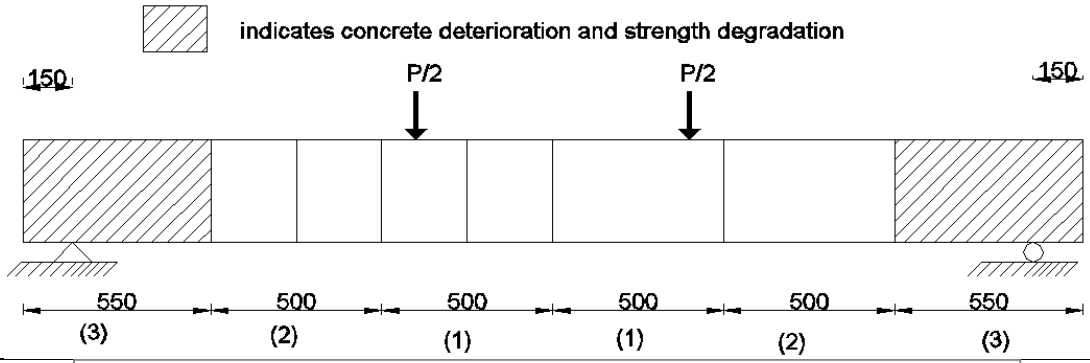

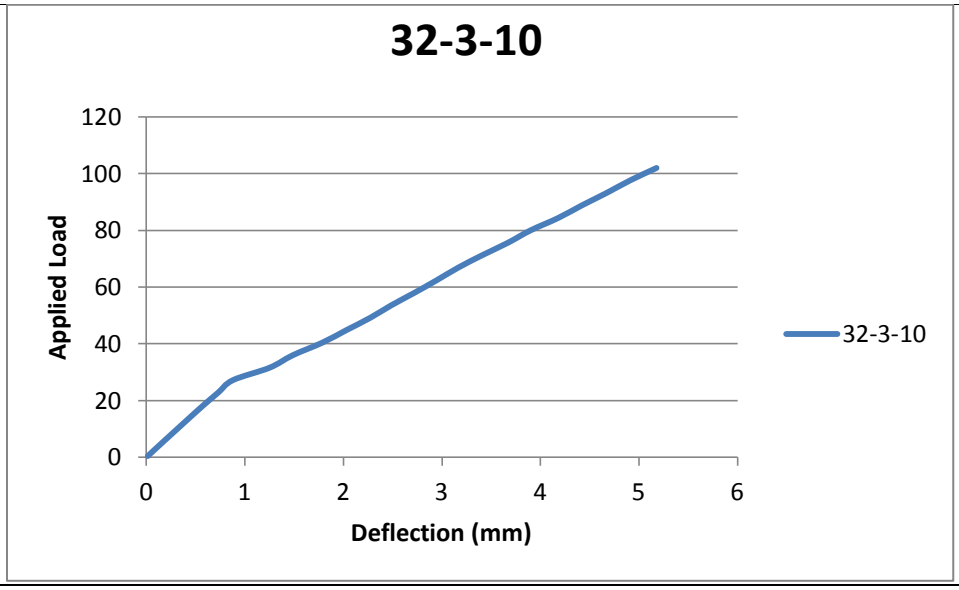

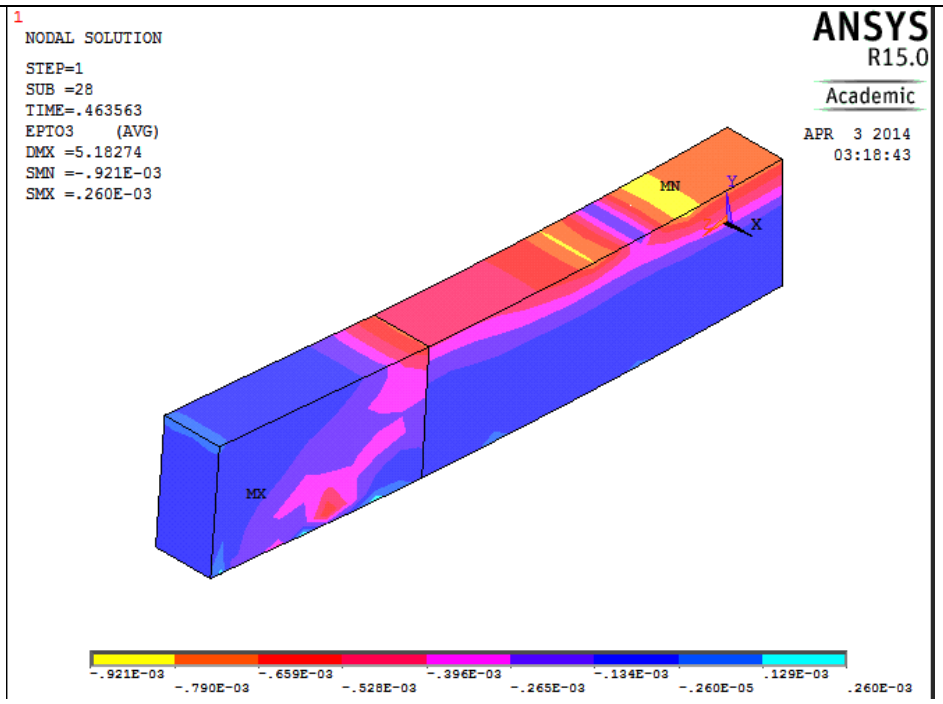

Figure D-217 Nodal solution – 3rd principal total mechanical strain for 32-3-10

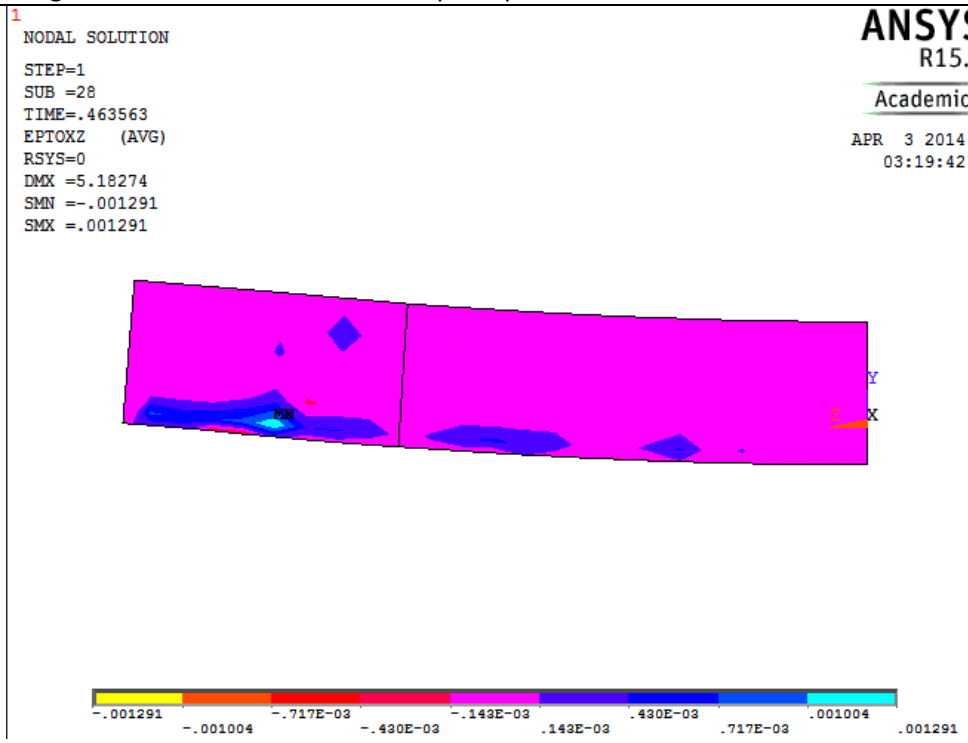

Figure D-218 Nodal Solution XZ shear total mechanical strain for 32-3-10

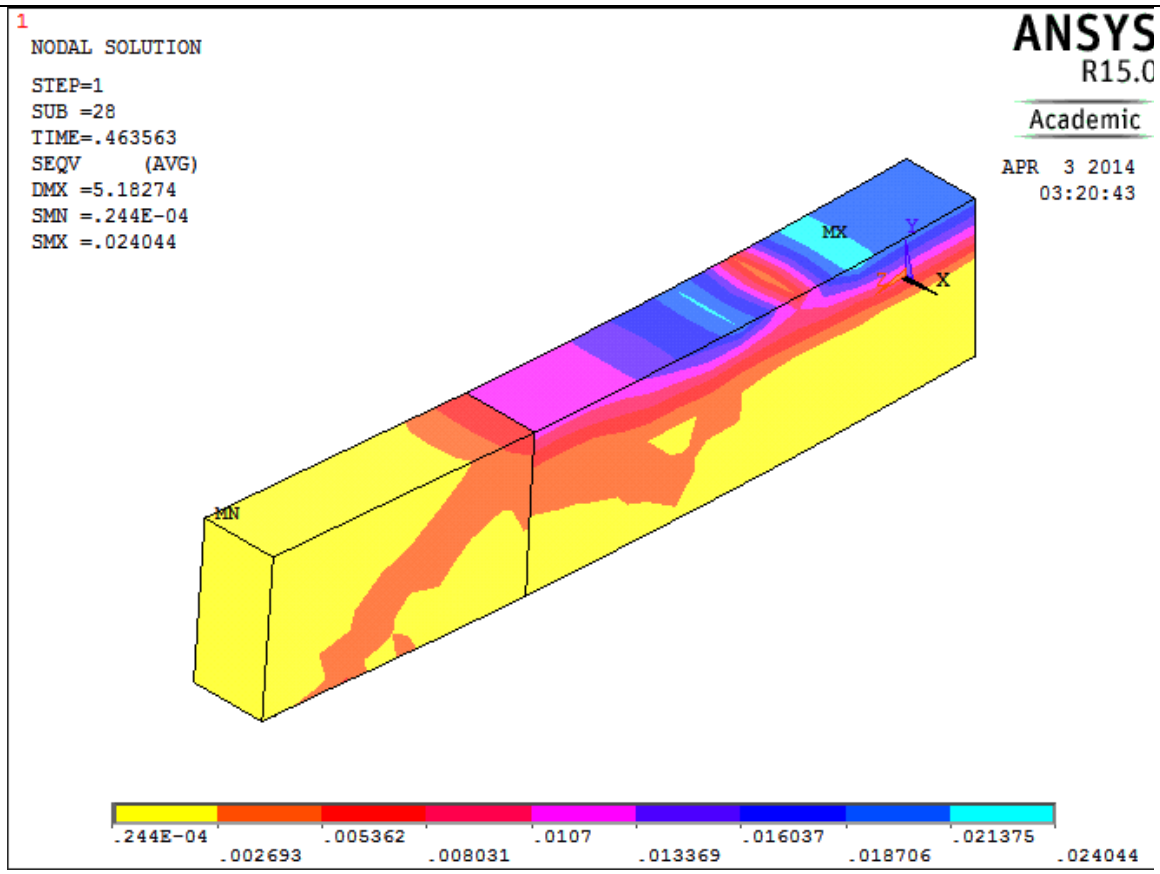

Figure D-219 Nodal Solution -Von Mises Stress for 32-3-10

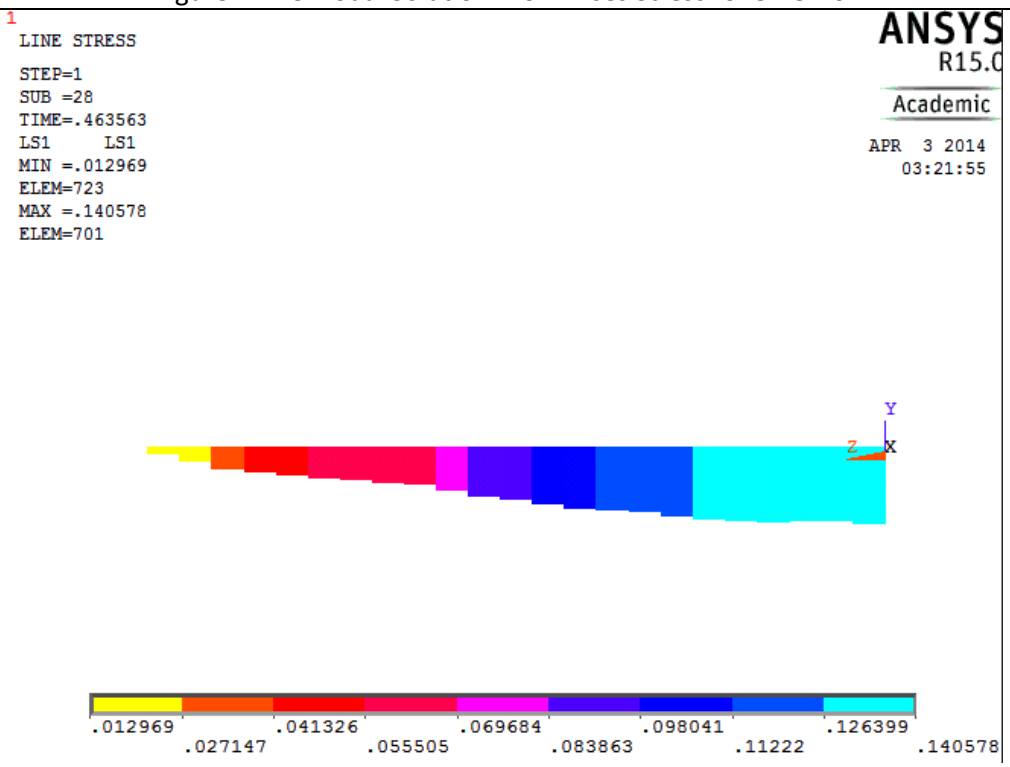

Figure D-220 Reinforcement Stress for 32-3-10

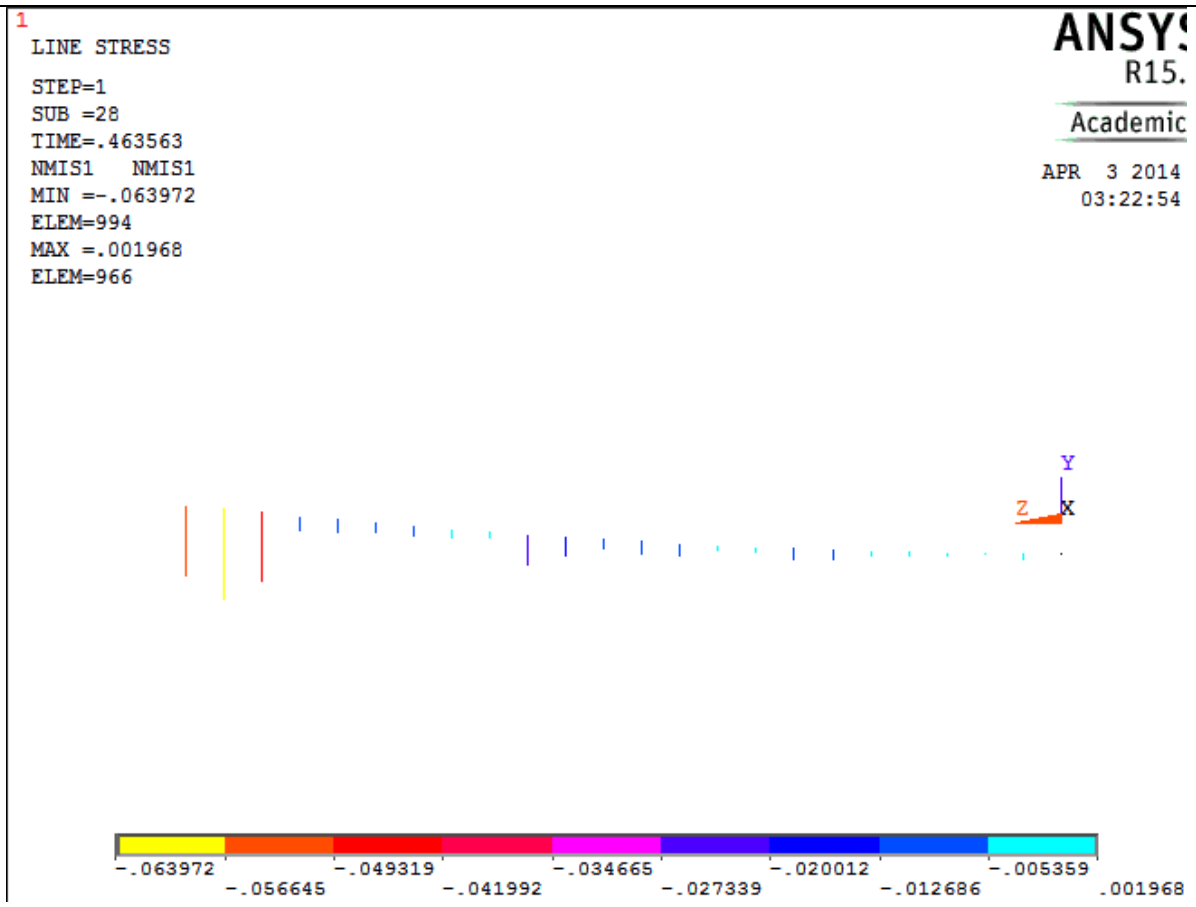

Figure D-221 Spring Stretch for 32-3-10

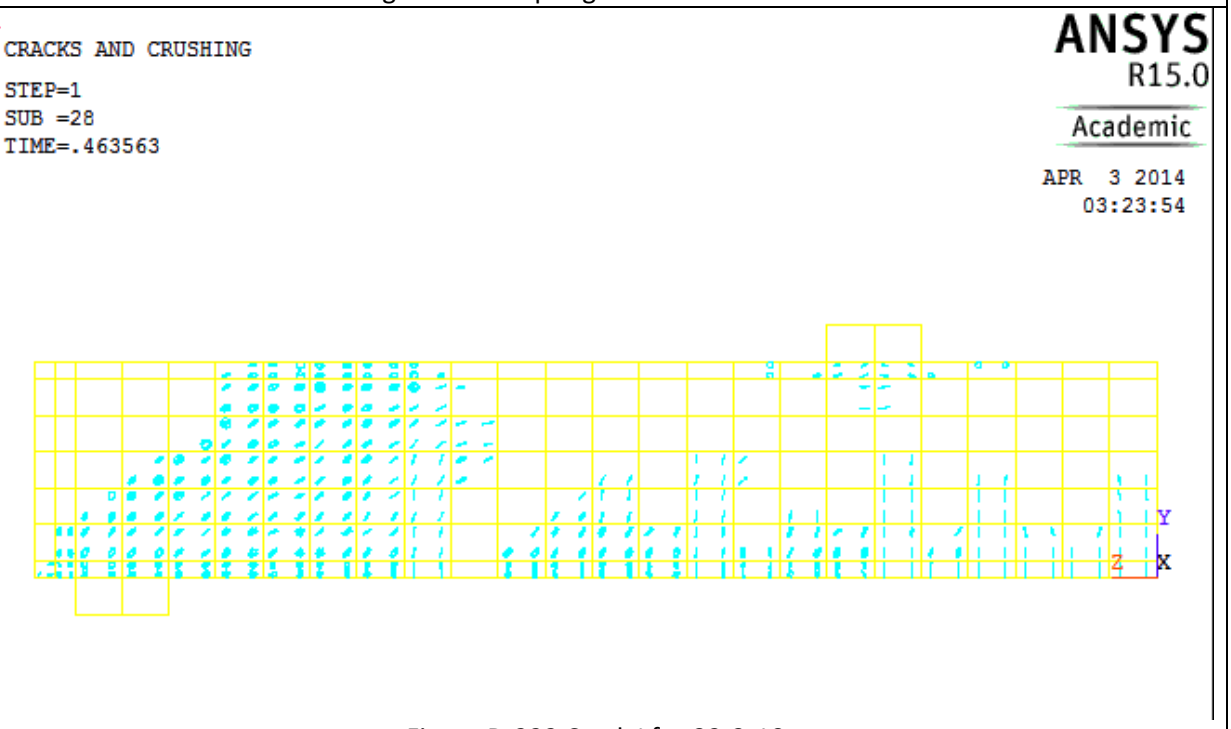

Figure D-222 Crack I for 32-3-10

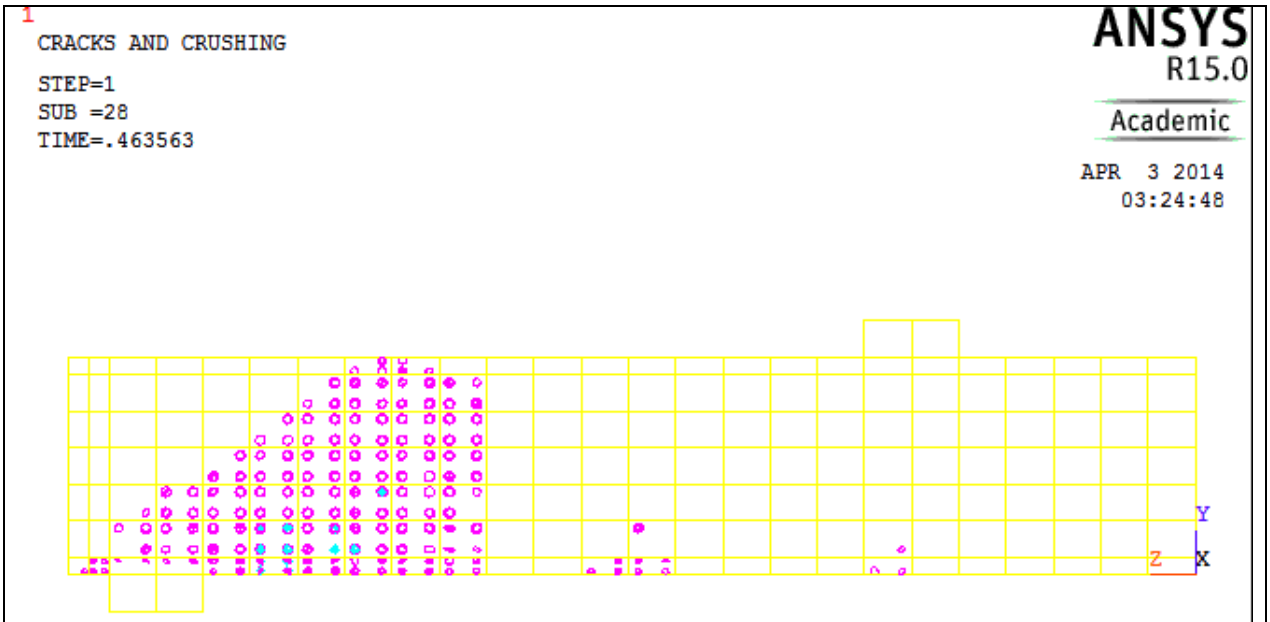

Figure D-223 Crack II for 32-3-10

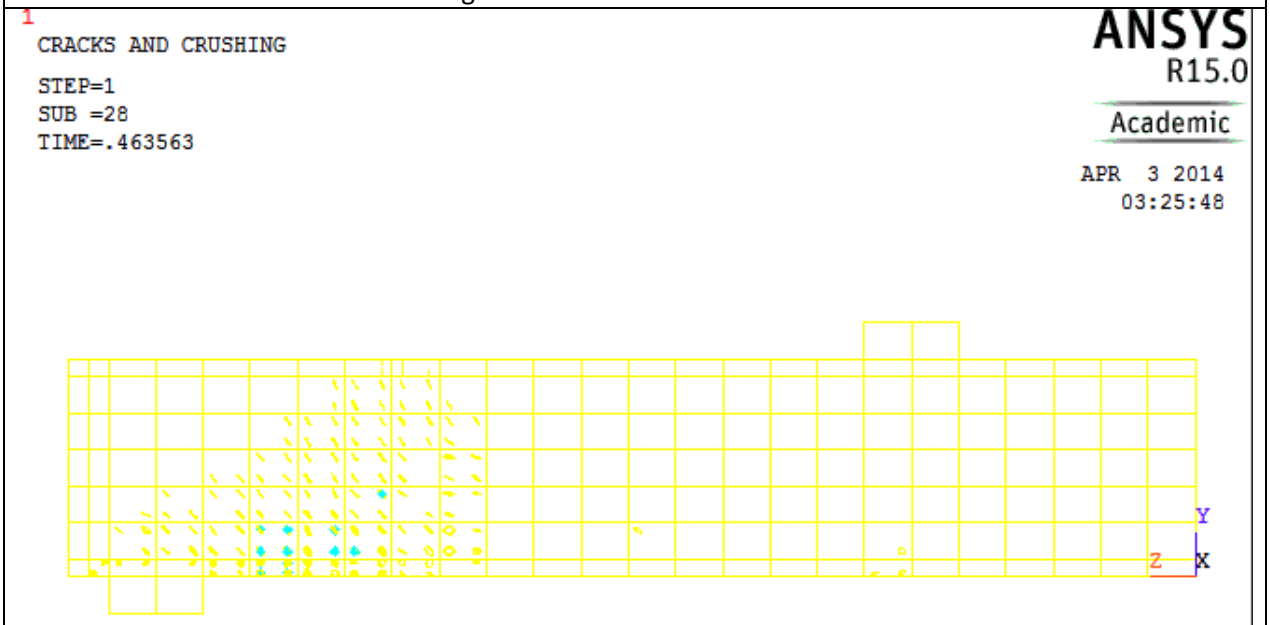

Figure D-224 Crack III for 32-3-10

Table D-29 Details of case 32-3-20

Case Name	Bottom Reinforcement	Honeycombing Location	Strength of Concrete(MPa)	Ultimate Load (kN)	Ultimate Deflection(mm)	Failure Mode
32-3-20	32mm	3	20	175.6832	9.56821	

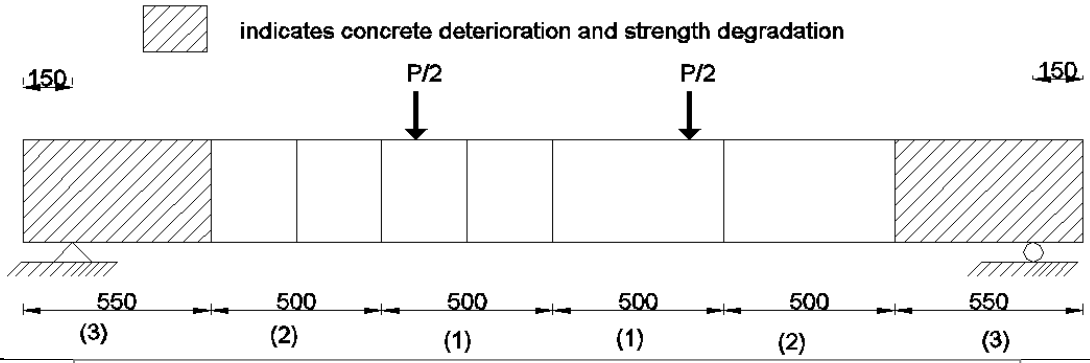

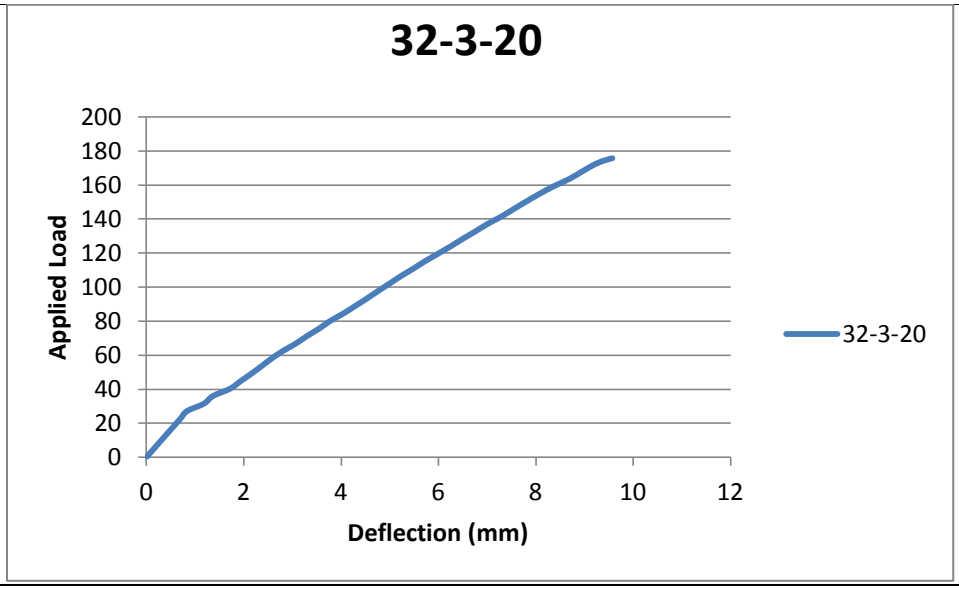

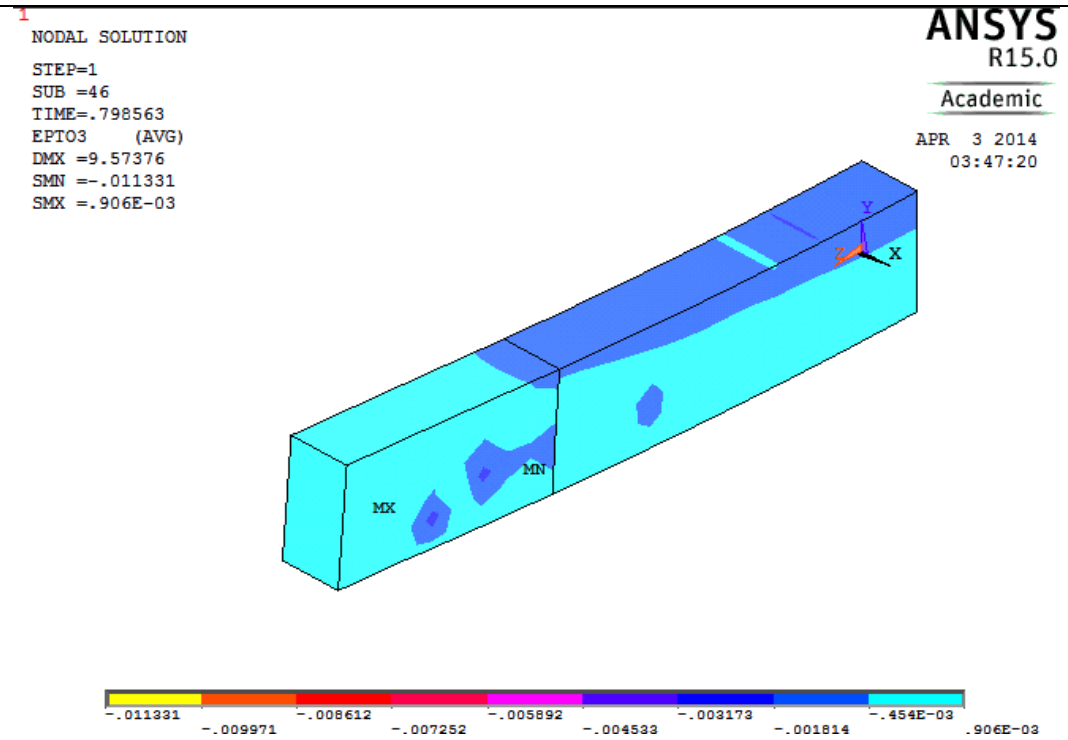

Figure D-225 Nodal solution – 3rd principal total mechanical strain for 32-3-20

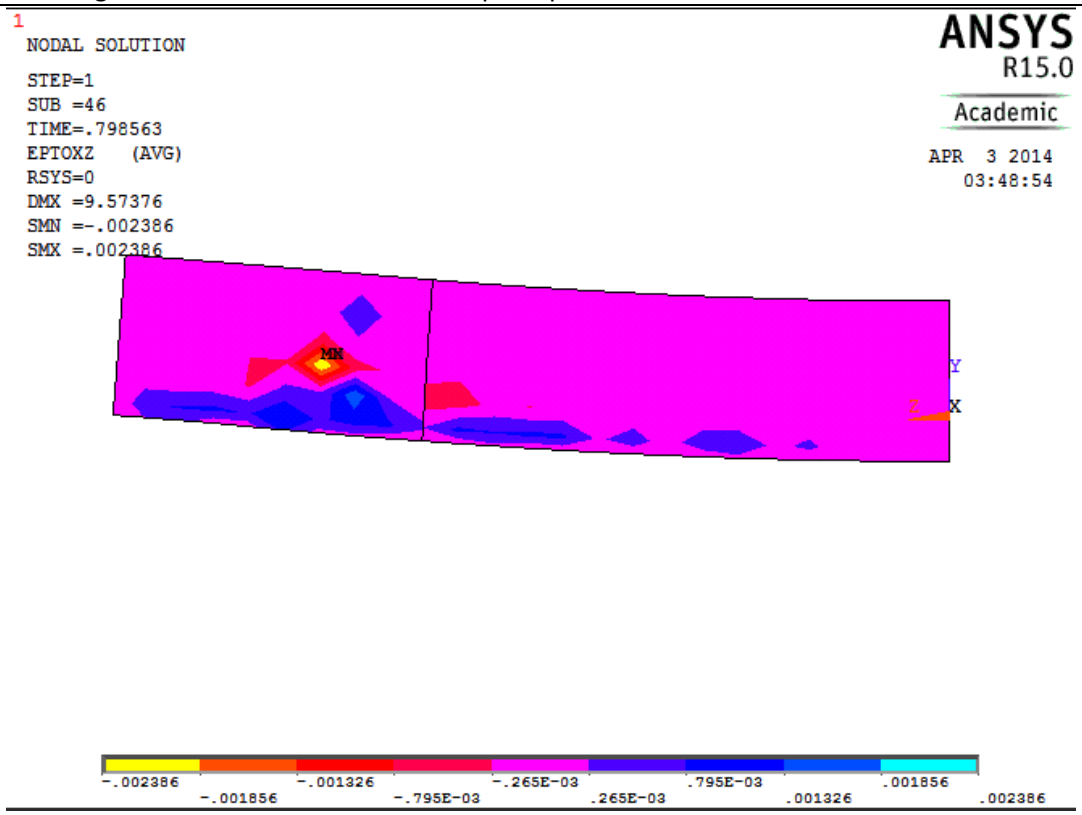

Figure D-226 Nodal Solution XZ shear total mechanical strain for 32-3-20

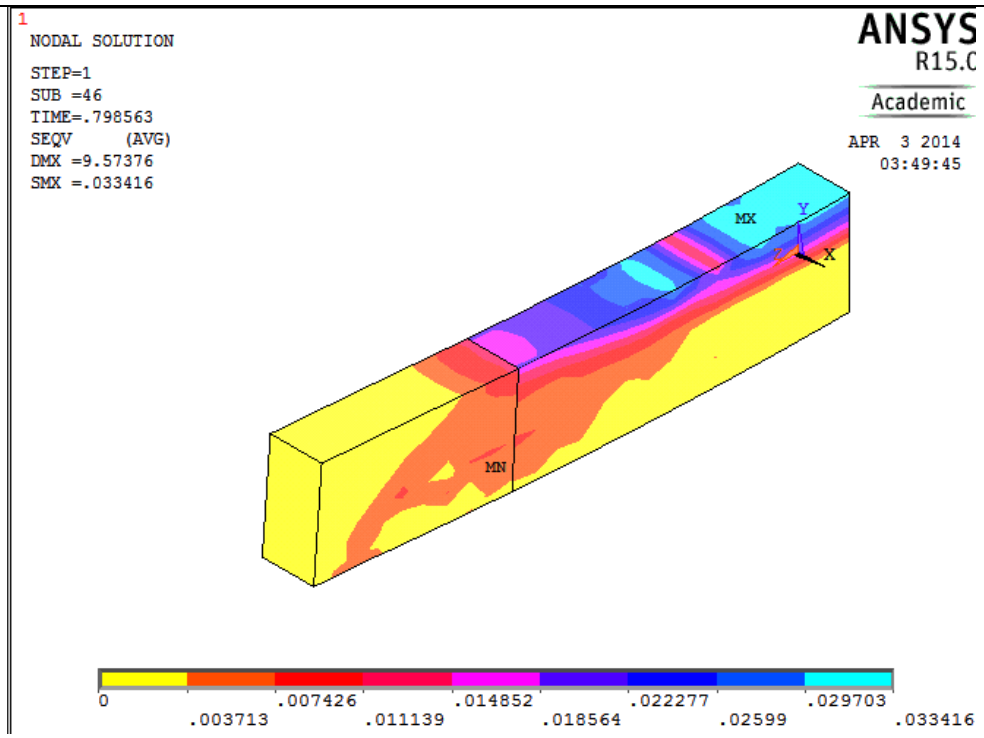

Figure D-227 Nodal Solution -Von Mises Stress for 32-3-20

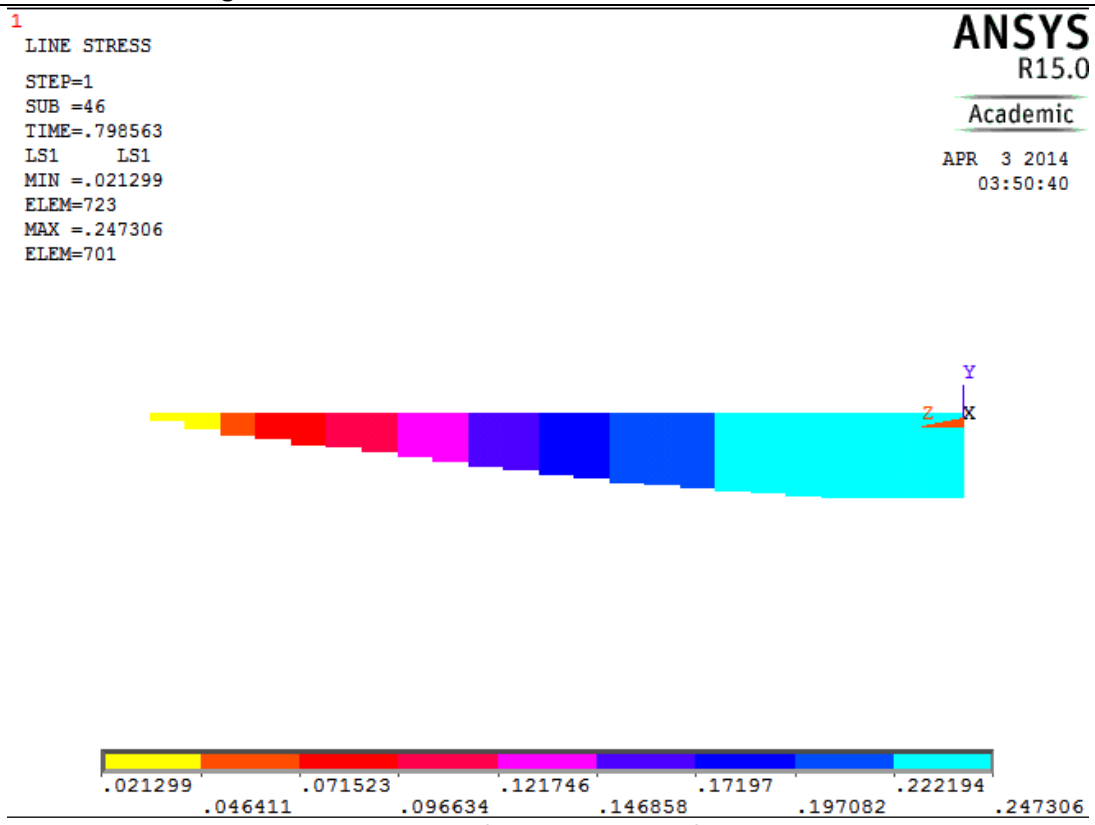

Figure D-228 Reinforcement Stress for 32-3-20

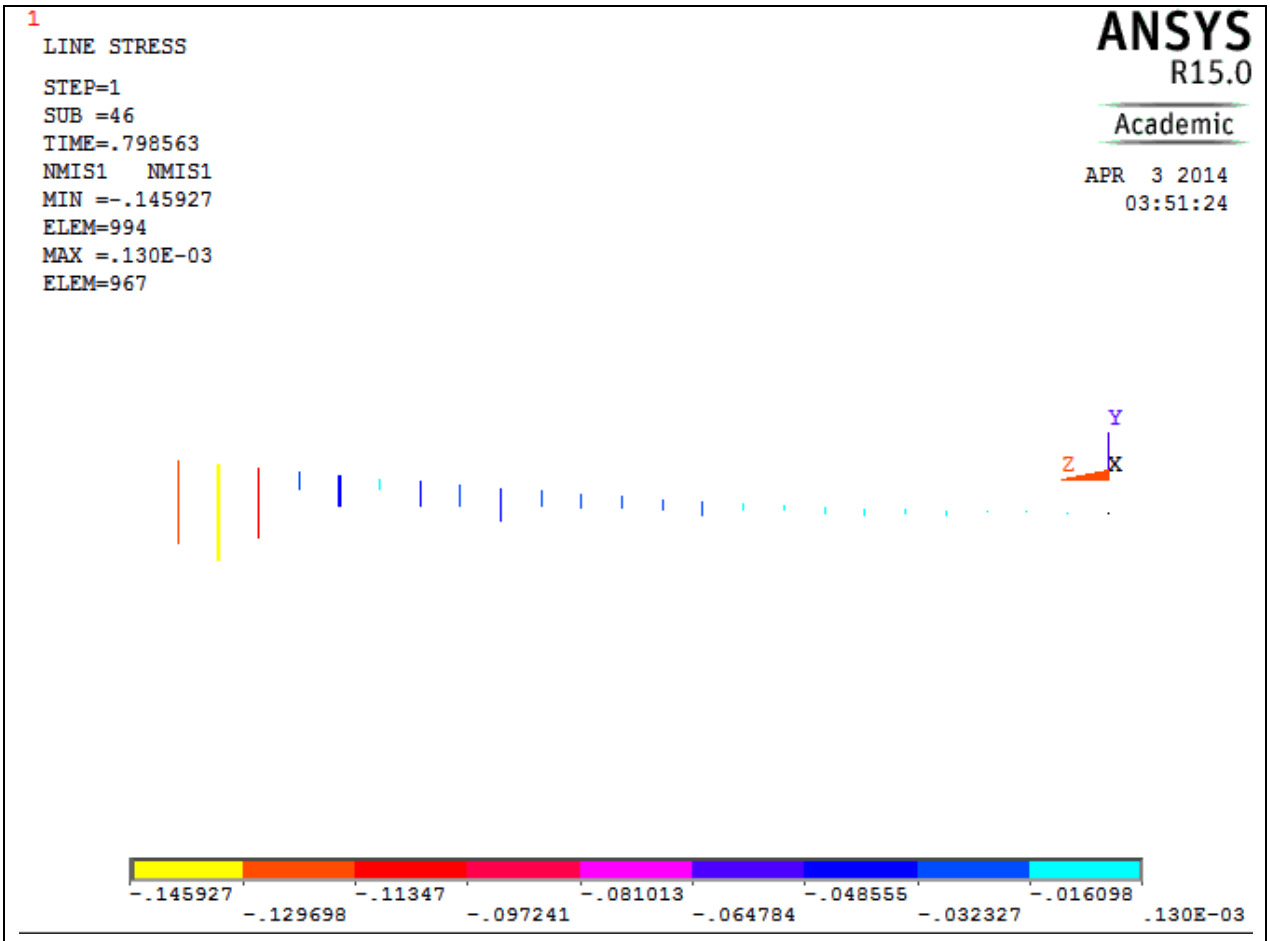

Figure D-229 Spring Stretch for 32-3-20

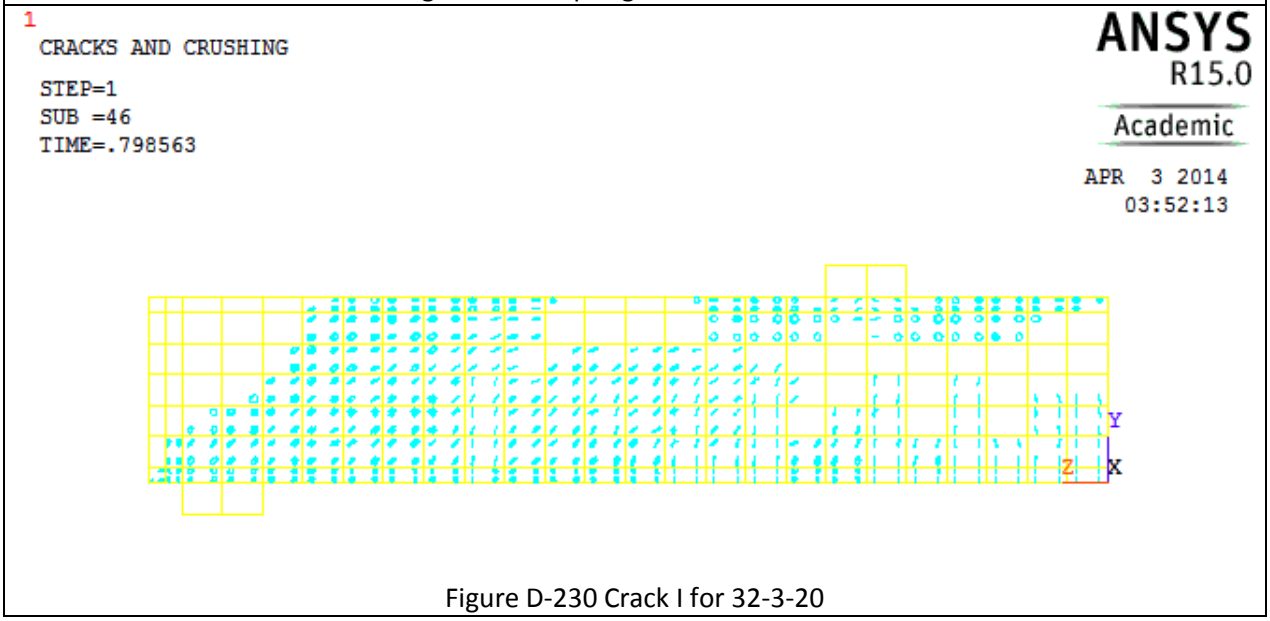

Figure D-230 Crack I for 32-3-20

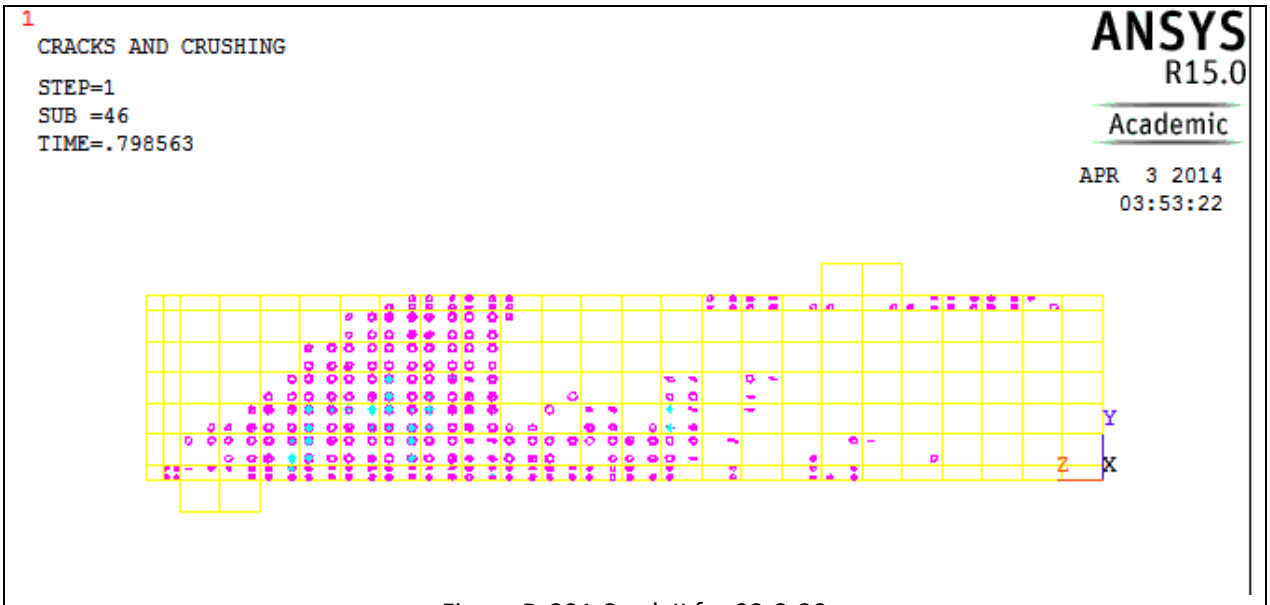

Figure D-231 Crack II for 32-3-20

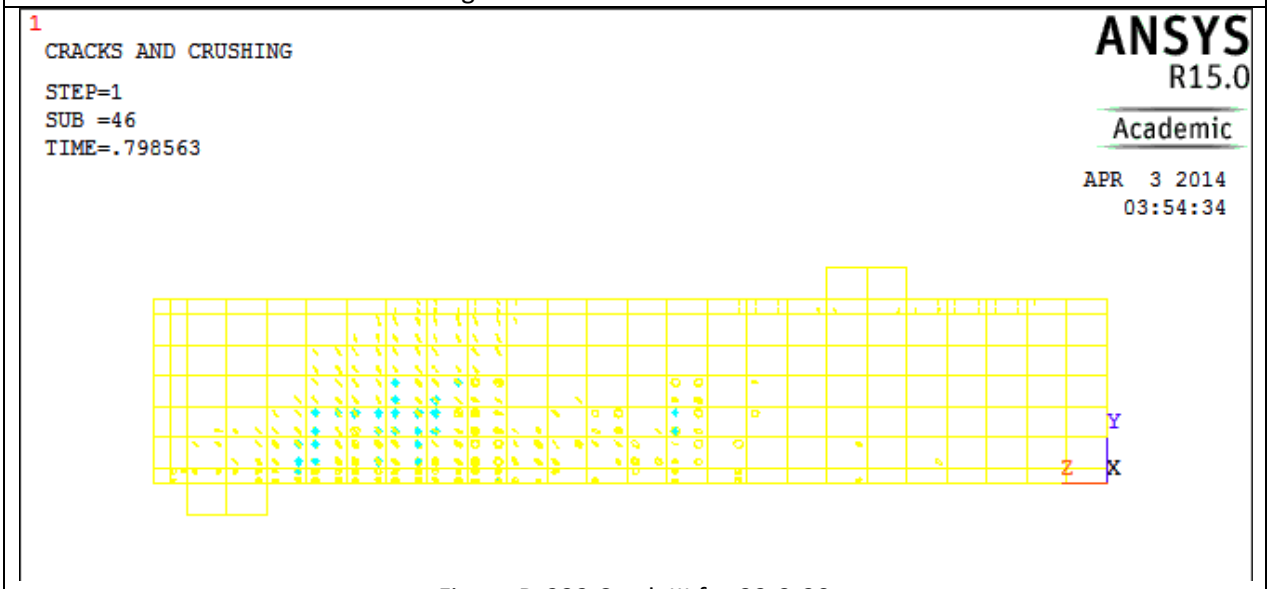

Figure D-232 Crack III for 32-3-20

Table D-30 Details of case 32-3-30

Case Name	Bottom Reinforcement	Honeycombing Location	Strength of Concrete(MPa)	Ultimate Load (kN)	Ultimate Deflection(mm)	Failure Mode
32-3-30	32mm	3	30	183.5592	9.93624	

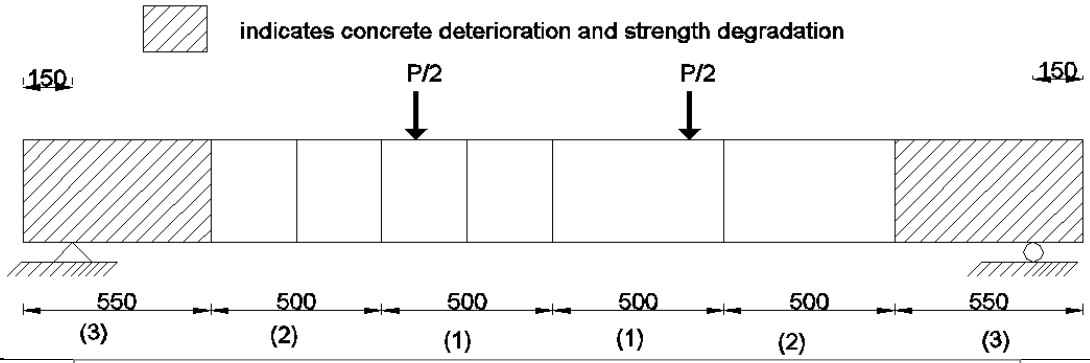

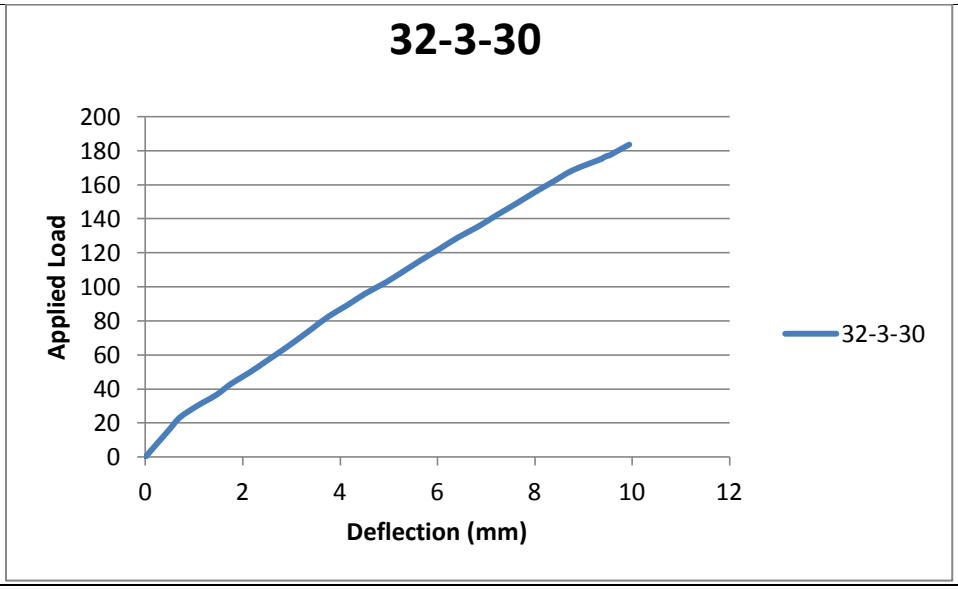

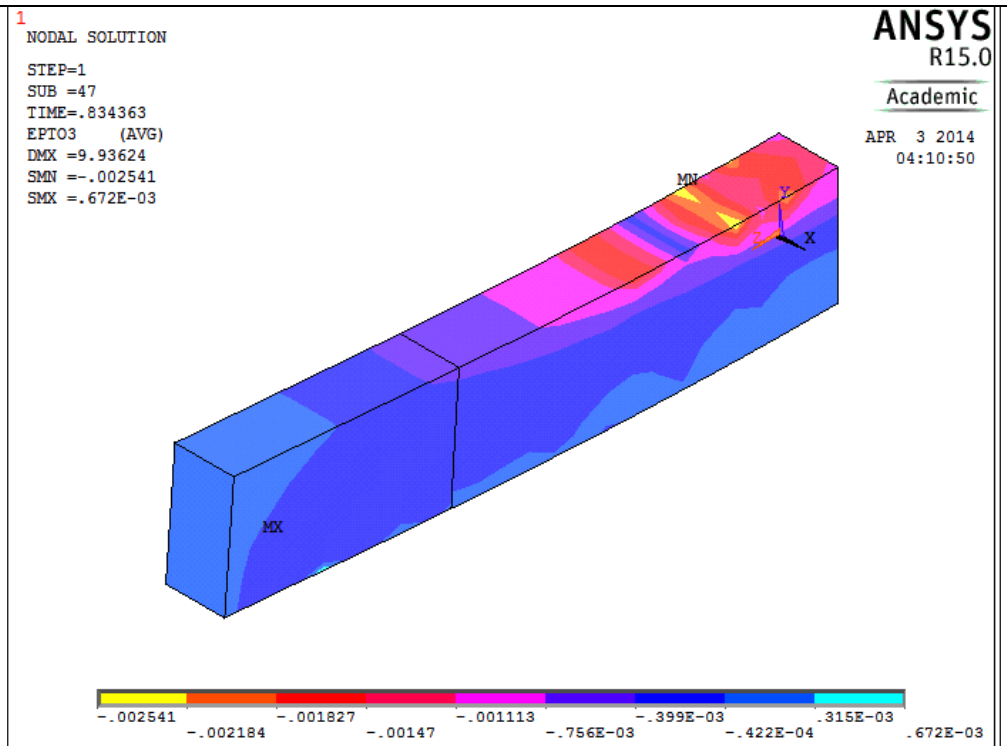

Figure D-233 Nodal solution – 3rd principal total mechanical strain for 32-3-30

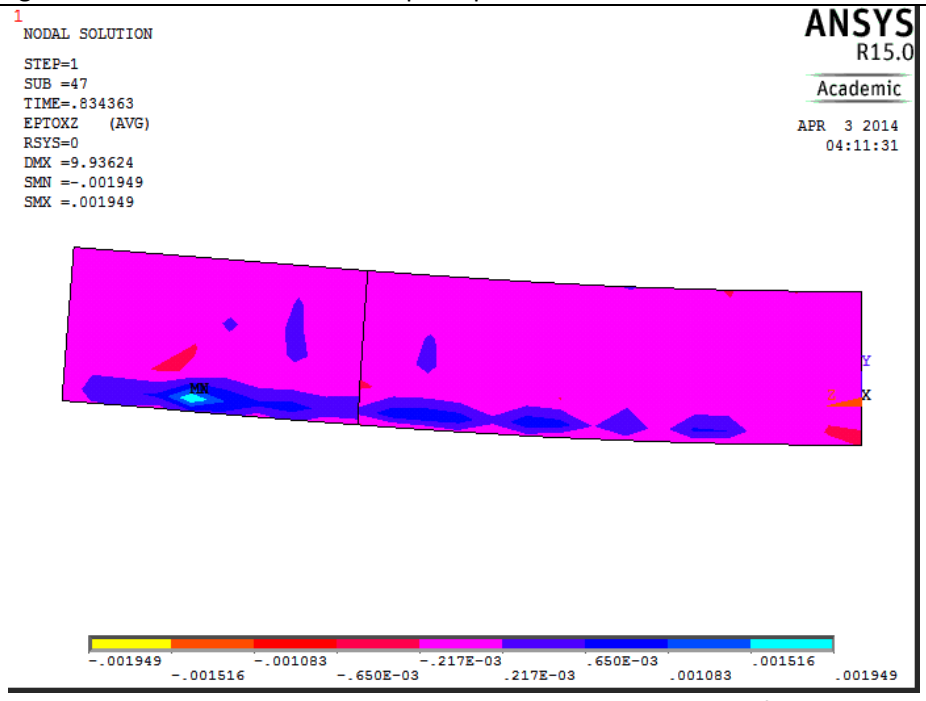

Figure D-234 Nodal Solution XZ shear total mechanical strain for 32-3-30

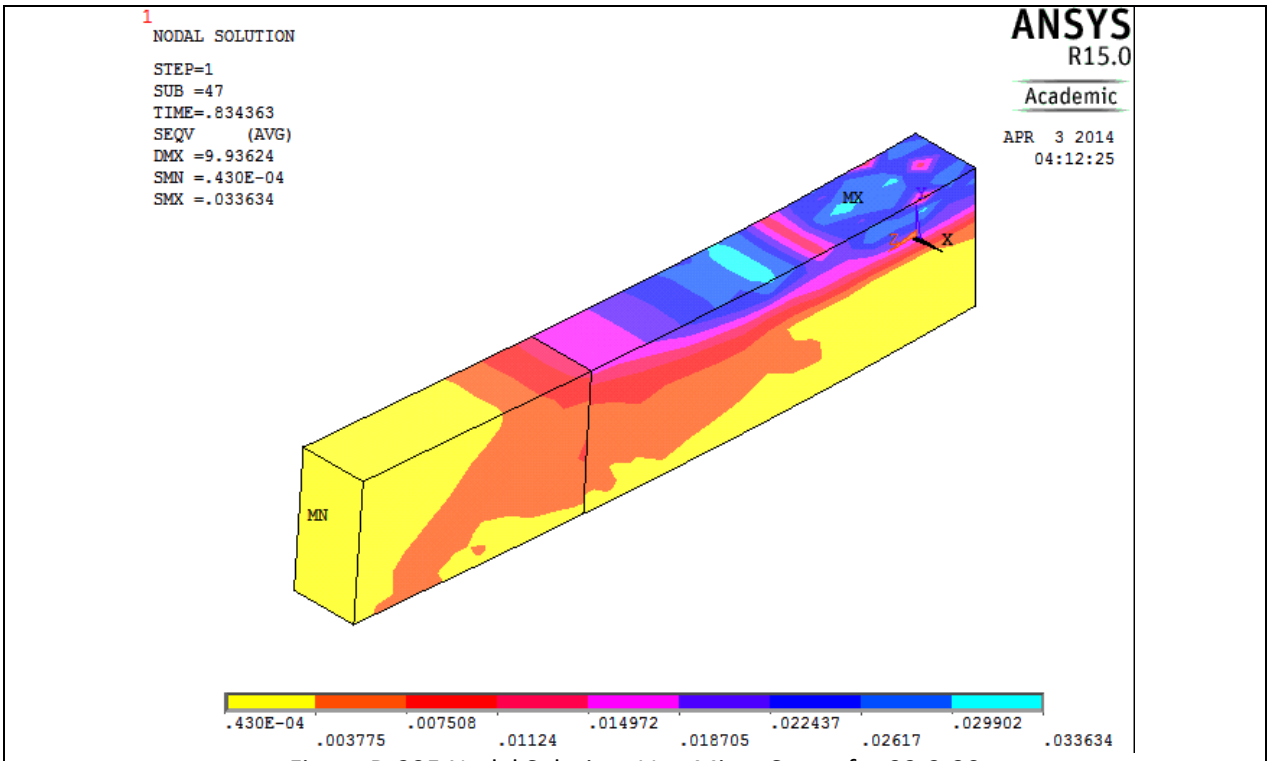

Figure D-235 Nodal Solution -Von Mises Stress for 32-3-30

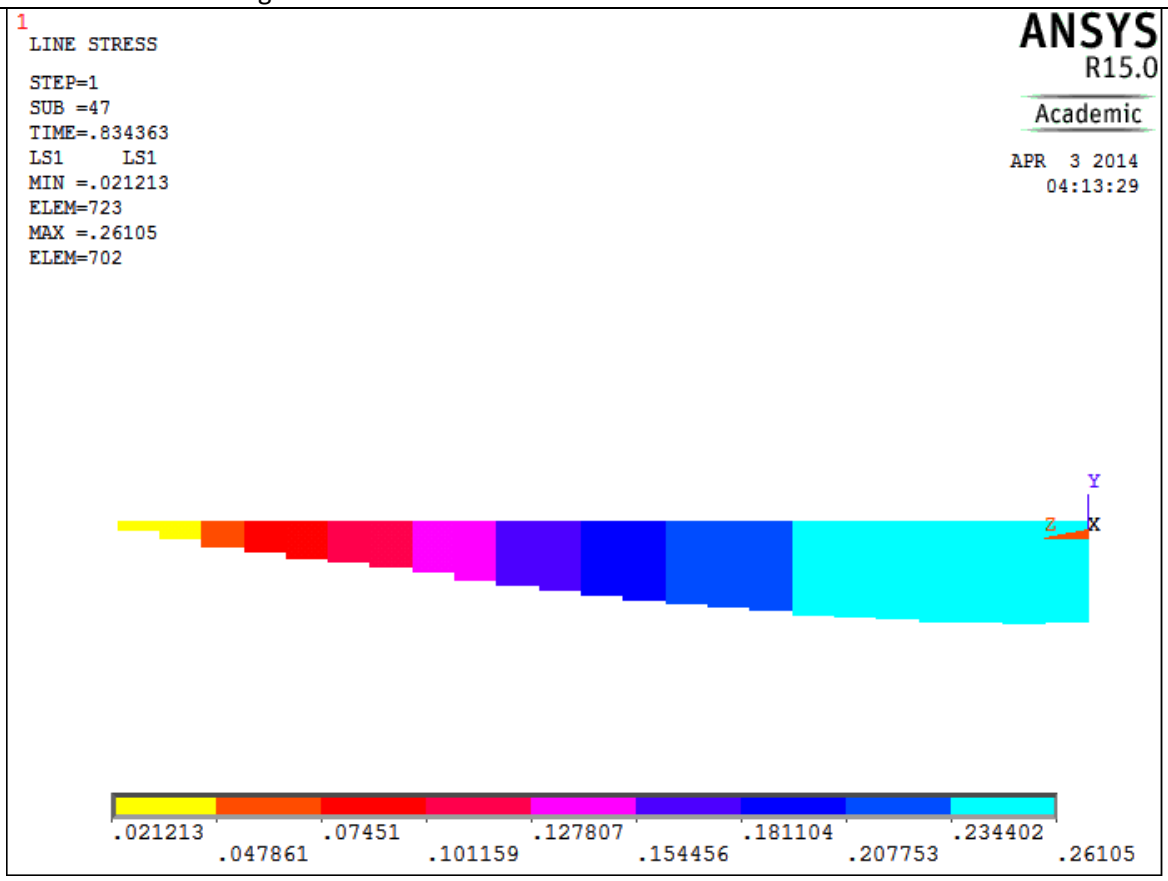

Figure D-236 Reinforcement Stress for 32-3-30

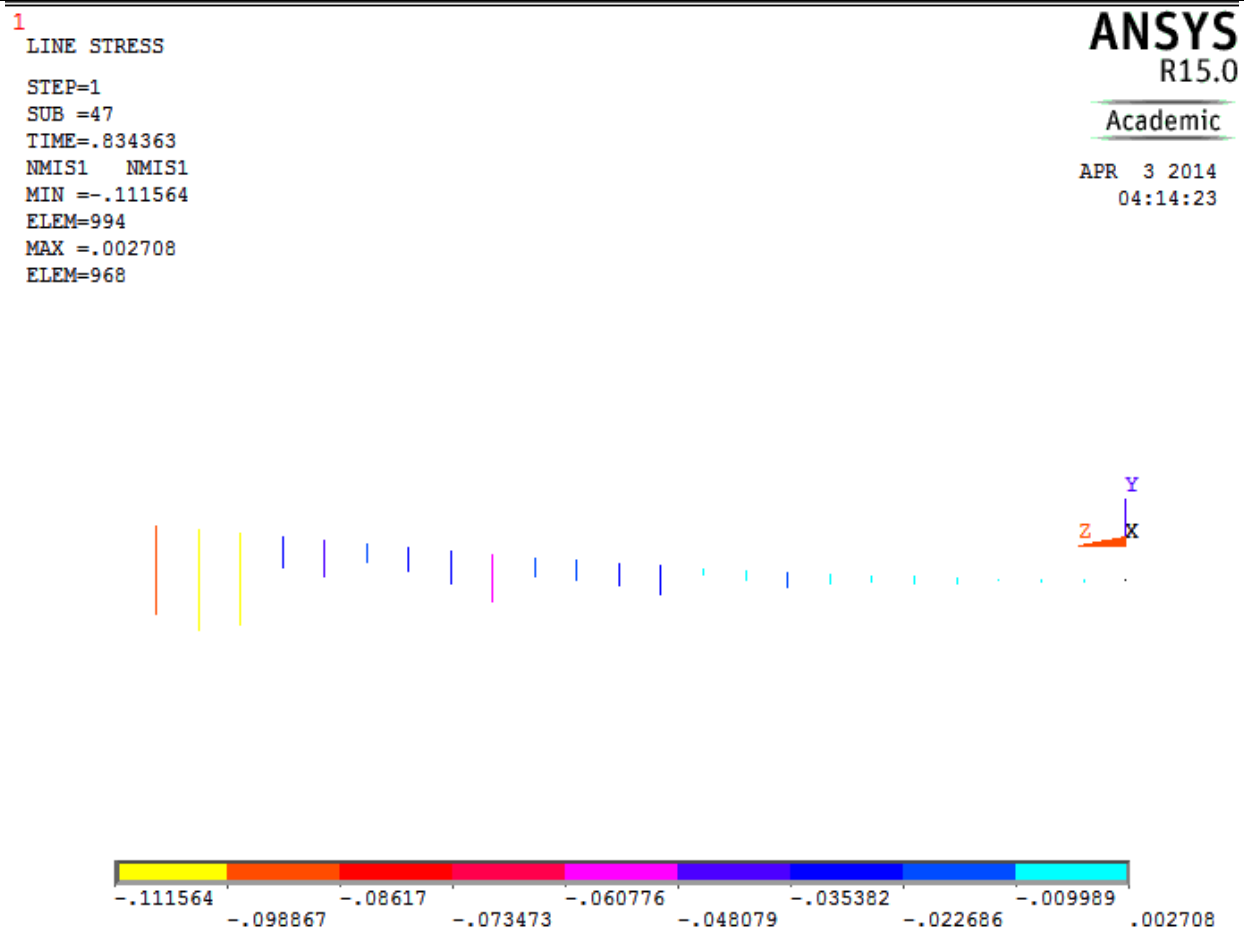

Figure D-237 Spring Stretch for 32-3-30

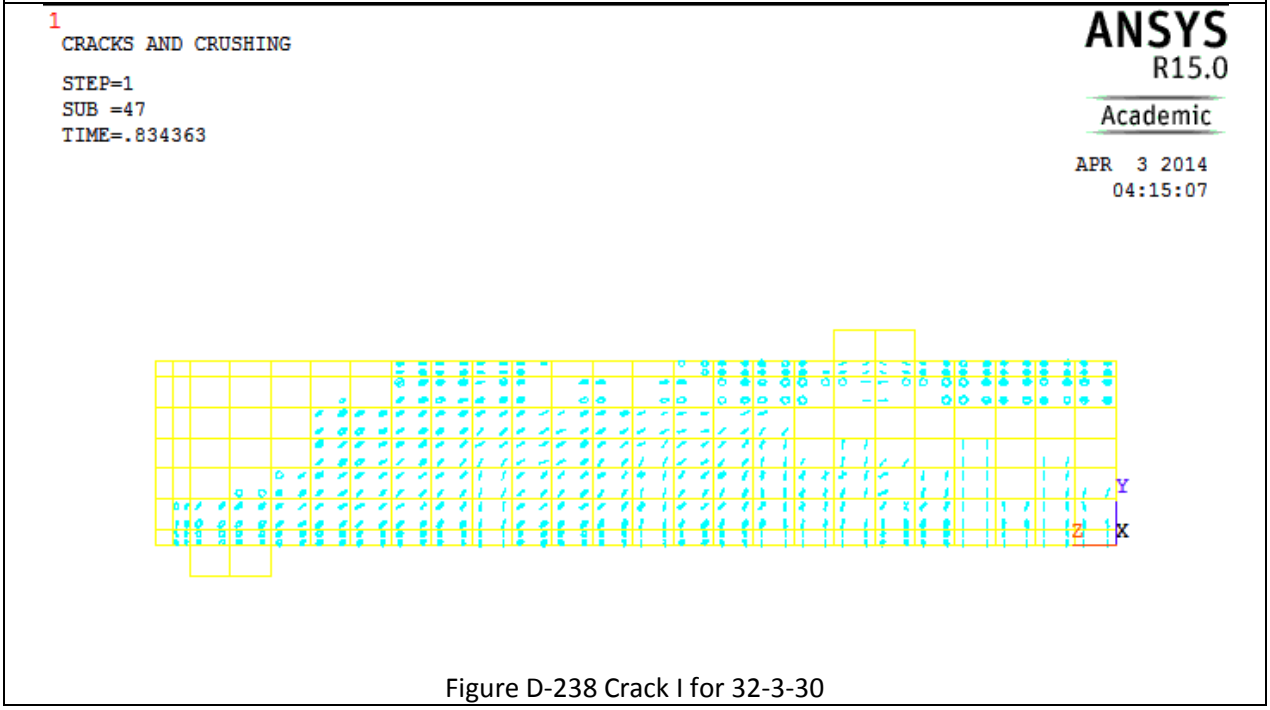

Figure D-238 Crack I for 32-3-30

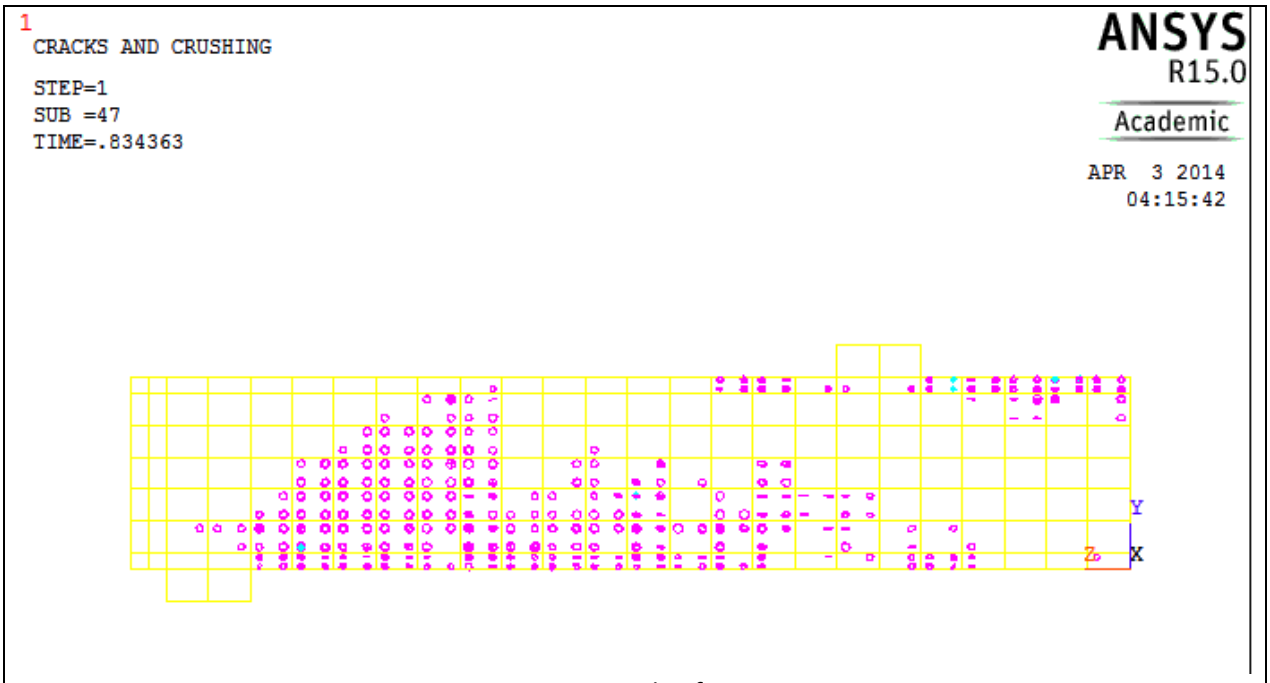

Figure D-239 Crack II for 32-3-30

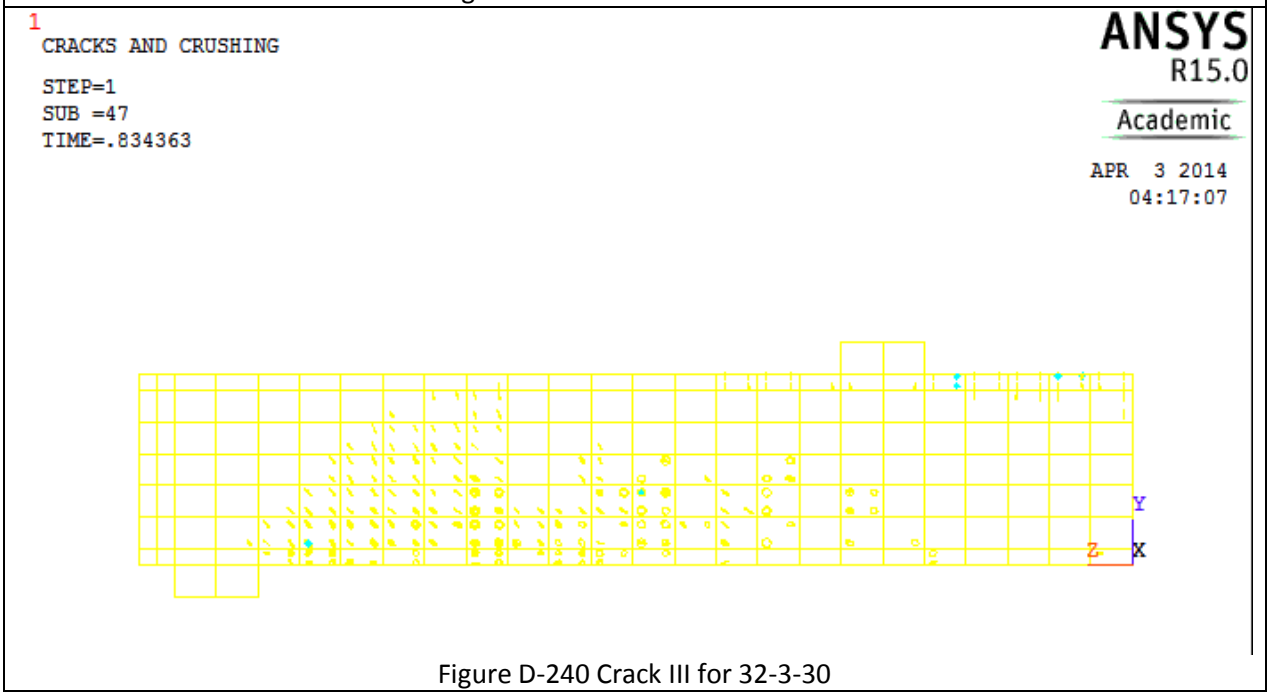

Figure D-240 Crack III for 32-3-30

VITA

Feng Xie was born in Hezhou, Guangxi Province, China, on March, 1989. Between 2008 and2012 he started his civil engineering study in China University of Geosciences majoring in civil engineering. In August, 2012 he came to Syracuse University for advanced civil engineering study and expected to achieve his master degree in May at Syracuse University.